

New Concepts of Reactivity in Photo- & Photoelectrocatalysis

Dissertation

Zur Erlangung des Doktorgrades der Naturwissenschaften

(Dr. rer. nat.)

an der Fakultät für Chemie und Pharmazie

der Universität Regensburg



vorgelegt von

Tobias Alwin Karl

aus Hohenfels

2023

The experimental work has been carried out between October 2018 and September 2022 under the supervision of Prof. Dr. Burkhard König at the University of Regensburg, Institute of Organic Chemistry.

Date of submission: 14.03.2023

Date of colloquium: 19.04.2023

Board of examiners:

Prof. Dr. Antje Bäumner (Chair)

Prof. Dr. Burkhard König (1st Referee)

Prof. Dr. Alexander Breder (2nd Referee)

Prof. Dr. Frank-Michael Matysik (Examiner)

„Ein Gipfel gehört dir erst, wenn du wieder unten bist, denn vorher gehörst du ihm.“

(Hans Kammerlander)

TABLE OF CONTENTS

1 Synthetic Molecular Photoelectrochemistry: New Frontiers in Synthetic Applications, Mechanistic Insights and Scalability	1
1.1 Abstract	2
1.2 Introduction	3
1.3 Electrochemically-mediated Photoredox Catalysis for Selective Super-Oxidations or Super-Reductions.....	5
1.4 Photocatalyst Electro-recycling.....	31
1.5 Photoelectrochemical HAT Reactions.....	43
1.6 Reactor Platforms	49
1.7 Summary and Outlook.....	51
1.8 References	52
2 Energy Harvesting: Synthetic Use of Recovered Energy in Electrochemical Late-Stage Functionalization.....	57
2.1 Abstract	58
2.2 Introduction	59
2.3 Results and Discussion	60
2.4 Conclusion.....	65
2.5 References	66
2.6 Experimental Part	67
2.6.1 General Remarks.....	67
2.6.2 Power Sources.....	67
2.6.3 Electrodes.....	68
2.6.4 Description of the EH Device	68
2.6.5 Characterization of Starting Materials	71
2.6.6 Characterization of Products.....	72
2.6.7 References.....	75

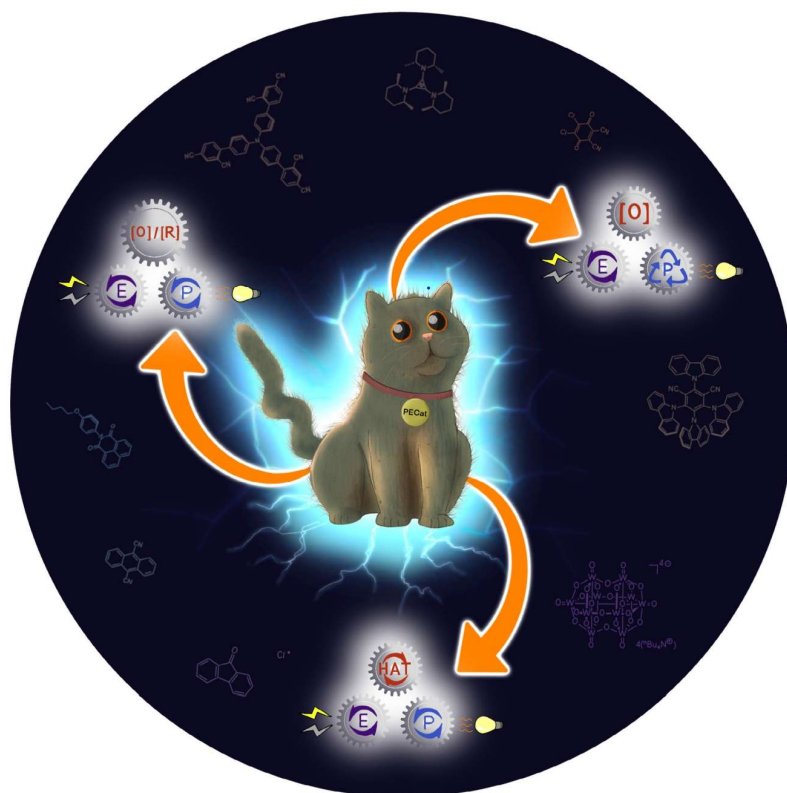
3 Electro-mediated Photoredox Catalysis for Selective C(sp³)-O Cleavages of Phosphinates to Carbanions.....	77
3.1 Abstract	78
3.2 Introduction	79
3.3 Results and Discussion	81
3.4 Conclusion.....	92
3.5 References	93
3.6 Experimental Part	95
3.6.1 General Remarks.....	95
3.6.2 Materials and Electrode Preparation.....	96
3.6.3 Synthesis of Catalysts	98
3.6.4 Synthesis of Phosphinate Substrates.....	99
3.6.5 Optimization of Reaction Conditions	102
3.6.6 Photoelectrochemical Isomerism Control Experiments.....	103
3.6.7 Characterization of Catalysts	105
3.6.8 Characterization of Phosphinate Substrates.....	107
3.6.9 Characterization of Products.....	119
3.6.10 Cyclic Voltammetry.....	128
3.6.11 Spectroelectrochemistry of Catalysts.....	131
3.6.12 UV-Vis Spectroscopy of Electrogenerated Radical Anions	132
3.6.13 Steady-State Luminescence Emission Spectroscopy.....	134
3.6.14 Lifetime Measurement	136
3.6.15 NMR Investigations of Preassociation.....	138
3.6.16 FT-IR Spectroscopy	142
3.6.17 Emission Spectra of LEDs.....	144
3.6.18 Electron Paramagnetic Spectroscopy Investigations	147
3.6.19 Computational Investigations	151
3.6.20 X-Ray Crystallography	164
3.6.21 References.....	166
4 Oxidative conPET Catalysis for Arene Functionalization	171

4.1	Abstract	172
4.2	Introduction	173
4.3	Results and Discussion	176
4.4	Conclusions	184
4.5	References	185
4.6	Experimental Part	186
4.6.1	General Remarks.....	186
4.6.2	Synthesis of Catalysts	186
4.6.3	Screening of Reaction Conditions.....	189
4.6.4	Electrochemical and Photophysical Characterization.....	191
4.6.5	Mass Spectroscopic Investigation.....	202
4.6.6	Characterization of Products.....	203
4.6.7	Unreactive Substrates and Nucleophiles.....	208
4.6.8	NMR Spectra of Isolated Compounds	209
4.6.9	References.....	235
5	Arene Hydrodehalogenation by Hydrogen-Terminated Diamond Semiconductor and Visible Light	237
5.1	Abstract	238
5.2	Introduction	239
5.3	Results and Discussion	240
5.4	Conclusion.....	248
5.5	References	249
5.6	Experimental Part	251
5.6.1	General Remarks.....	251
5.6.2	Synthesis and Description of DND Material	252
5.6.3	Description of Synthetic Procedures.....	252
5.6.4	Optimization and Control Reactions.....	253
5.6.5	Mass Spectroscopic Analysis.....	255
5.6.6	Catalyst Recycling	267
5.6.7	Substrate Synthesis	268

5.6.8	GC-FID Calibration	269
5.6.9	X-Ray Crystallography	270
5.6.10	GC-FID Spectra	272
5.6.11	NMR Spectra of Isolated Compounds	276
5.6.12	NMR Spectra of Crude Mixtures	278
5.6.13	References.....	297
6	A General Premise for Cross–Coupling Reactions with Adaptive Dynamic Homogeneous Catalysis	299
6.1	Abstract	300
6.2	Introduction	301
6.3	Results and Discussion.....	302
6.4	Conclusion.....	316
6.5	References	317
6.6	Experimental Part	318
6.6.1	General Remarks.....	318
6.6.2	Synthetic Procedures of Cross–Coupling Reactions.....	321
6.6.4	Characterization of Isolated Products	324
6.6.5	References.....	339
7	Summary.....	343
8	Zusammenfassung.....	349
9	Appendix.....	355
9.1	Abbreviations	355
9.2	Curriculum Vitae	359
10	Danksagung	365
11	Eidesstattliche Erklärung.....	369

CHAPTER 1

1 Synthetic Molecular Photoelectrochemistry: New Frontiers in Synthetic Applications, Mechanistic Insights and Scalability



This chapter has been published. For reference see: S. Wu, J. Kaur, T. A. Karl, X. Tian, J. P. Barham *Angew. Chem. Int Ed.* **2022**, *61*, (12), e202107811.

Tobias A. Karl wrote parts of the manuscript.

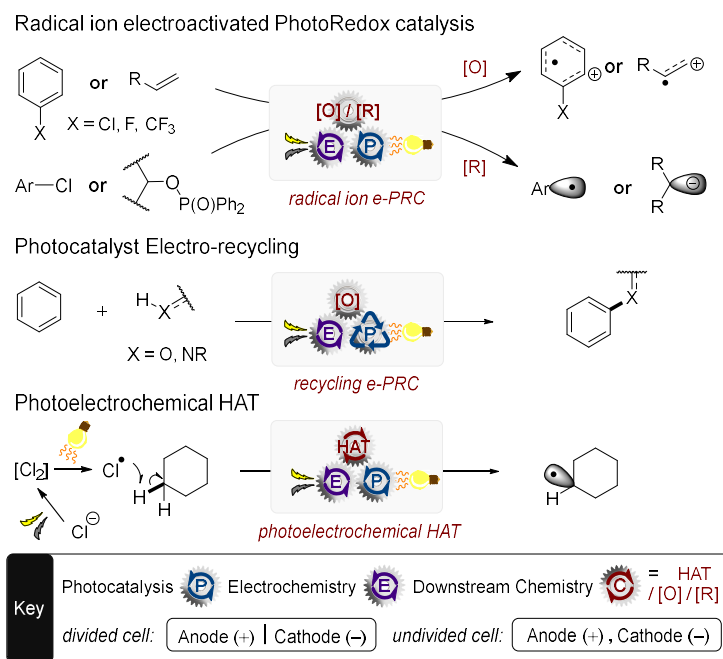
1.1 Abstract

Synthetic Photoelectrochemistry (PEC) is receiving increasing attention as a new frontier for the generation and handling of reactive intermediates. PEC permits selective single electron transfer (SET) reactions in a much greener way and broadens the redox window of possible transformations. Herein, the most recent contributions are reviewed, demonstrating exciting new opportunities. Namely, a combination of PEC with other reactivity paradigms (hydrogen atom transfer, radical polar crossover, energy transfer sensitization), scalability up to multigram scale, novel selectivities in SET super-oxidations/reductions, and the importance of precomplexation to temporally enable excited radical ion catalysis.

1.2 Introduction

The field of single electron transfer (SET) in organic synthesis and the late-stage functionalization of valuable compounds has expanded remarkably in the past two decades. Among this field, photoredox catalysis (PRC) and synthetic organic electrochemistry (SOE) are highly attractive to synthetic chemists due to i) their abilities to afford reactive intermediates under mild conditions and ii) their uses of light and electricity as sustainable energy sources to drive reactions.^[1-2] As powerful and generally applicable as PRC and SOE are, these chemistries present some issues on a fundamental level. PRC reactions are limited by the redox window of photocatalysts which is in most part defined by the energy of visible photons (ca. 1.8–3.1 eV).^[3] UV photons that access higher energy limits come with penalties of less energy- and cost-efficient reactors, safety and the direct exciting substrate molecules leading to deleterious pathways. Visible light PRC reactions utilizing multi-photon processes therefore came to the fore for overcoming the ‘redox energy limit’.^[4] To turnover PRC reactions, including these multi-photon paradigms, large excesses of sacrificial oxidants or reductants can be required to generate active forms of the catalyst or to turnover ‘spent’ photocatalyst. In SOE reactions, electrodes generally do not enjoy the ability to distinguish between different reaction components beyond inherent thermodynamic redox potentials of reaction components. Over-oxidations and over-reductions as well as solvent redox processes can plague reactions.

In this respect, engineering controls like tiny interelectrode distances,^[5] alternating potential,^[6] continuous flow manifolds^[7] or surface modifications,^[8] have shown promise in imparting selectivity in recent years. The merger of PRC and SOE, ‘synthetic photoelectrochemistry’, tackles these issues and has come to the forefront of methods for SET chemistry.^[9] By channeling electrochemical and photochemical energy through a homogeneous (or heterogeneous) catalyst, intriguing new reactivity and selectivity opportunities are manifested. The essence of this emerging field has been captured by highlights^[10] a full review^[9] and partially covered in other reviews.^[11] However, the field has expanded dramatically in the last couple of years in terms of its synthetic opportunities, reactivity concepts and mechanistic understanding. In the super-redox chemistry of electrogenerated radical ion (open shell) photocatalysts (Scheme 1), curious selectivities and reactivities unattainable by PRC or SOE chemistries have emerged, together with first pieces of evidence of catalyst-substrate precomplexation to rationalize otherwise time-forbidden excited-state reactivity. While the use of HAT as a reactivity paradigm is well established in PRC and SOE,^[12,13] its recent combination with PEC signals a broad scope of future synthetic applications. Finally, in (closed shell) photocatalyst electro-recycling, methods to upscale PEC to a productive level (multigram→multigram/h) are emerging, including various continuous photoflow and undivided cell batch setups.



Scheme 1. Focus of this review.

In the following sections, we categorize the new examples as follows: 1) Super-oxidations/reductions; 2) Photocatalyst Electro-recycling; 3) Photoelectrochemical HAT reactions. Interfacial photoelectrochemistry^[9] is not covered.^[14]

1.3 Electrochemically-mediated Photoredox Catalysis for Selective Super-Oxidations or Super-Reductions

The term ‘electrochemically-mediated photoredox catalysis’ (e-PRC) was coined as a blanket term to describe the category of PEC involving an intimate relationship of electro- and photochemical steps within the same catalytic cycle as subsequent steps.^[9] This broadly separates into two sub-categories, ‘radical ion e-PRC’ and ‘recycling e-PRC’ (Section 2) which, although technically are mechanistically identical, are conceptually different. Radical ion e-PRC involves electrogenerated radical ions which are photoexcited to yield super-oxidants or super-reductants. The key advantage is that radical ion e-PRC can engage compounds beyond the redox windows accessible to photoredox catalysis or synthetic electrochemistry alone (−3.0 V to +3.0 V), since photoexcited radical ion catalysts are oftentimes colored species that possess higher redox energy (ca. ~0.5-1.5 eV than conventional neutral (closed shell) photocatalyst excited states. Seminal contributions of Moutet and Reverdy^[15] first demonstrated this concept in the oxidations of diphenylethene and benzyl alcohol by an electrogenerated phenothiazine (PTZ) radical cation. These reports have been reviewed previously.^[9] Lund and Carlsson first demonstrated the reductive paradigm; dechlorination of chlorobenzene by electrogenerated pyrene radical anions.^[16] Inspired by this, the reductive dechlorination of chlorobiphenyls by 9,10-diphenylanthracene was studied by Rusling.^[17] While these reports established the fundamental concept of e-PRC, their focus was not synthetic and their conditions not synthetically applicable beyond a few catalytic turnovers. The field lay dormant for several decades until the recent dawn of its renaissance, driven by a combination of events: (i) an increasing interest in PRC and SOE,^[9] (ii) the realization of chemically-generated photoexcited radical ions as potent redox agents in synthesis^[4a-d] and (iii) seminal efforts in e-PRC in organic synthesis by synthetic groups^[18] that have been reviewed previously.^[9] A key platform that has underpinned rapid uptake of PRC by the synthetic community is the compilation of photocatalyst structures with their photophysical and redox properties, enabling chemists to logically plan reactions and provide best chances of success. Figure 1 depicts structures of historical and contemporary radical ion (pre)photocatalysts, while Table 1 summarizes their spectroscopic and redox properties as well as reported synthetic applications. Figure 2 summarizes the redox properties of radical ion photocatalysts compared to conventional photocatalysts and example substrates. While the focus of this section of the review is on e-PRC, this compilation of properties should equally assist practitioners of conPET photocatalysis in planning reactions.

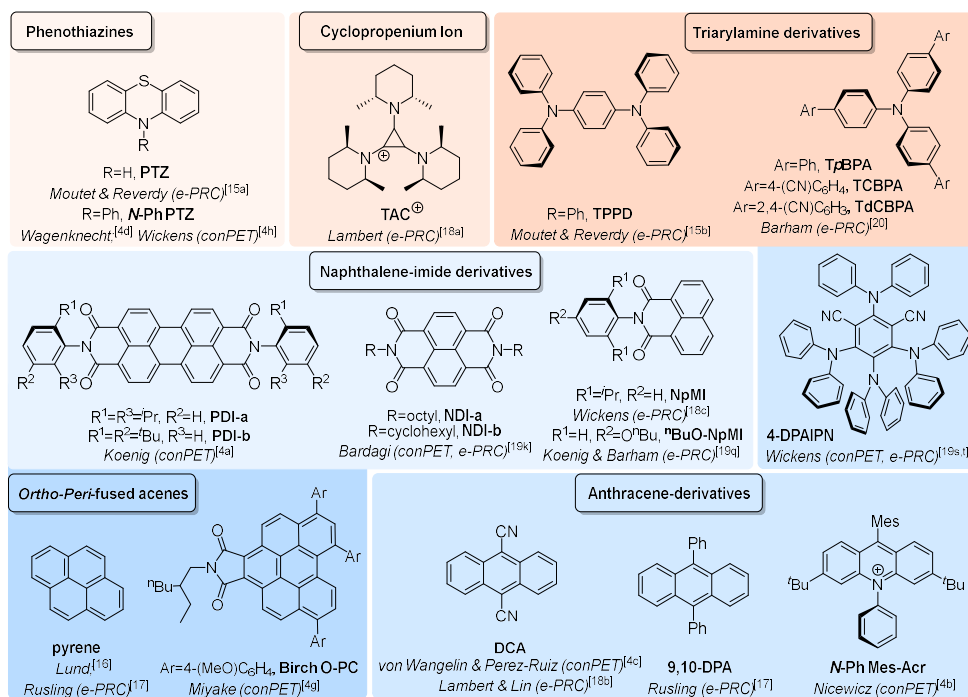


Figure 1. Radical ion/radical pre-catalysts grouped by molecular architecture: photooxidant pre-catalysts (red background) and photoreductant precatalysts (blue background). Shading corresponds to pre-catalyst family, is indicative of oxidizing/reducing power of radical ion forms of the family but not specific cases (Table 1).

Table 1. Properties and applications of radical ion/radical photocatalysts.

Pre-Catalysts							Radical Ion/Radical Photocatalyst						
PRC	λ_{max} (abs)	λ_{max} (em)	τ (ns)	E^{0-0} (eV)	$E_{1/2}^a$ (V)	$*E_{1/2}^{a,b}$	PRC	λ_{max} (abs)	λ_{max} (em)	τ	E^{0-0} (eV)	$*E_{1/2}$	Application
PTZ ^[19a]	<320	450	1.5 - 7.6 (S ₁)	3.20 (S ₁) ^[a]	+0.60	(-2.60)	PTZ ^{•+} ^[19b] [b]	834, 747 520	-	-	1.48(D ₁) ^[a] 2.38(D _n) ^[a]	+2.08 +2.98	Super [O] SET: styrenes; ^[4d,15a] alkylbenzenes, benzene ^[4h]
N-Ph PTZ ^[19c]	<380	510, 445	0.8 - 2.3(S ₁)	2.79(S ₁) 2.43(T ₁)	+0.68	(-2.10)	N-Ph PTZ ^{•+} ^[19d] , [c]	864, 514	-	<36 ps (D ₁)	1.39(D ₁) ^[d] 2.23(D _n) ^[d]	+2.10 +2.91	
TAC ⁺ [18a],[e]	<300	-	-	-	+1.26	-	TAC ^{•2+} [18a],[c],[e]	548, 497, 455	-	-	2.07(D ₁) ^[d] 2.72(D _n) ^[f]	+3.33 +3.98	Super [O] SET: ^[18a] styrenes; alkylbenzenes benzene, halobenzenes dihalobenzenes
TPPD [b]	320 [19e]	432 ^[19f]	-	3.10(S ₁) ^{[19g],[g]}	+0.61 ^[19e]	-	TPPD [19e],[b]	826 404	-	-	1.50(D ₁) ^[a] 3.07(D _n) ^[a]	+2.11 +3.68	Super [O] SET: ^[19b] benzyl alcohol
TpBPA [20],[b]	345	420	1.7	3.10(S ₁) ^[g]	+0.92	(-2.18)	TpBPA ^{•+}	856, 721, 419	-	4.6 ps (D ₁)	1.43(D ₁) ^[a] 3.10(D _n) ^[f]	+2.35 +4.02	Super [O] SET: ^[20] alkylbenzenes, benzene, halobenzenes,
TCBPA [20],[b]	374	435	2.2	2.99(S ₁) ^[g]	+1.03	(-1.96)	TCBPA ^{•+}	811, 695, 425	-	8.6 ps (D ₁)	1.52(D ₁) ^[a] 3.16(D _n) ^[f]	+2.55 +4.19	dihalobenzenes, trihalobenzenes, trifluorotoluene acetophenone
TdCBPA [20],[b],[c]	395	-	-	-	+1.34	-	TdCBPA ^{•+} ^{[20],[c]}	746 639, 404	-	-	1.66(D ₁) ^[a] 3.10(D _n) ^[f]	+3.00 +4.41	dihalobenzenes, trihalobenzenes, trifluorotoluene acetophenone
Pyrene [19g],[h]	<350	395	450(T ₁)	3.14(S ₁) ^[g] 2.00(T ₁) ^{[19h],[i]}	-2.10 ^{[19h],[i]}	-	Pyrene ^{•-} [19h],[i]	735, 495, 385	-	-	1.69(D ₁) ^[a] 3.22(D _n) ^[a]	-3.79 -5.32	Super [R] SET: e ⁻ -poor bromo /chloroarene C(sp ²)-X cleavage ^{[17],[19h]}
DPA ^{[19h],[i]}	<410	590 ^[19j] 426 ^[19j]	8.7(S ₁) ^[19i]	3.09(S ₁) ^{[19j],[g]} 1.77(T ₁) ^{[19h],[19j],[i]}	-1.94 ^[19i]	-	DPA ^{•-} ^{[19h],[i]}	800, 680, 610, 495	-	-	1.55(D ₁) ^[a] 2.50(D _n) ^[a]	-3.49 -4.44	Super [R] SET: e ⁻ -poor bromo /chloroarene C(sp ²)-X cleavage ^{[17],[19h]}
PDI-a ^[19i]	526, 487	573 532	3.9(S ₁)	2.35(S ₁) ^[d] 1.20(T ₁) ^[f]	-0.43 ^{[19k],[k],[l]}	-	PDI-b ^{•-} ^{[19k],[l]}	955 795, 700	-	≈145 ps (D ₁)	1.30(D ₁) ^[a] 1.77(D _n) ^[a]	-1.73 -2.20	Super [R] SET: e ⁻ -poor bromo /chloroarene C(sp ²)-X cleavage ^[19m]
NDI-a [19j],[b]	382	387	<20(S ₁) ^[19k]	3.23(S ₁) ^[g]	-0.48 ^{[19l],[l],[m]}	-	NDI-b ^{•-} ^[19k]	755 683, 605, 474	-	≈141 ps (D ₁)	1.60(D ₁) ^[a] 2.62(D _n) ^[a]	-2.08 -3.10	Super [R] SET: e ⁻ -poor bromo /chloroarene C(sp ²)-X cleavage ^[19m]

CHAPTER 1

Pre-Catalysts							Radical Ion/Radical Photocatalyst						
PRC	λ_{max} (abs)	λ_{max} (em)	τ (ns)	E^{0-0} (eV)	$E_{1/2}^a$ (V)	$*E_{1/2}^{a,b}$	PRC	λ_{max} (abs)	λ_{max} (em)	τ	E^{0-0} (eV)	$*E_{1/2}$	Application
DCA ^[19n]	415 394 <350	435, 460,	14.9(S ₁)	2.90(S ₁) ^[g] 1.80(T ₁) ^{[19o],[i]}	-0.91	(+1.99)	DCA ^{•-} [19p]	708, 645, 580	- ^[n]	- ^[n]	1.75(D ₁) ^[a] 2.13(D _n) ^[a]	-2.66 -3.04	Super [R] SET: e ⁻ -neutral/rich bromo/chloro arene C(sp ²)-X cleavage ^[18b,c]
NpMI ^[19q]	352 330	412	3.0(S ₁)	3.27(S ₁) ^[g]	-1.32	-	NpMI ^{•-} [19q]	840, 745, 490, 415	535	24 ps (D ₁) ^{[19j],[o]} 22 ns (ES ₁) ^{[p],[q]}	1.49(D ₁) ^[a] 2.99(D _n) ^[a] 2.45(Q _n) ^{[g],[q]}	-2.81 -4.31 -	
ⁿ BuO- NpMI ^[19q]	352 330	412	3.1(S ₁)	3.28(S ₁) ^[g]	-1.40	-	ⁿ BuO- NpMI ^{•-} [19q]	840, 745, 490, 415	548	- ^[o] (D ₁) 20 ns (ES ₁) ^{[p],[q]}	1.49(D ₁) ^[a] 2.99(D _n) ^[a] 2.45(Q _n) ^{[g],[q]}	-2.89 -4.39 -	Super [R] SET: chemoselective C(sp ³)- O cleavages; C(sp ²)-X tolerant ^[19q]
4- DPAIPN ^{[19s],[i]}	470, 380 350	525 ^[19u]	-	-	-1.52 ^[i]	(+1.12)	4-DPAIPN ^{•-} ^{[19s],[i]}	470, 380, 345	-	-	2.64(D ₁) 3.06(D ₂)	-4.16 -4.58	Super [R] SET: e ⁻ -neutral/rich chloroarene C(sp ²)-X cleavages; C(sp ²)-O and C(sp ²)-NR ₃ cleavages ^{[19s],[i]}
Birch O- PC ^{[4g],[s]}	507, 425, 355	595	-	-	-1.23	-	Birch O-PC ^{•-} ^{[4g],[i]}	715, 655, 580, 414 ^[c]	580	n.d. (D ₁) 40.1 μ s (ES ₁) ^{[p],[q]}	1.13(D ₁) ^[f] 3.11(D _n) ^[f] 2.36(ES ₁) ^{[f],[q]}	-2.43 -4.34 -	Super [R] SET: styrene, alkylbenzene Birch reductions; halostyrene dehalogenation ^[4g]
N-Ph Mes- Acr ^[4b]	420, 375	520	6.0(T ₁)	2.75(S ₁) ^[g]	-1.64	(+2.15)	N-Ph Mes-Acr [•] ^{[4b],[u]}	512, 492, \approx 385	-	\approx 100 ps (ES ₁) ^[p]	2.29(D ₁) ^[f] 2.92(D ₄) ^[f] 2.78(TICT) ^[f]	-2.87 -3.50 -3.36	Super [R] SET: e ⁻ -poor/neutral /rich haloarene dehalogenations; N-Ts cleavages ^[4b]

Unless otherwise stated, spectral data were measured in ACN solvent and cyclic voltammetry in 0.1 M ⁿBu₄N.PF₆ in ACN as solvent, see citations for exact conditions. ^[a] Especially where luminescence is not reported, ^[i] an estimation was made for E^{0-0} by taking the photon energy corresponding to $\lambda_{\text{max}}^{\text{abs}}$ for both the lowest and highest energy transition and $*E_{1/2}$ was calculated by the Rehm-Weller equation. ^[b] In DCM. ^[c] Spectral properties were determined from *in situ* electrogenerated species. ^[d] The red edge of the UV-Vis absorption band was taken for E^{0-0} . ^[e] Spectral data were obtained under the preparative reaction conditions. ^[f] Taken from the calculated TD-DFT vertical transition that corresponded most closely to the excitation wavelength in the preparative reactions. ^[g] E^{0-0} was determined by the intersection of absorption (most red-shifted) and emission (most blue-shifted) spectral bands. ^[h] In cyclohexane. ^[i] E^{0-0} was determined by another or unspecified means, see the cited study. ^[j] In DMSO. ^[k] For PDI-b. ^[l] In DMF. ^[m] NDI-a and NDI-b have the same redox potential. ^[n] Controversy exists over the reported luminescence/lifetimes of DCA^{•-} which likely derive from other species (10-cyanoanthrolate anion). ^[19p] ^[o] Transient absorption spectroscopy of a direct analog (2,4-disubstituted) of NpMI^{•-} reportedly afforded rapid photobleaching of the sample in 0.1 M ⁿBu₄N.PF₆ in DMF and the lifetime could not be determined, ^[19k] however, the lifetime of NpMI^{•-} itself was successfully determined in a recent study in 0.1 M ⁿBu₄N.PF₆ in DMAc. ^[19q] ^[q] This study^[19q] did not assign the measured lifetime to a specific excited state and the excited state was thus denoted 'ES₁'. ^[r] A quartet state was tentatively proposed as a candidate for the long-lived species. Since this state was found to be catalytically inactive in the PET step due to no lifetime quenching in the presence of substrate, an excited state potential is not given. ^[s] In 0.1 M ⁿBu₄N.PF₆ in DMF. ^[t] Spectral data measured in CHCl₃ and cyclic voltammetry in 0.1 M ⁿBu₄N.PF₆ in DMAc. ^[u] In THF. ^[v] In hexane.

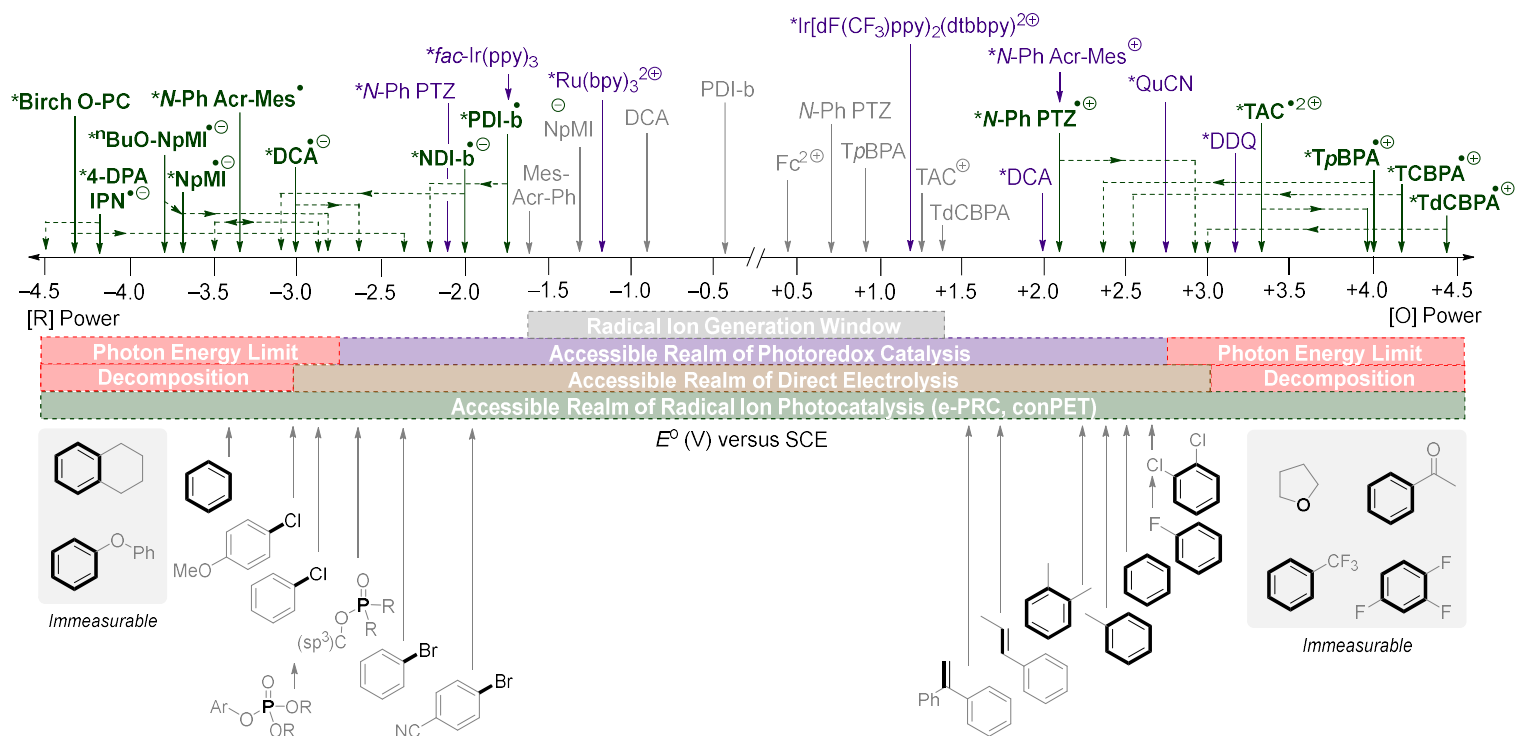


Figure 2. Redox benchmarking of contemporary radical ion photocatalysts compared to photoredox catalysts and redox-challenging target substrates. Unless otherwise specified in Table 1, all catalyst redox potentials are excited state half-wave potentials $*E_{1/2}$ taken from the literature.^[2c,e] Unless the excited state redox potential is explicitly claimed in the associated citation, solid lines (\rightarrow) represent either the upper-boundary excited doublet state redox potential (D_n) and assignments are guided by the redox scope of accessible substrates. Dotted lines (\leftrightarrow) represent upper or lower redox bounds for the excited doublet states (D_1 or D_n). Substrate redox potentials taken from the literature are irreversible peak redox potentials $E^{p/2}$,^[4c,18a-b,19q,21,22] or lie beyond the solvent redox window (>-3.0 V; $>+3.0$ V).^[9]

Comparison of conPET and e-PRC: While conPET and e-PRC methods are analogous in their active catalyst excited state and their scope of SET reactions, their downstream chemistry is fundamentally distinct and complementary. The reactivity paradigms are compared in the context of super-reductions (Figure 3). In both cases, following SET from the photoexcited radical ion catalyst, C-X bond cleavage affords a radical intermediate. In conPET, this radical intermediate, typically an aryl C(sp²) radical, can undergo (i) hydrogen atom transfer (with solvent or with by-products derived from sacrificial reductants in the radical ion catalyst generation step), (ii) addition to a heteroatom trapping agent or (iii) addition to an unsaturated partner (usually an electron-rich aromatic) in a C-C coupling reaction. In the case of (iii), the subsequent radical either reacts with a HAT agent (“Z•” → olefination) or is oxidized (by “Q•+”) and deprotonated, in both cases re-forming the unsaturation. The HAT agent (“Z•”) or oxidant (“Q•+”) is the by-product from the sacrificial electron donor that was required to form the radical anion photocatalyst. For example, the α -amino radical or *N*-radical cation of a trialkylamine electron donor.

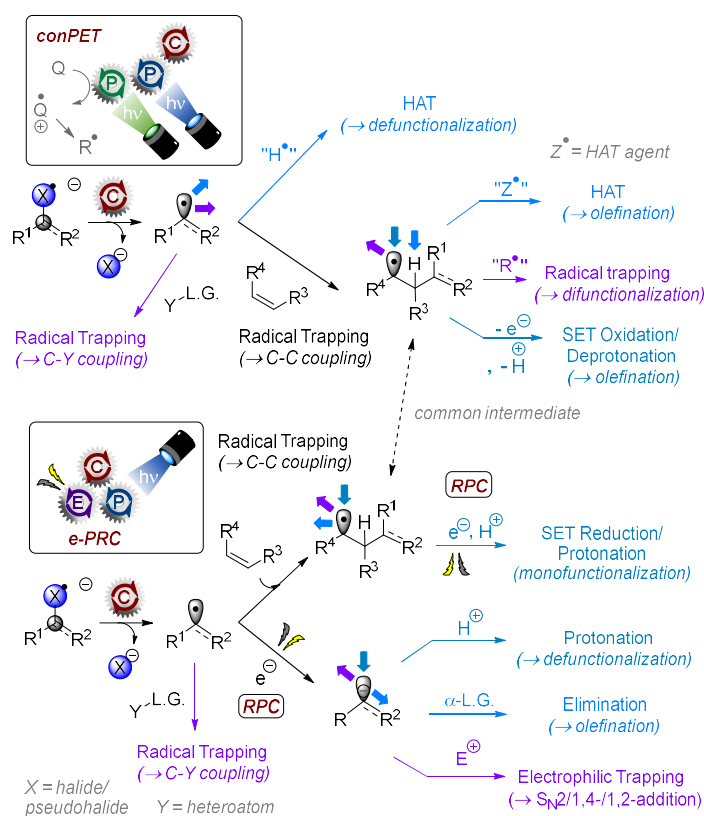


Figure 3. Downstream chemistry reactivity paradigms of conPET vs e-PRC. RPC, Radical Polar Crossover.

In e-PRC, different fates await the radical intermediate following initial SET and C-X bond cleavage, by virtue of the absence of sacrificial chemical reductant and their by-products. The radical can undergo the same radical trapping reactions as with conPET, but instead of HAT with solvent its electroreduction to a carbanion occurs in a radical polar crossover (RPC) fashion. The

resulting carbanion intermediate can undergo (i) protonation, (ii) elimination of an α -leaving group or (iii) electrophilic trapping. The radical intermediate following C-C coupling can undergo further reduction and subsequent protonation, or can engage in radical trapping depending on the applied potential. Thereby, e-PRC offers the unique advantage of a user-potentioccontrollable mechanism. While radical ion photocatalysts are a common theme in conPET and e-PRC chemistries, the focus of this review now turns to recent synthetic applications of the latter. Elegant, synthetic applications of conPET are reviewed elsewhere.^[2e,4i-k,11b]

C(sp²)-N bond formations: In the oxidative direction, e-PRC has witnessed impressive synthetic applications in C(sp²)-N bond formations. The Buchwald-Hartwig coupling is an important, widespread reaction for forging C(sp²)-N bonds, but relies on pre-functionalization of the C(sp²)-containing arene (an aryl halide or pseudohalide) for oxidative addition of a Pd-catalyst. A powerful alternative is the direct C(sp²)-H activation of arenes by SET oxidation to their radical cations that undergo S_NAr-type attack by *N*-containing nucleophiles. The Nicewicz group first demonstrated this concept using PRC with the Fukuzumi catalyst, an acridinium salt (Mes-Acr⁺) with a high excited state oxidation potential ($*E_{1/2} = +1.88$ V vs. SCE). Electron-rich arenes such as anisole underwent direct C(sp²)-N bond formations with azoles.

Elegant work by the Lambert group exemplified the power of e-PRC to breach the upper redox limit of single photon PRC^[18a] which has been reviewed elsewhere.^[9] They disclosed a trisaminocyclopropenium cation (TAC⁺) as an electroactivated photoredox catalyst (e-PRCat) whose excited state could oxidize benzene, chlorobenzene and up to dichlorobenzenes as arene partners. Trifluorotoluene gave no product, defining the upper limit of the excited state's oxidative power. While its scope of applications was broad, the exotic structural architecture of the catalyst does not seem amenable to modifications. Structural modification of a photoredox catalyst core to a family of derivatives with different photophysical and redox properties is a concept underpinning much of the success of field of PRC with transition metal or organic photocatalysts.^[2c,e] In the context of e-PRC, the Barham group disclosed tri(*p*-substituted)arylamines (TPAs) as a tunable class of e-PRCat for super-oxidations (Figure 4A).^[20] The TPAs are easily accessed and customized in a single step by Suzuki or Ullmann coupling reactions. A ubiquitous structural motif in hole-transport functional materials (OLEDs, photovoltaics)^[23] and as mediators in electrolysis,^[24] the photophysical and redox properties of TPAs and their bench-stable (isolable) radical cations^[25] have a rich history of characterization^[26] that backdates even that of Ruthenium polypyridyl complexes.^[27] In their e-PRC reactions, TPAs first undergo anodic oxidation to their corresponding strongly colored radical cations at a constant potential of +1.4 to 1.8 V (Figure 4B). Altering *para*-substituents on the TPA allows facile access to radical cation photocatalysts with different oxidative powers. Use of a moderate-power TPA (TpBPA) allowed C(sp²)-H amination of alkylbenzenes with high selectivity; aldehyde-bearing pyrazoles and arene benzylic positions were tolerated without oxidation. Introduction of a *para*-

cyano group on the peripheral aromatic ring gave a higher-power TPA (TCBPA) which allowed C-H amination of benzene and chlorobenzene in good yields and tolerated free carboxylic acids known to undergo decarboxylation in PRC^[28] and Kolbe oxidation pathways in SOE.^[29] Using the most powerful TPA (TdcBPA), the oxidative SET C-H aminations of dichlorobenzenes, fluorobenzene and even acetophenone were achieved. SET activations of very electron-poor trifluorobenzene and trifluorotoluene were achieved, leading to S_NAr-substitution reactivity (Figure 4C). The utility of triarylaminines as a family of e-PRCats that could be tuned to target substrates was successfully demonstrated. A key mechanistic question comes to mind when discussing the photochemistry of excited radical ions (doublet states), given that these species are well known to exhibit ultrashort (<1 ns) lifetimes that prohibit their diffusion-controlled photochemistry. It had been tentatively hypothesized in previous studies involving conPET reduction that a precomplexation of the substrate and radical ion photocatalyst occurs to rationalize otherwise temporally-forbidden photochemistry.^[4a,g]

A key advantage of TPAs as electroactivated photocatalysts is that they can be easily oxidized and isolated as their bench-stable radical cations.^[25c] This allowed the authors to measure lifetimes of TPA^{•+}s as short as <10 ps by transient absorption spectroscopy, clearly ruling out diffusion-controlled photochemistry. Precomplexation between TPA^{•+}s and arene substrates was proposed as the key to overcoming ultrashort (ps) lifetime (Figure 4B). It was postulated that steric effects in the precomplex formation rationalized both (i) the reactivity trend of xylene and dichlorobenzene isomers; since preparative reaction yields increased in the order: 1,4- < 1,2-disubstituted arenes, (ii) the lack of reactivity of iodobenzene. The increasing order of $E^{\text{p}_{\text{ox}}}$: 1,4- < 1,2-disubstituted arenes^[18a] and the highly accessible redox potential of iodobenzene meant that such behavior was unexpected and contra-thermodynamic.

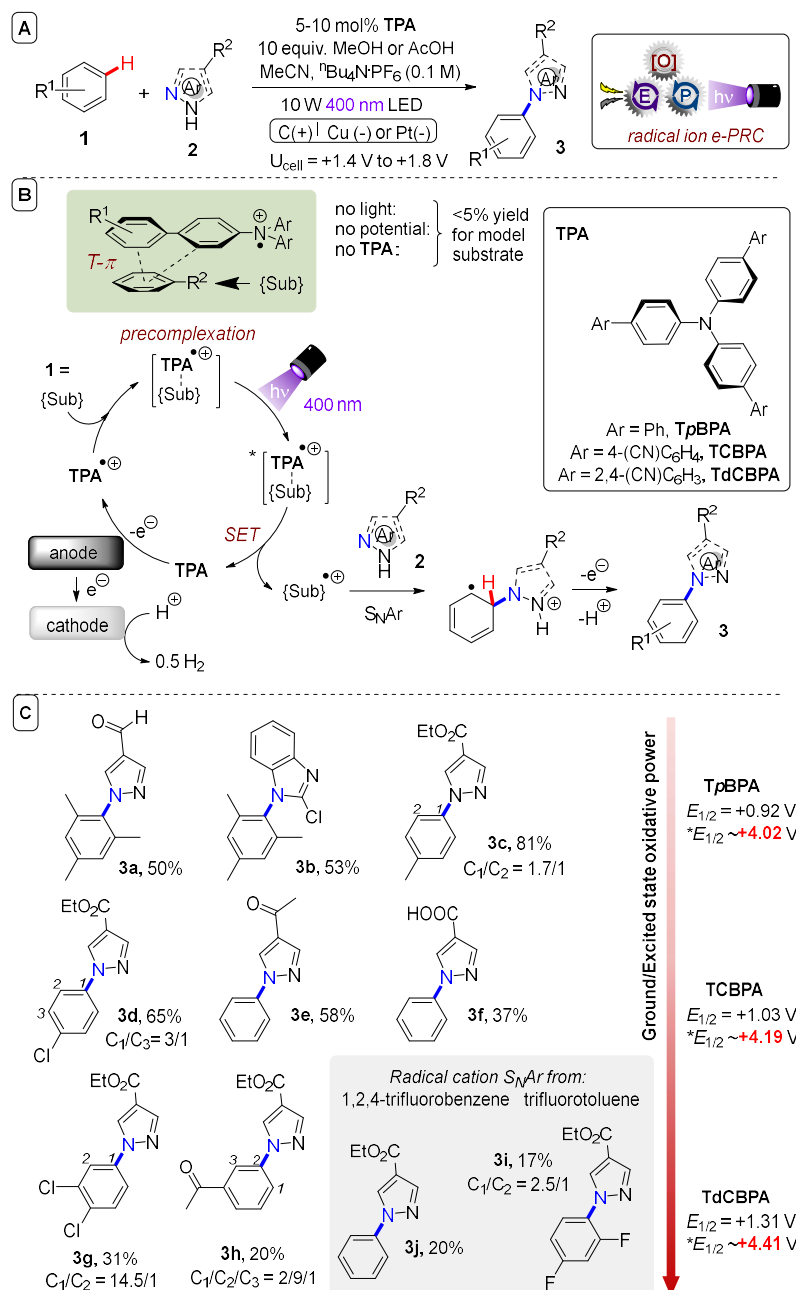


Figure 4. A) TPAs as a library of tunable super oxidative photocatalysts. B) Proposed precomplexation mechanism and TPA catalysts used in this study. C) Selected examples.

The presence of precomplexes was identified spectroscopically via changes in the UV-Vis spectra and EPR spectra of isolated $\text{TPA}^{\bullet+}$ s in the presence of arene substrates. The most striking comparison was when 1,2- or 1,4-dichlorobenzene substrates were added to $\text{TCBPA}^{\bullet+}$. The former ‘reactive’ substrate perturbed the EPR signal to a ‘triplet shape’, confirming spin density localization on the N atom in the precomplex. The latter ‘unreactive’ substrate perturbed the signal to a ‘broad singlet’, indicating another type of precomplex with spin density delocalization away from the N atom, that may stabilize the radical cation and decrease its excited state reactivity to SET. DFT calculations ($\omega\text{B97X-D}$ or B3LYP functionals) found optimized structures involving

T- π or π - π interactions. Relative binding energies revealed ‘reactive’ substrates favored T- π geometries and ‘unreactive’ substrates favored π - π geometries (Figure 5).

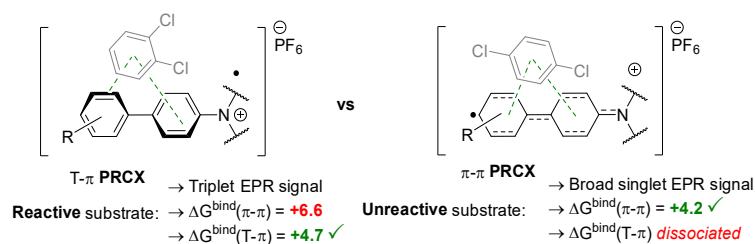


Figure 5. Candidate precomplexes of reactive (left) vs. unreactive (right) arenes.

In chlorobenzene’s precomplex with TCBPA $^{\bullet+}$, the calculated spin density changed when the Cl atom faced ‘in’ but did not change when facing ‘out’, providing a clue about the preferred geometry of precomplexes involving unsymmetrical haloarenes (Figure 6).^[30] Although TPA $^{\bullet+}$ s absorb strongly in the visible region (ca. 600-900 nm) corresponding to their first (doubly degenerate) excited states ($D_0 \rightarrow D_1$), only shorter wavelengths (400 nm) gave reactivity, suggesting anti-Kasha photochemistry.

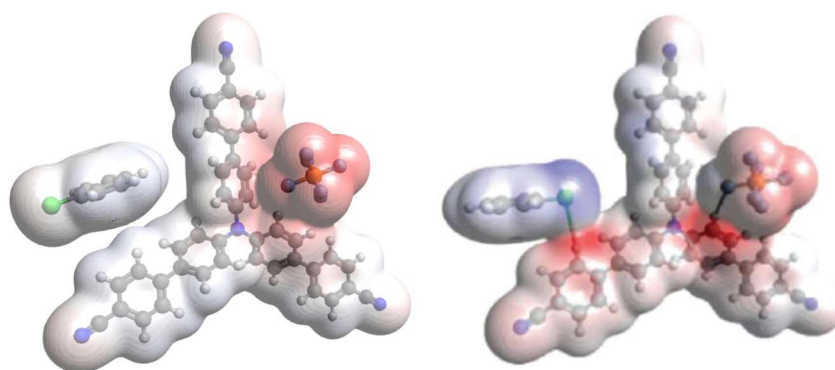


Figure 6. Calculated spin densities of T- π precomplexes of TCBPA $^{\bullet+}$ with chlorobenzene where the halogen faces “in” (left) or “out” (right).

The ability to access higher-order doublet photoexcited states of TPA $^{\bullet+}$ s with 400 nm provides as high as $^*E^{\text{p}}_{\text{ox}} = +4.4$ V vs. SCE as an upper boundary,^[31] and would rationalize the oxidation of arenes so electron-poor, that they exceed the measurable solvent window of cyclic voltammetry. TD-DFT calculations, which agreed well with UV-Vis spectra of TPA $^{\bullet+}$ s,^[32] revealed the near-IR transition ($D_0 \rightarrow D_1$) involved a π - π^* transition localized at the core aromatic rings (Figure 7). In contrast, the transition closest to ~ 400 nm ($D_0 \rightarrow D_n$) involved a π - π^* transition at the peripheral aromatic rings. This is precisely the binding location of substrate arenes as found by geometry optimizations. Precomplexation may rationalize synthetically productive anti-Kasha

photochemistry by the localization of hole density at the binding site of the substrate, priming the precomplex for ultrafast SET (faster than internal conversion; $D_n \rightarrow D_1$).

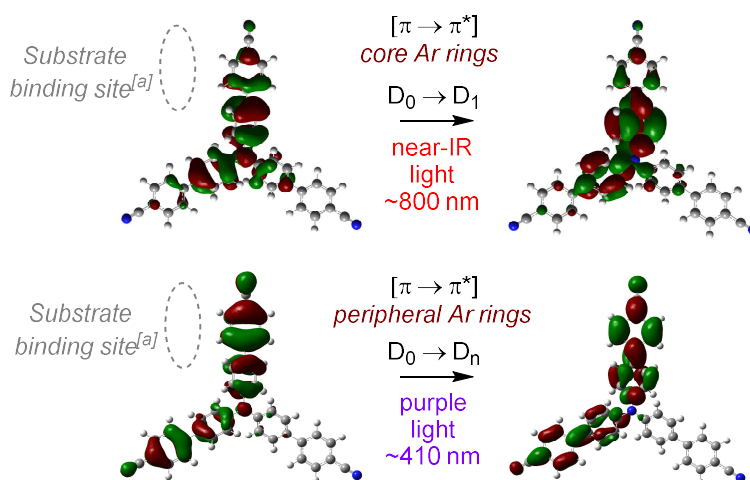


Figure 7. Orbital transitions for photoexcitation of $TCBPA^{\bullet+}$ corresponding to $D_0 \rightarrow D_1/D_n$. ^[a] Predicted by DFT.

While the simple computational model of precomplexes is consistent with experimental observations, deeper investigations with other DFT theory levels,^[33] different (non-DFT)^[34] theories and different precomplex candidates^[35] are warranted for a more holistic picture. Nonetheless, this study evidenced how radical ion-substrate precomplexes not only circumvent ultrashort lifetimes of doublet excited states, but even circumvent internal conversion allowing a greater proportion of the photon energy to be harnessed. Moreover, the study indicated how radical ion-substrate precomplexes give rise to different selectivities than SET chemistry involving diffusion-controlled SOE or PRC.

C(sp³)-N bond formations: In an impressive synthetic application of e-PRC, the Lambert group used TAC^+ for vicinal diamination of arylarenes (**4**, Figure 8A).^[36] Depending on the electrolyte, alkylated arenes undergo vicinal diamination either to afford 3,4-dihydroimidazoles (**5**) or oxazoline derivatives (**6** and **6'**). In the anodic chamber of a divided cell, TAC^+ is oxidized to its colored dication radical $TAC^{\bullet 2+}$. Upon photoexcitation, the highly oxidative $*TAC^{\bullet 2+}$ ($*E_{1/2} = +3.33$ V vs. SCE) engages arylarenes like cumene **4a** in SET (Figure 8B).

Upon loss of a proton from **4a**^{•+} and SET oxidation, benzylic carbenium ion **7** is generated and nucleophilic attack of the ACN solvent leads to Ritter-type amidation (Figure 8C). The resulting acetamide (**8**) undergoes acid-catalyzed elimination to α -methylstyrene (**9**). Subsequent e-PRC oxidation of **9** by $*TAC^{\bullet 2+}$ affords radical cation **9**^{•+} and acetonitrile solvent adds. Further oxidation and addition of a third equivalent of ACN were proposed to afford dihydroimidazole **5** in a Ritter-type fashion.^[37] Control reactions using α -methylstyrene (**9**) that led to polymerization

seemed to contradict this proposal. However, an equilibrium between **8** and **9** would generate small quantities of **9** *in situ*, mitigating against polymerization. LiClO₄ electrolyte presumably alters stability of cationic intermediates and the addition of H₂O to **9**⁺ or **10a** affords **6** and **6'**, respectively.

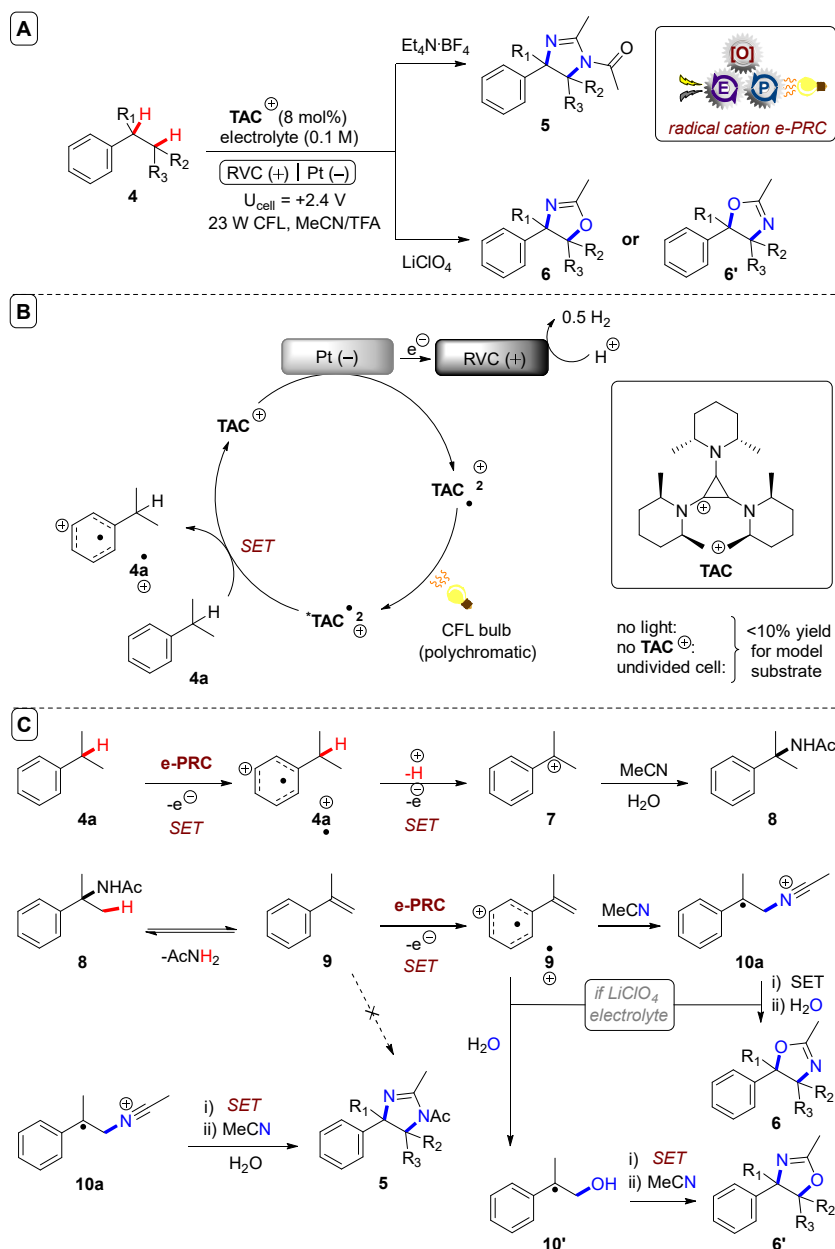


Figure 8. A) *e*-PRC vicinal diamination of alkylarenes. B) Catalytic cycle. C) Proposed downstream chemistry mechanism.

When applied to secondary alkylbenzenes, halide substitution was well-tolerated, while alkyl *para*-substitution on the arenes leads to formation of Ritter-type benzylic by-products (**5j**, Figure 9A). Cyclic systems were successfully functionalized, with preference for 4-phenylimidazoles over 5-phenylimidazoles. In primary alkylbenzenes, the regioselectivity was inverted.

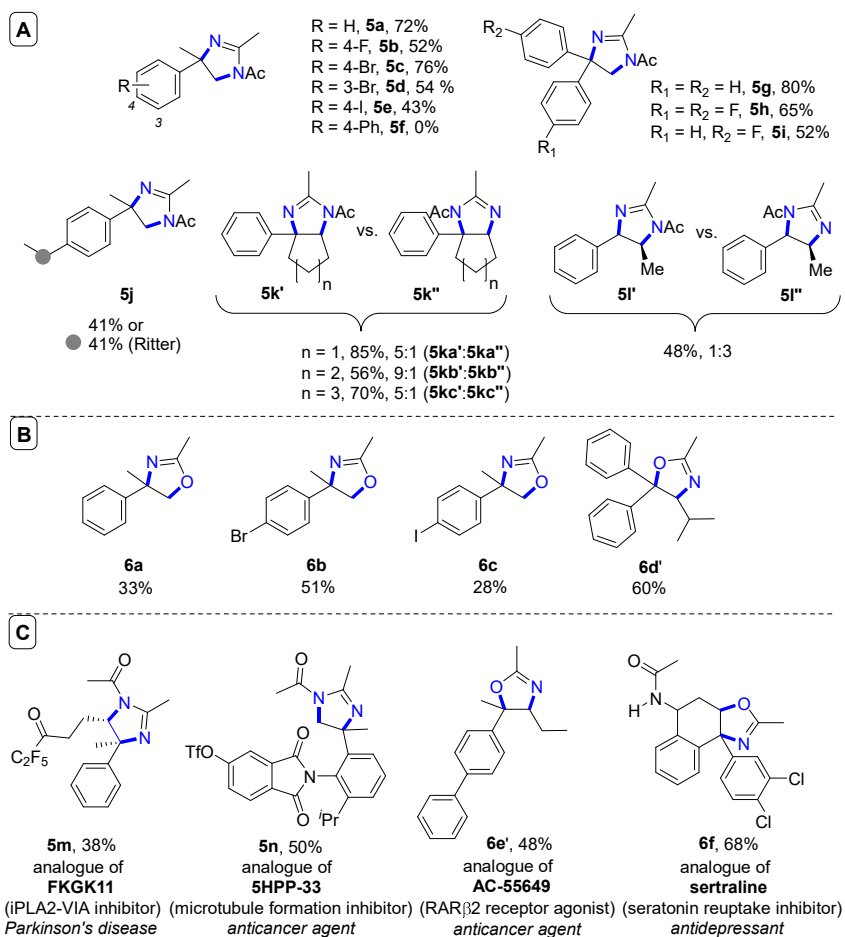


Figure 9. A) *e*-PRC vicinal diamination substrate scope of dihydroimidazoles. B) Substrate scope of oxazolines from using LiClO₄ electrolyte. C) Late-stage functionalizations of bioactive molecules.

Most impressively, the simple change of electrolyte from Et₄N⁺BF₄⁻ to LiClO₄ diverted the mechanism to form oxazolidines in an overall oxyamination. The methodology was amenable to late-stage functionalizations of pharmaceutical compound analogues (Figure 9C). Either dihydroimidazole or subsequent 1,2-diamine scaffolds could be accessed by a simple modification of the work up procedure, while β -amino alcohols derived from oxazolidine hydrolysis, signaling a broad and industrially-relevant scope of future applications for this chemistry.

In the context of C-H aminations, it is important to mention that DDQ as a neutral (closed-shell) photocatalyst^[38] can achieve C(sp²)-H aminations^[39] of electron-deficient arenes up to dichlorobenzenes, either under PRC^[39] with a co-oxidant or under recycling *e*-PRC (see later Section).^[40] However, larger, sub-stoichiometric quantities (10-20 mol%) are typically required and the evolution of hydrogen cyanide upon contact of this catalyst with moisture presents safety concerns.^[41] DDQ is a rather potent ground state oxidant that can react with *N*-nucleophiles,^[39] while TAC⁺ and TPA catalysts do not suffer such issues.

C-O bond formations: The Lambert group demonstrated the acetoxyhydroxylation of aryl olefins by radical ion e-PRC using TAC⁺. Transition metal-catalyzed dioxygenation reactions of olefins are well-known, but the authors noted the need for transition metal-free approaches to obviate the expense and toxicity of certain metals. While electrochemical approaches using ‘cation pool’ strategies are attractive,^[42] in dioxygenations they oftentimes lead to the cleavage of dioxygenated products to carbonyl and acetal-derived by-products (Figure 10A).^[43] Direct electrolysis employing DMSO and DMF as nucleophiles to attack electrogenerated olefin radical cations has successfully afforded dihydroxylated olefins.^[44] Lambert’s group use of radical ion e-PRC and acetic acid lead instead to acetoxyhydroxylation, and provides a mild platform to access products such as **12a** in 71% yield. Direct electrolysis likely occurs to an extent under the relatively high potential of +2.0 V; control reactions without light or TAC⁺ did afford product **12a** but in low yields. Direct electrolysis at +3.0 V increased the yield of **12a** to 40% but led to over-oxidation and cleavage to aldehyde, ketone and acetal by-products. In the mechanism, **11a** is oxidized by *TAC^{•2+} to its radical cation, which undergoes nucleophilic attack by AcOH to afford benzylic radical **13b** (Figure 10B). Oxidation of **13**, either by anodic potential or by *TAC^{•2+}, affords intramolecular cyclization to oxocarbenium **14**, primed for attack by H₂O to afford **12a**. Cyclic olefins were acetoxyhydroxylated to give **12b-12i** in good to excellent (52-82%) yields. A striking feature is the selectivity of this method compared to prior chemical and electrolytic reports. Benzylic methyls, alcohols and aldehydes were all tolerated (**12j-12l**). A free alkylsulfide, a Bpin ester, a product-bearing styrene and electron-rich heterocycles were all tolerated in the synthesis of **12m-12s** (31-78% yields). Yields of furan and thiophene-containing **12q** and **12r** were low (31%), but primarily due to lack of conversion.

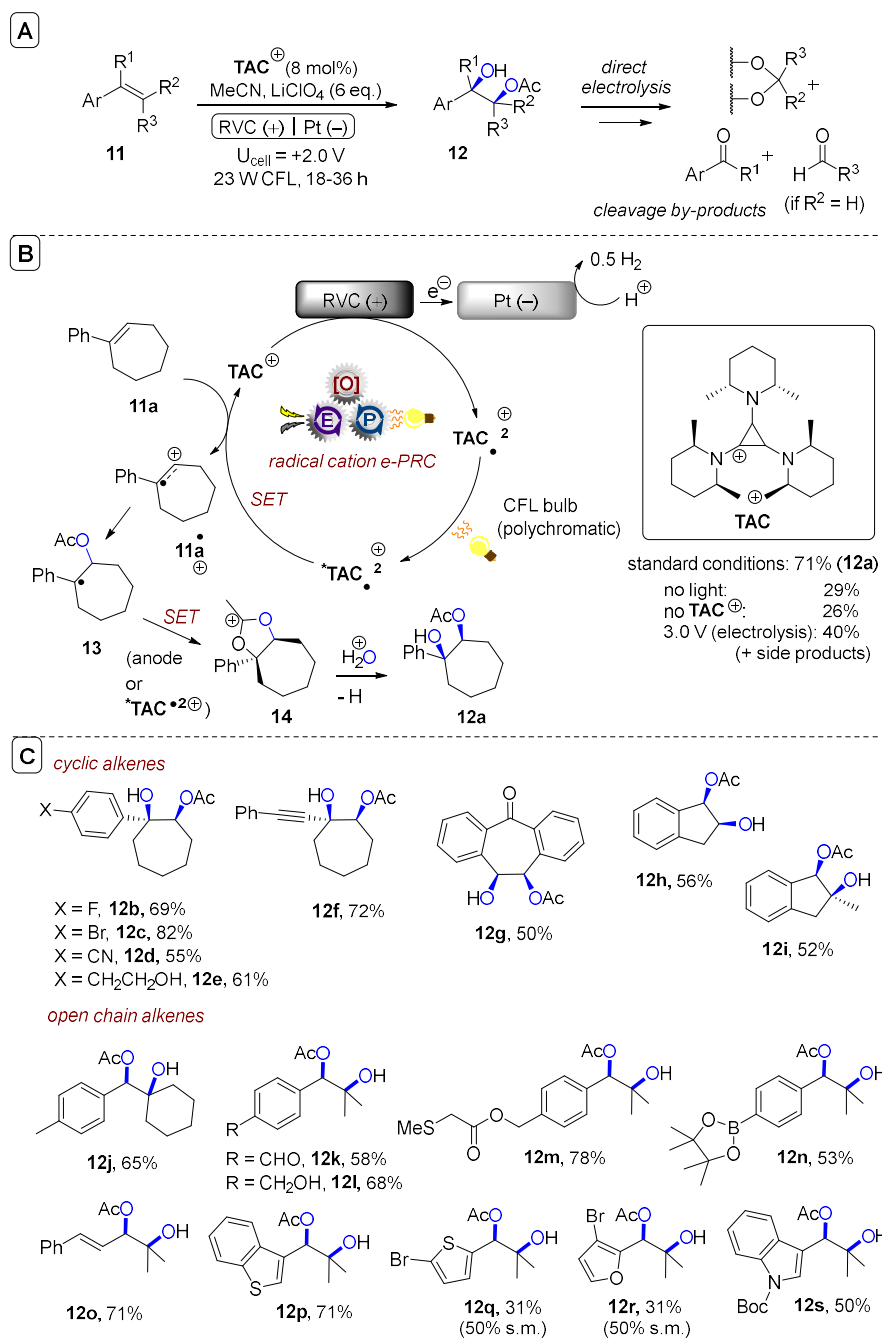


Figure 10. A) *e*-PRC acetoxyhydroxylation of aryl olefins. B) Proposed mechanism. C) Substrate scope of dihydroxylations, simple substrates.

Selectivity was further exemplified in the late-stage acetoxyhydroxylations of various aryl olefin-conjugated amino acids and complex molecules (Figure 11A). Other acids were tolerated, affording **13a-13e** in modest to good (38-55%) yields (Figure 11B). Interestingly, regioselectivity was inverted in these cases. Acrylic acid as a nucleophile underwent oligomerization in the synthesis of **13e**, which may be rationalized by Kolbe-type oxidation of acrylic acid and radical addition^[45] yet authors deemed this unlikely in absence of base. Finally, multigrams of products were achieved via a recirculated flow setup (Figure 11C). Electro-activation of TAC⁺ was done in a batch undivided cell and the reaction mixture was recirculated through three CFL-irradiated

coils with a total residence time of ($R_T =$) 3 min, affording up to 8.4 g of **12a** and 3.7 g of **12w** without appreciable yield losses after 20-36 h.

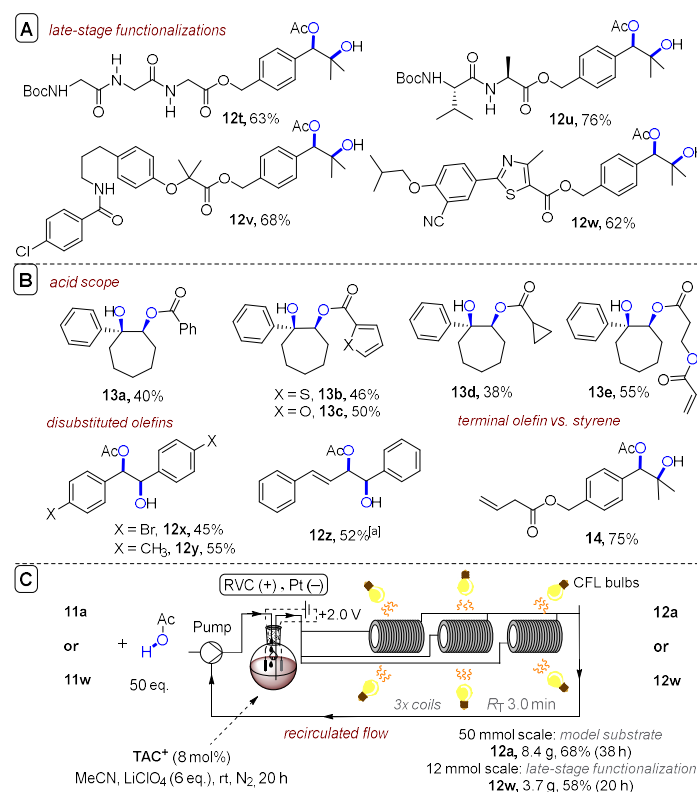


Figure 11. A) Late-stage acetoxyhydroxylation. B) Substrate scope acid partners, disubstituted olefins and terminal olefin tolerance. C) Recirculated flow recycling e-PRC acetoxy hydroxylation of the model substrate or a complex molecule.

C(sp²)-X cleavages: On the reduction side, Lambert and Lin disclosed dicyanoanthracene (DCA) as an electroactivated photoreductant for super-reductions of aryl halides,^[18b] which was previously reviewed.^[9] Simultaneously, the Wickens group reported an *N*-arylmaleimide (NpMI) as a catalyst that achieves this purpose (Figure 12).^[18c] Inspiration was drawn from seminal work of the König group on perylene diimide (PDI-b) photocatalysts, which are known to form stable radical anions (PDI-b^{•-}) that can be photoexcited to reduce electron-withdrawn aryl halides in a consecutive photoelectron transfer (conPET) mechanism.^[4a] e-PRC reactions with DCA and NpMI catalysts extended the scope of aryl halide partners to electron-neutral and electron-rich, and conditions provide substantial advantages for such challenging SET reductions over traditional Birch-type conditions which are practically undesirable (dissolving alkali metals in liquid ammonia).

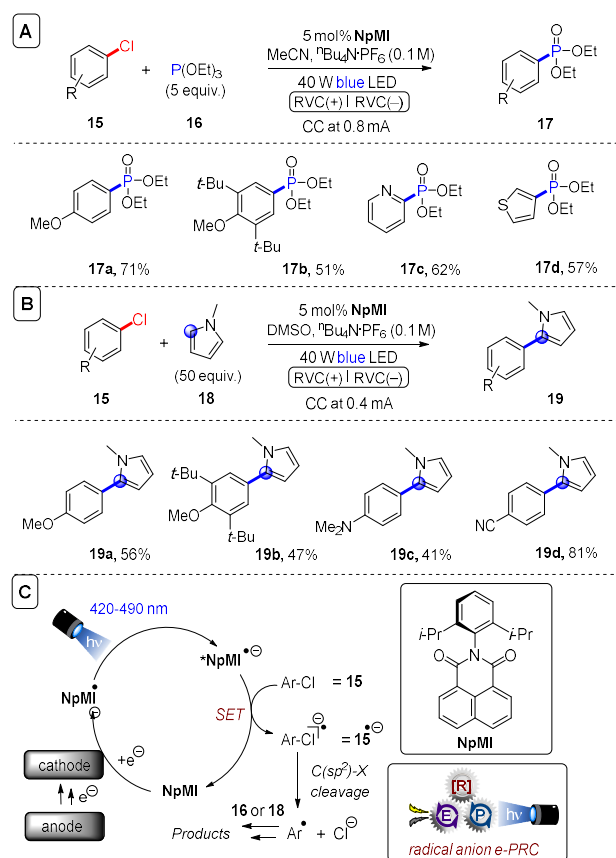


Figure 12. A) *e*-PRC reduction of aryl chlorides and trapping of aryl radicals, substrate scope with triethyl phosphite. B) Substrate scope trapping with *N*-methylpyrrole. C) Catalytic cycle.

In *e*-PRC, SET takes place in bulk solution where the electrogenerated catalyst is irradiated, not at the electrode surface due to the Beer-Lambert relationship. This leads to immediate deactivation of the photoexcited state, thus *e*-PRC exhibits a key benefit in harnessing the reactivity of aryl(sp²) radicals. Direct electrolytic reduction of aryl halides that takes place at the electrode surface suffers the issue that aryl(sp²) radicals are thermodynamically easier to reduce than their aryl halide precursors, leading inevitably to overall dehalogenation.^[21a] Wickens and co-workers found that diimide (PDI and naphthalene diimide, NDI) catalyst architectures were ineffective catalysts for the reduction of electron-neutral aryl halides,^[18c] likely due to the high stabilization of the radical anion prohibiting super-reductive chemistry in its photoexcited state. In their optimized *e*-PRC reaction conditions, the new catalyst *N*-(2,6-di-*iso*-propylphenyl)naphthalene monoimide (NpMI) is first reduced to its colored radical anion by a cathodic constant current of 0.8 mA. Upon photoexcitation with blue LEDs, photoexcited radical anion *NpMI^{•-} engages aryl chlorides as challenging as 4-chloroanisole (**15a**) in SET reduction to aryl radicals (Figure 12C). Aryl(sp²) radicals either underwent overall dehalogenation, or were trapped with triethylphosphite (Figure 12A) or *N*-methylpyrrole (Figure 12B) to afford products **17** and **19**. Notably higher preparative yields were obtained compared to direct electrolysis (which gave noticeable decomposition), demonstrating the key selectivity benefit of radical ion *e*-PRC.

When the debromination of 4-bromobiphenyl ($E_{\text{red}}^{\text{p}} \approx -2.43$ V vs. SCE)^[46] was used to optimize reaction conditions, a bis-*N*-(2,2',6,6'-di-*iso*-propyl)naphthalene diimide (NDI-d) precatalyst afforded dehalogenated product **21a** in a lower yield than NpMI (Figure 13A). Bardagi recently reported conPET and e-PRC reductions of 4-bromobenzonitrile ($E_{\text{red}}^{\text{p}} = -1.95$ V vs. SCE) using a modified naphthalene diimide precatalyst (NDI-c).^[19m] The aryl(sp²) radical was trapped by an excess of benzene and afforded desired products (such as **21b**) albeit in low yields (<20%) (Figure 13B). Though attention is needed to increase conversion and yields, this represents a potential alternative, milder set of conditions than transition metal-free arylations of haloarenes requiring KOtBu and organic additives. Such chemistry requires high temperatures to form electron donors *in situ* that initiate a base-assisted homolytic aromatic substitution (BHAS) chain reaction.^[47]

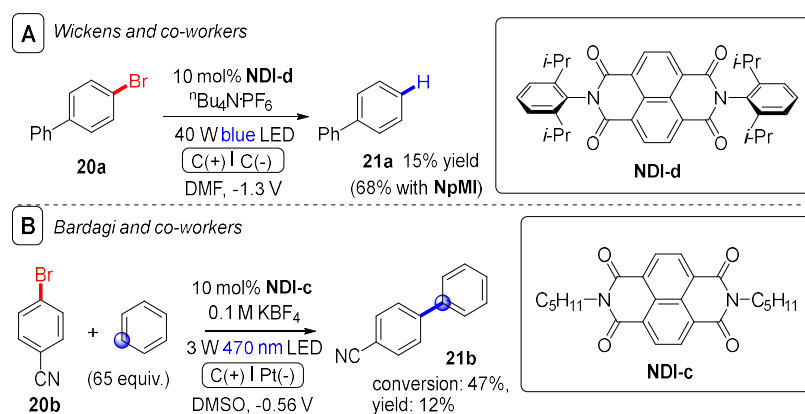


Figure 13. A) e-PRC dehalogenation of 4-bromobiphenyl using a naphthalene diimide precatalyst. B) e-PRC reduction of 4-bromo-1,1'-biphenyl using a naphthalene diimide precatalyst and trapping with benzene.

C(sp³)-O cleavages: Inspired by previous photocatalytic generations of carbanions^[48] and direct electrolytic reductions of phosphinates in overall deoxygenations,^[49] Barham, König and co-workers reported the first e-PRC reductive cleavage of C(sp³)-O bonds to access sp³-radicals and sp³-centered carbanions.^[19q] Phosphinates of aliphatic alcohols successfully underwent e-PRC reduction and C-O cleavage when *N*-(*para*-butoxyphenyl)naphthalene monoimide ($n\text{BuO-NpMI}$) was employed (Figure 14A). Following cathodic reduction to its radical anion and photoexcitation, $^*[\text{nBuO-NpMI}^{\bullet-}]$ engages phosphinates ($E_{\text{red}}^{\text{p}} \approx -2.4$ to -2.6 V vs. SCE) in SET. Then, C(sp³)-O bond cleavage of $\mathbf{22}^{\bullet-}$ forms a C(sp³) carbon radical, proposed to undergo further SET reduction likely by cathodic current (or by $^*[\text{nBuO-NpMI}^{\bullet-}]$) to afford a C(sp³) carbanion. In the presence of an α -leaving group (chloride, bromide), elimination occurs in an overall reductive olefination (Figure 14B). Since phosphinate substrates derive from α -chloro ketones and not aldehydes, the method has a different starting point to classic (Wittig-type) olefinations that can be leveraged to access cyclic and hindered olefins (Figure 14C). Compared to acid-catalyzed of base-dependent eliminations of alcohols, the method proceeds at ambient temperature, tolerates

base-sensitive functionality and allows user control over the direction of olefination. For example, a substrate containing free amide protons (**23i**) was tolerated, as were esters (**23p-r**) that risk hydrolysis or E₂ elimination under basic conditions. Formation of terminal olefin **23c** demonstrates the benefit over acid-catalyzed elimination of a 3° alcohol, which typically affords the most substituted olefin. In the absence of an α-leaving group, overall deoxygenation occurred as a mild and tin-free alternative to the Barton-McCombie reaction (Figure 14B). The presence of a carbanion intermediate was confirmed when a phosphinate with an α-chloro atom led to cyclopropanation. Stilbene **23l** could be accessed from the standard phosphinate, but also from a cyclic phosphinate derived from a diol in a photoelectrochemical Corey-Winter-type olefination reaction that avoids high temperatures and hazardous reagents normally associated with this reaction. Unsymmetrical stilbenes could also be readily accessed by this method, surprisingly with generally high Z-selectivities when ⁿBuO-NpMI was employed (Figure 14D). Olefinations and deoxygenations of phosphinates derived from benzylic or allylic alcohols were successful, while those derived from non-benzylic/allylic aliphatic alcohols did not react despite almost identical redox potentials. Remarkably, and in stark contrast to the previous report of Wickens,^[18c] aryl halides (chlorides and bromides) were tolerated under these conditions, despite their similar redox potentials to phosphinates ($E_{\text{red}}^{\text{P}}(\text{PhCl}) -2.78 \text{ V}$; $E_{\text{red}}^{\text{P}}(\text{PhBr}) = -2.44 \text{ vs. SCE}$). A phenol-derived phosphinate was also tolerated, contrasting with previous reports on C(sp²)-O cleavage by PRC with a phenothiazine catalyst.^[50] 4-Vinyl benzoates of terpene natural products that are liquid crystals or fragrance compounds could be prepared by late-stage e-PRC olefination from the phosphinates derived from the 4-acetylbenzoate esters of the terpenes, giving rise to potential monomers for polymerization (Figure 14E). Here, terminal olefination using base risks hydrolysis or E₂ elimination, while direct esterification is problematic due to thermal instability of 4-vinylbenzoic acid or its formulation with radical stabilizer (BHT). To probe the mechanism behind stilbene E-/Z-isomerism, control reactions with E-stilbene as an input revealed the critical importance of e-PRCat, light and potential on the E-/Z- isomerism. Luminescence spectroscopy revealed a nanosecond-lived emitting state from [ⁿBuO-NpMI^{•-}]*, that was catalytically inactive in the initial SET reduction step (its lifetime was not quenched by **22a**), but is likely responsible for E-/Z- isomerism. One candidate for this emitter is a quartet state, ⁴[ⁿBuO-NpMI^{•-}]* that results from intersystem crossing from a higher energy doublet state. The energy of this emitting state (E^{0-0}) was identical to transition metal photocatalyst triplet energies known to affect E-/Z- photoisomerism of olefins by triplet-triplet energy transfer,^[51] and was within range of the triplet energies of stilbenes.

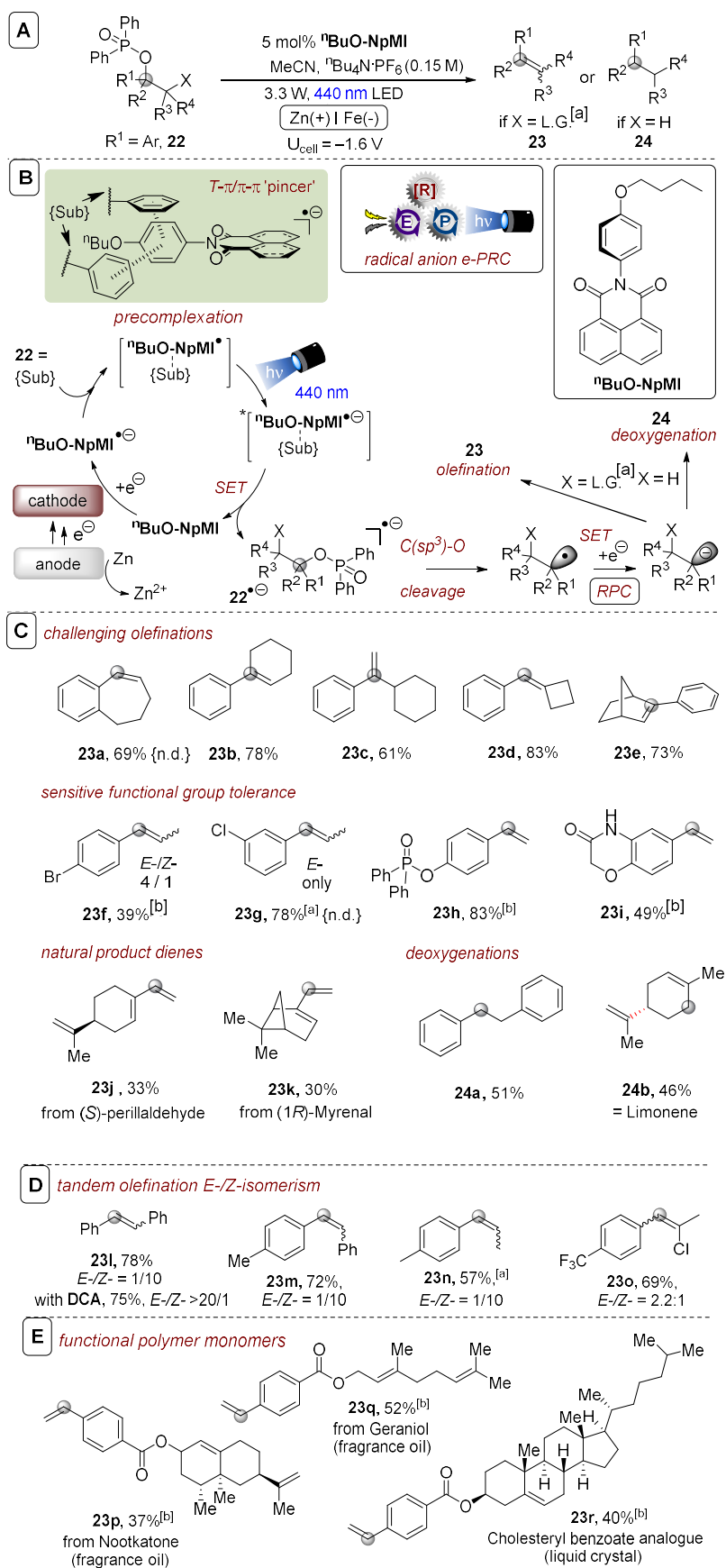


Figure 14. A) e-PRC reduction of phosphinates of aliphatic alcohols with ${}^n\text{BuO-NpMI}$. B) Catalytic cycle including proposed precomplexation. C) Selected olefination examples. D) Tandem photoelectrochemical olefination E-Z-isomerism, E) Application to functional polymer monomer synthesis. ^[a]Unless otherwise stated, phosphinate substrates with X = Cl; ^[b]from phosphinate with X = Br. n.d., not detected.

The authors sought to determine why ${}^n\text{BuO-NpMI}$ was an effective catalyst for all (benzylic/allylic) substrates attempted, while NpMI was ineffective for most substrates, despite the identical ground state reduction potentials ($E_{1/2} = -1.3$ V vs. SCE) and UV-Vis properties of both e-PRCats, as their neutral or radical anion forms. By a combination of CV, EPR and computational investigations examining $\text{C}(\text{sp}^3)\text{-O}$ bond dissociation free energies (BDFEs), the authors found that the $\text{C}(\text{sp}^3)\text{-O}$ bond cleavage was likely the reactivity-determining step, since the initial SET step was successful for both e-PRCats. Mirroring their study on $\text{TPA}^{\bullet+\text{s}}$,^[20] irradiation of the near-IR UV-Vis bands of the catalyst gave no conversion, suggesting anti-Kasha photochemistry from a higher order excited doublet state. Given i) the known ultrashort lifetimes of similar excited state radical anions (${}^*\text{PDI}^{\bullet-}$, ${}^*\text{NDI}^{\bullet-}$, Table 1) that prohibit their diffusion-controlled photochemistry, ii) the fact that catalyst architecture was able to influence a C-O bond cleavage step and iii) the involvement of higher order excited doublet states, the authors proposed a preassembly of phosphinate substrates with ${}^n\text{BuO-NpMI}^{\bullet-}$. However, in contrast to the authors' earlier study on $\text{TPA}^{\bullet+\text{s}}$,^[20] no spectroscopic (UV-Vis/EPR) changes were detected when electrogenerated ${}^n\text{BuO-NpMI}^{\bullet-}$ was mixed with phosphinate **22a**. The authors rationalized that precomplexation may occur at the *N*-aryl moiety, which is not spectroscopically detectable since the spin density and chromophore of the radical anion are localized on the naphthalene moiety, orthogonal and electronically disconnected from the *N*-aryl moiety. In support of this proposal, a strong correlation was found between decreasing steric hindrance at the *N*-aryl moiety *ortho*-positions of the e-PRCats and increasing reactivity of **22a** as a model substrate (Figure 15). Variations in the naphthalene moiety's electronics (e-PRCats **25a-b**) did not improve the activity compared to NpMI. An additional two alkoxy substituents at the *meta*-positions (**25c**) decreased activity relative to ${}^n\text{BuO-NpMI}$. DFT calculations ($\omega\text{B97X-D}$) found several candidate preassemblies between **22a** and both $\text{NpMI}^{\bullet-}$ and ${}^n\text{BuO-NpMI}^{\bullet-}$.

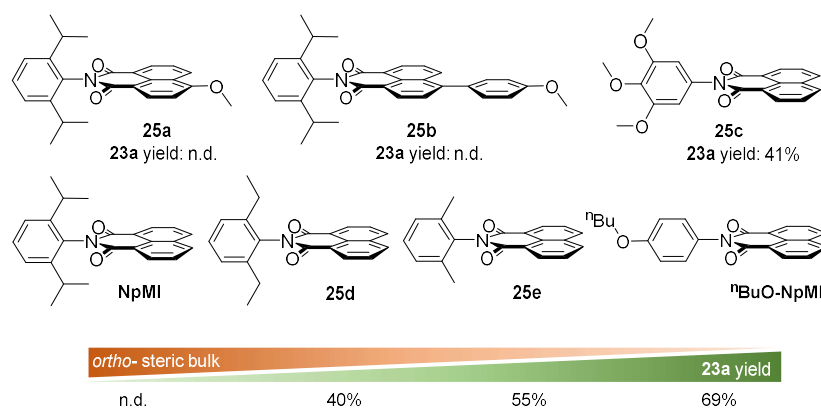


Figure 15. Relationship between catalyst structure and e-PRC activity. n.d., not detected.

In all cases, converged structures resembled a ‘pincer’ where two aromatic groups of **22a** interacted with the *N*-aniline moiety by a T - π and a π - π interaction (Figure 16). No matter the converged candidate structure, binding free energies (ΔG^{bind}) were always more favorable for ${}^n\text{BuO-NpMI}^{\bullet-}$ than $\text{NpMI}^{\bullet-}$. Finally, excited state calculations (DFT-MCRI), in good agreement with experimental UV-Vis of ${}^n\text{BuO-NpMI}^{\bullet-}$, revealed that the transition at ~ 430 nm ($D_0 \rightarrow D_n$) involved a charge transfer from the naphthalene moiety to the *N*-aniline moiety (Figure 17). Localization of electron density at the *N*-aniline in this excited state (D_n) is thus exactly where required for rapid intra-assembly SET. A more intimate precomplexation of **22a** and ${}^n\text{BuO-NpMI}^{\bullet-}$ likely promotes $\text{C}(\text{sp}^3)\text{-O}$ cleavage.

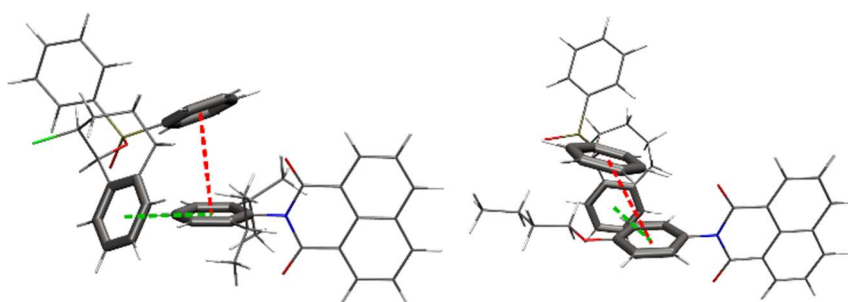


Figure 16. Example converged preassemblies for **22a** with $\text{NpMI}^{\bullet-}$ (left) or ${}^n\text{BuO-NpMI}^{\bullet-}$ (right). Two candidates are shown, for others see Ref. 19q.

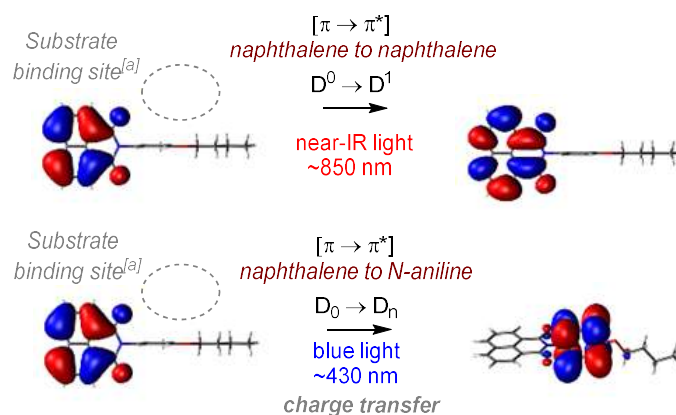


Figure 17. Orbital transitions for photoexcitation of ${}^n\text{BuO-NpMI}^{\bullet-}$ corresponding to $D_0 \rightarrow D_1/D_n$. ^[a]Predicted by DFT.

$\text{C}(\text{sp}^2)\text{-O}$ and $\text{C}(\text{sp}^3)\text{-NR}_3$ cleavages: Wickens and co-workers recently extended their aryl halide reduction methodology to the reduction of aryl pseudohalides.^[19i] Phosphonated phenols and anilinium salts could be reduced by e-PRC in an overall hydrodefunctionalization reaction as the main theme of the study (Figure 18A). Alternatively, the aryl radical could again be intercepted by triethylphosphite, *N*-methylpyrrole or B_2pin_2 (Figure 18B), inspired by the author’s previous work^[18c] and that by the groups of Larionov^[50] and König^[52] who demonstrated reductive

cleavages of strong bonds and borylation of aryl radicals via photocatalysis involving proton-coupled electron transfer^[50] or an EDA complex.^[52] Reactions were conducted in divided H-cells but (i) constant potential was employed, (ii) a higher loading (10 mol%) of e-PRCat was used and (iii) 2 equiv. of NEt₃ was present in the cathodic chamber as terminal reductant. As an example synthetic application, a phenol was used to direct the Friedel-Crafts reaction of **30** with **31** followed by e-PRC hydrodefunctionalization to **28e** and global O-demethylation to afford tricyclic resorcinol cannabinoid agonist **32** in 14% yield over 3 steps. This application followed the work of Makriyannis and co-workers^[53] but substituted dissolving Li metal reduction with e-PRC. Although isophthalonitrile structures are widely employed in PRC, this report,^[19q] together with a concurrently reported conPET variant,^[19s] constitute the first reports of isophthalonitrile radical anions in reductive catalytic transformations.

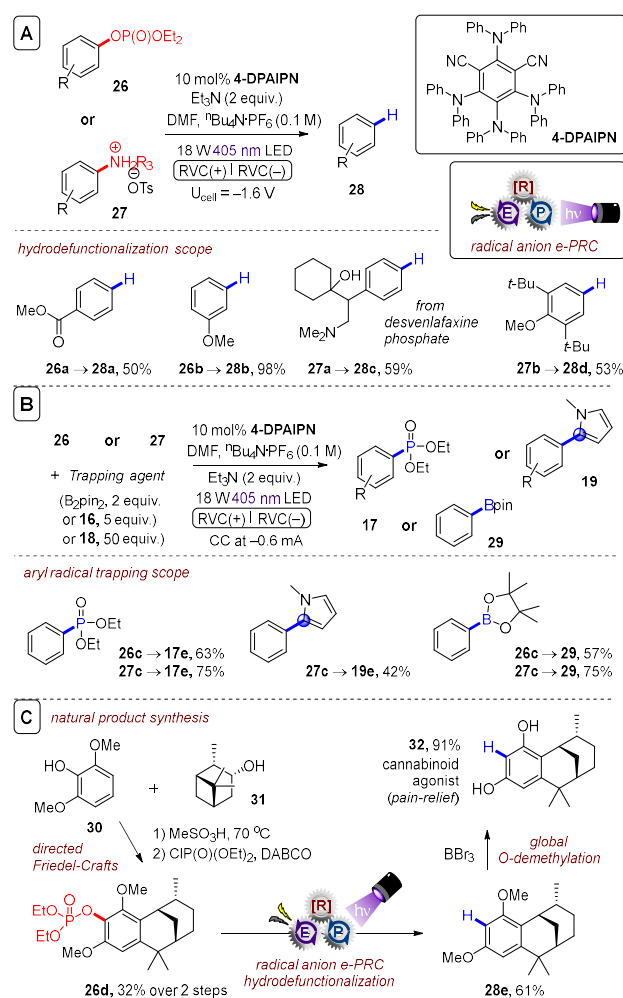
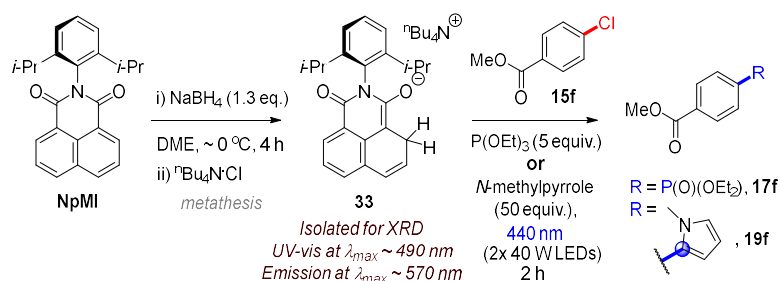


Figure 18. e-PRC reduction of phosphonated phenols and anilinium salts. A) Substrate scope of hydrodefunctionalization. B) Substrate scope of aryl radical trapping. C) Application in alkali metal-free synthesis of a cannabinoid agonist.

4-DPAIPN structurally resembles cyano-substituted triaryl amines used in oxidative e-PRC;^[20] it is interesting to find the acyclic triarylamine architectural family can be used in both reductive and oxidative e-PRC reactions. Current-based analysis of the reaction rate over time evidenced the enhanced stability of 4-DPAIPN compared to previously reported catalyst (NpMI). NpMI decomposed over time under the reaction conditions decreasing conversion rate. As the reaction progressed the rate increased again, meaning a decomposed form of the catalyst is also catalytically (albeit less) active. This concurs with Nocera and co-workers' recent report^[19r] which analyzed the electrodecomposition product of NpMI (irreversible CV wave at -2.3 V). Electrolysis at $U_{\text{cell}} = -3.0$ V provided a species absorbing at ($\lambda_{\text{max}}=480-500$) nm and luminescing at ($\lambda_{\text{max}}=560-580$ nm), which matched the spectra of a species formed when NpMI was chemically treated with NaBH_4 (in DME) or TBAF (in DMAc). XRD of the species chemically formed with NaBH_4 revealed a hydride adduct **33** (Scheme 2). Irradiating **33** with 440 nm in the presence of stoichiometric 4-methylchlorobenzoate (**15f**) and excesses of $\text{P}(\text{OEt})_3$ of *N*-methylpyrrole led to detection of **17f** and **19f** by ^1H NMR, confirming **33**'s ability to serve as a photoreductant. Nocera questioned the previously proposed involvement of radical anion photocatalysts,^[18c] claiming that $\text{NpMI}^{\bullet-}$ is too short-lived ($\tau = 24$ ps) to permit diffusion-controlled photochemistry yet the electrodecomposed emitting species assigned as **33** is sufficiently long-lived to do so ($\tau = 20$ ns). However, photoreductive activity of $\text{NpMI}^{\bullet-}$ is not ruled out since Wickens' kinetic analysis clearly evidenced the presence of multiple (at least two) active catalysts during e-PRC reactions.^[19i] Although **33**'s lifetime was effectively quenched by activated aryl chloride **15f**, PhCl was ineffective (radical trapping of PhCl was not reported). Adduct **33** or related species may be a candidate for the emitting state (ES_1) in Barham, König and co-workers' study,^[19q] but comparisons are still questionable due to (i) UV-Vis absorptions (λ_{max}) of $\text{NpMI}^{\bullet-}$ agreeing within ± 10 nm despite different solvents of DMAc^[19r] vs. ACN in both studies,^[19q] yet ES_1 differing in peak shape and λ_{max} (by ca. 40 nm);^[19q] (ii) notably lower cell potentials for electrolysis



Scheme 2. Chemical reduction of NpMI affords a hydride adduct which serves as a stoichiometric photoreductant in the coupling of an activated aryl chloride.

($U_{\text{cell}} = -1.6$ V) used both in spectroscopy and reactions where $U_{\text{cell}} = -3.0$ V led to intractable complex mixtures.^[19q] The proposal of diffusion-controlled SET photochemistry of adducts like **33**,^[19r] while intriguing, cannot rationalize (i) clear structure/activity relationships at the *N*-aniline of NpMI-type catalysts,^[19q] (ii) reduction of non-activated aryl chlorides like PhCl/4-chloroanisole (**15a**),^[18c] (iii) clear quenching of PRCat^{•-}s UV-Vis/EPR signals upon irradiation in the presence of substrates^[4a,19q,19s] and (iv) absence of quenching of longer(ns or μ s)-lived emitting species derived from radical anion PRCat^{•-}s in other reports.^[4g,19q] Closed shell anionic species may be reservoirs/precursors to radical anion photocatalysts as proposed by Miyake and co-workers.^[4g]

Future perspectives: Radical ion e-PRC is a rapidly-expanding field that offers (i) new opportunities in synthetic transformations, including complex molecule functionalizations, (ii) access to ultra-high-energy redox processes under exceedingly mild conditions to cleave or form strong bonds, and (iii) new opportunities for selectivity that differ from conventional parameters in SOE and PRC (redox potentials). While radical ion catalysts and their excited state behaviors are likely interchangeable concepts between conPET and e-PRC manifolds, downstream chemistry of a target substrate following its initial SET differs. Here, e-PRC offers an attractive and unique benefit of user-potential-controllable radical polar crossover. With the key importance of preassembly in radical ion photocatalysis establishing, a particularly exciting prospect is leveraging factors in preassembly formation to guide (i) SET chemoselectivity and/or (ii) following bond cleavages/formations; similar to the ‘lock and key’ concept of enzyme catalysis. Indeed, non-covalent interactions (dispersion, π - π stacking) historically viewed as ‘weak interactions’ are receiving increasing attention in catalysis.^[54]

Another emerging theme is access to excited states higher than the first excited state in anti-Kasha photochemistry.^[4,19q,20] This phenomenon in itself corroborates substrate/photocatalyst preassembly, to rationalize SET taking place more rapidly than internal conversion of the higher order excited state ($D_n \rightarrow D_1$). Thereby, anti-Kasha radical ion photochemistry harnesses the full visible photon redox energy, whereas in conventional PRC much is lost to internal conversion. Consequentially, the redox window of transformations is dramatically expanded - substrates beyond typical solvent windows (ACN/DMF) are engaged. The ultrafast timescale within which SET must occur shields the bulk reaction mixture from extreme redox potentials generated *in situ*; a clear benefit compared to high cell potentials constantly applied across reaction mixtures in direct electrolysis.

In theory, preassembly and anti-Kasha photochemistry should raise photochemical reaction (quantum) efficiency. In practice, long reaction times often plague radical ion e-PRC reactions. A greater understanding of factors involved in the preassembly is essential for the field to achieve higher quantum efficiencies. While it is straightforward to assign quantum yields and lifetimes to

closed-shell excited states, interrogation of open-shell doubled excited states is a challenging endeavor demanding more sophisticated spectroscopic and theoretical techniques. This said, solvated electrons^[4g] and decomposition of radical ion PRCats to closedshell PRCats as in *DCAC^{•-} and *NpMIC^{•-}^[19p,r] must be probed as alternative mechanisms as the field continues to evolve. Finally, limited reports of scalability in radical ion e-PRC are likely due to practitioners requiring 1) divided cell configurations to spatially mitigate nonproductive half-reactions and 2) constant potential desirable for selective e-PRCat activation

1.4 Photocatalyst Electro-recycling

The second subcategory of e-PRC, dubbed “recycling ePRC”, involves the turnover of a photocatalyst that is a known photoredox catalyst (PRCat) in PRC, and that is a colored species in its ground, neutral state. Figure 19 depicts the structures of PRCats used in recycling e-PRC; their photophysical properties are thoroughly detailed elsewhere. [2c,e, 38,55]

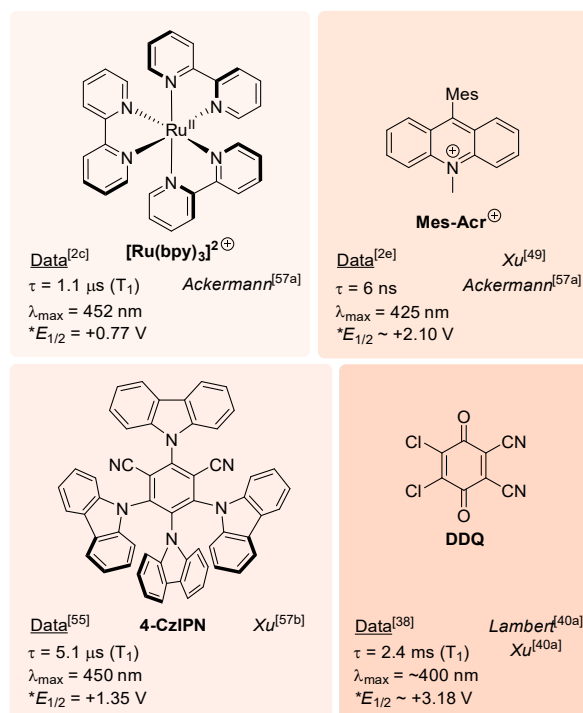


Figure 19. PRCats reported in recycling e-PRC. Red shading is indicative of oxidizing power. Selected photophysical and redox potential data are shown.

In recycling e-PRC, the available “redox window” is no wider than it is for PEC. Instead, the key benefit is the replacement of sacrificial oxidants or reductants in the photocatalyst turnover with electrochemistry (Figure 20), which can (or whose by-products can) interfere with downstream chemistry and/or complicate separation of desired products.^[9,56,57] This is not to say that sacrificial oxidants or reductants are *completely* avoided; they can be required by the counter-electrode’s reaction. However, here protons or water typically serve as much milder, atom economical sacrificial oxidants or reductants (respectively). Moreover, a divided cell configuration provides the opportunity to spatially separate sacrificial redox agents from the desired catalytic reaction in the product-forming chamber. In a seminal report that was previously reviewed elsewhere,^[9,10] Xu and co-workers reported recycling e-PRC using Fukuzumi’s catalyst Mes-Acr⁺ for a Minisci-type coupling of alkyltrifluoroborates with heteroarenes in an undivided cell.^[56] Inspired by this report, different applications of recycling e-PRC have emerged in recent years.^[40,57] Recycling e-

PRC benefits from the use of well-characterized and long-lived (nanosecond to millisecond) closed-shell excited states. As opposed to radical ion e-PRC where divided cells are generally employed, recycling e-PRC typically uses undivided cells or modular batch/recirculated flow setups. In fact, most reports on recycling e-PRC easily achieve gram to multigram-scale reactions - indicating the practical accessibility and robustness of this synthetic photoelectrochemical technology.

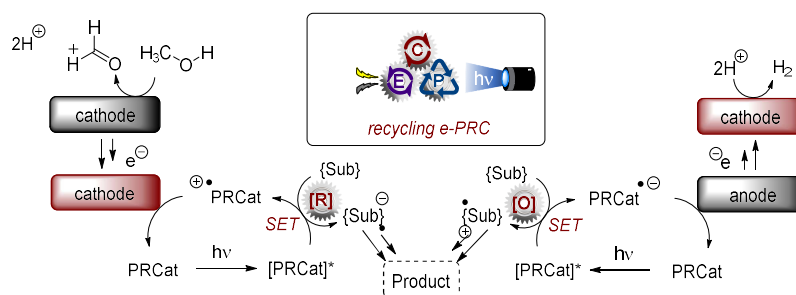


Figure 20. Concept of photocatalyst electrorecycling (recycling e-PRC).

C(sp²)-H trifluoromethylation: In an elegant example of photocatalyst electro-recycling, Ackermann and coworkers reported the PEC C(sp²)-H trifluoromethylation of arenes and heteroarenes under anodic current and with Langlois' reagent (**34**); CF₃SO₂Na (Figure 21).^[57a] Upon visible light photoexcitation of the Fukuzumi-type organic dye, **Mes-Acr⁺** (catalyst **a**) the authors proposed that the excited state ^{*}Mes-Acr⁺ engages in SET with the CF₃SO₂ anion to furnish the reduced acridinyl radical of the catalyst and form the CF₃SO₂ radical **34'**. Loss of SO₂ generates the active trifluoromethyl radical **36**, which attacks arene substrate **1a** to form arene radical **37**. SET oxidation of **37**, either by Mes-Acr⁺ or by the anode, forms cation **37⁺** which loses a proton to form the trifluoromethylated product **35a**. The protons generated could undergo cathodic reduction to form H₂ to complete the circuit. Meanwhile, ground state Mes-Acr⁺ photocatalyst is then regenerated by anodic oxidation of its acridinyl radical form at the C_(felt) anode under constant current conditions (4.0 mA). LiClO₄ was selected as an electrolyte which eases the separation of products, while another set of conditions was developed using Ru(bpy)₃²⁺ (catalyst **b**). This method enabled the C(sp²)-H trifluoromethylation of a range of arenes including electron-rich and electron-poor arenes and various heteroarenes (affording products such as **35b-35e**, Figure 21D). As a pioneering example of the transfer of PEC to a continuous flow setup, an electrochemical flow coil consisting of a C_(felt) and a nickel cathode and a photochemical fluoropolymer flow coil was used in sequence (Figure 21B). Recirculation of the reaction mixture over 12 h afforded **35a** in 76% using catalyst **a** (conditions employing catalyst **b** were inferior). Speaking to the facile integration of continuous flow with process analytical technologies (PATs),^[58] the authors used an in-line NMR spectrometer to monitor the reaction and observed

Wheland-type arenium cation **37**⁺ as a long-lived intermediate *via* ¹⁹F and ¹H NMR. This demonstrated a key opportunity for continuous flow in the investigation of SET reaction mechanisms by its ability to provide a steady state concentration of reactive species.

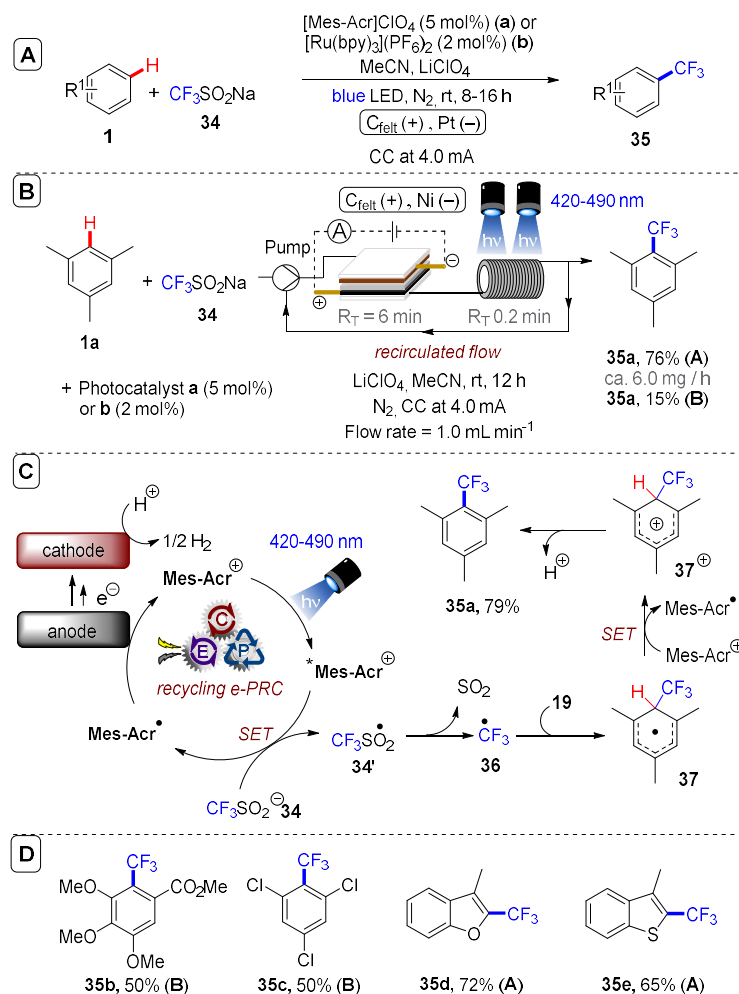


Figure 21. (a) C(sp²)-H trifluoromethylation using CF₃SO₂Na, graphite felt (C_{felt}) anode (Pt cathode) and a photocatalyst. (b) C-H trifluoromethylation in a flow setup with flow rate 1.0 mL min⁻¹ (R_T 'per pass' = 6 min). (c) Proposed mechanism. (d) Selected substrate scope.

C(sp²)-C(sp³) coupling: Building upon their previous work in photoelectrochemical C(sp²)-C(sp³) Minisci-type coupling of heteroarenes **30** with alkyl trifluoroborates,^[56] and as the first synergy of PEC with Cerium photocatalysis,^[59] Xu and coworkers reported direct decarboxylative C-H alkylation of heteroarenes **38** using RVC anode and CeCl₃·7H₂O as a photocatalyst precursor (Figure 22).^[57b] Initial anodic oxidation of Ce^{III} to Ce^{IV} occurs (Figure 22B), followed by coordination of Ce^{IV} by the carboxylic acid **39** to form complex **39'**. Photoinduced ligand-to-metal charge transfer (LMCT) regenerates Ce^{III} and simultaneously forms carboxyl radical **41**, which decarboxylates to afford alkyl radical **42**. Given the protic reaction conditions, the authors proposed the addition of alkyl radical **42** to protonated substrate **38-H** to give transient radical

cation **43**, which then loses a proton to form **44**. A highly exothermic oxidation of **44** by Ce^{IV} then affords product **40a-H**. The substrate scope demonstrated that various examples of carboxylic acids (primary, secondary, tertiary and α -alkoxy and aliphatic) could be tolerated, and the power of the method was demonstrated by the late-stage functionalizations of various *N*-heteroarenes including bioactive molecules such as **40f** (fasudil), a Rho-associate protein kinase inhibitor (Figure 22C).^[60]

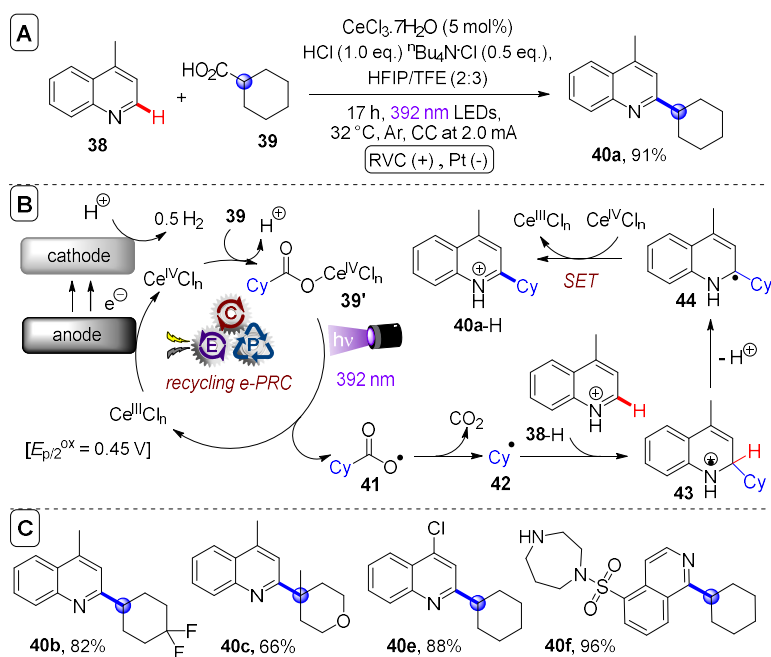


Figure 22. A) Decarboxylative C-H alkylation of heteroarenes using RVC anode (Pt cathode) and $\text{CeCl}_3 \cdot 7\text{H}_2\text{O}$. B) Proposed mechanism. C) Selected scope.

In the same report, Xu and coworkers further exploited decarboxylative radical formation in the PEC carbamoylation of heteroarenes using an RVC anode and a 4CzIPN photocatalyst (Figure 23).^[57b] Upon photoexcitation of 4CzIPN with blue LEDs, SET oxidation of oxamate substrate **45'** by ${}^34\text{CzIPN}^*$ forms $4\text{CzIPN}^{\bullet-}$ and, upon decarboxylation, carbamoyl radical **47** which adds to protonated substrate **38-H** resulting in radical cation **48** (Figure 23B). Reduction of **48**, either by the Pt cathode or by $4\text{CzIPN}^{\bullet-}$, affords intermediate **49**. Anodic oxidation of **49** with loss of H_2 was proposed to result in aromatization to protonated product **36-H**. Alternatively, the authors proposed deprotonation of **48** would afford radical **50** which could be oxidized by ground state 4CzIPN or by the anode. The substrate scope featured various examples of oxamic acids (bearing primary, secondary and tertiary *N*-substituents) and various electron-deficient *N*-heteroarenes (affording products such as **46a-d**), including the late-stage functionalization of antihistamine Loratadine^[61] to afford **46e** (Figure 23C). Finally, Xu and coworkers extended their method to alkyl oxalates as precursors to alkyl radicals in the absence of a transition metal catalyst (Figure

24).^[57e] Photoexcited 4CzIPN oxidizes alkyl oxalate **51** to generate alkyl radical **42** via double decarboxylation. The authors proposed similar downstream chemistry (Figure 24B) to that in the case of the carbamoyl radical (Figure 22) to afford **40a-h**. Although the reaction was amenable to various examples of secondary and tertiary oxalates (Figure 24C), primary oxalates were ineffective as alkyl radical precursors.

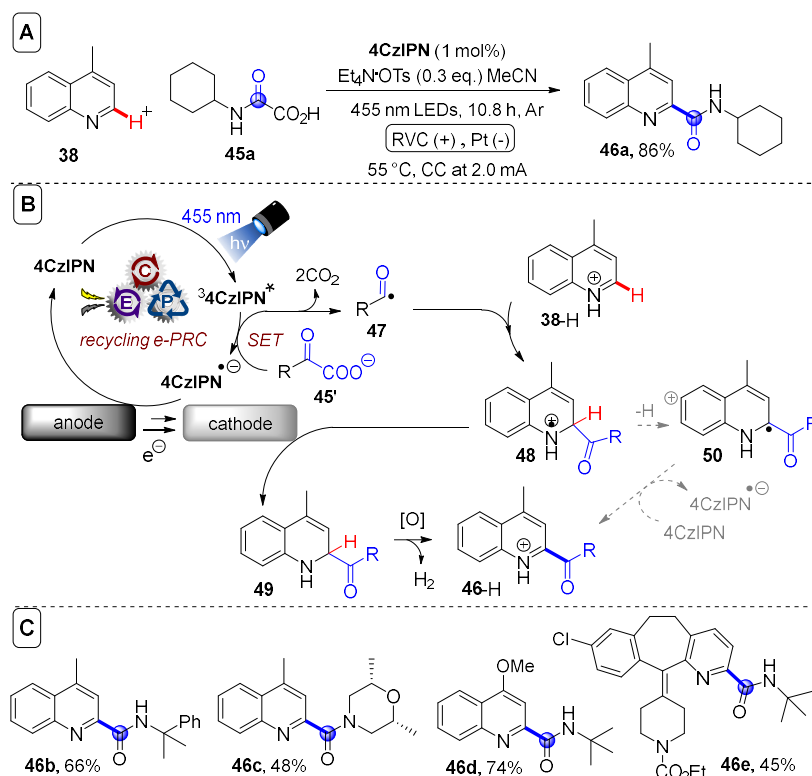


Figure 23. A) Decarboxylative C-H carbamoylation of heteroarenes using RVC anode (Pt cathode) and 4CzIPN as photocatalyst. B) Proposed mechanism. C) Selected scope.

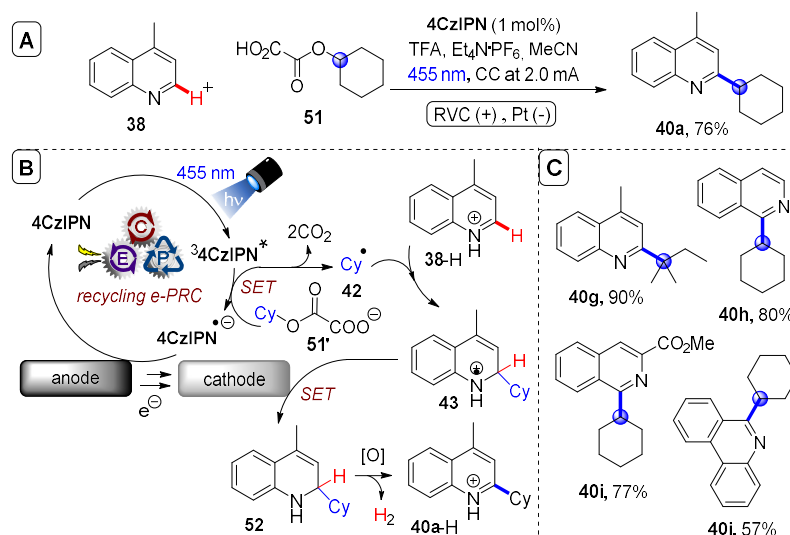


Figure 24. A) C–H alkylation of heteroarenes with alkyl oxalates using RVC anode (Pt cathode) and 4CzIPN as photocatalyst. B) Proposed mechanism. C) Selected scope.

C(sp²)-O/N bond formations: So far, examples covered have focused on C(sp²)-C bond formations. However, C(sp²)-O and C(sp²)-N bond formations can also be achieved under recycling e-PRC. DDQ as a neutral photocatalyst is a powerful oxidant in its long-lived triplet excited state (+3.18 V vs. SCE).^[38] Despite its absorbance maxima at ~400 nm, DDQ is successfully photoexcited with longer wavelength blue (455 nm) light. Prior to any contemporary reports of recycling e-PRC, König's group achieved the photocatalytic oxidation of electron-deficient arenes by ³DDQ* in the presence of *tert*-butyl nitrite and molecular oxygen,^[39] which was reviewed previously.^[9] Inspired by this work, and by their earlier work on recycling e-PRC for the S_NAr-type arene azolations^[62] (reviewed previously),^[9] the Lambert group recently reported arene acetoxylation using DDQ as photocatalyst under recycling e-PRC (Figure 25).^[40a] Benzene (**1c**) was hydroxylated to phenol (**54a**) in the optimization study. Control reactions confirmed the necessity of light, catalyst and potential in the reaction (Figure 25A). Direct electrolysis at a potential of $E_{\text{cell}} = +3.2$ V gave no product after 48 h (presumably, decomposition occurred, as previously reported in the radical ion e-PRC azolation of benzene)^[18a], confirming the superiority of photoelectrochemistry in this reaction. In the mechanism, SET oxidation of arene **1** by ³DDQ* was proposed (Figure 25B), followed by nucleophilic addition of heteroatom partner **53** to radical cation **1**^{•+}. DDQ^{•-} formed after SET is protonated and engages **55** in HAT to afford product **54**. A range of electron-deficient arenes were hydroxylated and acetoxylation to afford products **54a-f** in modest to very good (30-76%) yields (Figure 25C). Remarkable selectivities were observed; aliphatic alcohols, terminal alkynes and benzylic positions were all tolerated, where these positions would not likely tolerate direct electrolysis. Aminations were also possible with free amides, carbamates and ureas, affording products **56a-d** in satisfactory to high (49-80%) yields, although the scope of amination partner was relatively narrow in each of these

classes. In an intriguing competition experiment (Figure 26A), benzene (**1c**) was selectively hydroxylated while anisole (**1b**) and trifluorotoluene (**1e**) were untouched by the recycling e-PRC conditions. This highlights the importance of matching excited state PRCat redox potentials to the substrate. Trifluorotoluene is beyond the scope of ${}^3\text{DDQ}^*$ (and ${}^*\text{TAC}^{\bullet 2+}$, >3.3 V vs. SCE, but could be engaged by potent ${}^*\text{TdCBPA}^{\bullet +}$, up to $+4.4$ V vs. SCE). On the other hand, anisole is easily accessible and likely oxidized by ${}^3\text{DDQ}^*$. It is plausible that back electron transfer (BET) is rapid enough to prohibit downstream chemistry of **1b** $^{\bullet +}$.^[63]

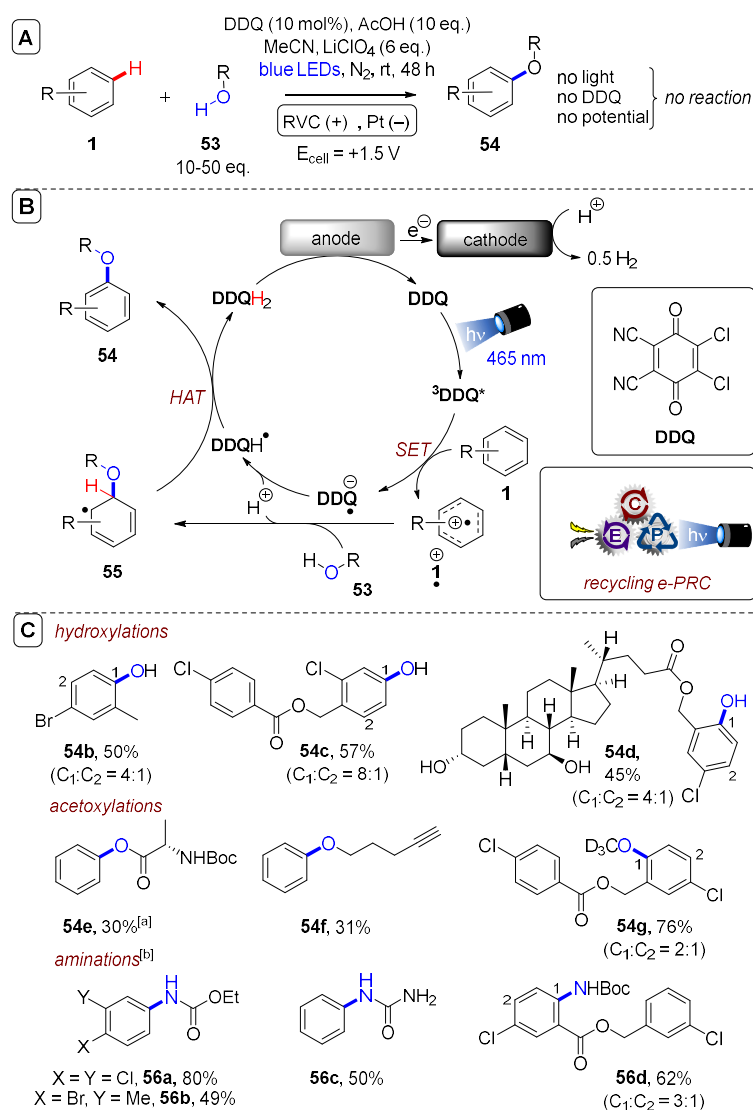


Figure 25. A) $C(\text{sp}^2)\text{-H}$ acetoxylation of arenes using RVC anode (Pt cathode) and DDQ as photocatalyst. B) Proposed mechanism. C) Selected substrate scope. ^[a]Boc-Ala-OH substituted for the AcOH additive. ^[b]3-15 eq. of amide/carbamate nucleophile was used.

In general, this recycling e-PRC gave superior to the preceding PRC-only report^[39] where cheap constant potential obviated the need for sacrificial oxidants molecular oxygen and expensive *tert*-butyl nitrite; both hazardous reactants that require considerable safety considerations for scaling

up.^[64] In this respect, the Lambert group successfully scaled the benzene to phenol hydroxylation reaction in a recirculated continuous flow setup (Figure 26B). Electro-regeneration of DDQ was achieved in a batch undivided cell, while the reaction mixture was recirculated through a blue LED-irradiated coil with a residence time of (R_T) 3 min ‘per pass’. By extending reaction time and adding additional photocoils, the reaction was successfully scaled from 0.4 to 15 mmol without appreciable loss in yield of **54a**. Thereby, recycling e-PRC benefitted safety and cost-efficiency.

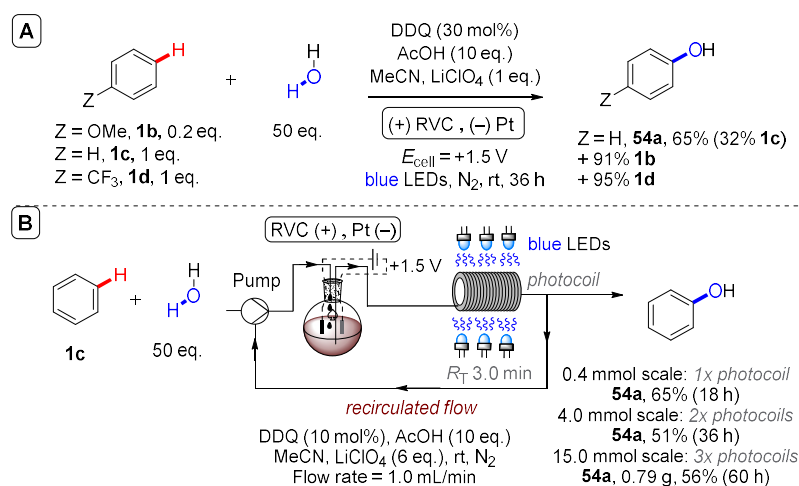


Figure 26. A) Competition experiments between arenes with different electronics in recycling e-PRC hydroxylation. B) Recirculated flow recycling e-PRC hydroxylation of benzene.

Xu and co-workers also reported arene heteroamination using DDQ under recycling e-PRC conditions (Figure 27A).^[40b] Compared to the Lambert group’s report, although conditions employed a loading of DDQ (20 mol%), the loadings of electrolyte (only 0.1 eq.) and amination partner (only 2 eq.) were markedly lower, possibly due to the use of constant current (2 mA) to drive the reaction. The focus was on aminations; hydroxylation and acetoxylation was not investigated. The mechanism proposed was as aforementioned (Figure 27B). A much broader scope of amination partners was explored, including azolations, affording products in modest to high (36-70%) yields (Figure 27C). Like Lambert’s report,^[40a] anisole was unreactive. ³DDQ* was not able to engage methyl benzoate - the upper limit was dihalobenzenes. Although these conditions^[40b] were unable to engage very electron-deficient arenes (radical ion e-PRC with TPAs were able to engage up to acetophenone),^[20] the yields of azolated dihaloarenes were higher than radical ion e-PRC reports^[18a,20] and, notably, arene **1** was the limiting reagent as opposed to a requirement of excesses of arene in radical ion e-PRC (typically 1 mL)^[18a,20] and conPET (typically 8 mL)^[4] previous reports. Excesses of arene required in radical cation e-PRC are likely due to the requirement of precomplexation between ground state radical cation and arene for successful photochemistry, whereas ³DDQ* is long-lived enough to engage in outer-sphere

Scalable acridinium salt library synthesis: Finally, recycling e-PRC was used by Xu's group to synthesize a library of 3/6-substituted acridinium PRCats from an acridinium core **60** using trifluoroborate salts (Figure 28A).^[57d,e] Reactions were conducted iteratively to either afford mono-substituted PRCats **61** in very good to excellent (74-97%) yields over one step (Figure 28B), or disubstituted PRCats **62/63** in modest to very good (31-83%) yields over two steps (Figure 28C).

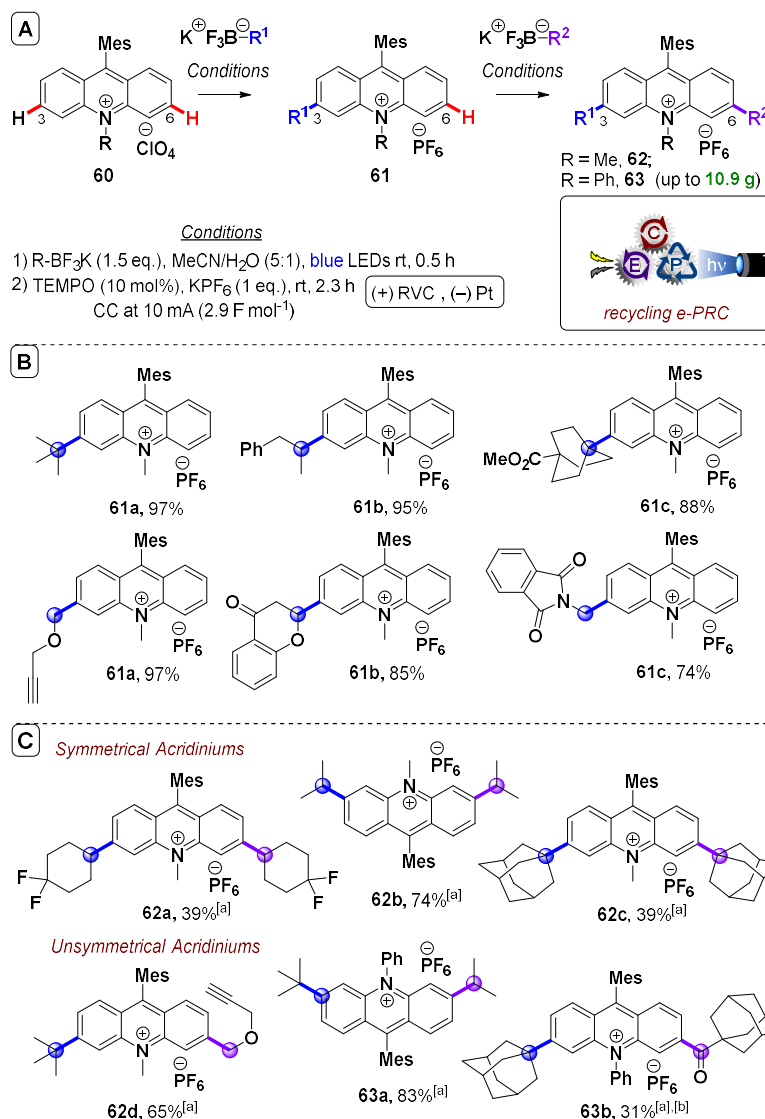


Figure 28. A) Iterative synthesis of 3,6-disubstituted acridinium PRCats. B) Selected scope of monosubstituted products. C) Selected scope of disubstituted products. ^[a]Overall yield after both steps. ^[b]A 1,4-dihydropyridine-based alkyl donor was used.

Impressively, different trifluoroborate salts can be employed at each step to furnish unsymmetrical 3,6-disubstituted acridinium salts. In the photochemical step (step 1) of the proposed mechanism (Figure 29A), photoexcitation of **60**, followed by SET reduction of ***60** by the alkyl trifluoroborate salt, affords reduced form **64**[•]. Addition of trifluoroborate-derived alkyl radical to **64**[•] affords **65**. In the electrochemical step (step 2), TEMPO engages **65** in HAT,

affording TEMPO-H and radical **66**. Oxidation of **66**, presumably by anodic current, affords product **61**. Meanwhile, TEMPO-H undergoes reduction at the cathode to liberate H₂ and TEMPO⁻, the latter of which is transformed back to TEMPO by SET at the anode. Passing a 0.05 M solution of **60** (R = Ph) through a flow photocoil into an electrochemical batch reactor for the first functionalization, then washing with KPF₆ before repeating for the second functionalization (see citation for details), 10.9 g (80% over both steps) of *N*-Ph Mes-Acr (structure in Figure 1) was successfully synthesized.

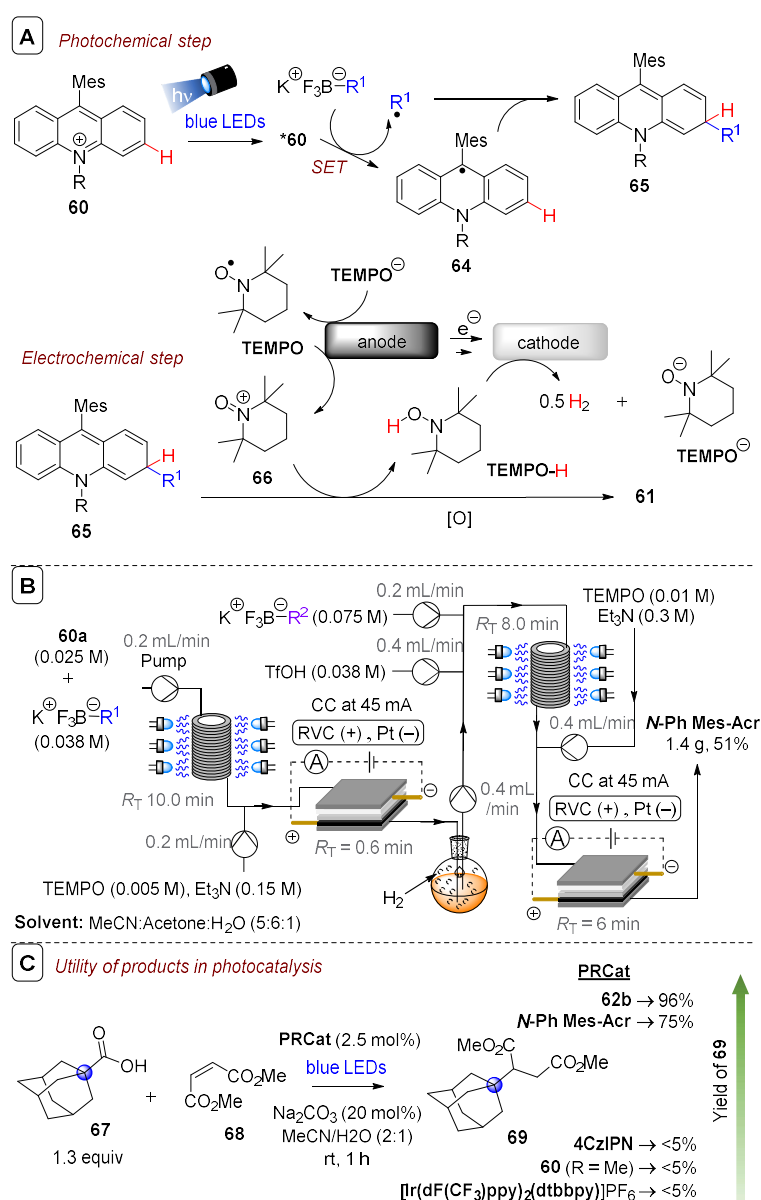


Figure 29. Proposed mechanism for each step. B) End-to-end continuous flow photoelectrochemical synthesis of functionalized acridinium salts. C) Utility of 3,6-disubstituted acridinium salts in photocatalysis.

In the first example of an end-to-end, semi-continuous homogeneous synthetic photoelectrochemical flow process, Xu and co-workers transformed 2.0 g of **53** (R = Ph) into 1.4 g (51% over both steps) of *N*-Ph Mes-Acr (Figure 29B). Here, the authors found that NEt₃ was necessary to improve conversion in the electro-mediated dehydrogenation of **58**. However, NEt₃ was detrimental to the photochemical step, so bases were neutralized *in situ* by TfOH before the subsequent photocell. A collection flask was required after the first electrochemical flow reactor in order to purge gas bubbles (H₂).

To demonstrate the value of their 3,6-disubstituted product acridinium salts (**62**), Xu and co-workers compared a variety of established photocatalysts in the photocatalytic decarboxylative conjugate addition of **67** to **68** (Figure 29C). While unsubstituted Mes-Acr⁺ (**60**, R = Me), an Iridium photocatalyst and 4CzIPN gave only trace products, the 3,6-*tert*-butyl disubstituted acridinium salt (*N*-Ph Mes-Acr) was effective and novel catalyst **62b** gave a near-quantitative yield of **69**. Interestingly, the nature of substituents at the 3,6-positions was found to dramatically influence the lifetime. The lifetime of *N*-Ph Mes-Acr (T₁) is ~6.1 ns (Table 1), while the lifetime of **62c** was much longer (τ = 30.7 ns) and is the longest lifetime ever reported for an acridinium salt. Enhanced lifetimes may provide a rationale for the increased activity of acridinium PRCat derivatives synthesized herein.

Future perspectives: Recycling e-PRC continues to pave the way to enhanced sustainability and safety in photocatalysis, by substituting sacrificial redox agents with cheap, non-hazardous electrochemistry. In contrast to radical ion e-PRC which typically uses 0.1 M of supporting electrolyte, a recurring theme is an ability to use lower electrolyte loadings, typically <1 to several equivalents, likely as a result of an undivided cell setup with shorter interelectrode distances. Applicability of the technology is clear; from late-stage functionalizations of pharmaceutically-relevant molecules to the synthesis of novel acridinium scaffolds as representing attractive functional materials and photocatalysts. Recent advances demonstrate how recycling e-PRC in recirculated or semi-continuous flow systems enables scalability of reactions, at least to multigram scales. However, the use of recycling e-PRC in the *reductive* direction is yet to be explored. Moreover, in most reports of oxidative recycling e-PRC, hydrogen gas is evolved and is not utilized downstream. Harnessing the by-product at the counter-electrode within a synthetic transformation (for example, utilizing H₂ in a subsequent catalytic hydrogenation,^[7b,65] isolating it, or conducting a paired electrolytic reaction^[66]) will improve Faradaic efficiency and enhance sustainability further. In a general sense, the elimination of sacrificial cathodic or anodic processes in favour of a paired electrolytic system is deemed necessary to encourage uptake of electro- and photoelectrochemistry in process chemistry.^[67]

1.5 Photoelectrochemical HAT Reactions

By circumventing high redox potentials, HAT is an efficient way to generate radicals which are hard to obtain from direct photocatalytic SET redox activations or where high applied electrochemical potentials would be inappropriate.^[68-69] Examples covered in this section include C(sp²)-C(sp³) and C(sp³)-N couplings.^[70] Photoelectrochemical HAT agents and selected properties^[18a,51a,68f,69-72] are displayed in Figure 30.

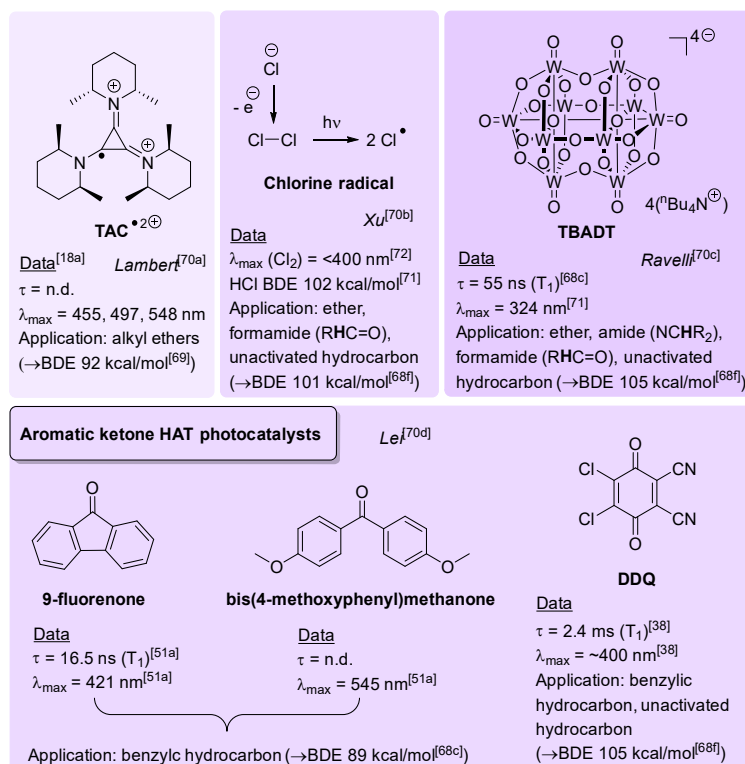


Figure 30. Photoelectrochemical HAT agents. Purple shading is indicative of C-H abstraction power. Selected photophysical and BDE data are shown.

Lambert and co-workers reported a photoelectrochemical HAT activation of C(sp³)-H bonds of alkyl ethers (**70**, **75**).^[70a] Here, the trisaminocyclopropenium ion (TAC⁺) developed by the group for radical ion e-PRC super-oxidations was employed as a catalyst. Upon anodic oxidation of TAC⁺ and photoexcitation of TAC•²⁺, the authors proposed that the excited radical dication *TAC•²⁺ engaged C(sp³)-H bonds of ethers in HAT to afford sp³ radical **79** (Figure 31D), which either 1) engaged in a Minisci-type reaction with quinoline derivatives like **71** to afford products **72-74** (Figure 31A); 2) underwent 1,4-addition to electron-deficient alkenes or alkynes **76** to afford products **77a-d** (Figure 31B); or 3) underwent further oxidation to oxocarbenium ions and then nucleophilic azolation with *N*-heteroarenes **2** to afford products **78a-d** (Figure 31C). Yields were generally satisfactory to excellent for all downstream transformations (31-89%). Following the proposed HAT step, TAC-H²⁺ releases a proton which is reduced to hydrogen at the cathode.

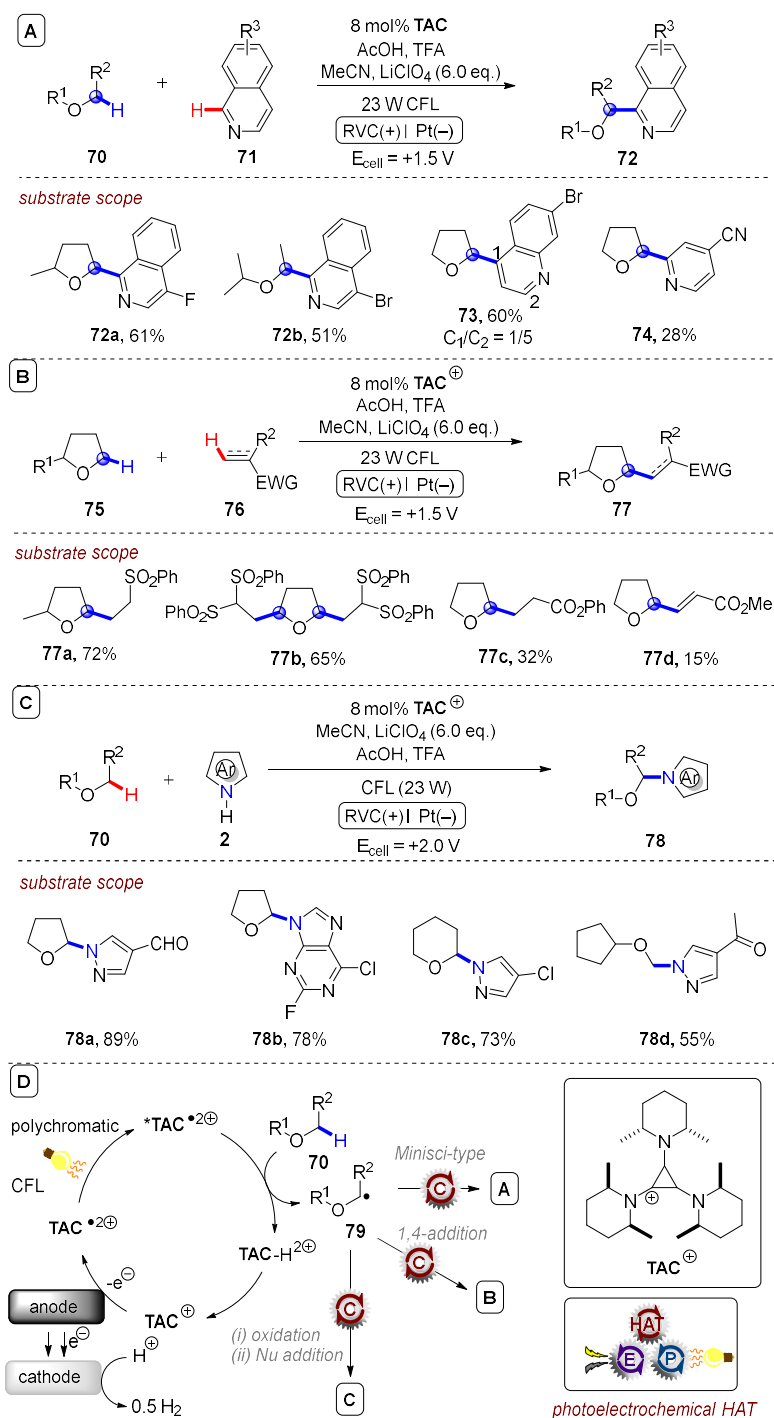


Figure 31. A) Photoelectrochemical HAT activation of alkyl ethers by a photoexcited cyclopropenium dication radical and participation of etheral sp^3 radicals in a Minisci-type reaction. B) 1,4-addition of etheral sp^3 radicals to electron-deficient alkenes or alkynes. C) Oxidation of etheral sp^3 radicals and nucleophilic azolations. D) Proposed photoelectrochemical HAT mechanism.

The observation of a kinetic isotopic effect (KIE, $k_{H/D} = 3.0$) confirmed rate-determining C-H cleavage. Despite the apparent bulkiness of $*TAC\bullet^{2+}$ as a HAT catalyst, the authors proposed that high selectivity for $2^\circ C(sp^3)\text{-H} > 3^\circ C(sp^3)\text{-H}$ corroborates HAT as the mechanism. However, the lifetime of $*TAC\bullet^{2+}$ is unknown, and as a doublet excited state, it is likely ultrashort-lived such that HAT might require preassembly of ethers and $TAC\bullet^{2+}$.

The Xu group reported an elegant photoelectrochemical pathway to activate C(sp³)-H bonds using chlorine radicals as HAT agents generated *in situ* within an undivided cell.^[70b] The generated C(sp³) radical (**83**) again participated in Minisci-type reaction with heteroarenes (Figure 32A). In their proposed mechanism, anodic oxidation of Cl⁻ to Cl₂ first occurs. Subsequent light irradiation leads to homolysis of Cl₂,^[73] generating Cl• as a powerful HAT reagent. Continuous *in situ* generation of Cl₂ by anodic oxidation and its consumption in the reaction avoids the direct use of toxic Cl₂ gas (Figure 32B). Since the bond dissociation enthalpy (BDE) of HCl is high (102 kcal/mol),^[71] Cl• is a powerful HAT agent and successfully engages various C(sp³)-H bonds in a thermodynamically favored process. As well as ethers, radicals were successfully accessed from C(sp²)-H positions of formamides and even C(sp³)-H positions of hydrocarbons were successfully engaged. Substrate scope with respect to both radical precursors and heteroarenes was relatively broad, tolerating many sensitive functional groups and affording products like **82a-f** generally in modest to excellent (40-94%) yields (Figure 32C). The ability to substitute photo- or electroactivated photocatalysts (TBADT, TAC) with Cl• from HCl readily available in all laboratories is a key advantage of this method. Without noticeable erosion in the yield of **82f**, a batch reaction was done on a 45 mmol scale. Even a 122 mmol batch reaction was achieved by recirculating the reaction mixture through a reservoir (Figure 32D). As per previous Minisci-type photoelectrochemical reactions (section 2), late-stage functionalization was achieved for complex and bioactive molecules such as dihydroinchonidine, fasudil, roflumilast and even an adenosine analogue (Figure 32C). While this process involved the photoelectrochemical generation of chlorine radicals, it is worth noting that the photoelectrochemical generation of iodine radicals for HAT at benzylic positions was reported earlier by Stahl and co-workers,^[74] and was reviewed previously.^[9]

It is well established that the photoexcited state of tetra-n-butylammonium decatungstate, TBADT ((ⁿBu₄N)₄[W₁₀O₃₂]) is one of the most powerful HAT agents reported. It engages challenging C(sp³)-H bonds in HAT, including alkyl ethers, alkyl nitriles and even light hydrocarbons like methane.^[68a,c,f] Ravelli and co-workers recently demonstrated electro-recycling of TBADT in a photoelectrochemical HAT process (Figure 33A).^[70c] Photoexcited TBADT engaged the remote C(sp³)-H bonds of nitriles and carbonyls as well as hydrocarbons in HAT to afford C(sp³) radicals and HTBADT. Bentothiazoles (**85**) were explored as the C(sp³) radical trapping partner, affording coupling products like **86a-d** (Figure 33C) TBADT is regenerated from TBADT-H by anodic oxidation at a very low applied potential ($\Delta E_{WE-RE} = +0.15$ V) in a divided cell (Figure 33B), such that the reaction could even be driven successfully by 2x AAA batteries. Laser flash photolysis confirmed the quenching of ³TBADT* by **81** and by a dihydro-precursor of **86**, but not by the LiNTf₂ electrolyte.

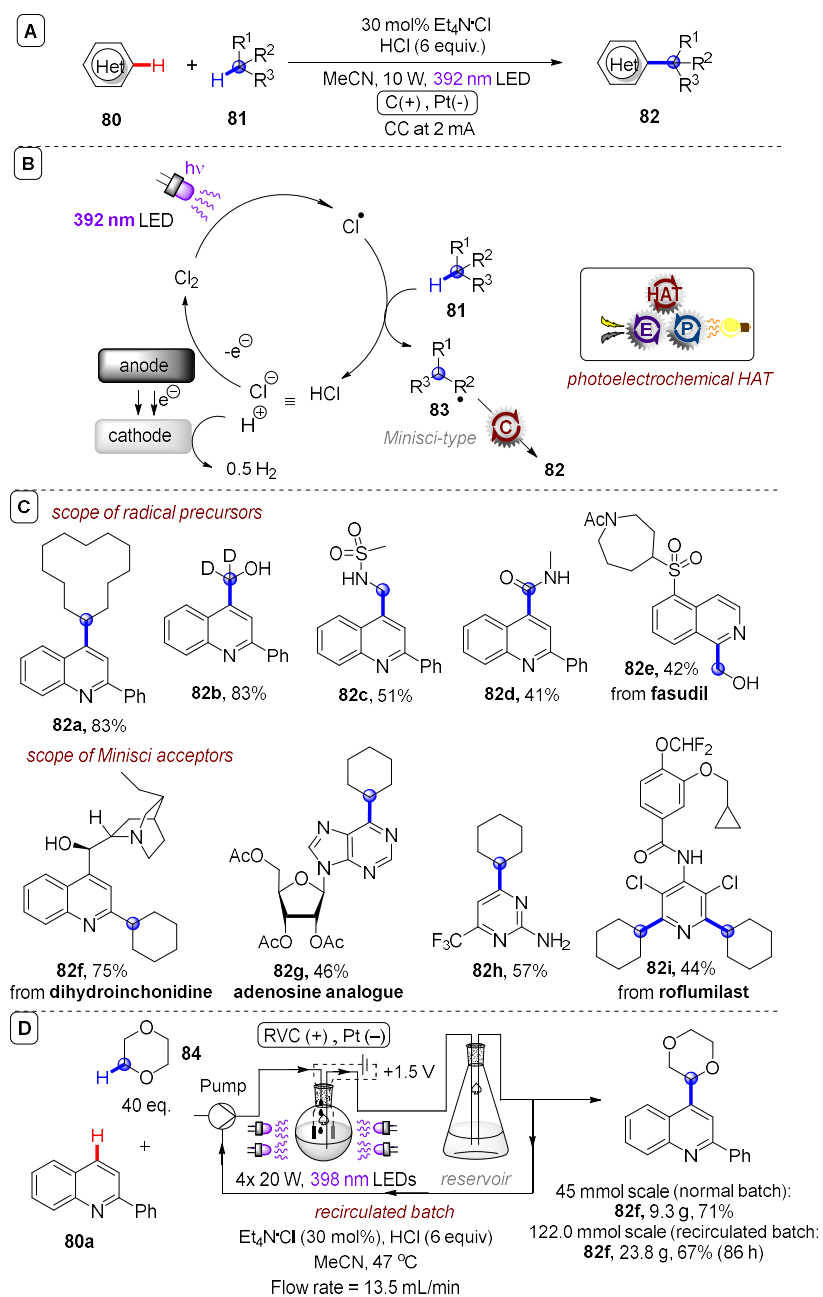


Figure 32. A) Photoelectrochemically-generated chlorine radicals in $C(sp^3)$ -H HAT activation for a Minisci-type reaction; B) Proposed mechanism; C) Selected examples; D) Recirculated flow photoelectrochemical HAT activation of 1,4-dioxane and Minisci-type reaction.

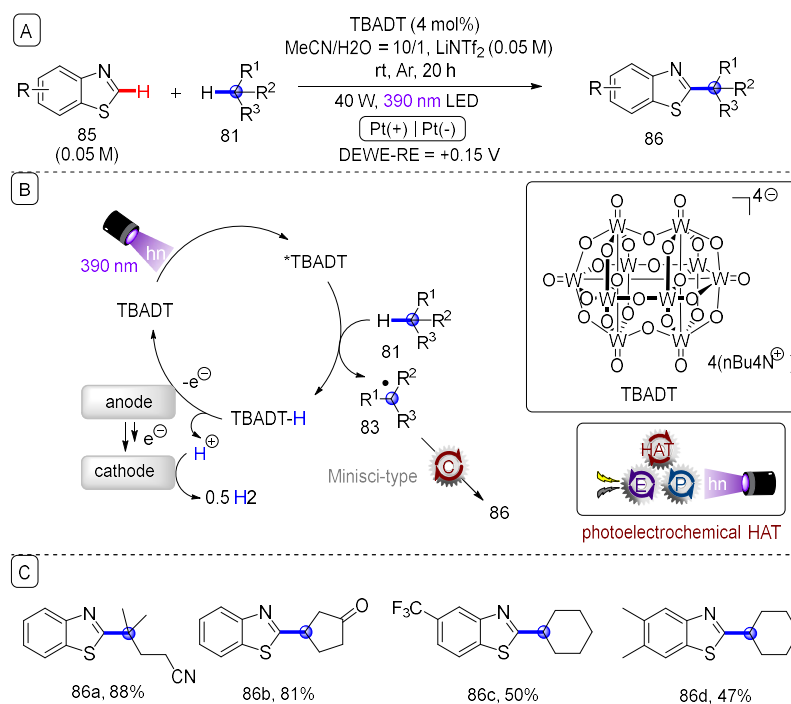


Figure 33. A) Photoelectrochemical HAT involving electro-recycling of TBADT ($(n\text{Bu}_4\text{N})_4[\text{W}_{10}\text{O}_{32}]$); B) Proposed mechanism. C) Selected examples.

Lei and co-workers group reported a photoelectrochemical oxidative azidation of $\text{C}(\text{sp}^3)\text{-H}$ bonds in an undivided cell, in which electrochemistry plays multiple roles (Figure 34A).^[70d] Upon photoexcitation of an aromatic ketone catalyst (Cat.) and intersystem crossing, the long-lived triplet excited state, the excited triplet state abstracts a $\text{C}(\text{sp}^3)\text{-H}$ atom from either activated benzylic positions (when Cat. = 9-fluorenone or bis(4-methoxyphenylmethanone) or unactivated hydrocarbons (when Cat. = DDQ), affording an $\text{C}(\text{sp}^3)$ radical **83** which reacts with a Mn(III)-azide complex species to form the azidated product **88**. This Mn(III)-azide complex is electrogenerated *in situ* from its precursor Mn(II)-azide complex. The authors proposed that, upon photoexcited-HAT, reoxidation back to the carbonyl is simultaneously mediated by anodic oxidation (Figure 34B), while liberated protons are reduced to hydrogen at the cathode. Benzylic and unactivated hydrocarbons were azidated to afford a broad scope of products such as **88a-e** in modest to excellent (31-99%) yields (Figure 34C). Reactivities and selectivities were generally higher for 3° benzylic $\text{C}(\text{sp}^3)\text{-H}$ azidation compared to 2° benzylic aziridinations. The azidation of a cumene derivative was successfully achieved on gram scale after extended reaction time (71% yield after 72 h). Late-stage azidation of bioactive molecules such as a different precursor and ibuprofen methyl ester (affording **88d,e**) when DDQ was used as a catalyst.

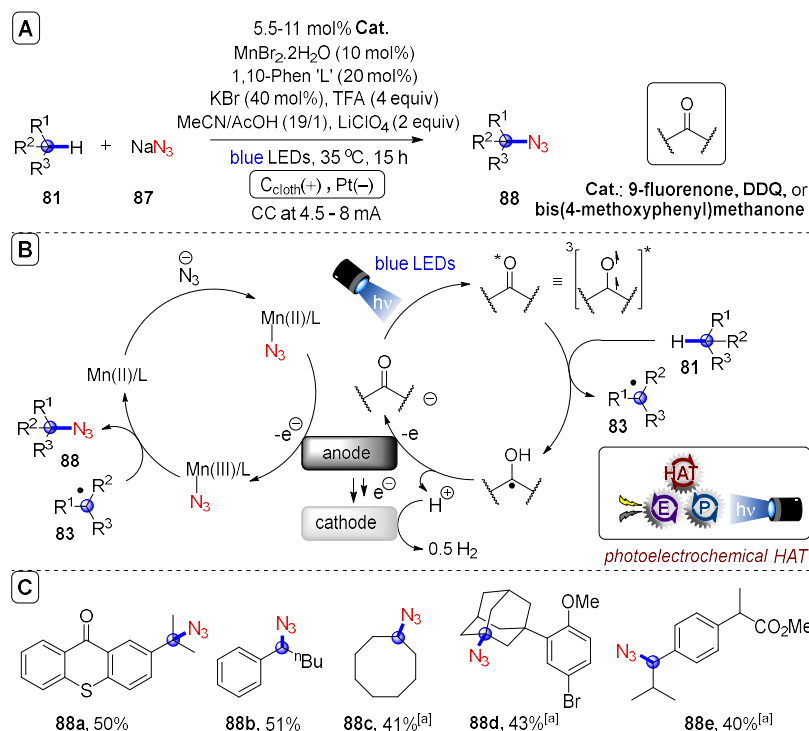


Figure 34. A) Photoelectrochemical HAT azidation of C(sp³)-H bonds; B) Proposed mechanism; C) Selected examples. ^[a]Cat. = DDQ.

In their mechanistic studies, the authors found by cyclic voltammetry that the oxidation of NaN₃ occurred at a lower potential than substrates and photocatalysts. This led them to suggest the azide radical was preferentially formed under the anodic conditions of the reaction. TEMPO was found to inhibit the reaction and by EPR the authors were able to detect the azide radical. In their optimization, authors found that the reaction did proceed appreciably in the dark without catalyst (45% yield), although the rate of reaction was markedly accelerated by irradiation (61%). To rationalize progress of the reaction in the dark, they suggested that the azide radical can also engage in HAT.

1.6 Reactor Platforms

Of key importance to the discovery of new PEC reactions and their uptake in industry is the requirement for robust reactor platforms that deliver reproducible chemistry. To this end, a 3D-printed photoreactor accommodating two interchangeable high-power commercial LED lamps and up to 6x vials was reported by Schiel and co-workers at Boehringer Ingelheim (Figure 35A).^[75] The reactor gave excellent reproducibility, both vial-to-vial and of literature PRC reaction yields. By exchanging the vial holder module, the reactor accommodated an undivided cell photoelectrochemical reactor vial driven externally by a benchtop commercial potentiostat.^[76] The recycling e-PRC heteroarene carbamoylation^[57b] was successfully reproduced, affording **38e** in 83% yield (Figure 35B). Since 3D printing has previously converted a commercial benchtop potentiostat into a compact flow electrochemical reactor;^[77] it is likely bespoke or commercial 3D printed photoelectrochemical batch and flow systems will soon be available to practitioners, both in divided and undivided modes.

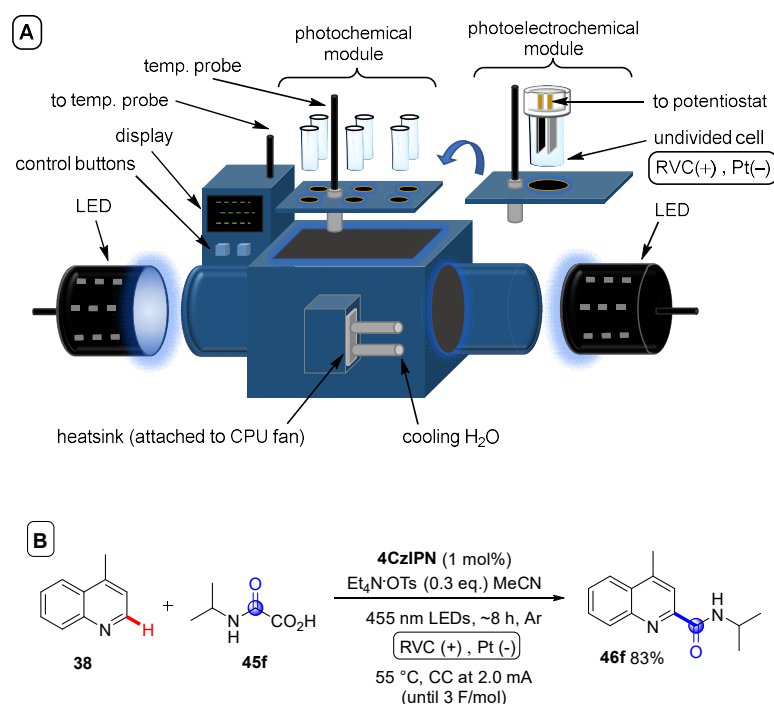


Figure 35. A) A 3D-printed reactor for photochemical and photoelectrochemical reactions; B) Application to recycling e-PRC carbamoylation of heteroarenes.

A key challenge in molecular photoelectrochemical reaction discovery is the number of variables that arise when combining SOE with PRC. Light wavelength, light intensity, current, potential, electrode materials, divided vs. undivided cell, temperature, catalyst choice and loading, electrolyte choice and loading all influence the reaction outcome. The critical influence of light intensity and reaction temperature in PRC has been recently highlighted.^[78] High throughput screening is a powerful tool for reaction discovery, allowing multiple variables to be

simultaneously explored.^[79] Lin, Lehnerr, Kalyani and co-workers developed a compact, high-throughput microscale electrochemical reactor that was successfully applied to screen up to 24 conditions at once in a radical ion e-PRC reaction under constant potential (Figure 36), including control reactions.^[80] The reactor increased the reaction rate 3-fold rate, likely due to increased transmission of light on the microscale and LED optical power. Vial-to-vial reproducibility was high (identical reactions with an average 75% yield gave a 5% standard deviation) confirming the robustness of the system for discovery.

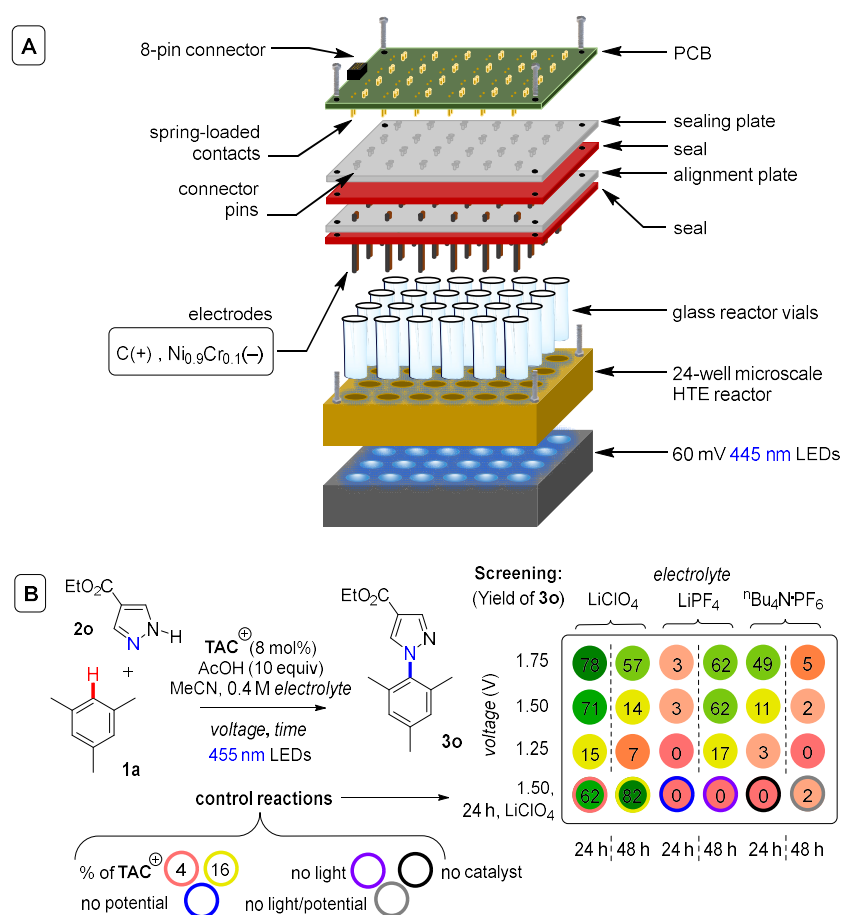


Figure 36. A) A compact, high throughput screening platform for photoelectrochemistry; B) Results of screening a radical ion e-PRC reaction.

1.7 Summary and Outlook

Synthetic photoelectrochemistry (PEC) involving *in situ* generated homogeneous photocatalysts is a rapidly-growing research frontier in single electron transfer chemistry and organic synthesis. Radical ion electrochemically-mediated photoredox catalysis (e-PRC) pushes the boundaries of the redox window further than ever before, achieving unprecedented oxidations and reductions in a controlled, selective manner that can be leveraged to construct, or cleave, strong bonds. While controversy continues to surround the operating mechanisms of reactions proposed to involve radical ion photocatalysts, substrate-catalyst preassembly provides a convincing interpretation of reactivity patterns and offers exciting new opportunities for selectivity control that challenge conventional parameters like the thermodynamic redox potential. Recycling electrochemically-mediated photoredox catalysis forges ahead of conventional photoredox catalysis in improving sustainability, scalability, safety and cost-efficiency of reaction conditions, with sacrificial chemical redox additives being substituted for cheap, benign electricity. Both sub-categories of e-PRC leverage the general selectivity benefits of substrate engagement with a photoexcited state in bulk solution, mitigating against over-reduction or over-oxidation processes and harnessing reactive intermediates that may normally undergo further redox chemistry at electrode surfaces or lead to grafting/passivation. The combination of PEC and HAT opens new opportunities for synthesis, including new photoexcited HAT agents or electro-recycling established ones, as well as providing new access to ground-state HAT agents from inexpensive, abundant precursors. Finally, in addition to promising initial efforts in the scale-up of these chemistries in recirculated or continuous flow, new reactor platforms designed for high reproducibility, control of reaction variables and high-throughput experimentation pave the way to photoelectrochemistry becoming a tool accessible to both academic and industrial chemists alike.

1.8 References

- [1] Selected reviews: (a) K. D. Moeller, *Tetrahedron* **2000**, *56*, 9527-9554; (b) J.-i. Yoshida, K. Kataoka, R. Horcajada, A. Nagaki, *Chem. Rev.* **2008**, *7*, 2265-2299; (c) B. A. Frontana-Urbe, R. D. Little, J. G. Ibanez, A. Palma, R. Vasquez-Medrano, *Green Chem.* **2010**, *12*, 2099-2119; (d) M. Yan, Y. Kawamata, P. S. Baran, *Chem. Rev.* **2017**, *117*, 13230-13319; (e) A. Weibe, T. Geishoff, S. Mohle, E. Rodrigo, M. Zirbes, Waldvogel, S., *Angew. Chem. Int. Ed.* **2018**, *57*, 5594-5619; *Angew. Chem.* **2018**, *130*, 5694-5721.
- [2] Selected reviews: (a) K. Zeitler, *Angew. Chem. Int. Ed.* **2009**, *48*, 9785-9789; (b) J. M. R. Narayanam, C. R. J. Stepenson, *Chem. Soc. Rev.* **2011**, *40*, 102-113; (c) C. Prier, D. Rankic, D. W. C. MacMillan, *Chem. Rev.* **2013**, *113*, 5322-5363; (d) S. Fukuzumi, K. Ohkubo, *Chem. Sci.* **2013**, *4*, 561-574; (e) N. A. Romero, D. A. Nicewicz, *Chem. Rev.* **2016**, *116*, 10075-10166; (f) K. L. Skubi, T. R. Blum, T. P. Yoon, *Chem. Rev.* **2016**, *116*, 10035-10074; (g) J. K. Matsui, S. B. Lang, D. R. Heitz, G. A. Molander, *ACS Catal.* **2017**, *7*, 2563-2575.
- [3] F. Glaser, C. Kerzig, O. S. Wenger, *Angew. Chem. Int. Ed.* **2020**, *59*, 10266-10284; *Angew. Chem.* **2020**, *132*, 10350-10370.
- [4] Selected examples: (a) I. Ghosh, T. Ghosh, J. I. Bardagi, B. König, *Science* **2014**, *346*, 725-728; (b) I. A. MacKenzie, L. Wang, N. P. R. Onuska, O. F. Williams, K. Begam, B. D. Duneitz, A. M. Moran, D. A. Nicewicz, *Nature* **2020**, *580*, 76-80; (c) M. Neumeier, D. Sampedro, M. Májek, V. A. De la Peña O'Shea, A. J. von Wangelin, R. Pérez-Ruiz, *Chem.-Eur. J.* **2015**, *21*, 15496-15501; (d) D. Rombach, H.-A. Wagenknecht, *Angew. Chem. Int. Ed.* **2019**, *59*, 300-303; *Angew. Chem.* **2020**, *132*, 306-310; (e) C. Kerzig, O. S. Wenger, *Chem. Sci.* **2019**, *10*, 11023-11029; (f) B. D. Ravetz, A. B. Pun, E. M. Churchill, D. N. Congreve, T. Rovis, L. M. Campos, *Nature* **2019**, *565*, 343-346; (g) J. P. Cole, D.-F. Chen, M. Kudisch, R. M. Pearson, C.-H. Lim, G. M. Miyake, *J. Am. Chem. Soc.* **2020**, *142*, 13573-13581; (h) K. Targos, O. P. Williams, Z. K. Wickens, *J. Am. Chem. Soc.* **2021**, *143*, 4125-4132; for a review, see: (i) J. Castellanos-Soriano, J. C. Herrera-Luna, D. D. Díaz, M. Consuelo Jiménez, R. Pérez-Ruiz, *Org. Chem. Front.* **2020**, *7*, 1709-1716; for partial coverage of consecutive photoinduced electron transfer (conPET) amongst other topics, see reviews: (j) M. Cybularczyk-Cecotka, J. Szczepanik, M. Giedyk, *Nat. Catal.* **2020**, *3*, 872-886; (k) S. Reischauer, B. Pieber, *iScience* **2021**, *24*, 102209.
- [5] Y. Mo, Z. Lu, G. Rughoobur, P. Patil, N. Gershenfeld, A. I. Akinwande, S. L. Buchwald, K. F. Jensen, *Science* **2020**, *368*, 1352-1357.
- [6] For examples of selectivity alterations observed during alternating potential electrolysis, see: (a) Y. Takahira, M. Chen, Y. Kawamata, P. Mykhailiuk, H. Nakamura, B. K. Peters, S. H. Reisberg, C. Li, L. Chen, T. Hoshikawa, S. Tomoyuki, P. S. Baran, *Synlett* **2019**, *30*, 1178-1182; (b) A. G. Wills, D. L. Poole, C. M. Alder, M. Reid, *ChemElectroChem* **2020**, *7*, 2771-2776; (c) Y. Kawamata, K. Hayashi, E. Carlson, S. Shaji, D. Waldmann, B. J. Simmons, J. Edwards, C. W. Zapf, M. Saito, P. S. Baran, *ChemRxiv* **2021**, DOI: 10.26434/chemrxiv.14394602.v1.
- [7] (a) G. Laudadio, N. J. W. Straathof, M. D. Lanting, B. Knoops, V. Hessel, T. Noël, *Green Chem.* **2017**, *19*, 4061-4066; (b) M. Oseka, G. Laodadio, N. P. van Leest, M. Dyga, A. de A. Bartolomeu, L. J. Gooßen, B. de Bruin, K. T. de Oliveira, T. Noël, *Chem* **2021**, *7*, 255-266.
- [8] Electrode materials with chiral additives can induce enantioselectivity, see: (a) M. Ghosh, V. S. Shinde, M. Rueping, *Beilstein J. Org. Chem.* **2019**, *15*, 2710-2746; (b) Q. Lin, L. Li, S. Luo, *Chem.-Eur. J.* **2019**, *25*, 10033-10044.
- [9] J. P. Barham, B. König, *Angew. Chem. Int. Ed.* **2020**, *59*, 11732-11747; *Angew. Chem.* **2020**, *1323*, 11828-11844.
- [10] For highlights of synthetic PEC, see: (a) L. Capaldo, L. L. Quadri, D. Ravelli, *Angew. Chem. Int. Ed.* **2019**, *58*, 17508-17510; *Angew. Chem.* **2019**, *131*, 17670-17672; (b) Y. Yu, P. Guo, J.-S. Zhong, Y. Yuan, K.-Y. Ye, *Org. Chem. Front.* **2020**, *7*, 131-135; (c) T. Hardwick, N. Ahmed, *ACS Sus. Chem. Eng.* **2021**, *9*, 4324-4340; during the preparation of this manuscript, a review partially covering recent synthetic examples appeared: (d) L. F. T. Novaes, J. Liu, Y. Shen, L. Lu, J. M. Meinhardt, S. Lin, *Chem. Soc. Rev.* **2021**, *50*, 7941-8002.
- [11] For partial coverage of synthetic PEC amongst other topics, see reviews: (a) R. H. Verschuere, W. M. De Borggraeve, *Molecules* **2019**, *24*, 2122; (b) J. Liu, L. Lu, D. Wood, S. Lin, *ACS Cent. Sci.* **2020**, *6*, 1317-1340; (c) N. Chen, H.-C. Xu, *Chem. Rec.* **2021**, DOI: 10.1002/tcr.202100048.
- [12] Selected recent examples in PRC: (a) K. Yamada, M. Okada, T. Fukuyama, D. Ravelli, M. Fagnoni, I. Ryu, *Org. Lett.* **2015**, *17*, 1292-1295; (b) M. H. Shaw, V. W. Shurffleff, J. A. Terrett, J. D. Cuthbertson, D. W. C. MacMillan, *Science* **2016**, *352*, 1304-1308; (c) I. B. Perry, T. F. Brewer, P. J. Sarver, D. M. Schultz, D. A. DiRocco, D. W. C. MacMillan, *Nature* **2018**, *560*, 70-75; (d) T. Ide, J. P. Barham, M. Fujita, Y. Kawato, H. Egami, Y. Hamashima; *Chem. Sci.* **2018**, *9*, 8453-8460; (e) J. Ye, I. Kalvet, F. Schoenebeck, T. Rovis, *Nat. Chem.* **2018**, *10*, 1037-1041; (f) S. Das, K. Murugesan, G. J. V. Rodríguez, J. Kaur, J. P. Barham, A. Savateev, M. Antonietti, B. König, *ACS Catal.* **2021**, *11*, 1593-1603. For a review, see: (g) L. Capaldo, D. Ravelli, *Eur. J. Org. Chem.* **2017**, 2056-2071.
- [13] Selected recent examples in SOE: (a) Y. Kawamata, M. Yan, Z. Liu, D. H. Bao, J. Chen, J. T. Starr, P. S. Baran, *J. Am. Chem. Soc.* **2017**, *139*, 7448-7451; (b) Y. Takahira, M. Chen, Y. Kawamata, P. Mykhailiuk, H. Nakamura, B. K. Peters, S. H. Reisberg, C. Li, L. Chen, T. Hoshikawa, T. Shibuguchi, P. S. Baran, *Synlett* **2019**, *30*, 1178-1182; (c) Y. Kurimoto, J. Yamashita, K. Mitsudo, E. Sato, S. Suga, *Org. Lett.* **2021**, *23*, 3120-3124.
- [14] Interfacial photoelectrochemistry concerns the use of photoelectrodes as heterogeneous catalysts rather than homogeneous catalysts. Examples of photoelectrodes in the context of organic synthesis are beyond the scope of this review and are comprehensively reviewed elsewhere, see: (a) Ref. 9; (b) T. Hardwick, A. Qurashi, B.

- Shirinfar, N. Ahmed, *ChemSusChem* **2020**, *13*, 1967-1973; (c) Y.-C. Wu, R.-J. Song, J.-H. Li, *Org. Chem. Front.* **2020**, *7*, 1895-1902.
- [15] (a) J.-C. Moutet, G. Reverdy, *Tetrahedron Lett.* **1979**, *20*, 2389-2393; (b) J.-C. Moutet, G. Reverdy, *J. Chem. Soc., Chem. Commun.* **1982**, 654-655.
- [16] H. Lund, H. S. Carlsson, *Acta Chem. Scand., Ser. B* **1978**, *32*, 505-509.
- [17] S. S. Shukla, J. F. Rusling, *J. Phys. Chem.* **1985**, *89*, 3353-3358.
- [18] (a) H. Huang, Z. M. Strater, M. Rauch, J. Shee, T. J. Sisto, C. Nickolls, T. H. Lambert, *Angew. Chem. Int. Ed.* **2019**, *58*, 13318-13322; *Angew. Chem.* **2019**, *131*, 13452-13456; (b) H. Kim, H. Kim, T. H. Lambert, S. Lin, *J. Am. Chem. Soc.* **2020**, *142*, 2087-2092; (c) N. G. W. Cowper, C. P. Chernowsky, O. P. Williams, Z. K. Wickens, *J. Am. Chem. Soc.* **2020**, *142*, 2093-2099.
- [19] (a) S. Jin, H. T. Dang, G. C. Haug, R. He, V. D. Nguyen, V. T. Nguyen, H. D. Arman, K. S. Schanze, O. V. Larianov, *J. Am. Chem. Soc.* **2020**, *142*, 1603-1613; (b) S. V. Rosokha, J. K. Kochi, *J. Am. Chem. Soc.* **2007**, *129*, 3683-3697; (c) E. H. Discekici, N. J. Treat, S. O. Poelma, K. M. Mattson, Z. M. Hudson, Y. Luo, C. J. Hawker, J. R. de Alaniz, *Chem. Commun.* **2015**, *51*, 11705-11708; (d) J. A. Christensen, B. T. Phelan, S. Chaudhuri, A. Acharya, V. S. Batista, M. R. Wasielewski, *J. Am. Chem. Soc.* **2018**, *140*, 5290-5299; (e) Y.-C. Chung, Y. O. Su, *J. Chin. Chem. Soc.* **2009**, *56*, 493-503; (f) X. Z. Yan, J. Pawlas, T. Goodson, J. F. Hartwig, *J. Am. Chem. Soc.* **2005**, *127*, 9105-9116; (g) A. C. Benniston, A. Harriman, D. J. Lawrie, S. A. Rostron, *Eur. J. Org. Chem.* **2004**, 2272-2276; (h) I. Ghosh, R. S. Shaikh, B. König, *Angew. Chem. Int. Ed.* **2017**, *56*, 8544-8549; *Angew. Chem.* **2017**, *129*, 8664-8669; (i) K. Kikuchi, T. Niwa, Y. Takahashi, H. Ikeda, T. Miyashi, *J. Phys. Chem.* **1993**, *97*, 5070-5073; (j) W. E. Ford, P. V. Kamat, *J. Phys. Chem.* **1987**, *91*, 6373-6380; (k) D. Gosztola, M. P. Niemczyk, W. Svec, A. S. Lukas, M. R. Wasielewski, *J. Phys. Chem. A* **2000**, *104*, 6545-6551; (l) S. Chopin, F. Chaignon, E. Blart, F. Odobel, *J. Mater. Chem.* **2007**, *17*, 4139-4146; (m) the NDI catalyst was not NDI-a/b, but was *N*-alkyl substituted and likely has similar properties: S. Caby, L. M. Bouchet, J. E. Argüello, R. A. Rossi, J. Bargadi, *ChemCatChem* **2021**, DOI: 10.1002/cctc.202100359; (n) S. Blanc, T. Pigot, C. Cugnet, R. Brown, S. Lacombe, *Phys. Chem. Chem. Phys.* **2010**, *12*, 11280-11290. (o) A. P. Darmanyan, *Chem. Phys. Lett.* **1984**, *110*, 89-94; (p) D. T. Breslin, M. A. Fox, *J. Am. Chem. Soc.* **1993**, *115*, 11716-11721; (q) X. Tian, T. A. Karl, S. Reiter, S. Yakubov, R. de Vivie-Riedle, B. König, J. P. Barham, *Angew. Chem. Int. Ed.* **2021**, ASAP, DOI: 10.1002/anie.202105895; (r) A. J. Rieth, M. I. Gonzalez, B. Kudisch, M. Nava, D. G. Nocera, *ChemRxiv* **2021**, DOI: 10.33774/chemrxiv-2021-pbxjq; (s) A. F. Chmiel, O. P. Williams, C. P. Chernowsky, C. S. Yeung, Z. K. Wickens, *J. Am. Chem. Soc.* **2021**, ASAP, DOI: 10.1021/jacs.1c05988; (t) C. Chernowsky, A. Chmiel, Z. Wickens, *ChemRxiv* **2021**, DOI: 10.26434/chemrxiv.14710398.v1.
- [20] S. Wu, J. Žurauskas, M. Domański, P. S. Hitzfeld, V. Butera, D. J. Scott, J. Rehbein, A. Kumar, E. Thyraug, J. Hauer, J. P. Barham, *Org. Chem. Front.* **2021**, *8*, 1132-1142.
- [21] (a) L. Pause, M. Robert, J.-M. Savéant, *J. Am. Chem. Soc.* **1999**, *121*, 7158-7159; (b) H. G. Roth, N. A. Romero, D. A. Nicewicz, *Synlett* **2016**, *27*, 714-723; (c) S. Fukuzumi, K. Ohkubo, T. Suenobu, K. Kato, M. Fujitsuka, O. Ito, *J. Am. Chem. Soc.* **2001**, *123*, 8459-8467.
- [22] The redox potential of PhCl in Ref. 21b is +0.33 V more positive than that in Ref. 18, likely due to systematic differences in measurement conditions. To ensure consistency, +0.33 V is added to values of Ref. 18.
- [23] (a) Z. Ning, N. Tian, *Chem. Commun.* **2009**, 5483-5495; (b) P. Cias, C. Slugovc, G. Gescheidt, *J. Phys. Chem. A* **2011**, *115*, 14519-14525.
- [24] Selected reports on the use of TPAs as mediators in electrolysis: (a) T. Fuchigami, M. Tetsu, T. Tajima, H. Ishii, *Synlett* **2001**, 1269-1271; (b) X. Wu, A. P. Davis, A. J. Fry, *Org. Lett.* **2007**, *9*, 5633-5636; (c) C.-Y. Cai, H.-C. Xu, *Nat. Commun.* **2018**, *9*, 3551.
- [25] Seminal reports on the use of TPA radical cations as ground state SET oxidants in organic synthesis: (a) R. A. Pabon, D. J. Bellville, N. L. Bauld, *J. Am. Chem. Soc.* **1983**, *105*, 5158-5159; (b) D. W. Reynolds, K. T. Lorenz, H. S. Chiou, D. J. Bellville, R. A. Pabon and N. L. Bauld, *J. Am. Chem. Soc.* **1987**, *109*, 4960-4968; (c) U. Jahn, S. Aussicker, *Org. Lett.* **1999**, *1*, 849-852; (d) J. P. Barham, M. P. John, J. A. Murphy, *J. Am. Chem. Soc.* **2016**, *138*, 15482-15487.
- [26] (a) R. I. Walter, *J. Am. Chem. Soc.* **1955**, *77*, 5999-6002; (b) L. Hagopian, G. Kohler, R. I. Walter, *J. Phys. Chem.* **1967**, *71*, 2290-2296.
- [27] (a) D. M. Klassen, G. A. Crosby, *J. Chem. Phys.* **1968**, *48*, 1853-1858; (b) G. A. Crosby, *Acc. Chem. Res.* **1975**, *8*, 231-238.
- [28] Recent examples: (a) L. Chu, C. Ohta, Z. Zuo, MacMillan, D. W. C. *J. Am. Chem. Soc.* **2014**, *136*, 10886-10889; (b) J. D. Griffin, M. A. Zeller, D. A. Nicewicz, *J. Am. Chem. Soc.* **2015**, *137*, 11340-11348; (c) L. Candish, M. Freitag, T. Gensch, F. Glorius, *Chem. Sci.* **2017**, *8*, 3618-3622.
- [29] Recent examples: (a) X. Ma, D. F. Dewez, L. Du, X. Luo, I. E. Markó, K. Lam, *J. Org. Chem.* **2018**, *83*, 12044-12055; (b) R. A. Green, R. C. D. Brown, D. Pletcher, *J. Flow Chem.* **2016**, *6*, 191-197; for a review of the Kolbe electrolysis: (c) H. J. Schäfer, *Top. Curr. Chem.* **1990**, *152*, 91-151.
- [30] Changes in EPR represent overall spin density changes in a *distribution* of precomplexes, whose rotational barriers are likely accessible at rt.
- [31] Since luminescence does not occur, one can only estimate the upper or lower 'boundary' of redox energy by interpretation of UV-Vis spectral bands or computed vertical transition energies. The 'upper bound' redox potential is reasonable to propose, considering that the nature of the SET event must be fast enough to outcompete internal conversion.
- [32] For typical agreements between TD-DFT and experimental UV-Vis transitions of related radical cations, see Ref. 19d and: Z. Zara, J. Iqbal, K. Ayub, M. Irfan, A. Mahmood, R. A. Khera, B. Eliasson, *J. Mol. Struct.* **2017**, *1149*, 282-298.

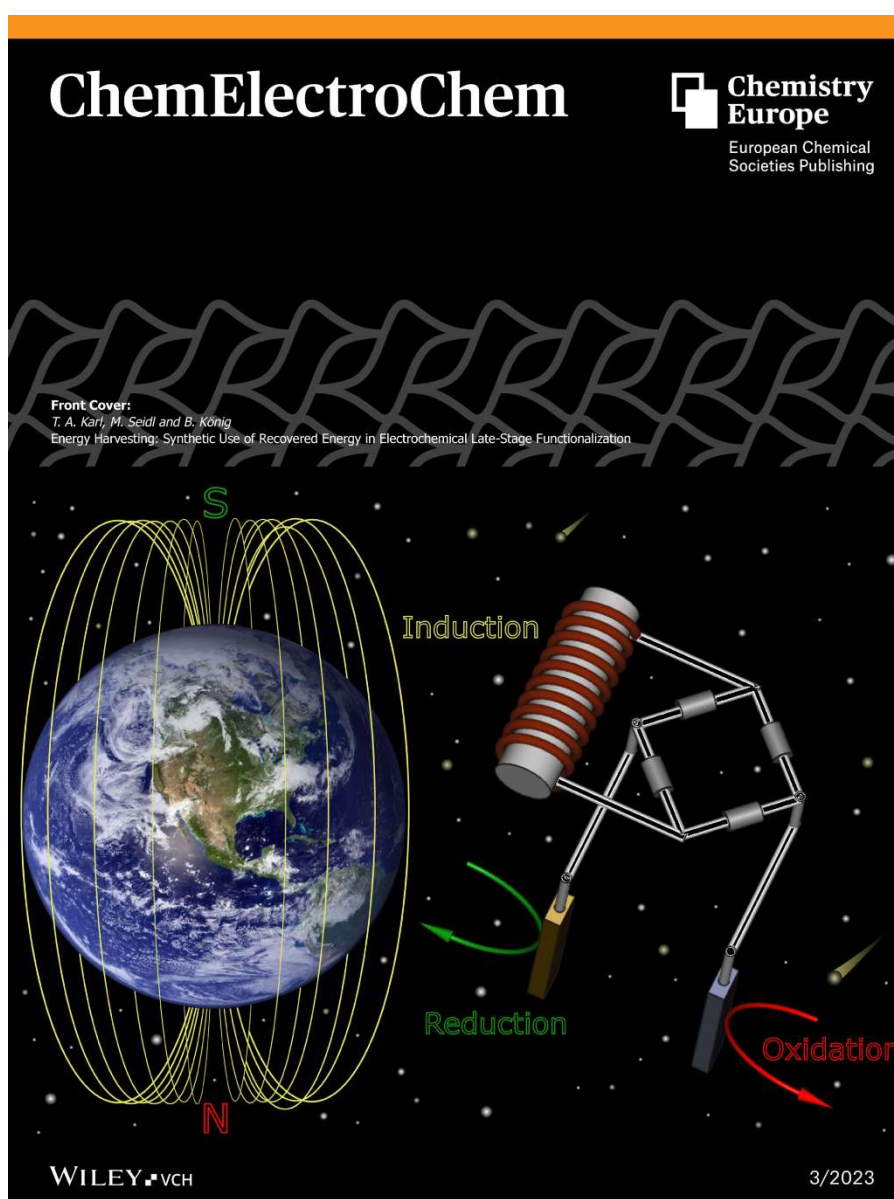
- [33] The long-range-corrected functional ω B97X-D includes dispersion corrections and provides comparable results to more expensive calculations for non-covalent interactions, see: (a) T. Gao, T. Li, W. Li, L. Li, C. Fang, H. Li, L. Hu, Y. Lu, Z.-M. Su, *J. Cheminf.* **2016**, *8*, 24; (b) K. Wang, J. Lv, J. Miao, *Theor. Chem. Acc.* **2015**, *134*, 5. This was used to compare a limited number of precomplex candidates in Ref. 20.
- [34] For a discussion on the comparison of quantum and molecular mechanical methods in modeling π -stacking interactions, see: R. Zhao, *Modeling of Nanotoxicity*, Springer, 2015, pp 169-188.
- [35] For example, modeling multiple substrate binding and explicit solvation.
- [36] T. Shen, T. H. Lambert, *Science* **2021**, *371*, 620-626.
- [37] H. J. P. de Lijser, D. Arnold, *J. Org. Chem.* **1997**, *62*, 8432-8438.
- [38] P. Natarajan, B. König, *Eur. J. Org. Chem.* **2021**, 2145-2161.
- [39] S. Das, P. Natarajan, B. König, *Chem.-Eur. J.* **2017**, *23*, 18161-18165.
- [40] (a) H. Huang, T. H. Lambert, *Angew. Chem. Int. Ed.* **2021**, *60*, 11163-11167; *Angew. Chem.* **2021**, *133*, 11263-11267; (b) Z.-W. Hou, H. Yan, J. Song, H.-C. Xu, *ChemRxiv* **2021**, DOI: 10.26434/chemrxiv.13718392.v1
- [41] D. Walker, J. D. Hiebert, *Chem. Rev.* **1967**, *67*, 153-195.
- [42] J.-i. Yoshida, A. Shimizu, R. Hayashi, *Chem. Rev.* **2018**, *118*, 4702-4730.
- [43] (a) X. Wu, A. P. David, A. J. Fry, *Org. Lett.* **2007**, *9*, 5633-5636; (b) C.-Y. Cai, H.-C. Xu, *Nat. Commun.* **2018**, *9*:3551; (c) E. A. Mayeda, L. L. Miller, J. F. Wolf, *J. Am. Chem. Soc.* **1972**, *94*, 6812-6816.
- [44] (a) Y. Ashikari, T. Nokami, J.-i. Yoshida, *Org. Lett.* **2012**, *14*, 938-941; (b) D. S. Chung, S. H. Park, S.-g. Lee, *H. Kim, Chem. Sci.* **2021**, *12*, 5892-5897.
- [45] F. D. Mango, W. A. Bonner, *J. Org. Chem.* **1964**, *29*, 1367-1371.
- [46] C. Constentin, M. Robert, J.-M. Savéant, *J. Am. Chem. Soc.* **2004**, *126*, 16051-16057.
- [47] (a) E. Shirakawa, K.-I. Ito, T. Higashino, T. Hayashi, *J. Am. Chem. Soc.* **2010**, *132*, 15537-15539; (b) C.-L. Sun, H. Li, D.-G. Yu, M. Yu, X. Zhao, X.-Y. Lu, K. Huang, S.-F. Zheng, B.-J. Li, Z.-J. Shi, *Nat. Chem.* **2010**, *2*, 1044-1049; (c) J. P. Barham, G. Coulthard, R. G. Kane, N. Delgado, M. P. John, J. A. Murphy, *Angew. Chem. Int. Ed.* **2016**, *55*, 4492-4496; *Angew. Chem.* **2016**, *128*, 4568-4572; (d) J. P. Barham, G. Coulthard, K. J. Emery, E. Doni, F. Cumine, G. Nocera, M. P. John, L. E. A. Berlouis, T. McGuire, T. Tuttle, J. A. Murphy, *J. Am. Chem. Soc.* **2016**, *138*, 7402-7410.
- [48] (a) K. Donabauer, M. Maity, A. L. Berger, G. S. Huff, S. Crespi, B. König, *Chem. Sci.* **2019**, *10*, 5162-5166; (b) Q.-Y. Meng, T. E. Schirmer, A. L. Berger, K. Donabauer, B. König, *J. Am. Chem. Soc.* **2019**, *141*, 11393-11397.
- [49] K. Lam, I. E. Markó, *Org. Lett.* **2011**, *13*, 406-409.
- [50] S. Jin, H. T. Dang, G. C. Haug, R. He, V. D. Nguyen, V. T. Nguyen, H. D. Arman, K. S. Schanze, O. V. Larianov, *J. Am. Chem. Soc.* **2020**, *142*, 1603-1613.
- [51] (a) S. Yakubov, J. P. Barham, *Beilstein J. Org. Chem.* **2020**, *16*, 2151-2192; (b) J. J. Molloy, T. Morack, R. Gilmour, *Angew. Chem. Int. Ed.* **2019**, *58*, 13654-13664; *Angew. Chem.* **2019**, *131*, 13789-13800; (c) D. C. Fabry, M. A. Ronge, M. Rueping, *Chem.-Eur. J.* **2014**, *21*, 5350-5354.
- [52] S. Wang, H. Wang, B. König, *Chem* **2021**, *7*, 1653-1665.
- [53] D. Lu, S. P. Nikas, X.-W. Han, D. A. Parrish, A. Makriyannis, *Tetrahedron Lett.* **2012**, *53*, 4636-4638.
- [54] Non-covalent interactions are gaining interest as a selectivity control parameter in catalysis. For comprehensive reviews, see: (a) J. P. Wagner, P. R. Schreiner, *Angew. Chem. Int. Ed.* **2015**, *54*, 12274-12296; *Angew. Chem.* **2015**, *127*, 12446-12471; (b) A. J. Neel, M. J. Hilton, M. S. Sigman, F. D. Toste, *Nature* **2017**, *543*, 637-646.
- [55] T.-Y. Shang, L.-H. Lu, Z. Cao, Y. Liu, W.-M. He, B. Yu, *Chem. Commun.* **2019**, *55*, 5408-5419.
- [56] H. Yan, Z.-W. Hour, H.-C. Xu, *Angew. Chem. Int. Ed.* **2019**, *131*, 4640-4643; *Angew. Chem.* **2019**, *131*, 4640-4643.
- [57] (a) Y. Qiu, A. Scheremetjew, L. H. Finger, L. Ackermann, *Chem.-Eur. J.* **2020**, *26*, 3241-3246; (b) X.-L. Lai, X.-M. Shu, J. Song, H.-C. Xu, *Angew. Chem. Int. Ed.* **2020**, *59*, 10626-10632; *Angew. Chem.* **2020**, *132*, 10713-10719; (c) F. Xu, X.-L. Lai, H.-C. Xu, *Synlett* **2020**, *31*, 369-372; (d) H. Yan, J. Song, S. Zhu, H.-C. Xu, *CCS Chem.* **2021**, *3*, 317-325; (e) H. Yan, S. Zhu, H.-C. Xu, *Org. Process Res. Dev.* **2021**, DOI: 10.1021/acs.oprd.1c00038.
- [58] (a) G. A. Price, D. Mallik, M. G. Organ, *J. Flow. Chem.* **2017**, *7*, 82-86; (b) P. Sagmeister, R. Lebl, I. Castollo, J. Rehr, J. Krusz, M. Sipek, M. Horn, S. Sacher, D. Cantillo, J. D. Williams, C. O. Kappe, *Angew. Chem. Int. Ed.* **2021**, *60*, 8139-8148; *Angew. Chem.* **2021**, *133*, 8220-8229.
- [59] (a) A. Hu, J.-J. Guo, H. Pan, Z. Zuo, *Science* **2018**, *361*, 668-672; (b) A. Hu, Y. Chen, J.-J. Guo, N. Yu, Q. An, Z. Zuo, *J. Am. Chem. Soc.* **2018**, *140*, 13580-13585; (c) J. Schwarz, B. König, *Chem. Commun.* **2019**, *55*, 486-488; (d) V. R. Yatham, P. Bellotti, B. König, *Chem. Commun.* **2019**, *55*, 3489-3482.
- [60] H. Nagumo, Y. Sasaki, Y. Ono, H. Okamoto, M. Seto, Y. Takuwa, *Am. J. Physiol. Cell Physiol.* **2000**, *278*, C57-65.
- [61] G. G. Kay, A. G. Harris, *Clin. Exp. Allergy* **2009**, *29*, 147-150.
- [62] H. Huang, T. H. Lambert, *Angew. Chem. Int. Ed.* **2019**, *59*, 658-662; *Angew. Chem.* **2020**, *132*, 668-672.
- [63] K. Ohkubo, K. Hirose, S. Fukuzumi, *Chem.-Eur. J.* **2015**, *21*, 2855-2861.
- [64] (a) D. Audisio, F. Taran, *tert-Butyl Nitrite*, *Encyclopedia of Reagents for Organic Synthesis*, Wiley, 2016; (b) S. Caron, R. W. Dugger, S. G. Ruggeri, J. A. Ragan, D. H. B. Ripin *Chem. Rev.* **2006**, *106*, 2943-2989; (c) C. A. Hone, D. M. Roberge, C. O. Kappe, *ChemSusChem* **2016**, *10*, 32-41.
- [65] R. S. Sherbo, R. S. Delima, V. A. Chikowski, B. P. MacLeod, C. P. Berlinguette, *Nat. Catal.* **2018**, *1*, 501-507.
- [66] (a) T. Wu, B. H. Nguyen, M. C. Daugherty, K. D. Moeller, *Angew. Chem. Int. Ed.* **2019**, *58*, 3562-3565; *Angew. Chem.* **2019**, *131*, 3600-3603; (b) T. Wu, K. D. Moeller, *Angew. Chem. Int. Ed.* **2021**, *60*, 12883-12890; *Angew. Chem.* **2021**, *133*, 12993-13000.
- [67] J. C. Vantourout, *Org. Process. Res. Dev.* **2021**, DOI: 10.1021/acs.oprd.1c00046.

- [68] Selected recent PRC examples: (a) K. Yamada, M. Okada, T. Fukuyama, D. Ravelli, M. Fagnoni, I. Ryu, *Org. Lett.* **2015**, *17*, 1292-1295; (b) M. H. Shaw, V. W. Shurffleff, J. A. Terrett, J. D. Cuthbertson, D. W. C. MacMillan, *Science* **2016**, *352*, 1304-1308; (c) I. B. Perry, T. F. Brewer, P. J. Sarver, D. M. Schultz, D. A. DiRocco, D. W. C. MacMillan, *Nature* **2018**, *560*, 70-75; (d) T. Ide, J. P. Barham, M. Fujita, Y. Kawato, H. Egami, Y. Hamashima; *Chem. Sci.* **2018**, *9*, 8453-8460; (e) J. Ye, I. Kalvet, F. Schoenebeck, T. Rovis, *Nat. Chem.* **2018**, *10*, 1037-1041; (f) G. Laudadio, Y. Deng, K. van der Wal, D. Ravelli, M. Nuño, M. Fagnoni, D. Guthrie, Y. Sun, T. Noël *Science* **2020**, *369*, 92-96; (g) S. Das, K. Murugesan, G. J. V. Rodríguez, J. Kaur, J. P. Barham, A. Savateev, M. Antonietti, B. König, *ACS Catal.* **2021**, *11*, 1593-1603. For a review: (h) L. Capaldo, D. Ravelli, *Eur. J. Org. Chem.* **2017**, 2056-2071.
- [69] Selected SOE examples: (a) Y. Kawamata, M. Yan, Z. Liu, D. H. Bao, J. Chen, J. T. Starr, P. S. Baran, *J. Am. Chem. Soc.* **2017**, *139*, 7448-7451; (b) Y. Takahira, M. Chen, Y. Kawamata, P. Mykhailiuk, H. Nakamura, B. K. Peters, S. H. Reisberg, C. Li, L. Chen, T. Hoshikawa, T. Shibuguchi, P. S. Baran, *Synlett* **2019**, *30*, 1178-1182; (c) Y. Kurimoto, J. Yamashita, K. Mitsudo, E. Sato, S. Suga, *Org. Lett.* **2021**, *23*, 3120-3124.
- [70] (a) H. Huang, Z. M. Strater, T. H. Lambert, *J. Am. Chem. Soc.* **2020**, *142*, 1698-1703; (b) P. Xu, P.-Y. Chen, H.-C. Xu, *Angew. Chem. Int. Ed.* **2020**, *59*, 14275-14280; *Angew. Chem.* **2020**, *132*, 14381-14386; (c) L. Capaldo, L. L. Quadri, D. Merli, D. Ravelli, *Chem. Commun.* **2021**, *57*, 4424-4427; (d) L. Niu, C. Jiang, Y. Liang, D. Liu, F. Bu, R. Shi, H. Chen, A. D. Chowdhury, A. Lei, *J. Am. Chem. Soc.* **2020**, *142*, 17693-17702.
- [71] B. J. Shields, A. G. Doyle, *J. Am. Chem. Soc.* **2016**, *138*, 12719-12722.
- [72] (a) D. J. Seery, D. Britton, *J. Phys. Chem.* **1964**, *68*, 2263-2266; (b) R. T. P. Sant'Anna, C. M. P. Santos, G. P. Silva, R. J. R. Ferreira, A. P. Oliveira, C. E. S. Côrtes, R. B. Faria, *J. Braz. Chem. Soc.* **2012**, *23*, 1543-1550.
- [73] D. C. Duncan, T. L. Netzel, C. L. Hill, *Inorg. Chem.* **1995**, *34*, 4640-4646.
- [74] F. Wang, S. Stahl, *Angew. Chem. Int. Ed.* **2019**, *58*, 6385-6390; *Angew. Chem.* **2019**, *131*, 6451-6456.
- [75] F. Schiel, C. Peinsipp, S. Kornigg, D. Böse, *ChemPhotoChem* **2021**, *5*, 431-437.
- [76] (a) [ika.com/en/Products-Lab-Eq/](https://www.ika.com/en/Products-Lab-Eq/) (b) For an application, see: C. Li, Y. Kawamata, H. Nakamura, J. C. Vantourout, Z. Liu, Q. Hou, D. Bao, J. T. Starr, J. Chen, M. Yan, P. S. Baran, *Angew. Chem. Int. Ed.* **2017**, *56*, 13088-13093; *Angew. Chem.* **2017**, *129*, 13268-13273.
- [77] C. G. W. van Melis, M. R. Penny, A. D. Garcia, A. Petti, A. P. Dobbs, S. T. Hilton, K. Lam, *ChemElectroChem* **2019**, *6*, 4144-4148.
- [78] T. D. Svejstrup, A. Chatterjee, D. Schekin, T. Wagner, J. Zach, M. J. Johansson, G. Bergonzini, B. König, *ChemPhotoChem* **2021**, DOI: 10.1002/cptc.202100059.
- [79] Selected accounts: (a) S. W. Krska, D. A. DiRocco, S. D. Dreher, M. Shevlin, *Acc. Chem. Res.* **2017**, *50*, 2976-2985; (b) S. M. Mennen, C. Alhambra, C. L. Allen, M. Barberis, S. Berritt, T. A. Brandt, A. D. Campbell, J. Castañón, A. H. Cherney, M. Christensen, D. B. Damon, J. Eugenio De Diego, S. García-Carrada, P. García-Losada, R. Haro, J. Janey, D. C. Leitch, L. Li, F. Liu, P. C. Lobben, D. W. C. MacMillan, J. Magano, E. McInturff, S. Monfette, R. J. Post, D. Schultz, B. J. Sitter, J. M. Stevens, I. I. Strambeanu, J. Twilton, K. Wang, M. A. Zajac, *Org. Process Res. Dev.* **2019**, *23*, 1213-1242.
- [80] J. Rein, J. R. Annand, M. K. Wismer, J. Fu, J. C. Siu, A. Klapars, N. A. Strotman, D. Kalyani, D. Lehnerr, S. Lin, *ChemRxiv* **2021**, DOI: 10.26434/chemrxiv.14173538.v2

From this review of recent developments in photoelectrocatalysis, it is clear that PEC is a promising approach for high redox potentials. As described above, the most obvious approach SOE has the disadvantage of over-oxidation/reduction and may cause problems in selectivity. Thus, we will not explore electrochemistry as a method for extreme redox potentials. However, PEC requires similar equipment to SOE to perform reactions. Therefore, alternative voltage sources from SOE may also facilitate access to photoelectrocatalysis. The following chapter contains our contribution to this topic.

CHAPTER 2

2 Energy Harvesting: Synthetic Use of Recovered Energy in Electrochemical Late-Stage Functionalization



This chapter has been published. For reference see: T. A. Karl, M. Seidl, B. König *ChemElectroChem* **2023**, *10*, (3) e202201097.

T. A. Karl performed all experiments and wrote the manuscript.

2.1 Abstract

An induction-based energy harvesting (EH) device was presented. It converted part of the rotational energy of magnetic stirrers back into electrical energy, making it accessible for electrochemical transformations. After rectification, the induced AC voltage was optionally provided as a constant voltage or constant current whereby the available voltage could directly be adjusted by the stirring rate of the reaction. The comparability of the results with reactions carried out with commercial power supplies has been demonstrated on six different late-stage functionalizations, including methylation, carboxylation, trifluoromethylation, imidation, hydrolysis, and keto-olefin coupling. Therefore, the described EH device is a low-cost, resource-efficient alternative to a commercial electrochemical set-up and enables laboratories without specialized equipment to perform electrochemical reactions.

2.2 Introduction

Energy Harvesting (EH) refers to a process in which ambient energy is captured, to power devices.^[1] In addition to recovering otherwise wasted energy, it also helps to decentralize the generation of electricity for more energy autonomy. Self-powered electrochemical and photoelectrochemical systems are used for waste stream treatment,^[2,3] sensor systems,^[4,5] corrosion protection^[6] and water splitting.^[7] To our knowledge, applications in the synthesis of organic molecules have not been described so far.^[8]

We report here the application of a self-powered rotary energy harvesting (EH) device (Figure 1) to power an electrolytic cell for the synthesis of complex organic molecules. Based on the concept of induction, which is defined as the occurrence of an electromotive force across an electrical conductor due to a changing magnetic flux, parts of the rotating magnetic field of laboratory stirring plates are converted back into electric energy.^[9] This method is not intended to reduce overall energy consumption, but to enable performance of electrochemical transformation without the need for additional power supplies. It may be therefore a cost-effective and resource-saving alternative for low-budget chemical laboratories. The approach simplifies operations in synthetic laboratories and allows performing electrochemical reactions with limited equipment. Simple design ensures that all components can be modified and repaired as easily as possible.

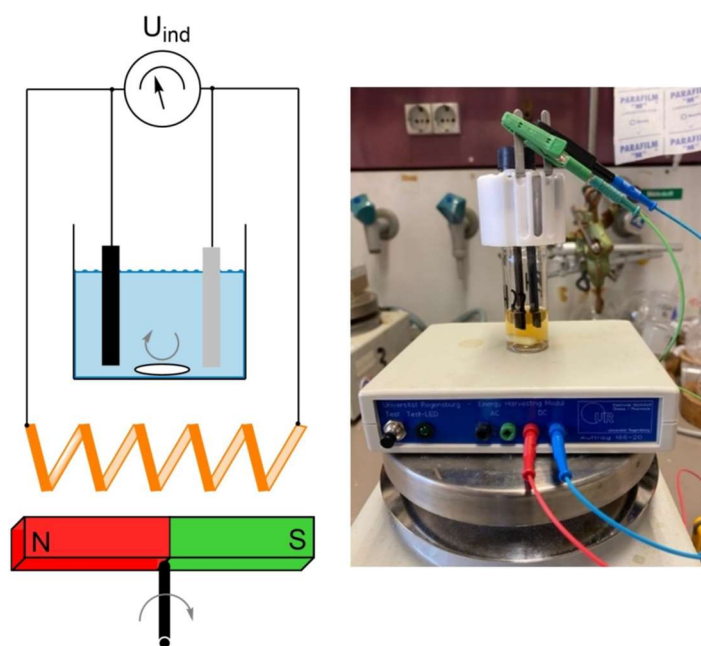


Figure 1. Energy Harvesting (EH) device. Left: schematic representation, right: Prototype on a magnetic stirring plate during the operation of an electrolysis.

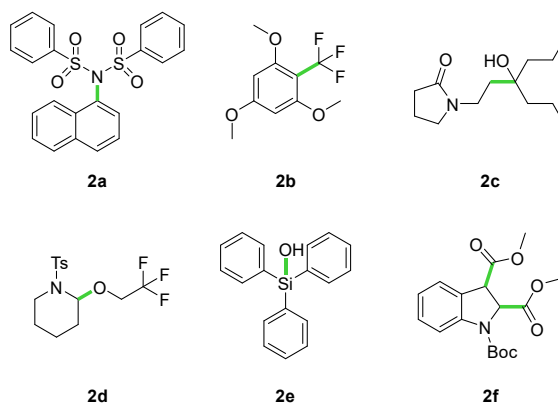
2.3 Results and Discussion

The EH device essentially consists of an induction coil inside a plastic housing, AC and DC outputs, a rectifier made of four diodes, a capacitor and a test LED with switch and ballast resistor (Figure S1, S2). Providing an open-circuit voltage of $U_{\text{ind}}=18\text{ V}$ and a current of $I_{\text{max}}=40\text{ mA}$, the requirements for most electrochemical reactions are fulfilled.^[10–13] The sinusoidal voltage is smoothed to a high level, ensuring operation in DC mode (Figure 2).



Figure 2. Oscillogram of the output voltage of the EH device. Left: open circuit without rectification, right: closed circuit under load with rectification.

An external module, consisting of a tunable rotary potentiometer was conceived for constant current (c.c.) operation mode. Connected to the DC-output of the EH device, constant current is delivered to the module's output jacks. In order to assess the viability of this EH concept in organic electrochemistry, a comparison between conventional power supply (PS) and the newly developed EH device was carried out as follows. To determine whether and to what extent the EH device can be used as a substitute for a commercial energy source, the yield was chosen as the decisive parameter. Due to their importance in the synthesis of natural products,^[14] pharmaceuticals,^[15,16] agrochemicals^[17] and new materials,^[16] six late-stage functionalization (Scheme 1) were selected as model reactions for this purpose.



Scheme 1. Selected late-stage functionalizations.

Nitrogen-containing aromatics are omnipresent and new approaches for Buchwald-Hartwig^[18] coupling and Ullman amination^[19,20] receive much attention.^[21] We employed a method for C-N cross-coupling, developed by Lei^[22] to demonstrate the direct dependency between rotational speed and induced voltage. Operating at constant voltage (c.v.) mode, a slow stirring speed of $f_{\text{rot}}=350$ rpm provides a voltage of 3.5 V, which furnishes the imidation of naphthalene in 18% yield. The control reaction with a conventional power supply led to similar low outcome. Higher temporal change of the magnetic field generates a higher output voltage $U_{\text{ind}}=4.0$ V, furnishing 50% respectively 47% yield at 550 rpm. An extreme stirring speed of 1050 rpm delivers $U_{\text{ind}}=8.0$ V, causing an overoxidation which in turn diminishes the yield (12%). Overall, the yields varied only slightly between the two power sources for all rotation speeds. Therefore, poor mixing at extremely high or low stirring speeds hardly has any effect, while the induced voltage does. Operation in c.c. mode enhanced the reaction outcome, as described by the authors.^[22] The reaction outcome is also almost identical for both power sources in this operating mode (Table 1).

Table 1. Influence of stirring speed on electrochemical reactions using the imidation of naphthalene as an example.

$\text{1a} \xrightarrow[\text{NBu}_4\text{OAc (1.0 eq), 25}^\circ\text{C}]{\text{c.v. (+) C | (-) Pt, DCM : MeCN : HFIP (20:4:1)}} \text{2a}$

Entry	Source	f_{rot} (rpm)	Mode	U (V)	I (mA)	Yield (%)
1	PS	350	c.v.	3.5		12
2	EH	350	c.v.	3.5		18
3	PS	550	c.v.	4.6		47
4	EH	550	c.v.	4.6		50
5	PS	1050	c.v.	8.0		11
6	EH	1050	c.v.	8.0		12
6	PS	550	c.c.		10	59
6	EH	550	c.c.		10	56

To confirm the initial findings, we applied our EH approach to other reactions like the trifluoromethylation of 1,3,5-trimethoxybenzene. The introduction of trifluoromethyl groups into organic compounds often improves properties related to bioavailability, lipophilicity, and metabolic stability which makes them appealing for all kinds of applications.^[23–25] There are numerous strategies for the installation of a trifluoromethyl functionality, including photoredox^[26,27] and electrochemical^[28,29] approaches. Processes that do not require an external oxidant are of particular interest. That is why we chose the work of Lei^[30] for another comparison between the different power sources in c.v. and c.c. mode. The applied voltage of 3.3 V corresponds to the initial voltage at 10 mA. Once again, no significant difference between the power sources has been observed, neither in c.v. nor in c.c. mode (Table 2). Both modes furnished the product formation in >60% yield. The deviation in yield in c.v. mode is slightly higher than in c.c. mode, which was also observed during the previous imidation.

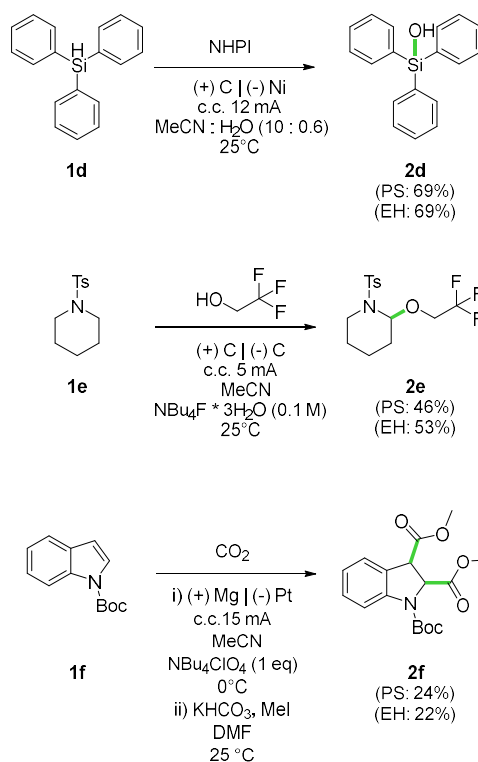
Table 2. Comparison of c.v. and c.c. operation using the example of the trifluoromethylation of 1,3,5-trimethoxybenzene.

Entry	Source	Mode	U (V)	I (mA)	Yield (%)
1	PS	c.v.	3.3		64
2	EH	c.v.	3.3		60
3	PS	c.c.		10	64
4	EH	c.c.		10	64

A keto olefin coupling of 1-vinylpyrrolidin-2-one with 4-heptanone was chosen for the last example in c.v. mode (Table 3). As carbonyl and olefin compounds are well available,^[31,32] such couplings have found use in complex molecule synthesis.^[33] Following an electro reductive procedure reported by Baran,^[32] we obtained the coupling product in fair yields. The yield in c.v. mode was on average by 14% lower than in c.c. mode and the fluctuation between PS and EH was double (4%) compared to those at c.c. mode (2 %). In conclusion, the c.v. mode is more reliable in terms of reaction outcome than the c.c. mode. Fluctuations seem to be smaller and yields tend to be higher. Photoelectrochemical reactions are an exception here.^[34] As a consequence, the last three examples (Scheme 2) were focusing on the comparisons of both power sources in c.c. mode.

Table 3. Comparison of c.v. and c.c. operation using the example of a keto-olefin coupling.

Entry	Source	Mode	U (V)	I (mA)	Yield (%)
1	PS	c.v.	1.9		54
2	EH	c.v.	1.9		50
3	PS	c.c.		10	68
4	EH	c.c.		10	66



Scheme 2. Comparison of yields from EH and classical electrolysis, based on the hydrolysis of triphenylsilane (top), the synthesis of an N,O-acetal as a methylation precursor (middle) and the dual carboxylation of Boc-indole.

Silanols are valuable compounds as they are employed in organic transformations, including metal-catalyzed cross-couplings,^[35] C-H functionalization,^[36,37] and organocatalysis.^[38] They are furthermore known from polymeric materials^[39] and as isosteres in bioactive molecules.^[40,41] One elegant way to access silanols is the hydrolysis of hydrosilane. Using NHPI (N-hydroxyphthalimide) as HAT mediator, we synthesized triphenylsilanol in satisfactory yield, without any detectable difference based on the power source used.^[42] For the provision of desirable intermediates in late-stage functionalization a Shono-oxidation of *N*-*p*-tosylpyridine gives access to the corresponding N,O-acetal, which acts as a methylation precursor. Methylations are an important modification to increase biological activity. Activity changes of more than two orders of magnitude have been observed for bioactive compounds^[43] and methyl groups are structural elements in top-selling drugs.^[44] We applied a procedure by Lin,^[45] which uses trifluoroethanol (TFE) to capture an iminium ion intermediate. TFE is more stable towards anodic oxidation than MeOH, while retaining its reactivity to undergo methylation when treated with organozinc reagents.^[45] Under low current electrolysis (5 mA) both PS and EH forged the protected N,O-acetal of piperidine in fair yield. After the applicability at low currents was demonstrated, the upper limit of the device was examined. Carbon dioxide is considered to be the most widespread source of carbon on the planet.^[46] CO₂ is omnipresent, but its extensive emission from fossil fuels is the main cause of global warming, leading to increased attention to CO₂-capturing syntheses.^[47] In this regard, Mita^[48] has developed an electrochemical carboxylation procedure for the esterification of indole derivatives. Even though the described method exceeds

the available current, provided by the EH device, we could demonstrate that under slightly modified conditions Boc-Indole was successfully converted. After presumably quantitative methylation with MeI, we managed to isolate the two-fold carboxylated product in 22% (EH) respectively 24% (PS) yield, manifesting that there are no significant drawbacks in terms of yield when a commercial PS is replaced by EH. For the application in small lab-scale organic synthesis, the EH performs equally well as potentiostat.

2.4 Conclusion

Six different late-stage functionalization reactions including C-CF₃, C-Me, C-CO₂Me, sp²C- sp³C, Si-O and C-N bond formation demonstrate that the EH of rotational energy of a conventional laboratory magnetic stirrer could be used to perform electrochemical reactions. We observed no significant deviation in yield within the individual operational modes, between conventional power sources and the EH device. The built-in rectifier was sufficient to smooth the induced AC voltage to the extent required for different organic transformations. The simple to operate and cost-effective set-up may allow more chemical laboratories including laboratories in developing countries to use electrochemical reactions in education and research. The overall cost for all parts of the EH device was estimated to be below 90 €.

2.5 References

- [1] Y. Zhang, M. Xie, V. Adamaki, H. Khanbarez, C. R. Bowen, *Chem. Soc. Rev.* **2017**, *46*, 7757–7786.
- [2] F. Dong, Z. Pang, S. Yang, Q. Lin, S. Song, C. Li, X. Ma, S. Nie, *ACS Nano* **2022**, *16*, 3449–3475.
- [3] J. Wang, X. Dai, X. Pei, L. Qi, F. Ning, J. Chen, Y. Li, J. Chen, Y. Zhao, *ACS Appl. Nano Mater.* **2022**, *5*, 12756–12764.
- [4] F. Wu, P. Yu, L. Mao, *Chem. Soc. Rev.* **2017**, *46*, 2692–2704.
- [5] L. Zhou, D. Liu, L. Liu, L. He, X. Cao, J. Wang, Z. L. Wang, *Research* **2021**, *2021*, 1–15.
- [6] M. Wu, W. Guo, S. Dong, A. Liu, Y. Cao, Z. Xu, C. Lin, J. Zhang, *npj Mater. Degrad.* **2022**, *6*, 73.
- [7] B. Zhang, C. Zhang, O. Yang, W. Yuan, Y. Liu, L. He, Y. Hu, Z. Zhao, L. Zhou, J. Wang, Z. L. Wang, *ACS Nano* **2022**, *16*, 15286–15296.
- [8] Y. Li, W. Liu, Z. Zhang, X. Du, L. Yu, Y. Deng, *Commun. Chem.* **2019**, *2*, 67.
- [9] P. Kinsler, *Physics* **2020**, *2*, 148–161.
- [10] A. Wiebe, T. Gieshoff, S. Möhle, E. Rodrigo, M. Zirbes, S. R. Waldvogel, *Angew. Chem. Int. Ed.* **2018**, *57*, 5594–5619; *Angew. Chem.* **2018**, *130*,
- [11] T. H. Meyer, I. Choi, C. Tian, L. Ackermann, *Chem.* **2020**, *6*, 2484–2496.
- [12] R. D. Little, *J. Org. Chem.* **2020**, *85*, 13375–13390.
- [13] M. Yan, Y. Kawamata, P. S. Baran, *Chem. Rev.* **2017**, *117*, 13230–13319.
- [14] P. S. Baran, *J. Am. Chem. Soc.* **2018**, *140*, 4751–4755.
- [15] L. Guillemard, N. Kaplaneris, L. Ackermann, M. J. Johansson, *Nat. Chem. Rev.* **2021**, *5*, 522–545.
- [16] J. Wencel-Delord, F. Glorius, *Nat. Chem.* **2013**, *5*, 369–375.
- [17] M. J. Tilby, D. F. Dewez, L. R. E. Pantaine, A. Hall, C. Martínez-Lamenca, M. C. Willis, *ACS Catal.* **2022**, 6060–6067.
- [18] R. Dorel, C. P. Grugel, A. M. Haydl, *Angew. Chem. Int. Ed.* **2019**, *58*, 17118–17129; *Angew. Chem.* **2019**, *131*, 17276–17287.
- [19] M.-L. Louillat, F. W. Patureau, *Chem. Soc. Rev.* **2014**, *43*, 901–910.
- [20] Q. Cai, W. Zhou, *Chin. J. Chem.* **2020**, *38*, 879–893.
- [21] A. Vijeta, C. Casadevall, E. Reisner, *Angew. Chem. Int. Ed.* **2022**, *61*.
- [22] X. Hu, G. Zhang, L. Nie, T. Kong, A. Lei, *Nat. Commun.* **2019**, *10*, 5467.
- [23] S. Purser, P. R. Moore, S. Swallow, V. Gouverneur, *Chem. Soc. Rev.* **2008**, *37*, 320–330.
- [24] T. Furuya, A. S. Kamlet, T. Ritter, *Nature* **2011**, *473*, 470–477.
- [25] K. Müller, C. Faeh, F. Diederich, *Science* **2007**, *317*, 1881–1886.
- [26] D. A. Nagib, D. W. C. MacMillan, *Nature* **2011**, *480*, 224–228.
- [27] Y. Ouyang, X.-H. Xu, F.-L. Qing, *Angew. Chem. Int. Ed.* **2018**, *57*, 6926–6929; *Angew. Chem.* **2018**, *130*, 7042–7045.
- [28] S. Rodrigo, C. Um, J. C. Mixdorf, D. Gunasekera, H. M. Nguyen, L. Luo, *Org. Lett.* **2020**, *22*, 6719–6723.
- [29] R. P. Bhaskaran, B. P. Babu, *Adv. Synth. Catal.* **2020**, *362*, 5219–5237.
- [30] Y. Deng, F. Lu, S. You, T. Xia, Y. Zheng, C. Lu, G. Yang, Z. Chen, M. Gao, A. Lei, *Chin. J. Chem.* **2019**, *37*, 817–820.
- [31] R. S. Doerksen, C. C. Meyer, M. J. Krische, *Angew. Chem. Int. Ed.* **2019**, *58*, 14055–14064; *Angew. Chem.* **2019**, *131*, 14193–14202.
- [32] P. Hu, B. K. Peters, C. A. Malapit, J. C. Vantourout, P. Wang, J. Li, L. Mele, P.-G. Echeverria, S. D. Minter, P. S. Baran, *J. Am. Chem. Soc.* **2020**, *142*, 20979–20986.
- [33] K. D. Nguyen, B. Y. Park, T. Luong, H. Sato, V. J. Garza, M. J. Krische, *Science* **2016**, *354*, 5133.
- [34] S. Wu, J. Kaur, T. A. Karl, X. Tian, J. P. Barham, *Angew. Chem. Int. Ed.* **2022**, *61*.
- [35] S. E. Denmark, C. S. Regens, *Acc. Chem. Res.* **2008**, *41*, 1486–1499.
- [36] M. Mewald, J. A. Schiffner, M. Oestreich, *Angew. Chem. Int. Ed.* **2012**, *51*, 1763–1765; *Angew. Chem.* **2012**, *124*, 1797–1799.
- [37] C. Huang, B. Chattopadhyay, V. Gevorgyan, *J. Am. Chem. Soc.* **2011**, *133*, 12406–12409.
- [38] T. Min, J. C. Fettinger, A. K. Franz, *ACS Catal.* **2012**, *2*, 1661–1666.
- [39] R. Murugavel, M. G. Walawalkar, M. Dan, H. W. Roesky, C. N. R. Rao, *Acc. Chem. Res.* **2004**, *37*, 763–774.
- [40] A. K. Franz, S. O. Wilson, *J. Med. Chem.* **2013**, *56*, 388–405.
- [41] S. Bähr, S. Brinkmann-Chen, M. Garcia-Borràs, J. M. Roberts, D. E. Katsoulis, K. N. Houk, F. H. Arnold, *Angew. Chem. Int. Ed.* **2020**, *59*, 15507–15511; *Angew. Chem.* **2020**, *132*, 15637–15641.
- [42] H. Liang, L. Wang, Y. Ji, H. Wang, B. Zhang, *Angew. Chem. Int. Ed.* **2021**, *60*, 1839–1844; *Angew. Chem.* **2021**, *133*, 1867–1872.
- [43] E. J. Barreiro, A. E. Kümmerle, C. A. M. Fraga, *Chem. Rev.* **2011**, *111*, 5215–5246.
- [44] H. Schönherr, T. Cernak, *Angew. Chem. Int. Ed.* **2013**, *52*, 12256–12267; *Angew. Chem.* **2013**, *125*, 12480–12492.
- [45] L. F. T. Novaes, J. S. K. Ho, K. Mao, K. Liu, M. Tanwar, M. Neurock, E. Villemure, J. A. Terrett, S. Lin, *J. Am. Chem. Soc.* **2022**, *144*, 1187–1197.
- [46] J. Luo, I. Larrosa, *ChemSusChem* **2017**, *10*, 3317–3332.
- [47] R. Martín, A. W. Kleij, *ChemSusChem* **2011**, *4*, 1259–1263.
- [48] Y. You, W. Kanna, H. Takano, H. Hayashi, S. Maeda, T. Mita, *J. Am. Chem. Soc.* **2022**, *144*, 3685–3695.

2.6 Experimental Part

2.6.1 General Remarks

All reactions were carried out with dry solvents unless otherwise stated. Dry nitrogen was used as inert gas atmosphere. All solvents and required chemicals were purchased from commercial suppliers (Acros, Alfa Aesar, Fluka, Fluorochem, Merck, Sigma Aldrich, TCI) as reagent grade or at the highest commercial quality and were used directly without further purification unless stated otherwise. Thin-layer chromatography (TLC) was performed on silica gel coated alumina plates (MN TLC sheets ALUGRAM®Xtra SIL G/UV254). Visualization was accomplished with UV light (254 nm or 366 nm) sources. All NMR spectra were recorded using a Bruker Avance 400 (400 MHz for ^1H , 101 MHz for ^{13}C , 376 MHz for ^{19}F) or Bruker Avance 600 (600 MHz for ^1H , 151 MHz for ^{13}C , 565 MHz for ^{19}F) NMR spectrometer in CDCl_3 , D_2O and DMSO-d^6 solutions with internal solvent signals (for ^1H and ^{13}C) as reference (7.26, 77.2 for CDCl_3 , 2.50, 4.8, NA for D_2O and 39.5 for DMSO-d^6). All chemical shifts are reported in δ -scale as parts per million [ppm] (multiplicity, coupling constant J , number of protons) relative to the solvent residual peaks as the internal standard. Coupling constants J are given in Hertz [Hz]. Abbreviations used for signal multiplicity: ^1H NMR: br = broad, s = singlet, d = doublet, t = triplet, q = quartet, p = quintet, dd = doublet of doublets, dt = doublet of triplets, dq = doublet of quartets and m = multiplet. High-resolution mass spectra (HRMS) were obtained from the central analytic mass spectrometry facilities of the Faculty of Chemistry and Pharmacy, University of Regensburg. All mass spectra were recorded on a Finnigan MAT 95, Thermo Quest Finnigan TSQ 7000, Finnigan MATSSQ 710 A or an Agilent Q-TOF 6540 UHD instrument.

2.6.2 Power Sources

All electrochemical transformations, powered by EH, were performed by placing the EH device in between the magnetic stirrer and the reaction vessel. If necessary, the c.c. module was additionally interposed. Voltage or current was set to the specific value via the speed of the stirrer and monitored by a connected multimeter. Reactions performed with a commercial device were powered by a PeakTech® 6080A digital DC power supply. If specifically indicated in literature, an IKA ElectraSyn® 2.0 was employed instead. Scale, vessel size and electrode surface may vary from literature procedures (due to availability), leading to slightly different results.^[1-6] All parameters were held constant within one series of reactions, ensuring the comparability of the yields achieved vial self-sustained (EH) and externally powered (PS) electrolysis.

2.6.3 Electrodes

The employed electrode materials were: reticulated vitreous carbon (RVC) foam electrodes, thickness: 6.35 mm, porosity: 96.5% (Goodfellow, Product Code: 613-422-20); Carbon from Faber-Castell 2.0 mm HB pencil lead, Pt 99.9 from Sigma Aldrich; Fe from DC01 CR1 (C 0.12, P 0.045, S 0.045, Mn 0.60, Ti 0.0) by Thyssen Krupp; Mg 99.9% from Sigma Aldrich, Zinc from MARAWE (part01-74-00000) (200 x 170 x 0.6 mm). Sn 99.9% (Aldrich).

2.6.4 Description of the EH Device

The EH device provides a tunable operational voltage $U_{\text{Ind}} = 18 \text{ V}$ and a maximum current of $I_{\text{max}} = 40 \text{ mA}$. The power is supplied to two pairs of banana jacks, one each for AC voltage and DC voltage. The installed components are an induction coil (steel screw M8x100 with 500 turns of copper wire $\varnothing = 0.05 \text{ mm}^2$) for voltage generation, a rectifier consisting of diodes (D_1 - D_4 : BAT41), a ballast resistor ($R_1 = 1 \text{ k}\Omega$), a capacitor (C_1 : $220 \mu\text{F}/35 \text{ V}$) and a test LED with switch. Circuitry is housed within a plastic enclosure. The cost of production amounted to 54.50 €.



Figure S 1. EH device. top: front view, bottom: view into the opened housing.

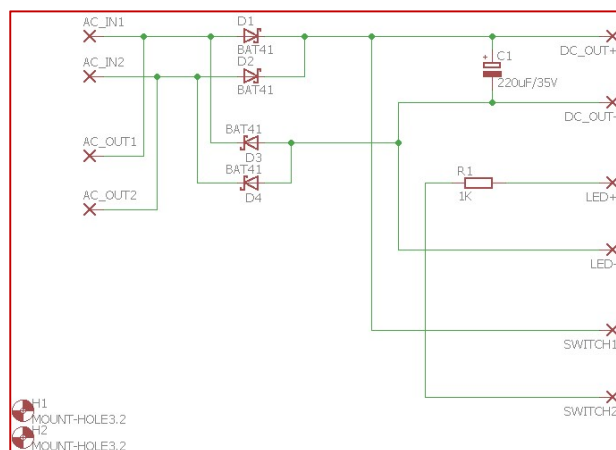


Figure S 2. Circuit diagram of the EH device including all installed components.

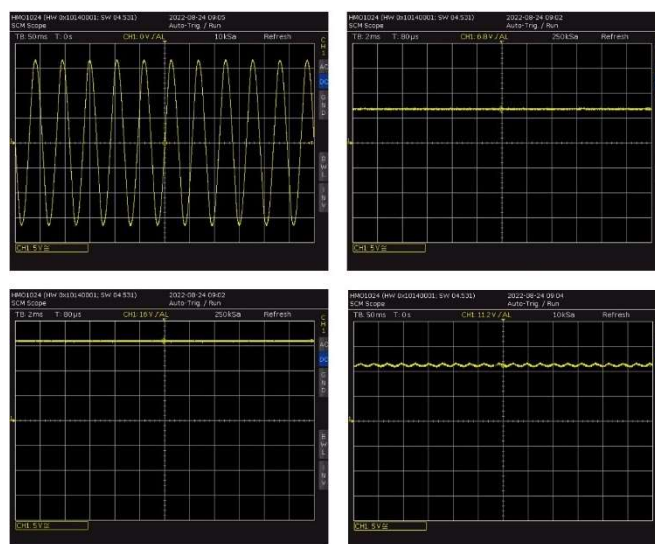


Figure S 3. Oscillogram of the output voltage of the EH device. top left: open circuit without rectification, bottom left: open circuit with rectification, top right: open circuit with rectification at lower stirring speed, bottom right: closed circuit under load with rectification.

The control module for reactions at constant current consists of a tunable rotary potentiometer in an alumina housing which is connected to two pairs of banana jacks (c.v.-input; c.c.-output). Once connected to the DC-output of the EH device, constant current is delivered to the module's output jacks. The cost of production amounted to 34.50 €.



Figure S 4. Current control module. Top: front and back view, bottom: opened and closed housing.

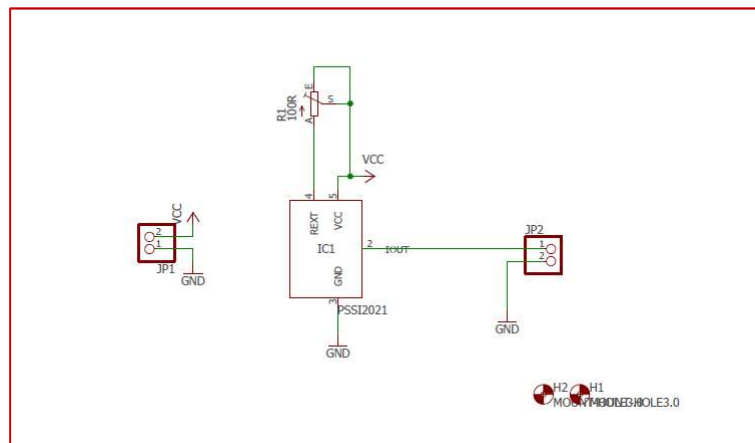
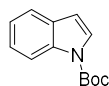


Figure S 5. Current control module. Top: front and back view, bottom: opened and closed housing.

2.6.5 Characterization of Starting Materials

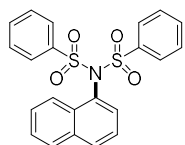


1-Tosylpiperidine (1e):^[1] In a 50 mL round bottom flask, *p*-toluolsulfonyl chloride (1.3 g, 7 mmol, 1.0 equiv.) was dissolved in ethanol (14 mL). Then the piperidine (1.4 mL, 14 mmol, 2.0 equiv.) was slowly added and the mixture was stirred at room temperature for 5 min. Solvent was removed under reduced pressure and the crude was purified with flash column chromatography (petroleum ether / ethyl acetate = 93/7) to give a white solid: 1.6 g, 96% yield. **¹H NMR (400 MHz, CDCl₃)** δ_H [ppm] = 7.64 (d, *J* = 8.3 Hz, 2H), 7.31 (d, *J* = 7.9 Hz, 2H), 2.97 (t, *J* = 6.0 Hz, 4H), 2.43 (s, 3H), 1.69 – 1.54 (m, 4H), 1.46 – 1.34 (m, 2H). **¹³C NMR (101 MHz, CDCl₃)** δ_C [ppm] = 143.41, 133.45, 129.67, 127.87, 47.08, 25.31, 23.67, 21.66; **HRMS (ESI+)** *m/z* calcd. for C₁₂H₁₈NO₂S⁺ [M+H]⁺ = 240.1053, found 240.1055; MP 99.0-100.5°C.

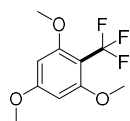


Synthesis of 1-Boc-indole (1f):^[2] In a 100 mL Schlenk flask, Boc-anhydride (1.9 g, 8.5 mmol, 1.0 equiv.), indole (1.0 g, 8.5 mmol, 1 equiv.) and DMAP (104 mg, 0.85 mmol, 0.1 equiv.) were dissolved in dry DCM (20 mL) and stirred at room temperature for 10 h. The reaction mixture was washed with brine (10 mL), dried over anhydrous Na₂SO₄ and the solvent was removed under reduced pressure. The crude was then purified by column chromatography (petroleum ether/ethyl acetate = 75/25) to receive a pale-yellow oil: 1.8 g, 95% yield. **¹H NMR (400 MHz, CDCl₃)** δ_H [ppm] = 8.32 (brs, 1H), 7.72 (s, 1H), 7.66 (d, *J* = 7.8 Hz, 1H), 7.44 (td, *J* = 7.8, 1.3 Hz, 1H), 7.34 (td, *J* = 7.8, 1.3 Hz, 1H), 6.66 (d, *J* = 3.1 Hz, 1H), 1.77 (s, 9H); **¹³C NMR (101 MHz, CDCl₃)** δ_C [ppm] = 149.74, 135.23, 130.59, 125.83, 124.19, 122.63, 120.93, 115.18, 107.28, 83.48, 28.12; **HRMS (APCI+)** *m/z* calcd. for C₁₃H₁₆NO₂⁺ [M+H]⁺ = 218.1176, found 218.1175.

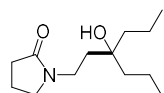
2.6.6 Characterization of Products



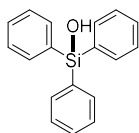
***N*-(Naphthalen-1-yl)-*N*-(phenylsulfonyl) benzene sulfonamide (2a):**^[3] In a 25 mL Schlenk tube, naphthalene (51.3 mg, 0.4 mmol, 1.0 equiv.), dibenzenesulfonimide (178 mg, 0.6 mmol, 1.5 equiv.) and ⁿBu₄NOAc (121 mg, 0.4 mmol, 1.0 equiv.) were added. The tube was sealed with a rubber septum, equipped with an RVC (15 mm x 5.0 mm x 5.0 mm) anode and a Pt-foil (10 mm x 5.0 mm x 0.1 mm) cathode. Dry, degassed DCM (2.5 mL), ACN (0.5 mL) and HFIP (0.125 mL) were added through the septum. Then, the mixture was stirred and electrolyzed at a constant current of 10 mA for 4 hours. The crude was purified by flash column chromatography on silica (hexane/EtOAc = 90/10 to 0/100) to receive a white solid: EHD: 94 mg, 56% yield; PS: 100 mg, 59% yield. **¹H NMR (400 MHz, CDCl₃)** δ_H [ppm] = 7.96 (dd, *J* = 8.5, 1.2 Hz, 5H), 7.85 (d, *J* = 8.2 Hz, 1H), 7.67 (t, *J* = 7.5 Hz, 2H), 7.59 – 7.49 (m, 5H), 7.48 – 7.38 (m, 2H), 7.29 (ddd, *J* = 8.3, 6.9, 1.1 Hz, 1H), 7.12 (dd, *J* = 7.4, 1.0 Hz, 1H); **¹³C NMR (101 MHz, CDCl₃)** δ_C [ppm] = 139.25, 134.78, 134.21, 132.92, 131.28, 131.13, 130.67, 129.18, 129.06, 128.23, 127.11, 126.66, 125.10, 124.06; **HRMS (ESI)** *m/z* calcd. for C₂₂H₁₈NO₄S₂⁺ [M+H]⁺ = 424.0672 found 424.0674. **MP** 197-198°C



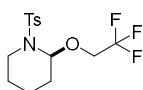
1,3,5-Trimethoxy-2-(trifluoromethyl) benzene (2b):^[4] In a 25 mL Schlenk tube 1,3,5-trimethoxybenzene (84.0 mg, 0.5 mmol, 1.0 equiv.), CF₃SO₂Na (156 mg, 1 mmol, 2.0 equiv.), ⁿBu₄NBF₄ (82.3 mg, 0.25 mmol, 5.0 equiv.) were dissolved in a mixture of ACN (10 mL) and water (1 mL) under nitrogen atmosphere. The tube was sealed with a rubber septum, equipped with a carbon (RVC: 20 mm x 5.0 mm x 5.0 mm) anode and a steel (20 mm x 5.0 mm x 0.2 mm) cathode. The mixture was degassed by purging with nitrogen for 5 min and electrolyzed at a constant current of 10 mA at room temperature for 5 h. Then water (10 mL) and ethyl acetate were added and the organic layer was separated. The aqueous phase was extracted in ethyl acetate (3x 20 mL) and the combined organic phase was washed with brine and dried over anhydrous Na₂SO₄. The solvent was removed under reduced pressure and the crude was purified by flash column chromatography (hexane/EtOAc = 95/5) to receive a white solid: EH: 76 mg, 64%; PS: 76 mg, 64% yield. **¹H NMR (400 MHz, CDCl₃)** δ_H [ppm] = 6.12 (s, 2H), 3.83 (s, 9H); **¹³C NMR (101 MHz, CDCl₃)** δ_C [ppm] = 163.67, 160.53, 160.52, 124.51 (q, *J*_{c-F}¹ = 182.81 Hz), 100.385 (q, *J*_{c-F}² = 20.20 Hz), 91.33, 56.31, 55.45; **¹⁹F NMR (377 MHz, CDCl₃)** δ_F [ppm] = -54.68; **HRMS (EI+)** *m/z* calcd. for C₁₀H₁₂O₃F₃⁺ [M+H]⁺ = 236.06548, found 236.06502; **MP** 60-63°C.



1-(3-Hydroxy-3-propylhexyl)pyrrolidin-2-one (2c):^[5] In a 2 mL Eppendorf® tube, 4-heptanon (98 μ L, 0.7 mmol, 2.0 equiv.), 1-vinyl-2-pyrrolidon (37 μ L, 0.35 mmol, 1.0 equiv.) and $^n\text{Bu}_4\text{NBr}$ (96.7mg, 0.3 mmol) were dissolved in DMF (1 mL). A zinc anode (10 mm x 5.0 mm x 0.3 mm) and a Sn-cathode (10 mm x 5.0 mm x 0.2 mm) were immersed. Then the mixture was electrolyzed at air with a constant current of 10 mA at room temperature for 4 h. The reaction mixture was filtered through a plug of silica, rinsed with EtOAc (30 mL) and dried over anhydrous Na_2SO_4 . The solvent was removed under reduced pressure and the crude was purified by flash column chromatography on silica (petroleum ether/EtOAc = 90/10) to receive a colorless oil: EH: 54 mg, 68% yield; PS: 54 mg, 68% yield. $^1\text{H NMR}$ (400 MHz, CDCl_3) δ_{H} [ppm] = 3.40 – 3.29 (m, 4H), 2.63 (brs, 1H), 2.33 (t, J = 8.1 Hz, 2H), 2.05 – 1.90 (m, 2H), 1.62 – 1.56 (m, 2H), 1.43 – 1.36 (m, 4H), 1.33 – 7.20 (m, 4H), 0.88 (t, J = 7.1 Hz, 6H). $^{13}\text{C NMR}$ (101 MHz, CDCl_3) δ_{C} [ppm] = 175.22, 73.36, 47.51, 41.62, 38.29, 36.16, 31.17, 17.95, 16.93, 14.74. **HRMS (EI+)** m/z calcd. for $\text{C}_{13}\text{H}_{26}\text{NO}_2$ + $[\text{M}+\text{H}]^+$ = 227.1885, found 227.1885

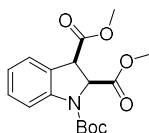


Triphenylsilanol (2d):^[6] In a 10 mL ElectraSyn® undivided cell, triphenylsilane (157 mg, 0.6 mmol, 1.0 equiv.), NHPI (98 mg, 0.6 mmol, 1.0 equiv.), and $^n\text{Bu}_4\text{NPF}_6$ (325 mg, 0.84 mmol, 1.4 equiv.) were dissolved in a mixture of ACN (7.0 mL) and water (0.4 mL). The vial was sealed with a cap, equipped with an RVC (20 mm x 5.0 mm x 3.0 mm) anode and a nickel foam (4.0 cm x 0.8 cm x 0.2 cm) cathode and the mixture was purged with nitrogen for 15 min. Then, the mixture was stirred and electrolyzed at a constant current of 12 mA for 8 hours at room temperature. After completion, the solvent was removed under reduced pressure and the crude was purified by flash column chromatography on silica (petroleum ether/EtOAc = 95/5) to receive a white solid: EH: 140 mg, 69% yield; PS: 140 mg, 69% yield. (400 MHz, CDCl_3) δ_{H} [ppm] = 7.66 (d, J = 6.5 Hz, 6H), 7.47 (t, J = 7.3 Hz, 3H), 7.40 (t, J = 7.2 Hz, 6H), 2.74 (brs, 1H); $^{13}\text{C NMR}$ (101 MHz, CDCl_3) δ_{C} [ppm] = 135.13, 130.24, 128.05; **HRMS (EI+)** m/z calcd. for $\text{C}_{18}\text{H}_{17}\text{OSi}$ + $[\text{M}+\text{H}]^+$ = 276.09649, found 276.09676; **MP:** 151-152°C.



Piperidine,1-[(4-methylphenyl)sulfonyl]-2-(2,2,2-trifluoroethoxy) (2e):^[7] In a 5 mL ElectraSyn vial, equipped with graphite (20 mm x 6.0 mm x 3.0 mm) anode and graphite (20 mm x 6.0 mm x 3.0 mm) cathode, 1-tosylpiperidine (**1f**) (239 mg, 1.0 mmol, 1.0 equiv.), trifluoroethanol (4 mL, 55 mmol, 55 equiv.) and TBAF trihydride (126 mg, 0.4 mmol) were added. The mixture was electrolyzed at a constant current of 5 mA at room temperature for 16 hours (2.9 F/mol). Then, the crude was purified by flash column chromatography (petroleum ether /DCM = 40/60) to receive a colorless oil: EH: 147 mg, 53% yield; PS:127 mg, 46% yield. $^1\text{H NMR}$ (400 MHz, CDCl_3) δ_{H} [ppm] = 7.70 (d, J = 8.3 Hz, 2H), 7.30 (d, J = 8.0 Hz, 2H), 5.33

(s, 1H), 3.98 – 3.83 (m, 2H), 3.59 (d, $J = 13.5$ Hz, 1H), 3.12 (td, $J = 13.3, 2.7$ Hz, 1H), 2.43 (s, 3H), 1.92 – 1.89 (m, 1H), 1.77 – 1.63 (m, 1H), 1.53 – 1.41 (m, 2H), 1.37 – 1.34 (m, 1H), 1.42 – 1.21 (m, 1H); ^{13}C NMR (101 MHz, CDCl_3) δ_{C} [ppm] = 143.73, 137.70, 129.92, 128.19, 124.05 (q, $J_{\text{C-F}} = 279.77$ Hz), 83.52, 64.65 (q, $J_{\text{C-F}} = 34.34$ Hz) 40.85, 29.61, 23.92, 21.65, 17.66; ^{19}F NMR (377 MHz, CDCl_3) δ_{F} [ppm] = -74.66 (s); HRMS (ESI+) m/z calcd. for $\text{C}_{14}\text{H}_{19}\text{F}_3\text{NO}_3\text{S}^+$ [M+H] $^+$ = 338.1032 found 338.1033.



1-(tert-Butyl) 2,3-dimethyl (2S,3S)-indoline-1,2,3-tricarboxylate (2f):^[8] In a 5

mL Schlenk tube, 1-Boc indole (**1f**) (43.5 mg, 0.2 mmol, 1.0 equiv.) and NBu_4ClO_4 (68.4 mg, 0.2 mmol, 1.0 equiv.) were dissolved in dry ACN (2 mL) under nitrogen atmosphere. The vial was capped with a septum, equipped with a magnesium foil (20 mm \times 3.0 mm \times 0.15 mm) anode and a platinum foil (10 mm \times 5.0 mm \times 0.1 mm) cathode. Then the mixture was sparged with CO_2 for 10 min and electrolyzed under a constant current of 15 mA and continuous CO_2 sparging at 0°C for 3 h. The reaction mixture was acidified with 1 N HCl (2 mL), extracted with ethyl acetate (3x 15 mL) and the combined organic phase was dried over anhydrous Na_2SO_4 . The solvent was removed under reduced pressure and the crude was methyl esterified as follows: In a 5 mL crimp cap vial, the crude dicarboxylic acid and KHCO_3 (80 mg, 0.8 mmol, 2 equiv.) were dissolved in anhydrous DMF (3 mL) under nitrogen atmosphere. Then MeI (38 μL , 0.6 mmol) was slowly added and the mixture was stirred at room temperature for 12 h. The reaction mixture was diluted with EtOAc (10 mL), washed with brine (10 mL) and dried over anhydrous Na_2SO_4 . The solvent was removed under reduced pressure and the crude product was purified flash column chromatography on silica (EtOAc–PE, 3:17) to give a colorless oil: EH: 15 mg, 22 % yield; PS: 16 mg, 24% yield ^1H NMR (600 MHz, CDCl_3) δ_{H} [ppm] = 7.33 (d, $J = 7.6$ Hz, 1H), 7.30 – 7.26 (m, 2H), 6.98 (t, $J = 7.4$ Hz, 1H), 5.34 (brs, 1H), 4.17 (brs, 1H), 3.79 (s, 3H), 3.76 (s, 3H), 1.51 (brs, 9H); ^{13}C NMR (151 MHz, CDCl_3) δ_{C} [ppm] = 171.42, 170.54, 151.37, 142.39, 129.65, 125.57, 125.18, 122.86, 115.14, 81.97, 62.80, 53.20, 52.73, 49.98, 28.38; HRMS (ESI+) m/z calcd. for $\text{C}_{17}\text{H}_{22}\text{NO}_6$ [M+H] $^+$ = 358.1261; found 358.1269.

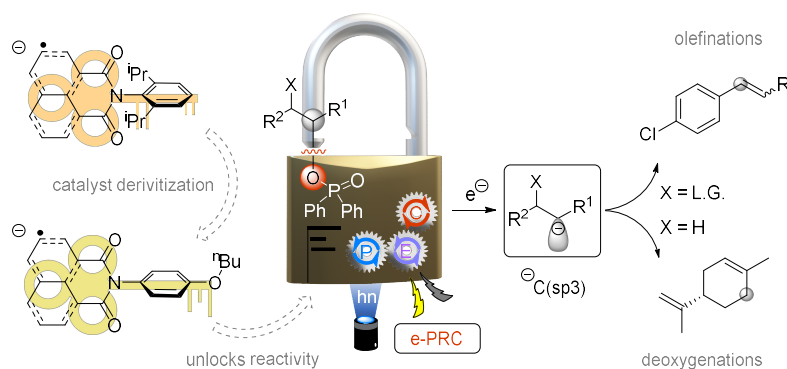
2.6.7 References

- [1] M. Jafarpour, A. Rezaeifard, T. Golshani, *Phosphorus Sulfur Silicon Relat. Elem.* **2010**, *186*, 140–148.
- [2] J. M. Fraile, K. Le Jeune, J. A. Mayoral, N. Ravasio, F. Zaccheria, *Org. Biomol. Chem.* **2013**, *11*, 4327.
- [3] X. Hu, G. Zhang, L. Nie, T. Kong, A. Lei, *Nat. Commun.* **2019**, *10*, 5467.
- [4] Y. Deng, F. Lu, S. You, T. Xia, Y. Zheng, C. Lu, G. Yang, Z. Chen, M. Gao, A. Lei, *Chin. J. Chem.* **2019**, *37*, 817–820.
- [5] P. Hu, B. K. Peters, C. A. Malapit, J. C. Vantourout, P. Wang, J. Li, L. Mele, P.-G. Echeverria, S. D. Minter, P. S. Baran, *J. Am. Chem. Soc.* **2020**, *142*, 20979–20986.
- [6] H. Liang, L. Wang, Y. Ji, H. Wang, B. Zhang, *Angew. Chem. Int. Ed.* **2021**, *60*, 1839–1844.
- [7] L. F. T. Novaes, J. S. K. Ho, K. Mao, K. Liu, M. Tanwar, M. Neurock, E. Villemure, J. A. Terrett, S. Lin, *J. Am. Chem. Soc.* **2022**, *144*, 1187–1197.
- [8] Y. You, W. Kanna, H. Takano, H. Hayashi, S. Maeda, T. Mita, *J. Am. Chem. Soc.* **2022**, *144*, 3685–3695.

As indicated above, the following chapters will focus less on the SOE and more on PRC and PEC. After this excursion into electrochemistry, the next chapter contains an example of how extreme redox potential and selective activation of specific bonds can be reconciled by e-PRC.

CHAPTER 3

3 Electro-mediated Photoredox Catalysis for Selective C(sp³)-O Cleavages of Phosphinates to Carbanions



This chapter has been published. For reference see: X. Tian, T. A. Karl, S. Reiter, S. Yakubov, R. Vivie-Riedle, B. Koenig, J. P. Barham, *Angew. Chem. Int Ed.* **2021**, *133*, (38), 20985-20993.

T. A. Karl developed the concept of phosphinate deoxygenation. He designed the α-chlorophosphinates and synthesized compound 1a and 4a. He further ran all the EPR, UV-Vis, emission and lifetime measurements and evaluated the data. All spectroelectrochemical and CV-data was processed and evaluated by T. A. Karl.

3.1 Abstract

We report a novel example of electro-mediated photoredox catalysis (e-PRC) in the reductive cleavage of C(sp³)-O bonds of phosphinates to alkyl carbanions. As well as deoxygenations, olefinations are reported which are *E*-selective and can be made *Z*-selective in a tandem reduction/photosensitization process where both steps are photoelectrochemically promoted. Spectroscopy, computation and catalyst structural variations reveal that our new naphthalene monoamide-type catalyst allows for a more intimate dispersive precomplexation of its radical anion form with the phosphinate substrate, facilitating a reactivity-determining C(sp³)-O cleavage. Surprisingly and in contrast to previously reported photoexcited radical anion chemistries, our conditions i) tolerate aryl chlorides/bromides and ii) do not give rise to Birch-type reductions.

3.2 Introduction

Synthetic methodologies involving single electron transfer (SET) are increasingly popular for the facile synthesis or modifications of important organic compounds. Photoredox catalysis (PRC)^[1] and synthetic organic electrochemistry (SOE)^[2] lead to easy SET processes, providing notable redox power for various organic transformations under mild conditions. Generally, visible-light PRC generates radical intermediates with good functional group tolerance in a mild manner. However, synthetic applications of PRC in terms of transformations needing highly oxidizing or reducing potentials are limited by the energetic limitations of visible light photons. One solution is to generate photoexcitable radical ions by multi-photon processes.^[3] Such photoexcited radical ions are highly oxidizing^[3a,b] or reducing species,^[3c-h] leading to a significantly expanded redox ‘window’ for activating inert substrates. Sacrificial redox additives (e.g. DIPEA) are employed in stoichiometric excesses in consecutive Photoinduced Electron Transfer (conPET) processes to prime catalysts prior to excitation. Their excesses and organic by-products can plague purification steps. In contrast, SOE allows direct access to high, user-controlled redox energy without involving photocatalysts or sacrificial redox additives, possessing a great advantage for net-oxidative/reductive reactions. However, the applied constant current or voltage can cause uncontrollable over-reductions/oxidations to afford by-products.

To address the aforementioned limitations in PRC and SOE, organic chemists have recently explored their combination.^[4] Merging the advantages of these two important techniques has made photoelectrochemistry a tool for greener, more challenging and more selective molecular activations.^[5] Pioneering reports by Xu,^[5b-c,o] Lambert,^[5g,h,i,k] Lin^[5h,j] and Wickens^[5f] have shown that introducing applied potential in photoredox catalysis is not only beneficial for accessing challenging redox reactions, but is also a green replacement for sacrificial redox additives.

Among the various strategies for combining photocatalysis and electrochemistry^[4a] the subcategory coined electrochemically-mediated photoredox catalysis (e-PRC) is highly attractive. In addition to turning over ‘spent’ closed-shell photocatalysts, e-PRC can also involve electrochemical generation of open-shell (radical ion) photocatalysts, followed by their photoexcitation to species with ultra-high redox potentials. A seminal report from the Lambert group demonstrated this strategy for super-oxidations of highly electron-poor arenes.^[5k] In the reductive direction, photoexcited radical anions of dicyanoanthracene (**DCA**)^[5h] and of 2,6-diisopropylphenyl-containing naphthalenemonoimide (**NpMI**)^[5f] are highly reducing species ($E^{\circ}_{red} < -3.0$ V vs. SCE) that reduce challenging aryl chlorides to their aryl radicals. Even *p*-chloroanisole was reduced, beyond reach of the photon energy limit of monophotonic PRC and where SOE inevitably leads to dehalogenation *via* subsequent aryl radical reduction (Scheme

3.3 Results and Discussion

To assess the viability of our proposed e-PRC alkyl phosphinate reduction, we employed 2-chloro-1,2-diphenylphosphinate **1a** as a model substrate for the olefination reaction (Table 1). By using DCA as an e-PRCat and Zn(+)/RVC(-) as the electrodes in a divided H-cell, we examined the reduction of **1a** under blue light irradiation and with different applied constant potentials. A high constant voltage ($U_{\text{cell}} = -3.2$ V) as used previously^[5h] for electron-priming DCA to its radical anion for photoexcitation gave notable decomposition, desired product *E*-stilbene (*E*-**2a**) in only 7% yield and a 25% yield of diphenylethane **3a**^[8] (Table 1, entry 1). A lower potential ($U_{\text{cell}} = -1.6$ V) led to a remarkable improvement in the reaction profile and yield of *E*-**2a** to 70% (Table 1, entry 2). The optimal yield of *E*-**2a** was obtained at an even lower potential ($U_{\text{cell}} = -1.0$ V). Cyclic phosphate ester **4a** was also a suitable substrate for preparing product *E*-**2a** (entry 4), offering an attractive Corey-Winter-type olefination that avoids explosive/toxic trimethylphosphite, harsh activating reagents, or high temperature. Control reactions omitting light, constant potential or e-PRCat confirmed the photoelectrochemical nature of the olefination reaction (entries 5-7). In contrast to DCA, NpMI as catalyst delivered higher amounts of *Z*-**2a** (entry 8).^[9] Allowing the reaction to proceed for 48 h (entry 9) increased the *E*-/*Z*- ratio to 1/10 (71% of *Z*-**2a**). Detailed investigations (see experimental part) revealed that light, constant potential and NpMI are all advantageous to the isomerization process, representing a novel photoelectroisomerism of alkenes.

Reaction scope was expanded to other substrates including precursors to unsymmetrical stilbenes as well as cyclic, hindered and terminal olefins. Phosphinate precursors are readily synthesized from their ketones *via* α -chlorination and one-pot NaBH₄ reduction/Cl-P(O)Ph₂ protection (see experimental part). Here we opted to use Fe instead of RVC as a cheaper, robust cathode material.^[10] However, it was quickly identified that DCA and NpMI were ineffective e-PRCats for the majority of phosphinates. For example, cyclic substrate **1d** underwent no reaction with these catalysts (entries 10-11). We synthesized ⁿBuO-NpMI as a novel e-PRCat which afforded the desired product **2d** in very good yield (entry 12). Control reactions confirmed the operation of e-PRC (entries 13-15), while cathode materials greatly impacted the reaction (for detailed optimizations see experimental part).^[11] Optimal conditions were examined for a range of olefination reactions (Scheme 2). Unsymmetrical *Z*-stilbenes **2b-2c** were prepared in high yields from the tandem e-PRC reduction/photoelectroisomerism process. Cyclic olefins **2d-2h**, rarely synthesized by the Wittig reaction due to the inconvenience of substrate preparations, were prepared in good to excellent (69-83%) yields. Terminal olefin **2i** could not be prepared in high selectivity by dehydration of its corresponding tertiary alcohol as such a method inevitably leads to the most substituted olefin,^[12] in this case, a tetrasubstituted instead of a terminal olefin.

Table 1. Optimization of the reaction conditions.

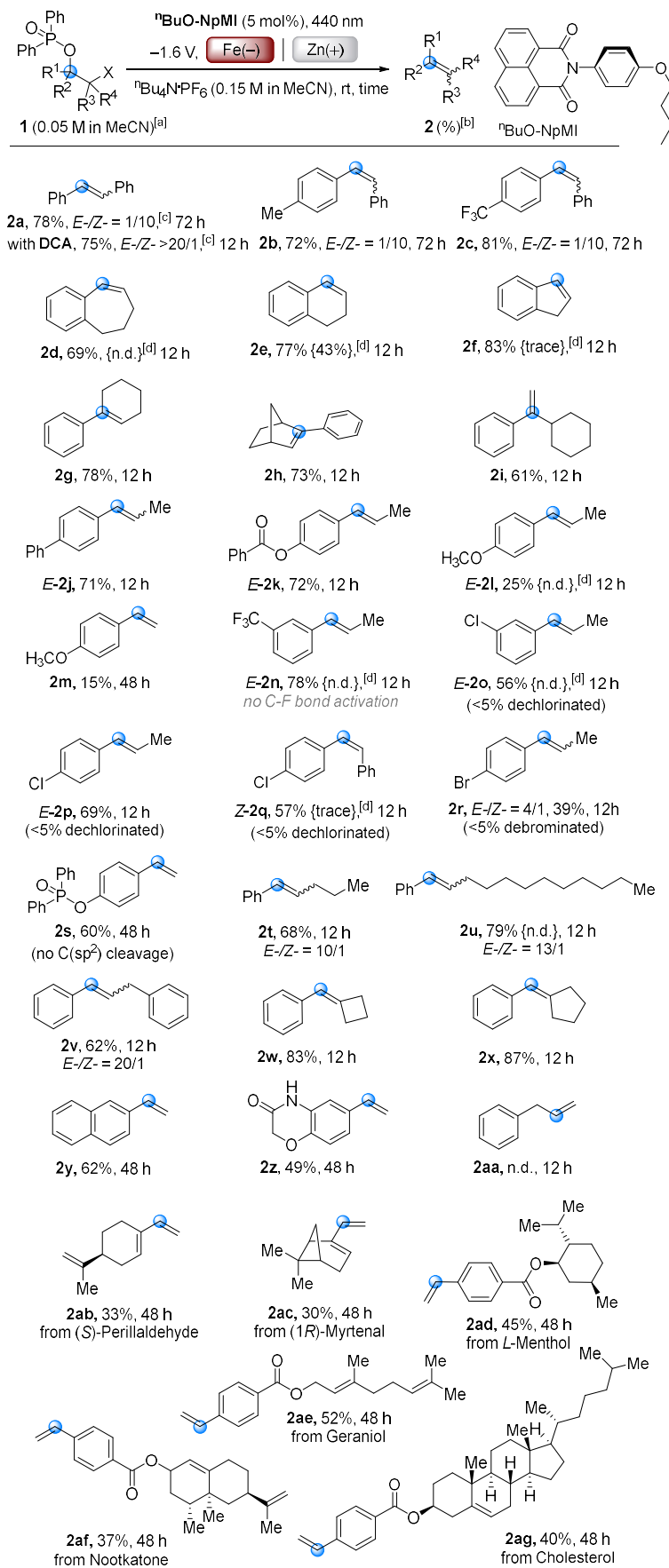
Entry	Substrate	e-PRCat	U _{cell} (V)	t (h)	product: yield (%) ^[a]
1	1a	DCA	-3.2	12	2a : 7%, <i>E</i> -/ <i>Z</i> -> 20:1 ^[b] 3a : 25%
2	1a	DCA	-1.6	12	2a : 70%, <i>E</i> -/ <i>Z</i> -> 20:1 ^[b] 3a : trace
3	1a	DCA	-1.0	12	2a : 79%, <i>E</i> -/ <i>Z</i> -> 20:1 ^[b] 3a : n.d.
4	4a	DCA	-1.0	24	2a : 79%, <i>E</i> -/ <i>Z</i> -> 20:1 ^[b] 3a : n.d.
5 ^[c]	1a	DCA	-1.0	12	2a : n.d. 3a : n.d.
6	1a	DCA	-	12	2a : n.d. 3a : n.d.
7	1a	-	-1.0	12	2a : trace 3a : n.d.
8	1a	NpMI	-1.6	12	2a : 80%, <i>E</i> -/ <i>Z</i> - = 1:1.3 ^[b] 3a : n.d.
9	1a	NpMI	-1.6	48	2a : 78%, <i>E</i> -/ <i>Z</i> - = 1:10 ^[b] 3a : n.d.
10 ^[d]	1d	DCA	-1.0	12	2d : n.d.
11 ^[d]	1d	NpMI	-1.6	12	2d : trace
12 ^[d]	1d	ⁿ BuONpMI	-1.6	12	2d : 75%
13 ^[d]	1d	ⁿ BuONpMI	-	12	2d : n.d.
14 ^{[c],[d]}	1d	ⁿ BuONpMI	-1.6	12	2d : n.d.
15 ^[d]	1d	-	-1.6	12	2d : < 5%

n.d., not detected; ^[a]Yields determined by ¹H NMR spectroscopy with 1,3,5-trimethoxybenzene as an internal standard; ^[b]*E*-/*Z*- ratios determined by ¹H NMR; ^[c]in the dark; ^[d]Fe cathode.

After the successful preparations of a series of *E*-styrene derivatives (exclusive isomers) bearing divergent substituents including -Ph (**2j**), -OBz(**2k**), -OMe(**2l**) and -CF₃(**2n**) at their arene rings, we questioned whether halogen substituents could be tolerated by our reaction. This is a highly challenging issue, since the reductions of aryl chlorides and bromides by photoexcited radical anions (either e-PRC or conPET-type) are highly efficient and heavily reported as discussed earlier (Scheme 1).^[3c-g,5f,5h] With this aim, we tested phosphinates bearing either a chloro- or bromo- substituent on their arene. To our delight, aryl chlorides **1o-1q** and aryl bromide **1r** underwent olefination in moderate to good (39-69%) yields with high or exclusive selectivity for their *E*- or *Z*- isomers; only traces of dehalogenated styrenes were observed (>10:1 in favor of olefination for **2p**). Compared with products **2o-2p**, *p*-chlorostilbene **2q** has a more conjugated π-system and is easier to reduce, yet still gave only traces of dechlorinated product **2a**. Substrate **1s**, bearing both an alkyl and aryl phosphinate,^[13] selectively underwent e-PRC reduction,^[13] of the alkyl phosphinate leading only to C(sp³)-O cleavage to afford **2s** in good yield. Our method retains reductively labile C(sp²)-O functionality, providing complementary selectivity to a recent report involving a phenothiazine photocatalyst.^[13]

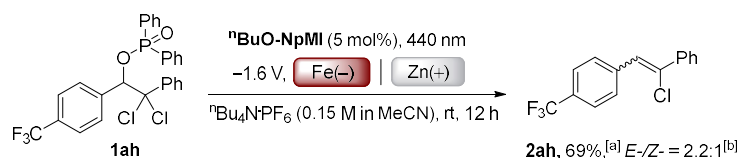
Styrene-forming substrates containing longer-chain aliphatic groups or a benzyl group retained high *E*-isomer selectivity, affording **2t-2v** in good to high (62-79%) yields and high selectivities (>10:1 in favor of their *E*-isomers). Olefin geometry is not impacted by the diastereomeric ratio of phosphinate precursors, but by the reaction conditions. For example, although the diastereomeric ratios of phosphinate precursors to **2r**, **2t** and **2v** were all >30 : 1, the *E*-/*Z*- ratios were 4:1, 10:1 and 20:1 respectively. Hindered olefins derived from carbocycles **1w-1x** were formed in high (83-87%) yields. In the synthesis of **2x**, our conditions offer an alternative to i) ⁿBuLi or Grignard chemistry with expensive bromocyclobutane and ii) expensive Wittig reagents/cyclobutanone, instead starting from commercial, inexpensive cyclobutyl phenyl ketone. Our e-PRC phosphinate reduction offers complementary selectivity to Birch-type photochemical reports involving SET,^[14] or E_nT.^[15] Naphthalene-based substrate **1y** was well-tolerated, affording **2y** in good (62%) yield without Birch-type reduction products. Amide **1z** was also well-tolerated, in spite of its free proton and labile heterocycle that would react with strong bases. Although an alkyl phosphinate derived from a non-benzylic alcohol **1aa** did not react, alkyl phosphinates derived from allylic alcohols were feasible. Allylic substrates **1ab-1ac** derived from naturally-occurring terpenes were found to be sluggish, but afforded dienes **2ab-2ac** in satisfactory (30-33%) yields in a complementary fashion to previous reports that require strong bases^[16] or transition metal catalysis.^[17]

Demonstrating the utility of our base-free approach, products **2ad-2ag** were synthesized from their alkyl *p*-acetylbenzoate precursors. Given the properties of Geraniol and Nootkatone as fragrance oils and cholesteryl benzoate as a liquid crystal, our reaction is a useful entry to terpene-loaded monomers for the synthesis of functional polymers.^[18] Strategies involving strong base - for example i) Wittig reaction of an aldehyde or ii) ketone reduction, mesylation and E₂-elimination - lead to hydrolysis or E₂ elimination of the benzoate,^[19] while direct esterification suffers from the caveats that 4-vinylbenzoic acid is thermally sensitive and formulated with BHT stabilizer. Further exemplifying utility, substrate **1ah**, readily prepared from its α -dichloroketone, underwent selective reduction to its unsymmetrical stilbene **2ah** in good yield while leaving the olefinic Cl atom untouched (Scheme 3).

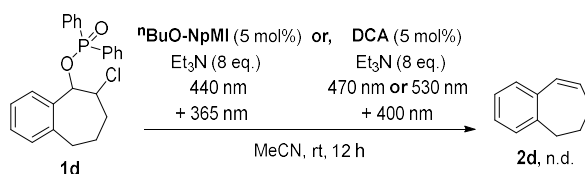


Scheme 2. *e*-PRC reductive olefination scope.^[a] for compounds **2a-2q**, **2t-2x**, **2aa-2ad**, *X* = Cl; for compounds **2r-2s**, **2y-2z**, **2ae-2ag**, *X* = Br; ^[b]Isolated yields; ^[c]*E*-*Z*- ratios determined by ¹H NMR; ^[d]Yields in parenthesis {} are ¹H NMR yields from NpMI as an *e*-PRCat.

This demonstrates the value of our method which retains reductively-labile halides for further functionalizations. The method provides alternative access to unsymmetrical halogenated stilbenes that does not rely on transition metal catalysis.^[20] While conPET photocatalysis and e-PRC are complementary approaches in the reductions of aryl halides/pseudohalides,^[3f,g] conPET conditions did not affect the net-reductive transformation herein (Scheme 4).

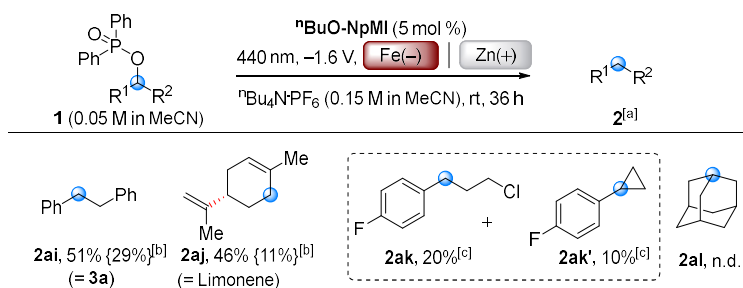


Scheme 3. e-PRC reduction of dichlorinated substrate **1ah**. ^[a]Yield of isolated product; ^[b]E-/Z- ratio was determined by ¹H NMR.



Scheme 4. Attempted reduction of **1d** under conPET conditions.

At this juncture, we wondered if overall deoxygenation would be possible by removing the α -Cl atom from **1a** (**1ai**) as the generated carbanion would be protonated. Photocatalytic deoxygenations of alcohols activated as their bis(trifluoromethyl)benzoates have been achieved with an iridium photocatalyst, but required stoichiometric Hantzsch ester, alkylamine and water at 40 °C.^[21] Direct electrolytic reduction of alkyl phosphinates is known, and required a constant current of 600 mA at 60-110 °C where a constant potential ($U_{\text{cell}} = -2.4 \text{ V vs. Ag/AgCl}$) was ineffective.^[22] Reductive functionality (styrenes, aryl halides, dienes, benzoates) would not tolerate these conditions. e-PRC deoxygenation afforded desired product **1ai** in good yield under standard conditions ($U_{\text{cell}} = -1.6 \text{ V}$) with extended time (Scheme 5). Allylic substrate **1aj** smoothly deoxygenated to **2aj** (Limonene). When a Cl atom was present β - to the phosphinate (**1ak**), deoxygenation afforded **2ak** and cyclopropane **2ak'**, confirming the intermediacy of a benzylic carbanion (see **1a''**, Scheme 1c). An alkyl phosphinate derived from non-benzylic/allylic alcohol (**1al**) did not react. We sought explanations as to two questions: 1) why e-PRC conditions herein could not engage non-benzylic substrates (**1aa** and **1al**, respectively) and 2) why ^tBuO-NpMI was a superior e-PRCat to NpMI; since NpMI as an e-PRCat gave no conversion of various substrates (**1f**, **1n**, **1o**, **1q**, **1u**) in olefinations (Scheme 2), and poor conversion of **1ai** and **1aj** in deoxygenations (Scheme 5).



Scheme 5. e-PRC reductive deoxygenation.^[a] Isolated yields of products **2ai** and **2aj**; ^[b]Yields in parenthesis {} are ¹H NMR yields from using NpMI as an e-PRCat; ^[c]Yields of **2ak** and **2ak'** are by ¹H NMR with 1,3,5-trimethoxybenzene as an internal standard, identified by literature comparisons and GC-MS traces.

Concerning the first question, measured reduction potentials ($E_{\text{red}}^{\text{p}}$) of the alkyl phosphinates - in good agreement with those calculated by DFT - did not correlate with reactivity (Table 2). Instead, comparison of the C(sp³)-O bond-dissociation free energies (BDFEs) of phosphinate radical anions correlated well with reactivity. This corroborated C(sp³)-O cleavage as the rate-limiting step and rationalized i) the unique tolerance of our conditions to aryl halides due to their less exergonic C-X BDFEs (entries 4,5; 6,7) and ii) the lack of reactivity of phosphinates derived from non-benzylic/allylic alcohols that require higher temperatures^[22] to assist C(sp³)-O cleavage (entries 9,10).

Table 2. Calculated properties of phosphinate radical anions vs. reactivity.

Entry	Radical anion	e-PRCat	Product yield (%) ^[a]	BDFE (kcal/ mol) ^[b]	$E_{\text{red}}^{\text{p}}(\text{V})$	
					$\Delta E^{\text{calc.}[c]}$	$\Delta E^{\text{exp.}[d]}$
1	1g	NpMI	78 (2g)	-39.8 (C-O)	-2.55	-2.47
2	1a	NpMI	78 (2a)	-39.2 (C-O)	-2.60	-2.23 / -2.34
3	1ai	ⁿ BuO-NpMI	51 (2ai)	-38.7 (C-O)	-2.62	ND
4	1o	ⁿ BuO-NpMI	56 (2o)	-38.1 (C-O)	-2.45	-2.60
5	1o	ⁿ BuO-NpMI	5 (de-Cl)	-26.9 (C-Cl)	-	-2.78 ^[f]
6	1r	ⁿ BuO-NpMI	39 (2r)	-38.2 (C-O)	-2.44	-2.33 / -2.46
7	1r	ⁿ BuO-NpMI	trace (de-Br)	-30.6 (C-Br)	-	-2.44 ^[f]
8	1d	ⁿ BuO-NpMI	69 (2d)	-34.5 (C-O)	-2.44	-2.41
9	1aa	ⁿ BuO-NpMI	n.d. (2aa)	-27.5 (C-O)	-2.40	-2.42
10	1al	ⁿ BuO-NpMI	n.d. (2al)	-22.1 (C-O)	-2.56	-2.68

^[a]Product yields as defined in Scheme 2; ^[b]bond dissociation free energies (ΔG) calculated at the ω B97X-D/6-311+G*, IEFPCM(ACN) theory level; ^[c]calculated at the ω B97X-D/6-311+G*, IEFPCM(ACN) theory level and calibrated to an experimental set, see experimental part; ^[d]measured at 10 mM [phosphinate] in 0.1 M ⁿBu₄N⁺PF₆⁻ in ACN using Fc as an internal standard and calibrated vs. SCE, see experimental part I; ^[f]Literature redox potentials of PhCl and PhBr are taken as surrogates.^[6]

As to the second question, NpMI and ⁿBuO-NpMI had identical redox potentials ($E_{1/2} = -1.3$ V vs. SCE, Figure 1, left) by cyclic voltammetry. Their radical anions are electrogenerated with equal efficiency, which is entirely consistent with the spin densities of their radical anions (Figure 1, right) being localized on the naphthalene and being unaffected by substitution on the *N*-aniline. Spectroelectrochemistry of both e-PRCats gave identical UV-Vis bands for their radical anions (Figure 2, left and see experimental part).

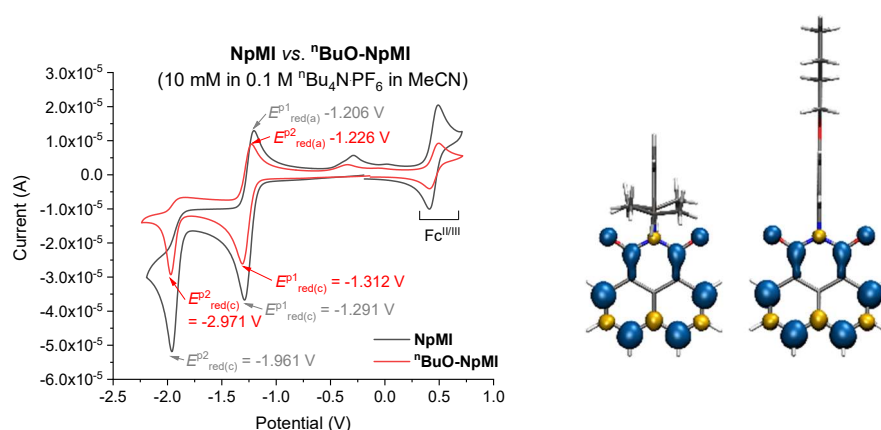


Figure 1. Cyclic voltammery of *e*-PRCats (10 mM [*e*-PRCat] in 0.1 M ⁿBu₄N·PF₆ in ACN) vs. Ag/AgCl (left). DFT calculated spin densities of NpMI^{•-} and ^tBuO-NpMI^{•-} (right), see experimental part for details.

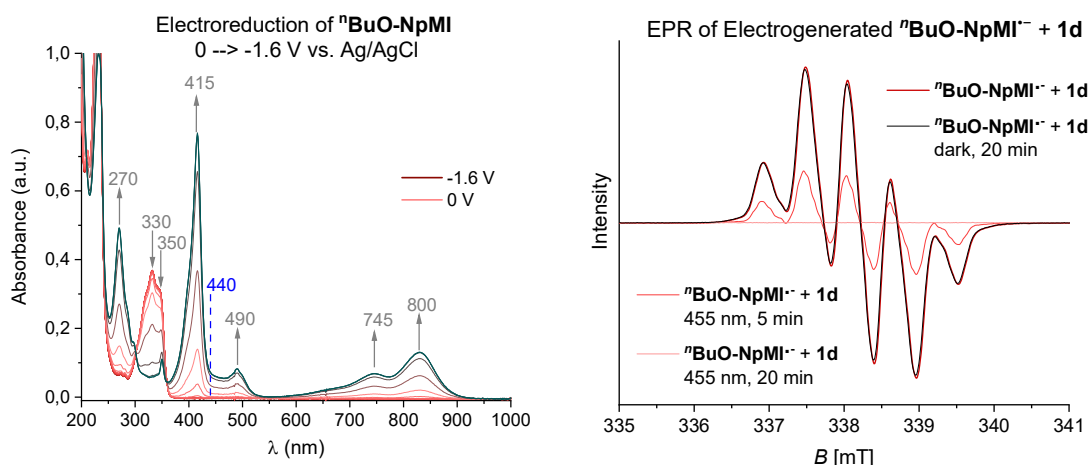


Figure 2. Spectroelectrochemistry of ^tBuO-NpMI (2.5 mM in 0.1 M ⁿBu₄N·PF₆ in ACN) from 0 to -1.6 V vs. Ag/AgCl (left). EPR spectrum of electrogenerated ^tBuO-NpMI^{•-} (2.5 mM in 0.1 M ⁿBu₄N·PF₆ in ACN at U_{cell} = -1.6 V for 1 h) in the presence of **1d** (10 eq.) and signal quenching upon light irradiation (right).

Taken together, these results indicate that their excited radical anions are equally potent reductants. To probe further, we electrochemically generated NpMI^{•-} and ^tBuO-NpMI^{•-} under inert conditions for analysis by EPR (Figure 2, right).^[23] In both cases, a pentet was observed whose intensity was unchanged upon irradiation with blue LEDs. In both cases, in the presence of **1d** (10 eq.), the EPR signal was identical in the dark (see experimental part), but upon irradiation by blue LEDs, the EPR signal quenched, corroborating successful SET from the doublet states (D_n) of both catalysts ²[NpMI^{•-}*] and ²[^tBuO-NpMI^{•-}*] to **1d**. Given that the reaction of **1d** is only successful with ^tBuO-NpMI^{•-} and taken together with the discussion of E_{red}^p and BDFEs in Table 2, this confirms SET is not the determining factor for the success of ^tBuO-NpMI^{•-}.

Neutral and electroreduced forms of NpMI and ⁿBuO-NpMI were probed by luminescence spectroscopy (Table 3). For neutral e-PRCats, absorbance and emission (fluorescence) spectra corresponded with the literature.^[24] Measured lifetimes were $\tau \approx 3.0$ ns in both cases. Although some *N*-arylnaphthalimide derivatives have ultrashort-lived singlet states, due to rapid intersystem crossing to triplet states,^[24] phosphorescence does not occur for the *N*-aryl-1,8-naphthalimides where *N*-aryl rotation becomes considerably hindered.^[24] Electroreduction for 1 h and selective excitation of the radical anions at 452 nm led to a new emission band (λ_{max} ca. 540 nm) and a longer-lived species for both NpMI^{•-} and ⁿBuO-NpMI^{•-} ($\tau = \sim 7$ and ~ 20 ns, respectively). The doublet (D₁) states of similar radical anions (naphthalene diimide radical anions, perylene diimide radical anions) are picosecond-lived and do not luminesce,^[25] and we confirmed by excitation spectra (see experimental part) that this emission was not deriving from the initially-formed excited state ²[ⁿBuO-NpMI^{•-*}] (Figure 2, left), but from a lower-lying, longer lived excited state, termed ‘ES₁’. Intersection of the longest wavelength absorption and shortest wavelength emission bands allows an estimation of E^{0-0} for photoexcited states.^[26] For these emitting excited states, estimated E^{0-0} values (E^{ES}) for both [NpMI^{•-*}] and [ⁿBuO-NpMI^{•-*}] were ($E^{\text{ES}} = 56.6$ kcal mol⁻¹) almost identical to the triplet energies (E^{T}) of *Ir^{III} photosensitizers used in olefin photoisomerisms.^[9a-c] It is therefore reasonable to propose *E*-/*Z*- photoisomerism occurs *via* energy transfer (E_nT) from ES₁. E_nT would be exergonic to *E*-stilbene and less so to *Z*-stilbene ($E^{\text{T}} = 51.0$ vs. $E^{\text{T}} = 55.5$ kcal mol⁻¹, respectively), rationalizing high *Z*-stilbene selectivity.^{[9b,c],[27]} However, the lifetime of ES₁ was unchanged in the presence of **1d** (10 eq.), confirming its catalytic inactivity in the initial SET step.

Table 3. Lifetimes of neutral and electroreduced^[a] e-PRCats.

Entry	e-PRCat	Conditions	$\lambda_{\text{max}}(\text{ex})$	$\lambda_{\text{max}}(\text{em})$	τ (ns)	E^{S/ES_1} (kcal mol ⁻¹)
1	NpMI	-	375	412	$\tau = 3.2$	(S ₁)75.4
2	NpMI	-1.6 V, 1 h ^[a]	452	535	T ₁ = 5.4 T ₂ = 21.7	(ES ₁) 56.6
3	ⁿ BuO-NpMI	-	375	412	$\tau = 3.2$	(S ₁)75.6
4	ⁿ BuO-NpMI	-1.6 V, 1 h ^[a]	452	548	T ₁ = 6.8 T ₂ = 19.5	(ES ₁) 56.6
5	ⁿ BuO-NpMI	-1.6 V, 1 h ^[a] +10 eq. 1d	452, 548		T ₁ = 8.1 T ₂ = 20.3	-

^[a]Electroreduced e-PRCat (2.5 mM in ACN (0.1 M ⁿBu₄N⁺PF₆⁻), diluted 8x.

In their study of photoexcited benzo[*ghi*]perylene monoamide (BPI) radical anions for Birch reductions, Miyake and co-workers made similar observations.^[14] They assigned the long-lived excited state as the lowest-lying quartet excited state (⁴BPI^{•-*}) arising from intersystem crossing (ISC) from the doublet state (²BPI^{•-*}). Therefore, the lowest-lying quartet state ⁴[ⁿBuO-NpMI^{•-*}] is a candidate for ES₁, which allows E_nT to be spin-conserved. However, Miyake similarly found that the putative ⁴BPI^{•-*} was not catalytically active in the Birch SET step. They hypothesized SET from a higher-lying excited doublet state ²BPI^{•-*} (D_n) in an anti-Kasha fashion. Consistent

with previously reported anti-Kasha photochemistry of doublet excited state photocatalysts,^[5a,14] excitation of the broad absorption of $^2[{}^n\text{BuO-NpMI}^{\bullet-*}]$ between 650-900 nm ($D_0 \rightarrow D_1$) with 740 nm or 850 nm LEDs gave only traces of **2d**.^[28] Ruling out participation of the first excited state (D_1), we predict ‘effective minimum’ potentials of $\text{NpMI}^{\bullet-*}$ (D_n) at -3.7 V vs. SCE and ${}^n\text{BuO-NpMI}^{\bullet-*}$ (D_n) at -3.8 V vs. SCE from the Rehm-Weller equation,^[29] easily reaching $E_{\text{red}}^{\text{p}}$ of all phosphinates herein as well as aryl halides.^{[30],[31]} Participation of a doublet excited state in SET is consistent with aforementioned quenching of the EPR signal (Figure 2). High-level DFT/MRCI calculations were carried out for ${}^n\text{BuO-NpMI}^-$ to characterize this D_n state. The computed spectrum (Figure 3, top) is in excellent agreement with the experimental absorption spectrum, especially at the band with $\lambda_{\text{max}} = 415$ nm comprising two bright $\pi\text{-}\pi^*$ states ($D_0 \rightarrow D_n$ and $D_0 \rightarrow D_{n+1}$). Contrary to the $D_0 \rightarrow D_1$ transition around 870 nm, both these excitations transfer electron density from the naphthalene to the *N*-aniline unit of ${}^n\text{BuO-NpMI}^-$ (Figure 3, bottom). Preassembly of ground state radical anion and substrate could explain (i) photochemistry of ultrashort-lived doublet states^[25] and (ii) faster than rates of diffusion.^[5a] Preassembly of ${}^n\text{BuO-NpMI}^{\bullet-}$ with **1d** being more favorable than that of $\text{NpMI}^{\bullet-}$ may explain the reactivity differences of the e-PRCats in effecting $\text{C}(\text{sp}^3)\text{-O}$ cleavage following SET, and may rationalize profound shift in the molecular site of reduction compared to previous reports.^[32] However, like Miyake and co-workers, we were unable to find spectroscopic evidence of preassembly by UV-Vis or EPR (see experimental). While the absence of spectroscopic perturbations does not rule out a preassociation,^[33] preassembly could occur at the *N*-aniline that is spin-disconnected from the naphthalene where the radical anion spin density is localized (Figure 1, right). Spin densities of favorable candidate preassemblies at the *N*-aniline unit of ${}^n\text{BuO-NpMI}^{\bullet-}$ found by computational geometry optimizations do not differ from that of ${}^n\text{BuO-NpMI}^{\bullet-}$ alone, while a favorable candidate preassembly at the naphthalene unit of ${}^n\text{BuO-NpMI}^{\bullet-}$ does differ (see experimental part). A preassembly at the *N*-aniline could also rationalize anti-Kasha photochemistry, since charge transfer to the *N*-aniline in the $D_{n/n+1}$ states is proximal to the bound substrate and promotes intermolecular SET upon photoexcitation (Figure 3). In contrast, the charge density of the lowest excited doublet state D_1 remains localized on the naphthalene and is not close to the substrate.

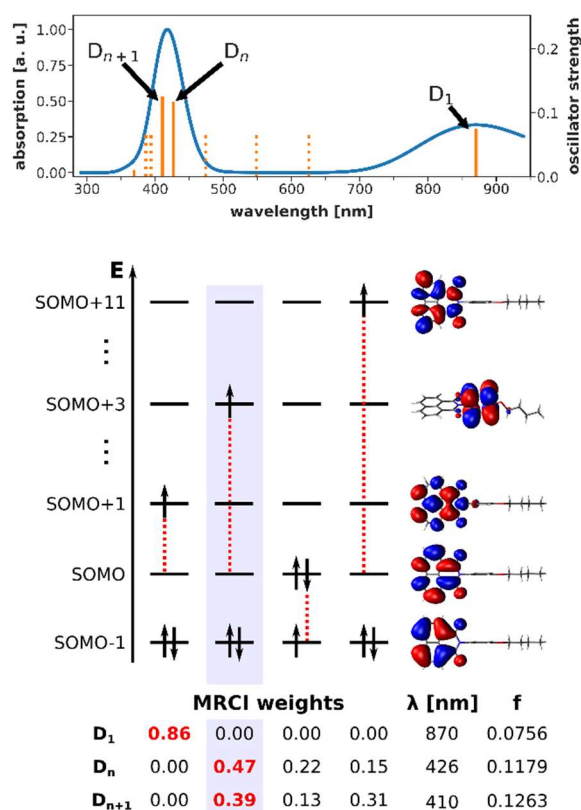
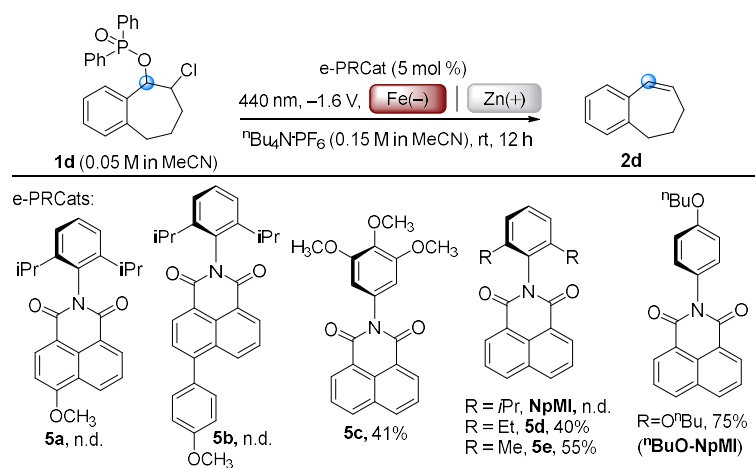


Figure 3. Calculated DFT/MRCI absorption spectrum for ${}^t\text{BuO-NpMI}^-$ (top). Dark states with oscillator strengths $f < 0.01$ are indicated by dotted orange lines. Leading electronic configurations for the bright excited states D_1 , D_n and D_{n+1} (bottom). Dotted red lines indicate single electron excitations from the ground state configuration.

Where spectroscopy offers little insight, a top-down approach varying catalyst structure and examining product yields has proven useful in investigating the mechanisms of reactions involving *in situ* formed organic electron donors.^[34] To probe the importance of a preassembly of **1d** at the *N*-aniline of the e-PRCat, we explored the influence of a series of e-PRCats with varying electronics and steric bulk (**5a-f**, Scheme 6). Compared to NpMI, catalysts with electron-donating alkoxy or *p*-aniso substituents on the naphthalene unit (**5a,5b**) gave no reaction. Compared to ${}^t\text{BuO-NpMI}$, a catalyst with additional alkoxy substituents on the *N*-aniline (**5c**) gave a lower (41%) yield of **2d**. The yield of **2d** increased with decreasing steric hindrance at the *ortho*-positions of the *N*-aniline (NpMI \ll **5d** < **5e**).^[35]

A decrease in ‘steric bulk’ likely promotes preassociation of radical anion e-PRCat and **1d**. In our computational investigations we found multiple stable ground-state preassemblies. Geometry optimizations (see experimental part) converged to pincer-like conformations for all candidates, where two of the substrate’s aryl groups coordinate to the *N*-aniline of the e-PRCat in a T- π and π - π orientation, respectively. The thermodynamics and kinetics of their formations (see experimental part) mirror reactivity trends in Scheme 6, corroborating a preassembly between e-PRCat and substrate before photoexcitation.



Scheme 6. *e*-PRC deoxygenation of **1d** with various *e*-PRCats. Yields of **2d** determined by ¹H NMR with 1,3,5-trimethoxybenzene as an internal standard.

3.4 Conclusion

In conclusion, we report an electro-mediated photoredox catalytic reduction of phosphinates derived from α -chloroketones toward selective olefinations and deoxygenations. This study reports reductive formation of alkyl carbanions *via* photoexcited radical anions as super-reductants. The selective reduction of C(sp³)-O bonds in the presence of C(sp²)-X bonds was achieved. Reactivity differences of various radical anion photocatalysts and anti-Kasha photochemistry, backed by computational insights, suggest the importance of a close catalyst-substrate interaction for an effective, selective reaction. In this context, our calculations indicate that intramolecular charge transfer in the catalyst radical anion upon photoexcitation promotes SET to the substrate. Photocatalyst-substrate preassemblies such as EDA complexes,^[36] non-covalent interactions,^[5a,37] hydrogen bonding^[38] and ordering of solvent^[39] are receiving increasing attention to unveil the next generation of photocatalytic transformations and offer new frontiers in selectivity and efficiency. Further studies into the nature of interactions and structure of preassemblies are ongoing.

3.5 References

- [1] Selected reviews on photochemistry: a) Q.-Q. Zhou, Y.-Q. Zou, L.-Q. Lu, W.-J. Xiao, *Angew. Chem. Int. Ed.* **2019**, *58*, 1586-1604; *Angew. Chem.* **2019**, *131*, 1600-1619; b) L. Marzo, S. K. Pagire, O. Reiser, B. König, *Angew. Chem. Int. Ed.* **2018**, *57*, 10034-10072; *Angew. Chem.* **2018**, *130*, 10188-10228; c) J. Xie, H. Jin, A. S. K. Hashmi, *Chem. Soc. Rev.* **2017**, *46*, 5193-5203; d) N. A. Romero, D. A. Nicewicz, *Chem. Rev.* **2016**, *116*, 10075-10166; e) C. K. Prier, D. A. Rankic, D. W. C. MacMillan, *Chem. Rev.* **2013**, *113*, 5322-5363.
- [2] Selected general reviews on electrochemistry: a) T. H. Meyer, I. Choi, C. Tian, L. Ackermann, *Chem.* **2020**, *6*, 2484-2496; b) P. Xiong, H.-C. Xu, *Acc. Chem. Res.* **2019**, *52*, 3339-3350; c) S. Tang, Y. Liu, A. Lei, *Chem.* **2018**, *4*, 27-45; d) A. Wiebe, T. Gieshoff, S. Möhle, E. Rodrigo, M. Zirbes, S. R. Waldvogel, *Angew. Chem. Int. Ed.* **2018**, *57*, 5594-5619; *Angew. Chem.* **2018**, *130*, 5694-5721; e) M. Yan, Y. Kawamata, P. S. Baran, *Chem. Rev.* **2017**, *117*, 13230-13319.
- [3] For selected representative examples, see: a) K. Targos, O. P. Williams, Z. Wickens, *J. Am. Chem. Soc.* **2021**, *143*, 4125-4132; b) D. Rombach, H.-A. Wagenknecht, *Angew. Chem. Int. Ed.* **2019**, *59*, 300-303; *Angew. Chem. Int. Ed.* **2019**, *132*, 306-310; c) J. I. Bardagi, I. Ghosh, M. Schmalzbauer, T. Ghosh, B. König, *Eur. J. Org. Chem.* **2018**, 34-40; d) M. Neumeier, D. Sampedro, M. Májek, V. A. de la Peña O'Shea, A. Jacobi von Wangelin, R. Pérez-Ruiz, *Chem. Eur. J.* **2018**, *24*, 105-108; e) L. Zeng, T. Liu, C. He, D. Shi, F. Zhang, C. Duan, *J. Am. Chem. Soc.* **2016**, *138*, 3958-3961; f) I. Ghosh, B. König, *Angew. Chem. Int. Ed.* **2016**, *55*, 7676-7679; *Angew. Chem.* **2016**, *128*, 7806-7810; g) I. Ghosh, T. Ghosh, J. I. Bardagi, B. König, *Science* **2014**, *346*, 725-728; h) H. Li, X. Tang, J. H. Pang, X. Wu, E. K. L. Yeow, J. Wu, S. Chiba, *J. Am. Chem. Soc.* **2021**, *143*, 481-487. For full reviews, see: i) F. Glaser, C. Kerzig, O. S. Wenger, *Angew. Chem. Int. Ed.* **2020**, *59*, 10266-10284; *Angew. Chem.* **2020**, *132*, 10350-10370; j) M. Schmalzbauer, M. Marcon, B. König, *Angew. Chem. Int. Ed.* **2020**, *60*, 6270-6292; *Angew. Chem.* **2020**, *133*, 6338-6363.
- [4] For a full review on the combination of photoredox catalysis and organic electrochemistry: a) J. P. Barham, B. König, *Angew. Chem. Int. Ed.* **2020**, *59*, 11732-11747; *Angew. Chem.* **2020**, *132*, 11828-11844. For highlights on this topic: b) J. Liu, L. Lu, D. Wood, S. Lin, *ACS Cent. Sci.* **2020**, *6*, 1317-1340; c) L. Capaldo, L. L. Quadri, D. Ravelli, *Angew. Chem. Int. Ed.* **2019**, *58*, 17508-17510; *Angew. Chem.* **2019**, *131*, 17670-17672; d) Y. Yu, P. Guo, J.-S. Zhong, Y. Yuan, K.-Y. Ye, *Org. Chem. Front.* **2020**, *7*, 131-135.
- [5] For recent examples on homogeneous photoelectrochemistry, see: a) S. Wu, J. Žurauskas, M. Domański, P. S. Hitzfeld, V. Butera, D. J. Scott, J. Rehbein, A. Kumar, E. Thyraug, J. Hauer, J. P. Barham, *Org. Chem. Front.* **2021**, *8*, 1132-1142; b) P. Xu, P.-Y. Chen, H.-C. Xu, *Angew. Chem. Int. Ed.* **2020**, *59*, 14275-14280; *Angew. Chem.* **2020**, *132*, 14381-14386; c) X.-L. Lai, X.-M. Shu, J. Song, H.-C. Xu, *Angew. Chem. Int. Ed.* **2020**, *59*, 10626-10632; *Angew. Chem.* **2020**, *132*, 10713-10719; d) L. Niu, C. Jiang, Y. Liang, D. Liu, F. Bu, R. Shi, H. Chen, A. D. Chowdhury, A. Lei, *J. Am. Chem. Soc.* **2020**, *142*, 17693-17702; e) Y. Qiu, A. Scheremetjew, L. H. Finger, L. Ackermann, *Chem. Eur. J.* **2020**, *26*, 3241-3246; f) N. G. W. Cowper, C. P. Chernowsky, O. P. Williams, Z. K. Wickens, *J. Am. Chem. Soc.* **2020**, *142*, 2093-2099; g) H. Huang, Z. M. Strater, T. H. Lambert, *J. Am. Chem. Soc.* **2020**, *142*, 1698-1703; h) H. Kim, H. Kim, T. H. Lambert, S. Lin, *J. Am. Chem. Soc.* **2020**, *142*, 2087-2092; i) H. Huang, T. H. Lambert, *Angew. Chem. Int. Ed.* **2020**, *59*, 658-662; *Angew. Chem.* **2020**, *132*, 668-672; j) W. Zhang, K. L. Carpenter, S. Lin, *Angew. Chem. Int. Ed.* **2020**, *59*, 409-417; *Angew. Chem.* **2020**, *132*, 417-425; k) H. Huang, Z. M. Strater, M. Rauch, J. Shee, T. J. Sisto, C. Nuckolls, T. H. Lambert, *Angew. Chem. Int. Ed.* **2019**, *58*, 13318-13322; *Angew. Chem.* **2019**, *131*, 13452-13456; l) J. H. Wang, X. B. Li, J. Li, T. Lei, H. L. Wu, X. L. Nan, C. H. Tung, L. Z. Wu, *Chem. Commun.* **2019**, *55*, 10376-10379; m) L. Zhang, L. Liardet, J. Luo, D. Ren, M. Grätzel, X. Hu, *Nat. Catal.* **2019**, *2*, 366-373; n) F. Wang, S. S. Stahl, *Angew. Chem. Int. Ed.* **2019**, *58*, 6385-6390; *Angew. Chem.* **2019**, *131*, 6451-6456; o) H. Yan, Z. W. Hou, H.-C. Xu, *Angew. Chem. Int. Ed.* **2019**, *58*, 4592-4595; *Angew. Chem.* **2019**, *131*, 4640-4643.
- [6] L. Pause, M. Robert, J.-M. Savéant, *J. Am. Chem. Soc.* **1999**, *121*, 7158-7159.
- [7] For reductions of benzyl radicals to benzyl anions by PRC: a) K. Donabauer, B. König, *Acc. Chem. Res.* **2021**, *54*, 242-252. For examples of electrochemical reports: b) W. Zhang, S. Lin, *J. Am. Chem. Soc.* **2020**, *142*, 20661-20670; c) L. Lu, J. C. Siu, Y. Lai, S. Lin, *J. Am. Chem. Soc.* **2020**, *142*, 21272-21278. For the reduction potential of a benzyl radical: d) J. Grimshaw, *Electrochemical Reactions and Mechanisms in Organic Chemistry*, Elsevier **2000**, pp. 89-157.
- [8] The alkane product likely forms via high-voltage-mediated C=C bond reduction, see: X. Liu, R. Liu, J. Qiu, X. Cheng, G. Li, *Angew. Chem. Int. Ed.* **2020**, *59*, 13962-13967; *Angew. Chem.* **2020**, *132*, 14066-14071.
- [9] For reviews on photosensitized TTET isomerizations of alkenes and their use in tandem strategies: a) J. J. Molloy, T. Morack, R. Gilmour, *Angew. Chem. Int. Ed.* **2019**, *58*, 13654-13664; *Angew. Chem.* **2019**, *131*, 13789-13800; b) S. Yakubov, J. P. Barham, *Beilstein J. Org. Chem.* **2020**, *16*, 2151-2192; c) D. C. Fabry, M. A. Ronge, M. Rueping, *Chem.-Eur. J.* **2014**, *21*, 5350-5354; d) J. J. Molloy, M. Schäfer, M. Wienhold, T. Morack, C. D. Daniliuc, R. Gilmour, *Science* **2020**, *369*, 302-306.
- [10] We found that although RVC (foam) electrodes provided a large surface area to the reaction and were superior to graphite felt, mechanical shearing oftentimes occurred. Fe plate was more robust and gave a similar yield of **2a** (see experimental part).
- [11] For reviews on electrode materials in organic electrochemistry: a) A. M. Couper, D. Pletcher, F. C. Walsh, *Chem. Rev.* **1990**, *90*, 857-865; b) D. M. Heard, A. J. J. Lennox, *Angew. Chem. Int. Ed.* **2020**, *59*, 18866-18884; *Angew. Chem.* **2020**, *132*, 19026-19044.
- [12] a) J. Iqbal, R. R. Srivastava, *J. Org. Chem.* **1992**, *57*, 2001-2007; b) H. A. Dabbagh, M. Zamani, *Appl. Catal. A.* **2011**, *404*, 141-148. A method for selective elimination to form terminal olefins was reported but requires triphosgene: *Org. Lett.* **2019**, *21*, 5611-5615.

- [13] S. Jin, H. T. Dang, G. C. Haug, R. He, V. D. Nguyen, V. T. Nguyen, H. D. Arman, K. S. Schanze, O. V. Larianov, *J. Am. Chem. Soc.* **2020**, *142*, 1603-1613.
- [14] J. P. Cole, D.-F. Chen, M. Kudisch, R. M. Pearson, C.-H. Lim, G. M. Miyake, *J. Am. Chem. Soc.* **2020**, *142*, 13573-13581.
- [15] A. Chatterjee, B. König, *Angew. Chem. Int. Ed.* **2019**, *58*, 14289-14294; *Angew. Chem.* **2019**, *131*, 14427-14432.
- [16] a) B. Harirchian, N. L. Bauld, *J. Am. Chem. Soc.* **1989**, *111*, 1826-1828; b) L. Liao, R. Guo, X. Zhao *Angew. Chem. Int. Ed.* **2017**, *56*, 3201-3205.
- [17] a) H. Lebel, M. Davi, S. Díez-González, S. P. Nolan, *J. Org. Chem.* **2007**, *72*, 144-149; b) H. Level, V. Paquet, *J. Am. Chem. Soc.* **2004**, *126*, 320-328.
- [18] a) T. Ganicz, W. Stańczyk, *Materials* **2009**, *2*, 95-128; b) G. Mishra, A. K. Srivastava, *Polym. Bull.* **2007**, *58*, 351-358; c) G. Castruita, V. García, E. Arias, I. Moggio, R. Ziolo, A. Ponce, V. González, J. E. Haley, J. L. Flikkema, T. Cooper *J. Mat. Chem.* **2012**, *22*, 3770-3780; (d) G. Misra, A. K. Srivastava, *Colloid and Polymer Science* **2008**, *286*, 445-451; K. Nilles, P. Theato, *Eur. Polym. J.* **2007**, *43*, 2901-2912.
- [19] Conversion of a *p*-acetylbenzoate to a *p*-vinylbenzoate is been reported only as a low-yielding side reaction: E. Tayama, K. Watanabe, S. Sotome, *Org. Biomol. Chem.* **2017**, *15*, 6668-6678.
- [20] For transition metal catalyzed approaches: (a) A. Minato, K. Suzuki, *J. Am. Chem. Soc.* **1987**, *109*, 1257-1258; (b) T. Iwai, T. Fujihara, J. Terao, Y. Tsuji, *J. Am. Chem. Soc.* **2009**, *131*, 6668-6669.
- [21] D. Rackl, V. Kais, P. Kreitmeier, O. Reiser, *Beilstein J. Org. Chem.* **2014**, *10*, 2157-2165.
- [22] K. Lam, I. E. Markó, *Org. Lett.* **2011**, *13*, 406-409.
- [23] For full EPR investigations on $\text{NpMI}^{\bullet-}$, see experimental part.
- [24] A. Demeter, T. Bercés, L. Biczók, V. Wintgens, P. Valat, J. Kossanyi, *J. Phys. Chem.* **1996**, *100*, 2001-2011.
- [25] a) D. Gosztola, M. P. Niemczyk, W. Svec, A. S. Lukas, M. R. Wasielewski, *J. Phys. Chem. A* **2000**, *104*, 6545-6551; b) C. Lu, M. Fujitsuka, A. Sugimoto, T. Majima, *J. Phys. Chem. C* **2016**, *120*, 12734-12741.
- [26] This can only be an estimation for measurements at rt, cryogenic measurements are required for accurate E^{0-0} determinations: F. Strieth-Kalthoff, M. J. James, M. Teders, L. Pitzer, F. Glorius, *Chem. Soc. Rev.* **2018**, *47*, 7190-7202.
- [27] SET reduction of the *E*-isomer by $^*[\text{NpMI}^{\bullet-}]$ cannot be ruled out, but redox potential differences between *E*/*Z*- isomers are deemed insufficient to provide high (>10:1) *Z*-selectivities. Literature precedent for photoisomerism by closed-shell photocatalysts favors E_nT .
- [28] See experimental part for full wavelength dependence experiments.
- [29] For a relevant example, see: C. J. Zeman IV, S. Kim, F. Zhang, K. S. Schanze, *J. Am. Chem. Soc.* **2020**, *142*, 2204-2207. Calculated by the sums of ground state redox potentials (vs. SCE) and the tail of the UV-Vis band at 490 nm ($525 \text{ nm} = 2.45 \text{ eV}$).
- [30] In Ref. 14, formation of solvated electrons is proposed. Herein, reactions take place in non-alcoholic solvents. Formation of solvated electrons cannot rationalize reactivity differences between catalysts. Substrate-catalyst preassociation could allow ultrashort lifetimes of excited doublet-state photocatalysts to be circumvented.
- [31] In Ref. 30a, an attempt to determine the lifetime of $^2[N\text{-arylnaphthalimide}^{\bullet-}]$ in ACN by transient absorption spectroscopy led to rapid bleaching, suggesting solvent redox processes.
- [32] π -stacking interactions were implicated by DFT to explain selective reduction of arenes over aliphatic esters by photoexcited neutral electron donors: E. Doni, B. Mondal, S. O'Sullivan, T. Tuttle, J. A. Murphy, *J. Am. Chem. Soc.* **2013**, *135*, 10934-10937.
- [33] Hunter and Sanders claimed that π - π stacking rarely leads to notable UV-Vis perturbations, and supported the participation of s - π interactions in favorable edge-to-face binding: C. A. Hunter, J. K. M. Sanders, *J. Am. Chem. Soc.* **1990**, *112*, 5525-5534.
- [34] a) S. Zhao, E. Doni, G. M. Anderson, R. G. Kane, S. W. MacDougall, V. M. Ironmonger, T. Tuttle, J. A. Murphy, *J. Am. Chem. Soc.* **2014**, *136*, 17818-17826; b) J. P. Barham, G. Coulthard, R. G. Kane, N. Delgado, M. P. John, J. A. Murphy, *Angew. Chem. Int. Ed.* **2016**, *55*, 4492-4496; *Angew. Chem.* **2016**, *128*, 4568-4572; c) J. P. Barham, G. Coulthard, K. J. Emery, E. Doni, F. Cumine, G. Nocera, M. P. John, L. E. A. Berlouis, T. McGuire, T. Tuttle, J. A. Murphy, *J. Am. Chem. Soc.* **2016**, *138*, 7402-7410.
- [35] When the reaction was attempted with the *N*-phenyl derivative (*N*-Ph NpMI , with no *para*- or *ortho*-substitution), no product was observed. We presume a certain degree of electron richness is required in the *N*-aniline moiety to render it sufficiently reductive in its higher order charge transfer excited state.
- [36] Selected reviews: a) C. G. S. Lima, T. de M. Lima, M. Duarte, I. D. Jurberg, M. W. Paxiã, *ACS Catal.* **2016**, *6*, 1389-1407; b) G.E. M. Crisenza, D. Mazzearella, P. Melchiorre, *J. Am. Chem. Soc.* **2020**, *142*, 5461-5476.
- [37] A. Bhattacharyya, S. De Sarkar, A. Das, *ACS Catal.* **2021**, *11*, 710-733.
- [38] Selected examples: a) N. Berg, S. Bergwinkl, P. Nuernberger, D. Horinek, R. M. Gschwind, *J. Am. Chem. Soc.* **2021**, *143*, 724-735; b) F. Burg, T. Bach, *J. Org. Chem.* **2019**, *84*, 8815-8836.
- [39] Selected examples: a) M. Giedyk, R. Narobe, S. Weiß, D. Touraud, W. Kunz, B. König, *Nat. Catal.* **2020**, *3*, 40-47; b) J. Kaur, A. Shahin, J. P. Barham, *Org. Lett.* **2021**, *23*, 2002-2006.

3.6 Experimental Part

3.6.1 General Remarks

Unless stated otherwise, reactions were carried out under an inert (N_2) atmosphere. Cryogenic conditions ($-78\text{ }^\circ\text{C}$) were achieved using dry ice/acetone baths. Temperatures of $0\text{ }^\circ\text{C}$ were obtained by means of an ice bath or ice/salt bath. ‘Room temperature’ (rt) indicates temperatures in the range of $20\text{--}25\text{ }^\circ\text{C}$. For purposes of thin layer chromatography (TLC), ALUGRAM® Xtra SIL G/UV₂₅₄ silica plates were used, with UV light ($\lambda = 254\text{ nm}$), near-UV light ($\lambda = 366\text{ nm}$) and potassium permanganate used for visualization. Purification was achieved by column chromatography using Macherey-Nagel silica gel 60 (0.063-0.2 mm) or Merck silica gel 60 (0.040-0.063 mm, 230-440 mesh). Removal of solvents (in vacuo) was achieved using Heidolph rotary evaporators or Vacuubrand high vacuum pumps. All NMR data were collected using a Bruker Avance 400 Ultrashield instrument (400 MHz, 376 MHz, 162 MHz and 101 MHz for ^1H , ^{19}F , ^{31}P and ^{13}C NMR), or a Bruker Avance 300 Ultrashield instrument (300 MHz, 282 MHz, 162 MHz and 75 MHz for ^1H , ^{19}F , ^{31}P and ^{13}C NMR) was used. ^{13}C NMR was run in ^1H -decoupled mode. Data were manipulated using MestReNova version 12.0.0. Multiplicities for coupled signals were denoted as: s = singlet, d = doublet, t = triplet, q = quartet, quint = quintet, sext = sextet, hept = heptet, dd = doublet of doublets, ddd = doublet of doublets of doublets, td = triplet of doublets, qd = quartet of doublets, m = multiplet, br. = broad, apt. = apparent. Coupling constants (J) are given in Hz and are uncorrected. Where appropriate, COSY, DEPT, HSQC and HMBC experiments were carried out to aid assignment. Infra-red measurements of electrogenerated radical anions were recorded on a Bruker Tensor 27 FT-IR Spectrophotometer (courtesy of Prof. Dr. Patrick Nürnberger’s group) as a thin film of solution between NaCl discs unless otherwise stated. Preparation of electrogenerated radical anions was done either using a MBRAUN UNIlab Plus glovebox (courtesy of Prof. Dr. Manfred Scheer’s group) or an MBRAUN UNIlab glovebox (courtesy of Prof. Dr. Robert Wolf’s group) under an N_2 atmosphere. UV-visible absorption measurements were performed either using an Otle Cell Chrono (optically transparent thin-layer electrochemical cell with a path length of 0.02 cm, see Section S12 for details on spectroelectrochemistry), or using a gastight quartz cuvette (path length of 1.0 cm), within an Agilent 8453 spectrometer unless otherwise stated. Online UV-Vis measurements were performed within the same spectrometer, using an ISMATEC ISM930C dosing pump to continuously pump the catholyte (1 mL/min) through a quartz flow cell (path length of 1.0 cm). EPR spectra of electrogenerated radical anions were measured on a Magnettech Miniscope MS 400 spectrometer (9.45 GHz) at $20\text{ }^\circ\text{C}$ (see Section S17 for EPR studies). High-resolution mass spectral analyses were carried out in EI or ESI mode on a Finnigan MAT 95, Thermo Quest Finnigan TSQ 7000, Finnigan MATSSQ 710 A or an Agilent Q-TOF 6540 UHD instrument,

masses observed are accurate to within ± 5 ppm. Melting points are uncorrected and were recorded using a Stuart melting point device up to 300 °C. All solvents and reagents were purchased from Sigma-Aldrich and used as supplied. All solvents and reagents were used as supplied or purified using standard techniques.^[1] As electrolyte in all preparative reactions and spectroscopic studies, *n*-tetrabutylammonium hexafluorophosphate ($n\text{Bu}_4\text{N}^+\text{PF}_6^-$ or 'TBAP' (98%+, TCI Chemicals)) was used as purchased (see Section S11 for cyclic voltammetry studies). Reactants and reagents were purchased at the highest commercial quality and used as received, from TCI, Sigma-Aldrich, Fischer Scientific, Fluorochem or ChemPur. All other solvents and reagents were used as supplied or purified using standard techniques.^[1]

3.6.2 Materials and Electrode Preparation

LEDs (Section S16 for characterization details):

365 nm: CCS (Creating Customer Satisfaction) Inc. (LDL-71X12UV12-365-N); 400 nm: LED Engin (LZ440UB00-00U4); 450 nm: 740 nm: LED Engin (LZ4-00R308); 850 nm: LED Engin (LZ4-00R608).

Materials:

Eluteng (12 V, 1 A) USB cooling fan (purchased from Amazon); Faber-Castell 2.0 mm 2B pencil lead (purchased from Amazon); PeakTech® 6080A digital DC power supply; Glassy Carbon Foam electrode, thickness: 6.35 mm, porosity: 96.5% (Goodfellow, Product Code: 613-422-20); Carbon felt electrode purchased from Alfa Aesar (1.27 cm, thick, 99.0%); Fe Cathode was manufactured in house from DC01 CR1 (C 0.12, P 0.045, S 0.045, Mn 0.60, Ti 0.0) by Thyssen Krupp; Cu Cathode was manufactured in house from CW021A (Cu min 99.5, Bi 0.0005, P 0.002-0.007, Pb 0.005) by Batz + Burgel oHG; Zinc Anode (for electroplating) purchased from MARAWE (part01-74-00000) (200 x 170 x 0.6 mm; Fabrication of divided H-cells was done by in-house by a glassblower. A built-in porous filter disc (\varnothing 1 cm, max. pore size 16 -40 μm) was purchased from Duran®; Set-up of divided cells for photoelectrochemical reactions followed a method previously reported^[2] and is summarized in Figure S1.



Figure S 1. Electrodes and H cell setup: Zn-electrode (left), steel-electrode (center), RVC-electrode (right).

Cathode (RVC foam) set-up: A 2B pencil lead was inserted through a septum with the help of a needle. A small square (around 7 mm x 7 mm) of carbon foam was cut from the carbon foam plate, and the pencil lead was pierced through the resulting foam cube. **Cathode (Fe) set-up:** A rectangular metal cathode (ca. 20 mm x 4 mm) was inserted into a conductive steel holder. With the help of a needle, the holder was inserted through a septum. **Anode (Zn) set-up:** A rectangular metal cathode (ca. 20 mm x 4 mm) was inserted into a conductive steel holder. With the help of a needle, the holder was inserted through a septum.

The assembled H cell, after charging with reactants, reagents and solvent and degassing *via* N₂ bubbling for 10 min, was stirred at room temperature above a water-cooled cooling block under irradiation of a 440 nm LED from beneath the cathodic chamber (Figure S2).

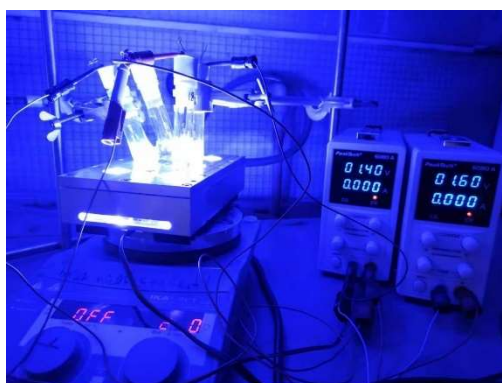


Figure S 2. Photoelectrochemical reaction setup

3.6.3 Synthesis of Catalysts

Procedure 1: ⁿBuO-NpMI and **5c-5e** were prepared according to a modified literature procedure.^[3] A mixture of 1,8-naphthalic anhydride (5.0 mmol, 1.0 eq.) and substituted aniline (10.0 mmol, 2.0 eq.) in CH₃COOH (25 mL) was charged to a pressure tube (50 mL in volume) with a stirrer bar and was heated to 120 °C. After being stirred at this temperature for 24 h, the reaction mixture was cooled down to rt and the precipitate was collected by filtration. The solid was then washed with Et₂O (5 × 5 mL) and dried under vacuum to afford the pure product as a solid.

Procedure 2: **5a** was prepared according to a modified literature procedure.^[4] A mixture of **5f** (435 mg, 1.0 mmol), sodium methoxide (432 mg, 8.0 mmol) and copper sulfate (37.5 mg, 0.15 mmol) in anhydrous methanol (5 mL) was refluxed under N₂ for 24 h. After cooling, solvent was evaporated under vacuum and the residue was dissolved in DCM (20 mL). The resulting mixture was sequentially washed by H₂O (20 mL), sat. aq. NaCl solution (20 mL), then dried over Na₂SO₄. The organic layer was evaporated under vacuum and the residue was purified by column chromatography on silica gel using a mixture of pentane and EtOAc as eluent to afford pure product **5a** in 90% yield as a light-yellow solid.

Procedure 3: **5b** was prepared according to a modified literature procedure.^[5] **5f** (435.0 mg, 1.0 mmol), 4-methoxyphenylboronic acid (304.0 mg, 2.0 mmol), Pd(PPh₃)₄ (58.0 mg, 0.05 mmol) and K₂CO₃ (690.0 mg, 5.0 mmol) were added to a mixture of toluene (12 mL), water (7 mL) and EtOH (5 mL). The resulting mixture was bubbled with N₂ for 10 min and then was heated at 90 °C for 12 h. After cooling, the organic solvents were removed under vacuum. DCM (20 mL) and H₂O (15 mL) were added to the residue. The organic layer was separated, and the aqueous layer was extracted with DCM (2 × 20 mL). The combined organic layers were dried over Na₂SO₄ and evaporated. The residue was purified by column chromatography on silica gel using a mixture of pentane and EtOAc as eluent to afford pure product **5b** in 75% yield as a yellow solid.

3.6.4 Synthesis of Phosphinate Substrates

Preparation of phosphinate **1a**.

Procedure 4: To a mixture of alcohols (3.0 mmol, 1.0 eq.) and NEt_3 (4.5 mmol, 1.5 eq.) in 20 mL anhydrous DCM was added diphenylphosphinic chloride (3.6 mmol, 1.2 eq.) dropwise followed by the addition of 4-dimethylamino pyridine (0.3 mmol, 0.1 eq.). The reaction mixture was stirred at rt overnight. The solvent was then removed under vacuum and the residue was purified by flash column chromatography using a mixture of pentane and EtOAc to give the desired phosphinates.

One-pot synthesis of phosphinates from α -halogenated ketones **1''**.

α -Halogenated ketones **1m''**, **1r''-1s''**, **1y''-1z''** are commercially available. Others were easily prepared using NXS (X = Cl or Br) according to literature procedures.^[6]

Procedure 5: At 0 °C, to a solution of α -halogenated ketone (3.0 mmol, 1.0 eq.) in 20 mL MeOH was added NaBH_4 (57.0 mg, 0.5 eq.) in 2 portions. The reaction mixture was stirred at 0 °C for 10 min and at room temperature for 2 h. Solvent was removed under vacuum and 10 mL H_2O was added to the residue. The resulting mixture was then extracted with DCM (3 \times 10 mL). The organic layers were dried over Na_2SO_4 and evaporated. At 0 °C, the residue was treated with 20 mL anhydrous DCM, NEt_3 (4.5 mmol, 1.5 eq.), diphenylphosphinic chloride (3.6 mmol, 1.2 eq.) and 4-dimethylamino pyridine (0.3 mmol, 0.1 eq.). The reaction mixture was stirred at room temperature overnight. Solvent was removed under vacuum and the residue was purified by flash column chromatography using a mixture of pentane and EtOAc to give the desired phosphinates.

Preparation of adamantane-based phosphinate **1al**.

Procedure 6: Prepared according to a literature procedure.^[6] At 0 °C, $n\text{BuLi}$ (1.6 M in hexane, 5.5 mmol, 1.1 eq.) was added dropwise to a solution of alcohol (5.0 mmol, 1.0 eq.) in 20 mL anhydrous THF under N_2 atmosphere. The resulting mixture was stirred at 0 °C for 30 min, followed by the addition of diphenylphosphinic chloride (6.0 mmol, 1.2 eq.) was added dropwise. Stirring continued for 1 h at 0 °C and then the reaction was allowed to warm to rt and stirred for 12 h. Afterwards, the mixture was quenched by sat. aq. NH_4Cl (10 mL). THF was removed under reduced pressure and the resulting mixture was extracted with DCM (3 \times 10 mL). The combined organic layers were washed with water, dried over anhydrous sodium sulfate and the solvent was evaporated under reduced pressure. The residue was purified by column chromatography on silica gel using a mixture of pentane and EtOAc as eluent to afford pure product **1al** as a white solid.

One-pot preparation of phosphinates from α -chloro ketones.

Procedure 7: At 0 °C, PhMgBr (1.0 M in THF, 5.5 mmol, 1.1 eq.) was added dropwise to a solution of α -chloro ketone (5.0 mmol, 1 eq.) in 20 mL anhydrous THF under N₂ atmosphere. The resulting mixture was stirred at 0 °C for 1 h, followed by the addition of diphenylphosphinic chloride (6.0 mmol, 1.2 eq.). Stirring continued for 1 h at 0 °C and then for 12 h at room temperature. Afterwards, the mixture was quenched by sat. aq. NH₄Cl (10 mL). THF was removed under reduced pressure and the resulting mixture was extracted with DCM (3 × 10 mL). The combined organic layers were washed with water, dried over anhydrous sodium sulfate and the solvent was evaporated under reduced pressure. The residue was purified by column chromatography on silica gel using a mixture of pentane and EtOAc as eluent.

One-pot preparation of phosphinate **1aa** from epichlorohydrin.

Procedure 8: At 0 °C, to a solution of PhMgBr (6.0 mmol in 20 mL anhydrous THF, 1.2 eq.) was added dropwise epichlorohydrin (5.0 mmol, 1 eq.) under N₂ atmosphere. The resulting mixture was stirred at 0 °C for 1 h, followed by the addition of diphenylphosphinic chloride (7.5 mmol, 1.5 eq.). Stirring continued for 1 h at 0 °C and then for 12 h at room temperature. The mixture was then quenched by sat. aq. NH₄Cl (10 mL). THF was removed under reduced pressure and the resulting mixture was extracted with DCM (3 × 10 mL). The combined organic layers were washed with water, dried over anhydrous sodium sulfate and the solvent was evaporated under reduced pressure. The residue was purified by column chromatography on silica gel using a mixture of pentane and EtOAc as eluent to afford product **1aa** as a white solid.

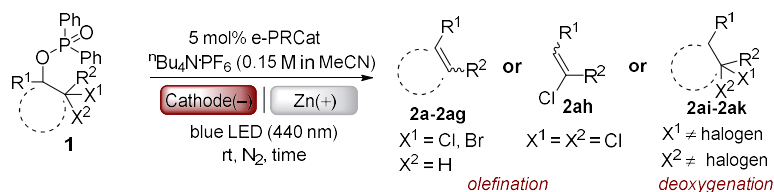
One-pot preparation of phosphinates **1ab-1ac** from chloriodomethane.

Procedure 9: At -78 °C, to a mixture of chloriodomethane (5.0 mmol, 1 eq.) and aldehyde (5.0 mmol, 1 eq) in 20 mL anhydrous THF was added dropwise ⁿBuLi (1.6 M in hexane, 5.0 mmol, 1.0 eq) under N₂ atmosphere. The resulting mixture was stirred at -78 °C for 30 min and then was allowed to warm to 0 °C for 1 h, followed by the addition of diphenylphosphinic chloride (6.0 mmol, 1.2 eq). Stirring continued for 1 h at 0 °C and then for 12 h at room temperature. The mixture was then quenched by sat. aq. NH₄Cl (10 mL). THF was removed under reduced pressure and the resulting mixture was extracted with DCM (3 × 10 mL). The combined organic layer was washed with water, dried over anhydrous sodium sulfate and the solvent was evaporated under reduced pressure. The residue was purified by column chromatography on silica gel using a mixture of pentane and EtOAc as eluent to afford the desired product.

Procedure 10: At 0 °C, to a stirred mixture of diol (10.0 mmol, 1.0 eq.) and NEt₃ (22.0 mmol, 2.2 eq.) in 50 mL anhydrous DCM was added dropwise phenylphosphonic dichloride (11.0 mmol, 1.1 eq.) under N₂ atmosphere. The resulting mixture was stirred at 0 °C for 10 min and then at room temperature for 12 h. The reaction mixture was washed with water (1 × 40 mL) and sat. aq.

NaCl solution (1 × 40 mL), dried over anhydrous sodium sulfate. Solvent was evaporated under reduced pressure. The residue was purified by column chromatography on silica gel using a mixture of pentane and EtOAc as eluent to afford the desired product **3a** as a white solid.

Procedure 11: Electrochemically-mediated Photoredox Catalyzed Phosphinate Reductions



An oven-dried *H*-Cell was equipped with magnetic stirring bars in both chambers. To the cathodic chamber was added substrate **1** (0.2 mmol) and e-PRC catalyst (0.01 mmol), followed by the additions of $t\text{Bu}_4\text{N}^+\text{PF}_6^-$ (232.0 mg) and 4 mL ACN in both chambers (resulting in 0.15 M $t\text{Bu}_4\text{N}^+\text{PF}_6^-$ in ACN as solvent). Both chambers were sealed using rubber septa pierced with wire-connected electrodes then bubbled with N_2 for 10 min. The resulting mixture was stirred at room temperature above a water-cooled cooling block under irradiation of 440 nm LED from beneath the anodic chamber (Figure S2). A constant potential of -1.6 V was applied across the cell. After the specified reaction time, the mixtures in both chambers were transferred into a flask and each chamber was washed with DCM (3 × 4 mL), the combined organics were evaporated under vacuum. After addition of Et_2O (20 mL) to the residue, $t\text{Bu}_4\text{N}^+\text{PF}_6^-$ was precipitated and removed by filtration. The filtrate was concentrated under vacuum and the residue was purified by column chromatography on silica gel using pentane or a mixture of pentane and EtOAc as eluent to afford pure product **2**.

3.6.5 Optimization of Reaction Conditions

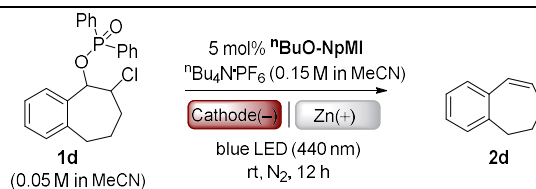
Table S 1. Optimization of light wavelength.



Entry	Wavelength / nm	NMR yield of 2d ^a
1	400	6%
2	440	75%
3	528	trace
4	740	trace
5	850	trace

^a Determined by ¹H NMR of the crude product using 1,3,5-trimethoxybenzene as an internal standard.

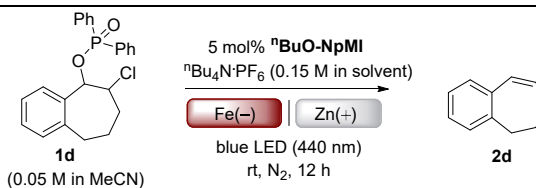
Table S 2. Optimization of cathodic material.



Entry	Cathode	NMR yield of 2d ^a
1	RVC foam	trace
2	Carbon felt	trace
3	Cu	20%
4	Fe	75%

^a Determined by ¹H NMR of the crude product using 1,3,5-trimethoxybenzene as an internal standard.

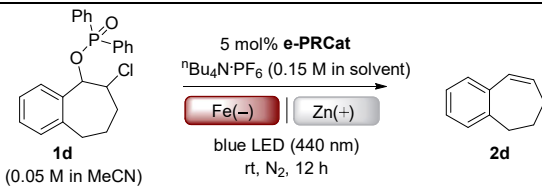
Table S 3. Optimization of solvent.



Entry	Solvent	NMR yield of 2d ^a
1	ACN	75%
2	DCM	n.d.

^a Determined by ¹H NMR of the crude product using 1,3,5-trimethoxybenzene as an internal standard. n.d., not detected.

Table S 4. Optimization of catalyst.



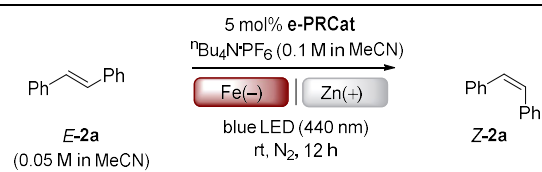
Entry	e-PRCat	NMR yield of 2d ^a
1	NpMI	n.d.
2	ⁿ BuO-NpMI	75%
3	5a	n.d.
4	5b	n.d.
5	5c	41%
6	5d	40%
7	5e	55%

^a Determined by ¹H NMR of the crude product using 1,3,5-trimethoxybenzene as an internal standard. n.d., not detected.

3.6.6 Photoelectrochemical Isomerism Control Experiments

In order to confirm the photoelectrochemical nature of the stilbene isomerism reaction, we subjected commercially available *E*-**2a** to the reaction conditions (Table S5). DCA as a catalyst gave no isomerism (entry 1), while NpMI gave isomerism marginally favoring *Z*-**2a** (entry 2). Upon extending the reaction time of this reaction, a 1:10 ratio of *E*-**2a** : *Z*-**2a** was achieved. The absence of light gave no isomerism (entry 3), while absence of potential gave marginal isomerism (entry 4). The triplet energy of ³[NpMI]* estimated from the UV-Vis absorption if NpMI and its steady-state emission spectra (75.4 kcal mol⁻¹), is higher than *E*-**2a** (51.0 kcal mol⁻¹)^[8] and *Z*-**2a** (55.5 kcal mol⁻¹)^[8]. Therefore triplet-triplet energy transfer (TTET) is highly exergonic in both cases and this may lead to less discrimination between the isomers. Moreover, the lifetime of ³[NpMI]* is only 3 ns. Interestingly, isomerism occurs in the absence of e-PRCat, marginally favoring *Z*-**2a** (entry 5). However, the ratio did not improve in favor of *Z*-**2a** upon running these conditions for a longer time and rather seemed to erode the selectivity (entry 6), in contrast to the enhancing effect of extending reaction time in the presence of NpMI (entry 3). The mechanism by which this catalyst-free photoelectrochemical isomerism occurs is currently elusive, but the addition of DCA catalyst clearly inhibits this mechanism (entry 1) and the reaction requires applied potential (entries 7-8). ⁿBuO-NpMI as an e-PRCat (entry 9) gave a similar result to NpMI (entry 3). Finally, a reaction was performed using 365 nm (entry 5). While this gave some isomerism, similar to entry 5, selectivity for the *Z*-isomer was lower than when 440 nm light was used.

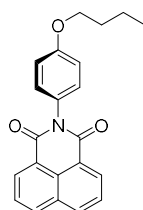
Table S 5. Photoelectrochemical isomerism.



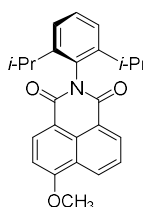
Entry	e-PRCat	λ (nm)	Electrolyte	Potential (V)	Time (h)	E-/Z- Ratio ^a	
						E-2a	Z-2a
1	DCA	440	ⁿ Bu ₄ N·PF ₆	-	10	100	n.d.
2	NpMI	440	ⁿ Bu ₄ N·PF ₆	-1.6	10	35	65
3	NpMI	440	ⁿ Bu ₄ N·PF ₆	-1.6	36	9	91
3	NpMI	-	ⁿ Bu ₄ N·PF ₆	-1.6	10	100	n.d.
4	NpMI	440	ⁿ Bu ₄ N·PF ₆	-	10	71	29
5	-	440	ⁿ Bu ₄ N·PF ₆	-1.6	10	33	67
6	-	440	ⁿ Bu ₄ N·PF ₆	-1.6	36	40	60
7	-	440	ⁿ Bu ₄ N·PF ₆	-	10	97	3
8	-	440	-	-	10	96	4
9	ⁿ BuO-NpMI	440	ⁿ Bu ₄ N·PF ₆	-1.6	36	12	88

^aE-/Z- Ratio was determined by ¹H NMR of the crude product

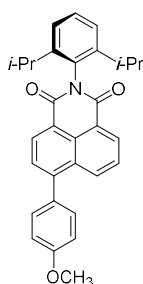
3.6.7 Characterization of Catalysts

**2-(4-butoxyphenyl)-1H-benzo[de]isoquinoline-1,3(2H)-dione (nBuO-NpMI):**

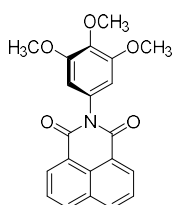
According to General Procedure 1. Yield: 1.54 g, 89%; light grey solid, m.p. 191 °C; $^1\text{H NMR}$ (400 MHz, CDCl_3) δ 8.70 (dd, $J = 0.8, 7.2$ Hz, 2H), 8.31 (dd, $J = 0.8, 8.4$ Hz, 2H), 7.87-7.80 (m, 2H), 7.30-7.24 (m, 2H), 7.12-7.08 (m, 2H), 4.08 (t, $J = 6.4$ Hz, 2H), 1.90-1.82 (m, 2H), 1.63-1.52 (m, 2H), 1.05 (t, $J = 7.2$ Hz, 3H) ppm; $^{13}\text{C NMR}$ (100 MHz, CDCl_3) δ 164.6, 159.2, 134.2, 131.8, 131.6, 129.5, 128.5, 127.7, 127.0, 122.9, 115.3, 67.9, 31.3, 19.3, 13.9 ppm; HRMS (ESI) (m/z) $[\text{M}+\text{H}]^+$ $\text{C}_{22}\text{H}_{20}\text{NO}_3$ calcd. for 346.1438, found 346.1443.

**2-(2,6-diisopropylphenyl)-6-methoxy-1H-benzo[de]isoquinoline - 1,3(2H)-**

dione (5a): According to Procedure 2. Yield: 348 mg, 90%; light yellow solid, m.p. 253-255 °C; $^1\text{H NMR}$ (400 MHz, CDCl_3) δ 8.70-8.61 (m, 3H), 7.79-7.73 (m, 1H), 7.49-7.43 (m, 1H), 7.33 (d, $J = 7.6$ Hz, 2H), 7.10 (d, $J = 8.0$ Hz, 1H), 4.16 (s, 3H), 2.76 (hept, $J = 6.4$ Hz, 2H), 1.16 (dd, $J = 6.8, 1.2$ Hz, 12H) ppm; $^{13}\text{C NMR}$ (100 MHz, CDCl_3) δ 164.6, 164.0, 161.1, 145.8, 134.0, 132.1, 131.2, 130.1, 129.4, 129.0, 126.1, 124.0, 123.8, 122.6, 115.2, 105.3, 56.4, 29.1, 24.0 ppm; HRMS (ESI) (m/z) $[\text{M}+\text{H}]^+$ $\text{C}_{25}\text{H}_{26}\text{NO}_3$ calcd. for 388.1907, found 388.1914.

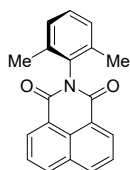
**2-(2,6-diisopropylphenyl)-6-(4-methoxyphenyl)-1H - benzo[de]isoquinoline-**

1,3(2H)-dione (5b): According to Procedure 3. Yield: 347 g, 75%; yellow solid, m.p. 216-217 °C; $^1\text{H NMR}$ (400 MHz, CDCl_3) δ 8.48 (d, $J = 7.6$ Hz, 2H), 8.17 (d, $J = 8.4$ Hz, 1H), 7.57-7.48 (m, 2H), 7.30-7.22 (m, 3H), 7.12 (d, $J = 7.6$ Hz, 2H), 6.89 (d, $J = 8.4$ Hz, 2H), 3.71 (s, 3H), 2.56 (hept, $J = 6.4$ Hz, 2H), 0.95 (d, $J = 6.4, 12\text{H}$) ppm; $^{13}\text{C NMR}$ (100 MHz, CDCl_3) δ 164.4, 164.2, 160.0, 147.1, 145.7, 133.1, 131.7, 131.4, 131.2 (one carbon was overlapped), 130.9, 130.5, 129.50, 129.45, 127.9, 126.8, 124.0, 123.0, 121.4, 114.3, 55.5, 29.2, 24.0 ppm; HRMS (ESI) (m/z) $[\text{M}+\text{H}]^+$ $\text{C}_{31}\text{H}_{30}\text{NO}_3$ calcd. for 464.2220, found 464.2224.

**2-(3,4,5-trimethoxyphenyl)-1H-benzo[de]isoquinoline-1,3(2H)-dione (5c):**

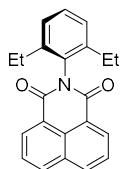
According to Procedure 1. Yield: 1.55 g, 85%; grey solid, m.p. > 300°C; $^1\text{H NMR}$ (400 MHz, CDCl_3) δ 8.66 (dd, $J = 7.2, 0.8$ Hz, 2H), 8.28 (dd, $J = 8.0, 0.8$ Hz, 2H), 7.80 (dd, $J = 8.0, 7.6$ Hz, 2H), 6.55 (s, 2H), 3.92 (s, 3H), 3.86 (s, 6H) ppm; $^{13}\text{C NMR}$ (100 MHz, CDCl_3) δ 164.5, 153.9, 138.1, 134.4, 131.8, 131.7,

131.1, 128.5, 127.1, 122.8, 105.9, 60.9, 56.1 ppm; **HRMS (ESI) (m/z)** $[M+H]^+$ $C_{21}H_{18}NO_5$ calcd. for 364.1179, found 364.1183. Data are consistent with the literature.^[9]



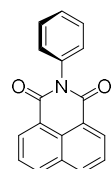
2-(2,6-dimethylphenyl)-1H-benzo[de]isoquinoline-1,3(2H)-dione (5d):

According to **Procedure 1**. Yield: 1.16 g, 77%; light brown solid, m.p. 227-229 °C; **1H NMR (400 MHz, $CDCl_3$)** δ 8.68 (dd, $J = 7.2, 0.8$ Hz, 2H), 8.30 (dd, $J = 8.4, 0.8$ Hz, 2H) ppm, 7.81 (dd, $J = 8.0, 7.2$ Hz, 2H), 7.32-7.27 (m, 1H), 7.25-7.21 (m, 2H), 2.16 (s, 6H) ppm; **^{13}C NMR (100 MHz, $CDCl_3$)** δ 163.5, 135.6, 134.4, 134.0, 131.9, 131.7, 128.9, 128.8, 128.6, 127.1, 122.8, 17.9 ppm; **HRMS (ESI) (m/z)** $[M+H]^+$ $C_{20}H_{16}NO_2$ calcd. for 302.1176, found 302.1182.



2-(2,6-diethylphenyl)-1H-benzo[de]isoquinoline-1,3(2H)-dione (5e):

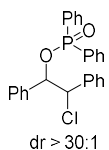
According to **Procedure 1**. Yield: 1.17 g, 71%; light brown solid, m.p. 225-226 °C; **1H NMR (400 MHz, $CDCl_3$)** δ 8.67 (dd, $J = 7.2, 0.8$ Hz, 2H), 8.30 (dd, $J = 8.4, 0.8$ Hz, 2H), 7.82 (dd, $J = 8.0, 7.2$ Hz, 2H), 7.42 (t, $J = 7.6$ Hz, 1H), 7.29 (d, $J = 7.6$ Hz, 2H), 2.48 (q, $J = 7.6$ Hz, 4H), 1.15 (t, $J = 7.6$ Hz, 6H) ppm; **^{13}C NMR (100 MHz, $CDCl_3$)** δ 164.1, 140.9, 134.3, 132.8, 131.9, 131.7, 129.2, 128.9, 127.1, 126.5, 122.8, 24.3, 14.0 ppm; **HRMS (ESI) (m/z)** $[M+H]^+$ $C_{22}H_{20}NO_2$ calcd. for 330.1489, found 330.1491. Data are consistent with the literature.^[10]



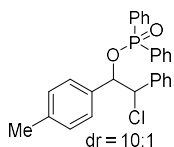
2-phenyl-1H-benzo[de]isoquinoline-1,3(2H)-dione (N-Ph NpMI):

According to **Procedure 1**. Yield: 821 mg, 60%; pale brown solid, m.p. 199 °C; **1H NMR (400 MHz, $CDCl_3$)** δ 8.65 (dd, $J = 0.8, 7.2$ Hz, 2H), 8.31 (dd, $J = 0.8, 8.4$ Hz, 2H), 7.82-7.75 (m, 2H), 7.59-7.53 (m, 2H), 7.52-7.46 (m, 1H), 7.36-7.30 (m, 2H) ppm; **^{13}C NMR (100 MHz, $CDCl_3$)** δ 164.5, 135.6, 134.4, 131.9, 131.7, 129.5, 128.82, 128.76, 128.66, 127.2, 123.0 ppm. 1H and ^{13}C data are consistent with the literature: H. J. Kim, J. Kim, S. H. Cho, S. Chang, *J. Am. Chem. Soc.* **2011**, *133*, 16382–16385.

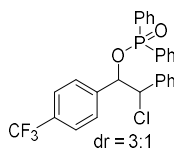
3.6.8 Characterization of Phosphinate Substrates



2-chloro-1,2-diphenylethyl diphenylphosphinate (1a): According to **Procedure 5**. Yield: 926.0 mg, 71%; dr > 30:1; white solid, m.p. 164-165 °C; $^1\text{H NMR}$ (400 MHz, CDCl_3) δ 7.50-7.39 (m, 5H), 7.35-7.23 (m, 8H), 7.22-7.11 (m, 7H), 5.70 (dd, $J = 9.2$, 6.8 Hz, 1H), 5.25 (d, $J = 6.8$ Hz, 1H) ppm; $^{13}\text{C NMR}$ (100 MHz, CDCl_3) δ 137.4, 136.3 (d, $J_{\text{C-P}} = 2.1$ Hz), 132.1 (d, $J_{\text{C-P}} = 2.7$ Hz), 132.0 (d, $J_{\text{C-P}} = 2.8$ Hz), 131.7 (d, $J_{\text{C-P}} = 10.4$ Hz), 131.44 (d, $J_{\text{C-P}} = 10.5$ Hz), 131.40 (d, $J_{\text{C-P}} = 137.6$ Hz), 131.0 (d, $J_{\text{C-P}} = 133.0$ Hz), 128.7, 128.6, 128.4, 128.3 (d, $J_{\text{C-P}} = 13.4$ Hz), 128.13, 128.09 (d, $J_{\text{C-P}} = 13.2$ Hz), 127.8, 80.1 (d, $J_{\text{C-P}} = 5.7$ Hz), 65.6 (d, $J_{\text{C-P}} = 6.6$ Hz) ppm; $^{31}\text{P NMR}$ (162 MHz, CDCl_3) δ 33.6 ppm; **HRMS (ESI)** (m/z) $[\text{M}+\text{H}]^+$ $\text{C}_{26}\text{H}_{23}^{35}\text{ClO}_2\text{P}$ calcd. for 433.1119, found 433.1122. Data are consistent with the literature^[11]

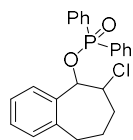


2-chloro-2-phenyl-1-(p-tolyl)ethyl diphenylphosphinate (1b): According to **Procedure 5**. Yield: 1.10 g, 82%; two diastereomers, dr = 10:1; white solid, m.p. 127-128 °C; $^1\text{H NMR}$ (400 MHz, CDCl_3) δ 7.92-7.76 (m, 2H), 7.62-7.42 (m, 5H), 7.39-7.33 (m, 1H), 7.27-7.17 (m, 3H), 7.14-7.03 (m, 3H), 7.02-6.93 (m, 5H), 5.76-5.72 (m, 0.1H, the minor isomer), 5.70-5.63 (m, 0.9H, the major isomer), 5.35-5.28 (m, 0.9H, the major isomer), 5.28-5.23 (m, 0.1H, the minor isomer), 2.28 (s, 0.27H, the minor isomer), 2.24 (s, 2.71H, the major isomer) ppm; $^{13}\text{C NMR}$ (100 MHz, CDCl_3) (not possible to assign every peak) δ 138.31, 136.22, 136.20, 133.60, 132.24, 132.22, 131.99, 131.96, 131.85, 131.79, 131.69, 128.77, 128.52, 128.48, 128.45, 128.39, 128.20, 128.17, 128.07, 127.94, 127.80, 80.74, 80.68, 77.46, 77.14, 76.82, 65.78, 65.72, 21.17 ppm; $^{31}\text{P NMR}$ (162 MHz, CDCl_3) δ 33.6 (0.1P, the minor isomer), 33.3 (0.9P, the major isomer) ppm; **HRMS (ESI)** (m/z) $[\text{M}+\text{H}]^+$ $\text{C}_{27}\text{H}_{25}^{35}\text{ClO}_2\text{P}$ calcd. for 447.1275, found 447.1281.



2,2-dichloro-2-phenyl-1-(4-(trifluoromethyl)phenyl)ethyl diphenyl phosphinate (1c) According to **Procedure 5**. Yield: 1.06 g, 65%; two diastereomers, dr = 3:1, white solid, m.p. 108-110 °C; $^1\text{H NMR}$ (400 MHz, CDCl_3) δ 7.88-7.57 (m, 4H), 7.55-7.30 (m, 7H), 7.29-6.98 (m, 8H), 5.83 (dd, $J = 9.2$, 6.8 Hz, 0.25H, the minor isomer), 5.71 (dd, $J = 9.2$, 6.8 Hz, 0.75H, the major isomer), 5.46 (d, $J = 6.8$ Hz, 0.75H, the major isomer), 5.33 (d, $J = 6.8$ Hz, 0.25H, the minor isomer) ppm; $^{13}\text{C NMR}$ (100 MHz, CDCl_3) (not possible to assign every peak) δ 141.39, 140.29, 136.05, 135.33, 135.30, 132.40, 132.38, 132.26, 132.23, 132.20, 132.17, 132.10, 132.06, 131.92, 131.82, 131.68, 131.57, 131.46, 131.34, 131.26, 131.16, 130.71, 130.38, 130.01, 129.19, 129.01, 128.98, 128.80, 128.61, 128.47, 128.39, 128.32, 128.26, 128.21, 128.19, 128.08, 128.03, 127.91, 127.83, 125.33, 125.29, 125.19, 124.93, 124.89, 124.86, 124.82, 122.49, 80.17, 80.11, 79.74, 79.69, 64.45, 64.40 ppm;

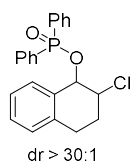
³¹P NMR (162 MHz, CDCl₃) δ 34.4 (0.33P, the minor isomer), 34.0 (1P, the major isomer) ppm; **¹⁹F NMR (377 MHz, CDCl₃)** δ -63.1 (0.33F, the minor isomer), -63.2 (1F, the minor isomer) ppm; **HRMS (ESI) (*m/z*)** [M+H]⁺ C₂₇H₂₂³⁵ClF₃O₂P calcd. for 501.0993, found 501.0998.



dr = 20:1

6-chloro-6,7,8,9-tetrahydro-5H-benzo[7]annulen-5-yl diphenylphosphinate (1d):

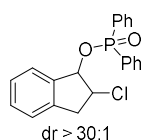
According to **Procedure 5**. Yield: 1.01 g, 85%; two diastereomers, dr = 20:1; white solid, m.p. 118-119 °C; **¹H NMR (400 MHz, CDCl₃)** δ 7.75-7.63 (m, 2H), 7.52-7.38 (m, 2H), 7.37-7.30 (m, 1H), 7.30-7.23 (m, 2H), 7.22-7.15 (m, 1H), 7.13-6.98 (m, 3H), 6.96-6.86 (m, 2H), 6.82-6.75 (m, 1H), 5.60 (d, *J* = 8.4 Hz, 1H), 4.53-4.05 (m, 1H), 2.94-2.64 (m, 1H), 2.45-2.33 (m, 1H), 2.32-2.15 (m, 1H), 2.13-2.00 (m, 1H), 1.75-1.54 (m, 1H), 1.49-1.29 (m, 1H) ppm; **¹³C NMR (100 MHz, CDCl₃)** (not possible to assign every peak) δ 135.70, 132.52, 132.33, 132.30, 132.07, 131.98, 131.88, 131.72, 131.70, 131.61, 131.60, 131.44, 131.34, 131.14, 130.63, 129.86, 129.75, 128.69, 128.62, 128.49, 128.36, 128.22, 126.23, 81.18, 79.11, 77.47, 77.15, 76.83, 63.19, 36.55, 34.86 ppm; **³¹P NMR (162 MHz, CDCl₃)** δ 33.4 (1P, the major isomer), 31.9 (0.05P, the minor isomer) ppm; **HRMS (ESI) (*m/z*)** [M+H]⁺ C₂₃H₂₃³⁵ClO₂P calcd. for 397.1119, found 397.1123.



dr > 30:1

2-chloro-1,2,3,4-tetrahydronaphthalen-1-yl diphenylphosphinate (1e):

According to **Procedure 5**. Yield: 982.0 mg, 81%; dr > 30/1; white solid, m.p. 149-151 °C; **¹H NMR (400 MHz, CDCl₃)** δ 7.80-7.66 (m, 2H), 7.64-7.53 (m, 2H), 7.36-7.22 (m, 4H), 7.22-7.12 (m, 3H), 7.01-6.93 (m, 1H), 6.92-6.82 (m, 2H), 5.54 (d, *J* = 6.0 Hz, 1H), 4.31-4.18 (m, 1H), 3.03-2.87 (m, 1H), 2.69-2.54 (m, 1H), 2.26-2.12 (m, 1H), 2.04-1.93 (m, 1H) ppm; **¹³C NMR (100 MHz, CDCl₃)** δ 135.2, 132.9 (d, *J*_{C-P} = 3.7 Hz), 132.03 (d, *J*_{C-P} = 136.2 Hz), 131.93 (d, *J*_{C-P} = 137.6 Hz), 132.24 (d, *J*_{C-P} = 13.0 Hz), 132.22 (d, *J*_{C-P} = 12.9 Hz), 131.89 (d, *J*_{C-P} = 10.6 Hz), 131.77 (d, *J*_{C-P} = 10.3 Hz), 129.1, 128.55, 128.52, 128.41, 128.38, 126.3, 73.6 (d, *J*_{C-P} = 5.7 Hz), 59.3 (d, *J*_{C-P} = 2.7 Hz), 27.9, 26.1 ppm; **³¹P NMR (162 MHz, CDCl₃)** δ 33.4 ppm; **HRMS (ESI) (*m/z*)** [M+H]⁺ C₂₂H₂₀³⁵ClNaO₂P calcd. for 405.0782, found 405.0779.

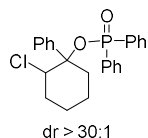


dr > 30:1

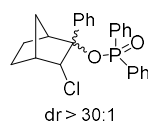
2-chloro-2,3-dihydro-1H-inden-1-yl diphenylphosphinate (1f):

According to **Procedure 5**. Yield: 883.0 mg, 80%; dr > 30:1; white solid, m.p. 102-105 °C; **¹H NMR (400 MHz, CDCl₃)** δ 8.02-7.91 (m, 2H), 7.90-7.81 (m, 2H), 7.57-7.40 (m, 6H), 7.37 (d, *J* = 7.6 Hz, 1H), 7.31-7.26 (m, 1H), 7.24-7.16 (m, 2H), 5.80 (dd, *J* = 8.8, 5.2 Hz, 1H), 4.64-4.58 (m, 1H), 3.32 (d, *J* = 5.2 Hz, 2H) ppm; **¹³C NMR (100 MHz, CDCl₃)** δ 139.4, 138.6 (d, *J*_{C-P} = 3.7 Hz), 132.4 (d, *J*_{C-P} = 2.8 Hz), 132.3 (d, *J*_{C-P} = 2.8 Hz), 132.1 (d, *J*_{C-P} = 10.4 Hz), 131.8 (d, *J*_{C-P} = 10.1 Hz), 131.7 (d, *J*_{C-P} = 137.8 Hz), 131.6 (d, *J*_{C-P} = 134.7 Hz), 129.4, 128.6

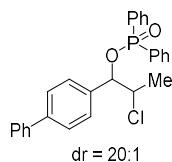
(d, $J_{C-P} = 3.4$ Hz), 128.5 (d, $J_{C-P} = 3.4$ Hz), 127.5, 125.9, 124.8, 77.8 (d, $J_{C-P} = 5.7$ Hz), 61.7 (d, $J_{C-P} = 4.6$ Hz), 40.2 ppm; ^{31}P NMR (162 MHz, CDCl_3) δ 33.5 ppm; HRMS (ESI) (m/z) $[\text{M}+\text{H}]^+$ $\text{C}_{21}\text{H}_{19}^{35}\text{ClO}_2\text{P}$ calcd. for 369.0806, found 369.0811.



2-chloro-1-phenylcyclohexyl diphenylphosphinate (1g): According to **Procedure 7**. Yield: 1.88 g, 87%; dr > 30:1; white solid, m.p. 180 °C; ^1H NMR (400 MHz, CDCl_3) δ 7.83-7.75 (m, 2H), 7.69-7.61 (m, 2H), 7.47-7.34 (m, 6H), 7.33-7.26 (m, 2H), 7.17-7.08 (m, 3H), 4.85-4.72 (m, 1H), 2.88-2.76 (m, 1H), 2.52-2.43 (m, 1H), 2.08-1.98 (m, 1H), 1.91-1.73 (m, 2H), 1.63-1.51 (m, 1H), 1.51-1.33 (m, 2H) ppm; ^{13}C NMR (100 MHz, CDCl_3) δ 139.4, 134.2 (d, $J_{C-P} = 138.7$ Hz), 134.0 (d, $J_{C-P} = 137.8$ Hz), 131.52, 131.51 (d, $J_{C-P} = 2.8$ Hz), 131.47 (d, $J_{C-P} = 10.2$ Hz), 131.37 (d, $J_{C-P} = 2.8$ Hz), 131.34 (d, $J_{C-P} = 10.3$ Hz), 128.25 (d, $J_{C-P} = 10.0$ Hz), 128.17, 128.11 (d, $J_{C-P} = 10.2$ Hz), 128.02, 127.28, 86.9 (d, $J_{C-P} = 8.6$ Hz), 66.9 (d, $J_{C-P} = 6.8$ Hz), 34.0, 32.0, 22.2, 22.0 ppm; ^{31}P NMR (162 MHz, CDCl_3) δ 28.0 ppm; HRMS (ESI) (m/z) $[\text{M}+\text{H}]^+$ $\text{C}_{24}\text{H}_{24}^{35}\text{ClNaO}_2\text{P}$ calcd. for 433.1095, found 433.1096.

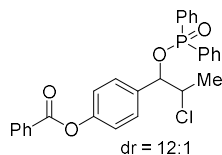


(1S,2R,3R,4R)-3-chloro-2-phenylbicyclo[2.2.1]heptan-2-yl diphenylphosphinate (1h): According to **Procedure 7**. Yield: 1.58 g, 71%; dr > 30:1; colorless oil; NEt_3 δ 7.80-7.72 (m, 2H), 7.34-7.24 (m, 5H), 7.20-7.13 (m, 2H), 7.08-7.01 (m, 1H), 6.96-6.88 (m, 2H), 6.87-6.78 (m, 3H), 4.18-4.08 (m, 1H), 3.68 (d, $J = 3.2$ Hz, 1H), 2.44-2.32 (m, 2H), 1.56-1.41 (m, 2H), 1.35-1.27 (m, 1H), 1.25-1.17 (m, 1H), 1.06-0.96 (m, 1H) ppm; ^{13}C NMR (100 MHz, CDCl_3) δ 136.3 (d, $J_{C-P} = 2.0$ Hz), 134.6 (d, $J_{C-P} = 179.9$ Hz), 133.2 (d, $J_{C-P} = 167.7$ Hz), 131.4 (d, $J_{C-P} = 2.8$ Hz), 131.3 (d, $J_{C-P} = 10.5$ Hz), 131.0 (d, $J_{C-P} = 10.0$ Hz), 130.5 (d, $J_{C-P} = 2.8$ Hz), 130.0, 128.5, 128.3 (d, $J_{C-P} = 13.3$ Hz), 127.7, 127.4 (d, $J_{C-P} = 13.3$ Hz), 91.7 (d, $J_{C-P} = 7.7$ Hz), 71.6 (d, $J_{C-P} = 7.2$ Hz), 47.0 (d, $J_{C-P} = 1.8$ Hz), 34.8, 28.6, 22.8 ppm; ^{31}P NMR (162 MHz, CDCl_3) δ 26.4 ppm; HRMS (ESI) (m/z) $[\text{M}+\text{H}]^+$ $\text{C}_{25}\text{H}_{24}^{35}\text{ClNaO}_2\text{P}$ calcd for 445.1095, found 445.1091.



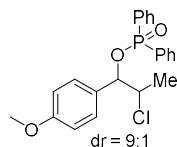
1-([1,1'-biphenyl]-4-yl)-2-chloropropyl diphenylphosphinate (1j): According to **Procedure 5**. Yield: 963.0 mg, 72%; two diastereomers, dr = 20:1 white solid, m.p. 116-117 °C; ^1H NMR (400 MHz, CDCl_3) δ 7.70 (dd, $J = 7.6, 12.0$ Hz, 2H), 7.42 (dd, $J = 8.0, 12.4$ Hz, 2H), 7.38-7.32 (m, 3H), 7.32-7.21 (m, 6H), 7.21-7.12 (m, 4H), 7.09-7.02 (m, 2H), 5.25 (dd, $J = 6.4, 8.8$ Hz, 1H), 4.32-4.21 (m, 1H), 1.38 (d, $J = 6.4$ Hz, 0.14H, the minor isomer), 1.24 (d, $J = 6.4$ Hz, 2.86H, the major isomer) ppm; ^{13}C NMR (100 MHz, CDCl_3) δ 141.5, 140.5, 135.6 (d, $J_{C-P} = 2.2$ Hz), 132.3 (d, $J_{C-P} = 2.6$ Hz), 132.02 (d, $J_{C-P} = 2.6$ Hz), 131.99 (d, $J_{C-P} = 14.2$ Hz), 131.7 (d, $J_{C-P} = 10.3$ Hz), 130.7 (d, $J_{C-P} = 48.5$ Hz), 128.8, 128.5 (d, $J_{C-P} = 13.3$ Hz), 128.2 (d, $J_{C-P} = 13.2$ Hz), 128.1, 127.54, 127.48 (d, $J_{C-P} = 145.7$ Hz),

127.1, 126.9, 80.4 (d, $J_{C-P} = 5.6$ Hz), 59.6 (d, $J_{C-P} = 5.5$ Hz), 20.7 ppm; ^{31}P NMR (162 MHz, CDCl_3) δ 33.2 ppm; HRMS (ESI) (m/z) $[\text{M}+\text{H}]^+$ $\text{C}_{27}\text{H}_{25}^{35}\text{ClO}_2\text{P}$ calcd. for 447.1275, found 447.1269.



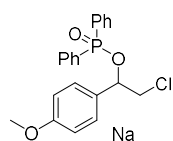
(E)-4-(prop-1-en-1-yl)phenyl benzoate (1k): According to Procedure 5.

Yield: 1.13 g, 77%; two diastereomers, dr = 12:1; white solid, m.p. 139-140 °C; ^1H NMR (400 MHz, CDCl_3) δ 8.17-8.07 (m, 2H), 7.85-7.75 (m, 2H), 7.60-7.50 (m, 3H), 7.50-7.32 (m, 6H), 7.30-7.20 (m, 4H), 7.06 (d, $J = 8.8$ Hz, 2H), 5.36 (d, $J = 9.2$, 5.6 Hz, 1H), 4.42-4.32 (m, 1H), 1.48 (d, $J = 6.8$ Hz, 0.23H, the minor isomer), 1.36 (d, $J = 6.8$ Hz, 2.77H, the major isomer) ppm; ^{13}C NMR (100 MHz, CDCl_3) δ 164.9, 151.1, 134.2 (d, $J_{C-P} = 2.8$ Hz), 133.7, 132.4 (d, $J_{C-P} = 2.8$ Hz), 132.23 (d, $J_{C-P} = 2.7$ Hz), 131.89 (d, $J_{C-P} = 10.4$ Hz), 131.61 (d, $J_{C-P} = 10.3$ Hz), 131.44 (d, $J_{C-P} = 139.3$ Hz), 130.77 (d, $J_{C-P} = 133.1$ Hz), 130.2, 129.4, 128.8, 128.65, 128.56 (d, $J_{C-P} = 13.5$ Hz), 128.33 (d, $J_{C-P} = 13.1$ Hz), 121.5, 79.9 (d, $J_{C-P} = 5.7$ Hz), 59.4 (d, $J_{C-P} = 5.2$ Hz), 20.5 ppm; ^{31}P NMR (162 MHz, CDCl_3) δ 33.5 ppm; HRMS (ESI) (m/z) $[\text{M}+\text{H}]^+$ $\text{C}_{28}\text{H}_{25}\text{ClO}_4\text{P}$ calcd for 491.1173, found 491.1171.



2-chloro-1-(4-methoxyphenyl)propyl diphenylphosphinate (1l): According to Procedure 5. Yield: 1.09 g, 86%; two diastereomers, dr = 9:1; colorless oil;

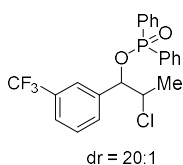
^1H NMR (400 MHz, CDCl_3) δ 7.88-7.81 (m, 2H), 7.62-7.56 (m, 2H), 7.54-7.51 (m, 1H), 7.49-7.43 (m, 2H), 7.42-7.37 (m, 1H), 7.33-7.22 (m, 3H), 7.22-7.12 (m, 2H), 6.80-6.75 (m, 1.8H, the major isomer), 6.73-6.70 (m, 0.2H, the minor isomer), 5.57 (dd, $J = 9.6$, 4.0 Hz, 0.1H, the minor isomer), 5.32 (dd, $J = 9.2$, 6.4 Hz, 0.9H, the major isomer), 4.45-4.35 (m, 1H), 3.86 (s, 0.3H, the minor isomer), 3.77 (s, 2.7H, the major isomer), 1.51 (d, $J = 6.8$ Hz, 0.27H), 1.35 (d, $J = 6.4$ Hz, 2.7H, the major isomer) ppm; ^{13}C NMR (100 MHz, CDCl_3) peaks of the major isomer δ 156.8, 132.2 (d, $J_{C-P} = 2.8$ Hz), 131.94 (d, $J_{C-P} = 2.8$ Hz), 131.89 (d, $J_{C-P} = 10.3$ Hz), 131.70 (d, $J_{C-P} = 138.8$ Hz), 131.65 (d, $J_{C-P} = 10.3$ Hz), 131.20 (d, $J_{C-P} = 135.6$ Hz), 128.9, 128.5 (d, $J_{C-P} = 13.3$ Hz), 128.1 (d, $J_{C-P} = 13.3$ Hz), 113.6, 80.5 (d, $J_{C-P} = 5.8$ Hz), 59.7 (d, $J_{C-P} = 5.7$ Hz), 55.3, 20.6 ppm; ^{31}P NMR (162 MHz, CDCl_3) δ 32.9 (0.1P, the minor isomer), 32.8 (1.0P, the major isomer) ppm; HRMS (ESI) (m/z) $[\text{M}+\text{H}]^+$ $\text{C}_{22}\text{H}_{22}^{35}\text{ClNaO}_3\text{P}$ calcd. for 423.0887, found 423.0887.



2-chloro-1-(4-methoxyphenyl)ethyl diphenylphosphinate (1m): According to Procedure 5. Yield: 961.0 mg, 83%; colorless oil; ^1H NMR (300 MHz, CDCl_3)

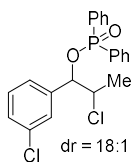
δ 7.94-7.86 (m, 2H), 7.75-7.67 (m, 2H), 7.62-7.56 (m, 1H), 7.54-7.47 (m, 3H), 7.42-7.35 (m, 2H), 7.30-7.24 (m, 2H), 6.91-6.84 (m, 2H), 5.51 (dt, $J = 9.3$, 3.3 Hz, 1H), 4.03 (dd, $J = 8.4$, 4.5 Hz, 1H), 3.85 (dd, $J = 8.4$, 4.5 Hz, 1H), 3.84 (s, 3H) ppm; ^{13}C NMR (100 MHz,

CDCl₃) δ 159.9, 132.3 (d, J_{C-P} = 2.9 Hz), 132.14 (d, J_{C-P} = 2.8 Hz), 132.06 (d, J_{C-P} = 150.2 Hz), 131.9 (d, J_{C-P} = 10.3 Hz), 131.62 (d, J_{C-P} = 10.3 Hz), 130.7 (d, J_{C-P} = 146.8 Hz), 129.5 (d, J_{C-P} = 3.6 Hz), 128.5 (d, J_{C-P} = 13.3 Hz), 128.31 (d, J_{C-P} = 13.1 Hz), 128.27, 113.9, 76.6 (d, J_{C-P} = 5.6 Hz), 55.3, 47.8 (d, J_{C-P} = 5.0 Hz) ppm; **³¹P NMR (162 MHz, CDCl₃)** δ 33.1 ppm; **HRMS (ESI) (*m/z*)** [M+Na]⁺ C₂₁H₂₀³⁵ClO₃PNa calcd. for 409.0736, found 409.0727.



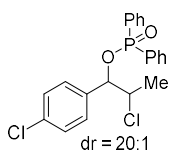
2-chloro-1-(3-(trifluoromethyl)phenyl)propyl diphenylphosphinate (1n):

According to **Procedure 5**. Yield: 972.0 mg, 74%; two diastereomers, dr = 20:1; white solid, m.p. 72-74 °C; **¹H NMR (300 MHz, CDCl₃)** δ 7.92-7.82 (m, 2H), 7.61-7.44 (m, 8H), 7.42-7.32 (m, 2H), 7.29-7.20 (m, 2H), 5.55-5.46 (m, 1H), 4.44-4.33 (m, 1H), 1.54 (d, J = 6.9 Hz, 0.14H), 1.42 (d, J = 6.9 Hz, 2.86H) ppm; **¹³C NMR (100 MHz, CDCl₃)** (not possible to assign every peak) δ 137.71, 137.69, 132.54, 132.51, 132.28, 132.26, 131.75, 131.65, 131.61, 131.51, 131.03, 128.33, 128.20, 127.87, 125.43, 125.39, 125.16, 124.35, 124.31, 124.27, 122.45, 119.75, 79.21, 79.16, 77.38, 77.07, 76.75, 59.18, 59.12, 20.56 ppm; **³¹P NMR (121 MHz, CDCl₃)** δ 33.8 (1P, the major isomer), 32.2 (0.05P, the minor isomer) ppm; **¹⁹F NMR (282 MHz, CDCl₃)** δ -63.2 ppm; **HRMS (ESI) (*m/z*)** [M+H]⁺ C₂₂H₂₀³⁵ClF₃O₂P calcd for 439.0836, found 439.0841.



According to **Procedure 5**. Yield: 957.0 mg, 79%; two diastereomers, dr = 18:1;

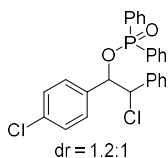
colorless oil; **¹H NMR (400 MHz, CDCl₃)** δ 8.02-7.92 (m, 2H), 7.73-7.66 (m, 2H), 7.65-7.60 (m, 1H), 7.59-7.53 (m, 2H), 7.51-7.45 (m, 1H), 7.40-7.33 (m, 3H), 7.32-7.27 (m, 1H), 7.27-7.22 (m, 2H), 4.51-4.42 (m, 1H), 1.61 (d, J = 6.4 Hz, 0.16H, the minor isomer), 1.49 (d, J = 6.4 Hz, 2.86H, the major isomer) ppm; **¹³C NMR (100 MHz, CDCl₃)** peaks of the major isomer δ 138.6 (d, J_{C-P} = 2.5 Hz), 134.1, 132.5 (d, J_{C-P} = 2.7 Hz), 132.3 (d, J_{C-P} = 2.8 Hz), 131.8 (d, J_{C-P} = 10.5 Hz), 131.6 (d, J_{C-P} = 10.4 Hz), 131.2 (d, J_{C-P} = 139.0 Hz), 130.7 (d, J_{C-P} = 133.1 Hz), 129.5, 128.8, 128.6 (d, J_{C-P} = 13.3 Hz), 128.3 (d, J_{C-P} = 13.2 Hz), 127.6, 125.8, 79.4 (d, J_{C-P} = 5.6 Hz), 59.2 (d, J_{C-P} = 5.6 Hz), 20.6 ppm; **³¹P NMR (162 MHz, CDCl₃)** δ 33.6 ppm; **HRMS (ESI) (*m/z*)** [M+H]⁺ C₂₁H₂₀³⁵Cl₂O₂P calcd. for 405.0572, found 405.0572.



2-chloro-1-(4-chlorophenyl)propyl diphenylphosphinate (1p): According to

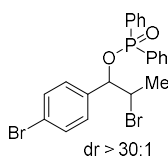
Procedure 5. Yield: 994.0 mg, 82%; two diastereomers, dr = 20:1; white solid, m.p. 96-98 °C; **¹H NMR (400 MHz, CDCl₃)** δ 7.94-7.85 (m, 2H), 7.67-7.64 (m, 1H), 7.64-7.61 (m, 1H), 7.61-7.55 (m, 1H), 7.54-7.42 (m, 3H), 7.35-7.29 (m, 2H), 7.27-7.25 (m, 4H), 5.42 (dd, J = 9.2, 5.6 Hz, 1H), 4.46-4.38 (m, 1H), 1.55 (d, J = 6.8 Hz, 0.14H, the minor isomer), 1.42 (d, J = 6.8 Hz, 2.8H, the major isomer) ppm; **¹³C NMR (100 MHz, CDCl₃)** peaks of the major isomer δ 135.1 (d, J_{C-P} = 2.6 Hz), 134.6, 132.4 (d, J_{C-P} = 2.8 Hz), 132.2

(d, J_{C-P} = 2.7 Hz), 131.77 (d, J_{C-P} = 10.4 Hz), 131.59 (d, J_{C-P} = 10.3 Hz), 131.25 (d, J_{C-P} = 138.7 Hz), 130.83 (d, J_{C-P} = 133.5 Hz), 128.9, 128.6 (d, J_{C-P} = 13.4 Hz), 128.4, 128.3 (d, J_{C-P} = 14.0 Hz), 79.6 (d, J_{C-P} = 5.6 Hz), 59.3 (d, J_{C-P} = 5.5 Hz), 20.4 ppm; ^{31}P NMR (162 MHz, CDCl_3) δ 33.5 ppm; HRMS (ESI) (m/z) $[\text{M}+\text{H}]^+$ $\text{C}_{21}\text{H}_{20}^{35}\text{Cl}_2\text{O}_2\text{P}$ calcd. for 405.0572, found 405.0573.



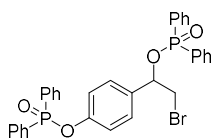
2-chloro-1-(4-chlorophenyl)-2-phenylethyl diphenylphosphinate (1q):

According to **Procedure 5**. Yield: 932.0 mg, 67%; two diastereomers, dr = 1.2:1; colorless oil; two diastereomers, dr = 1.2:1; ^1H NMR (400 MHz, CDCl_3) δ 7.85-7.74 (m, 1H), 7.60-7.41 (m, 5H), 7.39-7.31 (m, 2H), 7.29-7.20 (m, 5H), 7.16-7.10 (m, 2H), 7.09-7.04 (m, 2H), 7.03-6.98 (m, 1H), 6.89-6.85 (m, 1H), 5.68-5.58 (m, 1H), 5.28 (d, J = 7.6 Hz, 0.45H, the minor isomer), 5.23 (d, J = 6.4 Hz, 0.55H, the major isomer) ppm; ^{13}C NMR (100 MHz, CDCl_3) (difficult to assign every peak) δ 137.0 (the major isomer), 136.1 (the minor isomer), 134.83, 134.80, 134.60, 134.40, 132.42, 132.40, 132.29, 132.26, 132.21, 132.18, 132.15, 131.85, 131.75, 131.73, 131.72, 131.63, 131.62, 131.55, 131.50, 131.40, 130.69, 130.50, 130.38, 130.21, 129.93, 129.51, 129.24, 128.86, 128.70, 128.59, 128.49, 128.46, 128.36, 128.34, 128.30, 128.21, 128.17, 128.06, 128.01, 127.34, 79.9 (d, J_{C-P} = 5.8 Hz, the minor isomer), 79.3 (d, J_{C-P} = 5.7 Hz, the major isomer), 65.44 (d, J_{C-P} = 6.8 Hz, the minor isomer), 65.37 (d, J_{C-P} = 7.4 Hz, the major isomer) ppm; ^{31}P NMR (162 MHz, CDCl_3) δ 33.90 (1P, the major isomer), 33.70 (0.83P, the minor isomer) ppm; HRMS (ESI) (m/z) $[\text{M}+\text{H}]^+$ $\text{C}_{26}\text{H}_{22}^{35}\text{Cl}_2\text{O}_2\text{P}$ calcd. for 467.0729, found 467.0732.



2-bromo-1-(4-bromophenyl)propyl diphenylphosphinate (1r): According to

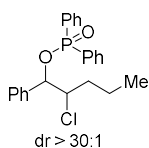
Procedure 5. Yield: 1.15 g, 78%; dr > 30:1; colorless oil; ^1H NMR (400 MHz, CDCl_3) δ 7.80-7.72 (m, 2H), 7.53-7.42 (m, 2H), 7.40-7.28 (m, 3H), 7.29-7.23 (m, 2H), 7.22-7.16 (m, 2H), 7.10-7.00 (m, 2H), 5.29 (dd, J = 9.2, 6.0 Hz, 1H), 4.37-4.29 (m, 1H), 1.48 (d, J = 6.8, 3H) ppm; ^{13}C NMR (100 MHz, CDCl_3) δ 135.8 (d, J_{C-P} = 2.6 Hz), 132.4 (d, J_{C-P} = 2.9 Hz), 132.2 (d, J_{C-P} = 2.7 Hz), 131.8 (d, J_{C-P} = 10.4 Hz), 131.6 (d, J_{C-P} = 10.4 Hz), 131.3, 131.2 (d, J_{C-P} = 138.6 Hz), 130.8 (d, J_{C-P} = 133.5 Hz), 129.2, 128.6 (d, J_{C-P} = 13.4 Hz), 128.3 (d, J_{C-P} = 13.2 Hz), 122.8, 79.6 (d, J_{C-P} = 5.6 Hz), 51.0 (d, J_{C-P} = 5.7 Hz), 21.5 ppm; ^{31}P NMR (162 MHz, CDCl_3) δ 33.4 ppm; HRMS (ESI) (m/z) $[\text{M}+\text{H}]^+$ $\text{C}_{21}\text{H}_{20}^{79}\text{Br}_2\text{O}_2\text{P}$ calcd. for 492.9562, found 492.9564.



2-bromo-1-(4-((diphenylphosphoryl)oxy)phenyl)ethyl diphenylphosphinate (1s): According to **Procedure 5**. Yield: 1.40 g, 76%; white solid, m.p. 155-157 °C; ^1H NMR (400 MHz, CDCl_3) δ 8.02-7.87 (m, 6H),

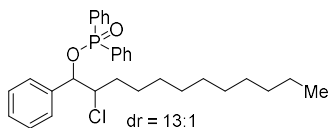
7.72-7.45 (m, 13H), 7.38-7.30 (m, 2H), 7.29-7.21 (m, 4H), 5.56-5.49 (m, 1H), 3.99 (dd, J = 7.6,

6.0 Hz, 1H), 3.85-3.79 (m, 1H) ppm; ^{13}C NMR (100 MHz, CDCl_3) δ 151.2 (d, $J_{\text{C-P}} = 8.2$ Hz), 133.7 (d, $J_{\text{C-P}} = 2.9$ Hz), 132.6 (d, $J_{\text{C-P}} = 2.8$ Hz), 132.4 (d, $J_{\text{C-P}} = 2.8$ Hz), 132.3 (d, $J_{\text{C-P}} = 2.7$ Hz), 131.82 (d, $J_{\text{C-P}} = 10.4$ Hz), 131.81 (d, $J_{\text{C-P}} = 1.7$ Hz), 131.7 (d, $J_{\text{C-P}} = 1.6$ Hz), 131.6 (d, $J_{\text{C-P}} = 10.3$ Hz), 131.13 (d, $J_{\text{C-P}} = 138.4$ Hz), 130.87 (d, $J_{\text{C-P}} = 137.2$ Hz), 130.74 (d, $J_{\text{C-P}} = 133.6$ Hz), 128.7 (d, $J_{\text{C-P}} = 13.4$ Hz), 128.5 (d, $J_{\text{C-P}} = 13.4$ Hz), 128.33 (d, $J_{\text{C-P}} = 13.2$ Hz), 128.31, 120.8 (d, $J_{\text{C-P}} = 4.9$ Hz), 76.0 (d, $J_{\text{C-P}} = 5.5$ Hz), 47.7 (d, $J_{\text{C-P}} = 4.7$ Hz) ppm; ^{31}P NMR (162 MHz, CDCl_3) δ 33.6, 31.5 ppm; HRMS (ESI) (m/z) $[\text{M}+\text{H}]^+$ $\text{C}_{32}\text{H}_{28}^{79}\text{BrO}_4\text{P}_2$ calcd. for 617.0641, found 617.0639.



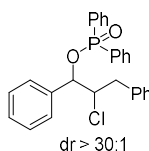
2-chloro-1-phenylpentyl diphenylphosphinate (1t): According to Procedure 5.

Yield: 979.0 mg, 82%; dr > 30:1; white solid, m.p. 75-76 °C; ^1H NMR (400 MHz, CDCl_3) δ 7.93-7.83 (m, 2H), 7.63-7.52 (m, 3H), 7.51-7.45 (m, 2H), 7.42-7.36 (m, 1H), 7.31-7.22 (m, 7H), 5.47 (dd, $J = 5.6, 9.2$ Hz, 1H), 4.31-4.21 (m, 1H), 1.74-1.64 (m, 1H), 1.63-1.45 (m, 2H), 1.44-1.32 (m, 1H), 0.83 (t, $J = 7.2$ Hz, 3H) ppm; ^{13}C NMR (100 MHz, CDCl_3) δ 137.0 (d, $J_{\text{C-P}} = 2.6$ Hz), 132.2 (d, $J_{\text{C-P}} = 2.7$ Hz), 132.0 (d, $J_{\text{C-P}} = 2.8$ Hz), 131.9 (d, $J_{\text{C-P}} = 10.5$ Hz), 131.7 (d, $J_{\text{C-P}} = 139.0$ Hz), 131.6 (d, $J_{\text{C-P}} = 10.3$ Hz), 131.1 (d, $J_{\text{C-P}} = 138.7$ Hz), 128.53, 128.49 (d, $J_{\text{C-P}} = 13.2$ Hz), 128.126, 128.124 (d, $J_{\text{C-P}} = 13.2$ Hz), 127.5, 79.7 (d, $J_{\text{C-P}} = 5.7$ Hz), 65.1 (d, $J_{\text{C-P}} = 5.3$ Hz), 35.5, 19.5, 13.4 ppm; ^{31}P NMR (162 MHz, CDCl_3) δ 33.0 ppm; HRMS (ESI) (m/z) $[\text{M}+\text{H}]^+$ $\text{C}_{23}\text{H}_{25}^{35}\text{ClO}_2\text{P}$ calcd. for 399.1275, found 399.1279.



2-chloro-1-phenyldodecyl diphenylphosphinate (1u):

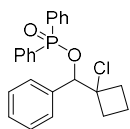
According to Procedure 5. Yield: 1.09 g, 73%; two diastereomers, dr = 13:1; colorless oil; ^1H NMR (400 MHz, CDCl_3) δ 7.91-7.82 (m, 2H), 7.62-7.50 (m, 3H), 7.49-7.42 (m, 2H), 7.40-7.33 (m, 1H), 7.30-7.20 (m, 2H), 7.46 (dd, $J = 9.6, 6.0$ Hz, 1H), 4.28-4.20 (m, 1H), 1.78-1.65 (m, 1H), 1.55-1.42 (m, 2H), 1.34-1.11 (m, 15H), 0.87 (t, $J = 6.8, 3\text{H}$) ppm; ^{13}C NMR (100 MHz, CDCl_3) (the major isomer) δ 137.1 (d, $J_{\text{C-P}} = 2.5$ Hz), 132.2 (d, $J_{\text{C-P}} = 2.7$ Hz), 132.0 (d, $J_{\text{C-P}} = 2.7$ Hz), 131.86 (d, $J_{\text{C-P}} = 10.4$ Hz), 131.76 (d, $J_{\text{C-P}} = 138.9$ Hz), 131.67 (d, $J_{\text{C-P}} = 10.3$ Hz), 131.2 (d, $J_{\text{C-P}} = 133.7$ Hz), 128.54, 128.49 (d, $J_{\text{C-P}} = 13.2$ Hz), 128.139, 128.136 (d, $J_{\text{C-P}} = 13.2$ Hz), 127.6, 79.7 (d, $J_{\text{C-P}} = 5.8$ Hz), 65.4 (d, $J_{\text{C-P}} = 5.4$ Hz), 33.5, 31.9, 29.57, 29.51, 29.38, 29.32, 28.9, 26.3, 22.7, 14.1 ppm; ^{31}P NMR (162 MHz, CDCl_3) δ 33.0 ppm; HRMS (ESI) (m/z) $[\text{M}+\text{H}]^+$ $\text{C}_{30}\text{H}_{39}^{35}\text{ClO}_2\text{P}$ calcd. for 497.2371, found 497.2372.



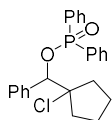
2-chloro-1,3-diphenylpropyl diphenylphosphinate (1v): According to

Procedure 5. Yield: 990.0 mg, 74%; dr > 30:1; white solid, m.p. 127-129 °C; ^1H NMR (400 MHz, CDCl_3) δ 7.95-7.85 (m, 2H), 7.64-7.43 (m, 5H), 7.42-7.16 (m, 12H), 7.15-7.07 (m, 2H), 5.62-5.22 (m, 1H), 4.48-4.42 (m, 1H), 3.30-3.18 (m, 1H),

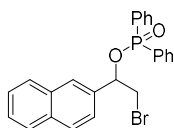
2.75-2.65 (m, 1H) ppm; ^{13}C NMR (100 MHz, CDCl_3) (the major isomer) δ ppm; 137.4, 136.7 (d, $J_{\text{C-P}} = 1.9$ Hz), 132.4, 132.2, 131.9 (d, $J_{\text{C-P}} = 10.2$ Hz), 131.73 (d, $J_{\text{C-P}} = 142.1$ Hz) 131.67 (d, $J_{\text{C-P}} = 10.0$ Hz), 131.0 (d, $J_{\text{C-P}} = 134.8$ Hz), 129.4, 128.72, 128.66 (d, $J_{\text{C-P}} = 12.0$ Hz), 128.4, 128.29 (d, $J_{\text{C-P}} = 13.2$ Hz), 128.25, 127.6, 126.8, 79.1 (d, $J_{\text{C-P}} = 4.9$ Hz), 66.0 (d, $J_{\text{C-P}} = 4.3$ Hz), 39.9 ppm; ^{31}P NMR (162 MHz, CDCl_3) δ 33.1 ppm; HRMS (ESI) (m/z) $[\text{M}+\text{H}]^+$ $\text{C}_{27}\text{H}_{25}^{35}\text{ClO}_2\text{P}$ calcd. for 447.1275, found 447.1275.



(1-chlorocyclobutyl)(phenyl)methyl diphenylphosphinate (1w): According to Procedure 5. Yield: 1.06 g, 89%; white solid, m.p. 124-125 °C; ^1H NMR (400 MHz, CDCl_3) δ 7.98-7.86 (m, 2H), 7.66-7.47 (m, 5H), 7.41-7.33 (m, 3H), 7.31-7.20 (m, 5H), 5.58 (d, $J = 10.8$ Hz, 1H), 3.00-2.89 (m, 1H), 2.76-2.66 (m, 1H), 2.46-2.37 (m, 1H), 2.35-2.26 (m, 1H), 2.26-2.15 (m, 1H), 1.93-1.81 (m, 1H) ppm; ^{13}C NMR (100 MHz, CDCl_3) δ 136.3 (d, $J_{\text{C-P}} = 2.1$ Hz), 132.26 (d, $J_{\text{C-P}} = 2.8$ Hz), 131.93 (d, $J_{\text{C-P}} = 2.5$ Hz), 131.88 (d, $J_{\text{C-P}} = 10.7$ Hz), 131.80 (d, $J_{\text{C-P}} = 140.4$ Hz), 131.51 (d, $J_{\text{C-P}} = 10.1$ Hz), 131.06 (d, $J_{\text{C-P}} = 142.2$ Hz), 128.5 (d, $J_{\text{C-P}} = 13.3$ Hz), 128.4, 128.3, 128.0 (d, $J_{\text{C-P}} = 13.2$ Hz), 127.6, 80.4 (d, $J_{\text{C-P}} = 5.9$ Hz), 72.7 (d, $J_{\text{C-P}} = 5.5$ Hz), 36.0, 35.1, 15.0 ppm; ^{31}P NMR (162 MHz, CDCl_3) δ 33.2 ppm; HRMS (ESI) (m/z) $[\text{M}+\text{H}]^+$ $\text{C}_{23}\text{H}_{23}^{35}\text{ClO}_2\text{P}$ calcd. for 397.1119, found 397.1119.

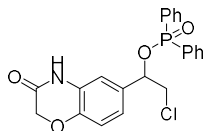


(1-chlorocyclobutyl)(phenyl)methyl diphenylphosphinate (1x): According to Procedure 5. Yield: 1.17 g, 95%; white solid, m.p. 92-93 °C; ^1H NMR (400 MHz, CDCl_3) δ 8.01-7.98 (m, 2H), 7.65-7.50 (m, 5H), 7.43-7.35 (m, 3H), 7.30-7.20 (m, 5H), 5.55 (d, $J = 10.8$ Hz, 1H), 2.31-2.20 (m, 2H), 2.17-2.07 (m, 1H), 2.06-1.92 (m, 2H), 1.89-1.73 (m, 3H) ppm; ^{13}C NMR (100 MHz, CDCl_3) δ 137.3 (d, $J_{\text{C-P}} = 1.7$ Hz), 132.25 (d, $J_{\text{C-P}} = 2.8$ Hz), 131.89 (d, $J_{\text{C-P}} = 10.4$ Hz), 131.85 (d, $J_{\text{C-P}} = 2.7$ Hz), 131.7 (d, $J_{\text{C-P}} = 140.8$ Hz), 131.5 (d, $J_{\text{C-P}} = 10.1$ Hz), 131.02 (d, $J_{\text{C-P}} = 132.0$ Hz), 128.5 (d, $J_{\text{C-P}} = 13.3$ Hz), 128.4, 128.3, 127.9 (d, $J_{\text{C-P}} = 13.2$ Hz), 127.5, 83.2 (d, $J_{\text{C-P}} = 5.9$ Hz), 81.6 (d, $J_{\text{C-P}} = 5.9$ Hz), 40.5, 39.4, 22.9 ppm; ^{31}P NMR (162 MHz, CDCl_3) δ 32.7 ppm; HRMS (ESI) (m/z) $[\text{M}+\text{H}]^+$ $\text{C}_{24}\text{H}_{25}^{35}\text{ClO}_2\text{P}$ calcd. for 411.1275, found 411.1277.

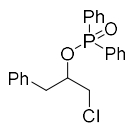


2-bromo-1-(naphthalen-2-yl)ethyl diphenylphosphinate (1y): According to Procedure 5. Yield: 1.00 g, 71%; white solid, m.p. 94-95 °C; ^1H NMR (400 MHz, CDCl_3) δ 7.72-7.64 (m, 2H), 7.63-7.52 (m, 3H), 7.49-7.41 (m, 3H), 7.37-7.31 (m, 1H), 7.30-7.20 (m, 5H), 7.20-7.13 (m, 1H), 7.07-6.99 (m, 2H), 5.55-5.44 (m, 1H), 3.73 (dd, $J = 6.0, 10.8$ Hz, 1H), 3.59 (dd, $J = 6.4, 10.8$ Hz, 1H) ppm; ^{13}C NMR (100 MHz, CDCl_3) δ 135.0 (d, $J_{\text{C-P}} = 3.7$ Hz), 133.4, 132.9, 132.4 (d, $J_{\text{C-P}} = 2.8$ Hz), 132.2 (d, $J_{\text{C-P}} = 2.7$ Hz), 131.9 (d, $J_{\text{C-P}} = 10.3$ Hz), 131.7 (d, $J_{\text{C-P}} = 10.3$ Hz), 131.5 (d, $J_{\text{C-P}} = 139.0$ Hz), 130.9 (d, $J_{\text{C-P}} = 133.8$ Hz),

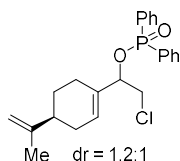
128.57 (d, $J_{C-P} = 13.4$ Hz), 128.53, 128.3 (d, $J_{C-P} = 13.2$ Hz), 128.2, 127.7, 126.8, 126.6, 126.4, 123.8, 76.7 (d, $J_{C-P} = 5.5$ Hz), 35.8 (d, $J_{C-P} = 4.7$ Hz) ppm; ^{31}P NMR (162 MHz, CDCl_3) δ 33.5 ppm; HRMS (ESI) (m/z) $[\text{M}+\text{H}]^+$ $\text{C}_{24}\text{H}_{20}^{79}\text{BrNaO}_2\text{P}$ calcd. for 473.0277, found 473.0274.



2-chloro-1-(3-oxo-3,4-dihydro-2H-benzo[*b*][1,4]oxazin-6-yl)ethyl diphenylphosphinate (1z): According to Procedure 5. Yield: 880.0 mg, 65%; light yellow oil; ^1H NMR (400 MHz, Acetone- d_6) δ 9.84 (brs, 1H), 7.93-7.85 (m, 2H), 7.77-7.68 (m, 2H), 7.64-7.58 (m, 1H), 7.56-7.48 (m, 3H), 7.44-7.37 (m, 2H), 7.07-7.02 (m, 1H), 6.97 (dd, $J = 8.4, 2.0$ Hz, 1H), 6.84 (d, $J = 8.4$ Hz, 1H), 5.48-5.39 (m, 1H), 4.53 (s, 2H), 3.98 (dd, $J = 6.4, 11.6$ Hz, 1H), 3.89 (dd, $J = 5.2, 11.6$ Hz, 1H) ppm; ^{13}C NMR (100 MHz, Acetone- d_6) δ 169.6, 149.0, 137.6, 137.5, 137.24 (d, $J_{C-P} = 3.0$ Hz), 137.15 (d, $J_{C-P} = 138.5$ Hz), 137.0 (d, $J_{C-P} = 135.5$ Hz), 136.9 (d, $J_{C-P} = 4.3$ Hz), 136.8 (d, $J_{C-P} = 3.4$ Hz), 133.9 (d, $J_{C-P} = 3.4$ Hz), 133.6 (d, $J_{C-P} = 3.2$ Hz), 132.6, 127.0, 121.3, 120.0, 76.23, 76.18, 66.94, 47.95, 47.89 ppm; ^{31}P NMR (162 MHz, Acetone- d_6) δ 32.5 ppm; HRMS (ESI) (m/z) $[\text{M}+\text{H}]^+$ $\text{C}_{22}\text{H}_{19}^{35}\text{ClNaO}_4\text{P}$ calcd. for 450.0632, found 450.0635.

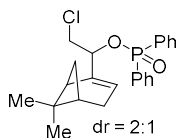


1-chloro-3-phenylpropan-2-yl diphenylphosphinate (1aa): According to Procedure 8. Yield: 1.57 g, 85%; white solid, m.p. 109-111 °C; ^1H NMR (400 MHz, CDCl_3) δ 7.86-7.76 (m, 2H), 7.65-7.56 (m, 2H), 7.55-7.42 (m, 4H), 7.41-7.33 (m, 2H), 7.31-7.22 (m, 3H), 7.21-7.14 (m, 2H), 4.80-4.70 (m, 1H), 3.74-3.65 (m, 2H), 3.24-3.05 (m, 2H) ppm; ^{13}C NMR (100 MHz, CDCl_3) δ 136.1, 132.3 (d, $J_{C-P} = 2.5$ Hz), 132.2 (d, $J_{C-P} = 2.5$ Hz), 131.73 (d, $J_{C-P} = 10.2$ Hz), 131.66 (d, $J_{C-P} = 135.2$ Hz), 131.29 (d, $J_{C-P} = 10.2$ Hz), 131.15 (d, $J_{C-P} = 134.5$ Hz), 129.7, 128.6 (d, $J_{C-P} = 13.0$ Hz), 128.5 (d, $J_{C-P} = 12.9$ Hz), 127.0, 75.6 (d, $J_{C-P} = 6.1$ Hz), 46.2 (d, $J_{C-P} = 2.7$ Hz), 39.2 (d, $J_{C-P} = 4.7$ Hz) ppm; ^{31}P NMR (162 MHz, CDCl_3) δ 32.8 ppm; HRMS (ESI) (m/z) $[\text{M}+\text{H}]^+$ $\text{C}_{21}\text{H}_{21}^{35}\text{ClO}_2\text{P}$ calcd. for 371.0962, found 371.0969.



2-chloro-1-((*S*)-4-(prop-1-en-2-yl)cyclohex-1-en-1-yl)ethyl diphenylphosphinate (1ab): According to Procedure 9. Yield: 852.0 mg, 71%; two diastereomers, dr = 1.2/1; colorless oil; ^1H NMR (400 MHz, CDCl_3) δ 7.68-7.55 (m, 4H), 7.37-7.19 (m, 6H), 5.57-5.44 (m, 1H), 4.79-4.67 (m, 1H), 4.55-4.41 (m, 2H), 3.67-3.56 (m, 1H), 3.48-3.39 (m, 1H), 2.05-1.60 (m, 5H), 1.59-1.51 (m, 2H), 1.51 (s, 1.4H, the minor isomer), 1.49 (s, 1.68H, the major isomer) ppm; ^{13}C NMR (100 MHz, CDCl_3) δ (not possible to assign every peak) 149.4, 149.1, 132.68, 132.66, 132.56, 132.52, 132.49, 132.40, 132.37, 132.24, 132.20, 132.17, 132.15, 132.10, 132.08, 132.05, 132.00, 131.90, 131.64, 131.54, 131.44, 131.17, 131.02, 129.85, 128.61, 128.54, 128.53, 128.41, 128.39, 128.36, 128.25, 128.23, 108.91, 108.85, 79.21, 79.15, 79.01, 78.96, 45.21, 45.15, 44.65, 44.59, 40.73, 40.26,

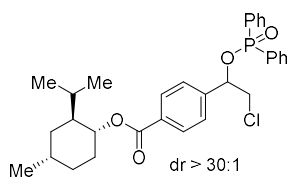
30.51, 30.25, 26.89, 26.83, 23.54, 23.24, 20.78, 20.56 ppm; ^{31}P NMR (162 MHz, CDCl_3) δ 31.9 (0.82P, the minor isomer), 31.7 (1P, the major isomer) ppm; HRMS (ESI) (m/z) $[\text{M}+\text{H}]^+$ $\text{C}_{23}\text{H}_{27}^{35}\text{ClO}_2\text{P}$ calcd. for 401.1432, found 401.1427.



2-chloro-1-((1R,5S)-6,6-dimethylbicyclo[3.1.1]hept-2-en-2-yl)ethyl

diphenylphosphinate (1ac): According to Procedure 9. Yield: 672.0 mg, 56%;

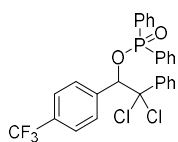
two diastereomers, dr = 2/1; colorless oil; ^1H NMR (400 MHz, CDCl_3) δ 7.70-7.58 (m, 4H), 7.37-7.30 (m, 2H), 7.30-7.22 (m, 4H), 5.42-5.32 (m, 1H), 4.77-4.63 (m, 1H), 3.58 (dd, J = 5.2, 8.4 Hz, 0.66H, the major isomer), 3.53 (dd, J = 6.4, 11.6 Hz, 0.34H, the minor isomer), 3.47-3.37 (m, 1H), 2.24-2.14 (m, 1H), 2.11-1.96 (m, 3H), 1.94-1.83 (m, 1H), 1.11 (s, 2H, the major isomer), 1.08 (s, 1H, the minor isomer), 0.94 (d, J = 8.8 Hz, 0.66H, the major isomer), 0.79 (d, J = 8.8 Hz, 0.36H, the minor isomer), 0.66 (s, 2H, the major isomer), 0.58 (s, 1H, the minor isomer) ppm; ^{13}C NMR (100 MHz, CDCl_3) δ (not possible to assign every peak) 143.40, 143.37, 143.12, 143.07, 132.59, 132.26, 132.23, 132.22, 132.19, 132.16, 132.13, 132.11, 132.01, 131.98, 131.90, 131.88, 131.68, 131.60, 131.58, 131.50, 131.21, 130.77, 128.52, 128.50, 128.47, 128.42, 128.39, 128.37, 128.34, 128.29, 123.75, 123.70, 77.35, 77.29, 45.57, 45.52, 44.56, 44.53, 41.88, 41.68, 40.69, 40.52, 38.02, 37.83, 31.74, 31.42, 31.22, 26.18, 26.12, 21.42 ppm; ^{31}P NMR (162 MHz, CDCl_3) δ 32.5 (2P, the major isomer), 32.0 (1P, the major isomer) ppm; HRMS (ESI) (m/z) $[\text{M}+\text{H}]^+$ $\text{C}_{23}\text{H}_{27}^{35}\text{ClO}_2\text{P}$ calcd. for 401.1432, found 423.1250.



(1R,2S,4S)-2-isopropyl-4-methylcyclohexyl 4-(2-chloro-1-

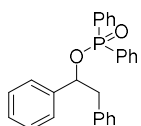
((diphenyl phosphoryl)oxy)ethyl) benzoate (1ad): According to Procedure 5. Yield: 1.45 g, 90%; dr > 30:1; colorless oil; ^1H NMR (400 MHz, CDCl_3) δ 7.85 (d, J = 7.6 Hz, 2H), 7.77-7.68 (m, 2H), 7.58-

7.49 (m, 2H), 7.45-7.38 (m, 1H), 7.37-7.29 (m, 3H), 7.25 (d, J = 8.4 Hz, 2H), 7.23-7.17 (m, 2H), 5.48-5.36 (m, 1H), 4.79 (dt, J = 4.4, 10.8 Hz, 1H), 3.87-3.78 (m, 1H), 3.74-3.63 (m, 1H), 2.01-1.92 (m, 1H), 1.86-1.74 (m, 1H), 1.65-1.54 (m, 2H), 1.49-1.35 (m, 2H), 1.07-0.90 (m, 2H), 0.86-0.81 (m, 1H), 0.79 (dd, J = 6.8, 2.4 Hz, 6H), 0.66 (d, J = 6.8 Hz, 3H) ppm; ^{13}C NMR (100 MHz, CDCl_3) δ 165.6, 142.0 (d, $J_{\text{C-P}}$ = 3.4 Hz), 132.5 (d, $J_{\text{C-P}}$ = 2.7 Hz), 132.4 (d, $J_{\text{C-P}}$ = 1.7 Hz), 131.8 (d, $J_{\text{C-P}}$ = 10.4 Hz), 131.6 (d, $J_{\text{C-P}}$ = 10.3 Hz), 131.3, 131.2 (d, $J_{\text{C-P}}$ = 137.7 Hz), 130.8 (d, $J_{\text{C-P}}$ = 134.2 Hz), 129.8 (d, $J_{\text{C-P}}$ = 0.8 Hz), 128.6 (d, $J_{\text{C-P}}$ = 13.3 Hz), 128.5 (d, $J_{\text{C-P}}$ = 13.2 Hz), 126.8, 76.0 (d, $J_{\text{C-P}}$ = 5.4 Hz), 75.0, 47.7 (d, $J_{\text{C-P}}$ = 4.5 Hz), 47.3, 41.0, 34.3, 31.5, 26.5, 23.6, 22.1, 20.8, 16.5 ppm; ^{31}P NMR (162 MHz, CDCl_3) δ 33.9 ppm; HRMS (EI) (m/z) $\text{C}_{31}\text{H}_{37}^{35}\text{ClO}_4\text{P}$ calcd. for 539.2113, found 539.2118.



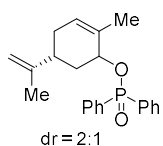
2,2-dichloro-2-phenyl-1-(4-(trifluoromethyl)phenyl)ethyl diphenylphosphinate (1ah): According to **Procedure 5**. Yield: 1.35 g, 84%; white solid,

m.p. 118-119 °C; $^1\text{H NMR}$ (400 MHz, CDCl_3) δ 7.76-7.65 (m, 4H), 7.57-7.52 (m, 1H), 7.51-7.41 (m, 6H), 7.37-7.31 (m, 1H), 7.23-7.13 (m, 3H), 7.09-7.02 (m, 4H), 6.01 (d, $J = 10.0$ Hz, 1H) ppm; $^{13}\text{C NMR}$ (100 MHz, CDCl_3) peaks of the major isomer δ 142.6, 133.8 (d, $J_{\text{C-P}} = 0.6$ Hz), 132.4 (d, $J_{\text{C-P}} = 2.8$ Hz), 132.1 (d, $J_{\text{C-P}} = 2.8$ Hz), 131.55 (d, $J_{\text{C-P}} = 10.6$ Hz), 131.4 (q, $J_{\text{C-F}} = 32.6$ Hz), 131.00 (d, $J_{\text{C-P}} = 134.4$ Hz), 130.80 (d, $J_{\text{C-P}} = 139.6$ Hz), 129.5, 129.1, 128.9, 128.5 (d, $J_{\text{C-P}} = 13.4$ Hz), 128.1 (d, $J_{\text{C-P}} = 13.4$ Hz), 127.3, 124.7 (q, $J_{\text{C-F}} = 3.6$ Hz), 123.7 (q, $J_{\text{C-F}} = 270.6$ Hz), 92.3 (d, $J_{\text{C-P}} = 7.8$ Hz), 83.7 (d, $J_{\text{C-P}} = 5.6$ Hz) ppm; $^{31}\text{P NMR}$ (162 MHz, CDCl_3) δ 34.4 ppm; $^{19}\text{F NMR}$ (377 MHz, CDCl_3) δ -63.2 ppm; **HRMS (ESI)** (m/z) $[\text{M}+\text{H}]^+$ $\text{C}_{27}\text{H}_{21}^{35}\text{Cl}_2\text{F}_3\text{O}_2\text{P}$ calcd. for 535.0603, found 535.0608.



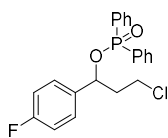
1,2-diphenylethyl diphenylphosphinate (1ai): According to **Procedure 4**. Yield: 860 mg, 72%; white solid, m.p. 140-141 °C; $^1\text{H NMR}$ (400 MHz, CDCl_3) δ 7.80-7.66 (m, 4H), 7.62-7.55 (m, 1H), 7.53-7.44 (m, 3H), 7.41-7.34 (m, 2H), 7.33-7.29

(m, 3H), 7.29-7.22 (m, 5H), 7.14-7.03 (m, 2H), 5.68-5.56 (m, 1H), 3.49 (dd, $J = 6.4, 13.2$ Hz, 1H), 3.31 (dd, $J = 6.8, 13.2$ Hz, 1H) ppm; $^{13}\text{C NMR}$ (100 MHz, CDCl_3) δ 140.0 (d, $J_{\text{C-P}} = 3.4$ Hz), 136.5, 132.05 (d, $J_{\text{C-P}} = 137.8$ Hz), 131.95 (d, $J_{\text{C-P}} = 2.7$ Hz), 131.88, 131.84 (d, $J_{\text{C-P}} = 10.3$ Hz), 131.57 (d, $J_{\text{C-P}} = 134.3$ Hz), 131.55 (d, $J_{\text{C-P}} = 10.2$ Hz), 130.0, 128.4 (d, $J_{\text{C-P}} = 13.1$ Hz), 128.19 (d, $J_{\text{C-P}} = 12.9$ Hz), 128.15 (one carbon is overlapping), 128.0, 126.7, 126.6, 79.0 (d, $J_{\text{C-P}} = 6.0$ Hz), 45.3 (d, $J_{\text{C-P}} = 4.6$ Hz) ppm; $^{31}\text{P NMR}$ (162 MHz, CDCl_3) δ 32.1 ppm; **HRMS (ESI)** (m/z) $[\text{M}+\text{H}]^+$ $\text{C}_{26}\text{H}_{24}\text{O}_2\text{P}$ calcd. for 399.1508, found 399.1508.

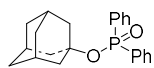


(5R)-2-methyl-5-(prop-1-en-2-yl)cyclohex-2-en-1-yl diphenylphosphinate (1aj): According to **Procedure 4**. Yield: 802.0 mg, 76%; two diastereomers, dr =

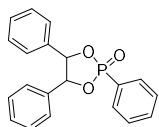
2:1; colorless oil; $^1\text{H NMR}$ (400 MHz, CDCl_3) δ 7.75-7.57 (m, 4H), 7.38-7.16 (m, 6H), 5.57-5.50 (m, 0.33H, the minor isomer), 5.45-5.37 (m, 0.67H, the major isomer), 4.94-4.83 (m, 0.67H, the major isomer), 4.73-4.67 (m, 0.33H, the minor isomer), 4.57-4.38 (m, 2H), 2.37-1.54 (m, 5H), 1.54 (s, 2H, the major isomer), 1.52 (s, 1H, the minor isomer), 1.46 (s, 3H) ppm; $^{13}\text{C NMR}$ (100 MHz, CDCl_3) (difficult to assign every peak) δ 148.4 (the minor isomer), 148.1 (the major isomer), 133.69, 133.63, 133.43, 133.30, 133.15, 132.80, 132.07, 132.04, 132.00, 131.97, 131.94, 131.80, 131.75, 131.70, 131.63, 131.61, 131.60, 131.53, 131.44, 128.49, 128.45, 128.36, 128.32, 128.02, 126.21, 109.38, 109.25, 75.63, 75.57, 73.25, 73.18, 40.37, 36.52, 35.40, 35.23, 30.74, 20.83, 20.40, 19.80 ppm; $^{31}\text{P NMR}$ (162 MHz, CDCl_3) δ 31.3 (1P, the major isomer), 31.1 (0.5P, the minor isomer) ppm; **HRMS (ESI)** (m/z) $[\text{M}+\text{H}]^+$ $\text{C}_{22}\text{H}_{26}\text{O}_2\text{P}$ calcd. for 353.1665, found 353.1664.



3-chloro-1-(4-fluorophenyl)propyl diphenylphosphinate (1ak): According to **Procedure 4**. Yield: 817.0 mg, 70%; colorless oil; $^1\text{H NMR}$ (400 MHz, CDCl_3) δ 7.91-7.81 (m, 2H), 7.67-7.54 (m, 3H), 7.54-7.42 (m, 3H), 7.37-7.29 (m, 2H), 7.29-7.22 (m, 2H), 7.05-6.93 (m, 2H), 5.60-5.48 (m, 1H), 3.73-3.60 (m, 1H), 3.53-3.42 (m, 1H), 2.67-2.53 (m, 1H), 2.32-2.21 (m, 1H) ppm; $^{13}\text{C NMR}$ (100 MHz, CDCl_3) δ 163.6 (d, $J_{\text{C-F}} = 245.6$ Hz), 135.4 (dd, $J = 3.1, 3.2$ Hz), 132.3 (d, $J_{\text{C-P}} = 2.8$ Hz), 132.1 (d, $J_{\text{C-P}} = 2.8$ Hz), 131.9 (d, $J_{\text{C-P}} = 10.3$ Hz), 131.7 (d, $J_{\text{C-P}} = 139.0$ Hz), 131.4 (d, $J_{\text{C-P}} = 10.1$ Hz), 131.0 (d, $J_{\text{C-P}} = 132.5$ Hz), 128.6 (d, $J_{\text{C-P}} = 13.2$ Hz), 128.4 (d, $J_{\text{C-F}} = 8.6$ Hz), 128.2 (d, $J_{\text{C-P}} = 13.3$ Hz), 115.5 (d, $J_{\text{C-F}} = 21.4$ Hz), 74.8 (d, $J_{\text{C-P}} = 5.8$ Hz), 41.1 (d, $J_{\text{C-P}} = 4.6$ Hz), 40.5 ppm; $^{31}\text{P NMR}$ (162 MHz, CDCl_3) δ 32.5 ppm; $^{19}\text{F NMR}$ (377 MHz, CDCl_3) δ -113.8 ppm; **HRMS (ESI)** (m/z) $[\text{M}+\text{H}]^+$ $\text{C}_{21}\text{H}_{20}^{35}\text{ClFO}_2\text{P}$ calcd. for 389.0868, found 389.0868.

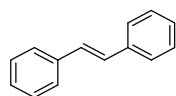


(3s,5s,7s)-adamantan-1-yl diphenylphosphinate (1al). According to **Procedure 6**. Yield: 1.32 g, 75%; white solid, m.p. 126-127 °C; $^1\text{H NMR}$ (400 MHz, CDCl_3) δ 7.69-7.60 (m, 4H), 7.35-7.22 (m, 6H), 2.00-1.90 (m, 9H), 1.45 (s, 6H) ppm; $^{13}\text{C NMR}$ (100 MHz, CDCl_3) δ 134.8 (d, $J_{\text{C-P}} = 137.5$ Hz), 131.5 (d, $J_{\text{C-P}} = 2.8$ Hz), 131.4 (d, $J_{\text{C-P}} = 10.2$ Hz), 128.3 (d, $J_{\text{C-P}} = 13.1$ Hz), 83.5 (d, $J_{\text{C-P}} = 8.7$ Hz), 44.6 (d, $J_{\text{C-P}} = 3.9$ Hz), 35.7, 31.2 ppm; $^{31}\text{P NMR}$ (162 MHz, CDCl_3) δ 26.5 ppm; **HRMS (ESI)** (m/z) $[\text{M}+\text{H}]^+$ $\text{C}_{22}\text{H}_{26}\text{O}_2\text{P}$ calcd. for 353.1665, found 353.1662.

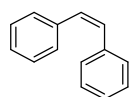


2,4,5-triphenyl-1,3,2-dioxaphospholane 2-oxide (4a). According to **Procedure 10**. Yield: 756.0 mg, 75%; white solid, m.p. 165-166 °C; $^1\text{H NMR}$ (400 MHz, CDCl_3) δ 7.95-7.85 (m, 2H), 7.57-7.51 (m, 1H), 7.49-7.41 (m, 2H), 7.31-7.20 (m, 8H), 7.12-7.04 (m, 2H), 5.42 (d, $J = 9.2$ Hz, 1H), 5.27 (dd, $J = 1.6, 9.2$ Hz, 1H) ppm; $^{13}\text{C NMR}$ (100 MHz, CDCl_3) δ 134.5 (d, $J_{\text{C-P}} = 10.0$ Hz), 134.3 (d, $J_{\text{C-P}} = 7.4$ Hz), 133.4 (d, $J_{\text{C-P}} = 3.2$ Hz), 132.3, 132.2, 129.5, 129.4, 128.98, 128.92, 128.88, 128.82, 127.0, 126.9 (d, $J_{\text{C-P}} = 184.5$ Hz), 126.5, 88.4 (d, $J_{\text{C-P}} = 1.7$ Hz), 85.3 ppm; $^{31}\text{P NMR}$ (162 MHz, CDCl_3) δ 34.07 ppm; **HRMS (ESI)** (m/z) $[\text{M}+\text{H}]^+$ $\text{C}_{20}\text{H}_{18}\text{O}_3\text{P}$ calcd. for 337.0988, found 337.0994. Literature NMR data is not available in CDCl_3 , but the compound has been previously reported.^[12]

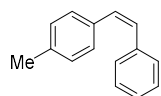
3.6.9 Characterization of Products



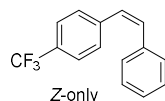
(E)-1,2-diphenylethene (E-2a): From the reaction of **1a** with DCA as e-PRCat according to **Procedure 11**, for 12 h. Yield: 28.0 mg, 75%; colorless solid, m.p. 124 °C; $^1\text{H NMR}$ (400 MHz, CDCl_3) δ 7.66 (d, $J = 7.6$ Hz, 4H), 7.54-7.46 (m, 4H), 7.43-7.38 (m, 2H), 7.26 (s, 2H) ppm; $^{13}\text{C NMR}$ (100 MHz, CDCl_3) δ 137.4, 128.73, 128.71, 127.7, 126.5 ppm; **HRMS (EI)** (m/z) [M] $\text{C}_{14}\text{H}_{12}$ calcd. for 180.0939, found 180.0939. Data are consistent with the literature.^[13]



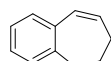
(Z)-1,2-diphenylethene (Z-2a): From the reaction of **1a** with $^n\text{BuO-NpMI}$ as e-PRCat according to **Procedure 11**, for 72 h. Yield: 25.0 mg, 78%; as a mixture of isomers with $E/Z = 1/10$; colorless liquid; $^1\text{H NMR}$ (400 MHz, CDCl_3) δ 7.29-7.18 (m, 10H), 6.62 (s, 2H) ppm; $^{13}\text{C NMR}$ (75 MHz, CDCl_3) δ 137.3, 130.3, 128.9, 128.2, 127.1 ppm; **HRMS (EI)** (m/z) [M] $\text{C}_{14}\text{H}_{12}$ calcd. for 180.0939, found 180.0941. Data are consistent with the literature.^[14]



(Z)-1-methyl-4-styrylbenzene (Z-2b): According to Procedure **11**. Yield: 28.0 mg, 72%; as a mixture of isomers with $E/Z = 1/10$; colorless liquid; $^1\text{H NMR}$ (400 MHz, CDCl_3) (Z - isomer) δ 7.30-7.19 (m, 5H), 7.17-7.13 (m, 2H), 7.04 (d, $J = 8.0$ Hz, 2H), 6.57 (s, 2H), 2.32 (s, 3H) ppm; $^{13}\text{C NMR}$ (100 MHz, CDCl_3) (Z - isomer) δ 137.5, 136.9, 134.3, 130.2, 129.6, 128.92, 128.86, 128.81, 128.2, 127.0, 21.3; **HRMS (ESI)** (m/z) [$\text{M}+\text{H}$] $^+$ $\text{C}_{15}\text{H}_{14}$ calcd. for 194.1096, found 194.1092. Data are consistent with the literature.^[15]

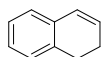


(Z)-1-styryl-4-(trifluoromethyl)benzene (Z-2c): According to Procedure **11**. Yield: 39.0 mg, 78%; colorless liquid; $^1\text{H NMR}$ (δ 7.50 (d, $J = 8.0$ Hz, 2H), 7.37 (d, $J = 8.0$ Hz, 2H), 7.32-7.20 (m, 5H), 6.76 (d, $J = 12.4$ Hz, 1H), 6.63 (d, $J = 12.4$ Hz, 1H) ppm; $^{13}\text{C NMR}$ (100 MHz, CDCl_3) δ 140.9, 136.6, 132.3, 129.2, 129.0 (d, $J_{C-P} = 139.6$ Hz), 128.97 (d, $J_{C-P} = 32.3$ Hz), 128.84, 128.76, 128.4, 127.6, 125.2 (q, $J_{C-F} = 3.7$ Hz), 124.2 (q, $J_{C-F} = 270.1$ Hz) ppm; $^{31}\text{P NMR}$ (162 MHz, CDCl_3) δ 34.4 (0.33P, the minor isomer), 34.0 (1P, the major isomer) ppm; $^{19}\text{F NMR}$ (377 MHz, CDCl_3) -63.1 (0.33F, the minor isomer), -63.2 (1F, the minor isomer) ppm; **HRMS (EI)** (m/z) [M] $\text{C}_{15}\text{H}_{11}\text{F}_3$ calcd. for 248.0813, found 248.0810. Data are consistent with the literature.^[16]



6,7-dihydro-5H-benzo[7]annulene (2d): According to Procedure **11**. Yield: 20.0 mg, 69%; colorless liquid; $^1\text{H NMR}$ (400 MHz, CDCl_3) δ 7.12-6.96 (m, 4H), 6.33 (d, $J =$

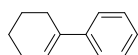
12.4 Hz, 1H), 5.82 (dd, $J = 12.4, 4.4$ Hz, 1H), 2.80-2.74 (m, 2H), 2.39-2.30 (m, 2H), 1.94-1.84 (m, 2H) ppm; ^{13}C NMR (100 MHz, CDCl_3) δ 141.7, 136.3, 132.3, 130.9, 129.8, 129.0, 126.6, 125.9, 36.2, 32.5, 27.0 ppm; HRMS (EI) (m/z) [M] $\text{C}_{11}\text{H}_{12}$ calcd. for 144.0939, found 144.0937. Data are consistent with the literature.^[17]



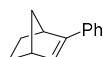
1,2-dihydronaphthalene (2e): According to Procedure 11. Yield: 20.0 mg, 77%; colorless liquid; ^1H NMR (400 MHz, CDCl_3) δ 7.34-7.23 (m, 3H), 7.20-7.15 (m, 1H), 6.62 (d, $J = 10.0$ Hz, 1H), 6.22-6.15 (m, 1H), 2.96 (t, $J = 8.0$ Hz, 2H), 2.52-2.44 (m, 2H) ppm; ^{13}C NMR (100 MHz, CDCl_3) δ 135.5, 134.2, 128.7, 127.8, 127.5, 126.9, 126.5, 125.9, 27.5, 23.2 ppm; HRMS (EI) (m/z) [M] $\text{C}_{10}\text{H}_{10}$ calcd. for 130.0783, found 130.0780. Data are consistent with the literature.^[18]



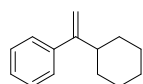
1H-indene (2f): According to Procedure 11. Yield: 19.0 mg, 83%; light yellow liquid; ^1H NMR (400 MHz, CDCl_3) δ 7.34 (d, $J = 7.6$ Hz, 1H), 7.27 (d, $J = 7.6$ Hz, 1H), 7.16-7.11 (m, 1H), 7.08-7.02 (m, 1H), 6.78-6.72 (m, 1H), 6.42 (dt, $J = 5.2, 2.0$ Hz, 1H), 3.26 (q, $J = 2.0$ Hz, 2H) ppm; ^{13}C NMR (100 MHz, CDCl_3) δ 144.9, 143.7, 134.2, 132.1, 126.3, 124.6, 123.7, 121.0, 39.1 ppm; HRMS (EI) (m/z) [M] C_9H_8 calcd. for 116.0626, found 116.0624. Data are consistent with the literature.^[18]



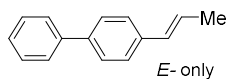
2,3,4,5-tetrahydro-1,1'-biphenyl (2g): According to Procedure 11. Yield: 25.0 mg, 78%; colorless liquid; ^1H NMR (300 MHz, CDCl_3) δ 7.43-7.37 (m, 2H), 7.35-7.28 (m, 2H), 7.26-7.19 (m, 1H), 6.17-6.09 (m, 1H), 2.47-2.37 (m, 2H), 2.27-2.16 (m, 2H), 1.85-1.75 (m, 2H), 1.73-1.63 (m, 2H) ppm; ^{13}C NMR (75 MHz, CDCl_3) δ 142.7, 136.6, 128.2, 126.5, 125.0, 124.8, 27.4, 25.9, 23.1, 22.2 ppm; HRMS (EI) (m/z) [M] $\text{C}_{12}\text{H}_{14}$ calcd. for 158.1096, found 158.1110. Data are consistent with the literature.^[19]



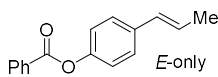
(1S,4R)-2-phenylbicyclo[2.2.1]hept-2-ene (2h): According to Procedure 11. Yield: 25.0 mg, 73%; colorless liquid; ^1H NMR (400 MHz, CDCl_3) δ 7.40-7.34 (m, 2H), 7.29-7.23 (m, 2H), 7.20-7.11 (m, 1H), 6.25 (d, $J = 3.2$ Hz, 1H), 3.30-3.24 (m, 1H), 2.98-2.92 (m, 1H), 1.77-1.71 (m, 2H), 1.50-1.45 (m, 1H), 1.26-1.17 (m, 1H), 1.13-1.08 (m, 2H) ppm; ^{13}C NMR (100 MHz, CDCl_3) δ 147.8, 135.8, 129.7, 128.4, 126.7, 124.9, 47.9, 43.4, 43.1, 26.8, 24.8 ppm; HRMS (EI) (m/z) [M] $\text{C}_{13}\text{H}_{14}$ calcd. for 170.1096, found 170.1088. Data are consistent with the literature.^[20]



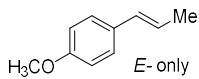
(1-cyclohexylvinyl)benzene (2i): According to Procedure 11. Yield: 23.0 mg, 61%; colorless liquid; $^1\text{H NMR}$ (400 MHz, CDCl_3) δ 7.29-7.16 (m, 5H), 5.09-5.03 (m, 1H), 4.97-4.90 (m, 1H), 2.40-2.30 (m, 1H), 1.82-1.68 (m, 4H), 1.67-1.59 (m, 1H), 1.33-1.19 (m, 2H), 1.18-1.03 (m, 3H) ppm; $^{13}\text{C NMR}$ (100 MHz, CDCl_3) δ 155.0, 143.0, 128.1, 127.0, 126.6, 110.3, 42.6, 32.7, 26.8, 26.5 ppm; **HRMS (EI)** (m/z) [M] $\text{C}_{14}\text{H}_{18}$ calcd. for 186.1409, found 186.1414. Data are consistent with the literature.^[21]



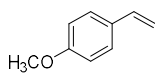
4-(prop-1-en-1-yl)-1,1'-biphenyl (2j): According to Procedure 11. Yield: 27.0 mg, 71%; white solid, m.p. 121-123 °C; $^1\text{H NMR}$ (400 MHz, CDCl_3) δ 7.46-7.42 (m, 2H), 7.40-7.36 (m, 1H), 7.30-7.23 (m, 4H), 7.21-7.15 (m, 1H), 6.29 (d, $J = 15.6$ Hz, 1H), 6.14 (dq, $J = 15.6, 6.4$ Hz, 1H), 1.76 (dd, $J = 6.4, 1.6$ Hz, 3H) ppm; $^{13}\text{C NMR}$ (100 MHz, CDCl_3) δ 140.9, 139.5, 137.0, 130.6, 128.8, 127.20, 127.15, 126.9, 126.2, 125.9, 18.6 ppm; **HRMS (EI)** (m/z) [M] $\text{C}_{15}\text{H}_{14}$ calcd. for 194.1096, found 194.1089. Data are consistent with the literature.^[22]



(E)-4-(prop-1-en-1-yl)phenyl benzoate (2k): According to Procedure 11. Yield: 32.0 mg, 72%; colorless oil; $^1\text{H NMR}$ (400 MHz, CDCl_3) δ 8.35-8.27 (m, 2H), 7.78-7.71 (m, 1H), 7.66-7.57 (m, 2H), 7.48 (d, $J = 8.4$ Hz, 2H), 7.25 (d, $J = 8.4$ Hz, 2H), 6.57-6.48 (m, 1H), 6.39-6.26 (m, 1H), 2.00 (dd, $J = 1.6, 6.4$ Hz, 3H) ppm; $^{13}\text{C NMR}$ (100 MHz, CDCl_3) δ 165.2, 149.7, 135.9, 133.6, 130.2, 130.2, 129.6, 128.6, 126.8, 126.0, 121.7, 18.5 ppm; **HRMS (EI)** (m/z) [M] $\text{C}_{16}\text{H}_{14}\text{O}_2$ calcd. for 238.0994, found 238.1001. Data are consistent with the literature.^[23]

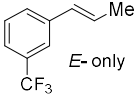


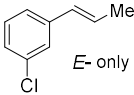
(E)-1-methoxy-4-(prop-1-en-1-yl)benzene (2l): According to Procedure 11. Yield: 7.4 mg, 25%; colorless liquid; $^1\text{H NMR}$ (400 MHz, CDCl_3) δ 7.30-7.24 (m, 2H), 6.88-6.81 (m, 2H), 6.35 (dq, $J = 15.6, 1.6$ Hz, 1H), 6.10 (dq, $J = 15.6, 6.8$ Hz, 1H), 3.81 (s, 3H), 1.87 (dd, $J = 1.6, 6.8$ Hz, 3H) ppm; $^{13}\text{C NMR}$ (100 MHz, CDCl_3) δ 158.6, 130.8, 130.4, 126.9, 123.5, 113.9, 55.3, 18.4 ppm; **HRMS (EI)** (m/z) [M] $\text{C}_{10}\text{H}_{12}\text{O}$ calcd. for 148.0888, found 148.0885. Data are consistent with the literature.^[24]

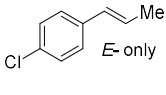


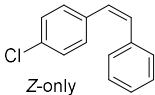
1-methoxy-4-vinylbenzene (2m): According to Procedure 11. Yield: 4.0 mg, 15%; colorless liquid; $^1\text{H NMR}$ (400 MHz, CDCl_3) δ 7.31-7.23 (m, 2H), 6.83-6.75 (m, 2H), 6.59 (dd, $J = 10.8, 17.6$ Hz, 1H), 5.53 (dd, $J = 0.8, 17.6$ Hz, 1H), 5.05 (dd, $J = 0.8, 10.8$ Hz, 1H), 3.73 (s, 3H) ppm; $^{13}\text{C NMR}$ (100 MHz, CDCl_3) δ 159.4, 136.2, 130.5, 127.4,

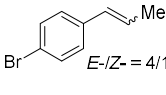
113.9, 111.6, 55.3 ppm; **HRMS (EI)** (m/z) [M] $C_9H_{10}O$ calcd. for 134.0732, found 134.0727. Data are consistent with the literature.^[25]

 **(E)-1-(prop-1-en-1-yl)-3-(trifluoromethyl)benzene (2n):** According to Procedure 11. Yield: 29.0 mg, 78%; colorless liquid; **¹H NMR (300 MHz, CDCl₃)** δ 7.49 (s, 1H), 7.46-7.28 (m, 3H), 6.36 (d, $J = 22.4$ Hz, 1H), 6.24 (dq, $J = 22.8, 8.0$ Hz, 1H), 1.83 (dd, $J = 1.2, 6.3$ Hz, 3H) ppm; **¹³C NMR (75 MHz, CDCl₃)** δ 138.7, 129.8, 129.0, 128.9, 127.9, 126.0, 124.7 (q, $J_{C-F} = 270.9$ Hz), 123.3 (q, $J_{C-F} = 15.6$ Hz), 122.5 (q, $J_{C-F} = 15.3$ Hz), 118.9, 118.2, 18.5 ppm; **¹⁹F NMR (282 MHz, CDCl₃)** δ -63.3 ppm; **HRMS (EI)** (m/z) [M] $C_{10}H_9F_3$ calcd. for 186.0656, found 186.0661. Data are consistent with the literature.^[26]

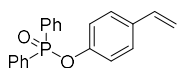
 **(E)-1-(prop-1-en-1-yl)-3-chlorobenzene (2o):** According to Procedure 11. Yield: 17.0 mg, 56%; colorless liquid; **¹H NMR (400 MHz, CDCl₃)** δ 7.32-7.29 (m, 1H), 7.24-7.13 (m, 3H), 6.34 (dq, $J = 15.6, 1.2$ Hz, 1H), 6.25 (dq, $J = 15.6, 6.0$ Hz, 1H), 1.88 (dd, $J = 6.4, 1.2$ Hz, 3H) ppm; **¹³C NMR (100 MHz, CDCl₃)** δ 139.8, 134.4, 129.8, 129.7, 127.4, 126.7, 125.8, 124.0, 18.5 ppm; **HRMS (EI)** (m/z) [M] C_9H_9Cl calcd. for 152.0393, found 152.0393. Data are consistent with the literature.^[27]

 **(E)-1-chloro-4-(prop-1-en-1-yl)benzene (2p):** According to Procedure 11. Yield: 21.0 mg, 69%; colorless liquid; **¹H NMR (400 MHz, CDCl₃)** δ 7.28-7.23 (m, 4H), 6.37 (dq, $J = 15.6, 1.6$ Hz, 1H), 6.23 (dq, $J = 15.6, 6.4$ Hz, 1H), 1.89 (dd, $J = 1.6, 6.4$ Hz, 3H) ppm; **¹³C NMR (100 MHz, CDCl₃)** δ 136.4, 132.3, 129.9, 128.6, 127.0, 126.5, 18.5 ppm; **HRMS (EI)** (m/z) [M] C_9H_9Cl calcd. for 152.0393, found 152.0393. Data are consistent with the literature.^[27]

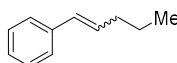
 **(Z)-1-chloro-4-styrylbenzene (2q):** According to Procedure 11. Yield: 24.0 mg, 57%; colorless liquid; **¹H NMR (300 MHz, CDCl₃)** δ 7.25-7.20 (m, 5H), 7.20-7.13 (m, 4H), 6.63 (d, $J = 12.3$ Hz, 1H), 6.53 (d, $J = 12.0$ Hz, 1H) ppm; **¹³C NMR (75 MHz, CDCl₃)** δ 136.9, 135.7, 132.8, 131.0, 130.2, 129.0, 128.8, 128.4, 128.4, 127.4 ppm; **HRMS (EI)** (m/z) [M] $C_{14}H_{11}^{35}Cl$ calcd. for 214.0549, found 214.0551. Data are consistent with the literature.^[28]

 **1-bromo-4-(prop-1-en-1-yl)benzene (2r):** According to Procedure 11. Yield: 15.0 mg, 39%; mixture of two isomers, $E/Z = 4/1$; colorless liquid; **¹H NMR (300 MHz, CDCl₃)** δ 7.47-7.43 (m, 0.4H, the *Z*- isomer), 7.42-7.37 (m, 1.6H, the *E*- isomer),

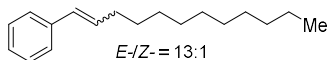
7.22-7.13 (m, 2H), 6.39-6.30 (m, 1H), 6.23 (dq, $J = 18.6, 5.6$ Hz ppm, 0.8H, the *E* isomer), 5.82 (dq, $J = 11.7, 7.2$ Hz, 0.2H, the *Z* isomer), 1.87 (dd, $J = 6.3, 1.2$ Hz, 3H) ppm; ^{13}C NMR (100 MHz, CDCl_3) (the *E* isomer) δ 136.9, 131.5, 129.9, 127.4, 126.6, 120.3, 18.5 ppm; HRMS (EI) (m/z) [M] $\text{C}_9\text{H}_9^{79}\text{Br}$ calcd. for 195.9888, found 195.9887. Data are consistent with the literature.^[29]



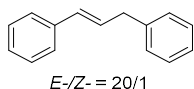
4-vinylphenyl diphenylphosphinate (2s): According to Procedure 11. Yield: 38.0 mg, 60%; white solid, m.p. 86-88 °C; ^1H NMR (400 MHz, CDCl_3) δ 7.93-7.86 (m, 4H), 7.55-7.49 (m, 2H), 7.47-7.42 (m, 4H), 7.29-7.23 (m, 2H), 7.19-7.13 (m, 2H), 6.60 (dd, $J = 17.6, 11.2$ Hz, 1H), 5.61 (d, $J = 17.6$ Hz, 1H), 5.16 (d, $J = 11.2$ Hz, 1H) ppm; ^{13}C NMR (100 MHz, CDCl_3) δ 150.5 (d, $J_{\text{C-P}} = 8.3$ Hz), 135.8, 134.1 (d, $J_{\text{C-P}} = 1.0$ Hz), 132.5 (d, $J_{\text{C-P}} = 2.8$ Hz), 131.8 (d, $J_{\text{C-P}} = 10.3$ Hz), 130.9 (d, $J_{\text{C-P}} = 137.3$ Hz), 128.6 (d, $J_{\text{C-P}} = 13.4$ Hz), 127.4, 120.8 (d, $J_{\text{C-P}} = 4.8$ Hz), 113.6 ppm ^{31}P NMR (162 MHz, CDCl_3) δ ppm; HRMS (ESI) (m/z) [M+H]⁺ $\text{C}_{20}\text{H}_{18}\text{O}_2\text{P}$ calcd. for 321.1039, found 321.1040.



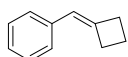
pent-1-en-1-ylbenzene (2t): According to Procedure 11. Yield: 20.0 mg, 68%; as a mixture of isomers, *E*-/*Z*- = 10:1; colorless liquid; ^1H NMR (300 MHz, CDCl_3) δ 7.36-7.26 (m, 4H), 7.23-7.16 (m, 1H), 6.43 (d, $J = 11.7$ Hz, 0.09H, the *Z*- isomer), 6.39 (d, $J = 15.9$ Hz, 0.91H, the *E*- isomer), 6.23 (dt, $J = 15.9, 6.9$ Hz, 0.92H, the *E*- isomer), 5.68 (dt, $J = 11.7, 7.2$ Hz, 0.09H, the *Z*- isomer), 2.37-2.27 (m, 0.20H, the *Z*- isomer), 2.24-2.15 (m, 1.88H, the *E*- isomer), 1.58-1.43 (m, 2H), 0.99-0.93 (m, 3H) ppm; ^{13}C NMR (75 MHz, CDCl_3) δ 138.0, 131.0, 129.9, 128.5, 126.8, 125.9, 35.2, 22.6, 13.8 ppm; HRMS (EI) (m/z) [M] $\text{C}_{11}\text{H}_{14}$ calcd. for 146.1096, found 146.1089. Data are consistent with the literature.^[30]



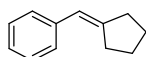
(*E*)-dodec-1-en-1-ylbenzene (2u): According to Procedure 11. Yield: 39.0 mg, 79%; *E*-/*Z*- = 13:1; colorless liquid; ^1H NMR (400 MHz, CDCl_3) δ 7.35-7.29 (m, 2H), 7.29-7.23 (m, 2H), 7.18-7.13 (m, 1H), 6.38 (d, $J = 11.6$ Hz, 0.07H, the *Z*- isomer), 6.35 (d, $J = 16.0$ Hz, 0.93H, the *E*- isomer), 6.20 (dt, d, $J = 15.6, 6.8$ Hz, 0.93H, the *E*- isomer), 5.64 (dt, $J = 11.6, 5.8$ Hz, 0.07H), 2.33-2.27 (m, 0.15H, the *Z*- isomer), 2.21-2.14 (m, 1.90H, the *E*- isomer), 1.47-1.38 (m, 2H), 1.31-1.21 (m, 14H), 0.86 (t, $J = 6.4$ Hz, 3H) ppm; ^{13}C NMR (100 MHz, CDCl_3) δ (peaks for the *E*- isomer only) 138.0, 131.3, 129.7, 128.5, 126.8, 125.9, 33.1, 32.0, 29.7 (one carbon is overlapping), 29.6, 29.4, 29.4, 29.3, 22.7, 14.2 ppm; HRMS (EI) (m/z) [M] $\text{C}_{18}\text{H}_{28}$ calcd. for 244.2191, found 244.2186. Data are consistent with the literature.^[31]



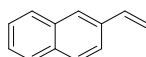
prop-1-ene-1,3-diyl dibenzene (2v): According to **Procedure 11**. Yield: 24.0 mg, 62%; *E*-/*Z*- = 20/1; colorless liquid; $^1\text{H NMR}$ (300 MHz, CDCl_3) δ 7.41-7.19 (m, 10H), 6.62 (dt, $J = 7.6, 2.0$ Hz, 0.05H, the *Z*- isomer), 6.49 (d, $J = 15.9$ Hz, 0.95H, the *E*- isomer), 6.38 (dt, $J = 15.9, 6.3$ Hz, 0.95H, the *E*- isomer), 5.89 (dt, $J = 11.7, 6.0$ Hz, 0.04H, the *Z*- isomer), 3.71 (d, $J = 7.5$ Hz, 0.09H), 3.58 (d, $J = 6.3$ Hz, 1.91H) ppm; $^{13}\text{C NMR}$ (75 MHz, CDCl_3) δ (*E*- isomer only) 140.2, 137.5, 131.1, 129.3, 128.7, 128.6 (one carbon is overlapping), 127.2, 126.23, 126.17 (2C), 39.4 ppm; **HRMS (EI)** (m/z) [M] $\text{C}_{15}\text{H}_{14}$ calcd. for 194.1096, found 194.1085. Data are consistent with the literature.^[32]



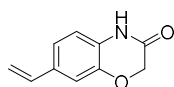
(cyclobutylidene)methyl benzene (2w): According to **Procedure 11**. Yield: 24.0 mg, 83%; colorless liquid; $^1\text{H NMR}$ (300 MHz, CDCl_3) δ 7.36-7.28 (m, 2H), 7.25-7.20 (m, 2H), 7.20-7.13 (m, 1H), 6.13-6.07 (m, 1H), 3.12-3.03 (m, 2H), 2.96-2.87 (m, 2H), 2.20-2.07 (m, 2H) ppm; $^{13}\text{C NMR}$ (75 MHz, CDCl_3) δ 144.9, 138.1, 128.4, 127.1, 125.8, 120.9, 32.8, 32.7, 18.4 ppm; **HRMS (EI)** (m/z) [M] $\text{C}_{11}\text{H}_{12}$ calcd. for 144.0939, found 144.0933. Data are consistent with the literature.^[33]



(cyclopentylidene)methyl benzene (2x): According to **Procedure 11**. Yield: 27.0 mg, 87%; colorless liquid; $^1\text{H NMR}$ (300 MHz, CDCl_3) δ 7.27-7.20 (m, 4H), 7.13-7.04 (m, 1H), 6.31-6.25 (m, 1H), 2.52-2.38 (m, 4H), 1.80-1.53 (m, 4H) ppm; $^{13}\text{C NMR}$ (75 MHz, CDCl_3) δ 147.3, 138.9, 128.2 (2C), 128.0 (2C), 125.6, 120.8, 36.0, 31.2, 27.3, 25.7 ppm; **HRMS (EI)** (m/z) [M] $\text{C}_{12}\text{H}_{14}$ calcd. for 158.1096, found 158.1090. Data are consistent with the literature.^[34]

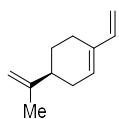


2-vinylnaphthalene (2y): According to **Procedure 11**. Yield: 19.0 mg, 62%; white solid, m.p. 64-66 °C; $^1\text{H NMR}$ (400 MHz, CDCl_3) δ 7.67-7.58 (m, 3H), 7.56 (s, 1H), 7.45 (dd, $J = 1.6, 8.8$ Hz, 1H), 7.35-7.21 (m, 2H), 6.70 (dd, $J = 10.8, 17.6$ Hz, 1H), 5.69 (d, $J = 17.6$ Hz, 1H), 5.15 (d, $J = 10.8$ Hz, 1H) ppm; $^{13}\text{C NMR}$ (100 MHz, CDCl_3) δ 137.0, 135.0, 133.6, 133.2, 128.2, 128.1, 127.7, 126.4, 126.3, 125.9, 123.2, 114.2 ppm; **HRMS (EI)** (m/z) [M] $\text{C}_{12}\text{H}_{10}$ calcd. for 154.0783, found 154.0785. Data are consistent with the literature.^[35]



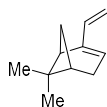
7-vinyl-2H-benzo[*b*][1,4]oxazin-3(4H)-one (2z): According to **Procedure 11**. Yield: 17.0 mg, 49%; light yellow solid, m.p. 187-188 °C; $^1\text{H NMR}$ (400 MHz, CDCl_3) δ 9.44 (s, 1H), 7.27 (dd, $J = 2.0, 8.4$ Hz, 1H), 7.20-7.10 (m, 2H), 6.86 (dd, $J = 10.8, 17.6$ Hz, 1H), 5.88 (d, $J = 17.6$ Hz, 1H), 5.44 (d, $J = 11.2$ Hz, 1H), 4.87 (s, 2H) ppm; $^{13}\text{C NMR}$ (100

MHz, CDCl₃) δ 166.2, 143.3, 135.5, 132.8, 126.1, 122.4, 116.8, 113.6, 113.4, 67.3 ppm; **HRMS (ESI) (*m/z*)** $[M+H]^+$ C₁₀H₁₀NO₂ calcd for 176.0633, found 175.0631.



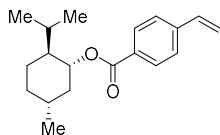
7(S)-4-(prop-1-en-2-yl)-1-vinylcyclohex-1-ene (2ab): According to **Procedure 11**.

Yield: 10.0 mg, 33%; colorless liquid; **¹H NMR (300 MHz, CDCl₃)** δ 6.37 (dd, $J = 10.8, 17.7$ Hz, 1H), 5.81-5.74 (m, 1H), 5.07 (d, $J = 17.4$ Hz, 1H), 4.92 (d, $J = 10.8$ Hz, 1H), 4.76-4.70 (m, 2H), 2.39-2.00 (m, 5H), 1.97-1.85 (m, 1H), 1.78-1.71 (m, 3H), 1.57-1.47 (m, 1H) ppm; **¹³C NMR (75 MHz, CDCl₃)** δ 149.8, 139.7, 135.8, 129.2, 110.1, 108.7, 41.2, 31.2, 27.3, 24.3, 20.8 ppm; **HRMS (EI) (*m/z*)** $[M]$ C₁₁H₁₆ calcd. for 148.1252, found 148.1251. Data are consistent with the literature.^[36]



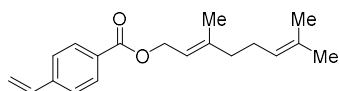
(1R,5S)-6,6-dimethyl-2-vinylbicyclo[3.1.1]hept-2-ene (2ac): According to

Procedure 11. Yield: 9.0 mg, 30%; colorless liquid; **¹H NMR (400 MHz, CDCl₃)** δ 6.37 (dd, $J = 10.8, 17.6$ Hz, 1H), 5.59-5.53 (m, 1H), 5.05 (d, $J = 17.2$ Hz, 1H), 4.89 (d, $J = 10.8$ Hz, 1H), 2.57 (t, $J = 5.2$ Hz, 1H), 2.46-2.41 (m, 1H), 2.39-2.27 (m, 2H), 2.17-2.09 (m, 1H), 1.33 (s, 3H), 1.14 (d, $J = 8.8$ Hz, 1H), 0.80 (s, 3H) ppm; **¹³C NMR (100 MHz, CDCl₃)** δ 146.8, 137.8, 124.5, 109.6, 41.0, 40.3, 37.69, 3.9, 31.2, 26.4, 20.7 ppm; **HRMS (EI) (*m/z*)** $[M]$ C₁₁H₁₆ calcd. for 148.1252, found 148.1251. Data are consistent with the literature.^[37]



(1R,2S,5R)-2-isopropyl-5-methylcyclohexyl 4-vinylbenzoate (2ad):

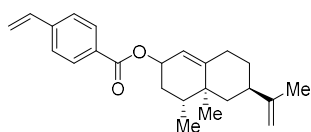
According to **Procedure 11**. Yield: 26.0 mg, 45%; colorless liquid; **¹H NMR (400 MHz, CDCl₃)** δ 7.85-7.74 (m, 2H), 7.30-7.20 (m, 2H), 6.54 (dd, $J = 10.8, 17.6$ Hz, 1H), 5.65 (d, $J = 17.6$ Hz, 1H), 5.16 (d, $J = 10.8$ Hz, 1H), 4.72 (dt, $J = 4.4, 10.8$ Hz, 1H), 1.96-1.88 (m, 1H), 1.80-1.70 (m, 1H), 1.57-1.47 (m, 2H), 1.41-1.29 (m, 2H), 0.98-0.84 (m, 2H), 0.79-0.73 (m, 1H), 0.73-0.69 (m, 6H), 0.59 (d, $J = 6.8$ Hz, 3H) ppm; **¹³C NMR (100 MHz, CDCl₃)** δ 165.9, 141.8, 136.1, 130.0, 129.9, 126.1, 116.3, 74.8, 47.3, 41.0, 34.4, 31.5, 26.6, 23.7, 22.1, 20.8, 16.6 ppm; **HRMS (ESI) (*m/z*)** $[M+H]^+$ C₁₉H₂₇O₂ calcd. for 287.1933, found 286.1920. Data are consistent with the literature.^[38]



(E)-3,7-dimethylocta-2,6-dien-1-yl 4-vinylbenzoate (2ae):

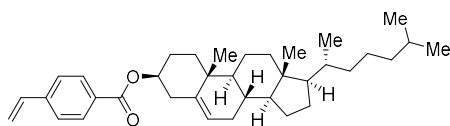
According to **Procedure 11**. Yield: 30.0 mg, 52%; colorless liquid; **¹H NMR (400 MHz, CDCl₃)** δ 7.84-7.76 (m, 2H), 7.29-7.21 (m, 2H), 6.55 (dd, $J = 10.8, 17.2$ Hz, 1H), 5.65 (d, $J = 17.2$ Hz, 1H), 5.32-5.23 (m, 1H), 5.17 (d, $J = 10.8$ Hz, 1H), 4.95-4.84 (m, 1H), 4.64 (d, $J = 7.2$ Hz, 2H), 1.97-1.83 (m, 4H), 1.57 (s, 3H), 1.48 (s, 3H), 1.40 (s, 3H) ppm; **¹³C NMR (100 MHz, CDCl₃)** δ 166.4, 142.3, 141.8, 136.1, 131.9, 129.9, 129.7, 126.1, 123.8,

118.5, 116.4, 61.9, 39.6, 26.3, 25.7, 17.7, 16.6 ppm; **HRMS (ESI)** (m/z) $[M+H]^+$ $C_{19}H_{25}O_2$ calcd. for 285.1849, found 285.1847.



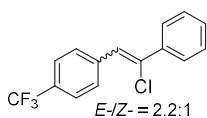
(4R,4aS,6R)-4,4a-dimethyl-6-(prop-1-en-2-yl)-2,3,4,4a,5,6,7,8-octahydronaphthalen-2-yl 4-vinylbenzoate (2af): According to **Procedure 11**. Yield: 26.0 mg, 37%; colorless liquid; 1H NMR (400

MHz, $CDCl_3$) δ 7.86-7.76 (m, 2H), 7.30-7.21 (m, 2H), 6.55 (dd, $J = 10.8, 17.6$ Hz, 1H), 5.66 (d, $J = 17.6$ Hz, 1H), 5.41-5.34 (m, 1H), 5.22-5.15 (m, 2H), 4.54-4.46 (m, 2H), 2.21-2.12 (m, 1H), 2.10-2.01 (m, 1H), 2.00-1.93 (m, 1H), 1.75-1.60 (m, 3H), 1.53 (s, 3H), 1.52-1.36 (m, 3H), 1.09-1.02 (m, 1H), 0.86 (s, 3H), 0.74 (d, $J = 6.0$ Hz, 1H) ppm; ^{13}C NMR (100 **MHz, $CDCl_3$)** δ 166.3, 150.1, 147.9, 141.8, 136.1, 129.9 (one carbon is overlapping), 126.0, 120.2, 116.3, 108.7, 71.6, 44.51, 40.8, 39.2, 38.2, 32.8, 32.7, 32.4, 20.8, 18.2, 15.4 ppm; **HRMS (ESI)** (m/z) $[M+Na]^+$ $C_{24}H_{30}NaO_2$ calcd. for 373.2138, found 373.2140.



(3S,8S,9S,10R,13R,14S,17R)-10,13-dimethyl-17-((R)-2,3,4,7,8,9,10,11,12,13,14,15,16,17-tetradecahydro-

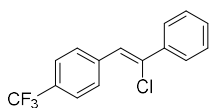
1H-cyclopenta[a]phenanthren-3-yl 4-vinylbenzoate (2ag): Yield: 41.0 mg, 40%; white solid, m.p. 179-181 °C; 1H NMR (400 **MHz, $CDCl_3$)** δ 7.80 (d, $J = 8.0$ Hz, 2H), 7.25 (d, $J = 8.4$ Hz, 2H), 6.55 (dd, $J = 10.8, 17.6$ Hz, 1H), 5.66 (d, $J = 17.6$ Hz, 1H), 5.22 (d, $J = 4.0$ Hz, 1H), 5.17 (d, $J = 11.2$ Hz, 1H), 4.72-4.58 (m, 1H), 2.27 (d, $J = 7.6$ Hz, 2H), 1.87-1.75 (m, 3H), 1.75-1.68 (m, 1H), 1.67-1.57 (m, 1H), 1.57-1.46 (m, 1H), 1.44-1.25 (m, 6H), 1.22-1.11 (m, 3H), 1.11-0.88 (m, 8H), 0.87 (s, 3H), 0.86-0.75 (m, 4H), 0.73 (d, $J = 6.4$ Hz, 3H), 0.68 (dd, $J = 2.0, 6.8$ Hz, 6H), 0.49 (s, 3H) ppm; ^{13}C NMR (100 **MHz, $CDCl_3$)** δ 165.8, 141.8, 139.7, 136.1, 130.0, 129.9, 126.0, 122.8, 116.3, 74.6, 56.7, 56.2, 50.1, 42.4, 39.8, 39.6, 38.3, 37.1, 36.7, 36.2, 35.8, 32.0, 31.9, 28.3, 28.1, 27.9, 24.3, 23.9, 22.9, 22.6, 21.1, 19.4, 18.8, 11.9 ppm; **HRMS (ESI)** (m/z) $[M]^+$ $C_{36}H_{52}O_2$ calcd. for 516.3967, found 516.3967. Data are consistent with the literature.^[39]



1-(2-chloro-2-phenylvinyl)-4-(trifluoromethyl)benzene (2ah): According to **Procedure 11**. Yield: 39 mg, 69%; as a mixture of isomers, $E/Z = 2.2:1$;

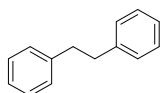
1H NMR (400 **MHz, $CDCl_3$)** δ 7.89 (d, $J = 8.4$ Hz, 0.63H, the Z - isomer), 7.84 (d, $J = 7.6$ Hz, 0.63H, the Z - isomer), 7.74 (d, $J = 8.4$ Hz, 0.66H, the Z - isomer), 7.64 (d, $J = 8.0$ Hz, 1.38H, the E - isomer), 7.57 (d, $J = 8.4$ Hz, 1.19H, the E - isomer), 7.50 (d, $J = 7.6$ Hz, 0.67H, the E isomer), 7.43 (d, $J = 7.2$ Hz, 0.32H, the Z - isomer), 7.29-7.25 (m, 1.19H, the E - isomer), 7.25-7.23 (m, 0.61H, the Z - isomer), 7.21 (s, 0.31H, the Z - isomer), 7.11 (s, 0.60H, the E - isomer), 7.07-7.02 (m, 1.22H, the E - isomer) ppm; ^{19}F NMR (377 **MHz, $CDCl_3$)** δ -63.2

(0.46F, the *E*- isomer), -63.3 (1F, the *Z*- isomer) ppm. The isomer below was isolated by careful chromatography for characterization and identity confirmation:



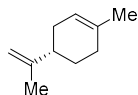
(Z)-1-(2-chloro-2-phenylvinyl)-4-(trifluoromethyl)benzene (Z-2ah):

According to **Procedure 11**. White solid, m.p. 143-144 °C; $^1\text{H NMR}$ (400 MHz, CDCl_3) δ 7.94 (d, $J = 8.0$ Hz, 2H), 7.88 (d, $J = 7.2$ Hz, 2H), 7.79 (d, $J = 8.0$ Hz, 2H), 7.58-7.52 (m, 2H), 7.50-7.44 (m, 1H), 7.26 (s, 1H) ppm; $^{13}\text{C NMR}$ (100 MHz, CDCl_3) δ 142.7, 134.7, 130.6 (q, $J_{\text{C-F}} = 32.4$ Hz), 130.5, 129.6, 128.6, 128.4, 128.0, 127.0, 125.5 (q, $J_{\text{C-F}} = 3.8$ Hz), 124.0 (q, $J_{\text{C-F}} = 270.4$ Hz); $^{19}\text{F NMR}$ (377 MHz, CDCl_3) δ -63.2 ppm; **HRMS (ESI)** (m/z) $[\text{M}+\text{H}]^+$ $\text{C}_{15}\text{H}_{11}^{35}\text{ClF}_3$ calcd. for 283.0496, found 283.0423.



1,2-diphenylethane (2ai): According to **Procedure 11**. Yield: 19.0 mg, 51%;

colorless crystal, m.p. 46 °C; $^1\text{H NMR}$ (400 MHz, CDCl_3) δ 7.38-7.32 (m, 4H), 7.29-7.23 (m, 6H), 2.99 (s, 4H) ppm; $^{13}\text{C NMR}$ (100 MHz, CDCl_3) δ 141.8, 128.5, 128.4, 125.9, 37.8 (2C) ppm; **HRMS (ESI)** (m/z) $[\text{M}]$ $\text{C}_{14}\text{H}_{14}$ calcd. for 182.1096, found 182.1101. Data are consistent with the literature.^[40]



(S)-1-methyl-4-(prop-1-en-2-yl)cyclohex-1-ene (2aj): According to **Procedure**

11. Yield: 12.5 mg, 46%; colorless liquid; $^1\text{H NMR}$ (400 MHz, CDCl_3) δ 5.46-5.35 (m, 1H), 4.71 (s, 2H), 2.15-2.00 (m, 3H), 2.00-1.87 (m, 2H), 1.84-1.76 (m, 1H), 1.75-1.71 (m, 3H), 1.68-1.62 (m, 3H), 1.54-1.40 (m, 1H) ppm; $^{13}\text{C NMR}$ (100 MHz, CDCl_3) δ 150.3, 133.8, 120.7, 108.4, 41.1, 30.8, 30.6, 27.9, 23.5, 20.8 ppm; **HRMS (ESI)** (m/z) $[\text{M}]$ $\text{C}_{10}\text{H}_{16}$ calcd. for 136.1252, found 136.1248. Data are consistent with the literature.^[41]

3.6.10 Cyclic Voltammetry

Cyclic voltammetry was conducted using a three-electrode setup consisting of a glassy carbon disc working electrode ‘WE’ ($d = 3.0$ mm, BASi MF-2012), an Ag/AgCl wire reference electrode ‘RE’ (containing sat. aq. KCl) and a platinum wire counter-electrode ‘CE’. Electrochemical measurements were carried out using an Metrohm Autolab PGSTAT 302N potentiostat at room temperature (298 K). Before use and between measurements, the WE was mechanically cleaned by polishing (Buehler Metadi Diamond polishing 1 Micron) and rinsed with distilled water repeatedly until its surface was reflective by eye, then allowed to air dry. The RE was washed with electrolyte solution and distilled water and stored in 3.0 M aq. KCl when not in use/between measurements. The CE was cleaned by soaking in 2.0 M HCl for 1-2 h, then rinsed with distilled water and allowed to air dry. Ferrocene was recrystallized twice from *n*-hexane prior to use. ${}^n\text{Bu}_4\text{N}^+\text{PF}_6^-$ (‘TBAP’) was used as supplied commercially from TCI (98%+). Unless otherwise stated, all solutions were prepared at 10.0 mM concentration (in 0.1 M TBAP that had been bubbled for 5 min with Ar prior to the analyte being added) and were purged with Ar bubbling for 5 min prior to recording CV. After measuring one CV scan, Ferrocene (2.2 mg, 12 μmol) was added and the mixture purged with Ar bubbling for 5 min prior to recording CV again. Data acquisition and processing were performed with Metrohm Autolab Nova 1.10.4. The given redox potentials were calculated as follows: Potential of sample vs. Ag/AgCl, minus potential of Ferrocene/Ferrocenium couple against Ag/AgCl, plus correction of +0.38 V for conversion to vs. saturated calomel electrode (vs. SCE). A peak height of 30 μA corresponds to a one-electron reduction event. Cyclic voltammograms of NpMI and ${}^n\text{BuO-NpMI}$ reveal reversible, one-electron reductions at -1.32 V (vs. SCE) for NpMI and -1.4 V (vs. SCE) for ${}^n\text{BuO-NpMI}$ (Figure S3). The second reductions of both catalysts are irreversible at a measured potential of > -2.0 V.

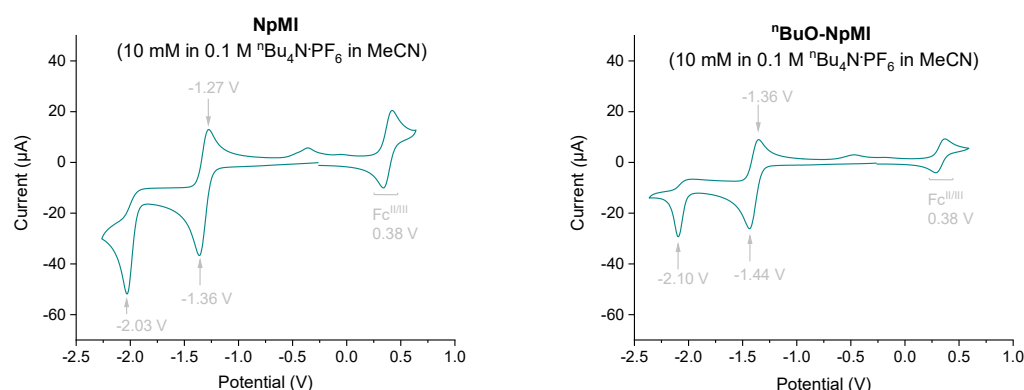


Figure S 3. Cyclic voltammograms of NpMI and ${}^n\text{BuO-NpMI}$ in ACN (0.1 M TBAP) vs. Ferrocene.

A peak height of 50 μA reveals a one-electron reduction event. Cyclic voltammograms of **1g**, **1ai** and **1d** with increasingly negative potential up to -3.00 V (vs. SCE) reveal single one-electron irreversible reductions (see Figure S4). For **1a**, an irreversible one-electron reduction occurs at -2.23 V , followed by a reversible one-electron reduction at -2.29 V . The former corresponds to irreversible one-electron reductions of the phosphinates, while the latter event may correspond to a reversible reduction of the stilbene product, given a similar value to the literature potential for this reduction ($E_{\text{red}}^{\text{p}} = -3.0\text{ V}$ vs. Ferrocene ($0.1\text{ M } ^n\text{Bu}_4\text{N}\cdot\text{Br}$ in ACN)).^[42] The DFT calculated phosphinate redox potential was $E_{\text{p red}} = -2.60\text{ V}$ vs. SCE (Section S18 for methods). For **1o**, a superposition of two irreversible one-electron reductions appears to occur at -2.60 V (vs. SCE). Given the calculated phosphinate redox potential ($E_{\text{red}}^{\text{p}} = -2.45\text{ V}$ vs. SCE) from DFT calculations (Section S18), together with the literature value for chlorobenzene ($E_{\text{red}}^{\text{p}} = -2.78\text{ V}$ vs. SCE),^[43] we propose that this peak may derive from the similar $E_{\text{red}}^{\text{p}}$ values of the phosphinate and aryl chloride moieties. A similar pattern occurs for **1r**, with a superposition of two irreversible one-electron reductions at -2.33 V and -2.46 V . The DFT calculated phosphinate redox potential is $E_{\text{p red}} = -2.44\text{ V}$ vs. SCE from DFT calculations (Section S18 for methods). The literature value for bromobenzene ($E_{\text{p red}} = -2.44\text{ V}$ vs. SCE),^[43] Given that the redox potential of all other phosphinates measured herein (except **1a**) exceed -2.40 V , and that the peak potential of aryl chloride **1o** was 0.18 V more positive than the literature potential of chlorobenzene, we presume the 44 first reduction peak corresponds to the aryl bromide (0.11 V more positive than the literature potential of bromobenzene) For **1o** and **1r**, at more negative potentials a third irreversible one-electron reduction occurs in each case at -2.95 V and -2.82 V , respectively. These peaks may derive from reduction of the halostyrene products, given that the styrenes require more negative potentials.^[44] For **1aa**, an irreversible two-electron reduction occurs at -2.42 V , followed by a reversible one-electron reduction at -2.54 V (vs. SCE) respectively. The behavior cannot be rationalized at this stage. Substrate **1al** exhibits a quasi-reversible one-electron reduction at -2.63 V (vs. SCE).

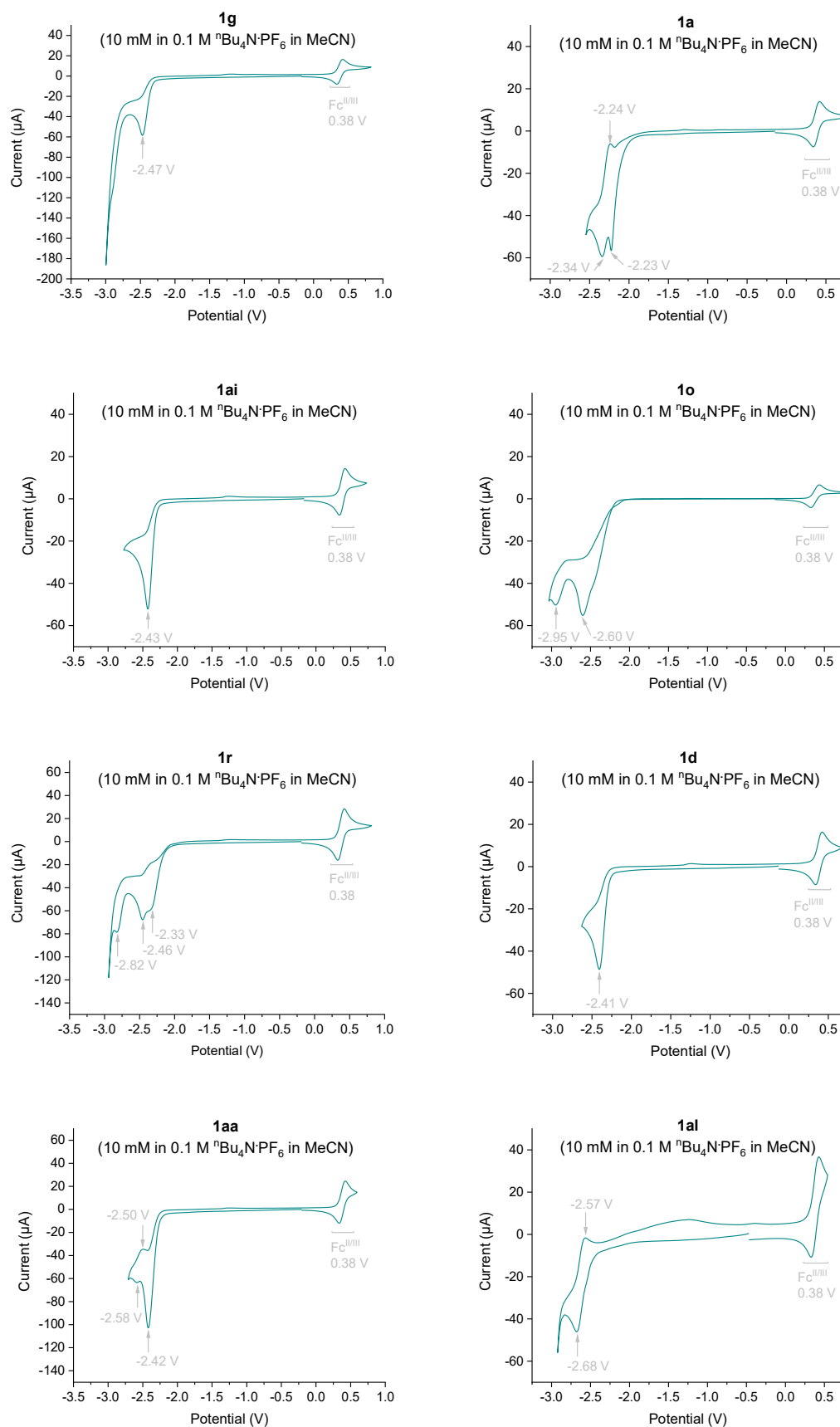
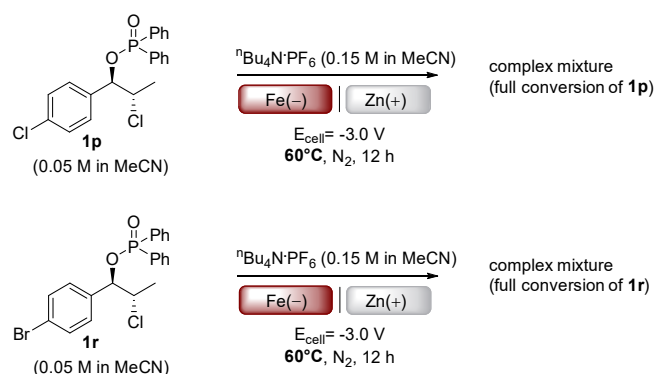


Figure S 4. Cyclic voltammograms of phosphinates in ACN (0.1 M TBAP) vs. Ferrocene.

3.6.11 Spectroelectrochemistry of Catalysts

To confirm the selectivity benefit of e-PRC, we subjected substrates **1p** and **1r** to direct electrolysis at -3.0 V in the absence of catalyst and light and at 60 °C (Scheme S1). The relevance for higher temperature comes from a previous report already showed that no reaction occurred at similar applied constant potentials at rt, and that 60 - 110 °C was required for C(sp³)-O cleavage.^[11] In both cases, full conversion occurred to a complex mixture of products. No olefination products were observed. The detrimental effect of high applied constant potentials in e-PRC reactions can also be found in the main manuscript, Table 1, entry 1.



Scheme S 1. Direct electrolysis at room temperature and 60°C .

Chrono amperometry was measured in an Otle Cell (optically transparent thin-layer electrochemical cell) with Pt mini-grid as working and counter electrode, an Ag wire as pseudo reference electrode and a path length of 0.02 cm. Samples were prepared as 1.5 mM or 2.5 mM solutions of **NpMI** and **ⁿBuO-NpMI**, respectively, in ACN (0.1 M $\text{Bu}_4\text{N}^+\text{PF}_6^-$). After degassing by bubbling the sample with Ar for 5 min, an increasingly negative potential from 0 to -1.6 V was applied and consecutive UV-Vis absorption spectra were recorded at 20 s intervals *via* the

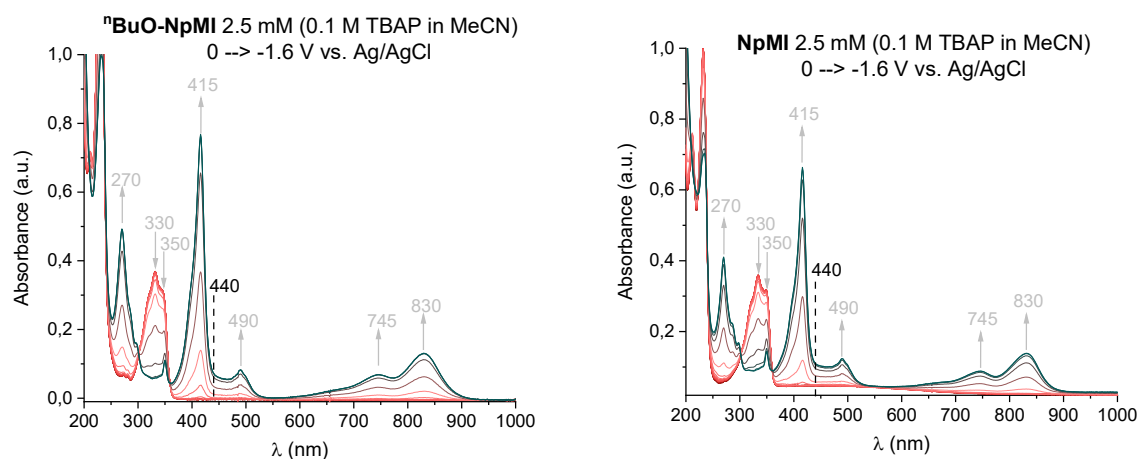


Figure S 5. Consecutive UV-Vis spectra (from red to teal) of **NpMI** (left) and **ⁿBuO-NpMI** (right) from chronoamperometry.

Agilent 8453 spectrometer. The UV-Vis spectra show, for both NpMI and ⁿBuO-NpMI (Figure S5), a decrease in the 330 - 350 nm band intensity accompanied by an increase in new bands at 270 nm, 415 nm, a broad band between 430-530 nm (with a peak at 490 nm) and a broad band between 600 - 900 nm (with peaks at 745 nm and 830 nm).

3.6.12 UV-Vis Spectroscopy of Electrogenerated Radical Anions

The reductions of NpMI and ⁿBuO-NpMI (2.5 mM in 0.1 M Bu₄N·PF₆) were performed accordingly to Procedure 11 without a phosphinate substrate. A green color was observed in the cathodic half-chamber of the divided cell. After 1 h, the contents of the cathodic chamber were taken for UV-Vis analysis. For samples in the presence of **1d**, the solid substrate was measured into a vial and the total cathodic chamber mixture was added to achieve the concentration of the preparative reactions. Then, 25.0 μL of this mixture were added to a quartz cuvette which was made up to 2.0 mL total volume with anhydrous, degassed ACN. Samples were then covered in aluminum foil to prevent penetration of ambient light. Samples that had been stored in the dark were analyzed by UV-Vis. Then, samples were irradiated with blue light by a 440 nm single-spot LED perpendicular to the beam path of the spectrometer.

The UV-Vis spectra of electrochemically reduced NpMI and ⁿBuO-NpMI show (Figure S6) the appearance of new bands for their radical anions with λ_{max} values (415 nm, 490 nm, 745 nm and 830 nm) in perfect agreement with their spectroelectrochemical analysis (Section S12). The radical anions are stable in the presence of **1d** in the dark (bordeaux line vs. black line are superimposed). Irradiation of the radical anions in the presence of **1d** leads to a clear decrease in the aforementioned peaks of the radical anion and regeneration of the neutral species NpMI and ⁿBuO-NpMI (333 nm and 350 nm bands). This confirms that SET is successful from both photoexcited radical anions to **1d**. No difference could be observed between the UV-Vis spectra of ⁿBuO-NpMI^{•-} vs. ⁿBuO-NpMI^{•-} + **1d** (Figure S7)

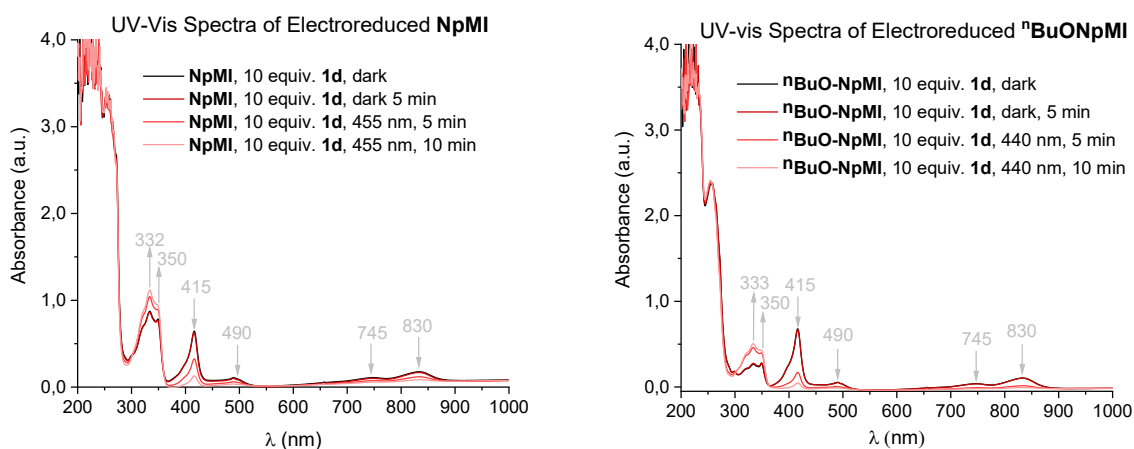


Figure S 6. UV-Vis spectra of electroreduced e-PRCats in the presence of substrate **1d**, in the dark and after 440 nm irradiation of samples.

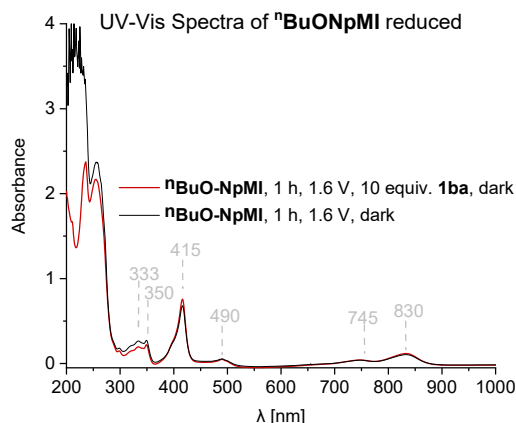


Figure S 7. UV-Vis spectra of electroreduced ⁿBuO-NpMI in the presence of substrate **1d**.

Online UV-Vis measurements were performed on an Agilent 8453 spectrometer using an ISMATEC ISM930C dosing pump to continuously pump the catholyte (1 mL/min) through a quartz flow cell (pathlength 1.0 cm). The concentration of ⁿBuO-NpMI was decreased to one-sixth of the conditions in Procedure 11, spectra were recorded at 10 min intervals. Monitoring the olefination reaction of **1d** under the preparative conditions *via* UV-Vis spectroscopy over a timescale of 100 min, the 330 nm and 350 nm bands of the neutral ⁿBuO-NpMI were increasing. The radical anion was difficult to observe at all. Since the radical anion is highly reactive under irradiation in the presence of **1d**, no buildup can be observed by UV-Vis spectroscopy. Instead, we observed a new feature arising between 450-600 nm ($\lambda_{\text{max}} = 510, 545$ nm), which might originate from oxidative processes (see Figure S8).

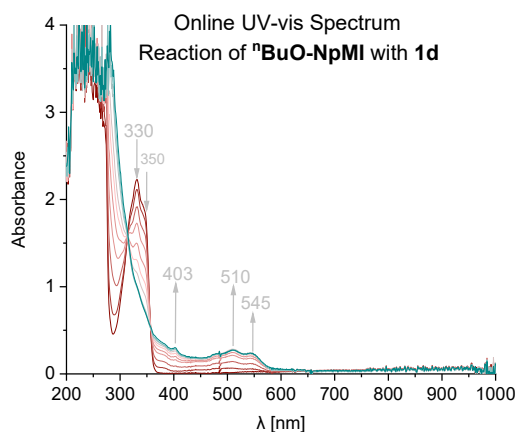


Figure S 8. Consecutively recorded online UV-Vis spectra (from red to teal) of the olefination of **1d** by ⁿBuO-NpMI.

3.6.13 Steady-State Luminescence Emission Spectroscopy

Steady-state luminescence measurements were performed on a Horiba® Scientific FluoroMax-4 instrument, which comprised a USHIO S150MO xenon short arc lamp as an excitation source, 200 - 900 nm double grating excitation and emission monochromators and a R298 Hamamatsu photomultiplier tube. The integration time was set to 0.1 s and the slit widths were 3 nm for both excitation and emission. For neutral e-PRCats, the excitation monochromator was set to 352 nm and emission was set to measure 360 - 600 nm. For electroreduced e-PRCats, the excitation monochromator was set to 440 nm and emission was set to measure 460 - 800 nm. A signal detector (S1) was enabled to measure the intensity signal (counts s^{-1}) and a reference detector (R1) was enabled to compensate for light source fluctuations (μA). Therefore, 'Counts' refers to S1/R1 with the unit $\text{s}^{-1} / \mu\text{A}$ but is given arbitrary units (a.u.) for simplicity. FluoroEssence V3.9 software was used for data acquisition and processing. Sample preparation follows that described in Section S13 for UV-Vis spectroscopy. The excitation spectra of neutral and electroreduced e-PRCats (NpMI and ⁿBuO-NpMI), determined by scanning excitation wavelength at the peak emission wavelength, are reported in this section as overlays with their steady-state emission spectra (Figure S9).

The emission bands of neutral NpMI and ⁿBuO-NpMI were identical ($\lambda_{\text{max}} = 412 \text{ nm}$) when excited at 352 nm (Figure S9). The emission band corresponded to the determined excitation, exhibiting maxima at 320 nm (both NpMI and ⁿBuO-NpMI), 355 nm (NpMI) and 360 nm (ⁿBuO-NpMI). The differences between excitation and emission band maxima were ca. 50 nm in both cases, corroborating fluorescence from the singlet state, rather than phosphorescence. The excitation emission spectra herein accord with the absorption fluorescence spectra of a previous report.^[50]

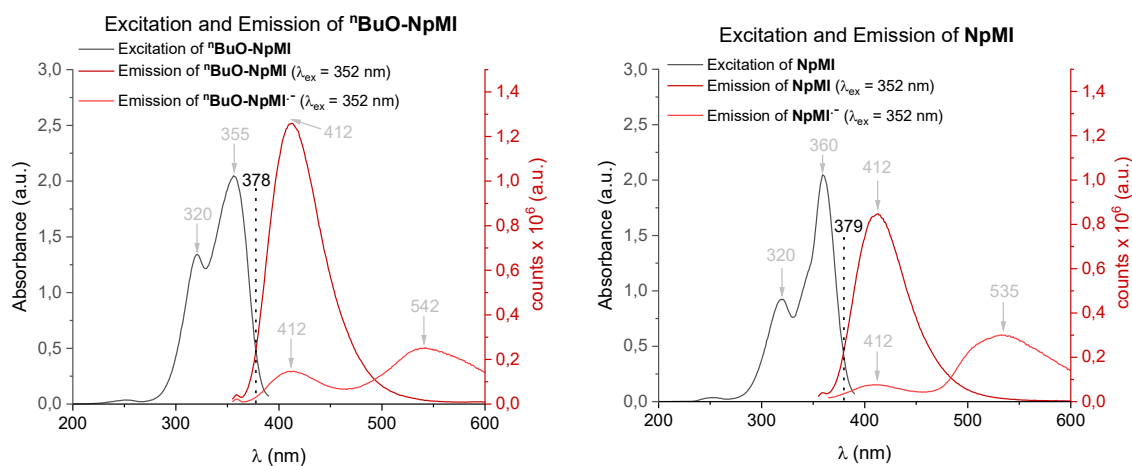


Figure S 9. Excitation and emission spectra of the used catalysts in neutral and reduced forms: ⁿBuO-NpMI (left), NpMI (right), at excitation of $\lambda = 352 \text{ nm}$.

The emission bands of NpMI^- and ${}^n\text{BuO-NpMI}^-$ were similar ($\lambda_{\text{max}} \approx 540 \text{ nm}$) when excited at 352 nm. The electroreduction step was not 100% efficient, since neutral NpMI and ${}^n\text{BuO-NpMI}$ remained (Figure S10). When excited at 440 nm, selective excitation of NpMI^- and ${}^n\text{BuO-NpMI}^-$ revealed only the longer wavelength emitting species ($\lambda_{\text{max}} \approx 540 \text{ nm}$). The emission band corresponded to the determined excitation, exhibiting maxima at ca. 282 nm (both NpMI^- and ${}^n\text{BuO-NpMI}^-$), at 378 nm (both NpMI^- and ${}^n\text{BuO-NpMI}^-$), at 460 nm (${}^n\text{BuO-NpMI}^-$) and 466 nm (NpMI^-). The differences between excitation and emission band maxima were ca. 90 nm in both cases, corroborating phosphorescence. The excitation band was different from the UV vis absorption bands of NpMI^- and ${}^n\text{BuO-NpMI}^-$ generated by spectroelectrochemical or preparative electrolytic measurements. Therefore, the emission belongs to a different photoactive species, not the doublet state of the radical anion, but a lower energy, longer-lived excited state (termed ES1).

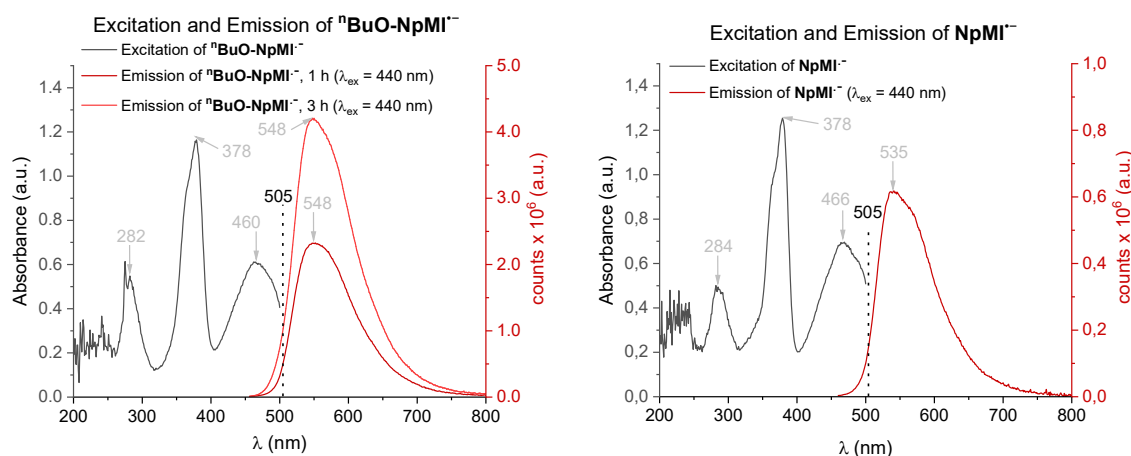


Figure S 10. Excitation and emission spectra of the used catalysts in the reduced forms: ${}^n\text{BuO-NpMI}^-$ (left), NpMI^- (right), at excitation of $\lambda = 440 \text{ nm}$.

The intersection wavelength of the excitation (most red-shifted) and emission (most blue-shifted) bands provides an estimate of the lowest excited state energy of the emitting species.^[45] On the basis of literature and recorded lifetimes covered in the following section, we propose the emitters derived from neutral e-PRCats are triplet states, while the emitters derived from electroreduced e-PRCats are quartet states. For NpMI and ${}^n\text{BuO-NpMI}$, these intersection wavelengths are 379 nm ($E^{\text{T}} = 75.4 \text{ kcal mol}^{-1}$) and 378 nm ($E^{\text{T}} = 75.6 \text{ kcal mol}^{-1}$) respectively. For NpMI^- and ${}^n\text{BuO-NpMI}^-$, this intersection wavelength is estimated by extrapolation to be 505 nm ($E^{\text{Q}} = 56.6 \text{ kcal mol}^{-1}$) in both cases.

3.6.14 Lifetime Measurement

Luminescence lifetimes were determined by time-correlated single photon counting (TCSPC) *via* a Horiba® Scientific DeltraPro™ system equipped with a Horiba Scientific DeltaDiode™ laser (pulsed excitation at 352 nm or 452 nm with a typical pulse width of 80 ps and a maximum repetition rate of 100 MHz). For neutral catalysts, $\lambda_{\text{ex}} = 352$ nm was used. For electroreduced catalysts, $\lambda_{\text{ex}} = 452$ nm was used. An emission monochromator was not employed. Instead, a bandpass filter was used and photons counted correspond to wavelengths from > 400 nm (neutral catalyst) or > 500 nm (electroreduced catalysts) measurement range. An ND1 filter Data were collected either on the 100 ns (neutral catalysts) or 400 ns (electroreduced catalysts) measurement range. Low absorption was maintained at the excitation wavelength ($A = 0.1$) by the use of ND1 cut-off filter at the excitation and lifetimes were measured at the magic angle (54.7°). Sample preparation follows that described in Section S13 for UV-Vis spectroscopy. Lifetimes were obtained using Horiba DAS6 decay analysis software where decays were fitted to one or two exponentials (as necessary to minimize the χ^2 fitting value).

NOTE – In this section, the labels NpMI^- and ${}^n\text{BuO-NpMI}^-$ are used which refer to the samples' spectral data measured after electroreduction of NpMI and ${}^n\text{BuO-NpMI}$. We do not claim to assign lifetimes to doublet states. The paragraphs below detail our proposals for luminescent species

Luminescence lifetime measurements on the reduced ${}^n\text{BuO-NpMI}$ revealed a biexponential decay for the emitting species. The lifetimes recorded for ${}^n\text{BuO-NpMI}^-$ ($\tau_1 = 6.8$ ns, $\tau_2 = 19.5$ ns) and NpMI^- ($\tau_1 = 8.1$ ns, $\tau_2 = 20.3$ ns) following electroreductions for 1 h, were very similar to each other, and were longer than their neutral precursors (Figure S11 and Figure S12, left vs. Figure S12, right). The longer contributor to the decay (ca. 20 ns) is likely to be longer lived than this number suggests due to the restricted measurement time domain. A quartet state (presumably, Q^1), resulting from rapid intersystem crossing from the excited doublet states (D^n) of the reduced e-PRCats, is one candidate for this emitting species, since our EPR studies confirm the radical anion's doublet state is initially formed and reactive to SET. EPR. However, other possibilities, such as aggregation of the radical anion^[46] or an excimer cannot be ruled out at this stage. The doublet states of similar species (perylene diimides and naphthalene diimides) are reported to be ultrashort(picosecond)-lived and do not undergo luminescence.^[47-49] A previously reported attempt to measure the lifetime of a ${}^2[\text{N-arylnaphthalimide}]^-*$ derived from a neutral precursor that is a direct analog of NpMI, was unsuccessful and led to rapid decomposition of the sample under the conditions of transient absorption spectroscopy.^[47]

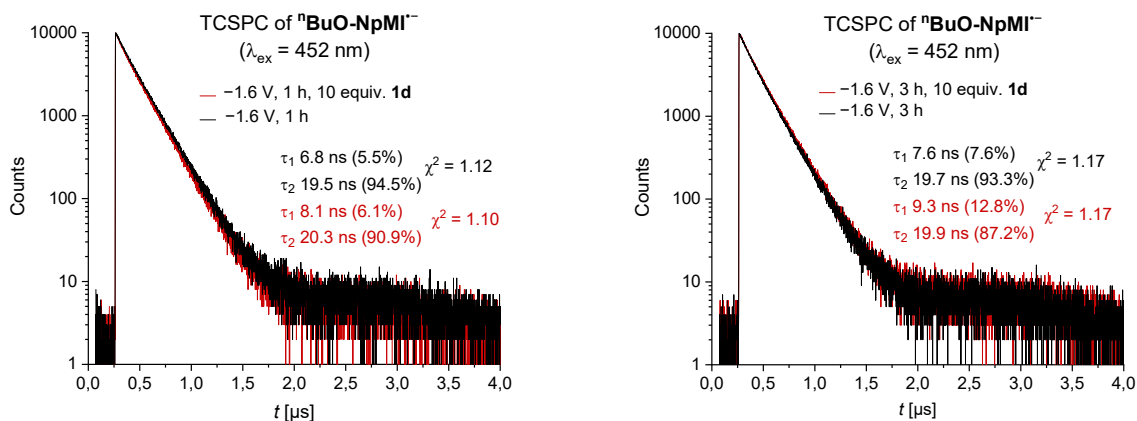


Figure S 11. TCSPC of electroreduced ${}^n\text{BuO-NpMI}^-$ after 1 h (left) and 3 h (right) at -1.6 V.

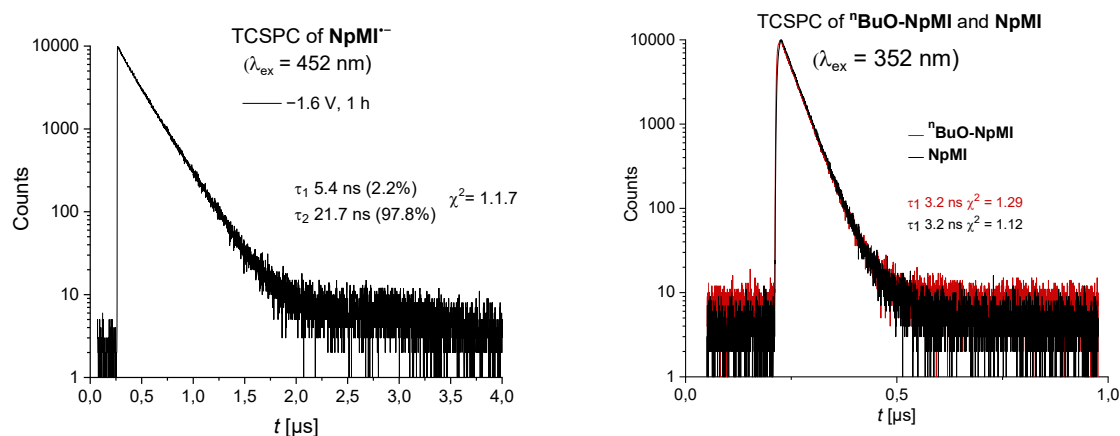


Figure S 12. TCSPC of electroreduced NpMI^- after 1 h at -1.6 V (left). TCSPC of ${}^n\text{BuO-NpMI}$ and NpMI neutral species (right).

The presence of **1d** (10 equiv.) did not significantly change the measured lifetime of ${}^n\text{BuO-NpMI}^-$. (Figure S11 left). We postulated whether the gradual color change from green to orange during an increased electroreduction time (from 1 - 3 h) would give rise to a different photoactive species, but similar results were obtained (Figure S11, right). A comparison of the neutral catalysts NpMI and ${}^n\text{BuO-NpMI}$ reveals similar lifetimes of 3.2 ns (Figure S12, right). These lifetimes are longer than previously reported lifetimes of singlet states of N -aryl-1,8-naphthalimides,^[50] where intersystem crossing is reported to occur to a triplet state (presumably, T1).^[51] However, phosphorescence is not reported for N -aryl-1,8-naphthalimides for which the N -aryl group rotation is considerably hindered. The discrepancy between lifetimes measured herein and therein^[50] could be due to different sample preparations (inert, glovebox conditions were used herein, no mention is present in the previous study), different solvent media (0.1 M $n\text{Bu}_4\text{N.PF}_6$ is present herein), or developments in TCSPC detector timing electronics over the

last two decades. Therefore, we assign the observed emitters are the singlet states (S_1) of NpMI and ${}^n\text{BuO-NpMI}$.

3.6.15 NMR Investigations of Preassociation

NOTE – In this section, the label ${}^n\text{BuO-NpMI}^-$ is used which refers to the samples' spectral data measured after electroreduction of ${}^n\text{BuO-NpMI}$.

${}^1\text{H}$ NMR of ${}^n\text{BuO-NpMI}^-$ was measured by performing the electroreduction of ${}^n\text{BuO-NpMI}$ (2.5 mM) in ACN-d_3 (0.1 M ${}^n\text{Bu}_4\text{N-PF}_6$) within a glovebox and then transferring the cathodic chamber solution to a sealed NMR tube. As expected for the open shell radical anion, the NMR was silent (Figures S13-14). The process was repeated, adding the cathodic chamber solution to **1d** (10 eq. with respect to neutral precursor ${}^n\text{BuO-NpMI}$) before transferring the resulting solution to a sealed NMR tube. The NMR of ${}^n\text{BuO-NpMI}^-$ again was silent and no significant shifts could be seen in the ${}^1\text{H}$ (aromatic or aliphatic) or ${}^{31}\text{P}$ NMR peaks of **1d** (Figures S15-19). Unfortunately, preassociation between ${}^n\text{BuO-NpMI}^-$ and **1d** could not be detected by NMR experiments.

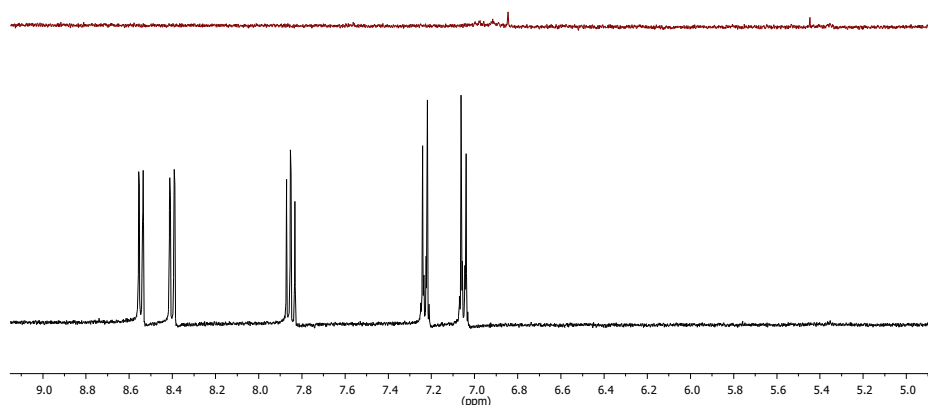


Figure S 13. ${}^1\text{H}$ NMR of ${}^n\text{BuO-NpMI}$ after (top) and before (bottom) electroreduction. Aromatic region.

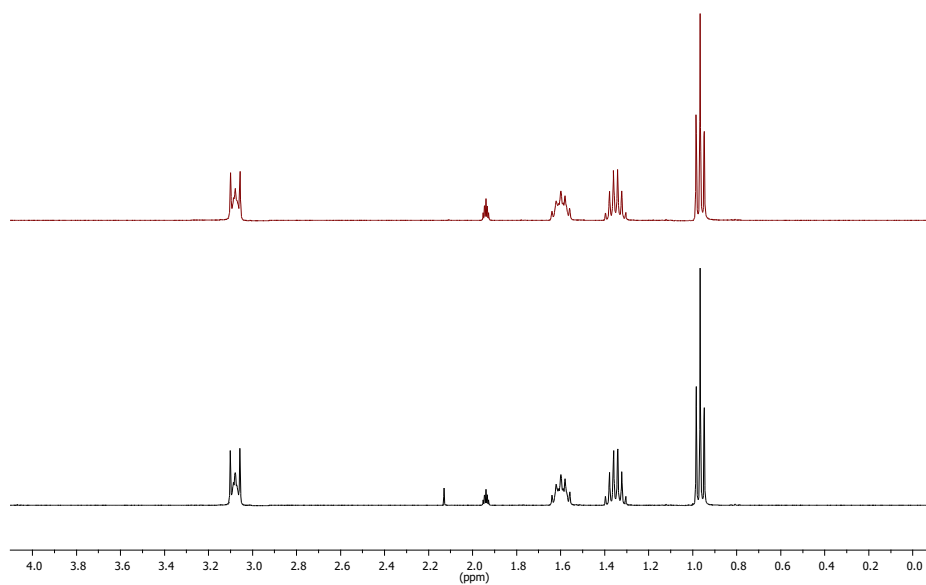


Figure S 14. ^1H NMR of $n\text{BuO-NpMI}$ after (top) and before (bottom) electroreduction. Aliphatic region.

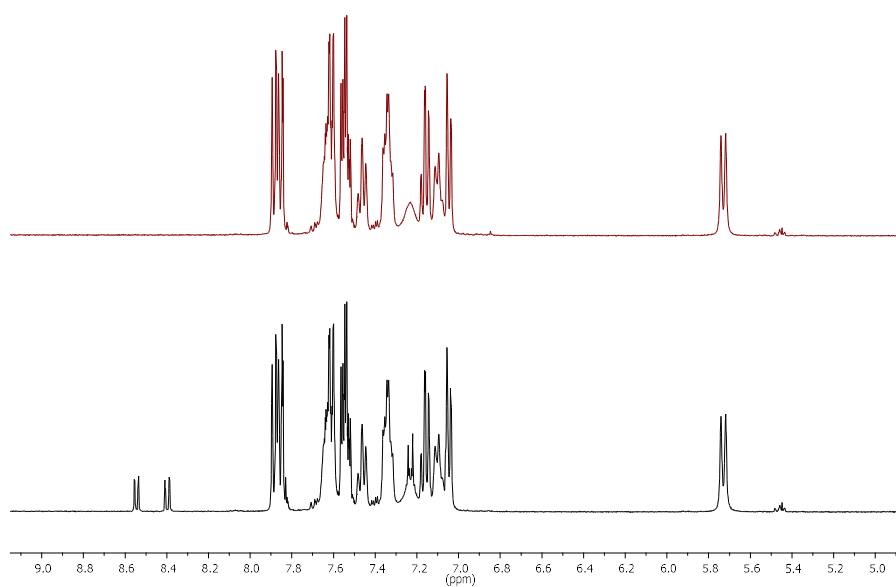


Figure S 15. ^1H NMR of $n\text{BuO-NpMI}$ in the presence of **1d** (10 eq.) after (top) and before (bottom) electroreduction. Aromatic region.

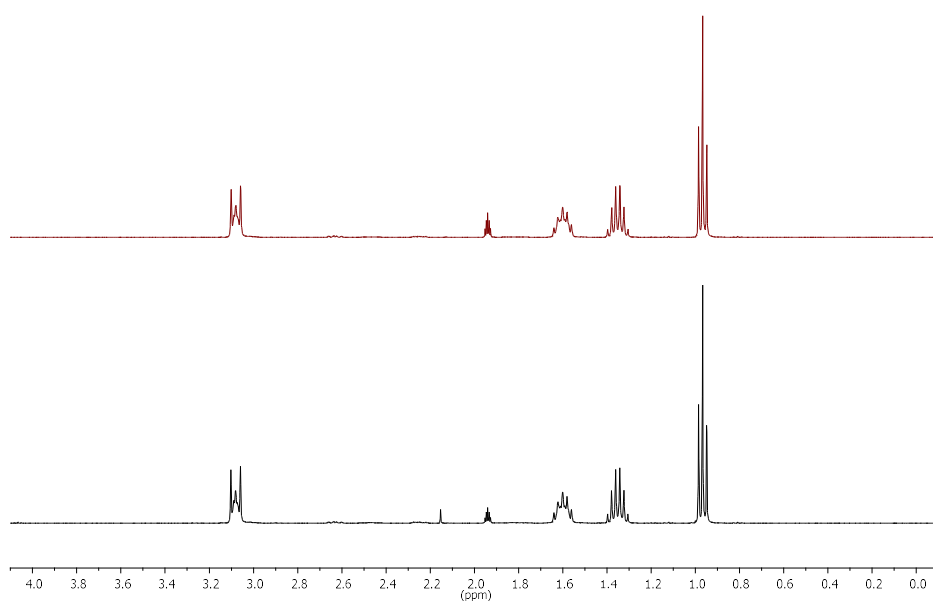


Figure S 16. ^1H NMR of $^n\text{BuO-NpMI}$ in the presence of **1d** (10 eq.) after (top) and before (bottom) electroreduction. Aliphatic region.

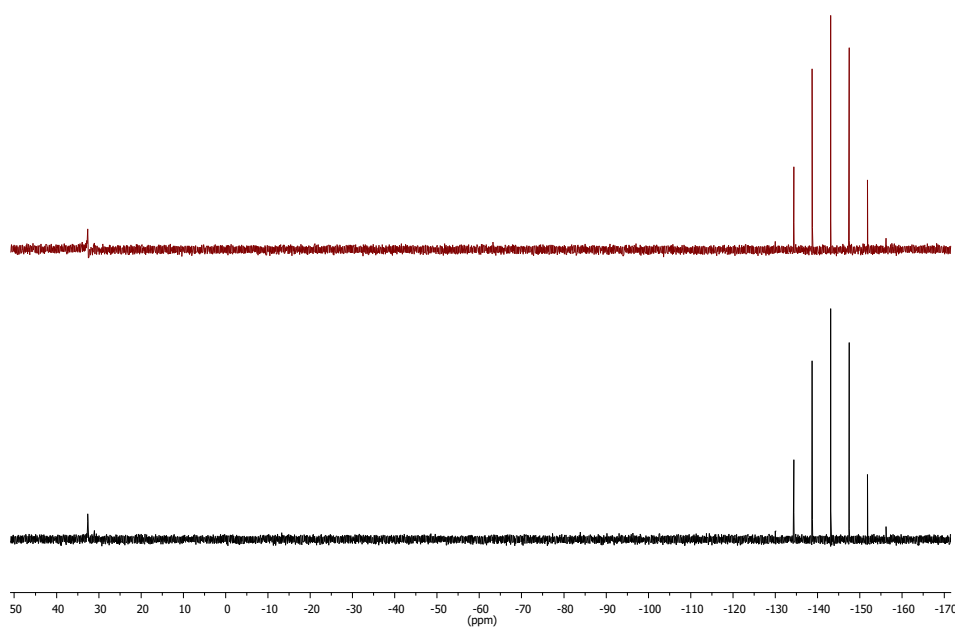


Figure S 17. ^{31}P NMR of $^n\text{BuO-NpMI}$ in the presence of **1d** (10 eq.) after (top) and before (bottom) electroreduction.

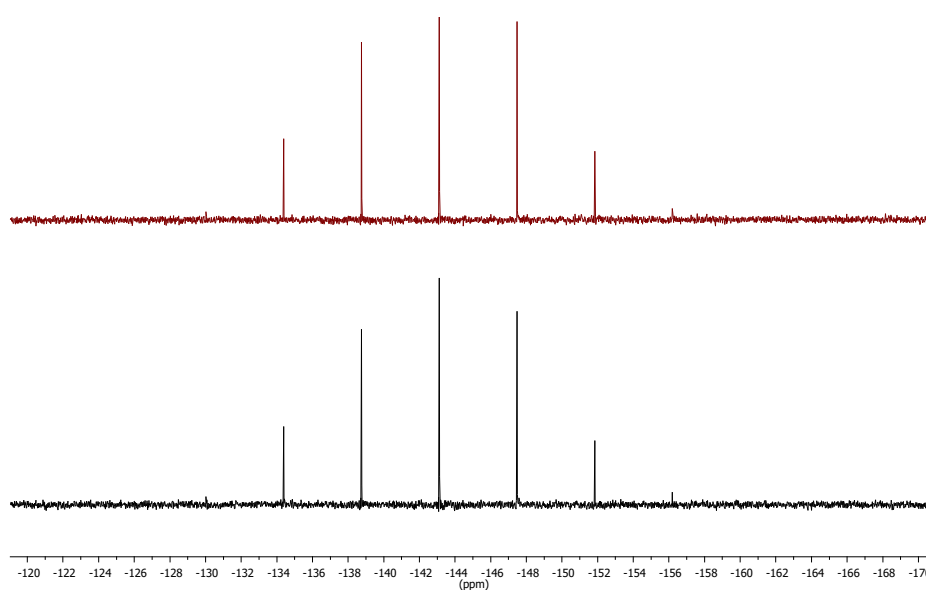


Figure S 18. ^{31}P NMR of $^n\text{BuO-NpMI}$ in the presence of **1d** (10 eq.) after (top) and before (bottom) electroreduction (expanded, electrolyte region).

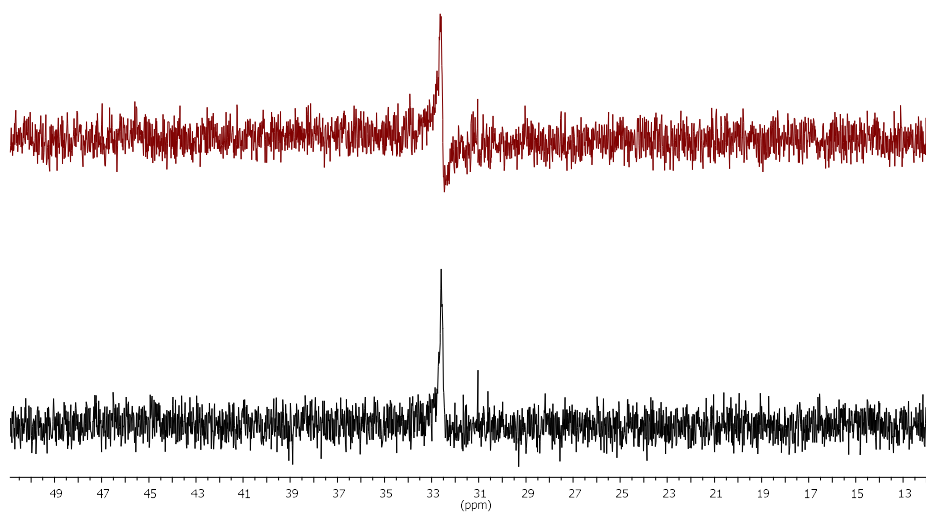


Figure S 19. ^{31}P NMR of $^n\text{BuO-NpMI}$ in the presence of **1d** (10 eq.) after (top) and before (bottom) electroreduction (expanded, **1d** region).

3.6.16 FT-IR Spectroscopy

*NOTE – In this section, the label ${}^n\text{BuO-NpMI}^-$ is used which refers to the *samples*' spectral data measured after electroreduction of ${}^n\text{BuO-NpMI}$.*

FT-IR spectra of ${}^n\text{BuO-NpMI}^-$ were measured by performing the electroreduction of ${}^n\text{BuO-NpMI}$ (2.5 mM) in ACN (0.1 M ${}^n\text{Bu}_4\text{N}^+\text{PF}_6^-$) within a glovebox and then transferring the cathodic chamber solution to a NaCl cell as a thin film. The process was repeated, adding the cathodic chamber solution to **1d** (1.0 eq. was used with respect to neutral precursor ${}^n\text{BuO-NpMI}$) before transferring the resulting solution to the FTIR cell between NaCl discs. Control samples of **1d** only or solvent only were prepared in the same way (without electroreduction). We opted for only 1.0 eq. of **1d** due to concerns that 10 eq. of **1d** (as used in ${}^1\text{H}$ NMR and UV-Vis studies) would swamp the IR signals of ${}^n\text{BuO-NpMI}^-$. The IR signals of the solvent (0.1 M ${}^n\text{Bu}_4\text{N}^+\text{PF}_6^-$ in ACN) dominated spectra and obvious shifts in the peak wavenumbers were not apparent (Figure S20). The only detectable small shifts occurred i) at 1668 cm^{-1} (${}^n\text{BuO-NpMI}^-$) which red-shifted to 1666 cm^{-1} in the presence of **1d**, and ii) at 1242 cm^{-1} (${}^n\text{BuO-NpMI}^-$) which red-shifted to 1239 cm^{-1} in the presence of **1d** (Figures S21-22). While these spectral shifts appear minor, they cannot be dismissed as experimental artifacts, since other peaks in the IR spectra overlay perfectly (1827, 1711, 1039, 918 cm^{-1}). FT-IR spectroscopy is a highly sensitive technique and has been utilized in the detection of non-covalent interactions, such as CH- π interactions in secondary folding of proteins.^[51] Shifts in vibrational frequencies of 2-5 cm^{-1} have been reported for dimers/trimers of aromatic compounds binding *via* noncovalent interactions.^[52]

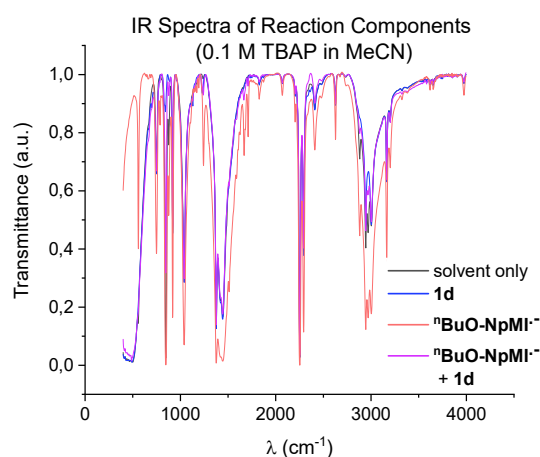


Figure S 20. IR spectra of electroreduced ${}^n\text{BuO-NpMI}$ in the presence of **1d** (1.0 eq.) and comparison to individual components.

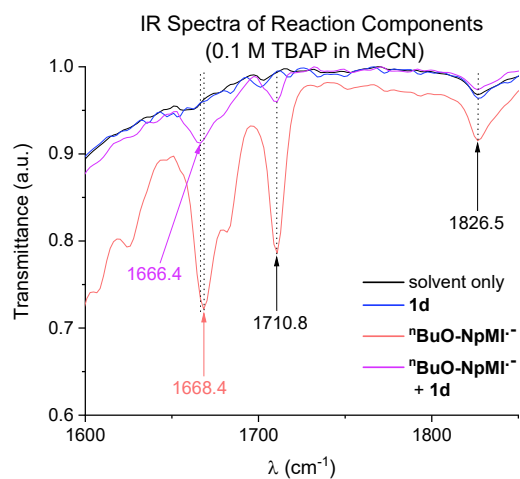


Figure S 21. IR spectra of electroreduced ${}^n\text{BuO-NpMI}$ in the presence of **1d** (1.0 eq.) and comparison to individual components. Expansion of 1600–1850 cm^{-1} region.

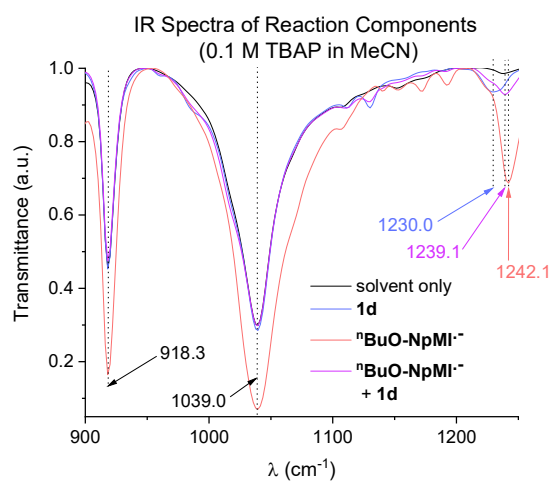
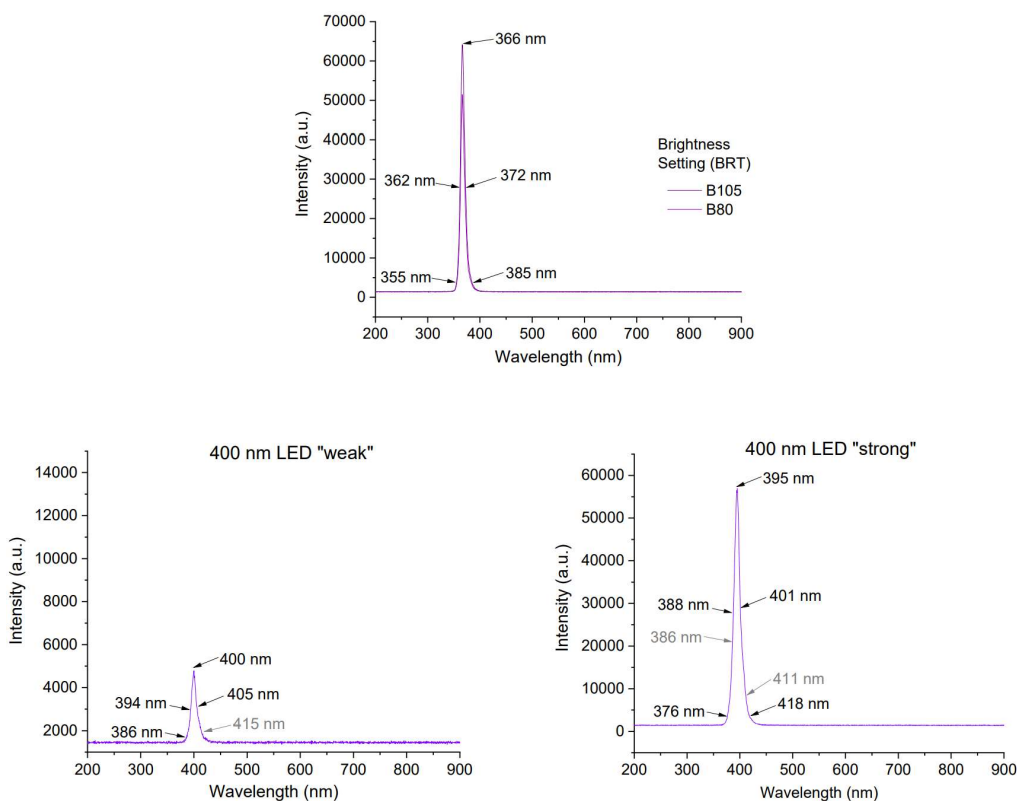


Figure S 22. IR spectra of electroreduced ${}^n\text{BuO-NpMI}$ in the presence of **1d** (1.0 eq.) and comparison to individual components. Expansion of 900–1250 cm^{-1} region.

3.6.17 Emission Spectra of LEDs

Our method to compare LED emission intensity was previously reported,^[2] using a BWTEK Inc. Exemplar LS optical fiber spectrometer. Reproducibility of the method was confirmed in our previous study by comparing different batches of commercially-supplied LEDs.^[2] The wavelengths and relative emission intensities of LEDs used in this study are reported in Table S6. The preparative yields of the reaction forming **2d** are shown earlier in Table S1.

Although the relative intensity maximum and relative intensity total peak area of the 440 nm LEDs is higher than other LEDs overall (Figure S23), the overlap of the 740 nm LED with the near-IR spectral bands of ⁿBuO-NpMI⁻ is similar to the overlap of the 440 nm LED with the near-UV band (Figure S24, right). However, no product was observed with 740 nm LED irradiation. This supports the conclusion of higher order photoexcited state participation to rationalize wavelength dependence on yield. Higher power LEDs (400 nm, 519 nm) gave improvements in product yields from trace levels, but the standard 440 nm LED was always superior. Although the high power 400 nm LED has the greatest overlap of any LED with the near-UV spectral band of ⁿBuO-NpMI⁻, we propose that either (i) the neutral ⁿBuO-NpMI also competes for light at this wavelength and shields photoexcitation of the ⁿBuO-NpMI⁻ or (ii) higher doublet states accessed at 400 nm do not exhibit charge transfer behavior as identified by DFT-MRCI calculations (Section 18).



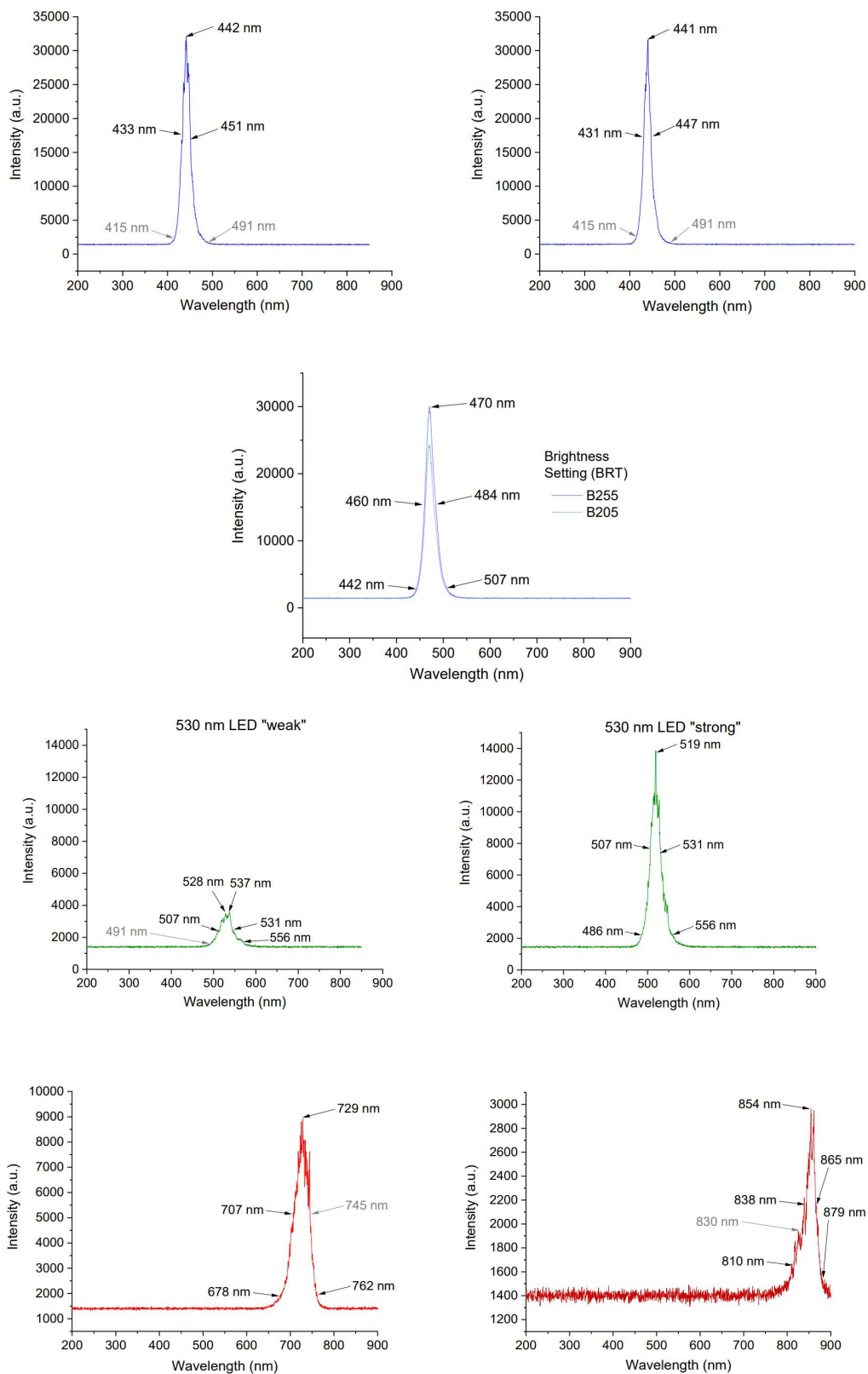


Figure S 23. Emission spectra of LEDs used throughout the study at a fixed measurement distance.

Table S 6. Characterization of LEDs used in this study and their measured wavelengths, optical powers and relative emitting intensities.

Manufacturer	Model/ Brand	Input Power per LED (W)	LED λ_{\max} (nm)	Luminous Flux	Peak intensity, directly above LED ^a (a.u.) at λ_{\max}	Peak area, directly above LED ^a (a.u.)	Peak intensity at λ_{\max} of ¹⁸ BuO-NpMI
CCS (Creating Customer Satisfaction) Inc.	LDL-71X12UV12-365-N	1.5	366	[70 mW / cm ²] ^b	57834 ^c	627320 ^c	-
Edison Edixeon	Edison EDEV-SLC1-03	3.5	400	0.35 W @ 700 mA	4788	43835	1859 (λ_{\max} = 415 nm)
OSRAM Oslon (batch 1)	Oslon SSL 80 LDCQ7P-2U3U LT1960	3.3	440	1.5 W @ 1000 mA	32040	693549	2215 (λ_{\max} = 415 nm)
OSRAM Oslon (batch 2)	Oslon SSL 80 LDCQ7P-2U3U LT1960	3.3	440	1.5 W @ 1000 mA	31542	610066	1698 (λ_{\max} = 491 nm)
OSRAM Oslon	Oslon SSL 80 LDCQ7P-2U3U LT1966	1.1	528	97 lm @ 350 mA	3508	89889	2618 (λ_{\max} = 415 nm)
LED Engin	LZ4-00R308	6.3	729	2.1 W @ 700 mA	8920	292177	1586 (λ_{\max} = 491 nm)
LED Engin	LZ4-00R608	8.7	854	3.8 W @ 700 mA	2965	49816	5198 (λ_{\max} = 745 nm)

^aMeasured by a BWTEC optical fiber spectrometer at a distance of 30 cm directly above the LED. The maximum observed intensity was recorded. The baseline (y axis) was ca. 1400 a.u. in each case. ^bMaximum intensity (mW / cm²) reported by supplier at a 3 cm distance from LED. ^cThe intensity-tunable LED was used at BRT100 setting for the preparative reaction. The mean average value of BRT105 and BRT80 (BRT95) was taken.

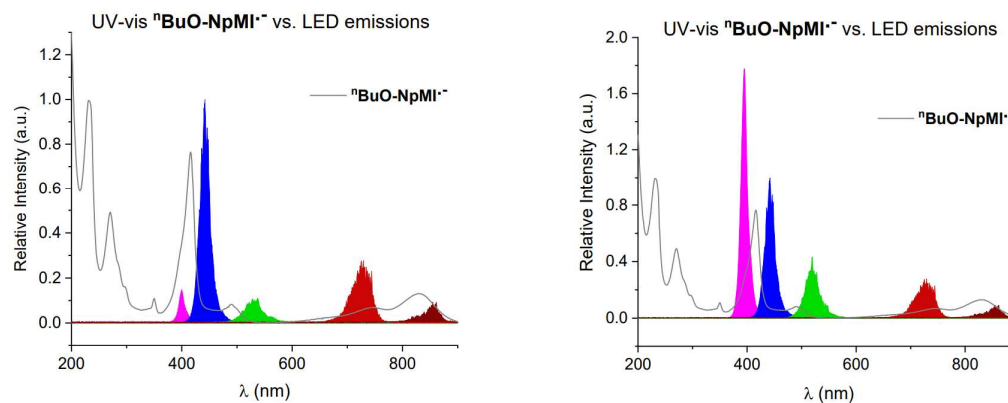


Figure S 24. Overlay of UV-Vis spectra of ¹⁸BuO-NpMI⁻ (spectroelectrochemistry) and LED emission spectra (calibrated relative intensities) of standard power LEDs used (left), or maximum available power LEDs (right).

3.6.18 Electron Paramagnetic Spectroscopy Investigations

As close as possible, EPR samples were prepared to mimic the photoelectrochemical reaction conditions. However, 10 eq. of **1d** was used instead of 20 eq. in the preparative reactions to ensure fully soluble conditions. EPR spectra were measured at 20 °C on a Magnetech MiniScope MS 400 spectrometer (9.45 GHz) which is a continuous-wave (CW) X-Band (9-10 GHz) spectrometer. Spectra were measured with a centered field of 340.7 G, a sweep width of 40.8 mT, a sweep time of 60 s, a resolution of 4096, a modulation amplitude of 0.2 mT, a microwave attenuation of 10.0 dB, a receiver gain of 20 and a time-constant of 0 s.

The electroreduction of NpMI and ⁿBuONpMI was performed in accordance with Procedure 11 without substrate, within nitrogen-filled glovebox (MBraun UNILAB Plus). The electrochemically reduced samples were taken from the cathodic half-cell, without diffusion of analyte into the sample, and transferred to Wilmad[®] quartz EPR tubes (O.D. = 1 mm, I.D. = 0.8 mm). Successful transfer was monitored by naked eye, as the reduced catholyte appears green (≤ 1 h, -1.6 V) or orange (>1 h, -1.6 V), exposure to air or contact with the anolyte vanishes the color instantly. The quartz EPR tubes were placed in a larger quartz tube (O.D. = 5 mm, I.D. = 4.5 mm), which was sealed by an NMR cap and parafilm. If measurements were performed in presence of **1d**, the catholyte was added to a vial containing solid **1d**. After complete dissolution, the mixture was given into the quartz EPR tube. The sample was then covered in aluminum foil to prevent penetration of ambient light. Irradiation with blue light was done by a 440 nm single spot LED outside of the EPR-spectrometer. After irradiation for the specified time, the sample was returned to the spectrometer for measurement. Hyperfine couplings were extracted from simulations done in WINSIM2002 (fitting correlation = >0.995 in each case)^[53]

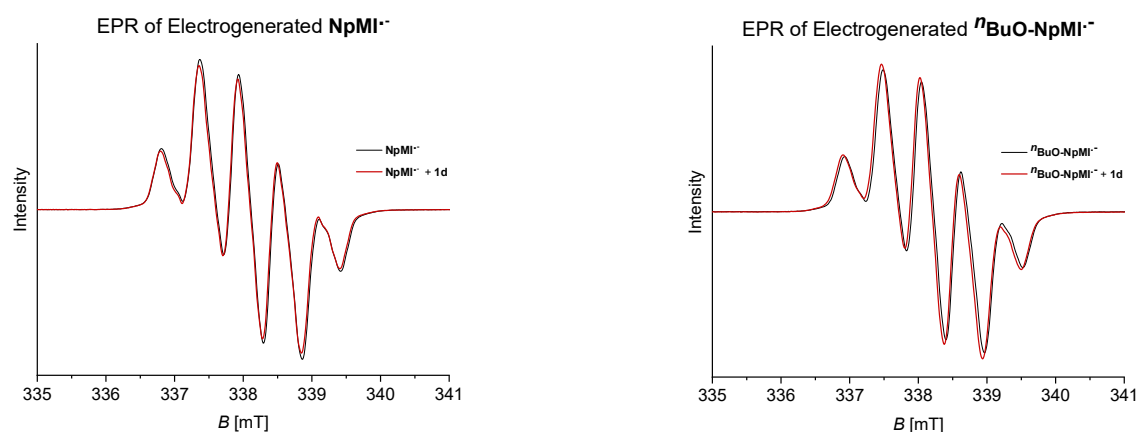


Figure S 25. EPR spectra of electrochemically-reduced NpMI (left) and ⁿBuO-NpMI (right) in the absence and presence of **1d** (10 eq).

Following electroreduction of NpMI for 1 h, a pentet signal at 337.8 mT was detected for NpMI^{•-}. Following electroreduction of ⁿBuO-NpMI for 1 h, ⁿBuO-NpMI^{•-} also appears as a pentet at 338.2 mT. Hyperfine couplings were consistent with the literature for *N*-phenylnaphthalimide radical anion.^[54]

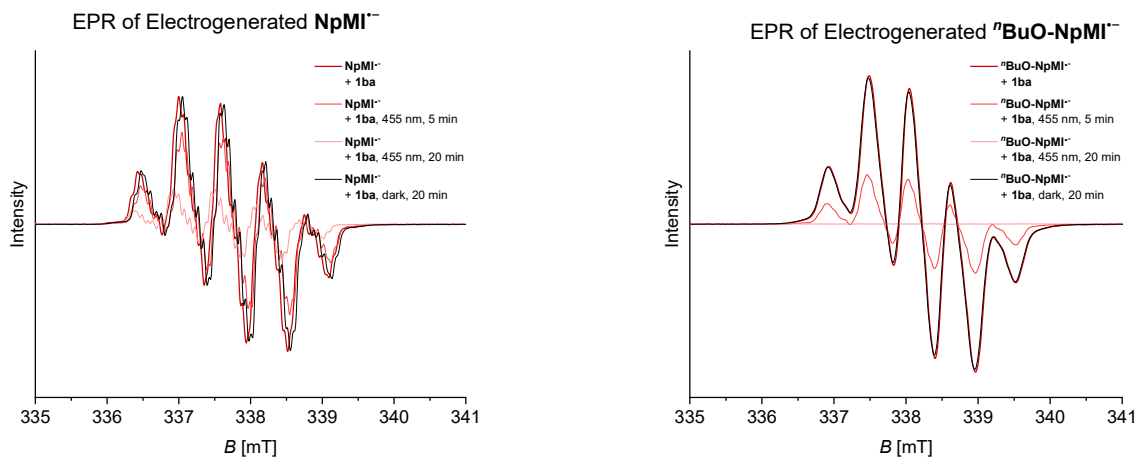


Figure S 26. EPR spectra of electrochemically-reduced NpMI (left) and ⁿBuO-NpMI (right) in the presence of **1d**.

In both cases, the intensity of the signal remains constant when kept in the dark (monitored for up to 20 min, Figure S26). However, for both NpMI^{•-} and ⁿBuO-NpMI^{•-}, in the presence of **1d** and upon irradiation with 440 nm for 5 min, signals are quenched to lower intensities. After 20 min of irradiation, signals almost completely disappear (Figure S26). Since both catalysts show similar behavior, SET from both NpMI^{•-} and ⁿBuO-NpMI^{•-} to **1d** must be successful. This was surprising at first, since NpMI is an ineffective e-PRCat in transforming **1d** to its olefin product **2d**. Therefore, a subsequent step in the mechanism (likely C(sp³)-O cleavage) must be rate-determining. For ⁿBuO-NpMI^{•-} in the absence of **1d**, irradiation with 440 nm leaves the signal unchanged (monitored for up to 20 min, Figure S26, bottom). This evidences against the possibility of SET from NpMI^{•-} and ⁿBuO-NpMI^{•-} to the solvent or conducting salt, or suggests rapid back electron transfer should such a process occur.

Table S 7. Simulated fitting of various EPR spectra and extracted hyperfine couplings.

Sample	$\alpha(\text{H}^{2,7})^a$	$\alpha(\text{H}^{3,6})^a$	$\alpha(\text{H}^{4,5})^a$	$\alpha(\text{N})^a$
NpMI ^{•-}	4.99	0.69	5.45	1.44
ⁿ BuO-NpMI ^{•-}	4.77	0.80	5.61	1.43
ⁿ BuO-NpMI ^{•-} + 1d	4.74	0.65	5.77	1.40

^aDetermined using WINSIM2002 by simulated fitting of the spectrum, fitting R > 0.975 in each case.^[23]

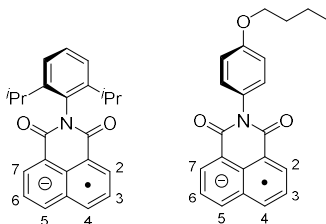


Figure S 27. Assignments of EPR hyperfine couplings.

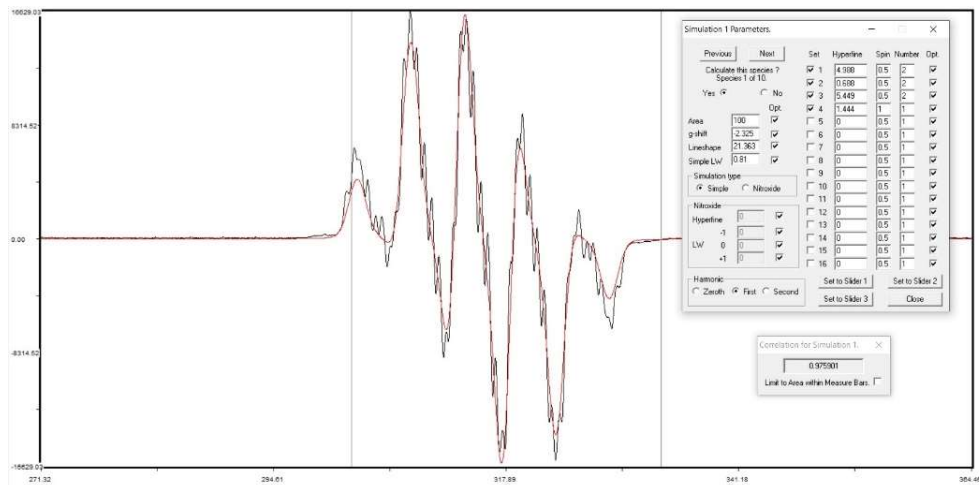


Figure S 28. Simulation of the EPR spectrum of NpMI^- .

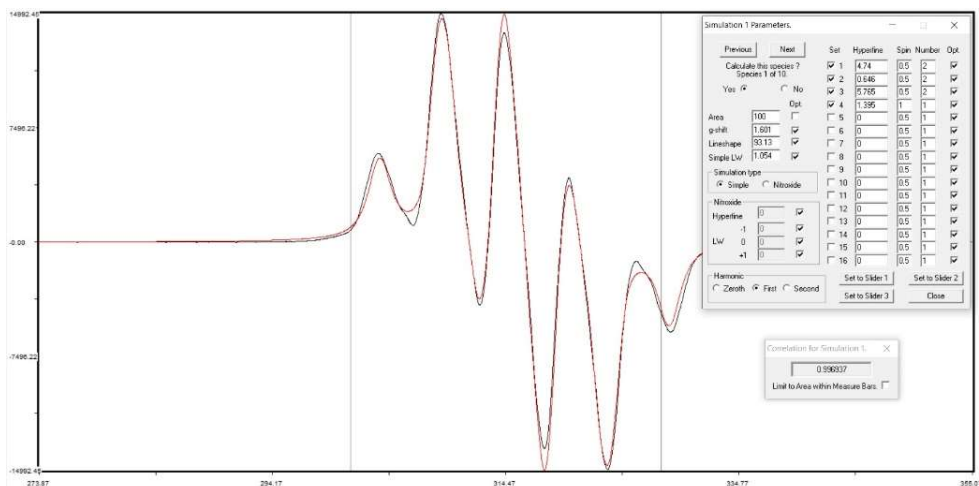


Figure S 29. Simulation of the EPR spectrum of ${}^n\text{BuO-NpMI}^-$.

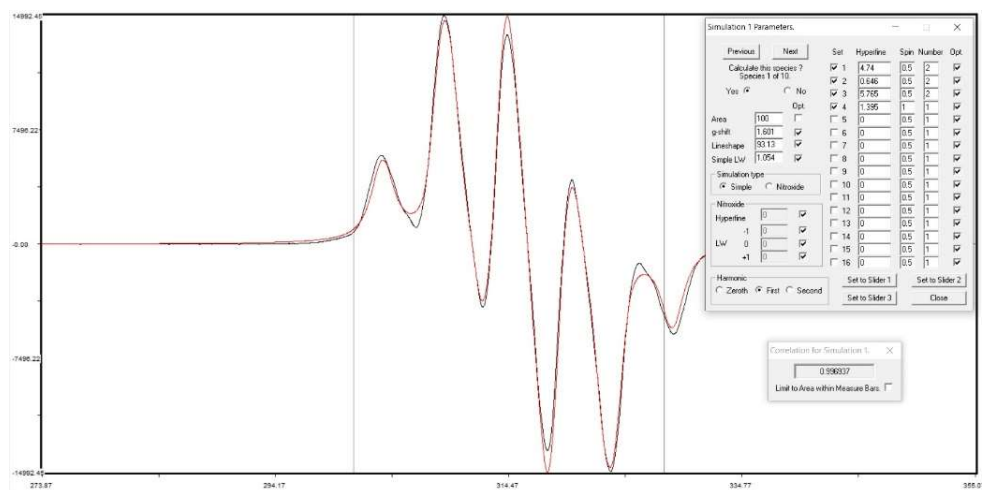


Figure S 30. Simulation of the EPR spectrum of $t\text{-BuO-NpMI}^-$.

3.6.19 Computational Investigations

3.6.19.1 General Information

All calculations were performed using Density Functional Theory (DFT)^[55] using the Gaussian16 software package.^[56] All minima were optimized using the ω B97X-D functional^[57] with the 6-311+G* basis set.^[58] Solvation effects were included with the integral equation formalism polarizable continuum model (IEFPCM),^[59] with default parameters for acetonitrile, in which preparative e-PRC reactions and spectroscopy were performed. Frequency calculations were performed on all optimized structures in order to characterize minima (zero imaginary frequencies). Spin densities and molecular orbitals depicted in the main article and herein were visualized using VMD 1.9.3^[60] with an iso-value of 0.004 and 0.02, respectively.

3.6.19.2 Bond Dissociation Free Energies

Benchmarks have shown^[61] that the range-separated and dispersion-corrected ω B97X-D functional^[57] is well-suited to main group thermochemistry, while the use of a triple-zeta basis set is generally recommended to mitigate basis set incompleteness errors.^[62,63] To further validate our DFT results, we calculated the bond dissociation energies of selected compounds with the open-shell DLPNOCCSD(T)^[64] method implemented in ORCA 4.2.1.^[65] We used the def2-TZVPPD^[66] basis set with the def2-TZVPPD/C^[67] correlation basis. Tight SCF and PNO convergence criteria were applied and solvation effects were treated with the conductor-like polarizable continuum model (C-PCM)^[68] using default parameters for acetonitrile, in which e-PRC reactions and spectroscopy were conducted. The DFT energies are on average 3.5 kcal/mol smaller than those obtained with DLPNO-CCSD(T) (Table S8), but the deviation is systematic and the trend is well reproduced, thus validating the use of DFT in this context.

Table S 8. Calculated C–O bond dissociation energies (kcal/mol) without thermodynamic corrections at the ω B97X-D/6-311+G* and DLPNO-CCSD(T)/def2-TZVPPD levels of theory.

Phosphinate radical anion	DFT	DLPNO-CCSD(T)	Difference
1bw	-23.44	-28.03	4.59
1d	-19.98	-23.47	3.49
1g	-25.77	-28.86	3.09
1o	-23.87	-27.53	3.66
1aa	-11.99	-15.10	3.10
1al	-8.69	-11.33	2.64

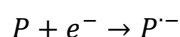
Optimized structures were obtained using the theory level (ω B97X-D/6-311+G*) and solvent model (IEFPCM) specified in the general part. Bond dissociation free energies ΔG were obtained from the frequency analysis at 298.15 K and 1 atm according to:

$$\Delta G = \Delta(E_{\text{elec}} + ZPVE + \Delta G_{\text{trans,rot,vib}} + \Delta G_{\text{solv}}).$$

Here, E_{elec} denotes the electronic energies, $ZPVE$ is the zero point vibrational energy, $\Delta G_{\text{trans,rot,vib}}$ includes thermal contributions from translations, rotations and vibrations as well as entropic terms and ΔG_{solv} is the free energy of solvation.

3.6.19.3 Redox Potentials

We investigated the reduction of a phosphinate substrate P by one electron, given by:



The free energy change ΔG of this reaction contains the thermally corrected energies G of reactant and product as well as the thermal contributions of the free electron. There are multiple conventions to include the latter^[69] and we have chosen the ionic convention where $G(e^-) = 0$ eV.

$$\Delta G = G(P'^-) - G(P) - G(e^-)$$

The absolute redox potential E_{abs}° is related to ΔG *via*:

$$E_{\text{abs}}^\circ = -\frac{\Delta G}{nF}$$

where n is the number of electrons involved in the redox process and F is the Faraday constant. Since we are only considering one-electron processes here, n is 1 in all cases. By supplying the energy in eV, the Faraday constant equals the elementary charge and the value of E_{abs}° is simply the negative change in free energy. ΔG is often calculated^[70] by an indirect approach *via* a thermodynamic cycle. There, the reaction free energy is calculated for the gas phase geometries and the free energy of solvation ΔG_{solv} is added separately, possibly at a different level of theory, while neglecting the structural relaxation in solution. The success of this strategy is rooted at least partially in error cancellation effects.^[71]

We therefore decided to use a simpler approach and calculated ΔG directly at the optimized geometries of reduced and oxidized species in solution,^[71a] using the theory level (ω B97X-D/6-311+G*) and solvent model (IEFPCM) specified in the general part. To compare the calculated potential E_{abs}° to experimental results, it must be referenced against a standard potential:

$$E^{\circ} = E_{\text{abs}}^{\circ} - E_{\text{ref}}$$

Here, we used the Fc^+/Fc couple as an internal standard against the saturated calomel electrode (SCE), whose absolute reduction potential in acetonitrile has been determined computationally as 4.988 V.^[72]

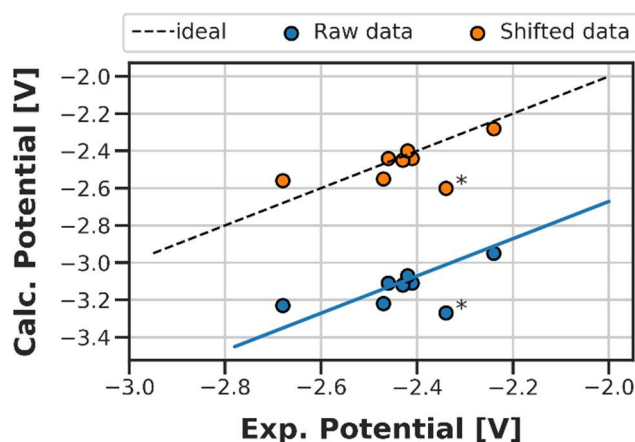


Figure S 31. Correlation between experimental and calculated redox potentials. The dashed black line represents the ideal correlation between experiment and theory (slope 1 and y-intercept 0). The blue points and line denote the raw data obtained from calculations and the orange points illustrate the final potentials reported in the paper. The starred point (**1a**) was omitted from the fit as an outlier. R^2 of the linear regression is 0.54.

The resulting redox potentials should ideally correlate 1:1 with the experimental ones (black line in Figure S31). However, because of experimental factors that cannot be reproduced well in calculations, such as conformational variations, as well as systematic errors specific to the chosen DFT functional and solvation model, we can expect a certain deviation from the ideal values. To correct for these deviations, we fitted a linear function with slope 1 to the data set of experimental and calculated potentials (blue line). In addition to the phosphinates in Table 2 of the main paper, we included compound **4a** ($\Delta E_{\text{exp}} = -2.24$ V, $\Delta E_{\text{calc}} = -2.27$ V) in the calibration protocol to enlarge the data set. In contrast, compound **1a** (marked with a star in Figure S31) was removed from the fit as an outlier. The y-intercept of the fit function (-0.67 V) represents the systematic shift of the calculated potentials and is on the higher end of the error margin reported for other DFT calculations.^[70a-b,73] Taking this into account, the final potentials reported in Table 2 are calculated as:

$$E^{\circ} = E_{\text{abs}}^{\circ} - E_{\text{ref}} + 0.67 \text{ V}$$

3.6.19.4 DFT/MRCI Calculations

The ground state geometry of nBuO-NpMI⁻ was optimized at the ω B97X-D/6-311+G* level of theory with Gaussian 16 (for xyz-coordinates, see Section 18). For excited state calculations, we employed the DFT/MRCI method^[74] with the R2018 Hamiltonian.^[74d] Here, the ground state DFT reference was calculated with ORCA 4.2.1^[65] using the BHLYP functional.^[75] The def2-TZVPD basis set^[66] was used on all atoms within the resolution-of-the-identity formalism for Coulomb and exchange integrals^[76] (RI-JK) in conjunction with the def2-TZVPD/C^[67a] and def2/JK^[77] auxiliary basis sets. Solvation effects were accounted for by the C-PCM model^[68] with default parameters for acetonitrile. Symmetry was turned off (keyword NoUseSym) and the SCF convergence threshold was set to 10⁻⁷ Eh (keyword SCFCONV7). The DFT orbitals for the radical anion were calculated in the unrestricted Kohn-Sham formalism and transformed to quasi-restricted orbitals^[78] prior to the MRCI calculation. Ten roots were 68 calculated in the MRCI step. The reference space was iteratively optimized using a tight selection threshold of 0.8 Eh (keywords \$esel 0.8, \$dftparam tight), until all leading configurations were contained in the reference space.

To identify the putative quartet state ES1, we performed CASSCF(11,10) calculations^[79-81] with Molpro 2021.1^[82-84] using the aug-cc-pVTZ^[85-86] basis set. Density fitting^[87] was used to approximate the two-electron integrals and speed up the calculations. To further reduce the computational cost, we built a model system for nBuO-NpMI⁻ by replacing the O-ether residue in the DFT-optimized structure with hydrogen and symmetrizing the resulting geometry to the C_{2v} point group. The active space was chosen to include correlating pairs of π and π^* orbitals as well as including a balanced amount of orbitals localized on the aniline and naphthalene subunits, respectively. The resulting active space contained 11 electrons in 10 orbitals (Figure S32). State averaging was performed over forty states, namely five doublet and five quartet states in each irreducible representation.

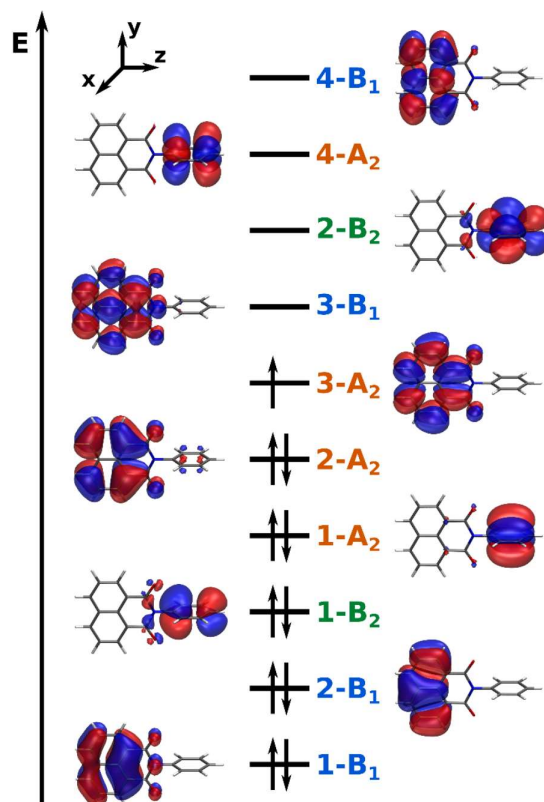


Figure S 32. Active space of the CASSCF(11,10) calculation used to determine the energy of the putative quartet excited state. The naphthalene subunit resides in the yz -plane with the N-C bond aligned along the z -axis. Orbitals were visualized with VMD 1.9.3 using an iso-value of 0.02. The figure depicts the doublet ground state configuration.

The first ten states are summarized in Table S9. Compared to the DFT/MRCI spectrum (see Figure 3, main manuscript), the CASSCF energies are blue-shifted by 1-2 eV. This is within the usual range for 69 vertical excitation energies computed with CASSCF, due to the lack of dynamical correlation.^[88] The tentative charge transfer doublet state, denoted Dn in the main manuscript is the fifth excited doublet D5, in agreement with the DFT/MRCI results. Its vertical excitation energy at the CASSCF(11,10) level of theory is 4.34 eV and its dominant contribution is the single electron excitation $3-A_2 \rightarrow 4-A_2$. The transition dipole moment of this state is lower than predicted by DFT/MRCI, which is likely due to the symmetry constraints used in the CASSCF calculation.

Table S 9. CASSCF(11,10) energies, norm of the transition dipole moments $|\mu|$ and dominant electronic transitions for the first ten electronic states of the *n*BuO-NpMI⁻ model system.

State	Sym.	ΔE (eV) ^[a]	$ \mu $ (a.u.)	Dominant transitions ^[b]
D ₀	² A ₂	0.00	/	ground state
D ₁	² B ₁	2.00	1.4219	3-A ₂ → 3-B ₁ (0.890)
D ₂	² B ₁	2.30	0.0480	3-A ₂ → 4-B ₁ (0.904)
D ₃	² A ₂	3.56	1.2666	1-A ₂ → 3-A ₂ (0.868)
Q ₁	⁴ B ₁	4.18	/	1-A ₂ → 3-A ₂ (0.936)
D ₄	² B ₂	4.19	0.0022	3-A ₂ → 2-B ₂ (0.933)
D ₅	² A ₂	4.43	0.0611	3-A ₂ → 4-A ₂ (0.927)
Q ₂	⁴ A ₂	4.72	/	1-B ₂ → 3-B ₂ (0.708) 2-A ₂ → 4-A ₂ (0.624)
D ₆	² A ₂	4.73	0.0077	1-B ₂ → 2-B ₂ (0.576) 2-A ₂ → 4-A ₂ (0.503)
D ₇	² B ₁	4.88	0.5000	2-B ₂ → 3-B ₂ (0.691) 1-B ₂ → 3-A ₂ (-0.307)

^[a]Relative energies and transition moments are reported with respect to the doublet ground state. ^[b]CI coefficients for each transition are given in parentheses.

The first excited quartet state Q₁ has a vertical excitation energy of 4.18 eV. Considering the aforementioned blue-shift of 1-2 eV in CASSCF as well as vibrational relaxation in the excited state, this is in reasonable agreement with the new emission band at 540 nm (2.29 eV). The excitation energy of Q₁ is 0.25 eV below that of D₅ and only 0.01 eV below that of D₄. This indicates that coupling to the quartet domain is a possibility after excitation into one of these doublet states, at least from an energetic point of view. In light of the luminescence spectra reported in Section S14, it is reasonable to assume that the long-lived emitting species is indeed the lowest excited quartet state. This state with B1 symmetry is characterized mainly by the single electron excitation 1-A₂ → 3-B₁, which corresponds to an opposite charge transfer from the aniline to the naphthalene subunit. EPR spectra (Section S17) and DFT calculations (Section S18.6) show that precomplexation of the substrate may occur on the aniline moiety. Therefore, Q₁ being the long-lived emitter state would explain why the luminescence is not quenched upon addition of substrate **1d** to the reaction mixture: In a precomplex, the charge would be shifted away from the substrate when the catalyst crosses to Q₁, thus impeding single electron transfer.

3.6.19.5 Computational Investigation of Preassembly Candidates

The variation of catalyst structure on the reactivity presented in the main article showed increasing yields for the reaction of **1d**, when reducing the steric bulk on the ortho-position of the catalyst's *N*-aniline moiety. Thus we performed DFT calculations to investigate possible arrangements for ground state precomplexation between substrate and the aniline unit of the catalyst radical anion. All calculations were performed at the ω B97X-D/6-311+G* level of theory with Gaussian16.^[56] Solvation effects were included with the IEFPCM model,^[59] with default parameters for acetonitrile. For the frequency analyses presented in this section, we reduced the two-electron integral accuracy threshold from 10-12 to 10-11 (keyword int=(acc2e=11)), because the

calculations would not converge otherwise. Due to their structural complexity, there are many ways for the phosphinate to dispersively bind to the radical anion catalyst. Assuming that the primary contributors to the binding mode are π -stacking interactions,^[89] the P-bound phenyl groups as well as the aryl moiety from the benzylic position (“O-CHR-aryl”) of the phosphinate may coordinate to the aniline or naphthalene moiety of the radical anion catalyst. Here, π - π stacked interactions (face-to-face, parallel displaced) as well as T- π shaped interactions (edge-to-face) are conceivable. We expect the strongest dispersive interactions when not just one but two of the substrate’s aromatic units coordinate to the *N*-aniline group in a pincer-like complex. Indeed, the geometry optimizations shown later in this section always converged to an orientation where one of the aromatic units of the substrate coordinates (π - π , face-to-face) to the aniline ring and another one to the side (T- π , edge-to-face), regardless of the starting structure. To assess the accessibility of such a complex starting from isolated molecules, we first performed a series of unrelaxed potential energy scans. The scan coordinate was chosen such that the O-CHR-aryl component of substrate 1d approaches the catalyst from the side and one of the P-bound phenyl units forms a T- π shaped complex with the aniline at small distances (Figure S32).

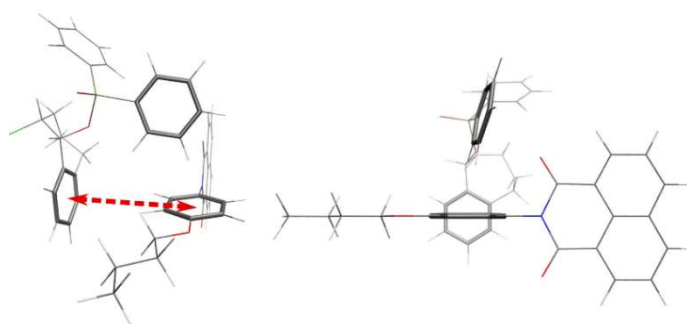


Figure S 33. Two views on the orientation of 1d and the catalyst (here *nBuO-NpMI*) were chosen for potential energy scans. The red arrow indicates the scan coordinate, i.e. the center-of-mass distance between the aniline moiety of the catalyst and the O-CHR-aryl moiety of the substrate. The three interacting aromatic rings are highlighted in bold.

Two energy minima emerge along the scan coordinate (Figure S33, left). Going from large to small distances, the first minimum appears when the P-bound phenyl starts to interact dispersively with the ortho-substituent groups. It is followed by an energy barrier when the imide-oxygen and/or the ortho-substituent groups come in closer contact with the phenyl unit and repulsive terms presumably start to predominate. As could be expected, this barrier rises with increasing “steric bulk” on the aniline and makes the second minimum entirely inaccessible for *NpMI* (Figure S33, left). This second energy minimum represents the fully formed pincer-like complex, where the O-CHR-aryl moiety of the substrate is close enough to form dispersive T- π -stacking interactions with the aniline unit, which stabilizes the energy.

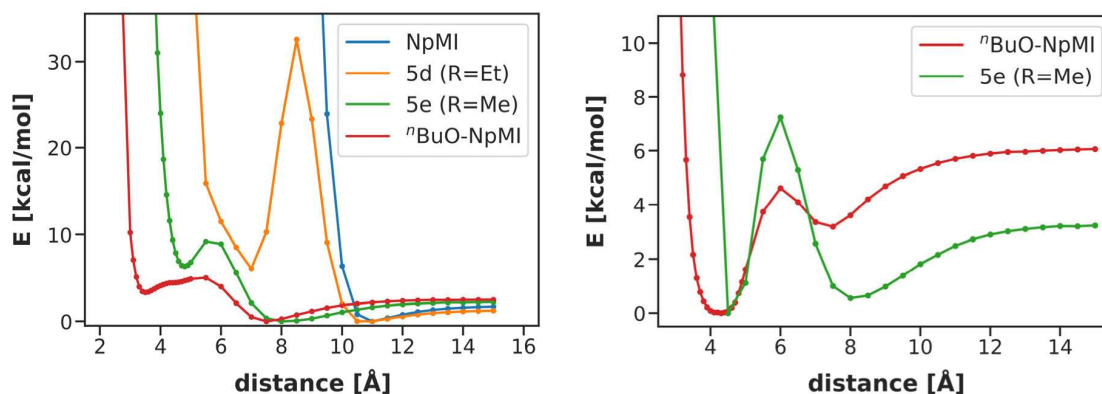


Figure S 34. Potential energy scans along the approach of substrate 1d towards the aniline unit of the catalyst. The scan coordinate refers to the center-of-mass distance between the O-CHR-aryl moiety and the aniline unit. Left: aniline and naphthalene units orthogonal, this is the ground state minimum of the catalyst. Right: naphthalene unit rotated by 90°, structure not relaxed. The minimum energy is shifted to zero in all scans.

For the less sterically hindered catalysts ⁿBuO-NpMI and 5e, the aniline unit can in principle rotate with respect to the imide group. We calculated the rotational barrier in nBuO-NpMI⁻ as 16 kcal/mol by performing a relaxed potential energy scan of the respective C-C-N-C dihedral angle between 90° and 180° with a step size of 2° at the same level of theory as before (Figure S34). In effect, the rotation of the aniline group decreases the repulsive “steric” interactions between one of the imide oxygens and the P-bound phenyls, thus lowering the energy barrier for precomplexation and stabilizing the complex (Figure S33, right) even more so than the initial dispersive interaction with the ortho-substituent.

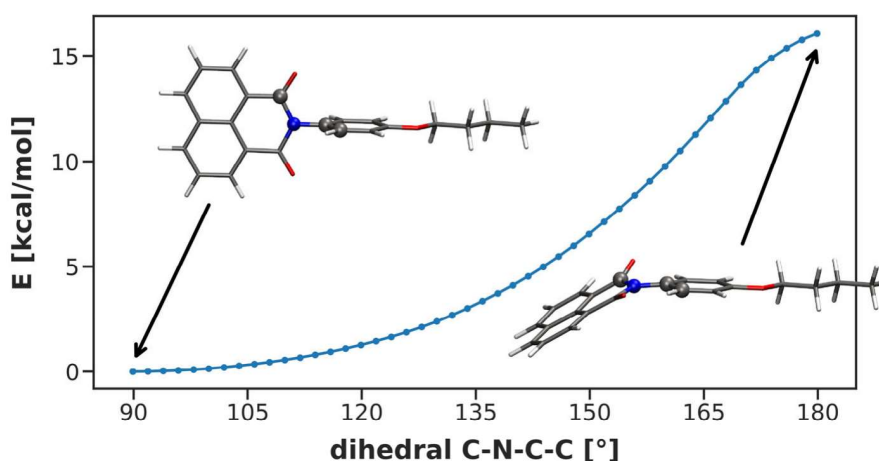


Figure S 35. Relaxed potential energy surface scan for the rotation of the aniline moiety in nBuO-NpMI. The four atoms defining the scanned dihedral angle are highlighted as spheres.

Assuming that a successful reaction requires formation of a precomplex, on the basis of arguments presented in the main manuscript: (i) known picosecond lifetime of doublet states, apparent anti-Kasha photochemistry, (ii) the likely rate-limiting C(sp³)-O cleavage and profound influence of

catalyst structure on this step, (iii) the identical redox, UV-Vis and emissive properties of **NpMI** and **^tBuO-NpMI** that confirm electronic differences cannot explain the success of the latter catalyst for most substrates, the potential energy scans depicted in Figure S33 could possibly explain the reactivity trend observed in the experimental SAR study. Increasing “steric bulk” at the ortho-position of the aniline impedes the formation of the most stable and intimate preassembly as the pincer-like π -stacking interaction becomes less accessible. Of course, an unrelaxed potential energy scan for complex molecular assemblies can only convey a rough picture of the real situation. For example, it neglects the internal flexibility of the substituents and the fact that the substrate can re-orient itself upon approaching the catalyst, thus minimizing clashes and stabilizing the complex. To take these effects into account, we optimized several candidate structures for a ground state precomplex. Using different catalysts and relative orientations, we were able to optimize 13 stable ground state preassemblies (Figures S35-39).

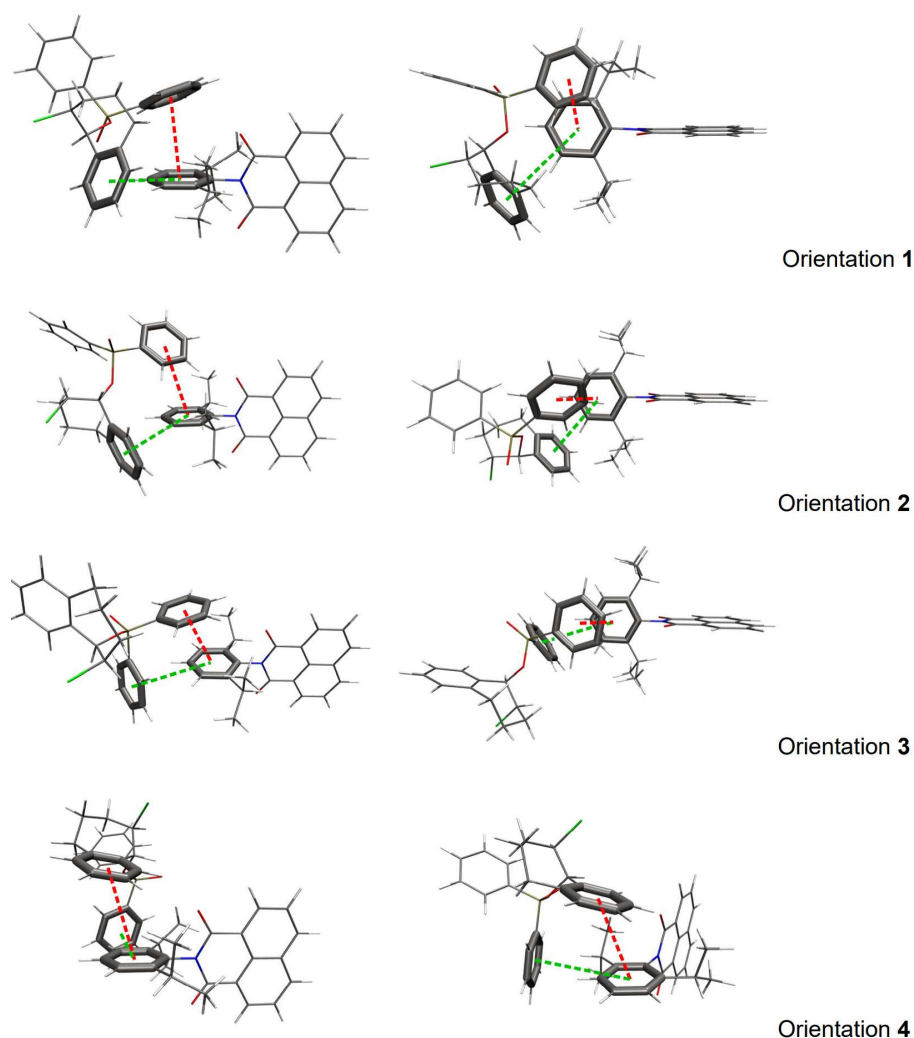


Figure S 36. Candidate preassemblies of **NpMI⁻/1d** at the *N*-aniline moiety.

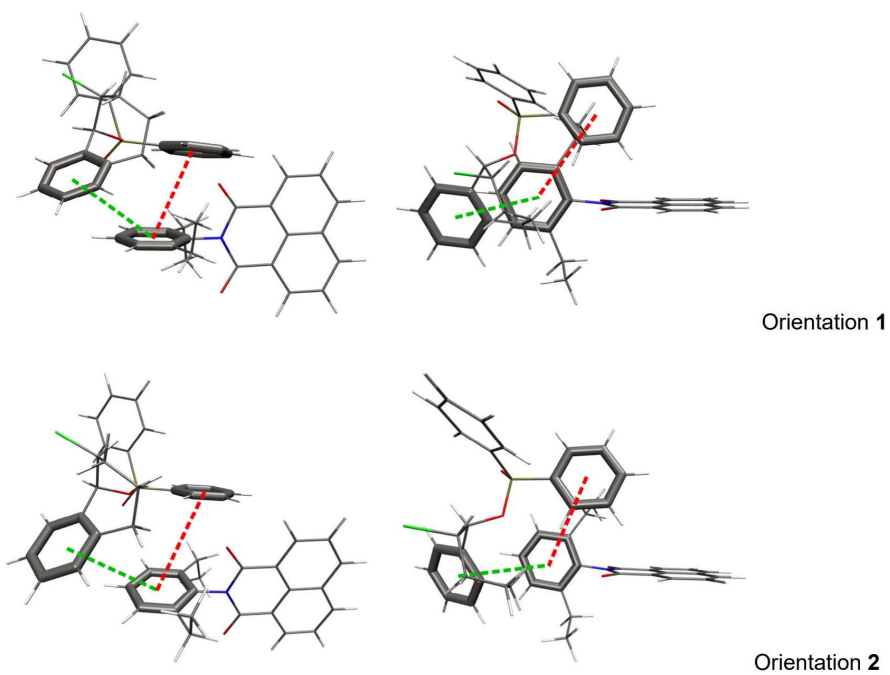


Figure S 37. Candidate preassemblies of $5d^+/1d$ at the *N*-aniline moiety.

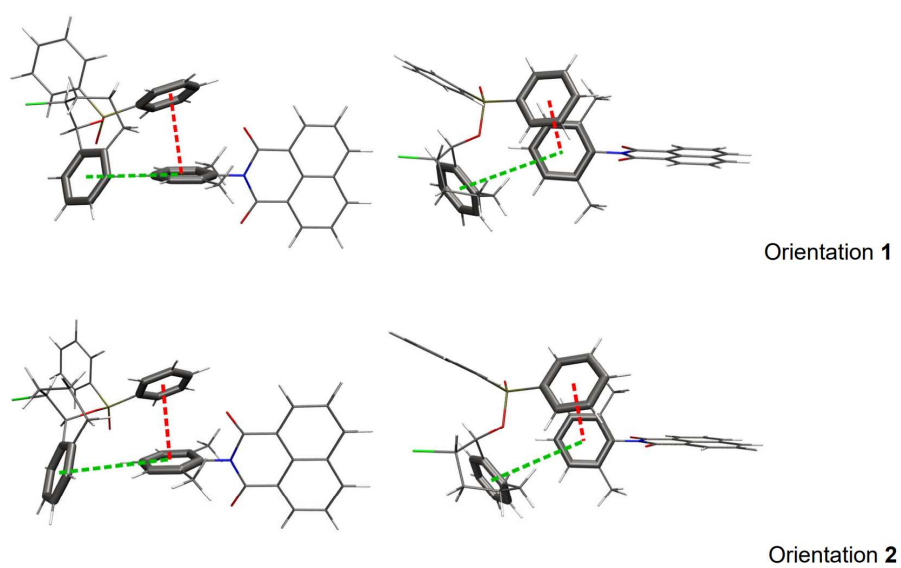


Figure S 38. Candidate preassemblies of $5e^-/1d$ at the *N*-aniline moiety.

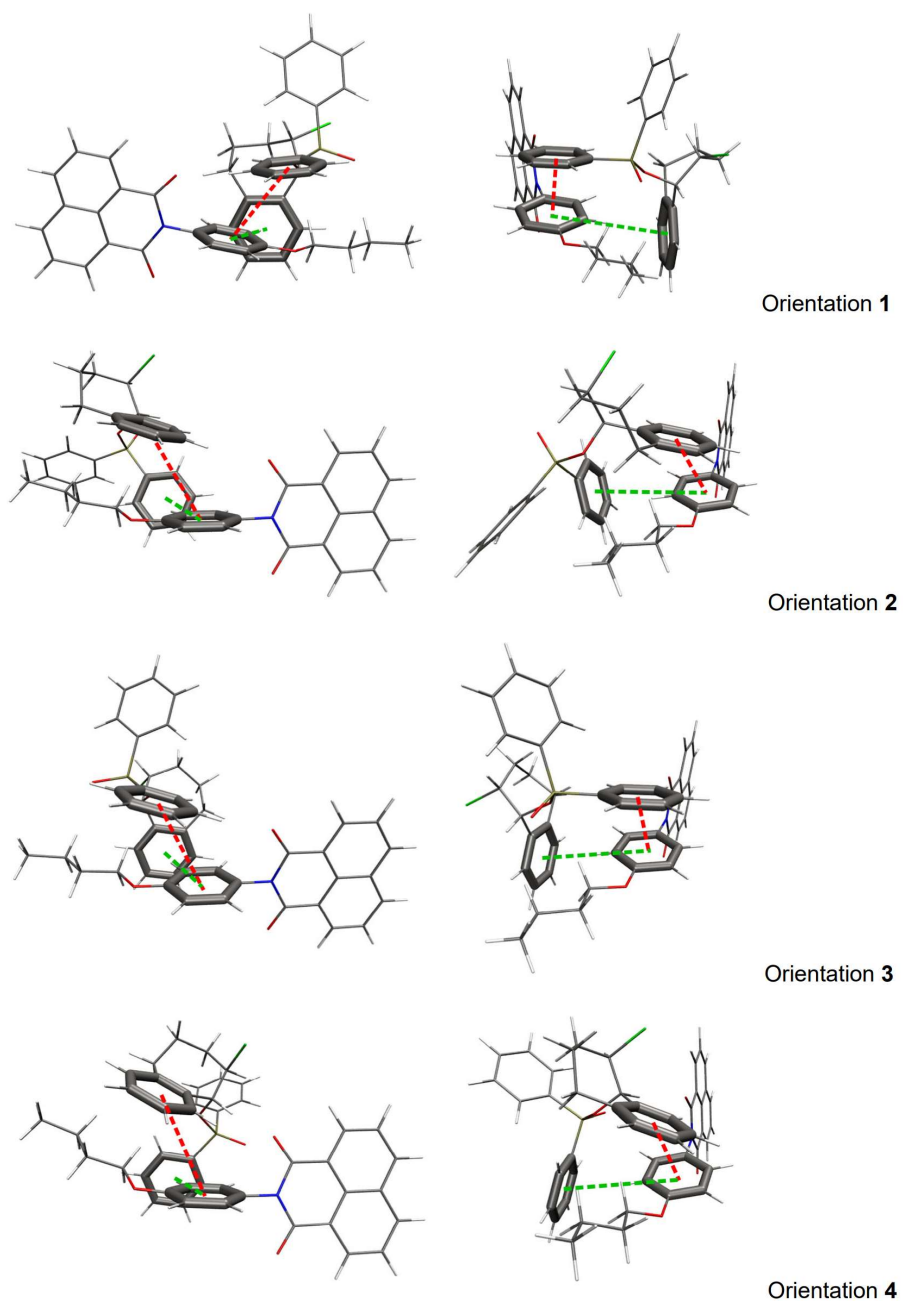


Figure S 39. Candidate preassemblies of $n\text{BuO-NpM}\Gamma^-/1d$ at the *N*-aniline moiety.

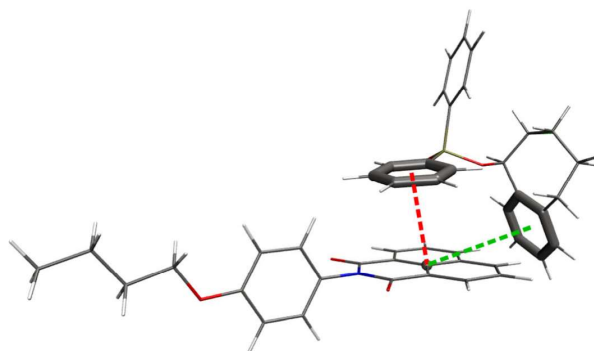


Figure S 40. Candidate preassembly of $n\text{BuO-NpM}\Gamma^-/1d$ at the naphthalene moiety.

As a quantitative measure for the stability of the converged structures, we defined the free energy of complexation ΔG_{compl} as the free energy difference between the optimized precomplex and its isolated components (Table S9). For the latter, we calculated the neutral form of phosphinate **1d** and the radical anion of the respective catalyst. In all cases, the optimized structures of isolated radical anion catalysts and preassemblies find the *N*-aniline moiety perpendicular to the naphthalene moiety. Multiple stable structures exist for the preassemblies, differing in the relative orientation of the substrate with respect to the catalyst and the calculations presented here are not intended to be comprehensive. However, comparing the relative energies of a few optimized structures^[76] is helpful to rationalize the observed SAR in the context of a potential preassembly. Regardless of initial input geometries, all optimizations converged to a pincer-like structure where one of the substrate-bound aromatic units coordinates to the side of the aniline and another is oriented parallel to the aniline and coordinates from the top.

Table S 10. Calculated free energies of complexation (kcal/mol) for ground state assemblies of substrate **1d** with various residues *R* on the ortho-position of the *N*-aniline unit of the catalyst (ω B97X-D/6-311+G*, IEFPCM(ACN)).

Components	Orientation	Complexation free energy ΔG^{compl} (kcal mol ⁻¹)	Intermolecular distance (Å) ^a	Preparative reaction yield (% 2d)
NpMI ⁻ (R=Pr) / 1d	1	+10.44	4.88 (<i>T</i> - π) ^b , 4.23 (π - π) ^c	n.d.
	2	+3.41	?	
	3	+5.35	?	
	4	+11.65	?	
5d ⁻ (R=Et) / 1d	1	+4.97	4.52 ^{b,d} , 5.37 ^{c,d}	40
	2	+4.66	4.63 ^{b,d} , 5.23 ^{c,d} ?	
5e ⁻ (R=Me) / 1d	1	+5.88	5.16 (<i>T</i> - π) ^b , 4.33 (π - π) ^c	55
	2	+6.11	5.17 (<i>T</i> - π) ^b , 4.32 (π - π) ^c	
ⁿ BuO-NpMI ⁻ (R=H) / 1d	1	+2.59	4.90 (<i>T</i> - π) ^b , 4.07 (π - π) ^c	75
	2	-0.18	5.14 (<i>T</i> - π) ^c , 4.26 (π - π) ^b	
	3	-0.33	4.89 (<i>T</i> - π) ^b , 4.06 (π - π) ^c	
	4	0.70	5.14 (<i>T</i> - π) ^c , 4.33 (π - π) ^b	
	Naphthalene complex	-0.16	4.50 (<i>T</i> - π) ^e , 4.52 (π - π) ^f	

n.d., not determined. ^aThe distances between the aromatic center points of each aromatic ring of **1d** to the center point of the *N*-aniline were taken. ^bInteraction between the *N*-aniline and the O-CHR-Ar arene. ^cInteraction between the *N*-aniline and the O-P(O)Ph arene. ^dThe interaction could not be assigned as *T*- π or π - π and resembled something in between.

Out of all the optimized complexes, the four orientational candidates for ⁿBuO-NpMI are consistently the most thermodynamically favorable, again supporting the hypothesis that precomplexation in the ground state is an important aspect of the catalytic process. The trend among the other catalysts is not as clear, however. It is difficult to draw a concrete relationship between increasingly bulky ortho-substituents and thermodynamics, since the substrate can rearrange to coordinate from a different direction. Nonetheless, formation of all complexes with ortho-substituted catalysts is endergonic at this level of theory, indicating that steric hindrance on the aniline unit indeed impedes the stacking interaction and destabilizes the complex.⁷⁷ The spin density in all of the optimized precomplex radical anions, where complexation occurs on the *N*-aniline unit of the catalyst, remains identical to those of the isolated catalysts. In contrast, the spin density of the one precomplex candidate, where the substrate coordinates to the naphthalene moiety of ⁿBuO-NpMI, is asymmetrical and thus deviates slightly from that of the isolated catalyst

(Figure S40). Such a change in the electronic structure should manifest in a different EPR signal, which we do not observe. This again supports the thesis that if preassociation occurs, it will involve the *N*-aniline moiety rather than the naphthalene moiety of the catalyst.

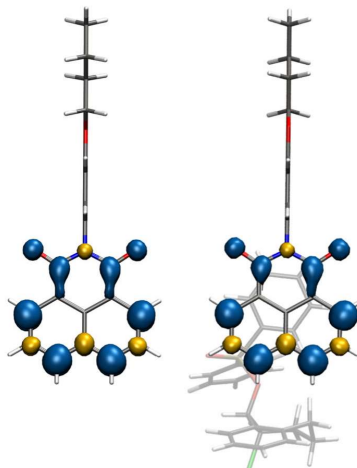


Figure S 41. Spin densities of *nBuO-NpMI*^{•-} (left) and an *nBuO-NpMI*^{•-}/*1d* precomplex structure where the substrate coordinates to the naphthalene moiety of the catalyst (right).

Note that the mere existence of a ground state minimum does not mean that it is catalytically active upon photoexcitation. For example, Barham and co-workers recently proposed the detection of two different triarylamine radical cation/haloarene precomplex geometries (edge-to-face T- π and face-to-face π - π) on the basis of changes in EPR spectra and DFT calculations.^[2] There, it was proposed the face-to-face π - π geometry was ‘unreactive’ upon photoexcitation. Therefore, the thermodynamics of precomplexation in the ground state is only one aspect to consider in a larger scheme. Our computational results demonstrate that there indeed are stable candidate preassemblies of phosphinate substrate and radical anion catalyst. Moreover, we show that the introduction of substituents at the ortho-position of the *N*-aniline moiety destabilizes these complexes and makes their formation less likely due to a higher kinetic barrier upon approach of the two molecules. Further studies are required to investigate the excited states of our optimized candidate structures and whether certain geometric factors can facilitate SET within preassemblies upon photoexcitation.

3.6.20 X-Ray Crystallography

Single crystal x-ray diffraction data were recorded for a suitable crystal of ⁿBuO-NpMI. The crystal was mounted on a MITIGEN holder with inert oil on a XtaLAB Synergy R, DW system, HyPix-Arc 150 diffractometer using Cu-K α radiation ($\lambda = 1.54184 \text{ \AA}$). The crystal was kept at a steady $T = 100.01(10) \text{ K}$ during data collection. Empirical multi-scan^[90] and analytical absorption corrections^[91] were applied to the data. Structures were solved using SHELXT^[92] using dual methods and Olex2 as the graphical interface,^[93] and least-squares refinements on F2 were carried out using SHELXL.^[92,94] All non-hydrogen atoms were refined anisotropically. Hydrogen atom positions were calculated geometrically and refined using the riding model. Most hydrogen atom positions were calculated geometrically and refined using the riding model, but some hydrogen atoms were refined freely. 2078961 (ⁿBuO-NpMI) contains the supplementary crystallographic data for this paper. These data are provided free of charge by The Cambridge Crystallographic Data Centre.

Compound	ⁿ BuO-NpMI
Empirical formula	C ₂₂ H ₁₉ NO ₃
$\rho_{\text{calc}}/(\text{g}/\text{cm}^3)$	1.363
μ/mm^{-1}	0.731
Formula weight	345.38 g mol ⁻¹
Crystal color	clear colorless
Crystal shape	plate
Crystal size/mm ³	0.18 × 0.13 × 0.05
Temperature/K	100.01(10)
Crystal system	triclinic
Space group	P-1
$a/\text{\AA}$	5.32030(10)
$b/\text{\AA}$	8.91200(10)
$c/\text{\AA}$	18.2867(2)
$\alpha/^\circ$	83.2940(10)
$\beta/^\circ$	84.9920(10)
$\gamma/^\circ$	78.2530(10)
Volume/ \AA^3	841.29(2)
Z	2
Z'	1
Wavelength/ \AA	1.54184
Radiation	Cu K α
$\Theta_{\text{min}}/^\circ$	2.438
$\Theta_{\text{max}}/^\circ$	74.411
Reflections collected	31649
Independent reflections	3319
Reflections $I \geq 2 \sigma(I)$	3018

R _{int}	0.0289
Parameters	300
Restraints	0
Largest peak	0.226
Deepest hole	-0.248
GooF	1.064
wR2 (all data)	0.0981
wR2	0.0961
R1 (all data)	0.0374
R1	0.0345

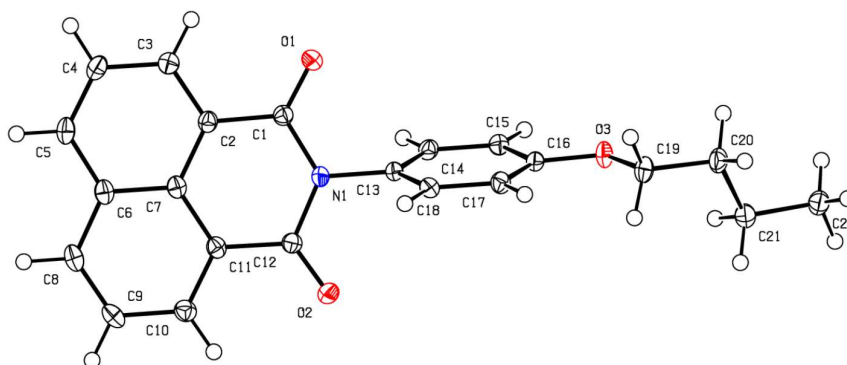


Figure S 42. Solid-state molecular structure of TCBPA, including atom numbering scheme. Thermal ellipsoids are set at the 50% probability level. C atoms are shown in grey, N atoms in blue and O atoms in red.

3.6.21 References

- [1] D. D. Perrin; L. F. Armarego, *Purification of Laboratory Compounds*, 3rd Ed.; Pergamon Press, New York, 1992.
- [2] S. Wu, J. Žurauskas, M. Domański, P. S. Hitzfeld, V. Butera, D. J. Scott, J. Rehbein, A. Kumar, E. Thyraug, J. Hauer, J. P. Barham, *Org. Chem. Front.* **2021**, *8*, 1132-1142.
- [3] N. G. W. Cowper, C. P. Chernowsky, O. P. Williams, Z. K. Wickens, *J. Am. Chem. Soc.* **2020** *142*, 2093-2099.
- [4] L. Song, Y. Yang, Q. Zhang, H. Tian, W. Zhu, *J. Phys. Chem. B* **2011**, *115*, 14648-14658.
- [5] W. Zhang, Y. Xu, M. Hanif, S. Zhang, J. Zhou, D. Hu, Z. Xie, Y. Ma, *J. Phys. Chem. C* **2017**, *121*, 23218-23223.
- [6] (a) I. Pravst, M. Zupan, S. Stavber, *Tetrahedron*, **2008**, *64*, 5191-5199; (b) J. C. Lee, Y. H. Bae, S.-K. Chang, *Bull. Korean Chem. Soc.* **2003**, *24*, 407-408.
- [7] K. Lam, I. E. Markó, *Org. Lett.* **2011**, *13*, 406-409.
- [8] S. Yakubov, J. P. Barham, *Beilstein J. Org. Chem.* **2020**, *16*, 2151-2192.
- [9] X. Chen, C. Xu, T. Wang, C. Zhou, J. Du, Z. Wang, H. Xu, T. Xie, G. Bi, J. Jiang, X. Zhang, J. N. Demas, C. O. Trindle, Y. Luo, G. Zhang, *Angew. Chem. Int. Ed.* **2016**, *55*, 9872-9876.
- [10] H. Kakuta, A. Tanatani, K. Nagasawa, Y. Hashimoto, *Chem. Pharm. Bull.* **2003**, *51*, 1273-1282.
- [11] D. J. Fox, D. S. Pedersen, A. B. Petersen, S. Warren, *Org. Biomol. Chem.* **2006**, *4*, 3117.
- [12] R. Chauvin, *Tetrahedron: Asymmetry*, **1990**, *1*, 737-742.
- [13] F. W. Lewis, T. C. McCabe, D. H. Grayson, *Tetrahedron*, **2011**, *67*, 7517-7528.
- [14] C. Belger, N. M. Neisius, B. Plietker, *Chem.-Eur. J.* **2010**, *16*, 12214-12220.
- [15] T. Shimasaki, Y. Konno, M. Tobisu, N. Chatani, *Org. Lett.* **2009**, *11*, 4890-4892.
- [16] T. Ljungdahl, T. Bennur, A. Dallas, H. Emtenäs, J. Mårtensson, *Organometallics* **2008**, *27*, 2490-2498.
- [17] M. Yasuda, R. Kojima, H. Tsutsui, D. Utsunomiya, K. Ishii, K. Jinnouchi, T. Shiragami, T. Yamashita, *J. Org. Chem.* **2003**, *68*, 7618-7624.
- [18] N. Taniguchi, *J. Org. Chem.* **2006**, *71*, 7874-7876.
- [19] B. Scheiper, M. Bonnekessel, H. Krause, A. Fürstner, *J. Org. Chem.* **2004**, *69*, 3943-3949.
- [20] P. Mayo, W. Tam, *Tetrahedron*, **2002**, *58*, 9527-9540.
- [21] A. L. Hansen, J.-P. Ebran, T. M. Gøsgig, T. Skrydstrup, *J. Org. Chem.* **2007**, *72*, 6464-6472.
- [22] R. Kumar, A. Sharma, N. Sharma, V. Kumar, A. K. Sinha, *Eur. J. Org. Chem.* **2008**, 5577-5582.
- [23] A. E. Díaz-Álvarez, P. Crochet, V. Cadierno, *Tetrahedron* **2012**, *68*, 2611-2620.
- [24] S. Fantauzzi, E. Gallo, A. Caselli, F. Ragaini, P. Macchi, N. Casati, S. Cenini, *Organometallics* **2005**, *24*, 4710-4713.
- [25] K. Ahmad, N. F. Thomas, M. R. Mukhtar, I. Noorbacha, J.-F. F. Weber, M. A. Nafiah, S. S. Velu, K. Takeya, H. Morita, C.-G. Lim, A. H. A. Hadi, K. Awang, *Tetrahedron* **2009**, *65*, 1504-1516.
- [26] B. M. Trost, H. C. Arndt, *J. Am. Chem. Soc.* **1973**, *95*, 5288-5298.
- [27] M. Al-Masum, S. Alam, *Tetrahedron Lett.* **2009**, *50*, 5201-5204.
- [28] Y. Zhao, Q. Liu, J. Li, Z. Liu, B. Zhou, *Synlett*, **2010**, 1870-1872.
- [29] U. P. N. Tran, G. Oss, D. P. Pace, J. Ho, T. V. Nguyen, *Chem. Sci.* **2018**, *9*, 5145-5151.
- [30] P. Batsomboon, W. Phakhodee, S. Ruchirawat, P. Ploypradith, *J. Org. Chem.* **2009**, *74*, 4009-4012.
- [31] D. M. Hodgson, M. J. Fleming, S. J. Stanway, *J. Am. Chem. Soc.* **2004**, *126*, 12250-12251.
- [32] E. Alacid, C. Nájera, *J. Org. Chem.* **2009**, *74*, 2321-2327.
- [33] T. Satoh, T. Kasuya, M. Ishigaki, M. Inumaru, T. Miyagawa, N. Nakaya, S. Sugiyama, *Synthesis* **2011**, 397-408.
- [34] N. Kambe, Y. Moriwaki, Y. Fujii, T. Iwasaki, J. Terao, *Org. Lett.* **2011**, *13*, 4656-4659.
- [35] S. E. Denmark, C. R. Butler, *Org. Lett.* **2006**, *8*, 63-66.
- [36] V. Paquet, H. Lebel, *Synthesis* **2005**, 1901-1905.
- [37] J. Y. Wu, B. Moreau, T. Ritter, *J. Am. Chem. Soc.* **2009**, *131*, 12915-12917.
- [38] M. Teraguchi, M. Ohtake, H. Inoue, A. Yoshida, T. Aoki, T. Kaneko, K. Yamada, *J. Polym. Sci., Part A: Polym. Chem.* **2005**, *43*, 2348-2357.
- [39] L. Chen, S. Jin, J. Gao, T. Liu, Y. Shao, J. Feng, K. Wang, T. Lu, D. Du, *Org. Lett.* **2021**, *23*, 394-399.
- [40] P. J. Black, M. G. Edwards, J. M. J. Williams, *Eur. J. Org. Chem.* **2006**, 4367-4378.
- [41] Y. Takada, J. Caner, S. Kaliyamoorthy, H. Naka, S. Saito, *Chem. Eur. J.* **2017**, *23*, 18025-18032.
- [42] O. Abdul-Rahim, A. N. Simonov, T. Rüther, J. F. Boas, A. A. J. Torriero, D. J. Collins, P. Perlmutter, A. M. Bond, *Anal. Chem.* **2013**, *85*, 6113-6120.
- [43] L. Pause, M. Robert, J.-M. Savéant, *J. Am. Chem. Soc.* **1999**, *121*, 7158-7159.
- [44] P. Cankar, D. Dubas, S. C. Banfield, M'hamed Chahma, T. Hudlicky, *Tetrahedron Lett.* **2005**, *46*, 6851-6854.
- [45] F. Strieth-Kalthoff, M. J. James, M. Teders, L. Pitzer, F. Glorius, *Chem. Soc. Rev.* **2018**, *47*, 7190-7202.
- [46] R. O. Marcon, S. Brochsztain, *J. Phys. Chem. A* **2009**, *113*, 1747-1752.
- [47] D. Gosztola, M. P. Niemczyk, W. Svec, A. S. Lukas, M. R. Wasielewski, *J. Phys. Chem. A* **2000**, *104*, 6545-6551.
- [48] C. Lu, M. Fujitsuka, A. Sugimoto, T. Majima, *J. Phys. Chem. C* **2016**, *120*, 12734-12741.
- [49] C. J. Zeman IV, S. Kim, F. Zhang, K. S. Schanze, *J. Am. Chem. Soc.* **2020**, *142*, 2204-2207.
- [50] A. Demeter, T. Bercés, L. Biczók, V. Wintgens, P. Valat, J. Kossanyi, *J. Phys. Chem.* **1996**, *100*, 2001-2011.
- [51] (a) J. Kong, S. Yu, *Acta Biochemica et Biophysica Sinica* **2007**, *39*, 549-559; (b) R. Chaudret, B. De Courcy, J. Contreras-García, E. Gloaguen, A. Zehnacker-Rentein, M. Mons, J.-P. Piquemal, *Phys. Chem. Chem. Phys.* **2014**, *16*, 9876-9891.

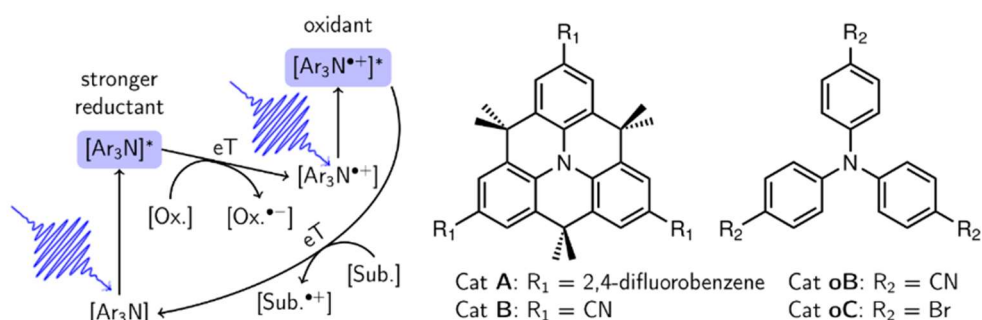
- [52] A. K. Lemmens, P. Chopra, D. Garg, A. L. Steber, M. Schnell, W. J. Buma, *Molecular Physics* **2021**, *119*, e1811908.
- [53] D. R. Duling *J. Mag. Reson.* **1994**, *104*, 105-110.
- [54] V. A. Ryabinin, V. F. Starichenko, G. N. Vorozhtsov, S. M. Shein, *J. Struct. Chem.* **1978**, *19*, 693-701.
- [55] (a) P. Hohenberg, W. Kohn, *Phys. Rev.* **1964**, *36*, 864-871; (b) W. Kohn, L. Sham *J. Phys. Rev.* **1965**, *140*, 1133-1138.
- [56] M. J. Frisch, G. W. Trucks, H. B. Schlegel, G. E. Scuseria, M. A. Robb, J. R. Cheeseman, G. Scalmani, V. Barone, G. A. Petersson, H. Nakatsuji, X. Li, M. Caricato, A. V. Marenich, J. Bloino, B. H. Janesko, R. Gomperts, B. Mennucci, H. P. Hratchian, J. V. Ortiz, A. F. Izmaylov, J. L. Sonnenberg, D. F. Williams, F. Lapparini, F. Egidi, J. Goings, B. Peng, A. Petrone, T. Henderson, D. Ranasinghe, V. G. Zakrzewski, J. Gao, N. Rega, G. Zheng, W. Liang, M. Hada, M. Ehara, K. Toyota, R. Fukuda, J. Hasegawa, M. Ishida, T. Nakajima, Y. Honda, O. Kitao, H. Nakai, T. Vreven, K. Throssell, J. A. Montgomery Jr., J. E. Peralta, F. Ogliaro, M. Bearpark, J. J. Heyd, E. N. Brothers, K. N. Kudin, V. N. Staroverov, R. Kobayashi, J. Normand, K. Raghavachari, A. P. Rendell, J. C. Burant, S. S. Iyengar, J. Tomasi, M. Cossi, J. M. Millam, M. Klene, C. Adamo, R. Cammi, J. W. Ochterski, R. L. Martin, K. Morokuma, Ö. Farkas, J. B. Foresman, D. J. Fox, Gaussian 16, Rev. C.01. Wallingford, CT, **2016**.
- [57] J.-D. Chai, M. Head-Gordon, *Phys. Chem. Chem. Phys.* **2008**, *10*, 6615-6620
- [58] (a) M. J. Frisch, J. A. Pople, J. S. Binkley, *J. Chem. Phys.* **1984**, *80*, 3265-3269; (b) R. Krishnan, J. S. Binkley, R. Seeger, J. A. Pople, *J. Chem. Phys.* **1980**, *72*, 650-654; (c) A. D. McLean, G. S. Chandler, *J. Chem. Phys.* **1980**, *72*, 5639-5648.
- [59] (a) J. Tomasi, B. Mennucci, R. Cammi, *Chem. Rev.* **2005**, *105*, 2999-3094; (b) G. Scalmani, M. J. Frisch, J. *Chem. Phys.* **2010**, *132*, 114110.
- [60] W. Humphrey, A. Dalke, K. Schulten, *J. Mol. Graph.* **1996**, *14*, 33-38.
- [61] (a) L. Goerigk, A. Hansen, C. Bauer, S. Ehrlich, A. Najibi, S. Grimme, *Phys. Chem. Chem. Phys.* **2017**, *19*, 32184-32215; (b) N. Mardirossian, M. Head-Gordon, *Mol. Phys.* **2017**, *115*, 2315-2372.
- [62] L. Goerigk, N. Mehta, Aust. *J. Chem.* **2019**, *72*, 563-573.
- [63] H. Kruse, L. Goerigk, S. Grimme, *J. Org. Chem.* **2012**, *77*, 10824-10834.
- [64] (a) D. G. Liakos, Y. Guo, F. Neese, *J. Phys. Chem. A* **2020**, *124*, 90-100; (b) M. Saitow, U. Becker, C. Riplinger, E. F. Valeev, F. Neese, *J. Chem. Phys.* **2017**, *146*, 164105.
- [65] (a) F. Neese, *WIREs Comput. Mol. Sci.* **2012**, *2*, 73-78; (b) F. Neese, *WIREs Comput. Mol. Sci.* **2018**, *8*, e1327.
- [66] (a) D. Rappoport, F. Furche, *J. Chem. Phys.* **2010**, *133*, 134105; (b) F. Weigend, R. Ahlrichs, *Phys. Chem. Chem. Phys.* **2005**, *7*, 3297-3305.
- [67] (a) A. Hellweg, C. Hättig, S. Höfener, W. Klopper, *Theor. Chem. Acc.* **2007**, *117*, 587-597; (b) A. Hellweg, D. Rappoport, *Phys. Chem. Chem. Phys.* **2015**, *17*, 1010-1017.
- [68] (a) V. Barone, M. Cossi, *J. Phys. Chem. A* **1998**, *102*, 1995-2001; (b) M. Cossi, N. Rega, G. Scalmani, V. Barone, *J. Comput. Chem.* **2003**, *24*, 669-681.
- [69] J. E. Bartmess, *J. Phys. Chem.* **1994**, *98*, 6420-6424.
- [70] (a) L. E. Roy, E. Jakubikova, M. G. Guthrie, E. R. Batista, *J. Phys. Chem. A* **2009**, *113*, 6745-6750; (b) D. G. Truhlar, C. J. Cramer, A. Lewis, J. A. Bumpus, *J. Chem. Educ.* **2004**, *81*, 596; (c) S. J. Konezny, M. D. Doherty, O. R. Luca, R. H. Crabtree, G. L. Soloveichik, V. S. Batista, *J. Phys. Chem. C* **2012**, *116*, 6349-6356; (d) S. Maier, B. Thapa, K. Raghavachari, *Phys. Chem. Chem. Phys.* **2020**, *22*, 4439-4452; (e) A. P. Davis, A. J. Fry, *J. Phys. Chem. A* **2010**, *114*, 12299-12304; (f) A. A. Isse, A. Gennaro, *J. Phys. Chem. B* **2010**, *114*, 7894-7899; (g) Y. Paukku, G. Hill, *J. Phys. Chem. A* **2011**, *115*, 4804-4810.
- [71] (a) A. Francisco da Silva, A. João da Silva Filho, M. L. A. A. Vasconcellos, O. Luís de Santana, *Molecules* **2018**, *23*, 2129; (b) J. Ho, A. Klamt, M. L. Coote, *J. Phys. Chem. A* **2010**, *114*, 13442-13444.
- [72] M. Namazian, C. Y. Lin, M. L. Coote, *J. Chem. Theory Comput.* **2010**, *6*, 2721-2725.
- [73] M. Isegawa, F. Neese, D. A. Pantazis, *J. Chem. Theory Comput.* **2016**, *12*, 2272-2284.
- [74] (a) S. Grimme, M. Waletzke, *J. Chem. Phys.* **1999**, *111*, 5645-5655. (b) I. Lyskov, M. Kleinschmidt, C. M. Marian, *J. Chem. Phys.* **2016**, *144*, 034104. (c) A. Heil, C. M. Marian, *J. Chem. Phys.* **2017**, *147*, 194104. (d) A. Heil, M. Kleinschmidt, C. M. Marian, *J. Chem. Phys.* **2018**, *149*, 164104. (e) C. M. Marian, A. Heil, M. Kleinschmidt, *WIREs Comput. Mol. Sci.* **2019**, *9*, e1394.
- [75] (a) C. Lee, W. Yang, R. G. Parr, *Phys. Rev. B* **1988**, *37*, 785-798. (b) A. D. Becke, *J. Chem. Phys.* **1993**, *98*, 1372-1377. (76) (a) F. Weigend, M. Kattannek, R. Ahlrichs, *J. Chem. Phys.* **2009**, *130*, 164106. (b) S. Kossmann, F. Neese, *Chem. Phys. Lett.* **2009**, *481*, 240-243.
- [77] F. Weigend, *J. Comput. Chem.* **2008**, *29*, 167-175.
- [78] F. Neese, *J. Am. Chem. Soc.* **2006**, *128*, 10213-10222.
- [79] H. Werner, W. Meyer, *J. Chem. Phys.* **1981**, *74*, 5794-5801.
- [80] H. Werner, P. J. Knowles, *J. Chem. Phys.* **1985**, *82*, 5053-5063. 222
- [81] D. A. Kreplin, P. J. Knowles, H.-J. Werner, *J. Chem. Phys.* **2020**, *152*, 074102.
- [82] H.-J. Werner, P. J. Knowles, G. Knizia, F. R. Manby, M. Schütz, P. Celani, W. Györffy, D. Kats, T. Korona, R. Lindh, A. Mitrushenkov, G. Rauhut, K. R. Shamasundar, T. B. Adler, R. D. Amos, S. J. Bennie, A. Bernhardsson, A. Berning, D. L. Cooper, M. J. O. Deegan, A. J. Dobbyn, F. Eckert, E. Goll, C. Hampel, A. Hesselmann, G. Hetzer, T. Hrenar, G. Jansen, C. Köppl, S. J. R. Lee, Y. Liu, A. W. Lloyd, Q. Ma, R. A. Mata, A. J. May, S. J. McNicholas, W. Meyer, T. F. Miller III, M. E. Mura, A. Nicklass, D. P. O'Neill, P. Palmieri, D. Peng, K. Pflüger, R. Pitzer, M. Reiher, T. Shiozaki, H. Stoll, A. J. Stone, R. Tarroni, T. Thorsteinsson, M. Wang, M. Welborn, *MOLPRO, Version 2021.1, a Package of Ab Initio Programs*, **2021**.
- [83] H.-J. Werner, P. J. Knowles, G. Knizia, F. R. Manby, M. Schütz, *WIREs Comput. Mol. Sci.* **2012**, *2*, 242-253.
- [84] H.-J. Werner, P. J. Knowles, F. R. Manby, J. A. Black, K. Doll, A. Heßelmann, D. Kats, A. Köhn, T. Korona, D.

- A. Kreplin, Q. Ma, T. F. Miller, A. Mitrushchenkov, K. A. Peterson, I. Polyak, G. Rauhut, M. Sibaev, *J. Chem. Phys.* **2020**, *152*, 144107.
- [85] T. H. Dunning, *J. Chem. Phys.* **1989**, *90*, 1007–1023.
- [86] R. A. Kendall, T. H. Dunning, R. J. Harrison, *J. Chem. Phys.* **1992**, *96*, 6796–6806.
- [87] W. Györfy, T. Shiozaki, G. Knizia, H.-J. Werner, *J. Chem. Phys.* **2013**, *138*, 104104.
- [88] B. Helmich-Paris, *J. Chem. Theory Comput.* **2019**, *15*, 4170–4179.
- [89] (a) C. A. Hunter, J. K. M. Sanders, *J. Am. Chem. Soc.* **1990**, *112*, 5525–5534; (b) C. R. Martinez, B. L. Iverson, *Chem. Sci.* **2012**, *3*, 2191–2201.
- [90] (a) SCALE3ABS, CrysAlisPro, Agilent Technologies Inc. Oxford and GB, **2015**. (b) Sheldrick, G. M. SADABS, Bruker AXS, Madison and USA, **2007**.
- [91] (a) R. C. Clark, J. S. Reid *Acta Cryst. A*, **1995**, *51*, 887–897. (b) CrysAlisPro, version 171.39.37b, Agilent Technologies Inc., Oxford and GB, **2017**.
- [92] G. M. Sheldrick *Acta Cryst. A*, **2015**, *71*, 3–8.
- [93] O. V. Dolomanov, L. J. Bourhis, R. J. Gildea, J. A. K. Howard, H. J. Puschmann, *Appl. Crystallogr.* **2009**, *42*, 339–341.
- [94] G. M. Sheldrick *Acta Cryst. A*, **2008**, *64*, 112–22.

After this first successful demonstration of the extreme reductive potential *via* e-PRC, we turn to an oxidative example. In the following chapter, another catalytic system capable of e-PRC is presented. However, the main focus is on its application as a conPET system. The consecutive accumulation of two photons and the use of molecular oxygen as a sacrificial electron donor make this an elegant approach with high oxidation power for the conversion of challenging organic molecules.

CHAPTER 4

4 Oxidative conPET Catalysis for Arene Functionalization



This chapter has been published. For reference see: B. Bieszczad, T. A. Karl, A. B. Rolka, P. Nuemberger, R. J. Kutta, B. Koenig, 10.26434/chemrxiv-2022-39x5l.

Tobias A. Karl performed all photoelectrochemical reactions. He performed parts of the optimization (Table S1, Entry 1-4, 8-10) and synthesized catalyst A. EPR, excitation, and emission spectra were recorded and evaluated by T. A. Karl. He also processed the CV and spectro-electrochemical results.

4.1 Abstract

We report the first successful use of consecutive two-photon accumulation of visible light energy to obtain ultra-high oxidation potentials enabled by a new class of rationally designed cyclic triarylamine photocatalysts. We demonstrate its practical and synthetic utility in a series of reactions of electron deficient arenes and fluoroarenes with *N*-nucleophiles. We identified that the photocatalytic reaction is initiated by the lowest excited state of the photocatalyst's radical cation which abstracts an electron from the substrate only at non-diffusive/direct contact encounters, *i.e.*, the omnipresence of substrate as co-solvent, since the excited radical cation lives only for ps. Neither pre-assembly nor a specific 'anti-Kasha' reactivity of a higher excited electronic state is observed. This method may serve as a promising basis for yet unexplored chemical reactions of substrates with very high oxidation potential and presents an attractive alternative to existing methods.

4.2 Introduction

Oxidations are fundamental to synthetic chemistry^[1] and natural processes,^[2] providing powerful tools for the functionalization of molecules and functional group interconversion.^[3] While routinely used in academic research, their application in pharmaceutical industry is surprisingly uncommon.^[4] This is due to the necessity of stoichiometric amounts of oxidizing agents, which are incompatible with most organic solvents and present significant explosion hazards.^[5] Additionally, they often produce undesirable waste products. Safe and environmentally benign oxidative systems are therefore highly sought-after.

Photoredox chemistry, a catalytic approach to harvesting visible light energy, provides a way out of this conundrum.^[6-10] In pioneering work in 2011 it was shown that benzene oxidation can be carried out photocatalytically to produce phenols with oxygen as a terminal oxidant.^[11,12] Subsequently a new reactivity paradigm for selective oxidative functionalization of arenes under mild conditions was established.^[13-22] However, such systems are confined to the energy of a single photon of visible light, *e.g.* 440 nm (2.82 eV, 65 kcal/mol), which limits their oxidative power.^[23] For example, the energy of excited state acridinium photocatalysts is lower than +2.5 V vs. SCE (saturated calomel electrode), which is insufficient to remove an electron from an electron-deficient arene.^[13] 2,3-dichloro-5,6-dicyano-1,4-benzoquinone (DDQ) as the only photocatalyst capable of reaching > +3 V vs. SCE is unstable, toxic, and reacting with water as well as with nucleophiles to release poisonous HCN gas.^[24] Furthermore, it must be used in stoichiometric or sub-stoichiometric amounts, which limits its applicability.^[22] Thus, alternative systems are highly desirable.

To overcome the limitation of a single photon excitation, one may learn from nature which for instance uses four photons of visible light cumulatively for the challenging task of water oxidation in the process of photosynthesis.^[25] A similar concept, consecutive photoinduced electron transfer (conPET) has recently been introduced to synthetic chemistry.^[26] Here, two approaches have been described to cumulate the energy of two photons of visible light to carry out thermodynamically challenging transformations (Figure 1A, B).^[27] On the one hand, electron transfer to an excited photocatalyst followed by exciting the just singly reduced photocatalyst generates a strong reductant excited species (Figure 1A) and on the other hand, photosensitized triplet formation of the photocatalyst that forms *via* triplet-triplet annihilation of two triplets one excited singlet and one ground state photocatalyst, where the former also represents a high reductive excited species (Figure 1B).

Reductive conPETs, where either a solvated electron is generated upon excitation of a radical anion in a chemical variant of the photoelectric effect^[28-31] or the excited single reduced photocatalyst transfers one electron directly to the substrate,^[32] allow difficult reactions such as reduction of aryl and alkyl halides or aromatic systems under mild conditions. By utilizing the

excited state chemistry of *N*-phenylphenothiazine the photocatalytic redox window of the conPET approach could be expanded.^[33,34] Recently, deazaflavins have been synthesized guided by mechanistic understanding that utilizes the internal heavy atom effect for more efficient conPET that achieves reductive powers comparable to lithium.^[35] However, the full potential of the conPET systems where two photons of visible light are cumulatively used to access oxidative powers of $\gg +3$ V vs. SCE for synthesis has yet to be realized. Here, we report the first successful attempt in this direction.

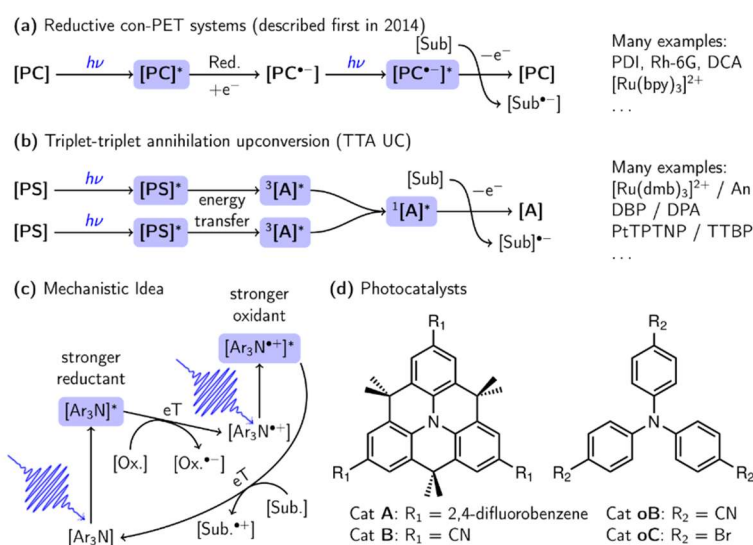


Figure 1. Examples of established and the here proposed photocatalytic system. a: Consecutive photo electron transfer (conPET), i.e., excitation of radical anions after initial photoreduction. b: triplet-triplet annihilation (TTA) upconversion, i.e., sensitized triplet formation that undergoes TTA forming one excited and one ground state photocatalyst. c: Mechanistic idea for oxidative conPET followed in this work. d: Novel photocatalysts **A** and **B** were used in this work. Legend: PDI = perylene diimide, Rh6G = rhodamine 6G, DCA = 9,10-dicyanoanthracene, bpy = 2,2'-bipyridine, dmb = 4,4'-dimethyl-2,2'-bipyridine, An = anthracene, DBP = diiodoBOPHY-like derivative, DPA = 9,10-diphenylanthracene, TPTNP = tetraphenyltetraphtho [2,3] porphyrin, TTBP = Tetraterbutylperylene, PC = Photocatalyst, Sub = Substrate, PS = Photosensitizer, A = Annihilator, Red. = reducing agent, Ox. = oxidizing agent, eT = electron transfer.

In our quest to find a suitable photocatalytic system for oxidative conPET, inspired by the recent work from the Wasielewski lab,^[36] we selected triarylmines (Ar_3N) as potential candidates.^[37] Prompted by their ability to form stable radical cations $Ar_3N^{\bullet+}$, which are used as stoichiometric oxidants,^[38] we envisaged that excitation of such radicals with visible light could dramatically enhance their oxidation power. Here, we investigated the possibility of the formation of stable $Ar_3N^{\bullet+}$ upon irradiation of Ar_3N in the presence of a terminal oxidant, such as molecular oxygen. Further, we explored if such stable $Ar_3N^{\bullet+}$ can subsequently be excited by a second photon to form a potential super-oxidant $Ar_3N^{\bullet+*}$ with a redox potential of $E_{ox} \gg +3.0$ V vs. SCE that will allow

for electron abstraction from a substrate regenerating the neutral form of the photocatalyst, closing the catalytic cycle, and initializing substrate transformation (Figure 1c).

As the expected lifetimes of excited radical species are generally in the picosecond range,^[39-40] an efficient diffusion-controlled reactivity at moderate substrate concentrations cannot be achieved and a bimolecular reaction may only occur, if the two reaction partners are already pre-assembled before photoexcitation. Since the relaxation of the $\text{Ar}_3\text{N}^{+\bullet}$ is facilitated mainly by rotation of the aromatic rings,^[41] we explored on the one hand if a rigid and cyclic architecture extends the excited state lifetime of the $\text{Ar}_3\text{N}^{+\bullet}$, and on the other hand if this triarylamine modification will also prevent its known photo-degradation.^[42] Additionally, we examined potential pre-organization of aryl substrates to the planar structure of $\text{Ar}_3\text{N}^{+\bullet}$ *via* cation- π interaction making electron transfer more feasible.

4.3 Results and Discussion

Inspired by the role of constrained Ar_3N species as hole transport materials in material science, we designed and prepared catalysts **A** and **B** (Figure 1D). Their key structural feature is the central and planar nitrogen atom, surrounded by three bridged aryl units, with para positions substituted to prevent their photo-degradation. Additionally, we synthesized the unbridged compounds **oB** and **oC** for investigations of the structural impact on the photophysics and the photocatalytic activity (Figure 1D). These compounds were prepared from readily available starting materials in 5 simple and scalable synthetic steps (see experimental part). To the best of our knowledge, **A** or **B** have not yet been used as photocatalysts.

The ground state absorption spectra ($S_n \leftarrow S_0$) as well as the emission spectra of **A** and **B** in ACN are shown in Figure 2A, B. Both molecules have their first electronic transition ($S_1 \leftarrow S_0$) below 400 nm and the excited state energies are 3.27 eV and 3.35 eV, respectively, as estimated from the crossing point of the absorption and emission spectra when both are normalized to their maxima. After excitation the first excited singlet states decay with 2.6 ns and 3.0 ns, respectively (Figure 2 and Figure S1). About 71% or 60% of the excitation energy is released *via* fluorescence and to *ca.* 25% or 30% the corresponding triplets are formed (see Figure 2 and experimental part including Figures S2 and S3). On a longer timescale in the absence of molecular oxygen, the triplet states of **A** and **B** decay back into the ground state with lifetimes in the order of tens of μs . However, in the presence of molecular oxygen, the triplet states of **A** and **B** evolve with lifetimes in the order of tens of ns into a further intermediate (Figure 3A, C and Figure S4). To note, the S_1 and the T_1 show both an excited state reaction with molecular oxygen, while only from the latter reaction an additional intermediate is observed. Considering an O_2 concentration in ACN of 2.4 mM;^[43] the corresponding bimolecular reaction rates for S_1 and T_1 quenching are in the order of $10^{10} \text{ M}^{-1}\text{s}^{-1}$, which is close to the expected full diffusion limit

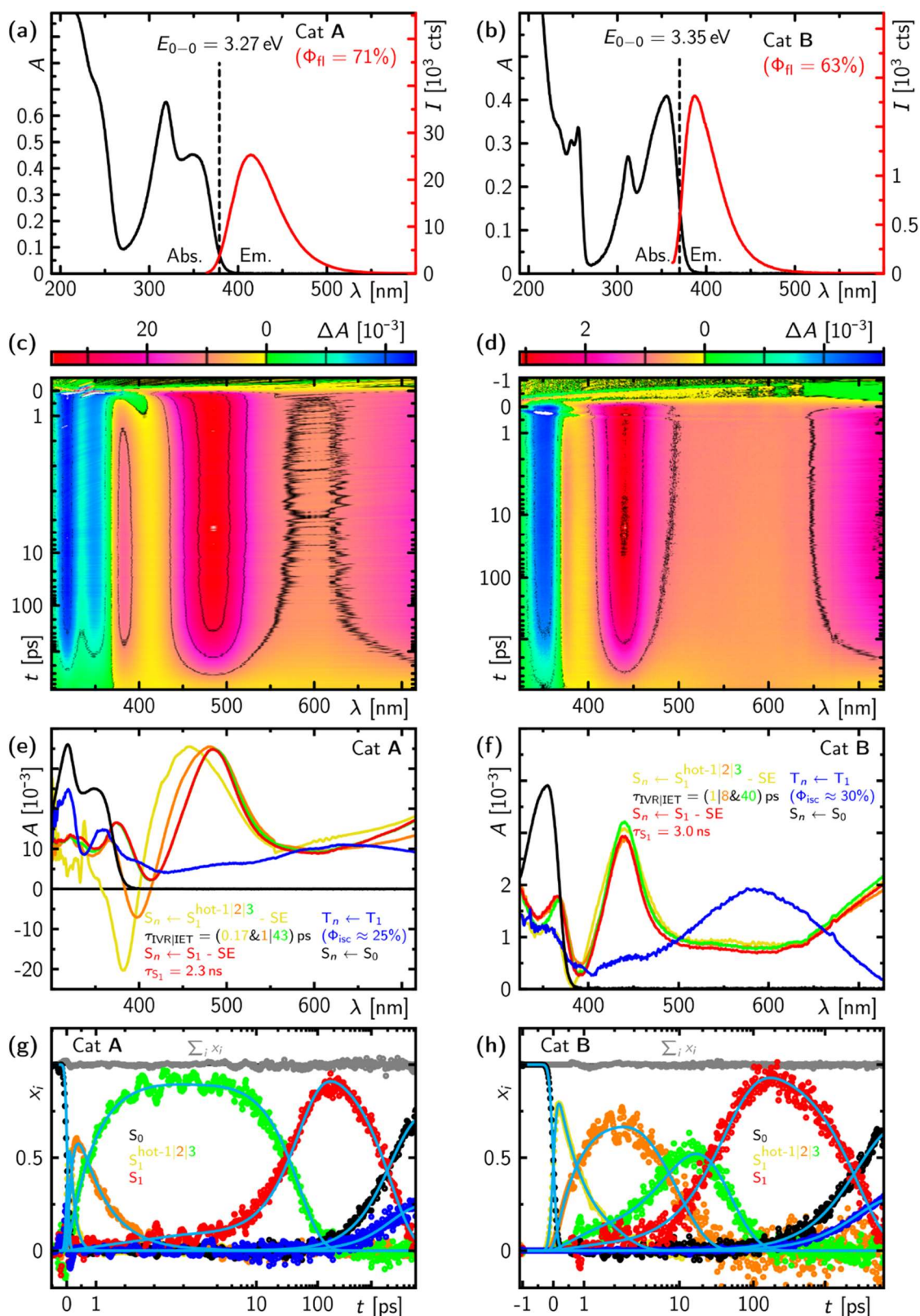


Figure 2. Steady-state and time-resolved optical spectroscopy of compounds **A** (a,c,e,g) and **B** (b,d,f,h) in ACN. a-b: Steady-state absorption and emission. c-d: Transient absorption after excitation either at 340 nm (c) or at 288 nm (d). e-h: Species-associated spectra and concentration-time profiles based on a photophysical model including only excited singlet, triplet, and ground state. To note, the relaxation dynamics due to IVR and IET of the vibrationally excited S_1^{hot} state to the relaxed S_1 are also shown. These are described and approximated by three subsequent exponential decays obtained from the data decomposition (for more information see experimental part).

The intermediate formed from the triplet in cases of **A** and **B** decays with lifetimes in the order of tens of μs in non-degassed and non-dried ACN showing dependence on the age of the used ACN, *i.e.*, the water content.

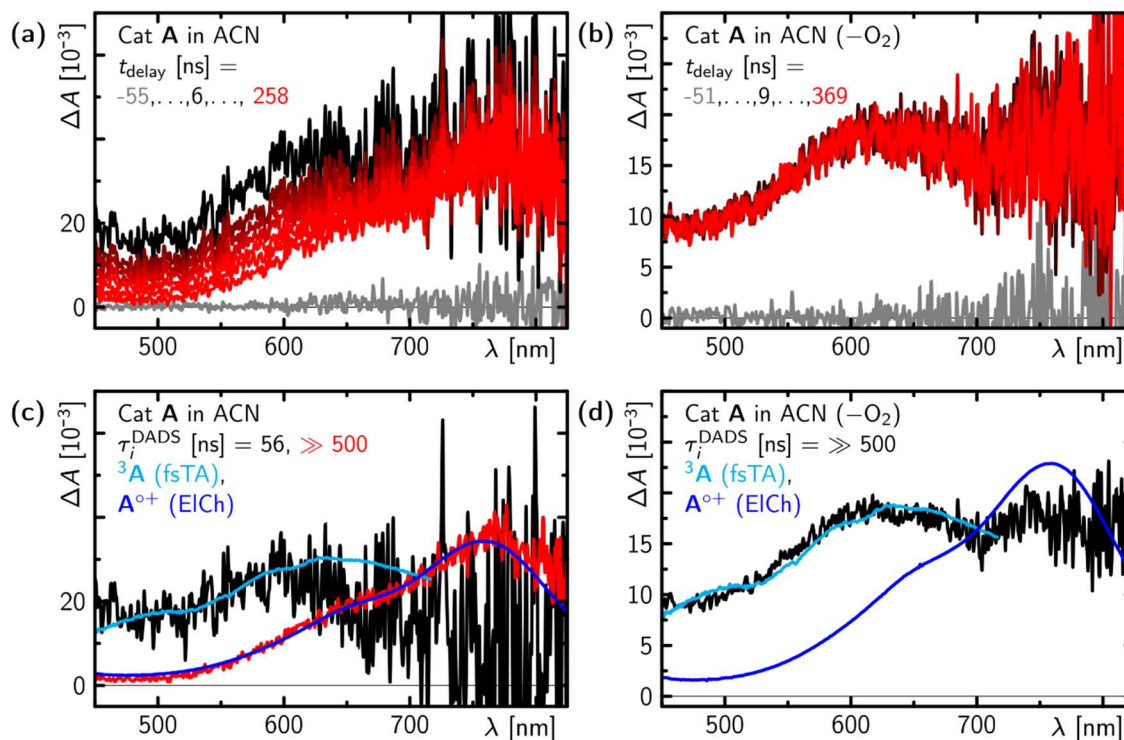


Figure 3. Time-resolved optical spectroscopy of compounds **A** in non-degassed (a) and degassed (b, degassed by four cycles of freeze pump and thaw) ACN after excitation at 355 nm in a 500 ns time window. c-d: Decay associated difference spectra (DADS) in comparison to the triplet ^3A spectrum from fs-TA (cyan) and the electrochemically generated radical cation $\text{A}^{\bullet+}$ spectrum as indicated (*vide infra*, for data on Cat **B** see Figure S4 in the experimental part).

At this point it was tempting to speculate that the formed intermediate corresponds to the $\text{Ar}_3\text{N}^{\bullet+}$ arising from electron transfer from Ar_3N to molecular oxygen. As both photocatalysts exhibit fully reversible redox states with anodic peaks at +0.66 V and +1.29 V vs. SCE respectively (Figure S5), the application of a potential of up to +1.7 V will lead to radical cation formation in both photocatalysts (Figure S6). Comparing the spectra of electrochemically generated $\text{Ar}_3\text{N}^{\bullet+}$ with the intermediate spectrum arising from the T_1 reaction with O_2 , a striking agreement proves transiently formed $\text{Ar}_3\text{N}^{\bullet+}$ when irradiating the neutral Ar_3N in the presence of O_2 (Figure 3C, D and Figure S4). To note, as residual water in the solvent environment leads to re-reduction of $\text{Ar}_3\text{N}^{\bullet+}$ to its neutral Ar_3N form, as demonstrated by adding a droplet of water to a sample of electrochemically formed $\text{Ar}_3\text{N}^{\bullet+}$ (Figure S6), the observed decay of the $\text{Ar}_3\text{N}^{\bullet+}$ on a μs timescale is ascribed to a reaction with water present in the non-dried ACN used in the time-resolved spectroscopic studies.

After exciting electrochemically formed Ar_3N^{++} (see Figure S7 in the experimental part for the electrochemical setup) either at 395 or 740 nm with *ca.* 100 fs resolution, first the excited Ar_3N^{++} in its lowest excited state is observed in both cases demonstrating that the higher excited doublet states relax within the temporal resolution (Figure 4). Accordingly, and expectedly, no reactivity from a higher excited electronic state (in terms of the latest IUPAC terminology: no ‘anti-Kasha’ behavior) is observed as was recently postulated to occur for non-cyclic triarylamine radical cations.^[44]

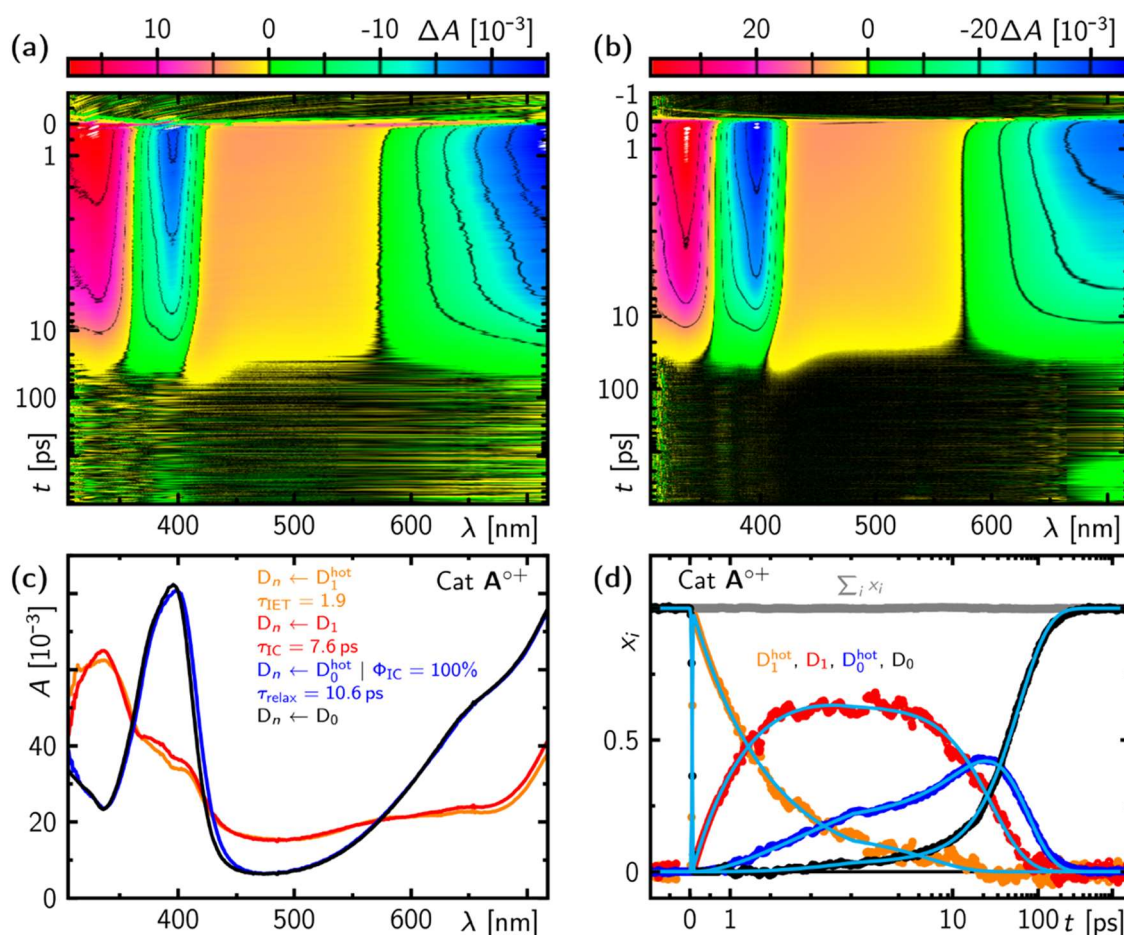


Figure 4. Transient absorption of the electrochemically formed radical cation of compounds *A* in ACN after excitation either at 395 nm (a) or 750 nm (b). c-d: Species-associated spectra and concentration-time profiles based on a photophysical model including an unrelaxed excited doublet (D_1^{hot}), a relaxed excited doublet (D_1), a thermally excited ground (D_0^{hot}), and a relaxed ground state (D_0).

In agreement with the expectation, the excited state lifetime of the Ar_3N^{++} is in the ps temporal range ($\tau_{\text{IC}} = 7.6$ ps; see experimental part including Figures S8 for the detailed global analysis). Interestingly, for both photocatalysts an additional intermediate arises from the excited state decay with a prominent absorption band peaking at *ca.* 410 nm, which decays back to the ground state with a lifetime of 10.6 ps. As the spectrum of this intermediate is very similar to the steady-state ground state spectrum of the radical cation, the second absorption band is redshifted. Due to the fact that the relaxation occurs on a ps timescale, one may speculate that a thermally excited

ground state of the $\text{Ar}_3\text{N}^{+\bullet}$ is observed (Figure 4). However, this is not further elucidated here, and attempts to identify the nature of this species are currently under investigation in our labs and will be presented elsewhere.

Knowing that the cyclic and rigid photocatalyst exhibit the photophysical and photochemical characteristics required for the proposed photocatalytic oxidative conPET mechanism, we selected C-N arene functionalization^[13] as a model reaction to test our hypothesis. As the excited state lifetime of the $\text{Ar}_3\text{N}^{+\bullet}$ is in the ps range, the substrate benzene was used as co-solvent (4.5 M) preventing the need for diffusive reaction encounters. To note, at such high substrate concentration there is no experimental indication of any pre-assembled complexes, which is in striking agreement with a detailed computational investigation on the ability of complex formation of this type of photocatalysts.^[45]

Already an initial trial showed that a catalytic amount of **A** catalyzed the reaction between benzene (4.5 M) and ethyl 1*H*-pyrazole-4-carboxylate (0.2 M) yielding 6% of the coupling product after 16 h hours of irradiation at 400 nm (LED, 160 mW/cm²) under ambient conditions (Table 1, entry 1). In contrast, using the non-cyclic amine, **oC** (see Table 1), resulted in no product formation (Table 1, entry 2). This low yield may indicate that *in situ* radical cation formation of the photocatalyst is rather inefficient for an overall substrate conversion. To test this hypothesis, SbCl_5 was added in catalytic amounts to the system, chemically oxidizing the photocatalyst to its radical cation prior to illumination. And indeed, almost full conversion could be achieved under otherwise identical conditions (Table 1, entry 3).

As a control, both in the absence of light and a photocatalyst no reactivity was observed (Table 1, entry 4, 5) demonstrating that the excited radical cation of the photocatalyst is a requirement for photocatalytic activity. Also using the non-cyclic version **oB** under otherwise identical conditions, resulted in significantly less yield of 19% (Table 1, entry 6) than with the corresponding cyclic photocatalyst indicating a prominent impact of the rigid, cyclic structure on the stability. As SbCl_5 is a very reactive species which itself absorbs light of 400 nm, giving even rise to some μs long-lived light-induced species (see Figure S9), we performed the model photocatalytic C-N coupling reaction without SbCl_5 and using electrochemically formed $\text{Ar}_3\text{N}^{+\bullet}$ instead, which yielded almost quantitative conversion of the starting material (Table 1, entry 7) independent of the presence or absence of molecular oxygen. This clearly identifies $\text{Ar}_3\text{N}^{+\bullet}$ as the photocatalytically active species and rules out any involvement of either SbCl_5 or O_2 in the coupling reaction.

In a recent study,^[44] the authors proposed the involvement of higher excited doublet states as a requisite for productive photocatalytic activity allowing for the formation of long-lived quartet states. A similar scenario may also apply here as in terms of energy considerations, the first excited quartet state becomes only available after excitation into the second prominent absorption

band at *ca.* 400 nm ($D_3 \leftarrow D_0$) (see Figure S10 and further information in the experimental part). Performing the model reaction exciting the system into its first electronic absorption band at 660 nm (LED, 200 mW), interestingly resulted in no product formation (Table 1, entry 8). However, it is to note, that the available excitation power at 660 nm is by a factor of *ca.* 10 lower compared to the power at 395 nm, and, thus, may explain this diminished activity.

Table 1. Screening for photocatalytic activity in C-N arene functionalization.

Entry	Deviation from standard conditions	Yield ^a (%)
1	No SbCl ₅	6
2	Cat oC ^d (2 mol%), No SbCl ₅	-
3	None	88 ^b
4	No catalyst	-
5	No light	-
6	Cat oB ^c (2 mol%)	19
7	Electrochemical generation of Ar ₃ N ⁺⁺⁺	97
8	Red LED (660 nm, 200 mW)	-

^aYield determined by GC with decane used as internal standard, ^bIsolated Yield, ^cCat **oB**: 4,4',4"-nitrilotribenzonitrile ^dCat **oC**: tris(4-bromophenyl) amine

The reactivity in general seems to follow the established pattern for radical cation accelerated arene C-H functionalization (Figure 5).^[13,14] The para selectivity, known for similar systems, indicates that the reactivity occurs *via* arene oxidation. Various the Ar₃N⁺⁺⁺ can be used in the reaction. When cat **A** was used, 9% of doubly substituted product was formed. Only small amounts of products were produced from extremely electron-poor arenes, like 2-chlorobenzonitriles (see experimental part).

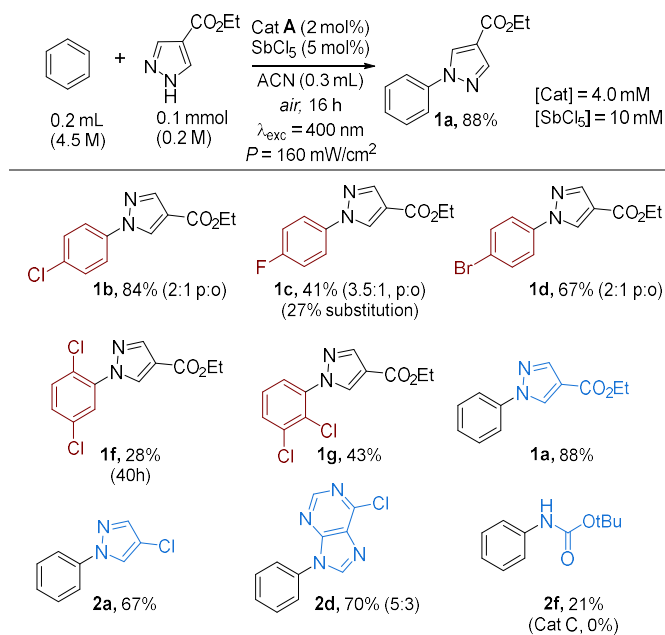


Figure 5. Examples of C-H functionalization of electron-deficient arenes under oxidative conPET conditions.

We also observed nucleophilic C-F substitution ($S_{\text{N}}\text{Ar}$) for fluorobenzene. We envisaged that this reactivity pattern may lead to a significant advantage over existing methods, which use substoichiometric and stoichiometric amounts of unstable and toxic DDQ.^[22] Several fluorobenzenes as well as different trapping reagents could be coupled with moderate to good yields and best performance for an electron-rich system. The photocatalyst **B** allowed activation of even strongly electron-deficient arenes, such as 1-chloro-2,4-difluorobenzene (Figure 6). These types of substrates are too electron-poor to be oxidized by known photocatalysts,^[46] but at the same time they do not undergo thermal $S_{\text{N}}\text{Ar}$ C-F substitution. Reactions were particularly clean, with no side reactions detected. We were also pleased to find that the catalyst can be recovered to 94% after a single cycle.

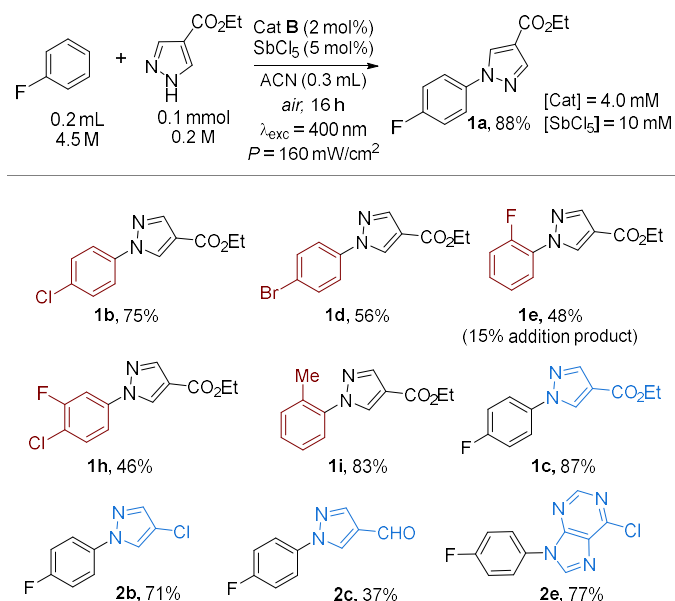


Figure 6. Examples of C-F functionalization of electron-deficient fluoroarenes under redox neutral conPET conditions.

As expected from the experimental findings discussed above, no reactivity between benzene and the excited species of neutral Ar₃N have been detected. However, considering that the overall efficiency of the coupling reaction is rather low, *i.e.*, 16 h of illumination at high fluence (395 nm, 2 W) was required for full conversion. As a result, the electron transfer from benzene to the excited state may represent the bottleneck of the reaction as SET from benzene to excited **A** or **B** may be simply too inefficient. Thus, as a proof of concept, we changed to 1,2-dimethoxy benzene as a substrate with a much lower redox potential. Repeating the C-N coupling model reaction at 660 nm (LED, 0.2 W) excitation and performing high-resolution mass spectrometry, indeed trace amounts of the coupling product could be detected (see Figure S11). Furthermore, when using 1,4-dimethoxybenzene as substrate even a significant amount of the corresponding product was identified (see Figure S12), giving evidence that the excitation into higher lying excited states is not required for productive conversion. Discrepancies in efficiencies are only due to dramatically different photo fluxes used in the experiments. Furthermore, this also demonstrates that involvement of electronic states with higher multiplicity can be ruled out since these are energetically not accessible

4.4 Conclusions

In summary, we have discovered a novel photocatalytic system using two photons of visible light to access high oxidative powers of $\gg +3$ V vs. SCE. The key component in the photocatalytic reaction is the lowest excited state of the radical cation, which shows a ps deactivation. Thus, requires the omnipresence of the substrate to avoid slow diffusive encounters for the rare event of bimolecular electron transfer between a substrate and such a short-lived excited state. Once the electron is abstracted from the substrate such as arenes, further downstream coupling events are initiated. The photostable catalysts of type **A** and **B** can be easily modified to tune their electronic and spectral properties for further improvements in the efficiency of the coupling reaction. The system provides a green alternative to existing methods, based on stoichiometric or sub-stoichiometric amounts of DDQ.

4.5 References

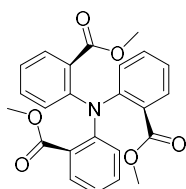
- [1] J. E. Backvall, *Modern Oxidation Methods*, Wiley-VCH, 2nd Edn, **2010**
- [2] E. T. Denisov and I. B. Afanas'ev, *Oxidations and Antioxidants in Organic Chemistry and Biology*, Taylor & Francis, Miami, **2005**
- [3] T. J. Donohoe, *Oxidation and Reduction in Organic Synthesis*, Oxford University Press, **2000**
- [4] R. W. Dugger, J. A. Ragan and D. H. Brown Rippin, *Org. Process Res. Dev.*, **2005**, *9*, 253–258
- [5] S. Caron, R. W. Dugger, S. G. Ruggeri, J. A. Ragan and D. H. Brown Ripin, *Chem. Rev.*, **2005**, *106*, 2943–2989
- [6] N. A. Romero and D. A. Nicewicz, *Chem. Rev.*, **2016**, *116*, 10075–10166
- [7] M. H. Shaw, J. Twilton and D. W. C. MacMillan, *J. Org. Chem.*, **2016**, *81*, 6898–6926
- [8] L. Marzo, S. K. Pagire, O. Reiser and B. König, *Angew. Chem., Int. Ed.*, **2018**, *57*, 10034–10072
- [9] J. K. Matsui, S. B. Lang, D. R. Heitz and G. A. Molander, *ACS Catal.*, **2017**, *7*, 2563–2575
- [10] L. Buzzetti, G. E. M. Crisenza and P. Melchiorre, *Angew. Chem., Int. Ed.*, **2019**, *58*, 3730–3747
- [11] K. Okhubo, T. Kobayashi, S. Fukuzumi, *Angew. Chem., Int. Ed.*, **2011**, *50*, 8652–8655
- [12] K. Okhubo, A. Fujimoto, S. Fukuzumi, *J. Am. Chem. Soc.*, **2013**, *135*, 5368–5371
- [13] N. A. Romero, K. A. Margrey, N. A. Tay and D. A. Nicewicz, *Science*, **2015**, *349*, 1326–1330
- [14] N. E. S. Tay and D. A. Nicewicz, *J. Am. Chem. Soc.*, **2017**, *139*, 16100–16104
- [15] W. Chen, Z. Huang, N. E. S. Tay, B. Giglio, M. Wang, H. Wang, W. Zhanhong, D. A. Nicewicz and L. Zibo, *Science*, **2019**, *364*, 1170–1174
- [16] Z. L. Huang, D. C. Zhang, X. Qi, X. T.; Z. Y. Yan, M. F. Wang, H. M. Yan and A. W. Lei, *Org. Lett.*, **2016**, *18*, 2351–2354
- [17] C. L. Song, H. Yi, B. W. Dou, Y. Y. Li, A. K. Singh and A. W. Lei, *Chem. Commun.*, **2017**, *53*, 3689–3692
- [18] S. Das, P. Natarajan, B. König, *Chem. Eur. J.*, **2017**, *23*, 18161–18165
- [19] H. Huang and T. H. Lambert, *Angew. Chem., Int. Ed.*, **2020**, *59*, 658–662
- [20] H. Huang, Z. M. Strater, M. Rauch, J. Shee, T. J. Sisto, C. Nuckolls and T. H. Lambert, *Angew. Chem., Int. Ed.*, **2019**, *58*, 13318–13322
- [21] Y.-W. Zheng, P. Ye, B. Chen, Q.-Y. Meng, K. Feng, W. Wang, L.-Z. Wu, C.-H. Tung, *Org. Lett.*, **2017**, *19*, 2206–2209
- [22] T. Sheridan, H. G. Yayla, Y. Lian, J. Genovino, N. Monck and J. W. Burton, *Eur. J. Org. Chem.*, **2020**, 2766–2770
- [23] F. Glasser, C. Kerzig and O. S. Wenger, *Angew. Chem., Int. Ed.*, **2020**, *59*, 10266–10284
- [24] D. R. Buckle, S. J. Collier and M. D. McLaws, 2,3-Dichloro-5,6-dicyano-1,4-benzo-quinone. In: *Encyclopedia of Reagents for Organic Synthesis*, (Ed.), Wiley **2006**
- [25] J. J. Conception, R. L. House, J. M. Papanikolas and T. J. Meyer, *Proc. Natl. Acad. Sci. USA*, **2012**, *109*, 15560–15564
- [26] I. Ghosh, T. Ghosh, J. I. Bardagi and B. König, *Science*, **2014**, *346*, 725–728
- [27] For a recent example of TTA-UC see: C. Kerzig and O. S. Wenger, *Chem. Sci*, **2018**, *9*, 6670–6678
- [28] C. Kerzig, X. Guo and O. S. Wenger, *J. Am. Chem. Soc.*, **2019**, *141*, 2122–2127
- [29] I. Ghosh and B. König, *Angew. Chem., Int. Ed.* **2016**, *55*, 7676–7679
- [30] R. Naumann, C. Kerzig and M. Goez, *Chem. Sci.*, **2017**, *8*, 7510–7520
- [31] M. Giedyk, R. Narobe, S. Weiß, D. Touraud, W. Kunz and B. König, *Nat. Catal.* **2020**, *3*, 40–47
- [32] A. Graml, T. Nevesely, R. J. Kutta, R. Cibulka and B. König, *Nat. Commun.*, **2020**, *11*, 3174
- [33] D. Rombach and H. -A. Wagenknecht, *ChemCatChem*, **2018**, *10*, 2955–2962
- [34] D. Rombach and H.-A. Wagenknecht, *Angew. Chem., Int. Ed.*, **2020**, *59*, 300–303
- [35] T. Pavlovska, D. K. Lesný, E. Svobodová, I. Hoskovcová, N. Archipowa, R. J. Kutta, R. Cibulka, *Chem. Eur. J.* **2022**, e202200768
- [36] J. A. Christensen, B. T. Phelan, S. Chauduri, A. Acharya, V. S. Batista and M. R. Wasielewski, *J. Am. Chem. Soc.*, **2018**, *140*, 5290–5299
- [37] K. Targos, O. P. Williams, and Z. K. Wickens, *J. Am. Chem. Soc.*, **2021**, *143*, 4125–4132
- [38] N. G. Connelly and W. E. Geiger, *Chem. Rev.*, **1996**, *96*, 877–910
- [39] J. C. Gumy and E. Vauthey, *J. Phys. Chem. A.*, **1997**, *101*, 8575–8580
- [40] J. Grilj, E. N. Laricheva, M. Olivucci and E. Vauthey, *Angew. Chem., Int. Ed.*, **2011**, *50*, 4496–4498
- [41] H. J. Shine and D.-C. Zhao, *J. Org. Chem.*, **1990**, *55*, 4086–4089
- [42] M. R. Talipov, M. M. Hossain, A. Boddeda, K. Thakur and R. Rahore, *Org. Biomol. Chem.*, **2016**, *14*, 2961–2968
- [43] C. Franco and J.-I. Olmsted., *Talanta.*, **1990**, *379*, 905–909
- [44] S. Wu, J. Zurauskas, M. Domanski, P. Hitzfeld, V. Butera, D. J. Scott, J. Rehbein, A. Kumar, E. Thyraug, J. Hauer, J. P. Barham, *Org. Chem. Front.* **2021**, *8*, 1132–1142
- [45] Lehner et al., Master thesis University of Regensburg, 2022.
- [46] V. A. Pistritto, M. E. Schutzbach-Horton and D. A. Nicewicz, *J. Am. Chem. Soc.*, **2020**, *142*, 17187–17194

4.6 Experimental Part

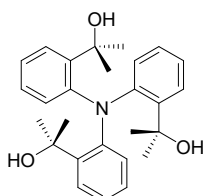
4.6.1 General Remarks

All reactions were carried with dry solvents unless otherwise stated. Reagents were purchased at the highest commercial quality and used without further purification, unless stated otherwise. Thin-layer chromatography was performed using silica gel plates 60 F254: Visualization was accomplished with short wavelength ultraviolet (UV) light (254 nm) and near UV light (366 nm) sources. Standard flash chromatography was performed on a Biotage® Isolera™ Spektra system automated with high-performance flash purification system using silica gel 60 M (particle size 40–63 μm , 230–440 mesh, Merck) or using forced flow chromatography (FC) on silica gel (35–70 mesh). Organic solutions were concentrated under reduced pressure on a Büchi rotary evaporator (in vacuo at 40 °C, *ca.* 5 mbar). The photochemical reactions were performed with commercial LEDs emitting with either $\lambda_{\text{max}} = 395 (\pm 15)$ nm (OSRAM, LZ4-40UB00-00U5; Optical Power @700mA: 3.8W) or $\lambda_{\text{max}} = 660 (\pm 15)$ nm (OSRAM, Oslon SSL 80 LHCP7P-2T3T (3T); Optical Power @700mA: 1 W).

4.6.2 Synthesis of Catalysts

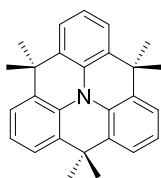


Trimethyl 2,2',2''-nitriлотрибензоате (II): Methyl 2-aminobenzoate (12 mL), methyl 2-iodobenzoate (40 mL), K_2CO_3 (29.5 g), Cu (0.68 g), CuI (1.73 g) was dissolved in diphenyl ether (110 mL) and heated under nitrogen at 190 °C for 48 h. The mixture was filtered through a plug of celite, washed with dichloromethane (DCM, 500 mL). The solvent was removed under reduced pressure. The residue was purified on silica gel using 4:1 petroleum ether / ethyl acetate as eluent to yield a yellow solid (23.7 g, 62%). $^1\text{H NMR}$ (300 MHz, CDCl_3), δ (ppm): 7.60 (m, 3H), 7.36 (m, 3H), 7.09 (m, 6H), 3.37 (s, 9H). Data are in accordance with literature.^[1]

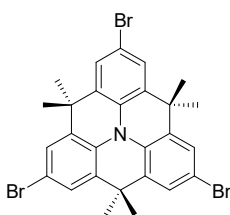


2,2',2''-(Nitriлотри(бенzene-2,1-диyl))три(пропан-2-ол) (I2): Solution of methyl iodide (11 mL) in dry Et_2O (100 mL) was added dropwise to magnesium turnings (4.1 g) activated with a small amount of iodine in dry Et_2O (20 mL) in a 3-neck round bottom flask, maintaining gentle reflux. After addition, the mixture was refluxed for 1 h. Solution of **II** (4.0 g) in dry toluene (120 mL) was added slowly to the Grignard reagent and the mixture was heated to reflux for 15 h. After cooling, the mixture was added to a saturated ammonium chloride solution (300 mL). The product was extracted with Et_2O (250 mL x 3), dried over anhydrous Na_2SO_4 . The residue was purified on silica gel using 5:1 petroleum ether / ethyl acetate as eluent to give a yellow solid (1.4 g, 37%).

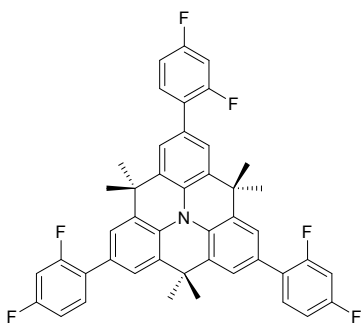
^1H NMR (300 MHz, CDCl_3), δ (ppm): 7.32 (m, 3H), 7.07 (m, 6H), 6.66 (m, 3H), 5.40 (broad, 3H), 1.67 (s, 9H), 0.85 (s, 9H). Data are in accordance with literature.^[1]



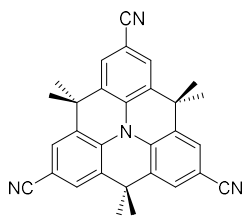
4,4,8,8,12,12-Hexamethyl-8,12-dihydro-4H-benzo[9,1]quinolizino[3,4,5,6,7-defg]acridine (I3): Compound **I2** (2.0 g) was suspended in H_3PO_4 (85%, 20 mL) and stirred for 2 h. The mixture was neutralized with *aq.* NaOH (2 M) and the product was extracted with DCM (100 mL x 2). The residue was purified on silica gel using petroleum ether as eluent to yield **I3** as a white solid (1.14 g, 66%). ^1H NMR (400 MHz, CDCl_3), δ (ppm): 7.38 (m, 6H), 7.12 (m, 3H), 1.63 (s, 18H). Data are in accordance with literature.^[1]



2,6,10-Tribromo-4,4,8,8,12,12-hexamethyl-8,12-dihydro-4H-benzo[9,1]quinolizino[3,4,5,6,7-defg]acridine (I4): Compound **I3** (1.0 g) was dissolved in CHCl_3 (20 mL) and *N*-bromo-succinimide (NBS) was added slowly (2.0 g). The mixture was stirred at room temperature overnight. Solvent was removed *in vacuo* and the residue was loaded directly on silica gel and purified using petroleum ether as eluent to yield **I4** as a white solid (1.54 g, 95%). ^1H NMR (400 MHz, CDCl_3), δ (ppm): 7.44 (m, 6H), 1.58 (s, 18H). Data are in accordance with literature.^[1]



2,6,10-Tris(2,4-difluorophenyl)-4,4,8,8,12,12-hexamethyl-8,12-dihydro-4H-benzo[9,1]quinolizino[3,4,5,6,7-defg]acridine (Cat A): Catalysts **A** was prepared according to a modified literature procedure.^[2] To a 20 mL microwave (MW) vial equipped with a stirrer bar, compound **I4** (250 mg, 0.42 mmol) was added, followed by $\text{Pd}(\text{PPh}_3)_4$ (42 mg, 0.04 mmol), difluorophenyl boronic acid (265 mg, 1.68 mmol, 4.0 *equiv.*), *aq.* Na_2CO_3 (4 M, 1 mL), toluene (2.5 mL) and ethanol (1.0 mL). The mixture was sparged with N_2 for 10 min, sealed, and heated to 160 °C for 7 min using microwave radiation. After completion, the mixture was quenched with water and the product was extracted with DCM (50 mL x 3). The solvent was removed *in vacuo* and the residue was purified on silica gel using petroleum ether as eluent to give **Cat A** as a slightly yellow solid (103 mg, 35%). ^1H NMR (400 MHz, CDCl_3), δ (ppm): 7.59 (s, 6H), 7.16 (m, 6H), 6.79 (m, 3H), 1.76 (s, 6H). ^{13}C NMR (75 MHz, CDCl_3), δ (ppm): 131.1, 130.9, 129.5, 125.1, 124.4, 118.2, 111.7, 111.4, 104.5, 104.1, 35.8, 33.6. ^{19}F NMR (121 MHz, CDCl_3), δ (ppm): 112.64 (s, 3F), 113.84 (s, 3F). HRMS: calculated for $\text{C}_{45}\text{H}_{33}\text{F}_6\text{N}^+$ ($\text{M}+\text{H}^+$): 701.2517, found 701.2531.



4,4,8,8,12,12-hexamethyl-8,12-dihydro-4H-benzo [9,1]quinolizino [3,4,5,6,7-defg] acridine-2,6,10-tricarbonitrile (cat B). To a 20 mL microwave vial equipped with a stirrer bar, compound **I4** (250 mg, 0.42 mmol) was added, followed by copper cyanide (500 mg, 5.58 mmol) and dry *N*-methyl-2-pyrrolidone (NMP, 6 mL). The mixture was sparged with N₂ for 10 min, sealed, and heated to 250 °C for 60 min using microwave radiation. After completion, the mixture was quenched with water and the product was extracted with ethyl acetate (100 mL x 3). The solvent was removed *in vacuo* and the residue was purified on silica gel using 1:5 petroleum ether / ethyl acetate as eluent to give **B** as a slightly yellow solid (104 mg, 57%). ¹H NMR (400 MHz, CDCl₃), δ (ppm): 7.68 (s, 6H), 1.64 (s, 18H). ¹³C NMR (75 MHz, CDCl₃), δ (ppm): 133.9, 131.0, 127.9, 118.9, 108.3, 35.7, 32.9. HRMS: calculated for C₃₀H₂₄N₄⁺ (M⁺): 440.2001, found 440.1975.

Synthesis of catalyst **oB**

The catalyst **oB** was prepared according to a method described in literature.^[3]

4.6.3 Screening of Reaction Conditions

4.6.3.1 General Procedure for Photochemical C-H Oxidation of Arenes

In 7 mL crimp cap vial equipped with a stirring bar, a catalyst **A** (1.2 mg, 2 μ mol, 2 mol%) and a nucleophile (0.1 mmol, 1.0 *equiv.*) were added. The vial was capped, followed by the addition of an arene (0.2 mL) and dry ACN (0.2 mL). SbCl₅ (0.1 mL of 50 mM in dry ACN, 5 mol%) was added. The reaction mixture was pressurized by adding 20 mL of air using a syringe and the vial was irradiated through the plane bottom side with HP LED (395 nm), with irradiance of 160 mW/cm² for 16 h. The residue was purified by flash chromatography (\varnothing = 1.5 cm, height SiO₂ = 13 cm) upon direct loading on silica column to afford products in stated yields.

Table S 1. Screening of reaction conditions

Entry	Deviation from standard conditions	Yield ^a
1	None	88%
2	No catalyst	-
3	No light	-
4	No SbCl ₅	6%
5	Cat oB ^b (2 mol%)	12%
6	Cat oC ^c (2 mol%)	39%
7	Cat B (2 mol%)	76%
8	Lower intensity - 40 mW/cm ²	33%
9	0.1 mL benzene	51%
10	5 eq. benzene	50%
11	0.2 mmol scale	64%
12	1 mol% Cat A	43%

^aMeasured by GC-FID, using decane as an internal standard, ^bCat **oB** - 4,4',4"-nitrilotribenzonitrile, ^cCat **oC** - tris(4-bromophenyl)amine

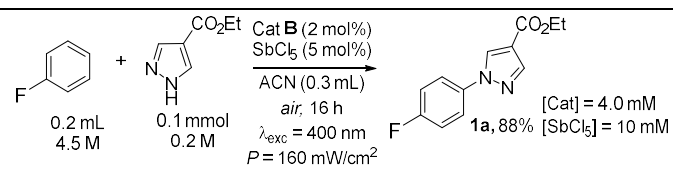
4.6.3.2 General Procedure for Photochemical C-F Substitution of Arenes

In 5 mL crimp cap vial equipped with a stirring bar, a catalyst **B** (0.8 mg, 2 μ mol, 2 mol%) and a nucleophile (0.1 mmol, 1.0 *equiv.*) were added. The vial was capped, followed by the addition of a fluoroarene (0.1 mL) and dry ACN (0.2 mL). SbCl₅ (0.1 mL of 50 mM in dry ACN, 5 mol%) was added. The vial was irradiated through the plane bottom side with a high-power LED emitting at 395 nm with an irradiance of 160 mW/cm² for 16 h. The residue was purified by flash chromatography (\varnothing = 1.5 cm, height of SiO₂ = 13 cm) upon direct loading on silica column to afford products in stated yields.

Table S 2. Screening of reaction conditions

Entry	Deviation from standard conditions	Yield ^a
1	None	87%
2	No catalyst	-
3	No light	-
4	No SbCl ₅	80%
5	Cat oBb (2 mol%)	19%
6	Cat oCc (2 mol%)	32%
7	Cat B (2 mol%)	41%
8	Lower intensity - 40 mW/cm ²	traces
9	5 eq. fluorobenzene	58%
10	0.2 mmol scale	76%
11	1 mol% Cat A	53%

^aMeasured by GC-FID, using decane as internal standard, ^bCat oB - 4,4'-nitrotribenzonitrile, ^cCat oC - tris(4-bromophenyl)amine



4.6.4 Electrochemical and Photophysical Characterization

4.6.4.1 Stationary Absorption with Stepwise Illumination, Emission and Time-Resolved Emission Spectroscopy

ACN (Carl Roth, spectroscopic grade) was used as solvent in all performed steady-state photophysical measurements. The steady-state absorption spectra in the UV/Vis were recorded with referenced single-beam photo-spectrometer (Cary 60, Agilent). For the photostability determination, the photo-spectrometer was equipped with a self-build sample compartment allowing for the usage of self-constructed sample cell holders and light-emitting diodes (LED) for sample excitation. The photo-stability of **A**, **B**, and **oB** in ACN was followed by recording absorption spectra after stepwise temporally and geometrically defined illumination into the $S_1 \leftarrow S_0$ transition (LED; M340L4, Thorlabs) of the sample in a 10 x 2 mm quartz cell. The rectangular excitation pulses were collimated using an anti-reflection coated aspheric lens (COP-A, Thorlabs) and delivered along the 2 mm path length of the cuvette orthogonal to the detection beam. The sample volume was 120 μL ensuring homogeneous illumination of the entire sample volume and, thus, avoiding possible effects of diffusion during the recording of the spectra.

The emission spectra were recorded at room temperature with a steady-state fluorescence spectrometer (Horiba Jobin Yvon Fluorolog-3). The emission decays were measured using a self-constructed time-correlated single photon counting (TCSPC) setup^[4] with single wavelength detection. The sample set to an optical density of 0.1 over 10 mm pathlength was excited along a 10 mm pathlength at $\lambda_{\text{exc}} = 280$ nm and the emission was recorded orthogonally to this along a 2 mm pathlength at the wavelength of maximum emission as given in the corresponding Figures. Removal of molecular oxygen from the sample was achieved *via* four cycles of freeze pump and thaw at vacuum pressure in the order of 10^{-5} mbar. The fluorescence quantum yield was determined *via* total integration of the excitation profile and the emission spectrum (Hamamatsu C9920-02 system equipped with a Spectralon® integrating sphere).

4.6.4.2 Time-Resolved UV/Vis Absorption Spectroscopy

Sub-ps Pump/Supercontinuum-Probe Spectroscopy

The transient absorption (TA) in the UV/Vis on fs to ns time range was recorded with an in-house build setup as described in.^[5] In short, the most important characteristics of the setup: The neutral Ar₃N samples were excited into the S₁←S₀ absorption band, *i.e.*, $\lambda_{\text{exc}} = 340$ nm, and the electrochemically generated radical cation species were excited into either the D₁←D₀ absorption band, *i.e.*, $\lambda_{\text{exc}} = 750$ nm, or the D₃←D₀ absorption band, *i.e.*, $\lambda_{\text{exc}} = 395$ nm. The radical cation species were generated in the photoelectrochemical cell (Figure S6) and pumped in circles *via* peristaltic pump (ecoline, Ismatec). The pulse energy was set to *ca.* 300 nJ at the sample position focused to *ca.* 80 μm in all cases. As a probe, a white-light supercontinuum (WLSC) was used and generated by focusing 800 nm pulses of *ca.* 1 mJ into a 5 mm thick CaF₂ disc. To maintain a linear polarization of the WLSC across the spectrum and over time the disc is rotated in an eccentric motion keeping the orientation of the crystal axes relative to the polarization of the fundamental constant. At the sample position the spot size of the probe pulse is *ca.* 40 μm . A flow sample cell (Starna) of 500 μm was used in all experiments. The spectral resolution over the entire spectral range was ± 50 cm⁻¹, *i.e.*, ± 0.5 nm at 300 nm and ± 2.5 nm at 700 nm. Typically, the time axis is chosen to be linear from -1 ps up to 2.0 ps in 20 fs steps and logarithmic afterwards, until the end of the delay stage of 6.5 ns with typically 400 time points. At each delay position of a scan an average of over 200 transient absorption spectra was recorded, each calculated for a baseline-corrected and referenced single shot. Averaging of at least five independent scans, if not stated otherwise, results in the final spectra. For recording the pure population dynamics of all excited states, the polarization between pump and probe pulses was set to magic angle (54.73°) *via* a $\lambda/2$ plate in the pump beam path. The averaged pre- t_0 laser scatter signal was subtracted from the data and the *ca.* 2 ps chirp of the WLSC is corrected before analysis using the coherent artifact as an indicator for time zero at each wavelength. No smoothing or filtering procedures were applied to the data.

Transient Absorption Spectroscopy in the ns to ms Time Range

The in-house build transient absorption spectrometer using a streak camera-based detection system was used,^{4,6-7} in which a laser pulse excites the sample and a Xe flash lamp pulses probes the excited sample. Only the neutral Ar₃N catalysts were investigated on this ns to ms timescale using the 355 nm (10 mJ, *ca.* 10 ns) pulses for excitation generated third harmonic of a Nd:YAG laser (10 Hz, Surelite II, Continuum). A pulsed 150 W Xe-flash lamp (Applied Photophysics) was used as probe pulse. The sample was pumped with a peristaltic pump (ecoline, Ismatec) in circles from a 5 mL reservoir through the 2 mm (excitation path) x 10 mm (probe path) flow cell (Starna) ensuring a total replacement of the sample prior to each individual measurement. No significant degradation of the photocatalyst was observed under the used conditions. Typically, 100 to 400

excitation cycles were recorded, and the corresponding data sets were averaged. To obtain data under molecular oxygen-free conditions for each compound, the corresponding sample was degassed prior to the measurement by either cycles of freeze pump and thaw at vacuum pressure in the order of 10^{-5} mbar or by bubbling N_2 through the sample solution.

Transient Absorption Data Analysis and Modelling

All transient absorption data recorded in this work include either a one-component system or a two-component system under pseudo-first-order conditions which justifies an analysis by a global fit to the data using an exponential ansatz. The global fits were performed using an in-house written program, of which details are provided in.^[4,6-7] In the program the time-resolved absorption data matrix $\Delta\mathbf{A}$ is decomposed into matrix \mathbf{F} containing the analytical functions accounting for the temporal changes in the data, *i.e.* exponential decays (convoluted with the instrument response, typically a Gaussian function) and a Gaussian together with its first to third derivative with identical temporal widths allowing to account for the coherent artifact (equation (1): Here, $\otimes g_{\text{app}}(t - t_0)$ means convolution with the apparatus function approximated by a Gaussian, $\delta(t)$ is the Dirac delta function, and N is the number of exponentials describing the dynamics of the TA change over time.),

$$f_k(t) = \sum_{i=0}^3 \frac{d^i}{dt^i} g_{\text{art}}(t - t_0) + \left(\delta(t) + \sum_{j=1}^N \exp(-\kappa_k t) \right) \otimes g_{\text{app}}(t - t_0) \quad (1)$$

and matrix \mathbf{B} containing the to be determined spectra *via* the linear least squares problem in equation (2) is solved.

$$\chi^2 = \|\Delta\mathbf{A} - \mathbf{FB}\|^2 = \text{Min} \quad (2)$$

The parameters of the temporal function in \mathbf{F} are optimized by a nonlinear least squares algorithm further optimizing χ^2 and resulting in so-called decay-associated difference spectra (DADS in matrix \mathbf{B}) and their associated optimized rate constants. As these DADS are the unique result of the global fit, no model is applied for the kinetics involved in the transient processes. SVD-based rank analysis allows determining the number of exponentials in the global fit, which is described elsewhere.^[8] Any model that may relate to the actual species kinetics to the elementary function is applied afterwards yielding species-associated spectra (SAS). Decision on the appropriateness of a model is obtained by the shape of the SAS in terms of identity with well-known spectra or following physical laws. As this step does not change the χ^2 value obtained in the global fit, this procedure has the advantage of drawing any interpretation with the same quality of fit.

Alternatively, known species spectra, taken either from literature or recorded in this work, may be taken to decompose the recorded time-resolved data matrix using the transpose of the data matrix in equation (2) and using the basis spectra instead of analytical functions. The resulting concentration-time profiles inform about the appropriateness of the basis spectra and the physical reasonability, *e.g.*, total sum of species being constant to 1.

General photophysical model

Both photocatalysts investigated show a mono-exponential decay of their excited singlet state emission in the absence and the presence of molecular oxygen showing that the bimolecular reaction between the first excited singlet and molecular oxygen is of pseudo-first order (see Figure S1). Accordingly, the decay rate of the clean excited singlet state decay in the absence of O₂ may be described *via* $k_{S_1} = k_{ic} + k_{rad} + k_{isc}$. The radiative rate k_{rad} can be determined *via* $k_{rad} = \Phi_{rad} k_{S_1}$ after measuring the corresponding fluorescence quantum yield of the S₁ emission of each photocatalyst.

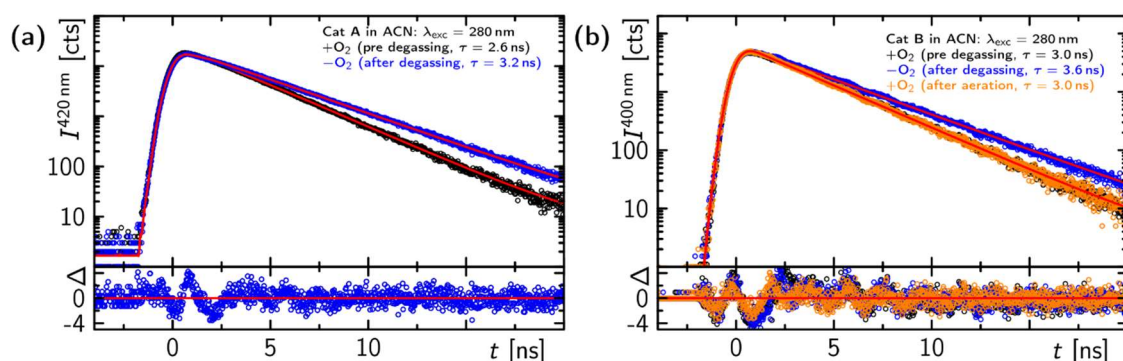


Figure S1. Excited singlet state decay recorded via the time-resolved emission of **A** (a) and **B** (b) in (non) degassed ACN. The emission was recorded either at 420 nm or at 400 nm after excitation at 280 nm with (black, orange = when the degassed sample was re-aerated) and without O₂ (blue).

The triplet formation of **A** and **B** was recorded *via* time-resolved absorption spectroscopy on fs to ns temporal window (Figure 1 in the main text) and each yield was estimated from a standard photophysical model, in which the rate constants κ_i , which are absolutely obtained from a bi-exponential global fit on the data (see Figure S2), represent:

$$\kappa_1 = k_{ic} + k_{rad} + k_{isc} \quad (3)$$

$$\kappa_2 = k_{bisc} \quad (4)$$

To note, three more exponentials were actually needed to describe the data best. These additional components are of small amplitude, resemble generally the first derivative of the main transient contributions, and have lifetimes in the range of *ca.* 1 ps to *ca.* 40 ps. Thus, these spectral

dynamics describe small spectral shifts arising from intramolecular vibrational energy redistribution (IVR) and intermolecular vibronic energy transfer (IET) to the environment. The decay of the thermally and electronically excited species into the equilibrated excited singlet state occurs in three phases for both compounds and the corresponding three spectra may be approximated by adding subsequently each of the three DADS, that describe the small spectral shifts, to the determined equilibrated S_1 state (*vide infra*). The SAS of thermally equilibrated excited singlet and triplet are determined as follows:

Considering the ground state contribution, S_{S_0} , one obtains the following relationship between the SAS, S_i , and the DADS, D_i :

$$S_{S_1} = \frac{(D_1 + D_2)}{c_0} + S_{S_0} \quad (5)$$

$$S_{T_1} = \frac{(\kappa_1 - \kappa_2)D_2}{c_0 \Phi_{isc} \kappa_1} + S_{S_0} \quad (6)$$

Only the parameters c_0 and Φ_{isc} are undetermined. The requirement that the resulting SAS must be positive and should not show any of the characteristic bands of the other species allows to find upper and lower bounds for these parameters. In particular, the negative peaks from the ground state bleach should disappear in the SAS. Figure S3 shows the *in-silico* titration of those two parameters for estimating the best values for both photocatalysts. The spectra of the thermally and electronically excited $S_1^{\text{hot-}i}$ states were calculated following equations 7 to 9, where the D'_i represent the three additional DADS that attribute to the small spectral changes due to IVR and IET (see Figure 1 in the main text).

$$S_{S_1^{\text{hot-1}}} = D'_1 + D'_2 + D'_3 + S_{S_1} \quad (7)$$

$$S_{S_1^{\text{hot-2}}} = D'_2 + D'_3 + S_{S_1} \quad (8)$$

$$S_{S_1^{\text{hot-3}}} = D'_3 + S_{S_1} \quad (9)$$

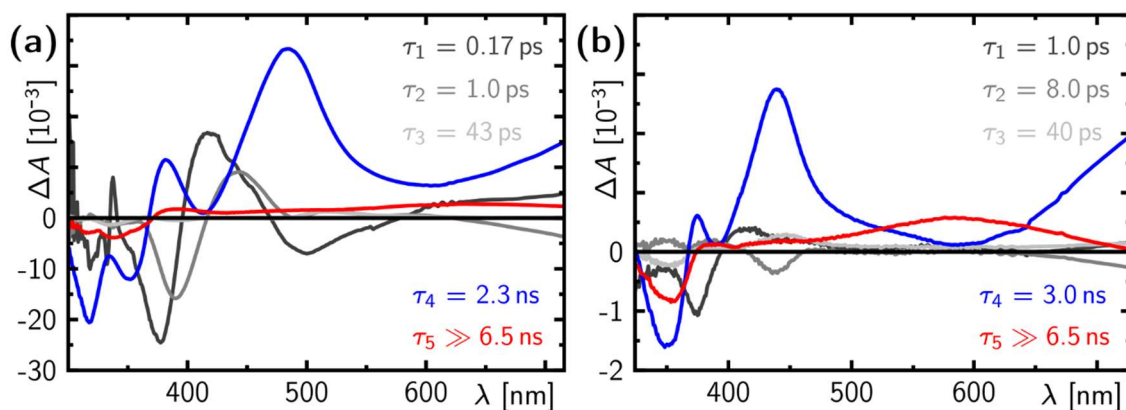


Figure S 2. Decay-associated difference spectra resulting from a global exponential fit with five components to the transient absorption data obtained for **A** (a) and **B** (b) in ACN.

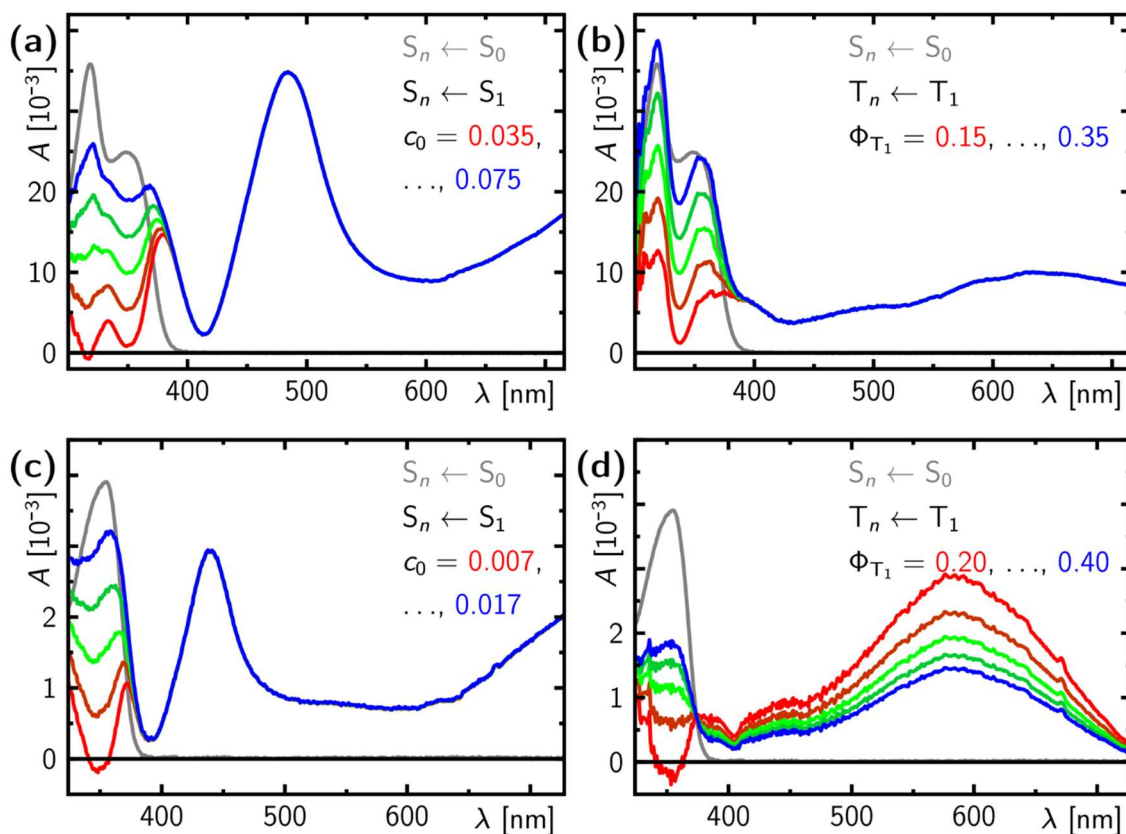


Figure S 3. Main contributing SAS of compounds **A** (a-b) and **B** (c-d) in ACN contributing to the transient absorption data based on the model described in the SI text. The S_1 state, $S_n \leftarrow S_1$ transitions, (left panels), and the T_1 state, $T_n \leftarrow T_1$ transitions, (right panels) are determined by varying the ground state contribution, c_0 , and the triplet yield, Φ_{T_1} , between lower and upper bounds, respectively. At the lower bounds the corresponding spectrum becomes negative and above the contributions of the S_0 state spectrum, $S_n \leftarrow S_0$ transitions, arise. The S_0 spectrum is plotted in grey in all panels for comparison.

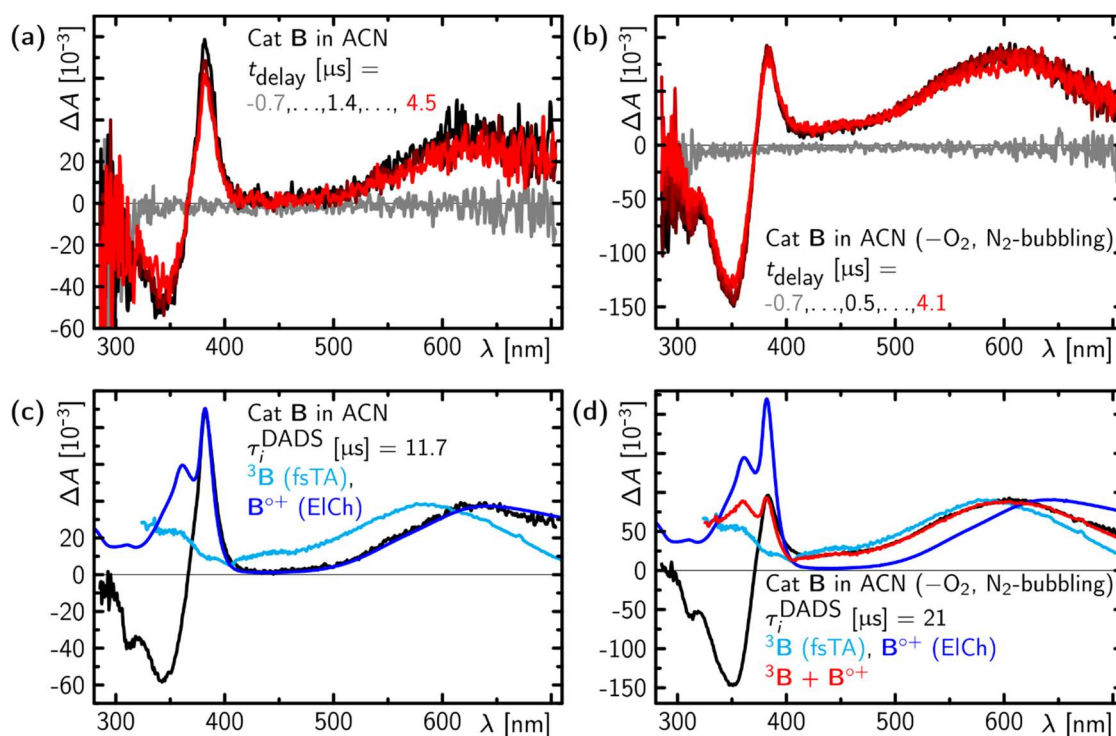


Figure S 4. Time-resolved optical spectroscopy of compounds **B** in non-degassed (a) and degassed (b) ACN after excitation at 355 nm in a 5 μs time window. c-d: Decay associated difference spectra (DADS) in comparison to the triplet ^3B spectrum from fs-TA (cyan) and the electrochemically generated radical cation $\text{B}^{\bullet+}$ spectrum as indicated. To note, here the data were recorded in a longer time window than for the data for compound **A** shown in Figure 3.

Cyclic voltammograms for **A** and **B** in ACN (Figure S5) were recorded against ferrocene using NBu_4PF_6 (0.1 M) as supporting electrolyte, glassy carbon anode, Pt cathode and Ag reference electrode. The corresponding redox potentials were calculated as follows: potential of sample against Ag electrode minus potential of ferrocene reference system against Ag electrode plus correction of +0.38 V for conversion to the potential against saturated calomel electrode (SCE).

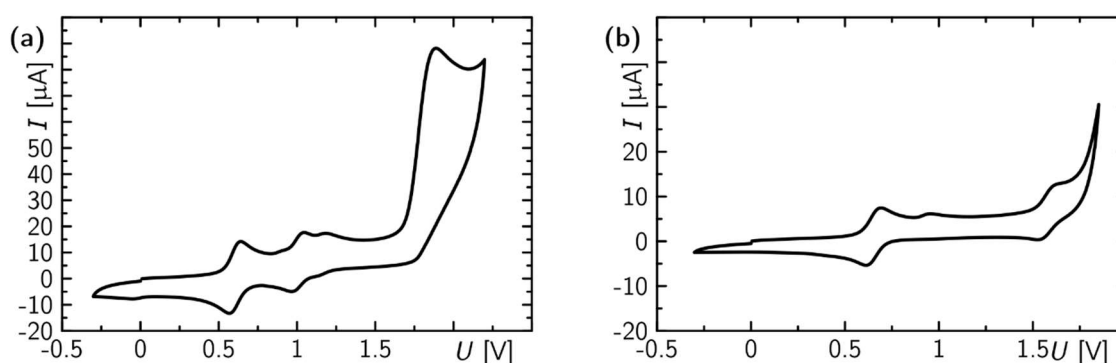


Figure S 5. Cyclic voltammogram of compounds **A** (a; $E_{\text{pc}}^{\text{Ox-1}} = 1.03 \text{ V}$, $E_{\text{pa}}^{\text{Ox-1}} = 0.98 \text{ V}$) and **B** (b; $E_{\text{pc}}^{\text{Ox-1}} = 1.61 \text{ V}$, $E_{\text{pa}}^{\text{Ox-1}} = 1.52 \text{ V}$) in relation to the Fc/Fc^+ (in a: $E_{\text{pc}}^{\text{Ox-1}} = 0.63 \text{ V}$, $E_{\text{pa}}^{\text{Ox-1}} = 0.60 \text{ V}$; in b: $E_{\text{pc}}^{\text{Ox-1}} = 0.69 \text{ V}$, $E_{\text{pa}}^{\text{Ox-1}} = 0.61 \text{ V}$) redox couple. Cat (A/A^+) = $1.00 - 0.62 + 0.38 = 0.76 \text{ V}$ vs. SCE. Cat (B/B^+) = $1.56 - 0.65 + 0.38 = 1.29 \text{ V}$ vs. SCE.

The sequence of UV/Vis absorption spectra for **A** and **B** after stepwise application of an increasingly positive voltage up to 1.6 V or 1.7 V (vs. Ag electrode), respectively, is shown Figure S6. In both cases isosbestic points indicate a clean stoichiometric conversion.

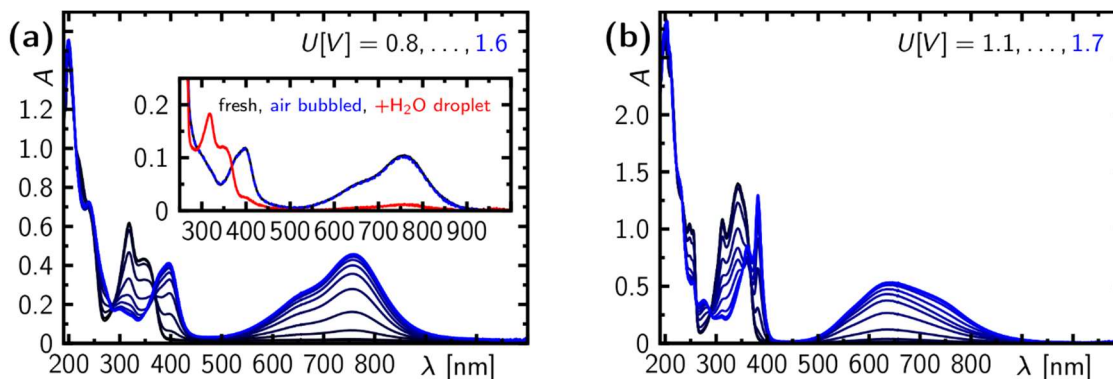


Figure S 6. Electrochemical characterization of **A** (a) and **B** (b) in ACN. **a,b**: The sequence of UV/Vis absorption spectra for **A** (a) and **B** (b) in ACN after stepwise application of an increasingly positive voltage up to 1.6 V or 1.7 V (vs. Ag electrode), respectively. Inset in **a**: **A** in ACN after applying a constant voltage of 1.5 V to a carbon electrode (black), after bubbling air through the sample (blue dashed), and immediately after addition of one droplet of water (red).

All reactions were carried with dry solvents unless otherwise stated. Reagents were purchased at the highest commercial quality and used without further purification, unless stated otherwise. Graphite electrodes were purchased from Faber-Castell (TK 9071, HB) and Pt-foil from Alfa Aesar (0.01 mm, 99.99%). The power supply was purchased from PekTech® (6080A, 0-15 V, 0-3 A DC) and the electrodes were connected *via* red (+) and black (-) mini hook clamps. Precision Seal® rubber septa were purchased by Sigma-Aldrich. Fabrication of divided half-cells was done in-house. Built-in porous filter disc (\varnothing 1 cm, max. pore size 16-40 μ m) was purchased from Duran®.

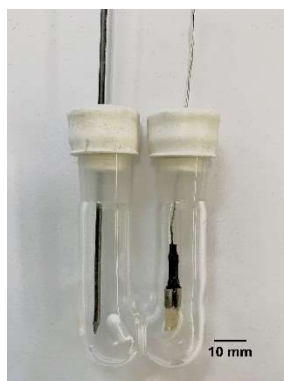


Figure S 7. Photoelectrochemical cell showing the two half cells connected via a porous filter disc. Shown are the left half-cell for the sample equipped with the carbon working electrode and the right half-cell equipped with the platinum counter electrode.

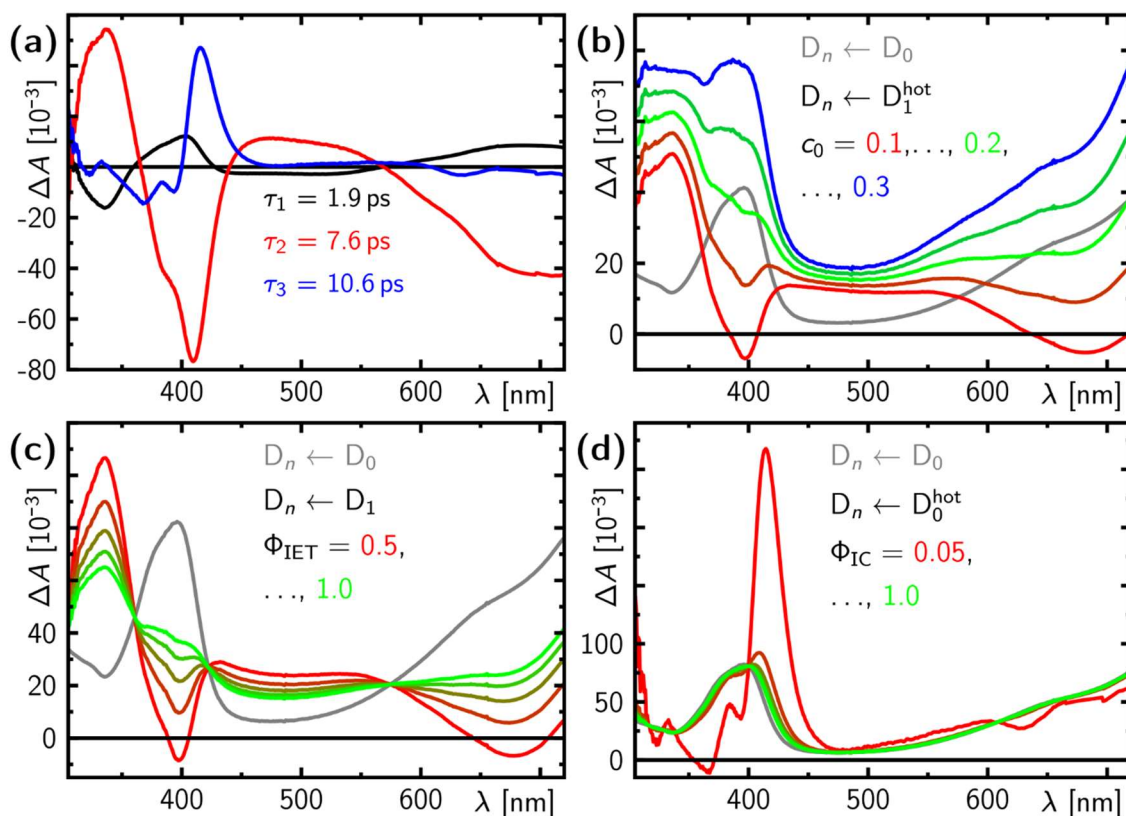


Figure S 8. Decay-associated difference spectra resulting from a global exponential fit with three components to the transient absorption data obtained for A^+ in ACN from data in Figure 4B (a) and the corresponding contributing SAS based on a sequential model of relaxation processes (b-d): The thermally and electronically excited doublet state D_1^{hot} , $D_n \leftarrow D_1^{\text{hot}}$ transitions, (b) relaxes via intramolecular vibrational energy redistribution (IVR) and intermolecular vibronic energy transfer (IET) into the relaxed excited doublet state D_1 ($D_n \leftarrow D_1$ transitions, c). Finally, internal conversion (IC) leads to formation of the thermally excited ground state doublet D_0^{hot} ($D_n \leftarrow D_0^{\text{hot}}$ transitions, d), which relaxes to the equilibrated doublet ground state D_0 ($D_n \leftarrow D_0$ transitions, grey line in each panel). The ground state contribution, c_0 , was determined by varying between lower and upper bounds so that the spectrum neither is negative nor shows contributions of the D_0 spectrum. The yields for IET and IC reveal only reasonable spectra when equal to one, which is also justified by the fact that no further long-lived transient absorption signal is observed.

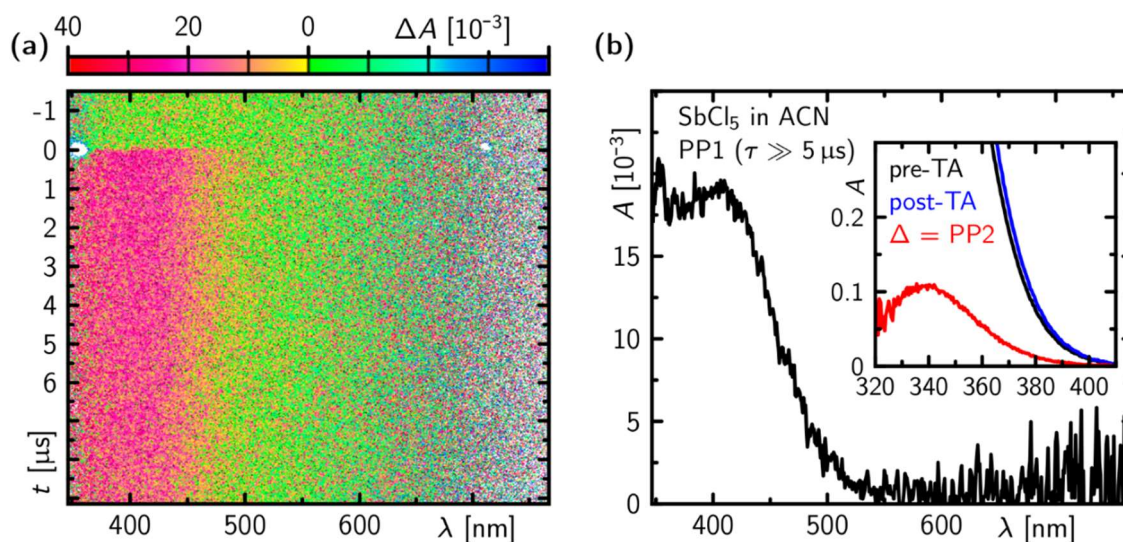


Figure S 9. Transient absorption of SbCl_5 in ACN following excitation at 355 nm showing a light-induced first photoproduct (PP1) with a lifetime in μs timescale, which converts further into a second photoproduct (PP2, difference spectrum between the spectra prior (pre-TA) and post (post-TA) the transient absorption measurement in the inset).

4.6.4.3 Computational Investigations

Quantum-mechanical calculations on a bridged triaryl amine unsubstituted in para position as well as on Cat **B** were performed using the Orca package.^[9-10] The geometries of their lowest doublet and quartet states were optimized on the level of unrestricted closed shell density functional theory URHF-DFT using the B3LYP functional and the DEF2-TZVP basis set with D_4 dispersion correction. To note, in the quartet state the planar configuration of the doublet state twists along one phenyl ring. For all optimized species the first 40 excited states in each spin state were calculated on the TD-DFT(B3LYP)/D4//DEF2-TZVP level of theory and the electronic states were connected by parabolas as a simplified harmonic approximation in configurational space (see Figure S11).

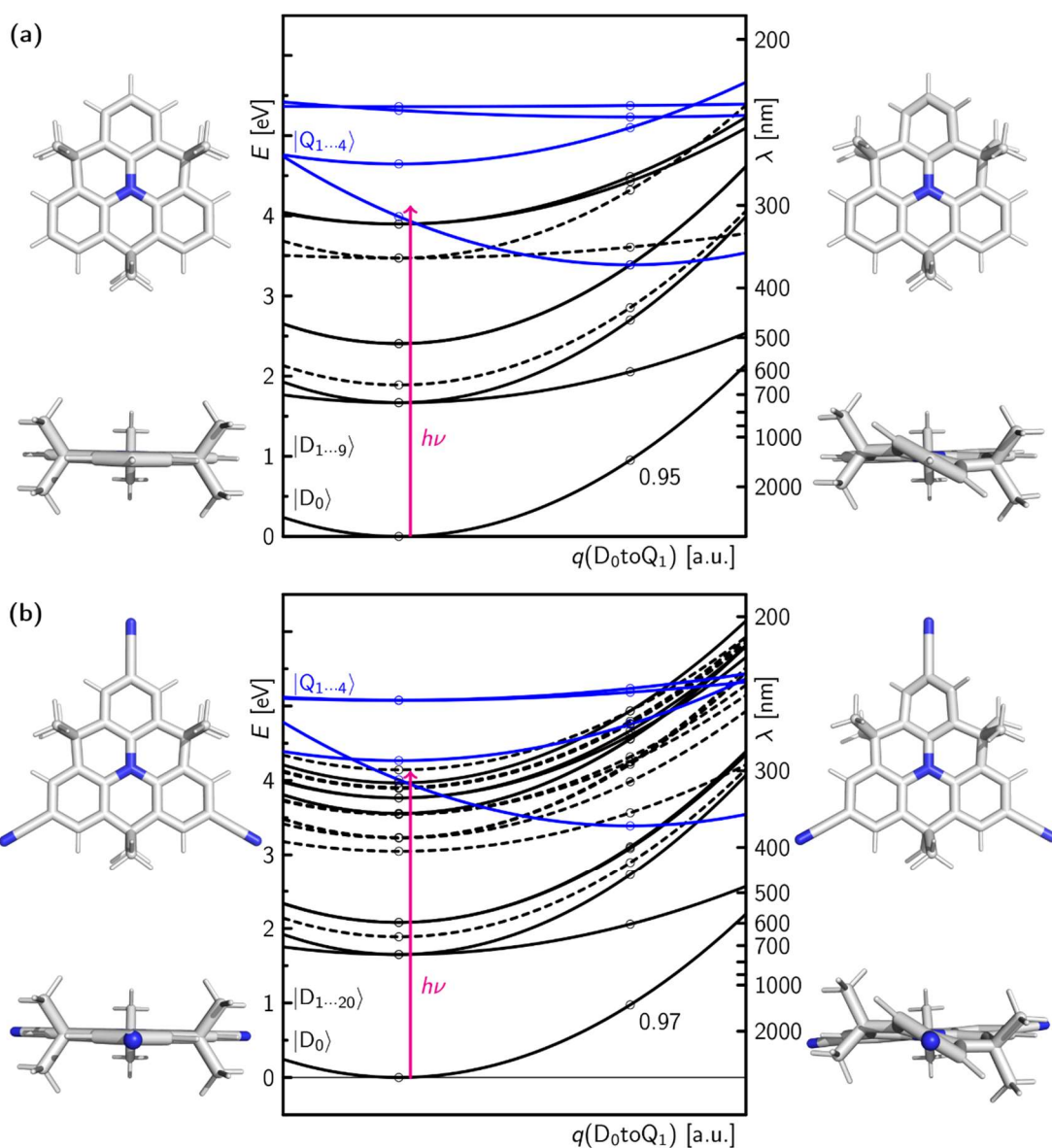


Figure S 10. Quantum-chemical calculation of the bridged triaryl amines in their doublet (left, black) and quartet states (right, blue). **a:** Derivative unsubstituted in para position. **b:** Cat **B** was investigated also experimentally in this work. The geometries of D_0 and Q_1 were optimized on the DFT-B3LYP-D4//DEF2-TZVP level in the gas phase. For each geometry the first 20 excited states were calculated on the TD-DFT-B3LYP-D4//DEF2-TZVP level of theory. As a simplified harmonic approximation in configurational space, the electronic states in the two corresponding geometries are connected by a parabola. Those states to which the transition probability is very low are shown in dashed lines and the experimentally relevant excitation energy is shown by a magenta arrow indicating that intersystem crossing to the lowest quartet state is in principle energetically accessible.

4.6.5 Mass Spectroscopic Investigation

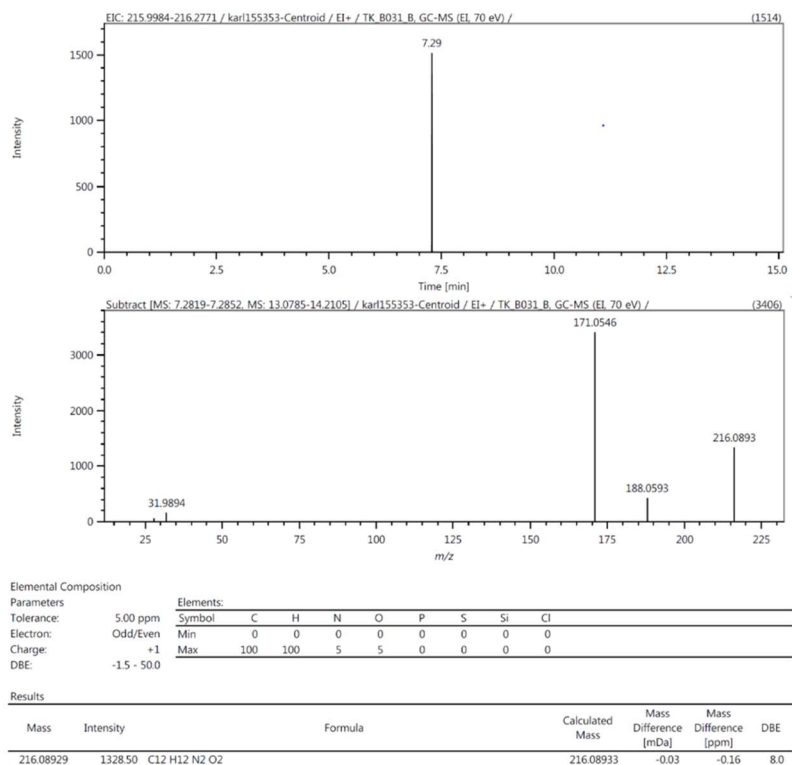


Figure S 11. High-resolution mass spectrum of a sample consisting of the electrochemically formed A^{+} , benzene, ethyl-1H-pyrazole-4-carboxylate, and the conducting salt Bu_4NPF_6 in ACN after irradiation for 72 h with 640 nm light.

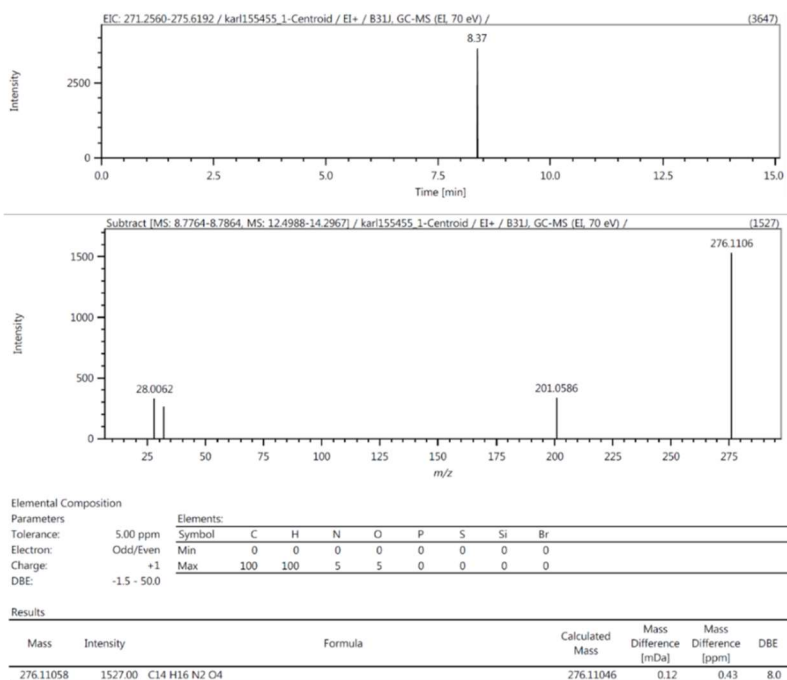
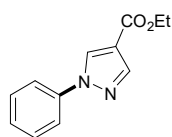
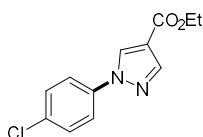


Figure S 12. High-resolution mass spectrum of a sample consisting of the electrochemically formed A^{+} , 1,4-dimethoxybenzene, ethyl-1H-pyrazole-4-carboxylate, and the conducting salt Bu_4NPF_6 in ACN after irradiation for 72 h with 640 nm light.

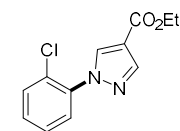
4.6.6 Characterization of Products



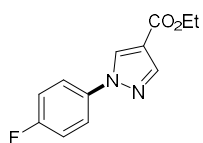
Ethyl 1-phenyl-1H-pyrazole-4-carboxylate (1a): Ethyl 1-phenyl-1H-pyrazole-4-carboxylate **1a** was prepared according to *General Procedure B*. The residue was purified by flash chromatography upon direct loading on silica column (petroleum ether/ethyl acetate, gradient from 90:10 to 70:30) to yield colorless crystalline needles (19 mg, 88%). $^1\text{H NMR}$ (300 MHz, CDCl_3), δ (ppm): 8.41 (s, 1H), 8.10 (s, 1H), 7.76 – 7.62 (m, 2H), 7.56 – 7.40 (m, 2H), 7.38-7.34 (m, 1H), 4.34 (q, $J = 7.1$ Hz, 2H), 1.38 (t, $J = 7.1$ Hz, 3H). $^{13}\text{C NMR}$ (75 MHz, CDCl_3), δ (ppm): 162.9, 142.2, 139.4, 130.0, 129.6, 127.6, 119.6, 118.2, 60.5, 14.4). Data in accordance with literature.^[11]



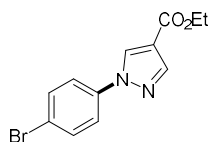
Ethyl 1-(4-chlorophenyl)-1H-pyrazole-4-carboxylate (1b): Ethyl 1-(4-chlorophenyl)-1H-pyrazole-4-carboxylate **1b** was prepared according to *General Procedure B*. The residue was purified by flash chromatography upon direct loading on silica column (petroleum ether/ethyl acetate, gradient from 90:10 to 70:30) to yield a white crystalline solid (21 mg, 84%, 2:1 para/ortho). Para isomer: $^1\text{H NMR}$ (300 MHz, CDCl_3), δ (ppm): 8.37 (s, 1H), 8.09 (s, 1H), 7.65 (d, $J = 9.0$ Hz, 2H), 7.45 – (d, $J = 9.0$ Hz, 2H), 4.34 (q, $J = 7.1$ Hz, 2H), 1.37 (t, $J = 7.1$ Hz, 3H). $^{13}\text{C NMR}$ (75 MHz, CDCl_3), δ (ppm): 162.7, 142.4, 138.0, 133.2, 130.0, 129.8, 120.8, 117.3, 60.6, 14.4). Data in accordance with literature.^[11]



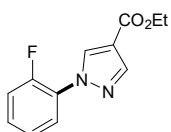
Ortho isomer: $^1\text{H NMR}$ (300 MHz, CDCl_3), δ (ppm): 8.35 (s, 1H), 8.13 (s, 1H), 7.65 – 7.48 (m, 2H), 7.49 – 7.35 (m, 2H), 4.34 (q, $J = 7.1$ Hz, 2H), 1.37 (t, $J = 7.1$ Hz, 3H). $^{13}\text{C NMR}$ (75 MHz, CDCl_3), δ (ppm): 162.5, 142.1, 135.0, 134.7, 130.8, 129.9, 128.5, 127.7, 60.5, 14.4). Data in accordance with literature.^[11]



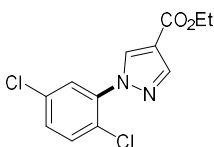
Ethyl 1-(4-fluorophenyl)-1H-pyrazole-4-carboxylate (1c): Ethyl 1-(4-fluorophenyl)-1H-pyrazole-4-carboxylate **1c** was prepared according to *General Procedure C*. The residue was purified by flash chromatography upon direct loading on silica column (petroleum ether/ethyl acetate, gradient from 90:10 to 70:30) to yield a white crystalline solid (20 mg, 87%). $^1\text{H NMR}$ (400 MHz, CDCl_3), δ (ppm): 8.43 (s, 1H), 8.17 (s, 1H), 7.82 – 7.70 (m, 2H), 7.30 – 7.24 (m, 2H), 4.42 (q, $J = 7.1$ Hz, 2H), 1.46 (t, $J = 7.1$ Hz, 3H). $^{13}\text{C NMR}$ (101 MHz, CDCl_3), δ (ppm): 163.0, 162.8, 142.2, 135.8, 130.1, 121.6, 121.5, 117.0, 116.4, 60.5, 14.4. $^{19}\text{F NMR}$ (377 MHz, CDCl_3), δ (ppm): -114.64. Data in accordance with literature.^[12]



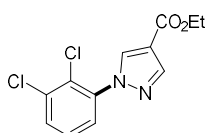
Ethyl 1-(4-bromophenyl)-1H-pyrazole-4-carboxylate (1d): Ethyl 1-(4-bromophenyl)-1H-pyrazole-4-carboxylate **1d** was prepared according to General Procedure C. The residue was purified by flash chromatography upon direct loading on silica column (petroleum ether/ethyl acetate, gradient from 90:10 to 70:30) to yield a white solid (16.5 mg, 56%). ¹H NMR (400 MHz, CDCl₃), δ (ppm): 8.37 (s, 1H), 8.11 (s, 1H), 7.60 (s, 4H), 4.34 (q, J = 7.1 Hz, 2H), 1.37 (t, J = 7.1 Hz, 3H). ¹³C NMR (101 MHz, CDCl₃), δ (ppm): 163.7, 142.4, 138.4, 132.7, 129.9, 121.0, 120.9, 117.3, 60.6, 14.4. Data in accordance with literature.^[13]



Ethyl 1-(2-fluorophenyl)-1H-pyrazole-4-carboxylate (1e): Ethyl 1-(2-fluorophenyl)-1H-pyrazole-4-carboxylate **1e** was prepared according to General Procedure C. The residue was purified by flash chromatography upon direct loading on silica column (petroleum ether/ethyl acetate, gradient from 90:10 to 70:30) to yield a white solid (11 mg, 48%). ¹H NMR (400 MHz, CDCl₃), δ (ppm): 8.48 (d, J = 2.5 Hz, 1H), 8.12 (s, 1H), 7.95 – 7.85 (m, 1H), 7.38 – 7.31 (m, 1H), 7.25-7.31 (m, 2H), 4.34 (q, J = 7.1 Hz, 2H), 1.38 (t, J = 7.1 Hz, 3H). ¹³C NMR (101 MHz, CDCl₃), δ (ppm): 162.8, 143.6, 142.0, 140.9, 134.1, 128.8, 117.0, 116.49, 60.5, 14.4. ¹⁹F NMR (377 MHz, CDCl₃), δ (ppm): -125.25. HRMS: calculated for B₂H₁₂FN₂O₂⁺ (M+H⁺): 235.0805, found 235.088.

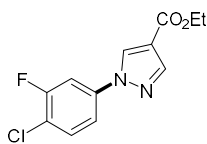


Ethyl 1-(2,5-dichlorophenyl)-1H-pyrazole-4-carboxylate (1f): Ethyl 1-(2,5-dichlorophenyl)-1H-pyrazole-4-carboxylate **1f** was prepared according to General Procedure B. The residue was purified by flash chromatography upon direct loading on silica column (petroleum ether/ethyl acetate, gradient from 90:10 to 70:30) to yield a white crystalline solid (8 mg, 28%). ¹H NMR (400 MHz, CDCl₃), δ (ppm): 8.39 (s, 1H), 8.13 (s, 1H), 7.65 (d, J = 2.4 Hz, 1H), 7.51-7.45 (m, 1H), 7.38 (d, J = 2.4 Hz, 1H), 4.33 (q, J = 7.1 Hz, 2H), 1.38 (t, J = 7.1 Hz, 3H). ¹³C NMR (101 MHz, CDCl₃), δ (ppm): 162.9, 142.4, 134.6, 133.6, 131.7, 129.8, 127.6, 127.7, 119.7, 116.9, 60.6, 14.4. HRMS: calculated for C₁₂H₁₁Cl₂N₂O₂⁺ (M+H⁺): 285.0192, found 285.0193.

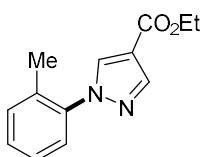


Ethyl 1-(2,3-dichlorophenyl)-1H-pyrazole-4-carboxylate (1g) Ethyl 1-(2,3-dichlorophenyl)-1H-pyrazole-4-carboxylate **1g** was prepared according to General Procedure B. The residue was purified by flash chromatography upon direct loading on silica column (petroleum ether/ethyl acetate, gradient from 90:10 to 70:30) to yield a white crystalline solid (12 mg, 43%). ¹H NMR (300 MHz, CDCl₃), δ (ppm): 8.38 (s, 1H), 8.10 (s, 1H), 7.69-7.62(m, 1H), 7.59-7.51 (m, 2H), 7.38 4.34 (q, J = 7.1 Hz, 2H), 1.38 (t, J = 7.1

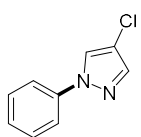
Hz, 3H). ^{13}C NMR (75 MHz, CDCl_3), δ (ppm): 165.5, 142.7, 131.3, 129.9, 121.4, 118.4, 60.7, 14.4. HRMS: calculated for $\text{C}_{12}\text{H}_{11}\text{Cl}_2\text{N}_2\text{O}_2^+$ ($\text{M}+\text{H}^+$): 285.0192, found 285.0194.



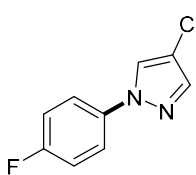
Ethyl 1-(4-chloro-3-fluorophenyl)-1H-pyrazole-4-carboxylate (1h): Ethyl 1-(4-chloro-3-fluorophenyl)-1H-pyrazole-4-carboxylate **1h** was prepared according to General Procedure C. The residue was purified by flash chromatography upon direct loading on silica column (petroleum ether/ethyl acetate, gradient from 90:10 to 70:30) to yield a crystalline white solid (13 mg, 48%). ^1H NMR (300 MHz, CDCl_3), δ (ppm): 8.38 (s, 1H), 8.09 (s, 1H), 7.65 – 7.55 (m, 1H), 7.54 – 7.40 (m, 2H), 4.33 (q, $J = 7.1$ Hz, 2H), 1.39 (t, $J = 7.1$ Hz, 3H). ^{13}C NMR (75 MHz, CDCl_3), δ (ppm): 162.5, 142.6, 131.4, 130.0, 118.2, 117.7, 115.2, 108.6, 60.7, 14.4. ^{19}F NMR (282 MHz, CDCl_3), δ (ppm): -112.08. HRMS: calculated for $\text{C}_{12}\text{H}_{10}\text{ClFN}_2\text{O}_2^+$ (M): 268.0415, found 268.0412



Ethyl 1-(o-tolyl)-1H-pyrazole-4-carboxylate (1i): Ethyl 1-(o-tolyl)-1H-pyrazole-4-carboxylate **1i** was prepared according to General Procedure C. The residue was purified by flash chromatography upon direct loading on silica column (petroleum ether/ethyl acetate, gradient from 90:10 to 70:30) to yield a white solid (19 mg, 83%). ^1H NMR (300 MHz, CDCl_3), δ (ppm): 8.11 (s, 1H), 8.09 (s, 1H), 7.38-7.26 (m, 4H), 4.34 (q, $J = 7.1$ Hz, 2H), 2.25 (s, 3H), 1.37 (t, $J = 7.1$ Hz, 3H). ^{13}C NMR (75 MHz, CDCl_3), δ (ppm): 141.7, 133.9, 133.7, 131.5, 129.2, 126.8, 126.0, 118.2, 115.9, 60.4, 14.4. Data in accordance with literature.^[14]

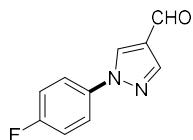


4-Chloro-1-phenyl-1H-pyrazole (2a): 4-Chloro-1-phenyl-1H-pyrazole **2a** was prepared according to General Procedure B. The residue was purified by flash chromatography upon direct loading on silica column (petroleum ether/ethyl acetate, gradient from 90:10 to 70:30) to yield a white crystalline solid (12 mg, 67%). ^1H NMR (300 MHz, CDCl_3), δ (ppm): 7.91 (s, 1H), 7.67 – 7.60 (m, 3H), 7.50 - 7.42 (m, 2H), 7.35-7.28 (m, 1H). ^{13}C NMR (75 MHz, CDCl_3), δ (ppm): 139.7, 139.5, 129.6, 127.0, 124.9, 119.0, 112.4. Data in accordance with literature.^[11]



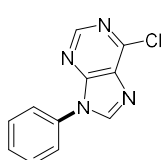
4-Chloro-1-(4-fluorophenyl)-1H-pyrazole (2b): 4-Chloro-1-(4-fluoro phenyl)-1H-pyrazole **2b** was prepared according to General Procedure C. The residue was purified by flash chromatography upon direct loading on silica column (petroleum ether/ethyl acetate, gradient from 90:10 to 70:30) to yield a white solid (14 mg, 71%). ^1H NMR (300 MHz, CDCl_3), δ (ppm): 7.84 (d, $J = 0.4$ Hz, 1H), 7.63

(s, 1H), 7.66-7.52 (m, 2H), 7.20 – 7.10 (m, 2H). ^{13}C NMR (75 MHz, CDCl_3), δ (ppm): 163.0, 159.8, 139.6, 125.0, 120.9, 120.8, 116.6, 116.3, 112.7. ^{19}F NMR (282 MHz, CDCl_3), δ (ppm): -115.43. Data in accordance with literature.^[15]



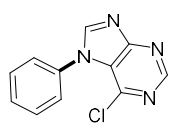
1-(4-Fluorophenyl)-1H-pyrazole-4-carbaldehyde (2c): 1-(4-fluorophenyl)-1H-pyrazole-4-carbaldehyde **2c** was prepared according to General Procedure

C. The residue was purified by flash chromatography upon direct loading on silica column (petroleum ether/ethyl acetate, gradient from 90:10 to 70:30) to yield a white solid (7 mg, 37%). ^1H NMR (400 MHz, CDCl_3), δ (ppm): 10.02 (s, 1H), 8.44 (s, 1H), 8.21 (s, 1H), 7.78 – 7.72 (m, 2H), 7.29 – 7.23 (m, 2H). ^{13}C NMR (101 MHz, CDCl_3), δ (ppm): 184.0, 162.2, 160.8, 141.8, 130.0, 125.8, 121.8, 121.7, 116.8, 116.6. ^{19}F NMR (282 MHz, CDCl_3), δ (ppm): -113.78. Data in accordance with literature.^[11]



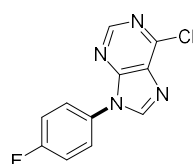
6-Chloro-9-phenyl-9H-purine (2d): 6-Chloro-9-phenyl-9H-purine **2d** was prepared according to General Procedure B. The residue was purified by flash chromatography upon direct loading on silica column (petroleum ether/ethyl acetate, gradient from 90:10 to 95:5) to yield a yellow solid (16 mg, 70%, 5:3 9H

to 7H isomer) ^1H NMR (300 MHz, CDCl_3), δ (ppm): 8.83 (s, 1H), 8.42 (s, 1H), 7.71 (d, $J = 7.9$ Hz, 2H), 7.63 (t, $J = 7.6$ Hz, 2H), 7.54 (d, $J = 7.6$ Hz, 1H). ^{13}C NMR (75 MHz, CDCl_3), δ (ppm): 152.7, 151.6, 151.4, 144.2, 133.9, 131.5, 130.2, 129.1, 123.7. Data in accordance with literature.^[16]



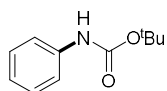
7H isomer: ^1H NMR (300 MHz, CDCl_3), δ (ppm): 8.97 (s, 1H), 8.35 (s, 1H), 7.65-7.55 (m, 3H), 7.49 – 7.43 (m, 2H). ^{13}C NMR (75 MHz, CDCl_3), δ (ppm): 152.8, 149.0, 134.7, 130.3, 129.6, 126.3. HRMS: calculated for $\text{C}_{11}\text{H}_8\text{ClN}_4^+$

($\text{M}+\text{H}^+$): 231.0432, found 231.0435.



6-Chloro-9-(4-fluorophenyl)-9H-purine (2e): 6-Chloro-9-(4-fluorophenyl)-9H-purine **2e** was prepared according to General Procedure C. The residue was purified by flash chromatography upon direct loading on silica column (DCM/MeOH, gradient from 100:0 to 95:5) to yield a yellow solid (19 mg,

77%, 2:1 9H to 7H isomer). ^1H NMR (300 MHz, CDCl_3), δ (ppm): 8.78 (s, 1H), 8.33 (s, 1H), 7.68-7.63 (m, 2H), 7.30 – 7.22 (m, 2H). ^{13}C NMR (75 MHz, CDCl_3), δ (ppm): 164.2, 152.8, 151.9, 144.0, 129.9, 125.8, 125.7, 118.2, 117.4, 117.1. ^{19}F NMR (282 MHz, CDCl_3), δ (ppm): -111.58. HRMS: calculated for $\text{CH}_7\text{ClFN}_4^+$ ($\text{M}+\text{H}^+$): 249.0338, found 249.0339.

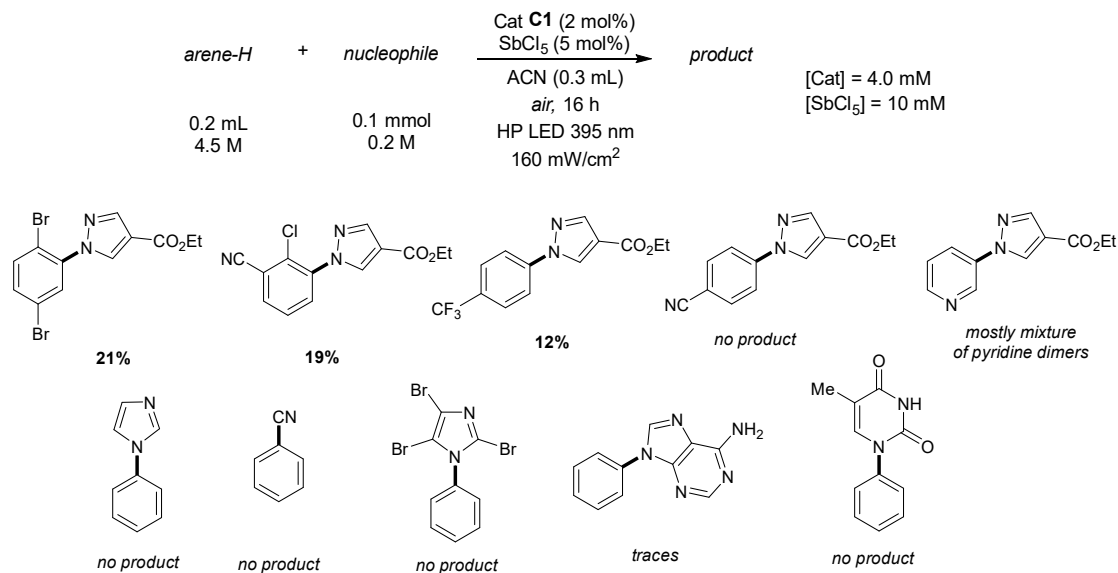


tert-Butyl phenylcarbamate (2f): tert-Butyl phenylcarbamate **2f** was prepared according to General Procedure B. The residue was purified by flash chromatography upon direct loading on silica column (petroleum ether/ethyl acetate, gradient from 90:10 to 70:30) to yield a white solid (4 mg, 21%). $^1\text{H NMR}$ (400 MHz, CDCl_3), δ (ppm): 7.41 – 7.26 (m, 4H), 7.03 (t, $J = 7.3$ Hz, 1H), 6.52 (s, 1H), 1.52 (s, 9H). $^{13}\text{C NMR}$ (101 MHz, CDCl_3), δ (ppm): 152.6, 138.3, 128.9, 123.0, 120.8, 118.5, 28.3. Data in accordance with literature.^[17]

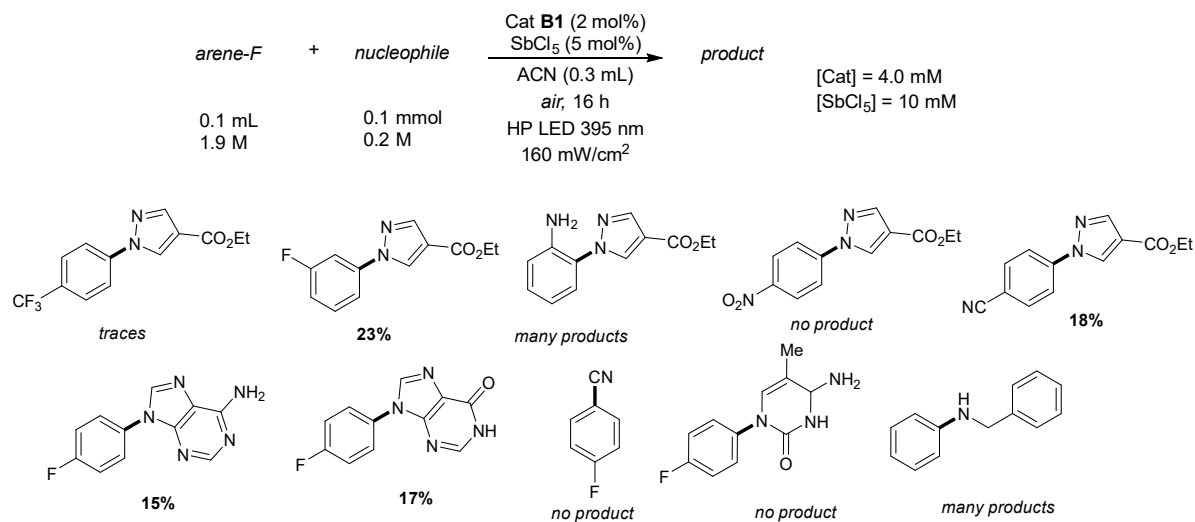
4.6.7 Unreactive Substrates and Nucleophiles

The screening conditions were evaluated with a variety of substrates and nucleophiles. Those shown below did not result in product formation or delivered product in low yields.

4.6.7.1 C-H Oxidation

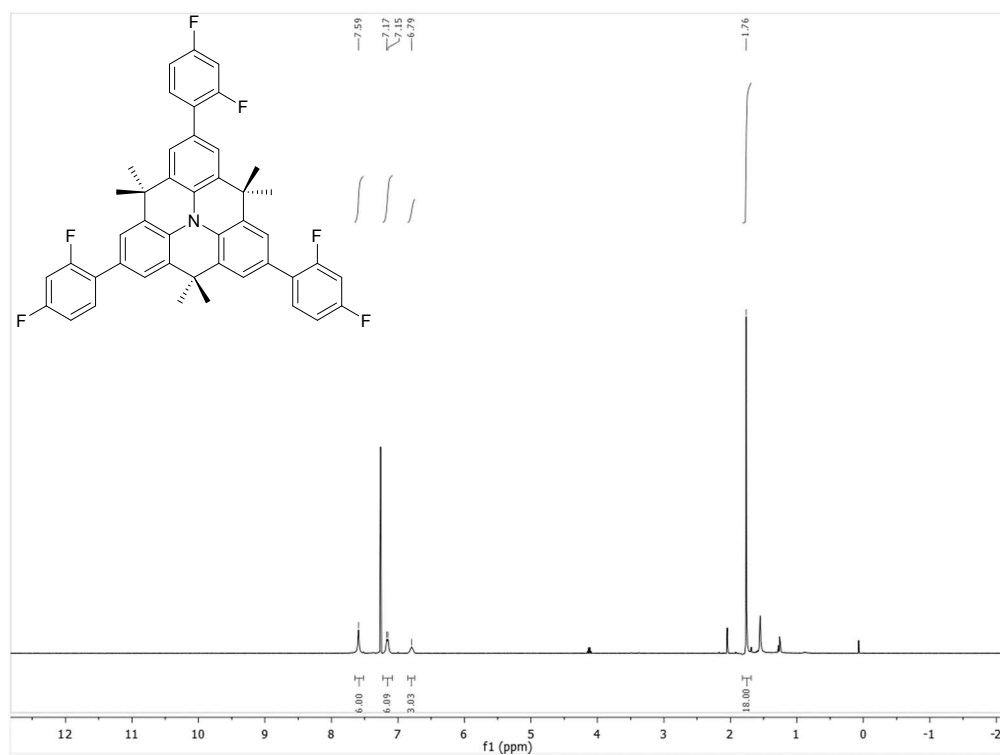


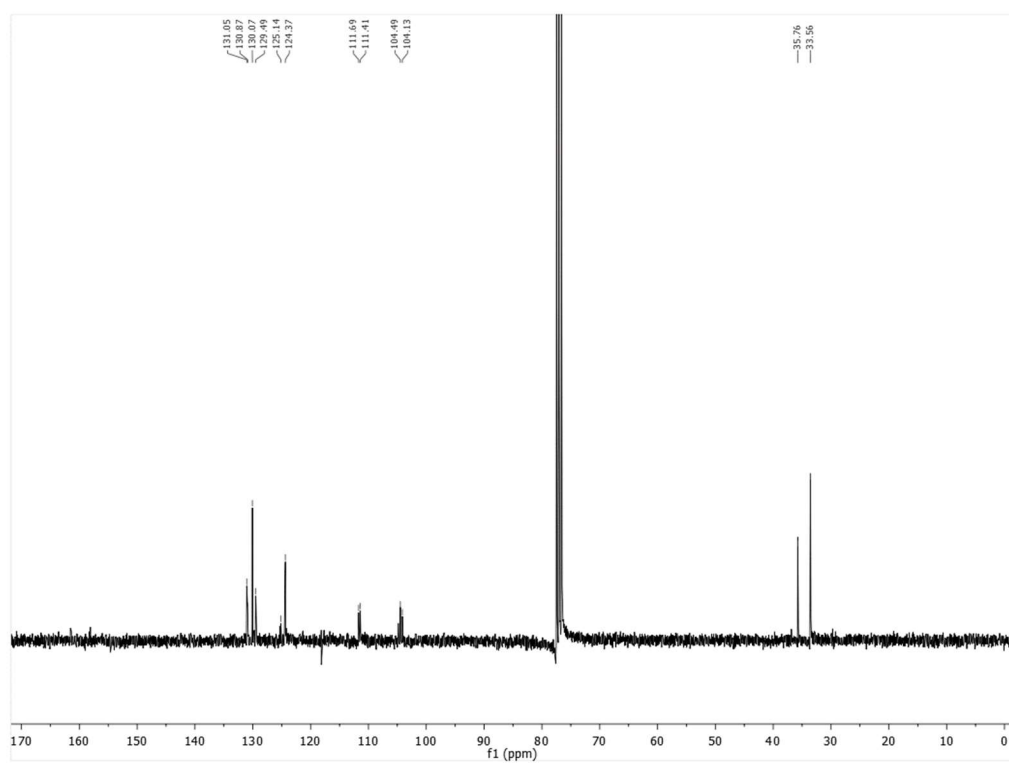
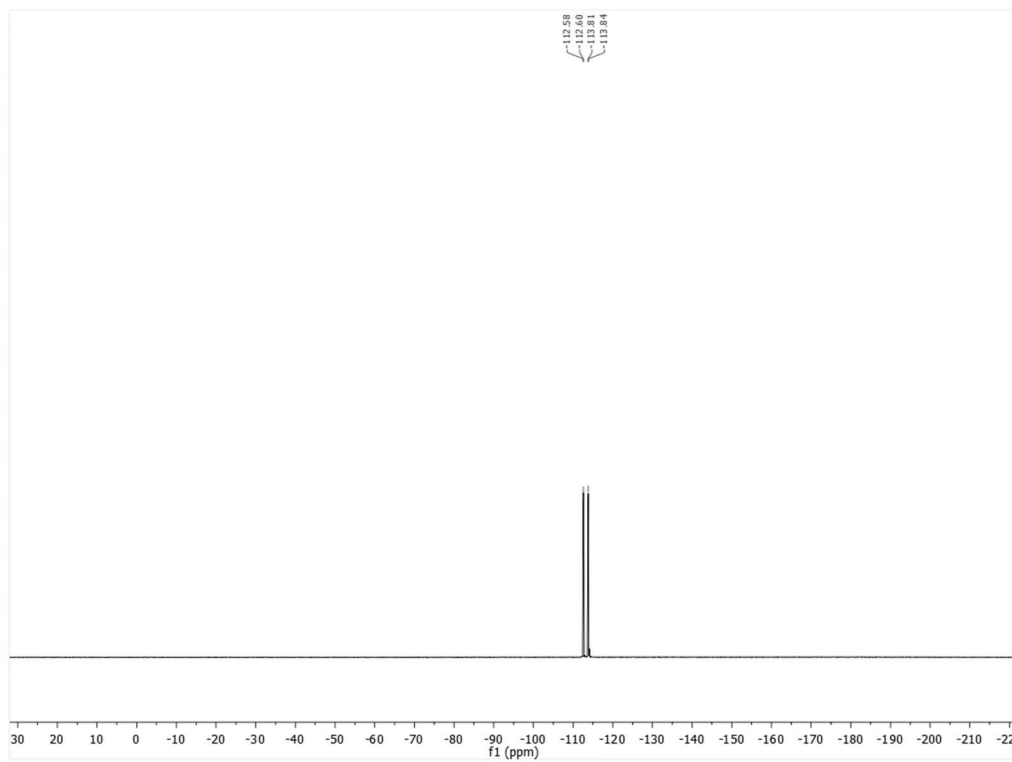
4.6.7.2 C-F Substitution

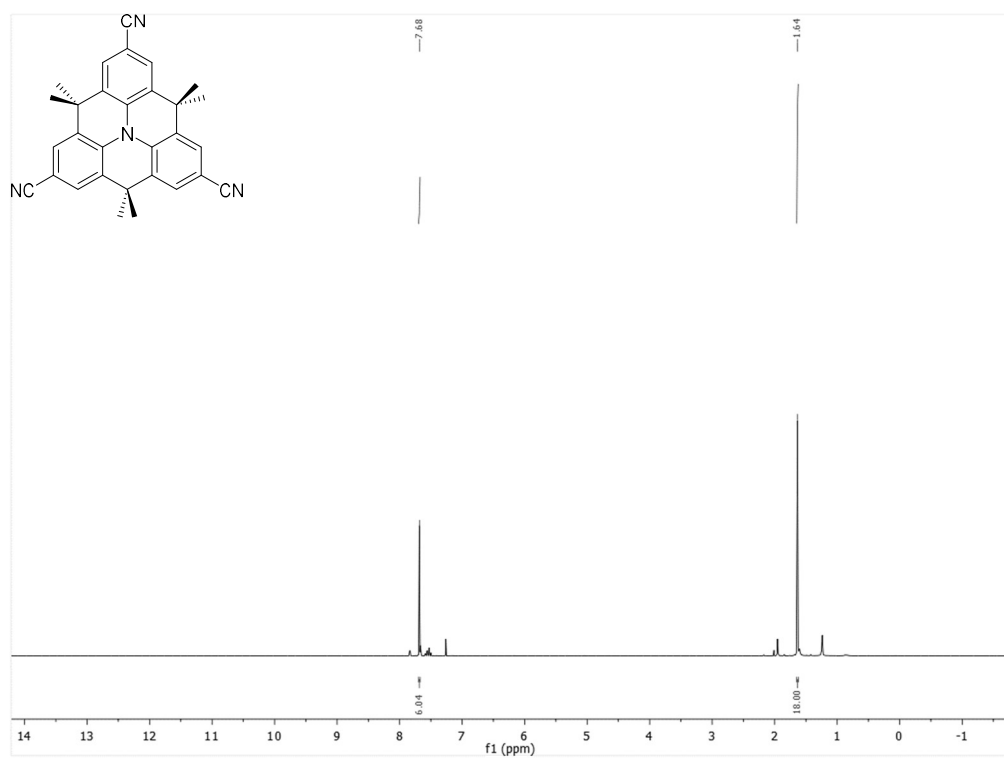
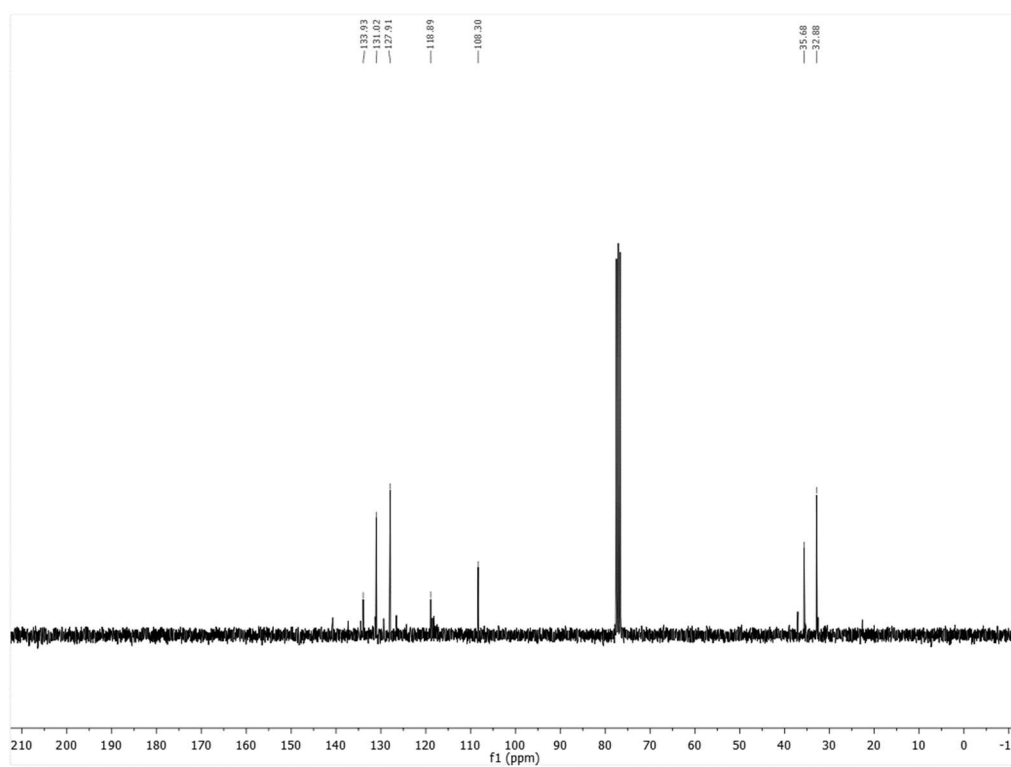


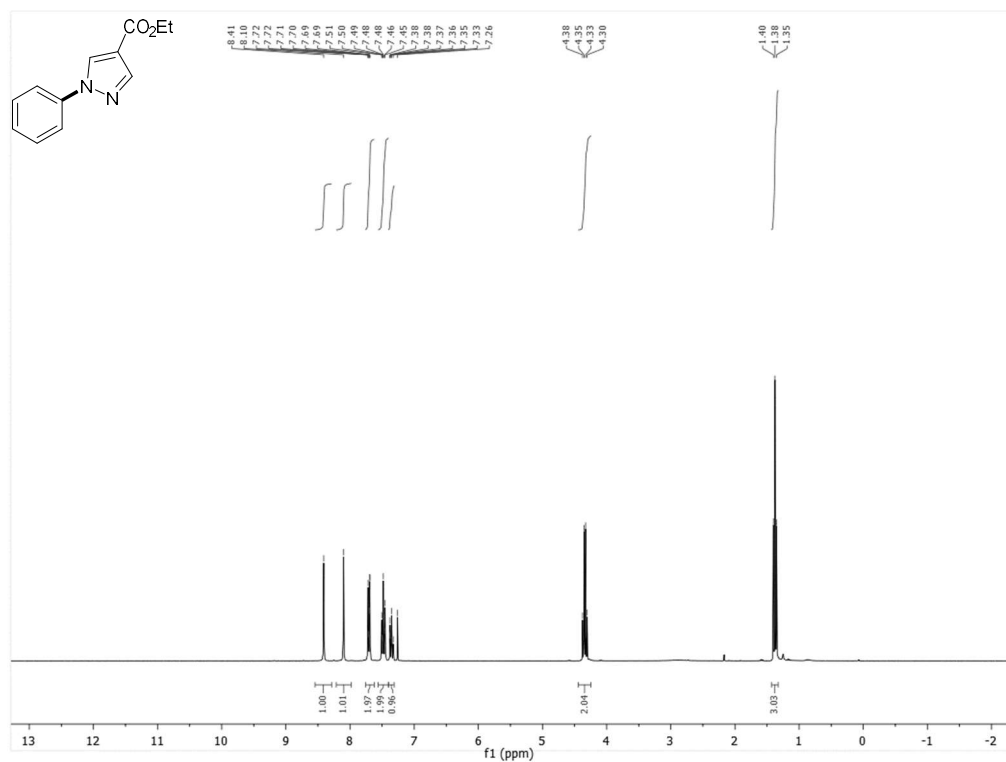
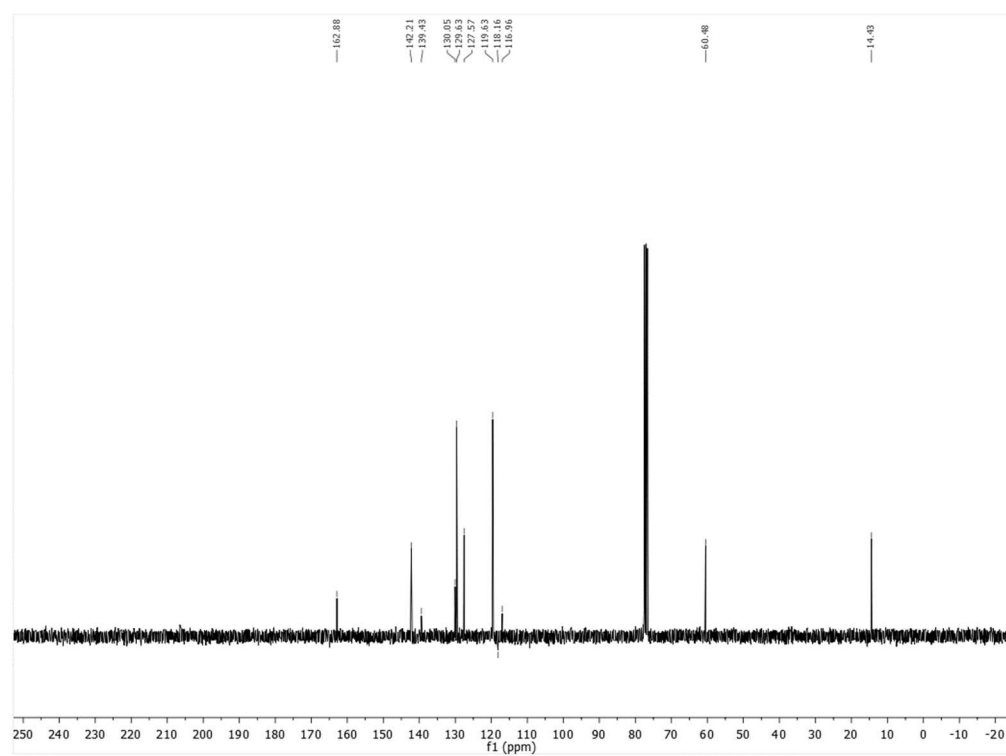
4.6.8 NMR Spectra of Isolated Compounds

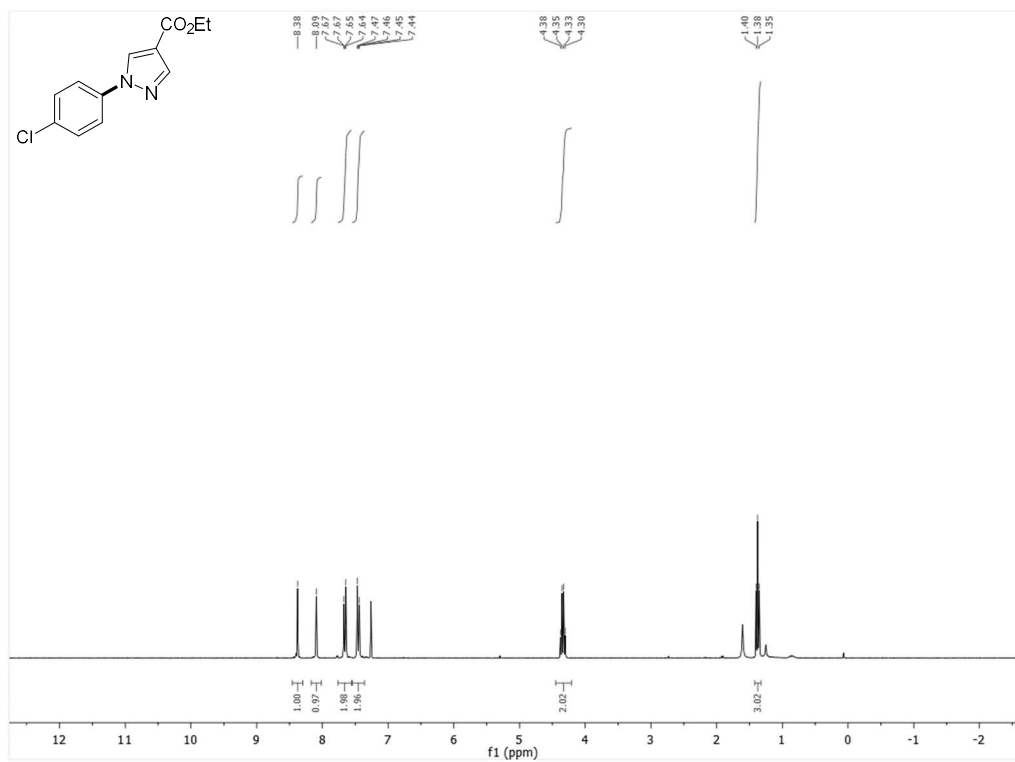
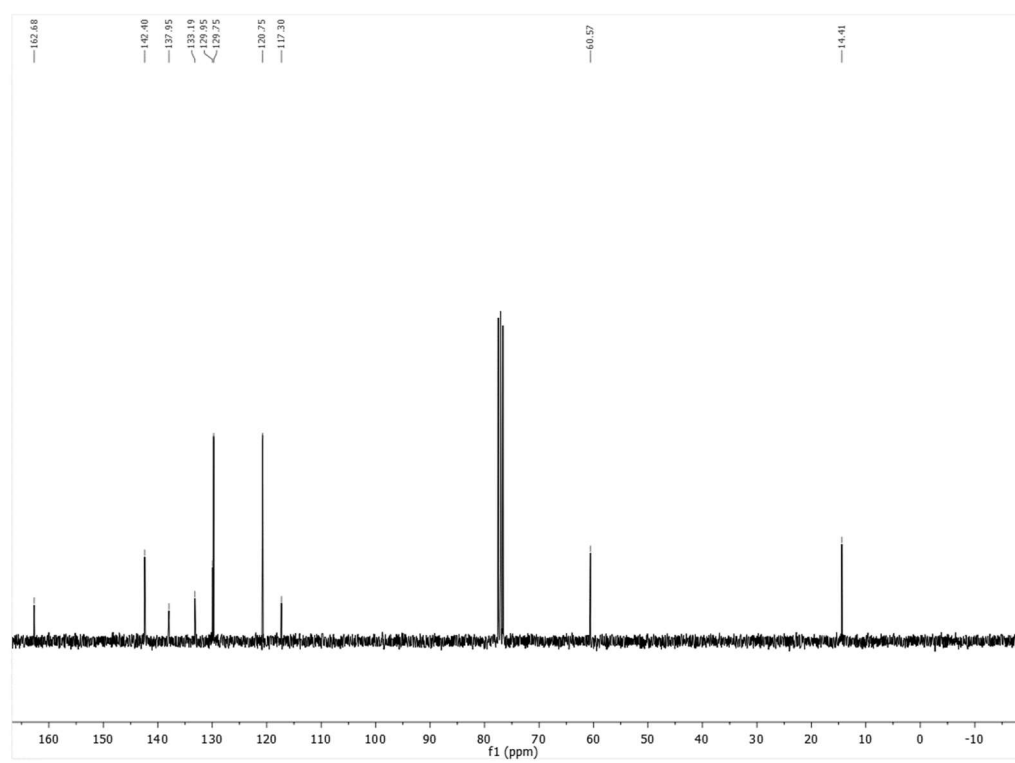
2,6,10-tris(2,4-difluorophenyl)-4,4,8,8,12,12-hexamethyl-8,12-dihydro-4H benzo [9,1] quinolizino [3,4,5,6,7-defg] acridine (Cat A)

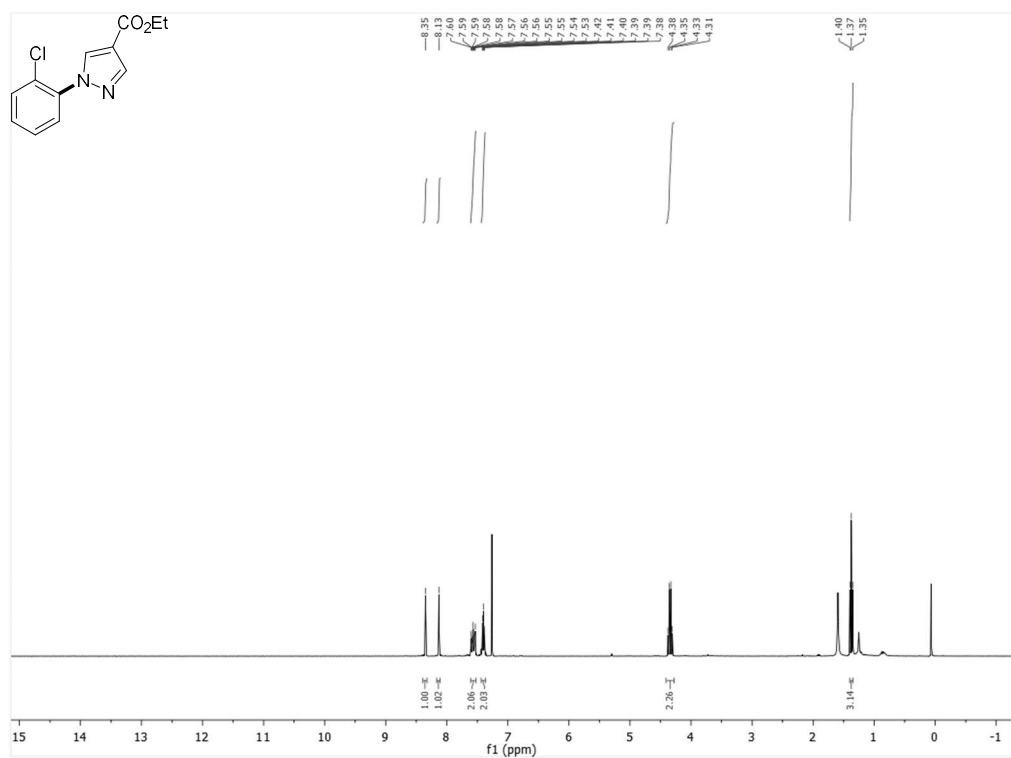
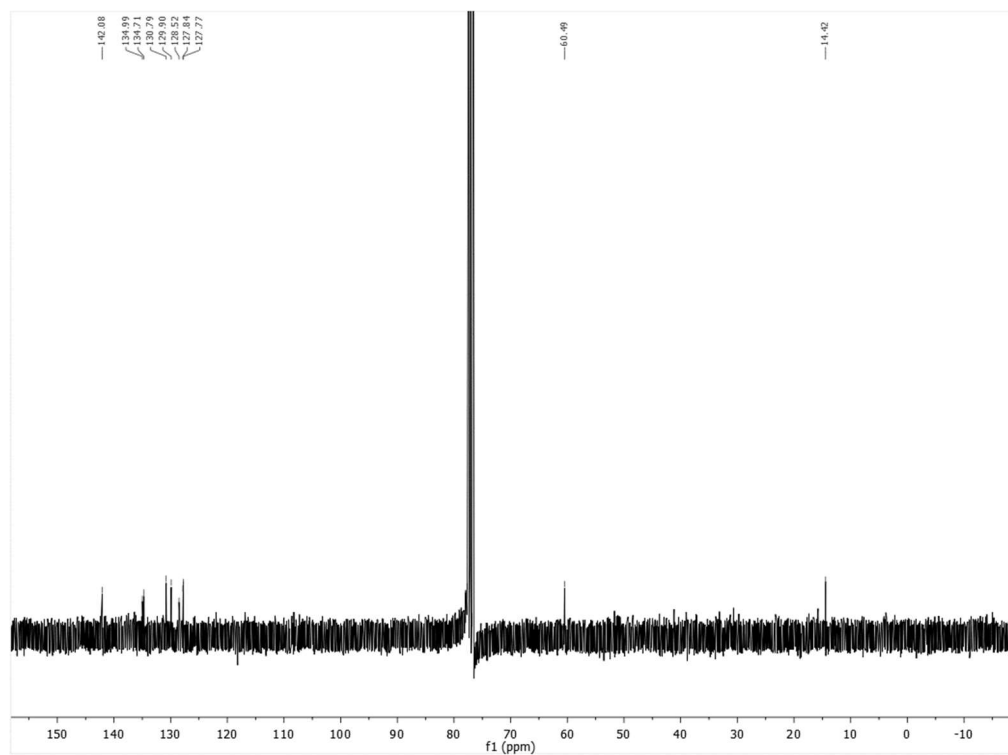
 ^1H NMR (400 MHz, CDCl_3)

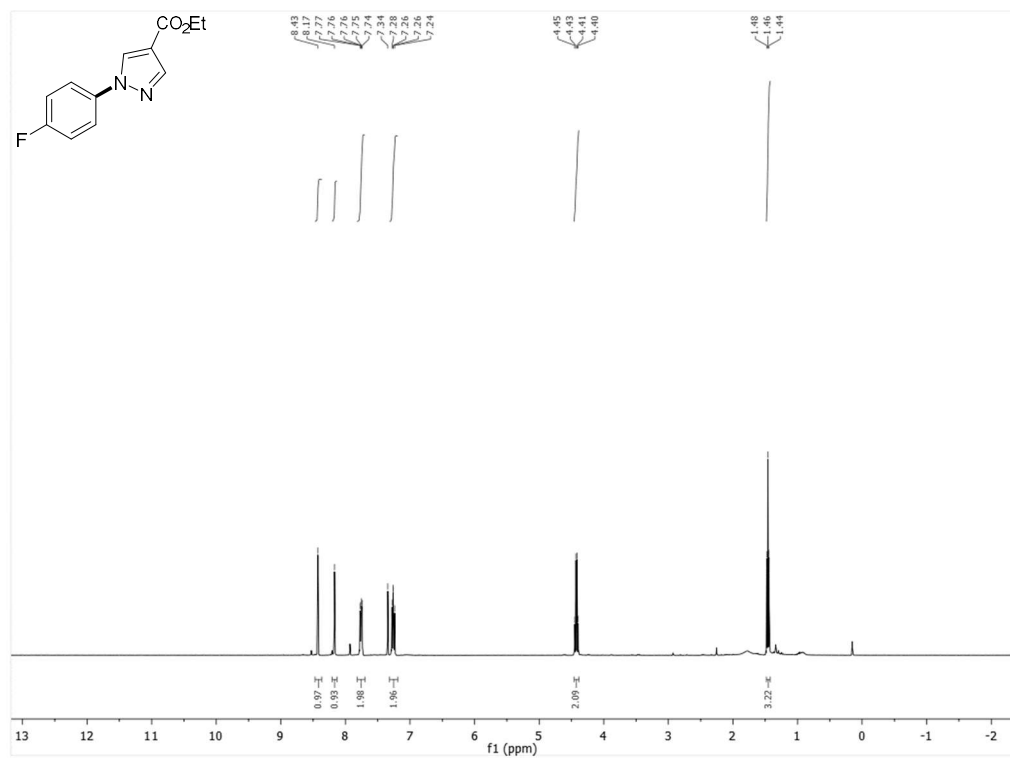
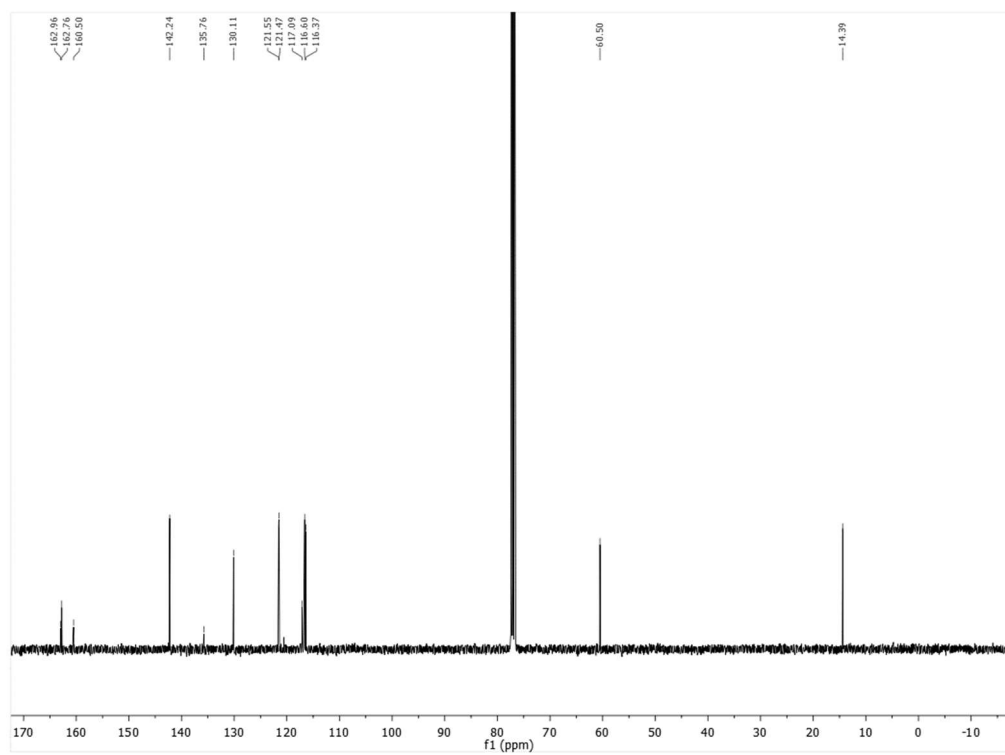
^{13}C NMR (75 MHz, CDCl_3) ^{19}F NMR (121 MHz, CDCl_3)

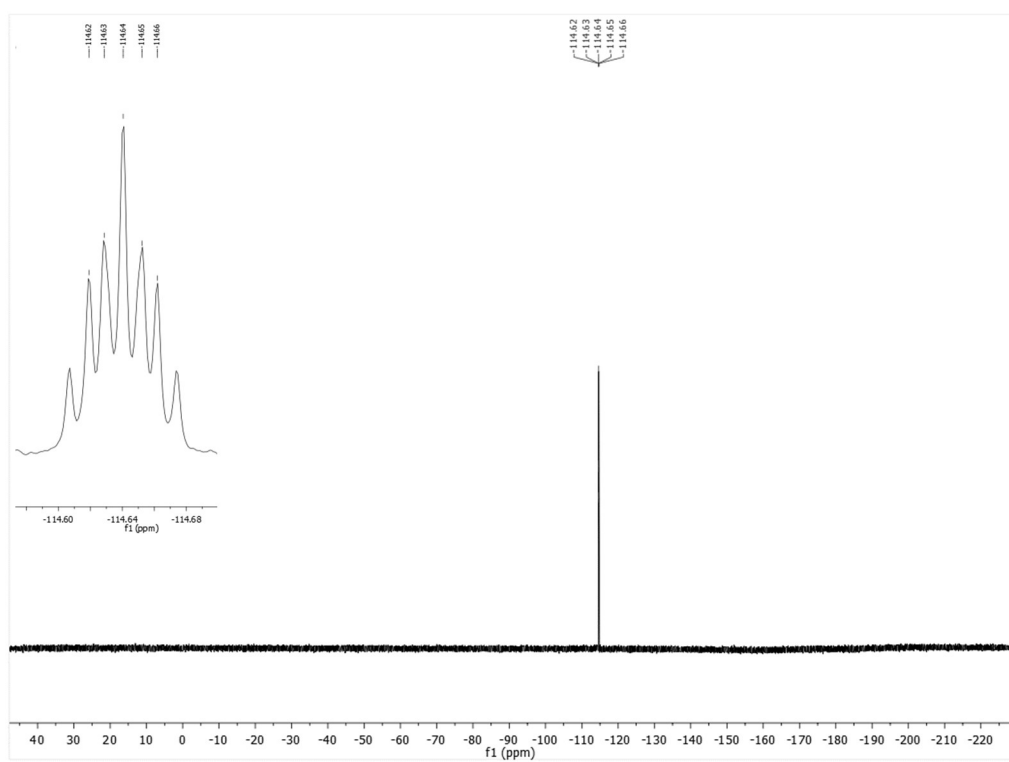
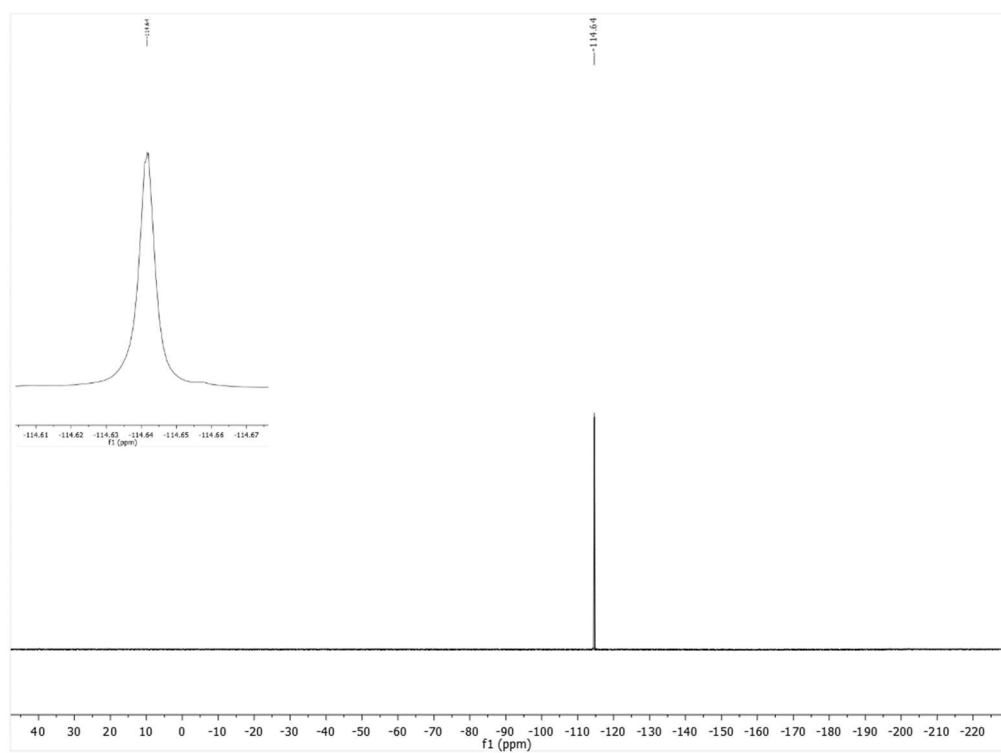
4,4,8,12,12-Hexamethyl-8,12-dihydro-4H-benzo[9,1]quinolizino[3,4,5,6,7-defg]acridine-2,6,10-tricarbonitrile (Cat B) ^1H NMR (400 MHz, CDCl_3) ^{13}C NMR (75 MHz, CDCl_3)

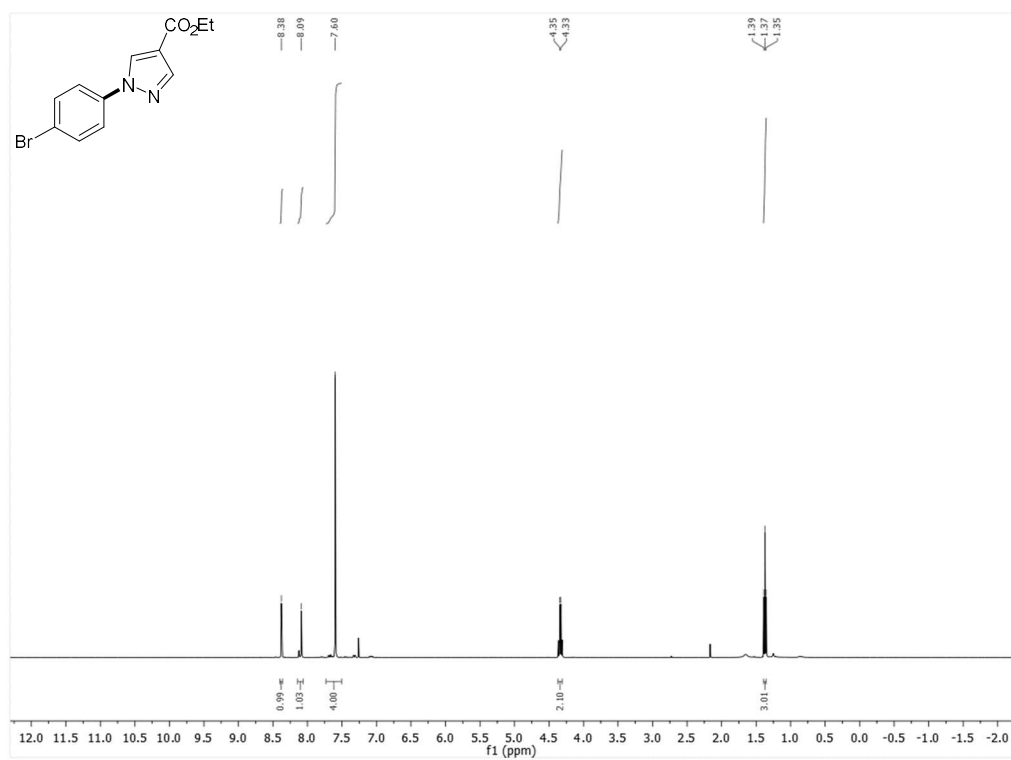
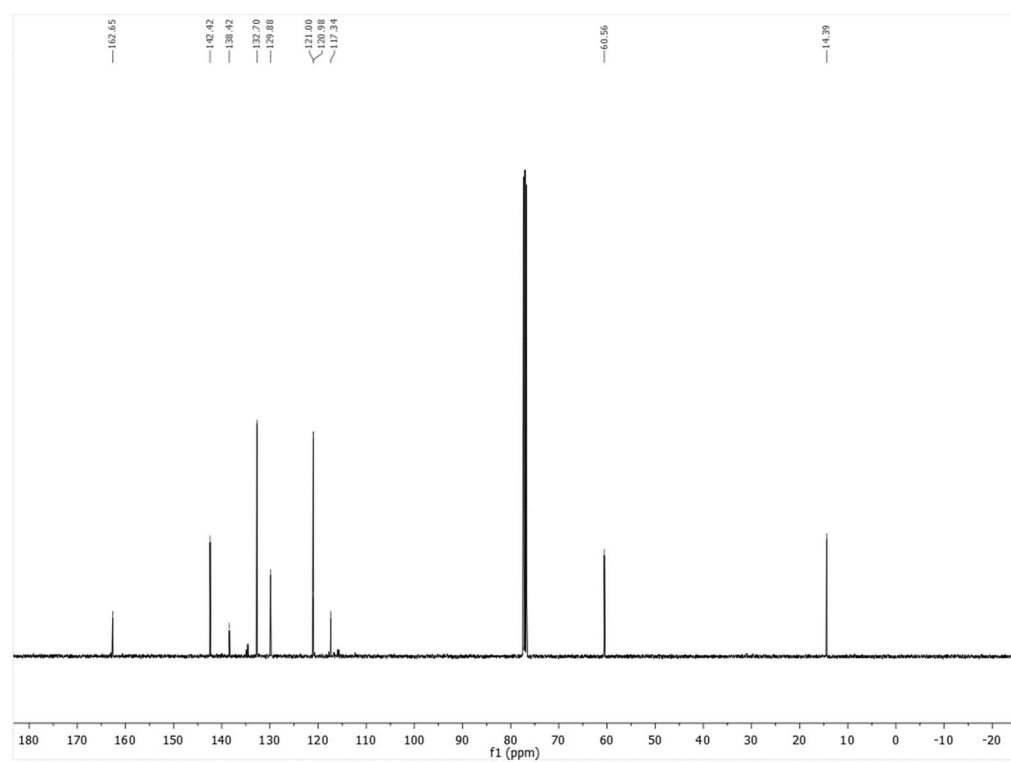
Ethyl 1-phenyl-1H-pyrazole-4-carboxylate (1a) ^1H NMR (300 MHz, CDCl_3) ^{13}C NMR (75 MHz, CDCl_3)

Ethyl 1-(4-chlorophenyl)-1H-pyrazole-4-carboxylate (1b) ^1H NMR (300 MHz, CDCl_3) ^{13}C NMR (75 MHz, CDCl_3)

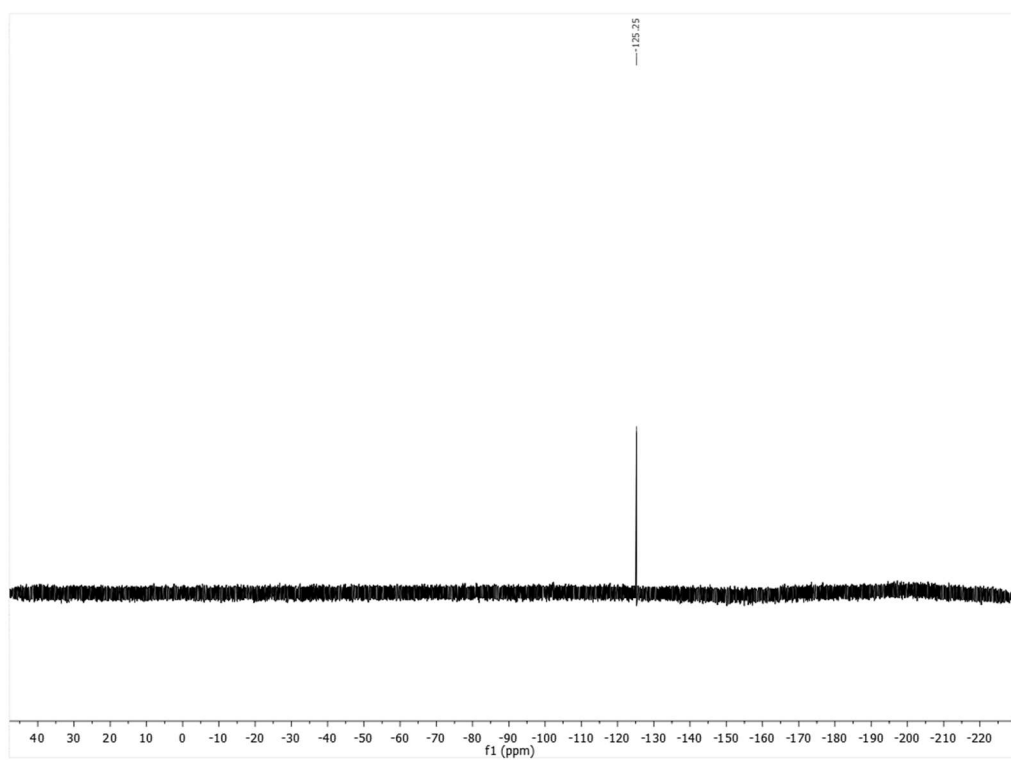
Ethyl 1-(2-chlorophenyl)-1H-pyrazole-4-carboxylate¹H NMR (300 MHz, CDCl₃)¹³C NMR (75 MHz, CDCl₃)

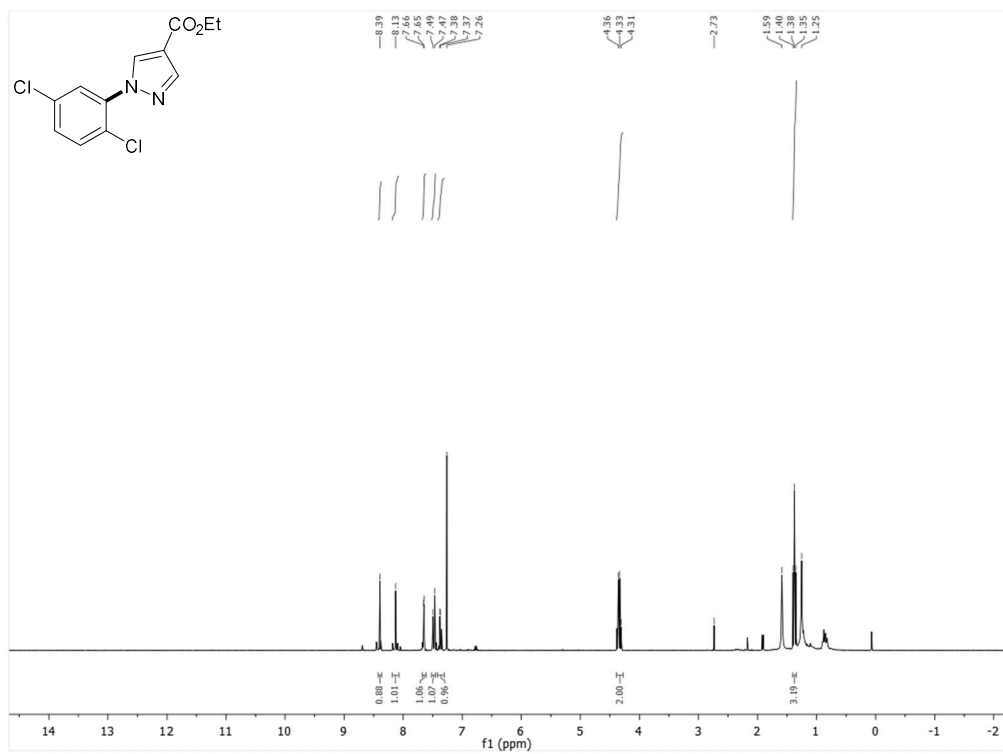
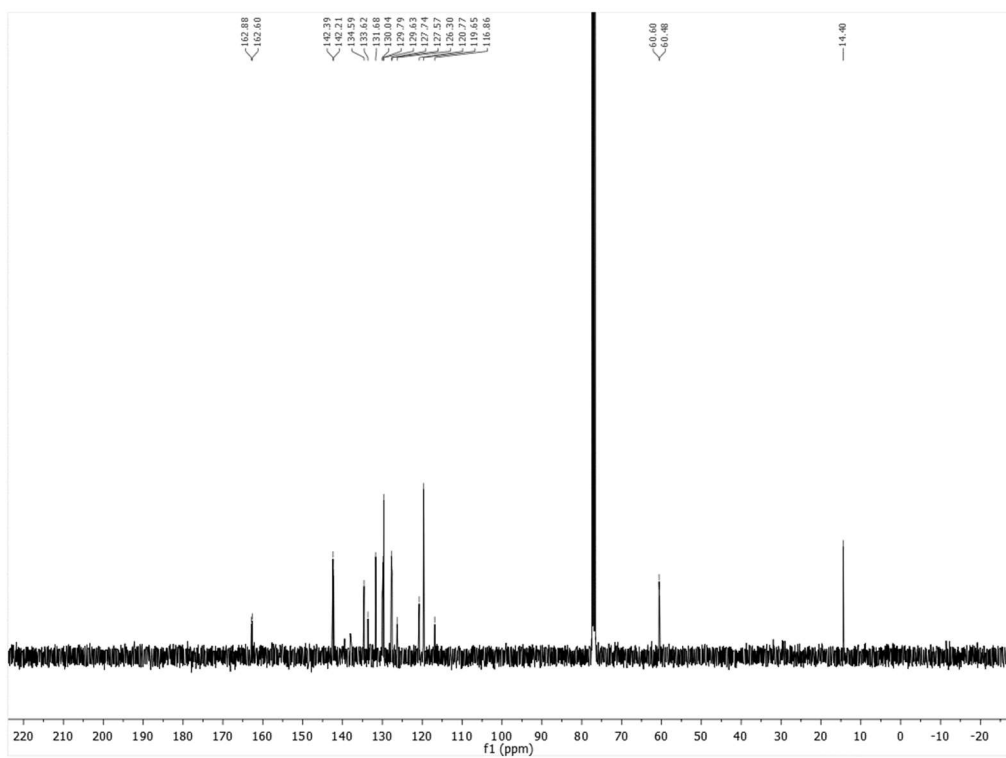
Ethyl 1-(4-fluorophenyl)-1H-pyrazole-4-carboxylate (1c)¹H NMR (400 MHz, CDCl₃)¹³C NMR (101 MHz, CDCl₃)

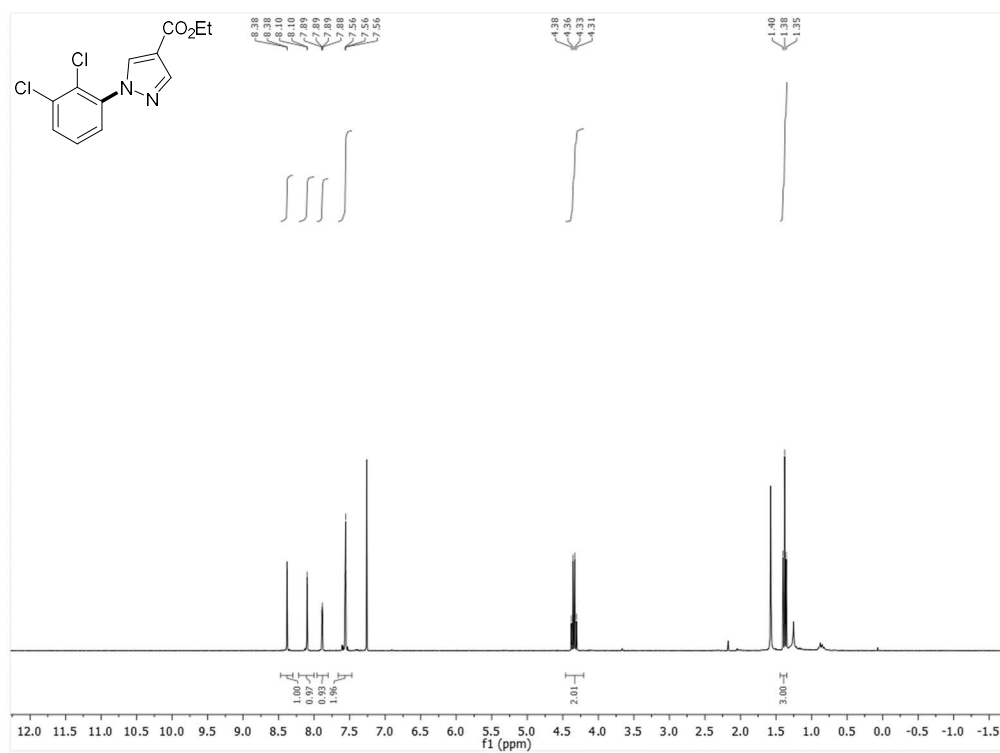
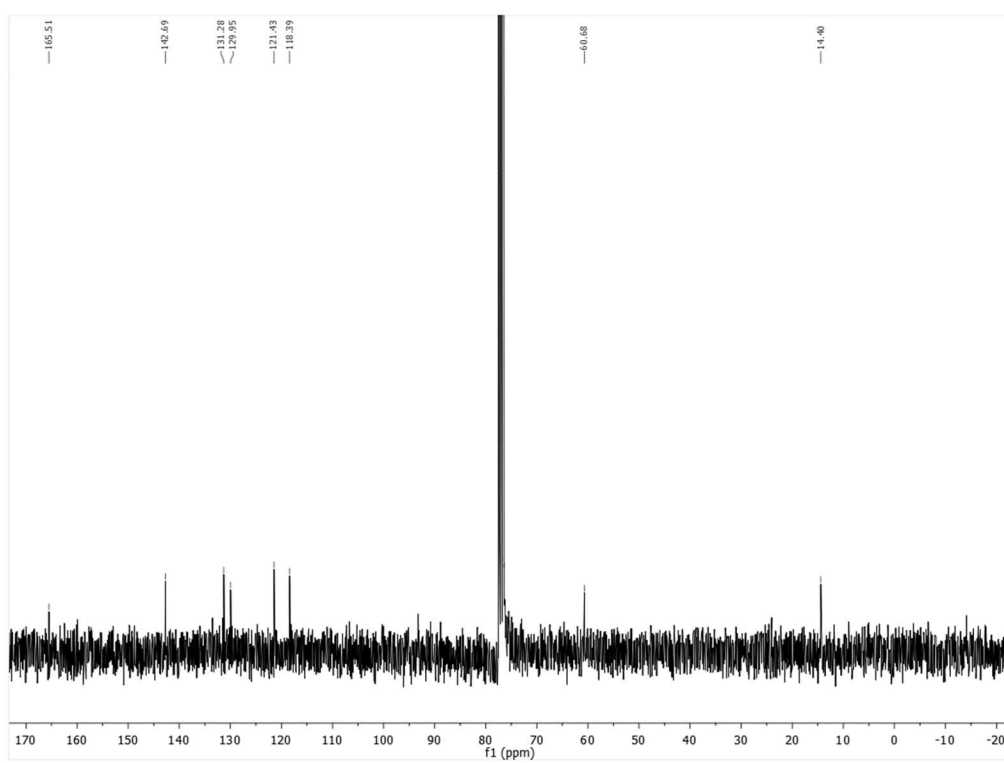
^{19}F NMR (376 MHz, CDCl_3) ^{19}F NMR (376 MHz, CDCl_3) $\{^1\text{H}\}$ 

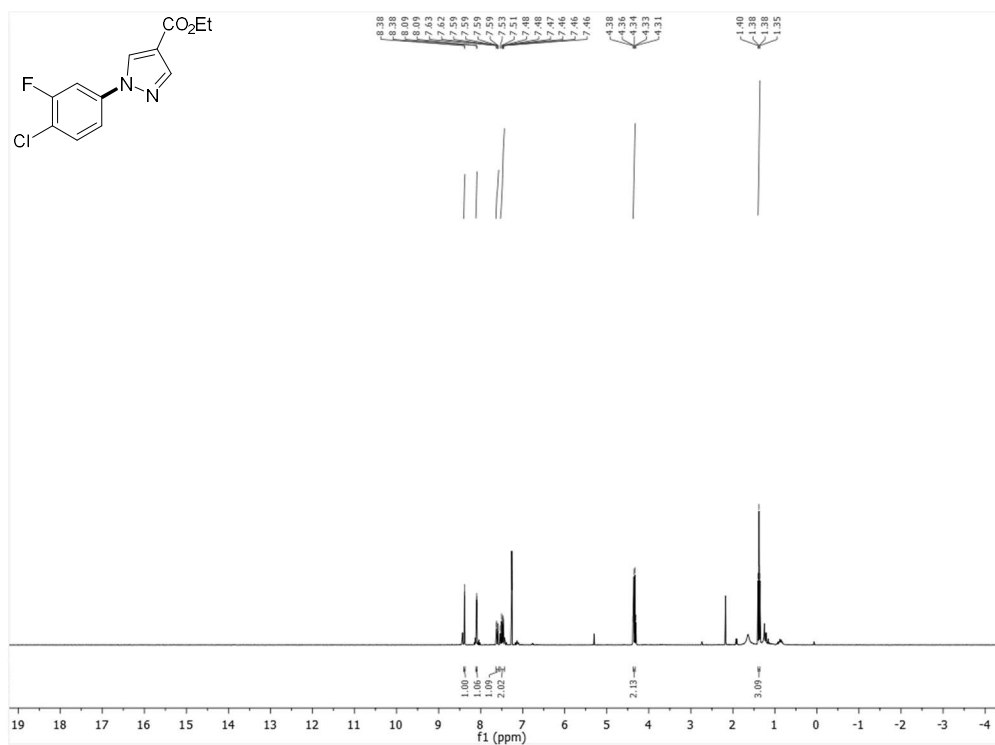
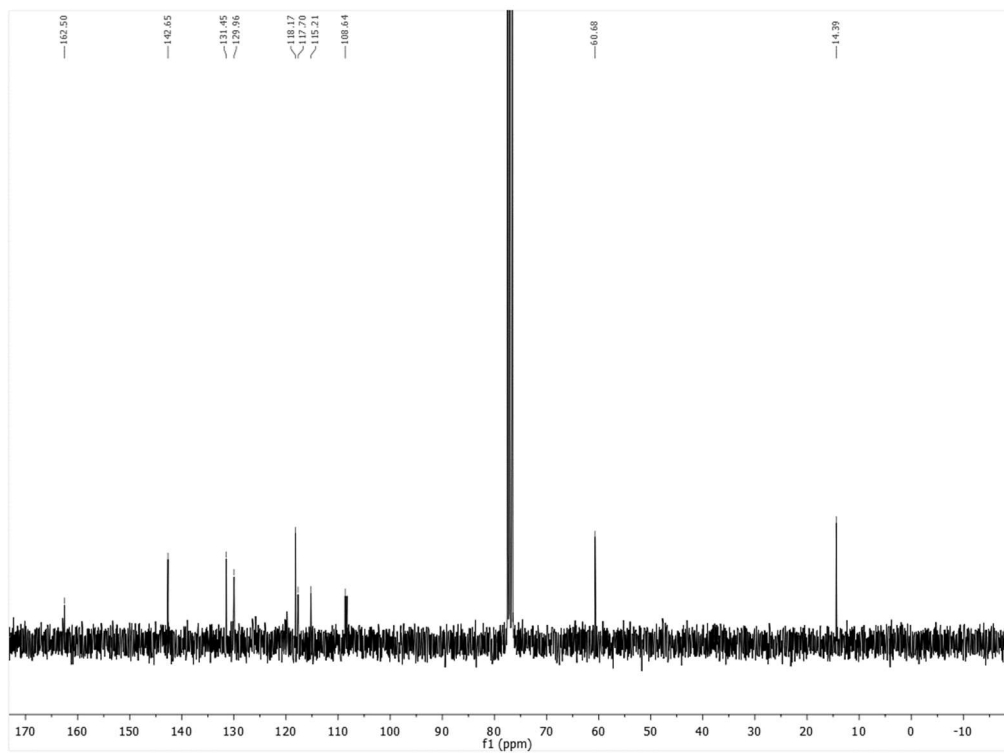
Ethyl 1-(4-bromophenyl)-1H-pyrazole-4-carboxylate (1d)¹H NMR (400 MHz, CDCl₃)¹³C NMR (101 MHz, CDCl₃)

^{19}F NMR (376 MHz, CDCl_3)

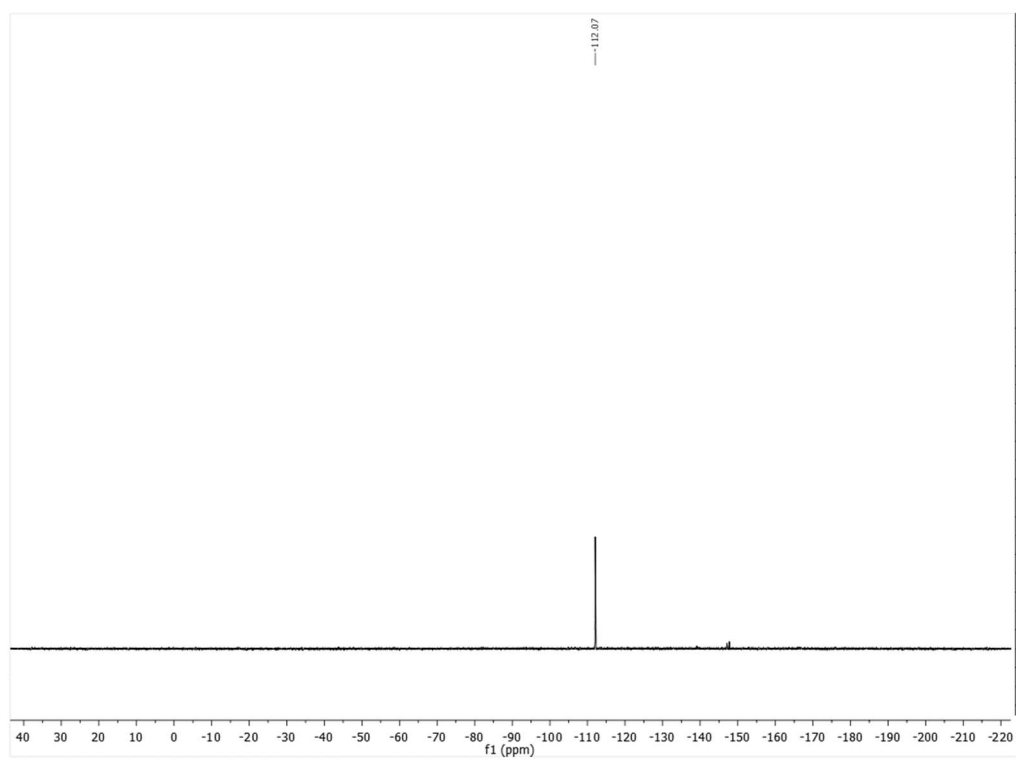


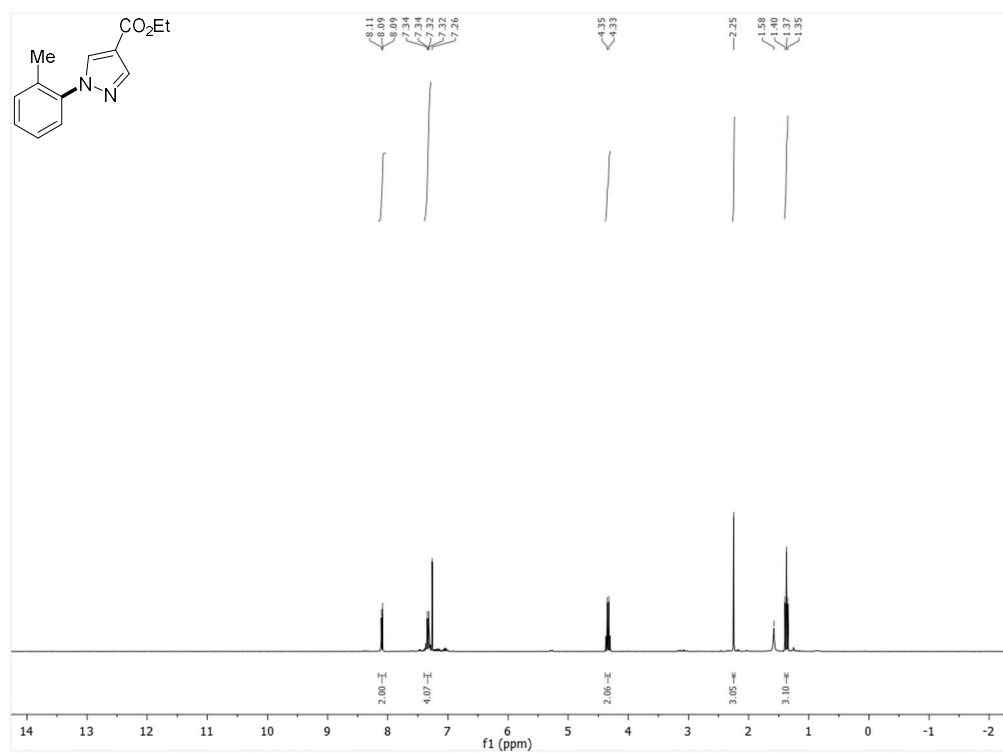
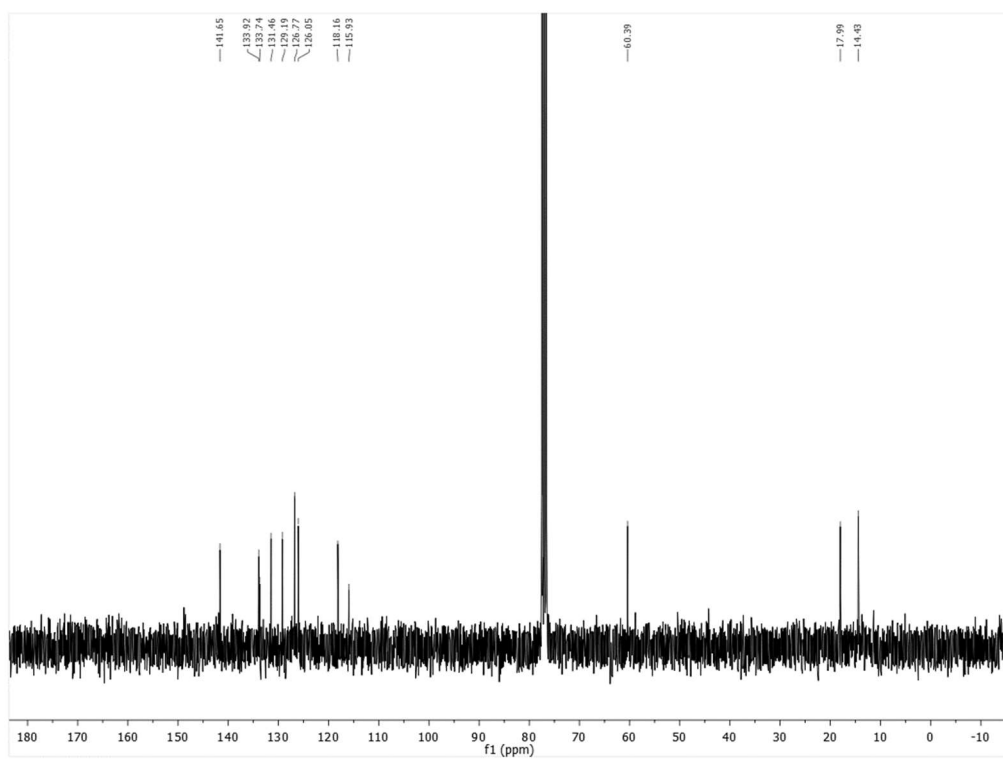
Ethyl 1-(2,5-dichlorophenyl)-1H-pyrazole-4-carboxylate (1f)¹H NMR (400 MHz, CDCl₃)¹³C NMR (101 MHz, CDCl₃)

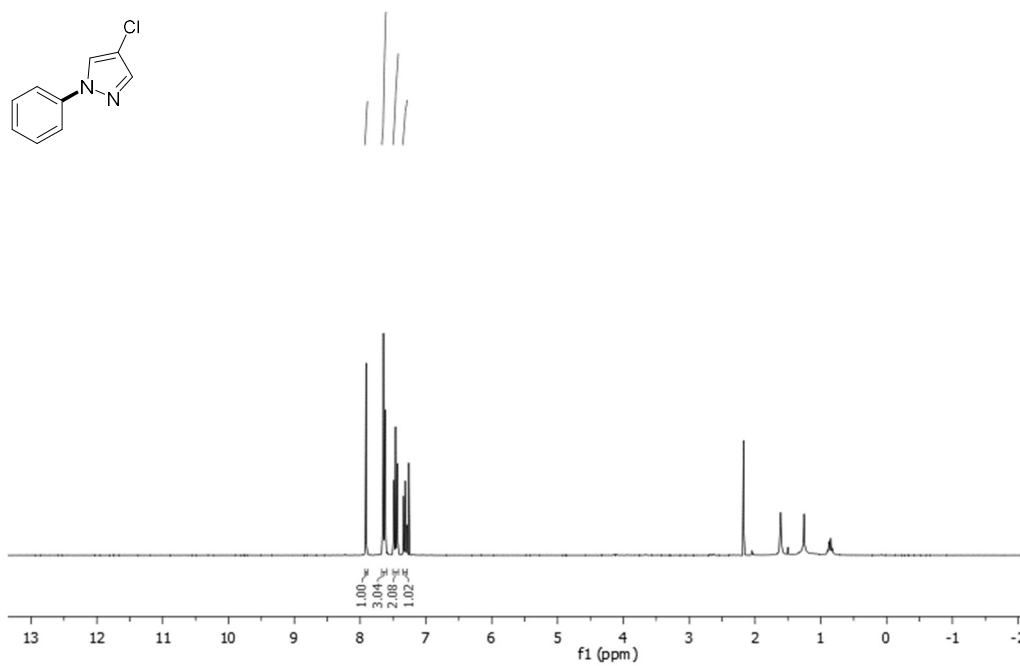
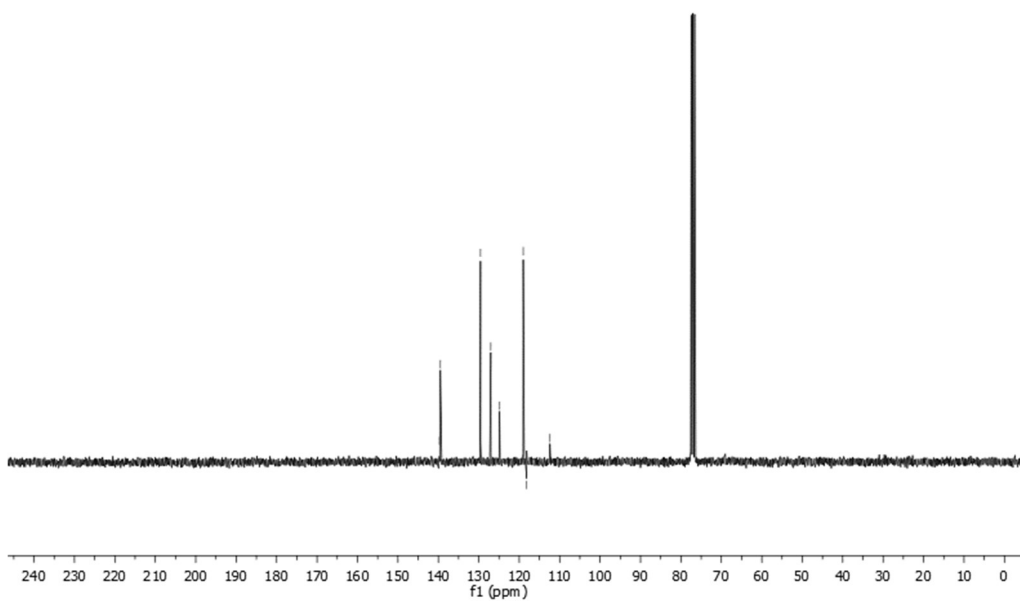
Ethyl 1-(2,3-dichlorophenyl)-1H-pyrazole-4-carboxylate (1g) ^1H NMR (300 MHz, CDCl_3) ^{13}C NMR (75 MHz, CDCl_3)

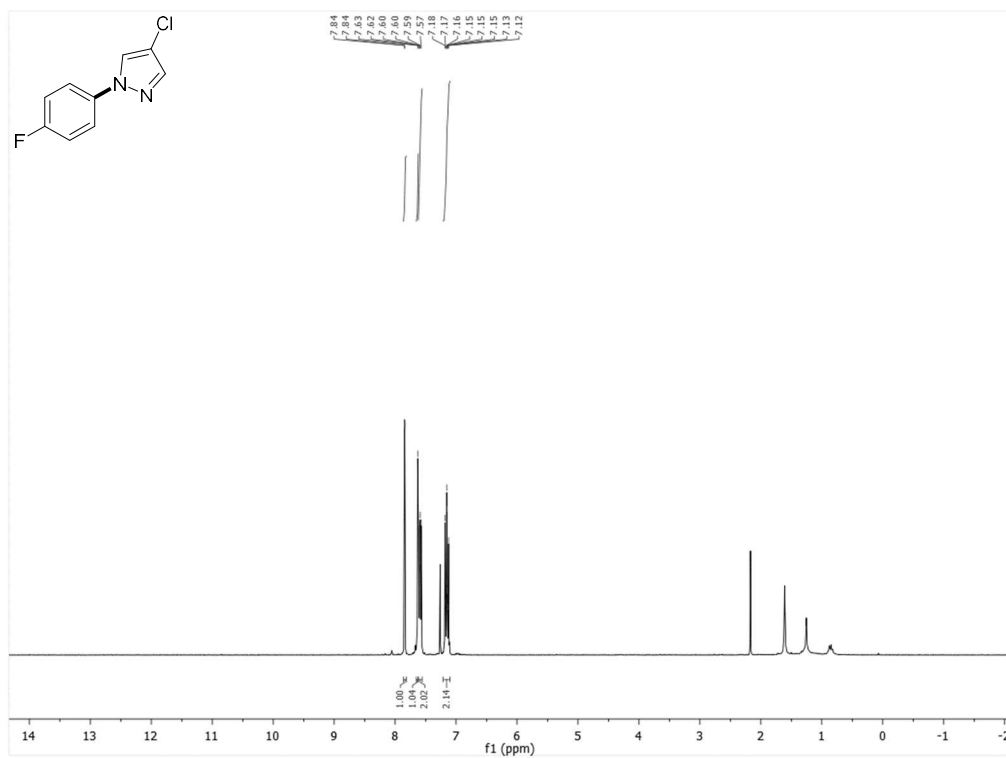
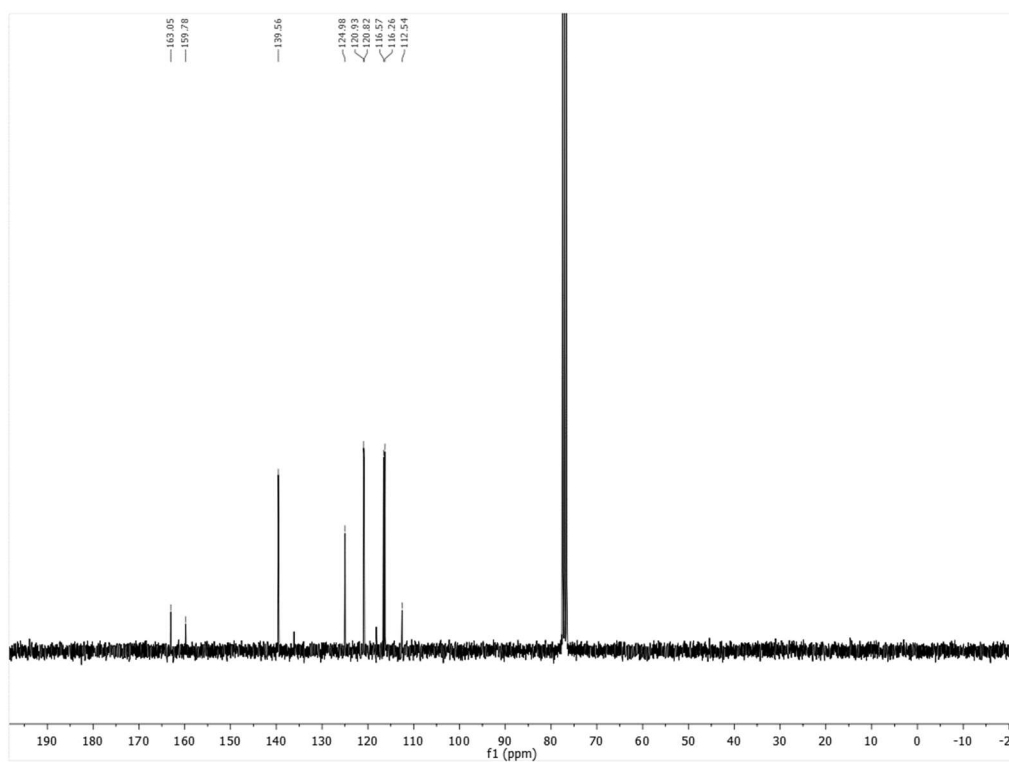
Ethyl 1-(4-chloro-3-fluorophenyl)-1H-pyrazole-4-carboxylate (1h)¹H NMR (300 MHz, CDCl₃)¹³C NMR (101 MHz, CDCl₃)

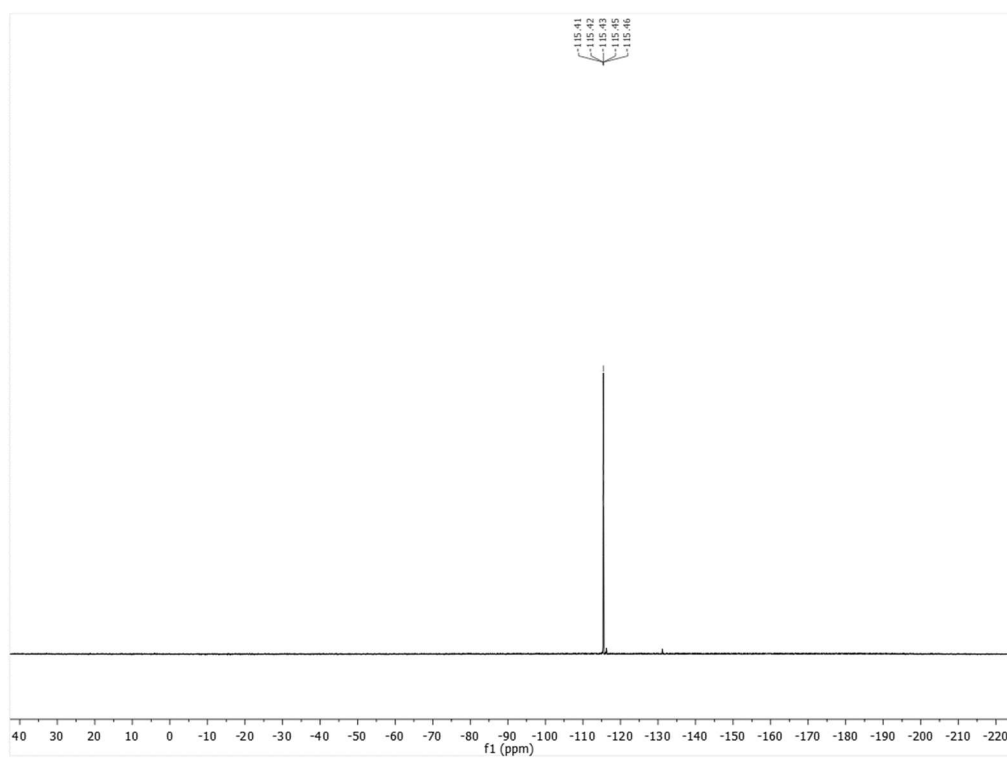
^{19}F NMR (282 MHz, CDCl_3)

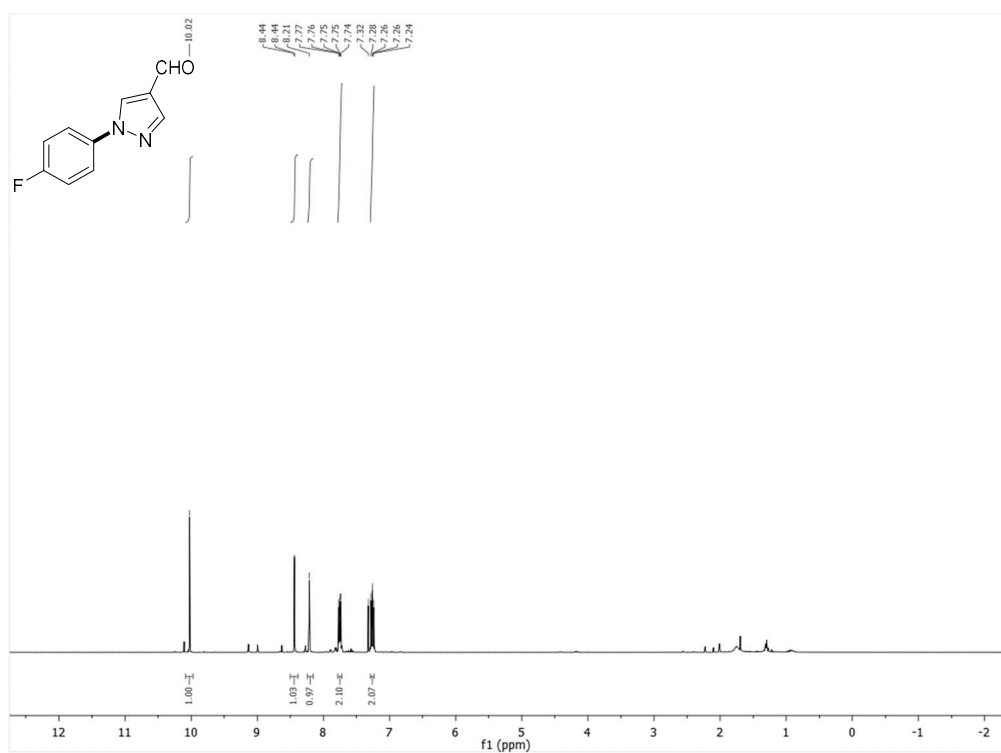
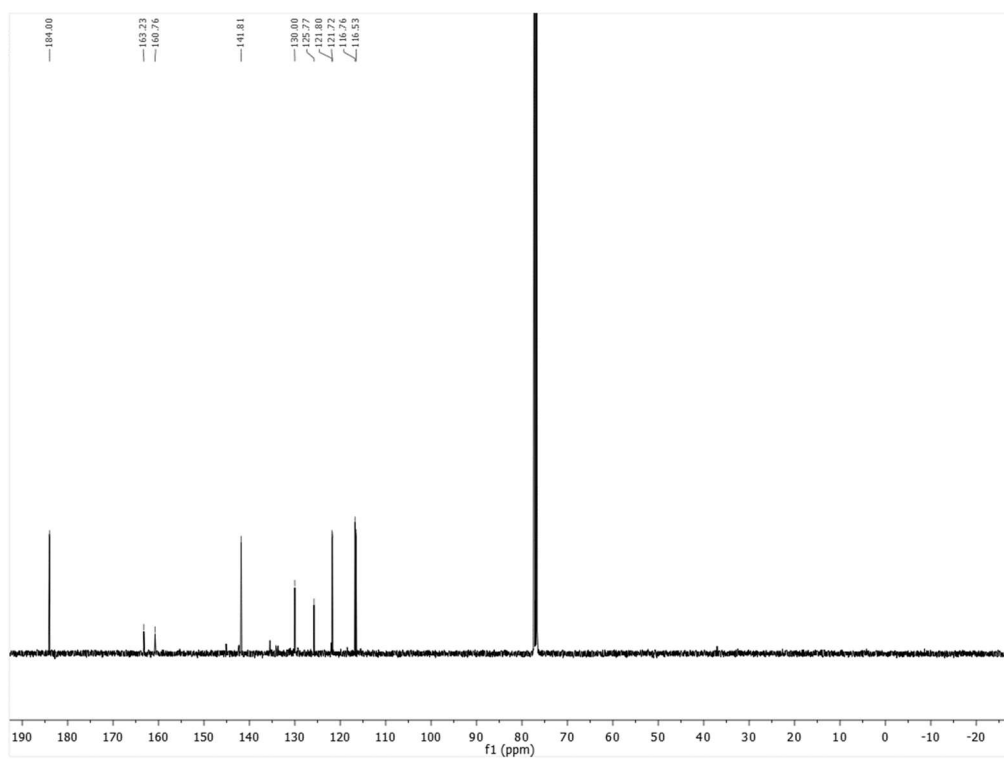


Ethyl 1-(o-tolyl)-1H-pyrazole-4-carboxylate (1i) ^1H NMR (300 MHz, CDCl_3) ^{13}C NMR (75 MHz, CDCl_3)

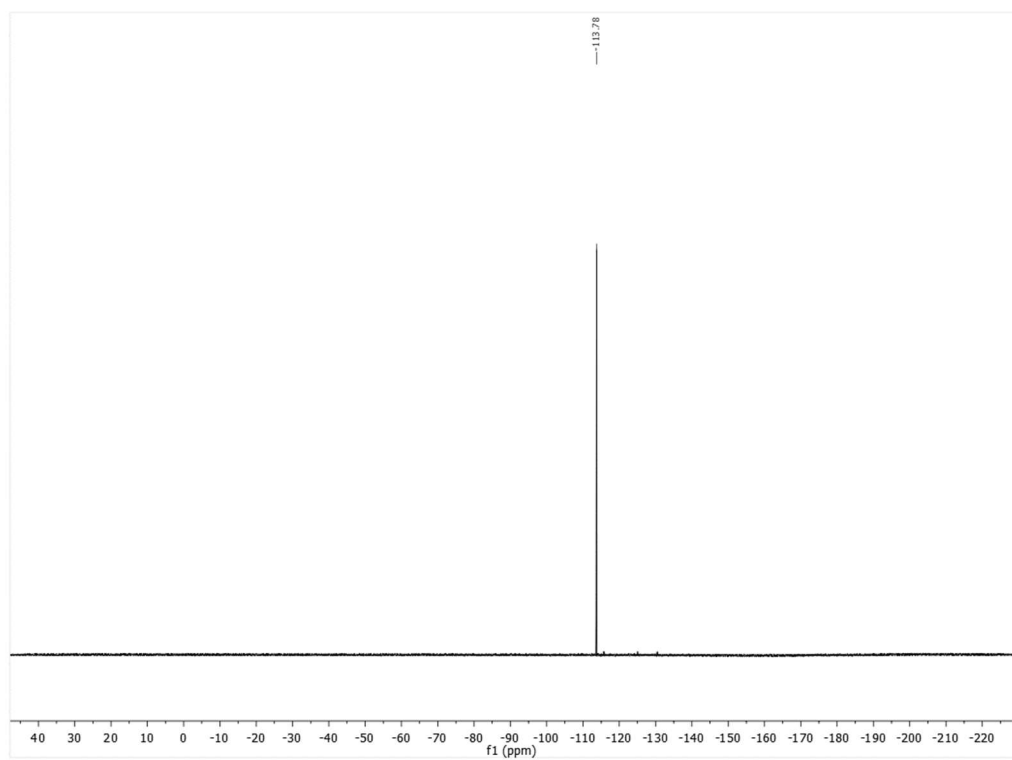
4-Chloro-1-phenyl-1H-pyrazole (2a) ^1H NMR (300 MHz, CDCl_3) ^{13}C NMR (75 MHz, CDCl_3)

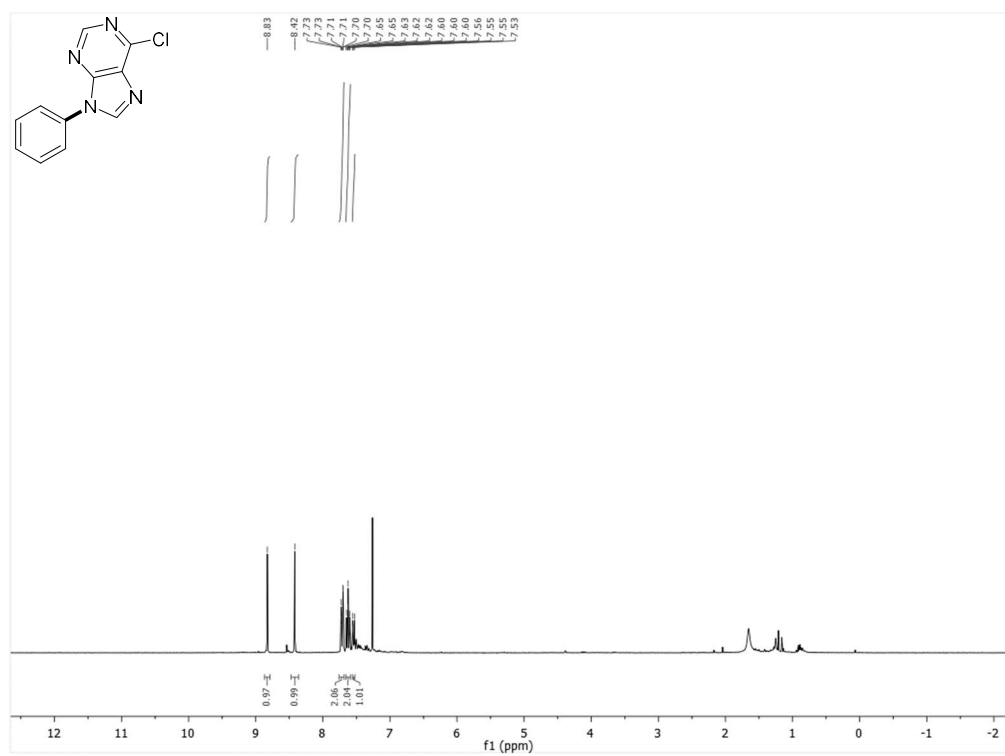
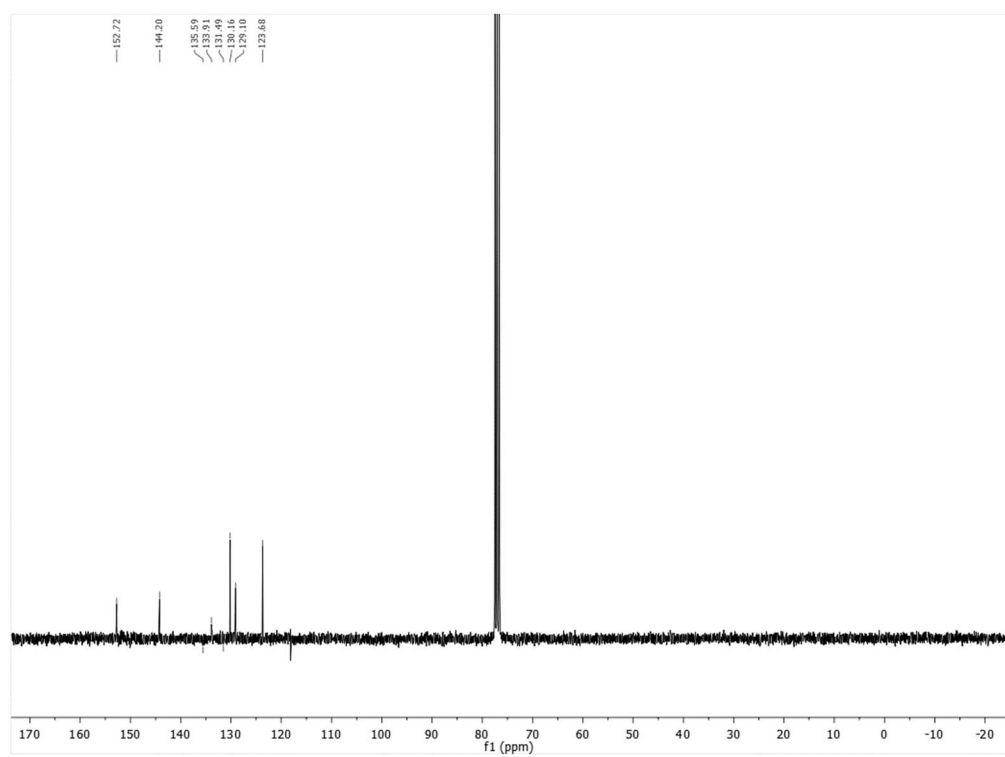
4-Chloro-1-(4-fluorophenyl)-1H-pyrazole (2b)¹H NMR (400 MHz, CDCl₃)¹³C NMR (75 MHz, CDCl₃)

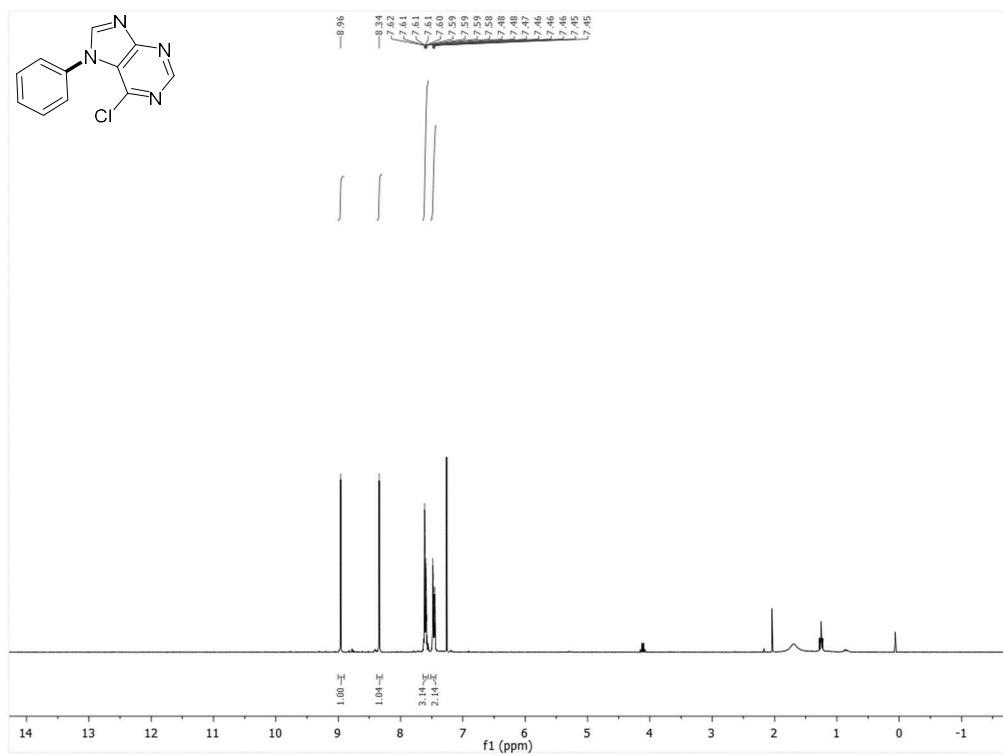
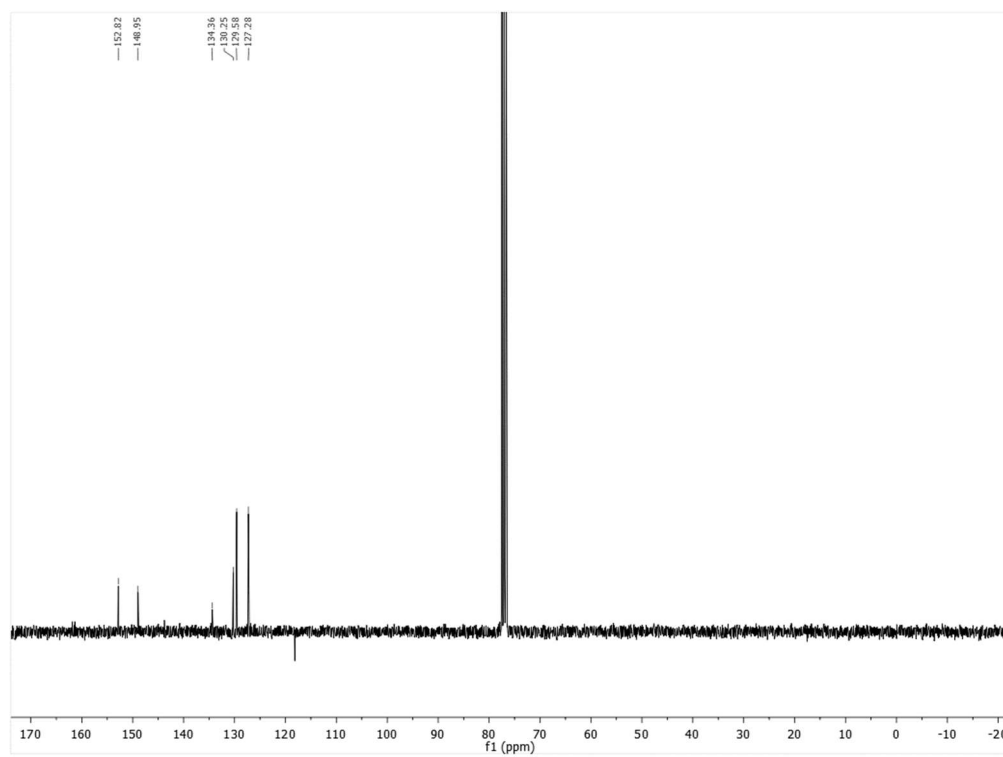
^{19}F NMR (282 MHz, CDCl_3)

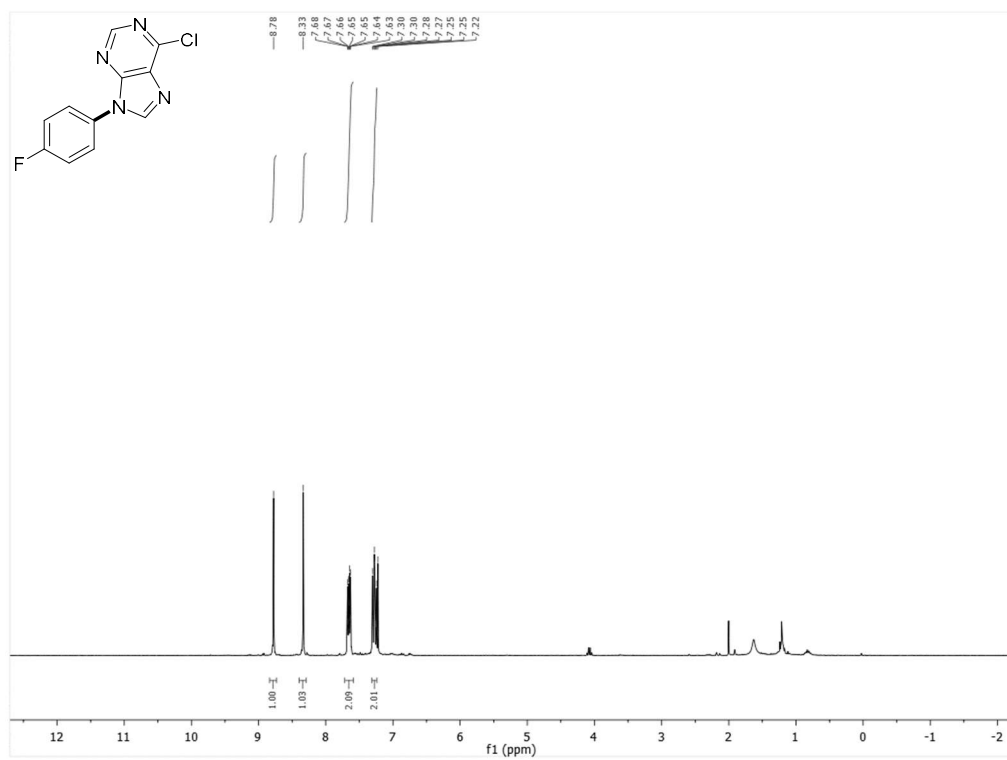
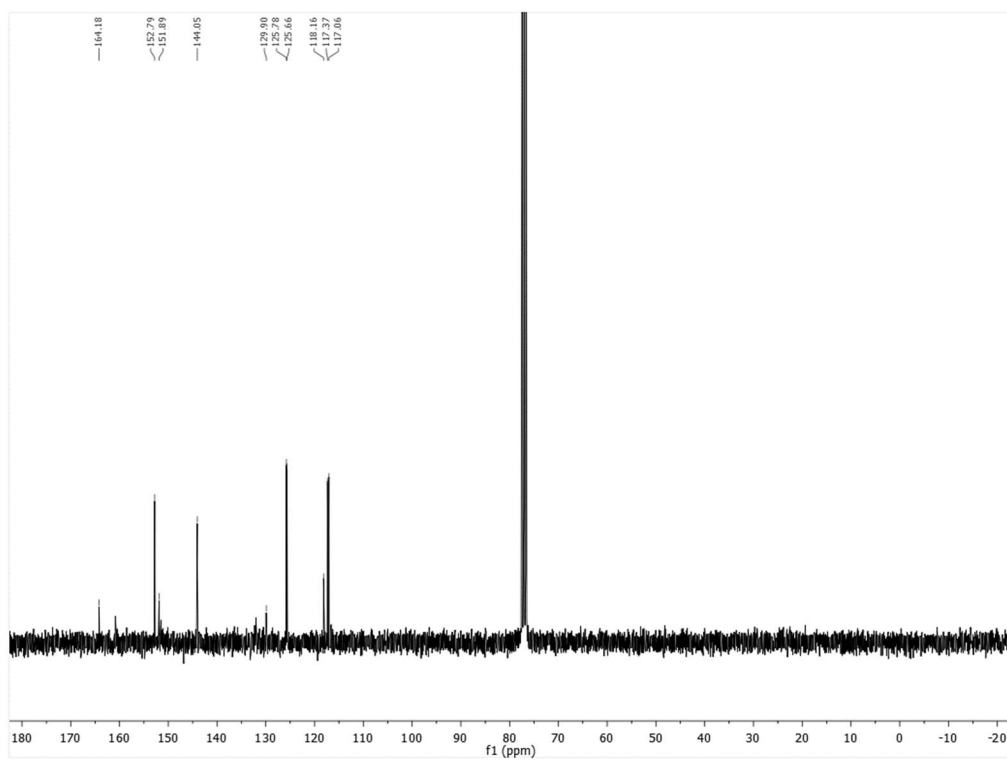
1-(4-Fluorophenyl)-1H-pyrazole-4-carbaldehyde (2c) ^1H NMR (400 MHz, CDCl_3) ^{13}C NMR (75 MHz, CDCl_3)

^{19}F NMR (282 MHz, CDCl_3)

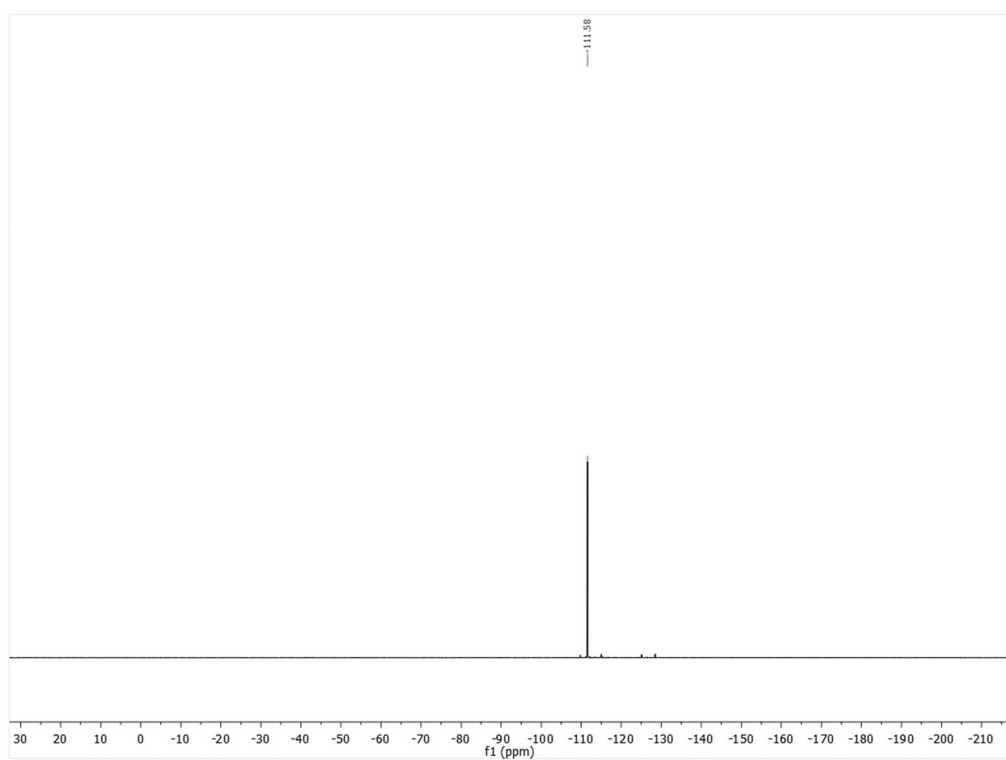


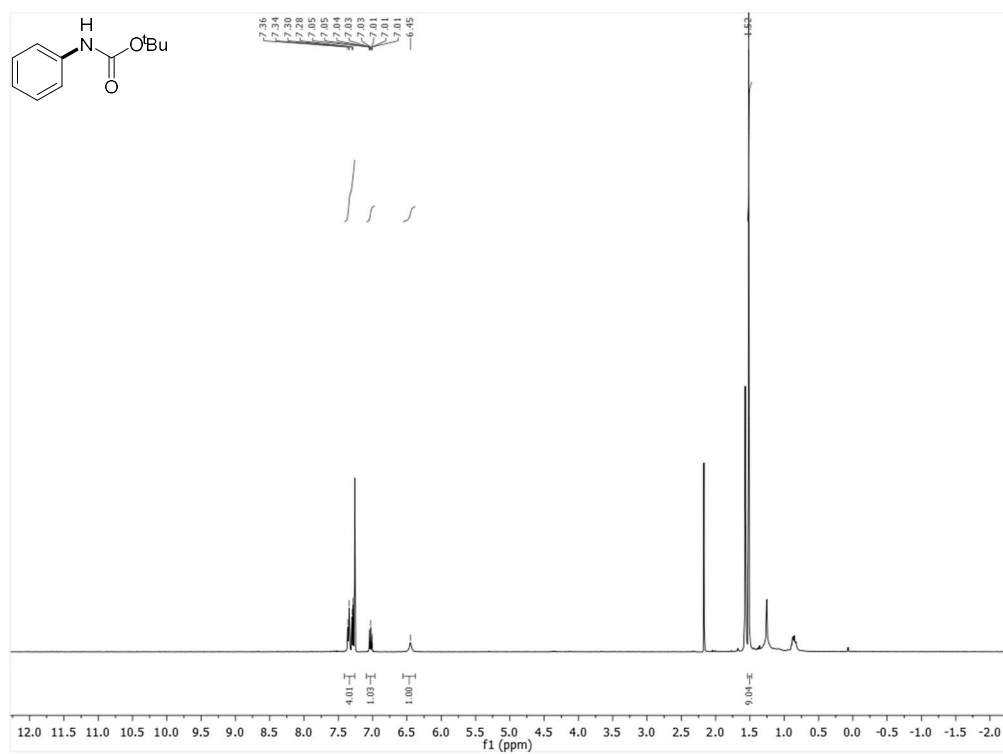
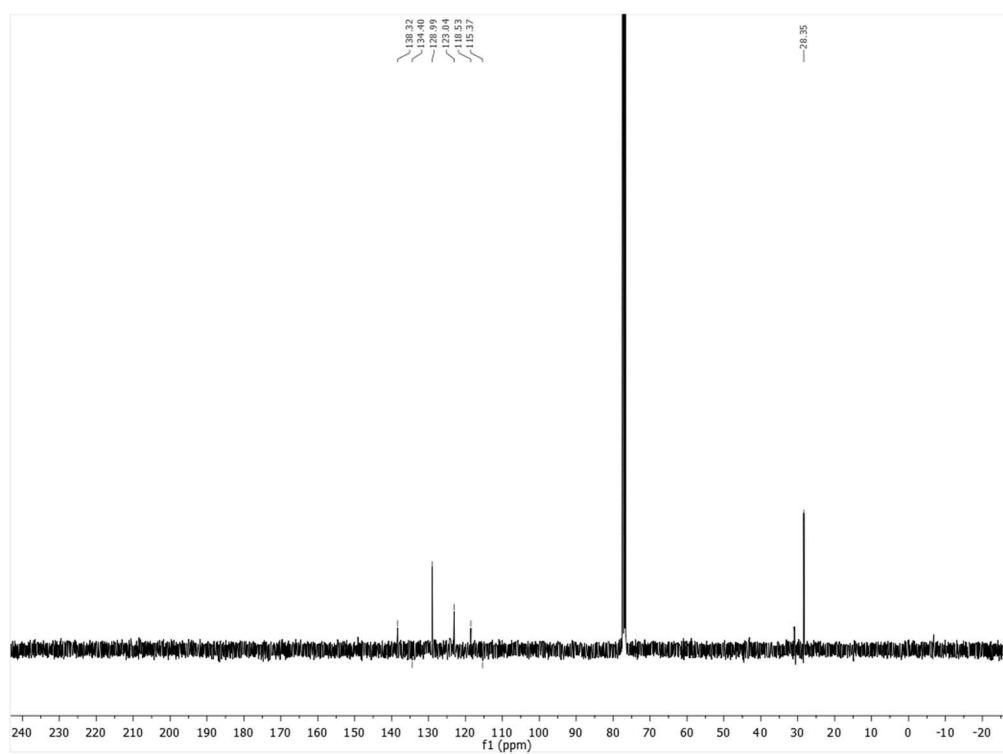
6-Chloro-9-phenyl-9H-purine (2d) ^1H NMR (300 MHz, CDCl_3) ^{13}C NMR (75 MHz, CDCl_3)

6-Chloro-7-phenyl-7H-purine ^1H NMR (300 MHz, CDCl_3) ^{13}C NMR (75 MHz, CDCl_3)

6-Chloro-9-(4-fluorophenyl)-9H-purine (2e) ^1H NMR (300 MHz, CDCl_3) ^{13}C NMR (75 MHz, CDCl_3)

^{19}F NMR (282 MHz, CDCl_3)



***tert*-Butyl phenylcarbamate (2f)** ^1H NMR (400 MHz, CDCl_3) ^{13}C NMR (101 MHz, CDCl_3)

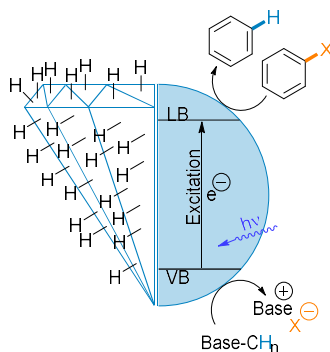
4.6.9 References

- [1] Z. Fang, V. Chellappan, R. D. Webster, L. Ke, T. Zhang, B. Liu, Y.-H. Lai, *J. Mater. Chem.* **2012**, *22*, 15397–15404.
- [2] J. S. Ward, N. A. Kuhta, P. L. dos Santos, D. G. Congrave, A. S. Batsanov, A. P. Monkman, *Chem. Mater.* **2019**, *31*, 6684–6695.
- [3] W. Yang, J. Wang, H. Wang, Z. Bao, J. C.-G. Zhao, B. Chen, *Cryst. Growth Des.* **2017**, *17*, 6132–6137.
- [4] R. J. Kutta - Blitzlichtphotolyse - *Untersuchung zu LOV-Domänen und photochromen Systemen*. Dissertation, Universität Regensburg, **2012**.
- [5] T. Pavlovska, D. Král Lesný, E. Svobodová, I. Hoskovcová, N. Archipowa, R. J. Kutta, R. Cibulka, *Chem. Eur. J.* **2022**, *28*, e202200768.
- [6] R. J. Kutta, T. Langenbacher, U. Kensity, B. Dick, *Appl. Phys. B*, **2013**, *111*, 203–216.
- [7] R. J. Kutta, U. Kensity, B. Dick, *Transient Absorption. in Chemical Photocatalysis* (ed. B. König) 295–318 (De Gruyter, **2013**).
- [8] K. Lanzl, M. v. Sanden-Flohe, R. J. Kutta, B. Dick, *Phys. Chem. Chem. Phys.*, **2010**, *12*, 6594–6604.
- [9] Neese, F., *WIREs. Comput. Mol. Sci.*, **2012**, *2*, 73–78.
- [10] Neese, F., *WIREs Comput. Mol. Sci.*, **2018**, *8*, e1327.
- [11] H. Huang, Z. M. Strater, M. Rauch, J. Shee, T. J. Sisto, C. Nuckolls, T. H. Lambert, *Angew. Chem. Int. Ed.* **2019**, *58*, 13318
- [12] J. Comas-Barceló, R. S. Foster, B. Fiser, E. Gomez-Bengoa, J. P. A. Harrity, *Chem. Eur. J.* **2015**, *21*, 3257–3263.
- [13] F. S. Byanca, S. C. Rafaela, S. A. Bernardo, M. dos Santos Silva, *Lett. Org. Chem.* **2021**, *18*.
- [14] J. C. Antilla, J. M. Baskin, T. E. Barder, S. L. Buchwald, *J. Org. Chem.* **2004**, *69*, 5578–5587.
- [15] B. S. Gerstenberger, M. R. Rauckhorst, J. T. Starr, *Org. Lett.* **2009**, *11*, 2097–2100.
- [16] L. E. Evans, M. D. Cheeseman, K. Jones, *Org. Lett.* **2012**, *14*, 3546–3549.
- [17] H. Lebel and O. Leogane, *Org. Lett.* **2006**, *8*, 5717–5720.

After two examples of homogeneous catalysis, we looked at heterogeneous approaches. To generate extreme redox potentials, the band structure of the semiconductor material must meet certain criteria. With hydrogen-terminated nanodiamonds (DND-H) we got our hands on a promising material. Chapter 5 shows how it can be successfully used in photocatalysis.

CHAPTER 5

5 Arene Hydrodehalogenation by Hydrogen-Terminated Diamond Semiconductor and Visible Light



This chapter has not been published. The manuscript for peer review is in preparation.
Authors listed: T. A. Karl, A. Krueger, B. Koenig.

All experiments were performed by T. A. Karl.

5.1 Abstract

Diamond semiconductors are promising materials to engage in redox reactions. Boron doping and surface termination offer a variety of options to tune the material for specific applications. Already established in electrochemistry, the use of diamond in photoredox catalysis has not yet been studied in detail. Herein, we report that hydrogen-terminated detonation nanodiamond (DND-H) shows photoredox activity, giving access to redox potentials of about 3 V (*vs* SCE). Irradiated at 395 nm it mediates the dehalogenation of electron-rich aryl halides *via* a radical mechanism, which makes DND-H suitable for the catalytic dehalogenation of dioxins, PCB's and pesticides. The diamond catalyst material is available on kilogram scale, can be recovered by a simple centrifugation and reused at least five times.

5.2 Introduction

Diamond materials have found applications in organic electrochemistry^[7] and photoelectrocatalysis.^[8] The chemical inertness and its mechanical strength make the carbon allotrope special. The most common modification, doping with boron or nitrogen, transforms the insulator into a semiconductor^[9] with applications ranging from electrode material for organic transformations^[10–12] and analytics^[13] to the use in electrical components like capacitors^[14] or transistors^[15,16]. Alternatively, the material properties are manipulated by nanostructuring and surface modification.^[17–19] Generated *via* blast, such detonation nanodiamonds (DND)^[20] most commonly undergo a hydrogen termination, even though alcohol, ketone, or acid functionalities are easy to access.^[21] The reason is that hydrogen-terminated nanodiamonds (DND-H) exhibit unique negative electron affinity and high p-type surface conductivity.^[22,23] Optically, the properties change in such a way that a transparency peak between zone-center optical phonon and free carriers (holes) at 1328 cm⁻¹ (Fano-type effect)^[24] is created. Defects in bulk and surface, uncomplete termination, surface roughness and ionic adsorbates create electronic disorder in the 2D-system which decreases the resistance by four orders of magnitude^[25] and thereby enables the photoemission of electrons.^[22,26–29] With an absorption at 395 nm, DND-H provides a theoretical redox potential of -3.2 eV, representing one of the most negative values known in photoredox catalysis.^[30] To our knowledge only Mes-Acr* (-2.9 V respectively -3.36 V vs SCE) can provide a similar reduction power, which has been proven experimentally by reductive hydrodehalogenation of electron-rich arenes.^[30] Polychlorinated biphenyls (PCBs), Dioxins and several halide-bearing pesticides are, even though some of them are long banned, a current issue.^[31,32] Due to their persistency, those toxins^[33] bioaccumulate within the food chain and new decontamination processes including physical^[34] photo-^[30,35] and electrochemical^[36] processes are in demand.^[35,37–43] Harsh conditions including high temperature,^[39,40,43] the use of sodium hydride,^[39] high H₂-pressure^[40] or the need for a metal catalyst^[35,37,38,40–43] should be avoided and light-driven dehalogenation may be considered as a valuable alternative.

5.3 Results and Discussion

With a more negative potential than -2.7 V vs. SCE,^[30] 1-bromo-4-tert-butylbenzene is at the upper limit of the redox window of DND-H and was therefore chosen to act as standard substrate (Table 1). Under optimized conditions, 30% of tert-butylbenzene **2a** can be obtained within 16 h, and 50 % within 48 h. Light, DND-H and a sacrificial electron donor (SED) are indispensable. The standard conditions were fixed to a high concentration of substrate (400 μ mol, 0.8 M). Higher dilution (400 μ mol, 0.4 M) significantly reduces the yield (18%), whereas a lower addition of SM (200 μ mol, 0.4 M) has hardly any effect (36%). The amount of catalyst was set to 3 mg, as smaller quantities are both difficult to weigh and deliver slightly lower yields (Table S1). A catalyst loading of 5 mg or more decreases the yield (20%) drastically, most probably by blocking light from entering the suspension. Light of shorter wavelength (365 nm) can directly excite various aromatic compounds, leading to uncontrollable side reactions.^[44] Longer wavelengths (455 nm) are not energetic enough to excite an electron into the conducting band of the semiconductor – no reaction occurs (Table S2). Out of all the organic and inorganic bases tested (Table S3), DIPEA worked best when added in two equivalents. Although previous work on boron-doped diamond reported the formation of solvated electrons in water,^[45] no productive dehalogenation was observed. In general, organic aprotic solvents are more suitable than protic solvents for this reaction (Table S4). The atmosphere must be free of oxygen, since the yield decreases with an increasing proportion of oxygen (Table S5).

Table 1. Reaction conditions & control reactions^a

Entry	Deviation from standard conditions	Yield /% ^b
1	non	30
2	48 h	50
3	no catalyst	-
4	no DIPEA	-
5	dark	-
6	DIPEA (2.5 equiv.)	31
7	NEt ₃ (2.0 equiv.)	14
	1 mL ACN (0.4M)	18
8	0.5 mL ACN (0.4 M)	36

^a Reaction condition: **1a** (0.4 mmol), DIPEA (0.8 mmol), DND-H (3 mg), ACN (0.5 mL), 395 nm LED (2 W), 25°C, 16 h, N₂. ^b Yield was determined by GC-FID analysis against n-heptane as an internal standard.

The scope of the reaction was investigated for various aryl halides, mainly focusing on bromides and chlorides (Figure 2). In most cases, fair to excellent yields were obtained after 48 h. Within the series of aryl halides (**1at**, **1au**, **1av** respectively **1f**, **1g**, **1h**), iodides are the most reactive species, followed by bromides and chlorides. As expected, the electron-donating or -withdrawing nature of the substituent influences the redox potential and thus the reaction outcome as follows:

Benzonitriles (**1ae**, **1af**) as well as aryl halides bearing a trifluoromethyl functionality (**1r**, **1s**) are easier to reduce and exhibit higher yields than electron-rich (**1a** to **1m**) substrates. For alkyl-substituted substrates, ortho-bromides exhibit higher yields than their meta counterpart (**1b**, **1c**). This known trend is evident for electron-rich aromatics. Examples **1g** and **1i** use anisoles to show the preference for the para position over the meta position. In addition to alkyl-substituted aryl bromides (**1a**, **1c**, **1d**), anisoles (**1f**, **1j**, **1k**, **1l**, **1m**), diphenyl ether (**1n**) (84%), thioether (**1t**) (93%) and trifluoromethyl ether (**1q**) (65%) are converted in mostly fair to very good yields. The corresponding chloro- variants (**1g**, **1i**, **1o**, **1u**, **1w**) give poor to fair yields. Examples **1l** and **1n** illustrate the preference for benzylic bromides over aryl bromides. In presence of two leaving groups, only the benzylic halide was cleaved. Larger aromatics such as naphthalenes (**1x**, **1y**) and biphenyls (**1aa** to **1ad**) are hydrodehalogenated in good to quantitative yields. Even the double hydrodehalogenation (**1ad**) is very efficient when using twice the amount of DIPEA. This high conversion of diphenyl bromides is particularly interesting regarding the possible application of the process for the degradation of PCBs. The poor yield of 1-iodonaphthalin (**1z**) is contrary to our expectations and can be explained by the observation of large amounts of unidentified, solid by-product which was separated during catalyst centrifugation. To demonstrate an example of a synthetic application for the degradation of environmental toxins, dicofol, a common acaricide, was successfully dechlorinated. The tolerance towards acids (**1ag**, **1ah**), amines (**1ar**) and trimethylsilanes (**1aq**) further extends the potential applications to late-stage modification of molecules.^[42] The reaction of heteroaromatic substrates, such as pyridines (**1ai** to **1am**) and pyrazines (**1am**), leads to fair to good yields, while furans (**1ao**) give only trace amounts and isoxazoles (**1an**) no product at all. Thiophene **1ap** gave a low yield (35%) of the dehalogenated product. In the presence of several different halide leaving groups (I, Br, Cl), the above-mentioned reactivity differences within the seventh main group are corroborated (**1aw** to **1az**). The iodo-leaving group is always completely cleaved, bromo- and chloro- substituents follow in the expected order.

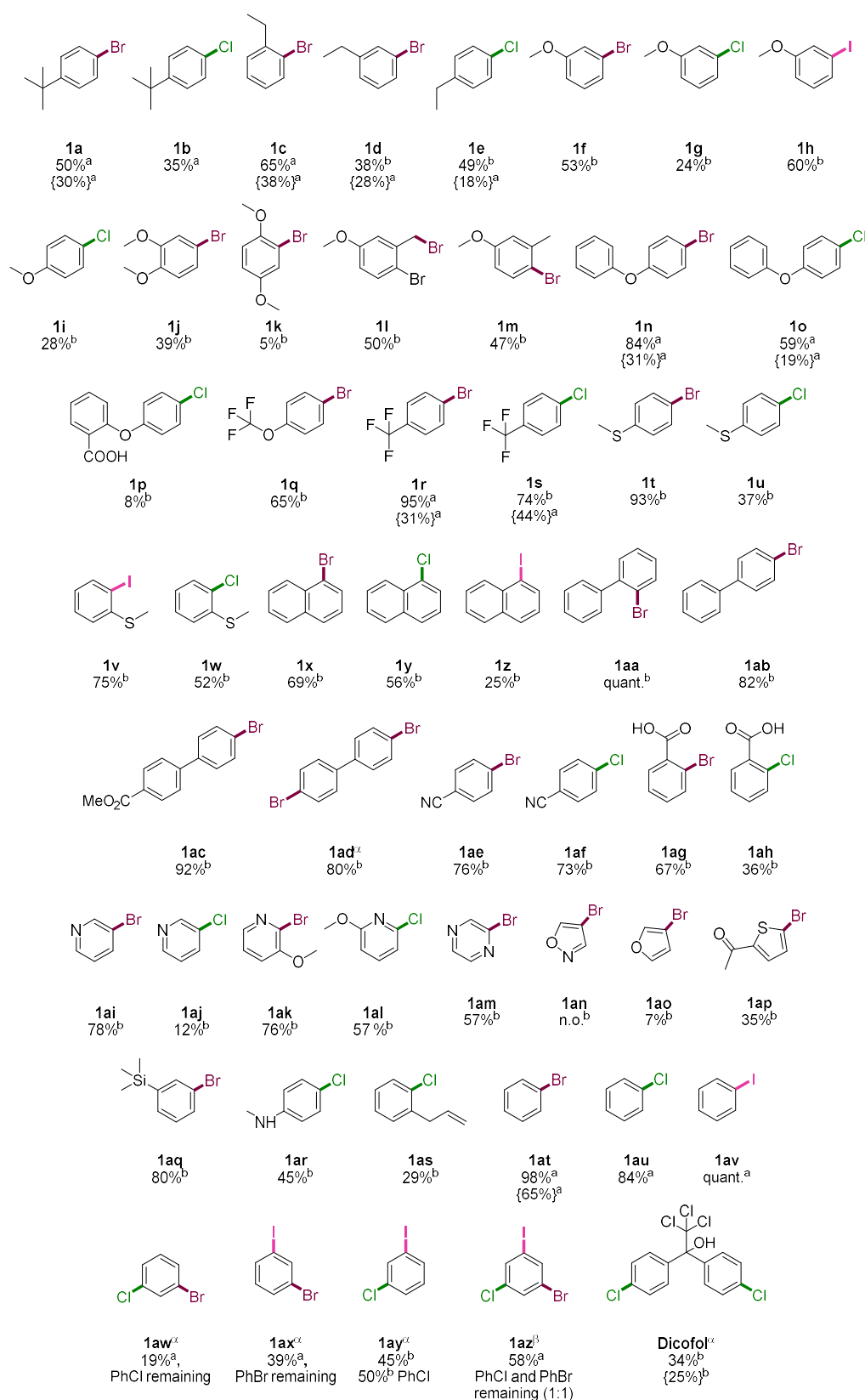


Figure 1. Substrate scope of the reductive hydrodehalogenation of aryl halides under DND-H photocatalysis. Yields are given in respect of the hydrodehalogenation of the color-indicated bond. Reaction condition: aryl halide (0.4 mmol), DIPEA (0.8 mmol), DND-H (3 mg), ACN (0.5 mL), 395 nm LED (2 W), 48 h, 25°C, N₂. The yields in parentheses were determined after 16 hours of reaction time. ^a 1.6 mmol of DIPEA. ^b 2.4 mmol of DIPEA. ^a Yields were determined by GC-FID analysis against *n*-heptane as internal standard. ^b Yields were determined by NMR analysis against hexamethyldisiloxane (HMDSO) as internal standard. Note: Tests on PCBs were not performed for safety reasons and to avoid the production and distribution of such substances.

The process of dehalogenation, as a unimolecular reaction, follows first-order kinetics (Figure 2). After a short phase (5 h) of concentration independence, the turnover rate decreases as the reaction proceeds. The rate of substrate conversion was determined to be $k = -6.71 \times 10^{-6} \text{ M}^{-1} \text{ s}^{-1}$ based on the calculated substrate concentration ($c_{\text{Sub}} = 1 - c_{\text{Prod}}$). We assume that the reduction of the aryl halide represents the rate-determining step.^[46] Whether the light input or the SET itself is responsible for this has not yet been clarified.

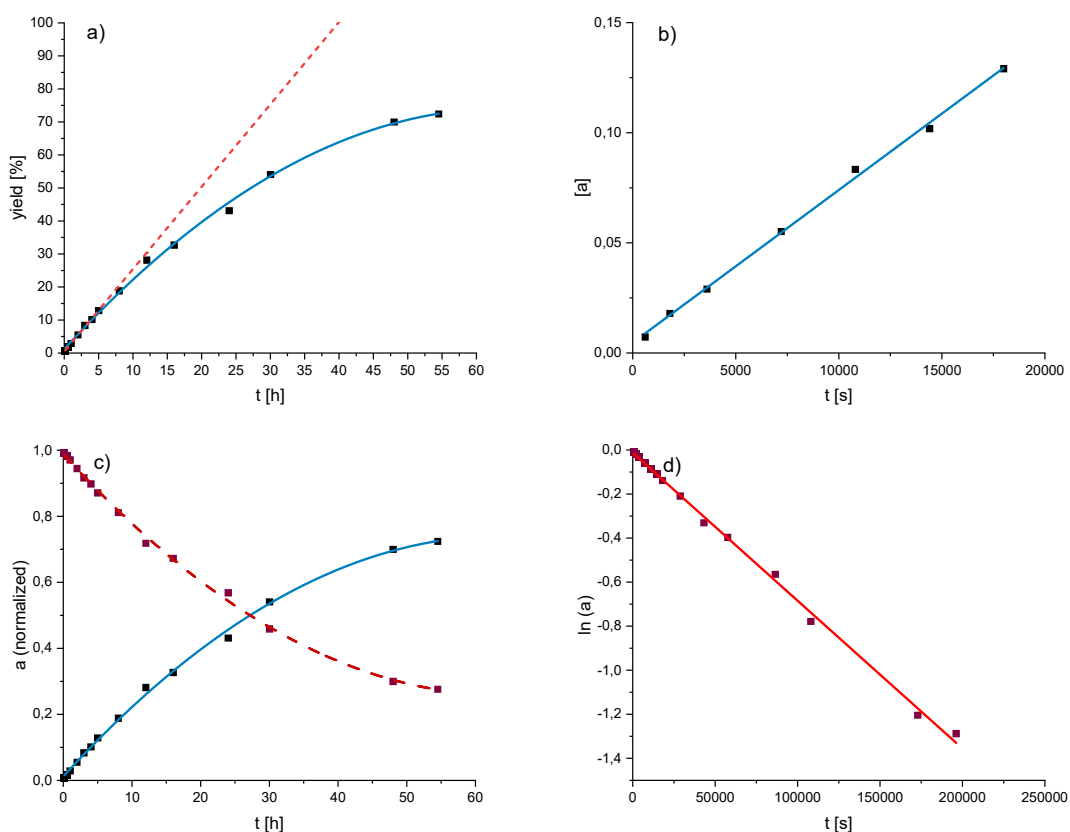


Figure 2. Kinetic data for the reaction of 4-bromophenylether under DND-H photocatalysis. Reaction condition: aryl halide (0.4 mmol), DIPEA (0.8 mmol), DND-H (3 mg), ACN (0.5 mL), 395 nm LED (2 W), 25°C, N₂. a) Yields (black cubes) determined by GC-FID analysis against n-heptane as internal standard. Second order polygonal fit (blue) and tangent (red dashed) of the concentration-independent section (0 h to 5 h). b) Yields (black cubes) determined by GC-FID analysis against n-heptane as internal standard. Linear fit (blue) of the concentration independent section (0 h to 5 h) $y = 6,9304 \text{ E-}6x + 0,00471$. c) Yields (black cubes) determined by GC-FID analysis against n-heptane as internal standard and second order polygonal fit (blue). Calculated ($c_{\text{Sub}} = 1 - c_{\text{Prod}}$) conversion of the arly halide (bordeaux cubes) and second order polygonal fit (red dashed). d) Calculated first derivation of the activity (1st order) of the calculated aryl halide conversion (bordeaux cubes) and the corresponding function (red).

A light-initiated radical chain mechanism is not supported by light on-off experiments (Figure 3). If the reaction is stored in the dark for 2 h after an initial irradiation with 395 nm, the yield does not increase. Renewed irradiation leads to a yield almost identical to that of a sample constantly illuminated for 4 hours. This result confirms that the DND-H and neither an anionic side-product, nor a persistent radical, drives the reaction.

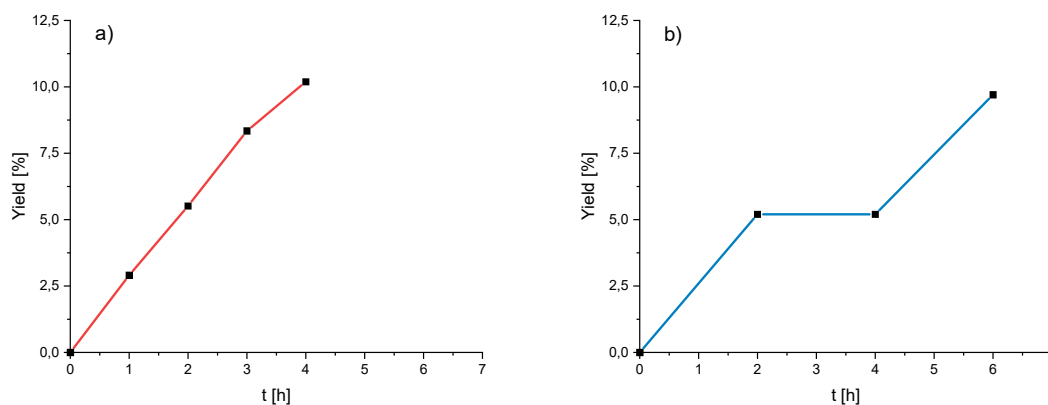


Figure 3. On-off experiment. Reaction condition: aryl halide (0.4 mmol), DIPEA (0.8 mmol), DND-H (3 mg), ACN (0.5 mL), 395 nm LED (2 W), 25°C, N₂. a) Yields (black cubes) determined by GC-FID analysis against *n*-heptane as internal standard. a) Yield obtained under constant irradiation with 395 nm for the given time. b) Yield obtained under irradiation (on-off-on) with 395 nm for 2 h each.

Further insights, into the mechanism was gained by a deuteration experiment (Figure 4A), performed in ACN-d³. Under the chosen conditions only DIPEA or the DND-H itself can act as proton source, respectively hydrogen atom source. Involvement of the solvent would lead to formation of deuterated product. As the level of deuteration is in strong alignment with the natural abundance of deuterium, we can conclude, that ACN does not react under our conditions. To exclude the catalyst from being oxidized during a HAT or proton transfer, we employed acid-terminated catalyst (DND-COOH). Being unable to undergo a HAT mechanism, the successful reduction of **1a** means that either DIPEA donates a hydrogen atom after its oxidation, or the reaction proceeds *via* an ionic pathway.

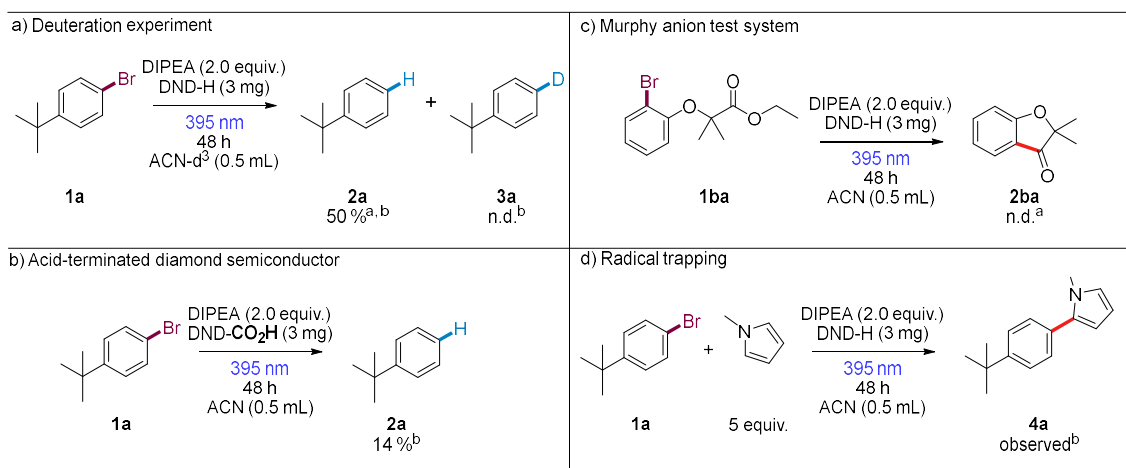


Figure 4. Mechanistic investigation: a) Deuteration experiment. Reaction condition: aryl halide (0.4 mmol), DIPEA (0.8 mmol), DND-H (3 mg), ACN-d³ (0.5 mL), 395 nm LED (2 W), 48 h, 25°C, N₂. b) Model reaction under DND-CO₂H Photocatalysis. Reaction condition: aryl halide (0.4 mmol), DIPEA (0.8 mmol), DND-CO₂H (3 mg), ACN (0.5 mL), 395 nm LED (2 W), 48 h, 25°C, N₂. c) Carbanion test reaction. Reaction condition: aryl halide (0.4 mmol), DIPEA (0.8 mmol), DND-H (3 mg), ACN (0.5 mL), 395 nm LED (2 W), 48 h, 25°C, N₂. d) Radical trapping test reaction. Reaction condition: aryl halide (0.4 mmol), DIPEA (0.8 mmol), *N*-Methylpyrrol (2.0 mmol), (DND-H (3 mg), ACN (0.5 mL), 395 nm LED (2 W), 48 h, 25°C, N₂. ^aYields determined by GC-FID analysis against *n*-heptane as internal standard. ^b Product identification via GC-MS and HR-MS.

Even though to the best of our knowledge there is no literature report on the formation of phenylanions under such conditions, we excluded this option by employing an anion trapping reagent. According to Murphy,^[47] radical species cannot be trapped by an ester functionality. Under our standard conditions, test compound **1ba** did not undergo any intramolecular ring closure, disproving an anionic mechanism. This was additionally confirmed in presence of acetone (Figure S4)^[48]. On the other hand, the successful capture *via* *N*-methylpyrrole (Figure 4D), thiophene (Figure S7) and an intramolecular system (Figure S5) are clear indicators of a phenyl radical intermediate. Aldehydes and Ketones (Figure S8 to S11) have shown to undergo pinacol coupling, esters and carboxylic acids (Figure S12, S13) are not reduced.

As major by-product of the hydrodebromination reaction, diisopropylammonium bromide was crystallized from the DCM washing solution after catalyst recycling (Figure 5).

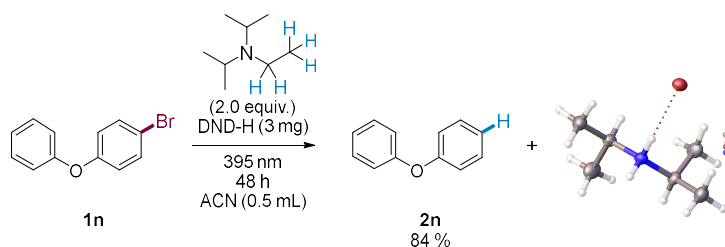


Figure 5. Reaction and crystal structure of diisopropylammonium bromide. Reaction condition: aryl halide (0.4 mmol), DIPEA (0.8 mmol), DND-H (3 mg), ACN (0.5 mL), 395 nm LED (2 W), 48 h, 25°C, N₂. Diisopropylammonium bromide was recrystallized from DCM.

This supports our mechanistic proposal, depicted in Figure 6. Upon absorption of blue (395 nm) light, an electron is excited from the valence band (VB) into the conducting band (CB7) of the DND-catalyst. Single electron transfer (SET) reduces substrate **A** to a radical anion, which upon C-X cleavage generates a phenyl radical **A**[•]. The hole, generated in the VB oxidizes DIPEA to its radical cation. This species then serves as a hydrogen atom source for **A**[•] to complete the hydrodehalogenation to **B**. The DIPEA cation then undergoes further degradation processes to furnish diisopropylamin bromide.

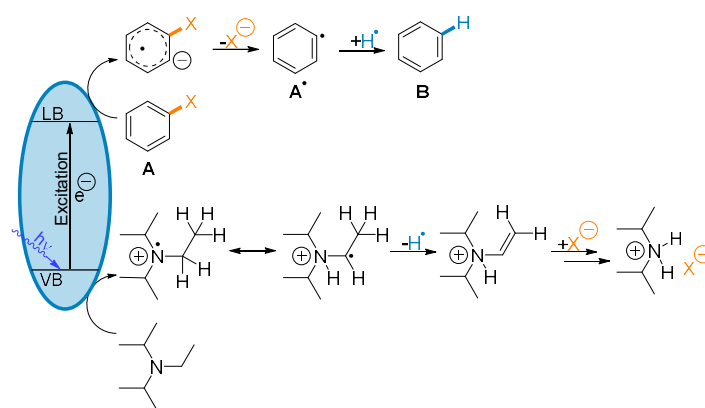


Figure 6. Proposed reaction mechanism.

Solvated electrons, known to be ejected from diamond semiconductors into aqueous media, can be excluded in ACN.^[45] In water, DND-H gave no product as the hydrophobic catalyst aggregates at interfaces. The acid-terminated variant suspends better, so we expected a higher possibility for generation of solvated electrons (Table 2).

Table 2. Effect of acid termination in aqueous media.^a

Entry	Deviation from standard conditions	Yield (%) ^b
1	non	86
2	H ₂ O	-
3	ACN : H ₂ O (1:1)	-
4	ACN : H ₂ O (2:1)	55
5	Sodium ascorbate	-
6	Sodium ascorbate, H ₂ O	-
7	Sodium ascorbate, ACN : H ₂ O (1:1)	-
8	Sodium ascorbate, ACN : H ₂ O (2:1)	-

^a Reaction condition: **1ab** (0.4 mmol), DIPEA (0.8 mmol), DND-CO₂H (2 mg), Solvent (0.5 mL), 395 nm LED (2 W), 25°C, 48 h, N₂.

^b Yields were determined by NMR analysis against hexamethyldisiloxane (HMDSO) as internal standard.

Substrate **1ab** was chosen as the model compound, as both starting material and product are solids and water can easily be removed *via* lyophilization. In strong agreement with our results on DND-H, the acid-terminated catalyst works best in ACN and does not facilitate the reaction in water or mixtures with high water content. The use of sodium ascorbate to repress a biphasic system had no positive effect on the reaction outcome. Under our standard conditions, a similar yield for **1ab** was obtained as with the DND-H catalyst. However, a small set of more difficult substrates (Figure 7) proves that DND-H is significantly more efficient.

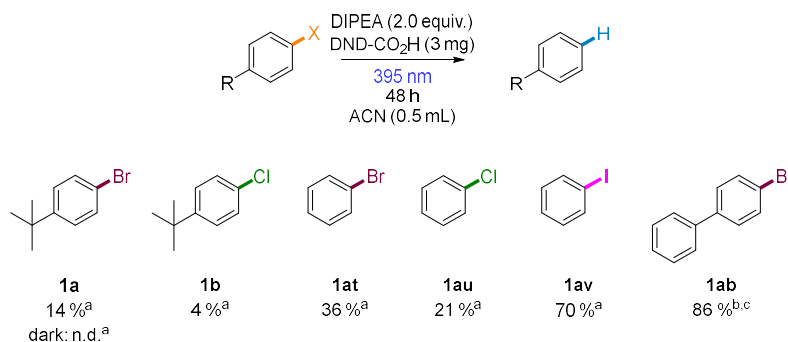


Figure 7. Substrate scope of the reductive hydrodehalogenation of aryl halides under DND-CO₂H photocatalysis. Yields are given in respect of the hydrodehalogenation of the color-indicated bond. Reaction condition: aryl halide (0.4 mmol), DIPEA (0.8 mmol), DND-CO₂H (3 mg), ACN (0.5 mL), 395 nm LED (2 W), 48 h, 25°C, N₂.^a Yields were determined by GC-FID analysis against *n*-heptane as internal standard. ^b Yields were determined by NMR analysis against HMDSO as internal standard. ^c DND-CO₂H (2 mg)

Finally, we investigated the reusability of the catalyst material. The heterogeneous photocatalyst can be separated from the mixture by centrifugation after the reaction.^[49] Washed with organic solvents (DCM, acetone, PE) and dried at 60°C, the catalyst retains its reactivity for at least five cycles (Figure 8). The slightly higher yield at the beginning is due to the presumably higher catalyst loading. During the recycling process, quaternary ammonium salts (Figure 5), may adsorb on the surface, increasing the absolute mass, respectively decreasing the amount of active catalyst of the next batch. Therefore, the small increase in yield (run 3 to 5) is probably due to better results in washing the catalyst. IR and thermogravimetric analysis (TGA) to prove or disprove this theory are in process.

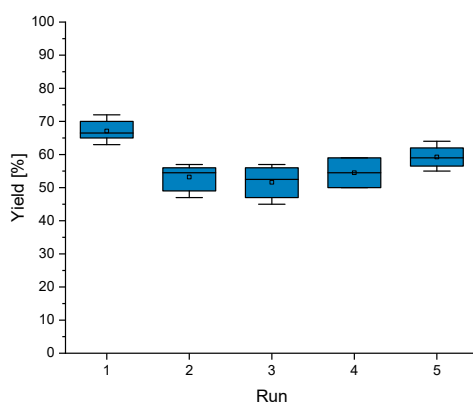


Figure 8. Box plot of the yields received for the hydrodehalogenation of **1n** with new and recycled DND-H. Lower end of whisker: the smallest value of the data set; upper end of whisker: the highest value of the data set; median (line inside the box): the smallest 50% of the data values are smaller than or equal to this characteristic value; beginning of the box: the smallest 25% of the data values are smaller than or equal to this characteristic value; end of the box: the smallest 75% of the data values are smaller than or equal to this characteristic value. Reaction condition: aryl halide (0.4 mmol), DIPEA (0.8 mmol), DND-H (3 mg), ACN (0.5 mL), 395 nm LED (2 W), 48 h, 25°C, N₂. Yields were determined by GC-FID analysis against *n*-heptane as an internal standard.

5.4 Conclusion

Considering its reusability, availability and low cost, diamond-based semiconductors can find applications in heterogeneous photoredox catalysis. The demonstration of more than 50 successful dehalogenations under very mild, visible light conditions demonstrates the potential of diamond nanomaterial in photocatalysis. With an estimated redox potential of about 3 V (vs. SCE), it is a non-toxic, metal-free alternative to existing homogeneous and heterogeneous photocatalysts. The possibility of surface modification allows for fine-tuned heterogeneous materials. Deposition on an electron surface may further extend its applicability to photoelectrocatalysis^[50].

5.5 References

- [1] X. Hu, G. Zhang, L. Nie, T. Kong, A. Lei, *Nat. Commun.* **2019**, *10*, 5467.
- [2] Y. Deng, F. Lu, S. You, T. Xia, Y. Zheng, C. Lu, G. Yang, Z. Chen, M. Gao, A. Lei, *Chin. J. Chem.* **2019**, *37*, 817–820.
- [3] P. Hu, B. K. Peters, C. A. Malapit, J. C. Vantourout, P. Wang, J. Li, L. Mele, P.-G. Echeverria, S. D. Minter, P. S. Baran, *J. Am. Chem. Soc.* **2020**, *142*, 20979–20986.
- [4] H. Liang, L. Wang, Y. Ji, H. Wang, B. Zhang, *Angew. Chem. Int. Ed.* **2021**, *60*, 1839–1844.
- [5] L. F. T. Novaes, J. S. K. Ho, K. Mao, K. Liu, M. Tanwar, M. Neurock, E. Villemure, J. A. Terrett, S. Lin, *J. Am. Chem. Soc.* **2022**, *144*, 1187–1197.
- [6] Y. You, W. Kanna, H. Takano, H. Hayashi, S. Maeda, T. Mita, *J. Am. Chem. Soc.* **2022**, *144*, 3685–3695.
- [7] S. Lips, S. R. Waldvogel, *ChemElectroChem* **2019**, *6*, 1649–1660.
- [8] Z. Wang, S. Xu, J. Cai, J. Ma, G. Zhao, *ACS EST Eng.* **2022**, *2*, 1001–1014.
- [9] D. J. Poferl, N. C. Gardner, J. C. Angus, *Journal of Applied Physics* **1973**, *44*, 1428–1434.
- [10] M. Dörr, J. L. Röckl, J. Rein, D. Schollmeyer, S. R. Waldvogel, *Chem. Eur. J.* **2020**, *26*, 10195–10198.
- [11] S. Herold, S. Möhle, M. Zirbes, F. Richter, H. Nefzger, S. R. Waldvogel, *Eur. J. Org. Chem.* **2016**, *2016*, 1274–1278.
- [12] B. K. Wilk, M. Szopińska, M. Sobaszek, M. Pierpaoli, A. Błaszczuk, A. Luczkiewicz, S. Fudala-Ksiażek, *Environ Sci Pollut Res* **2022**, *29*, 65625–65641.
- [13] K. Muzyka, J. Sun, T. H. Fereja, Y. Lan, W. Zhang, G. Xu, *Anal. Methods* **2019**, *11*, 397–414.
- [14] K. Miyashita, T. Kondo, S. Sugai, T. Tei, M. Nishikawa, T. Tojo, M. Yuasa, *Sci Rep* **2019**, *9*, 17846.
- [15] U. Choi, T. Kwak, S. Han, S.-W. Kim, O. Nam, *Diamond and Related Materials* **2022**, *121*, 108782.
- [16] S. J. Cobb, Z. J. Ayres, J. V. Macpherson, *Annual Rev. Anal. Chem.* **2018**, *11*, 463–484.
- [17] A. M. Panich, *Critical Reviews in Solid State and Materials Sciences* **2012**, *37*, 276–303.
- [18] J. Ackermann, A. Krueger, *Carbon* **2020**, *163*, 56–62.
- [19] A. J. Shirley, S. Schweeberg, T. Waag, M. Peindl, G. Dandekar, H. Walles, F. Jakob, A. Krueger, R. Ebert, *J. Mater. Chem. B* **2021**, *9*, 9395–9405.
- [20] É. M. Galimov, A. M. Kudin, V. N. Skorobogatskii, V. G. Plotnichenko, O. L. Bondarev, B. G. Zarubin, V. V. Strazdovskii, A. S. Aronin, A. V. Fisenko, I. V. Bykov, A. Yu. Barinov, *Dokl. Phys.* **2004**, *49*, 150–153.
- [21] J. Ackermann, A. Krueger, *Nanoscale* **2019**, *11*, 8012–8019.
- [22] D. Takeuchi, H. Kato, G. S. Ri, T. Yamada, P. R. Vinod, D. Hwang, C. E. Nebel, H. Okushi, S. Yamasaki, *Appl. Phys. Lett.* **2005**, *86*, 152103.
- [23] D. Takeuchi, M. Riedel, J. Ristein, L. Ley, *Phys. Rev. B* **2003**, *68*, 041304.
- [24] O. S. Kudryavtsev, R. H. Bagramov, A. M. Satanin, A. A. Shiryaev, O. I. Lebedev, A. M. Romshin, D. G. Pasternak, A. V. Nikolaev, V. P. Filonenko, I. I. Vlasov, *Nano Lett.* **2022**, *22*, 2589–2594.
- [25] S. Su, J. Li, V. Kundra, A. M. Abbot, H. Ye, *Journal of Applied Physics* **2013**, *113*, 023707.
- [26] C. E. Nebel, B. Rezek, A. Zrenner, *phys. stat. sol. (a)* **2004**, *201*, 2432–2438.
- [27] D. Takeuchi, C. E. Nebel, S. Yamasaki, *phys. stat. sol. (a)* **2006**, *203*, 3100–3106.
- [28] J. D. Rameau, J. Smedley, E. M. Muller, T. E. Kidd, P. D. Johnson, *Phys. Rev. Lett.* **2011**, *106*, 137602.
- [29] D. Takeuchi, S.-G. Ri, H. Kato, C. E. Nebel, S. Yamasaki, *phys. stat. sol. (a)* **2005**, *202*, 2098–2103.
- [30] I. A. MacKenzie, L. Wang, N. P. R. Onuska, O. F. Williams, K. Begam, A. M. Moran, B. D. Dunietz, D. A. Nicewicz, *Nature* **2020**, *580*, 76–80.
- [31] G. Barone, A. Storelli, A. Busco, R. Mallamaci, M. M. Storelli, *Journal of Food Science* **2021**, *86*, 4741–4753.
- [32] J. Castro-Jiménez, C. Gonzalez, *J. Environ. Monit.* **2011**, *13*, 894.
- [33] C. Singleman, A. Zimmerman, E. Harrison, N. K. Roy, I. Wirgin, N. G. Holtzman, *Environ Toxicol Chem* **2021**, *40*, 187–201.
- [34] EFSA Panel on Contaminants in the Food Chain (CONTAM), D. Schrenk, M. Bignami, L. Bodin, J. K. Chipman, J. del Mazo, B. Grasl-Kraupp, L. (Ron) Hoogenboom, J. Leblanc, C. S. Nebbia, E. Nielsen, E. Ntzani, A. Petersen, S. Sand, T. Schwerdtle, C. Vleminckx, H. Wallace, M. Rose, B. Cottrill, A. K. Lundebye, M. Metzler, A. Christodoulidou, C. Hogstrand, *EFSA* **2022**, *20*, DOI 10.2903/j.efsa.2022.7524.
- [35] Y. Wang, Y. Wei, W. Song, C. Chen, J. Zhao, *ChemCatChem* **2019**, *11*, 258–268.
- [36] J. Ke, H. Wang, L. Zhou, C. Mou, J. Zhang, L. Pan, Y. R. Chi, *Chem. Eur. J.* **2019**, *25*, 6911–6914.
- [37] J. Deng, T. Xue, H. Wu, P. Wu, *New J. Chem.* **2022**, *46*, 12169–12176.
- [38] X. Guo, C. Yu, Z. Yin, S. Sun, C. T. Seto, *ChemSusChem* **2018**, *11*, 1617–1620.
- [39] T. Hokamp, A. Dewanji, M. Lübbsmeyer, C. Mück-Lichtenfeld, E.-U. Würthwein, A. Studer, *Angew. Chem. Int. Ed.* **2017**, *56*, 13275–13278.
- [40] D. K. Leonard, P. Ryabchuk, M. Anwar, S. Dastgir, K. Junge, M. Beller, *ChemSusChem* **2022**, *15*, DOI 10.1002/cssc.202102315.
- [41] P. Wang, X. Shi, C. Fu, X. Li, J. Li, X. Lv, Y. Chu, F. Dong, G. Jiang, *Nanoscale* **2020**, *12*, 843–850.
- [42] B. Sahoo, A.-E. Surkus, M.-M. Pohl, J. Radnik, M. Schneider, S. Bachmann, M. Scalone, K. Junge, M. Beller, *Angew. Chem. Int. Ed.* **2017**, *56*, 11242–11247.
- [43] J. Jiang, L. Du, Y. Ding, *ChemistrySelect* **2021**, *6*, 1372–1377.
- [44] A. Elhage, P. Costa, A. Nasim, A. E. Lanterna, J. C. Scaiano, *J. Phys. Chem. A* **2019**, *123*, 10224–10229.
- [45] B. F. Bachman, D. Zhu, J. Bandy, L. Zhang, R. J. Hamers, *ACS Meas. Au* **2022**, *2*, 46–56.
- [46] C. J. Zeman, S. Kim, F. Zhang, K. S. Schanze, *J. Am. Chem. Soc.* **2020**, *142*, 2204–2207.
- [47] J. A. Murphy, J. Garnier, S. R. Park, F. Schoenebeck, S. Zhou, A. T. Turner, *Org. Lett.* **2008**, *10*, 1227–1230.
- [48] K. Donabauer, M. Maity, A. L. Berger, G. S. Huff, S. Crespi, B. König, *Chem. Sci.* **2019**, *10*, 5162–5166.

- [49] I. Ghosh, J. Khamrai, A. Savateev, N. Shlapakov, M. Antonietti, B. König, *Science* **2019**, *365*, 360–366.
- [50] S. Wu, J. Kaur, T. A. Karl, X. Tian, J. P. Barham, *Angew. Chem. Int. Ed.* **2022**, *61*.

5.6 Experimental Part

5.6.1 General Remarks

All reactions were carried out with dry solvents unless otherwise stated. Dry nitrogen was used as inert gas atmosphere. All solvents and required chemicals were purchased from commercial suppliers (Acros, Alfa Aesar, Fluka, Fluorochem, Merck, Sigma Aldrich, TCI) as reagent grade or at the highest commercial quality and were used directly without further purification unless stated otherwise. Thin-layer chromatography (TLC) was performed on silica gel coated alumina plates (MN TLC sheets ALUGRAM®Xtra SIL G/UV254). Visualization was accomplished with UV light (254 nm or 366 nm) sources. Photocatalytic reactions were performed using a water-cooled photoreactor equipped with violet LEDs (OSRAM® LED Engine LZ4-40UB00-00U5, $\lambda=395\text{ nm} \pm 15\text{ nm}$, 2W optical power), unless stated otherwise. The optical power of LEDs was determined using a FieldMaxII-TOTM laser power meter equipped with PM3 sensor GC-MS measurements were performed on a 7890A GC system from Agilent Technologies with an Agilent 5975 MSD Detector. Data acquisition and evaluation was done with MSD Chem Station E.02.02.1431. GC measurements were performed on a GC 9000 from Agilent Technologies. Data acquisition and evaluation was done with OpenLAB CDS ChemStation from Agilent (version 2.2). A capillary column Agilent 19091S-433UI-INT (US20300220) and hydrogen as carrier gas (flow rate of 1.4 mL/min) were used. The injector temperature (split injection: 30:1 split) was 280°C, detection temperature 300°C (FID). GC measurements were made and investigated *via* integration of the signal obtained. The GC oven temperature program was adjusted as follows: initial temperature of 40°C was kept for 3 minutes, the temperature was increased at a rate of 25°C/min until 280°C was reached and kept for 5 minutes, the temperature was again increased at a rate of 42°C/min until the final temperature (300°C) was reached and kept for 5 minutes. All NMR spectra were recorded at room temperature using a Bruker Avance 300 (300 MHz for ^1H , 75 MHz for ^{13}C , 282 MHz for ^{19}F), Bruker Avance 400 (400 MHz for ^1H , 101 MHz for ^{13}C , 376 MHz for ^{19}F) or Bruker Avance 600 (600 MHz for ^1H , 151 MHz for ^{13}C , 565 MHz for ^{19}F) NMR spectrometer in CDCl_3 , D_2O and DMSO-d^6 solutions with internal solvent signals (for ^1H and ^{13}C) as reference (7.26, 77.2 for CDCl_3 , 2.50, 4.8, NA for D_2O and 39.5 for DMSO-d^6). All chemical shifts are reported in δ -scale as parts per million [ppm] (multiplicity, coupling constant J , number of protons) relative to the solvent residual peaks as the internal standard. Coupling constants J are given in Hertz [Hz]. Abbreviations used for signal multiplicity: ^1H NMR: b = broad, s = singlet, d = doublet, t = triplet, q = quartet, p = quintet, dd = doublet of doublets, dt = doublet of triplets, dq = doublet of quartets and m = multiplet. High-resolution mass spectra (HRMS) were obtained from the central analytic mass spectrometry facilities of the Faculty of Chemistry and Pharmacy, University of Regensburg. All mass spectra were recorded on a

Finnigan MAT 95, Thermo Quest Finnigan TSQ 7000, Finnigan MATSSQ 710 A or an Agilent Q-TOF 6540 UHD instrument. The glass vial with reaction mixture and LED cooling block were thermostatic at 25 °C.

5.6.2 Synthesis and Description of DND Material

This data has not been provided by our collaboration partner so far. We will include detailed information, as soon as we receive any.

5.6.3 Description of Synthetic Procedures

General procedure A

A 5 mL crimp cap vial equipped with a magnetic stirring bar was charged with DND-H photocatalyst (3 mg) (Lot. No. 700110), solid aryl halide (0.4 mmol) and anhydrous ACN (0.5 ml). The vial was sealed, evacuated, and backfilled with N₂ three times before adding DIPEA (136 μL, 800 μmol, 2.0 equiv.) and liquid aryl halide (0.4 mmol) to the reaction vial. Subsequently, the reaction mixture was introduced to a nitrogen atmosphere *via* vacuum (500 mbar) nitrogen backfill cycles (×3). For volatile components "freeze-pump-thaw" cycles (×3 approx. 7 mbar) are necessary. The reaction mixture was irradiated with 2 W 395 (± 15) nm LEDs through the plane bottom side of the crimp cap vial (Figure S1) for 16 h to 48 h and stirred intensely

General procedure B

For GC-FID Analysis heptane (60 μL, 400 μmol) was added as internal standard. Then chloroform (0.5 mL) was added and the mixture was transferred into a 1.5 mL Eppendorf Tube® and centrifuged (2000 rpm) for 2 min. The top layer solution was filtered with a CHROMAFIL® 0-20/15 MS disposable syringe filter (pore size 20 μm) and submitted to GC-FID analysis (Figure S1). Yields were calculated according to the product calibration (Figure S13 A-D)

General procedure C

For NMR-Analysis hexamethyldisiloxane (42.5 μL, 200 μmol) was added as internal standard. Then Chloroform-d (0.5 mL) was added and the mixture was transferred into a

1.5 mL Eppendorf Tube® and centrifuged (2000 rpm) for 2 min. Then top layer solution was submitted to NMR analysis (Figure S1). The yields were calculated according to the integrals in the ^1H -spectrum.

Image guide



Figure S 1. Image guide of the sample preparation for product analysis via procedures B and C.

5.6.4 Optimization and Control Reactions

All optimizations were performed under general procedure A for 16 h and analyzed with procedure B.

Table S 1. Optimization of catalyst loading

Entry	Catalyst loading m_{DND} (mg)	Yield (%)
1	-	-
2	1	18
3	2	24
4	3	30
5	5	20

Table S 2. Optimization of irradiation wavelength

Entry	λ (nm)	Yield (%)
1	dark	-
2	395	30
3	455	-
4	528	-

Table S 3. Optimization of sacrificial electron donor (SED).

Entry	Sacrificial electron donor	Yield (%)
1	-	-
2	DIPEA (2.0 equiv)	30
3	DIPEA (2.0 equiv) for 48 h	50
4	DIPEA (2.5 equiv.)	31
5	DIPEA (1.0 equiv)	22
6	NEt_3 (2.0 equiv.)	14
7	Pyrrolidine (2.0 equiv.)	13
8	Na_2SO_3	-
9	Sodium ascorbate	-
10	Cs_2CO_3	4
11	DABCO	2

Table S 4. Optimization of Solvent.

Entry	Solvent	Yield (%)
1	ACN	30
2	THF	5
3	DMSO	14
4	DMA	20
5	MeOH	2
6	HFIP	-
7	Water	1
8	Acetone	12
9	DCM	2
10	Chloroform	17
11	EA	0

Table S 5. Control reactions at oxygen.

Entry	Atmosphere	Yield (%)
1	N ₂	30
2	Air	20
3	O ₂	12

Table S 6. Optimization of reaction temperature.

Entry	T (°C)	Yield (%)
1	0	24
2	25	30
3	50	35

Table S 7. Control reactions of particle scattering effect.

Entry	Particle material	Yield (%)
1	DND-H	30
2	Silica (3 mg): 60 M (40-63 μm, mesh)	-
3	Molecular sieves (3 mg, grinded) : 4 Å	1

5.6.5 Mass Spectroscopic Analysis

5.6.5.1 Deuteration Experiment

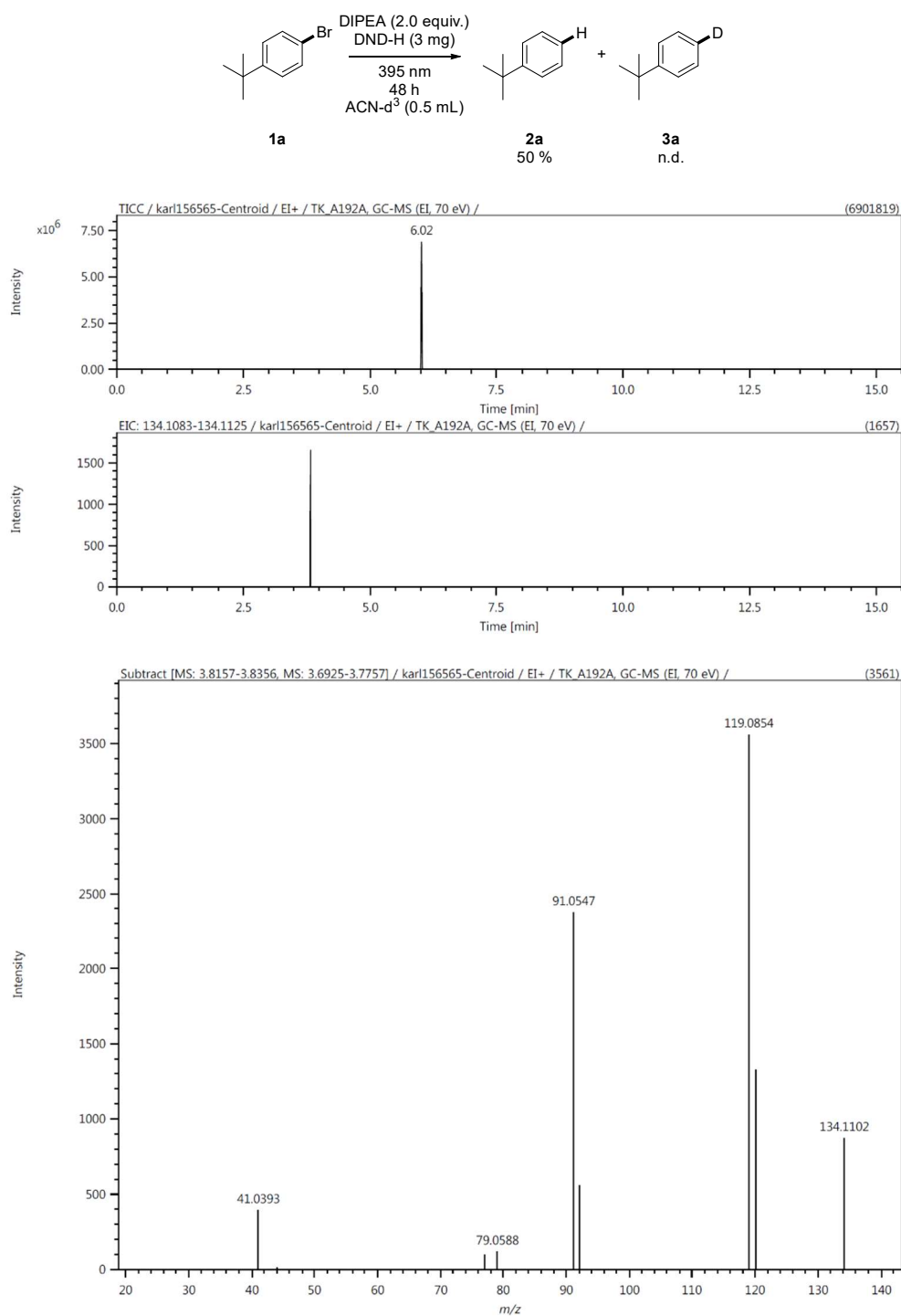


Figure S 2. Deuteration experiment: GC-MS trace and HRMS.

5.6.5.2 Carbanion Trapping

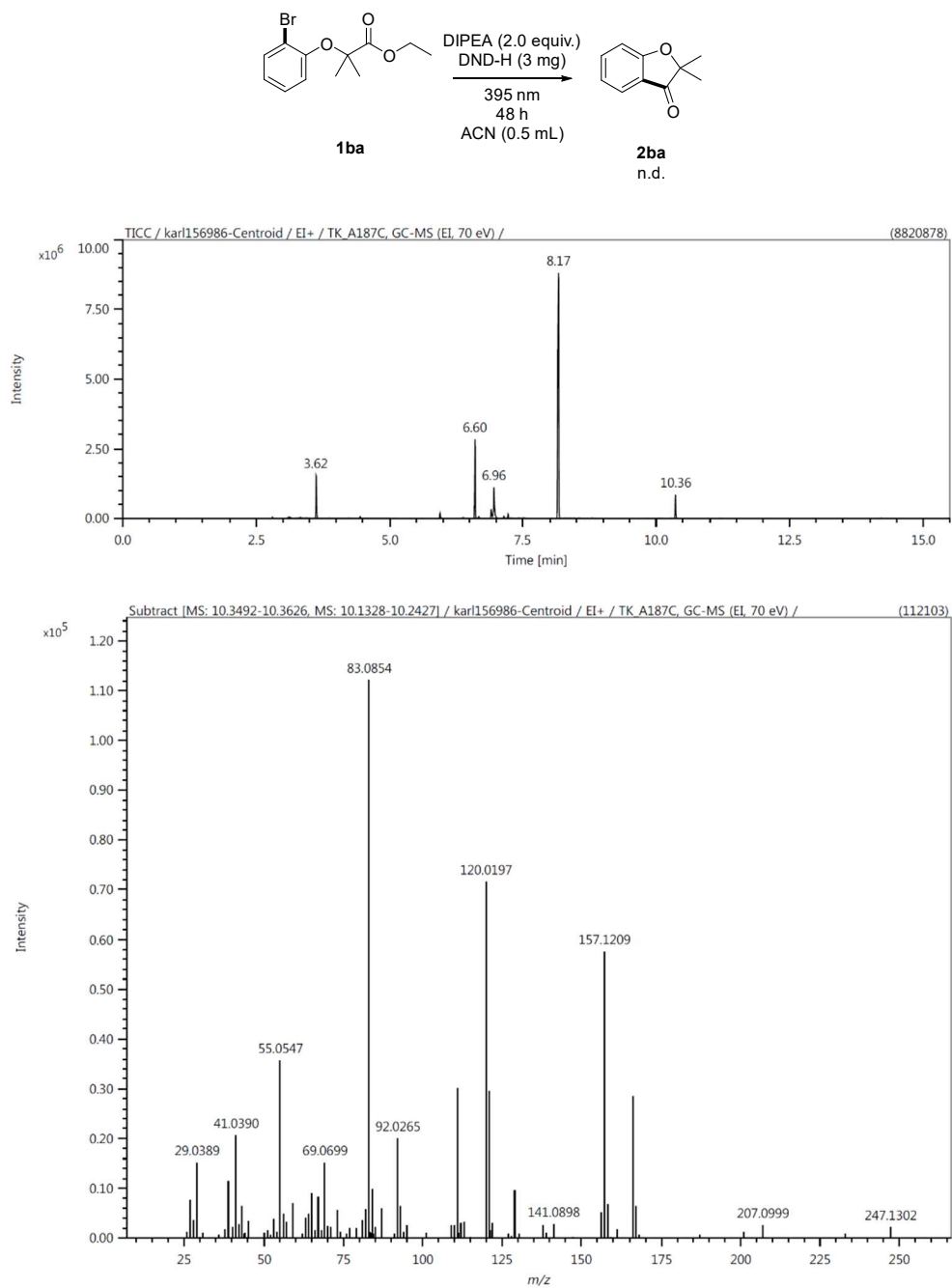


Figure S 3. Intramolecular carbanion trapping: GC-MS trace and HRMS.

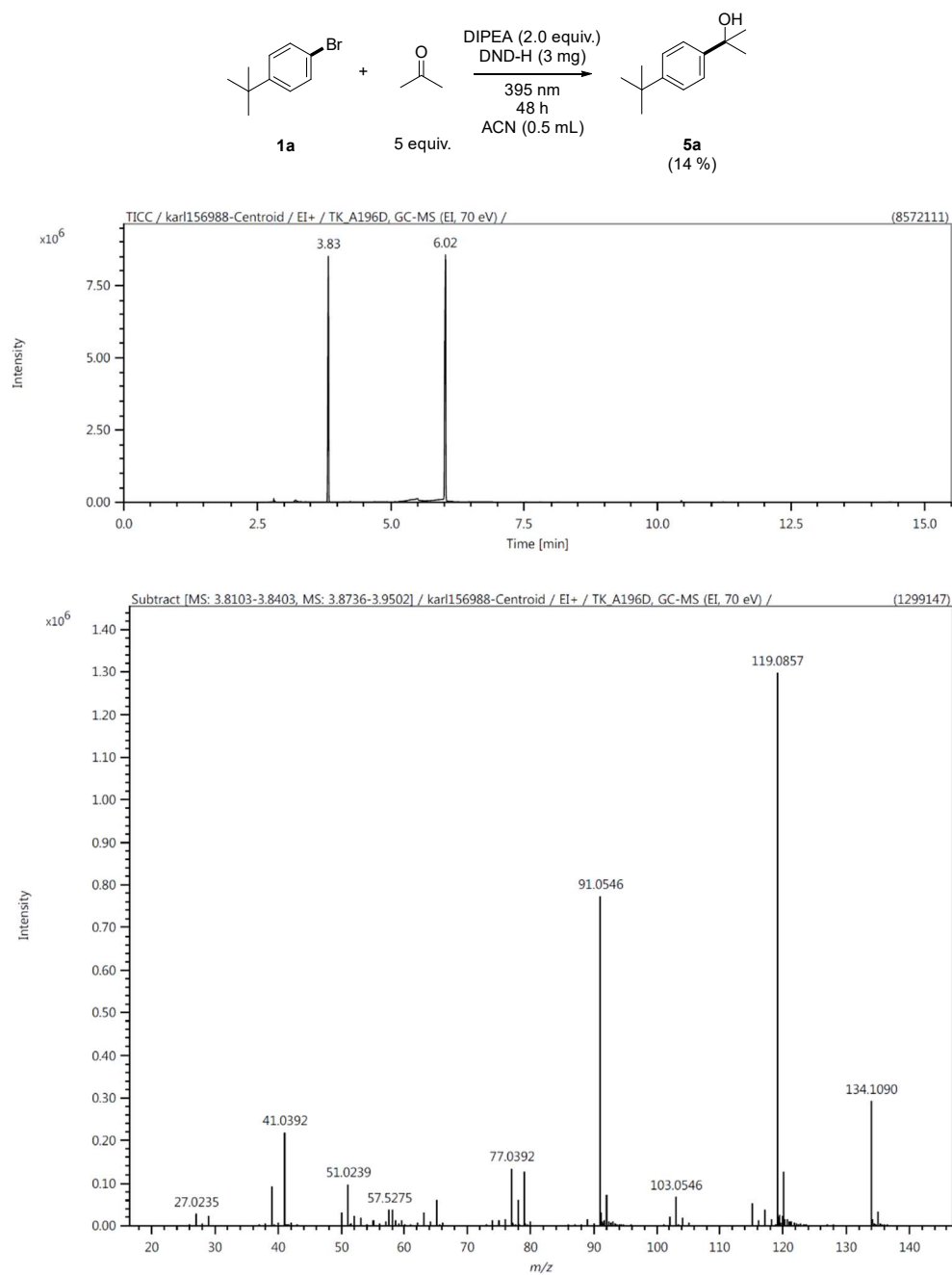
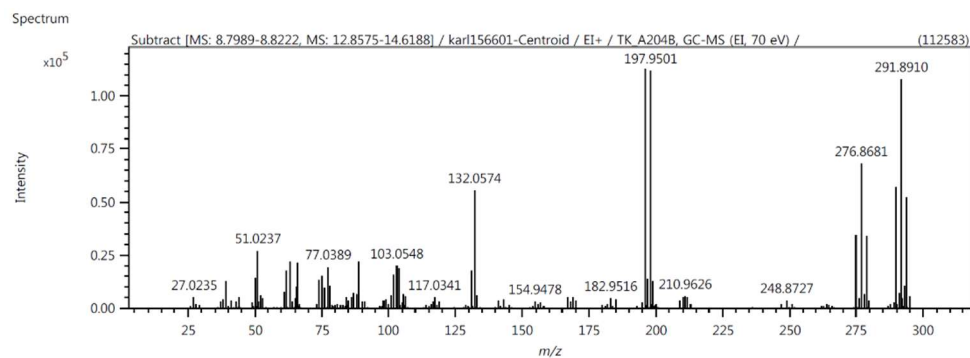
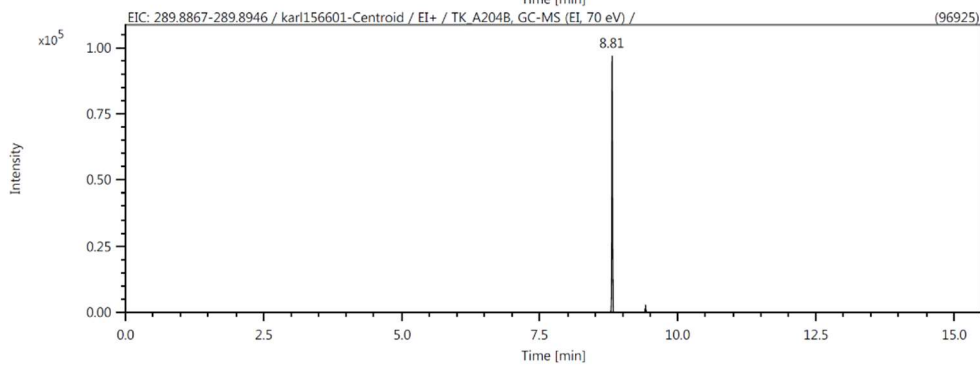
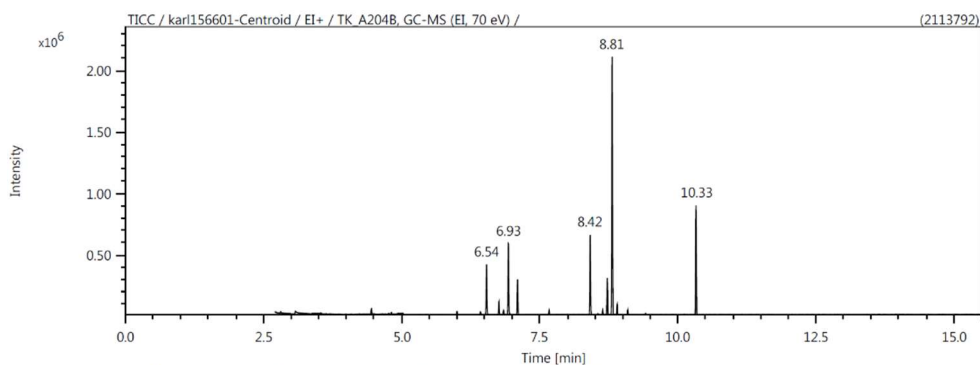
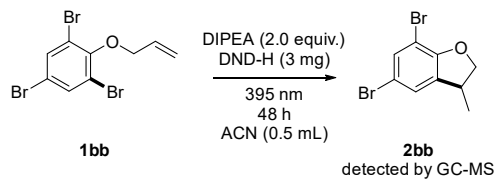


Figure S 4. Intermolecular carbanion trapping: GC-MS trace and HRMS.

5.6.5.3 Radical Trapping



Elemental Composition

Parameters

Tolerance:	10.00 ppm
Electron:	Odd/Even
Charge:	+1
DBE:	-1.5 - 50.0

Elements:

Symbol	C	H	N	O	S	Si	P	Br
Min	0	0	0	0	0	0	0	0
Max	100	100	0	5	0	0	0	5

Results

Mass	Intensity	Formula	Calculated Mass	Mass Difference [mDa]	Mass Difference [ppm]	DBE
289.89286	56866.25	C ₉ H ₈ OBr ₂	289.89364	-0.78	-2.69	5.0

Figure S 5. Intramolecular radical trapping: GC-MS trace and HRMS.

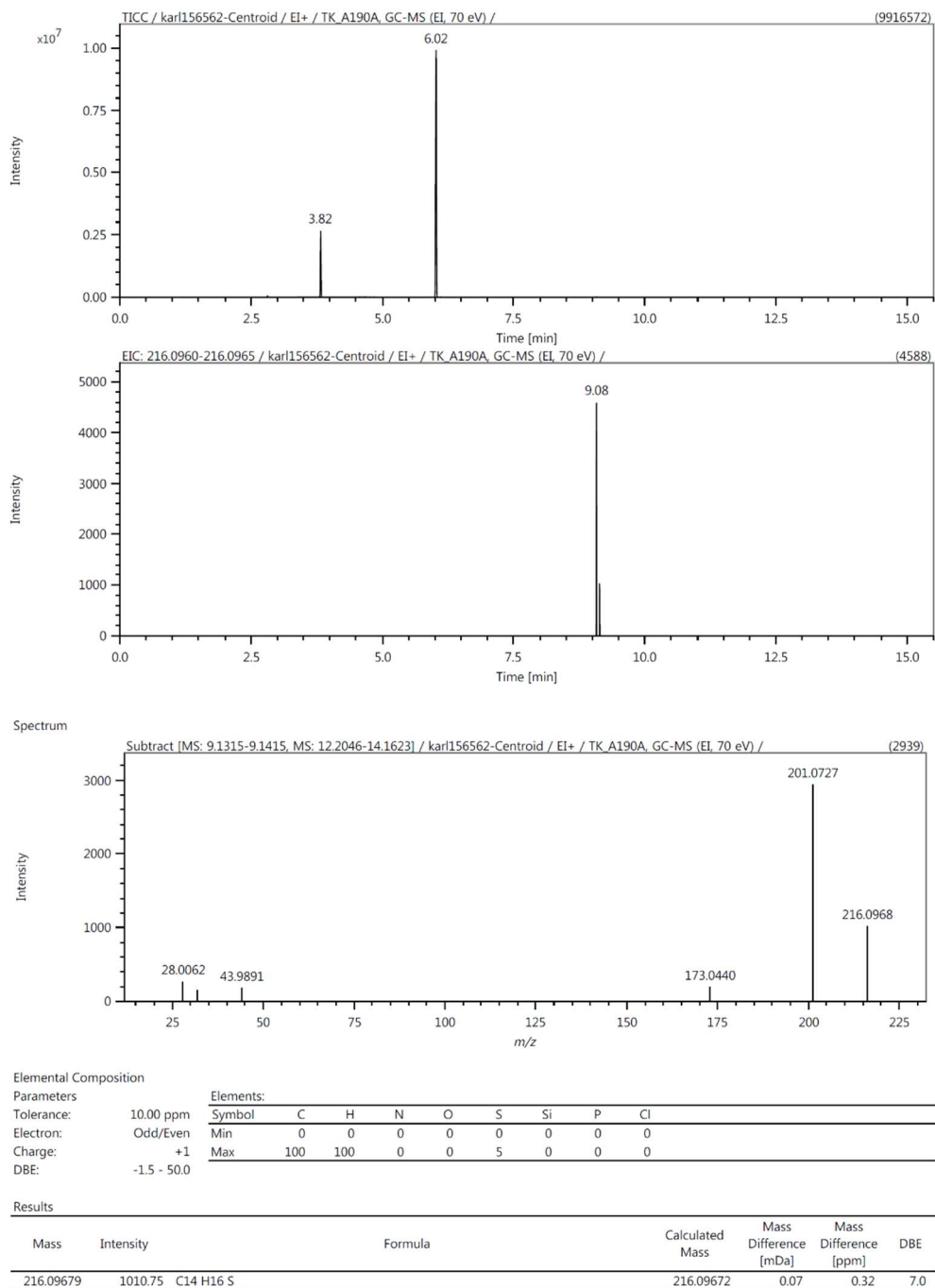
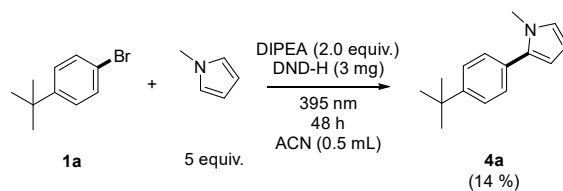


Figure S 6. Intermolecular radical trapping with *N*-methylpyrrole: GC-MS trace and HRMS.

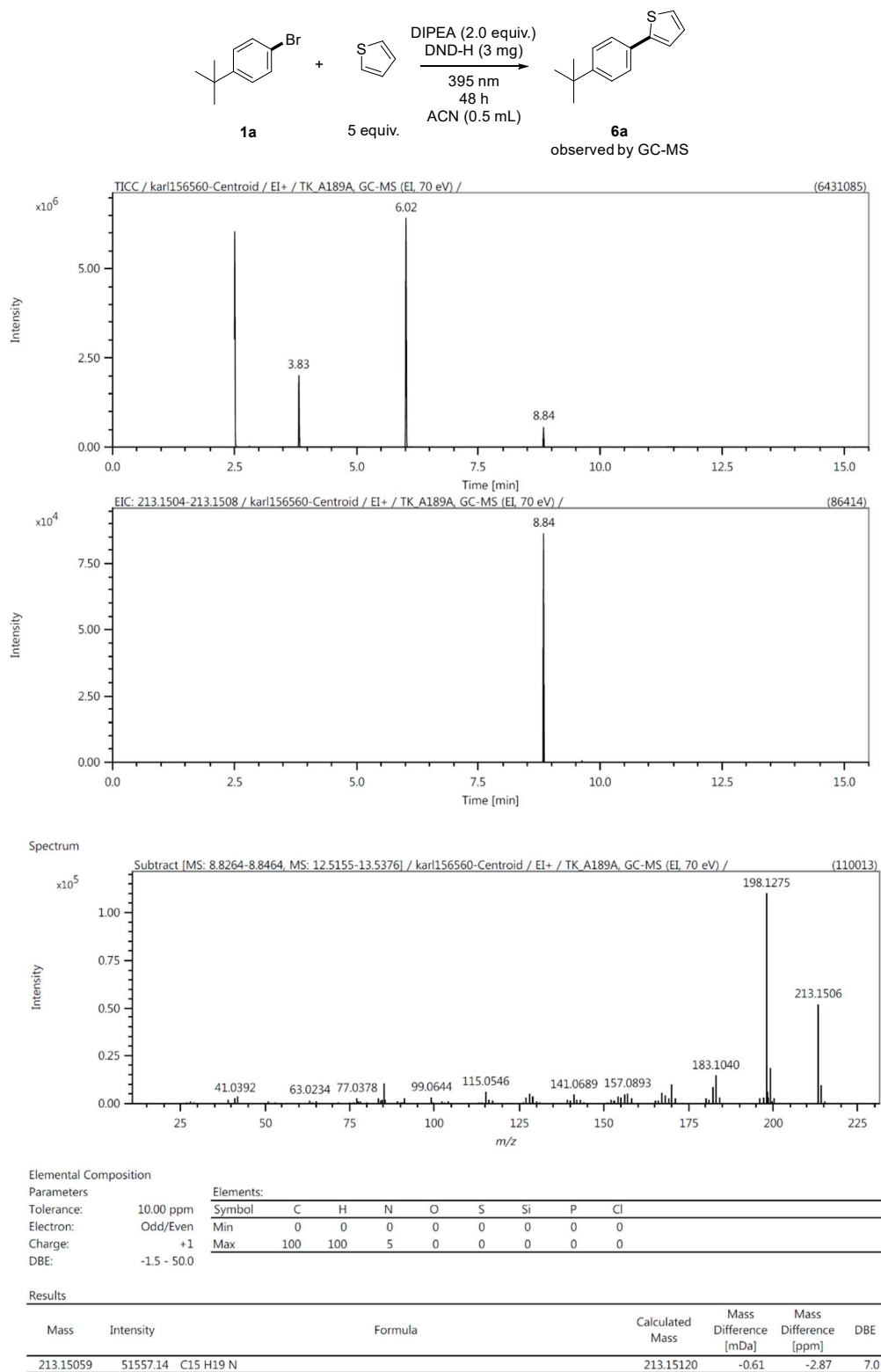


Figure S 7. Intermolecular radical trapping with thiophene: GC-MS trace and HRMS.

5.6.5.4 Pinacol Coupling

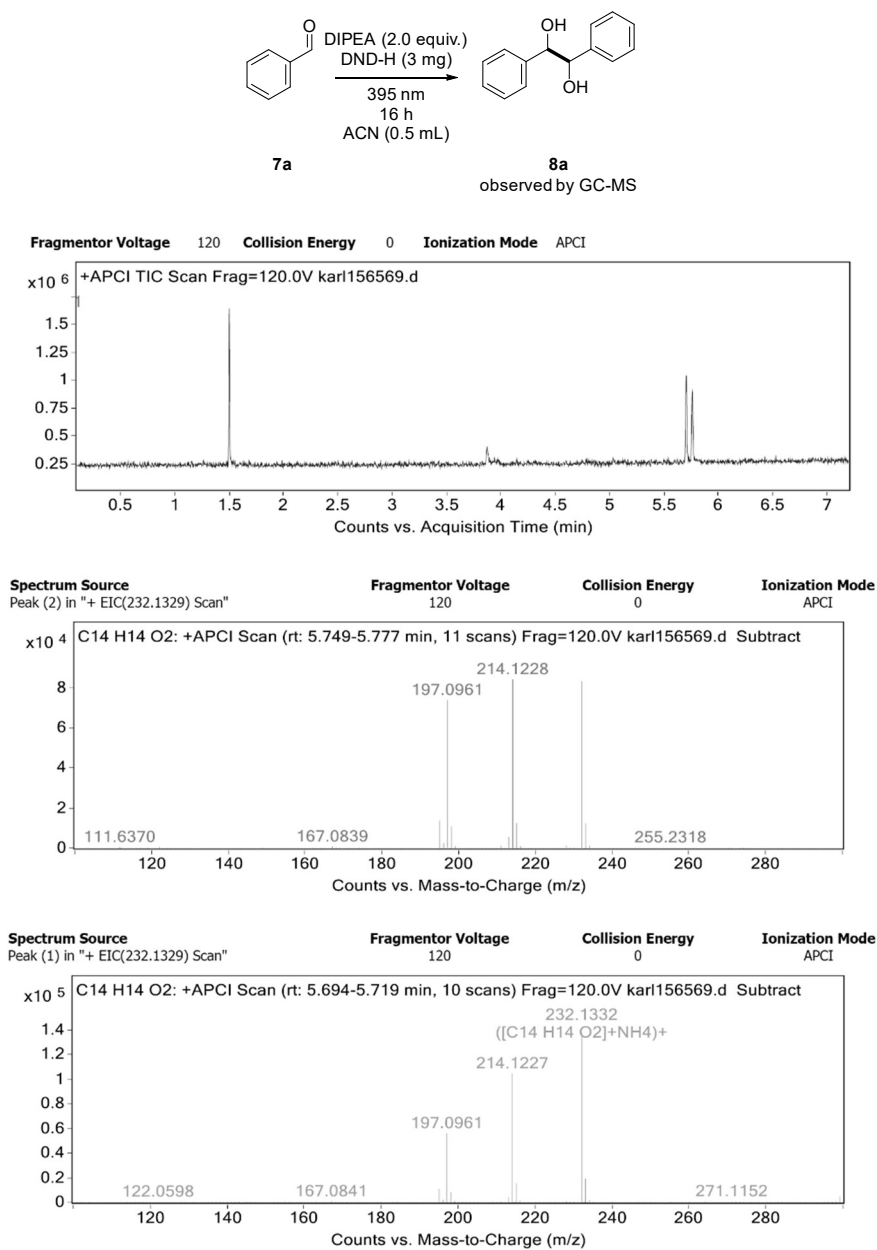


Figure S 8. Pinacol coupling of benzaldehyde: GC-MS trace and HRMS.

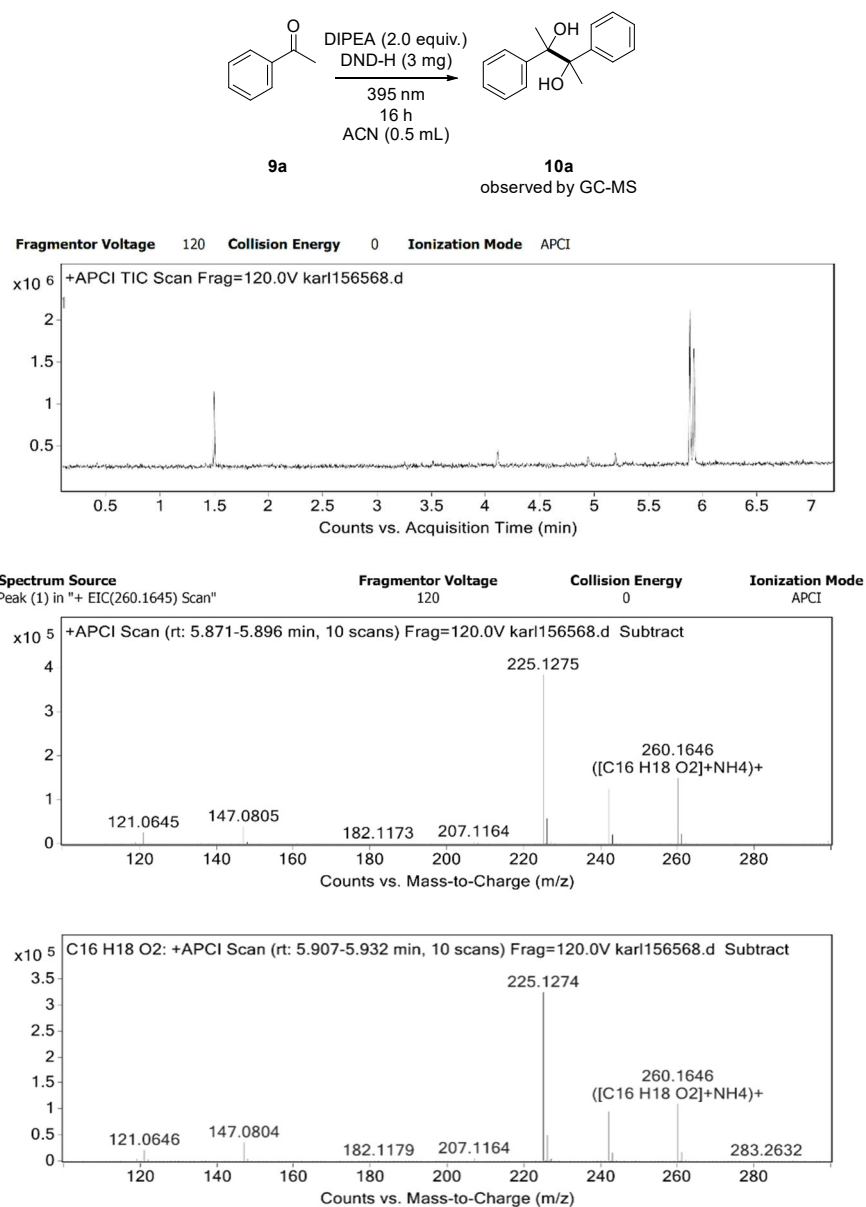


Figure S 9. Pinacol coupling of acetophenone: GC-MS trace and HRMS.

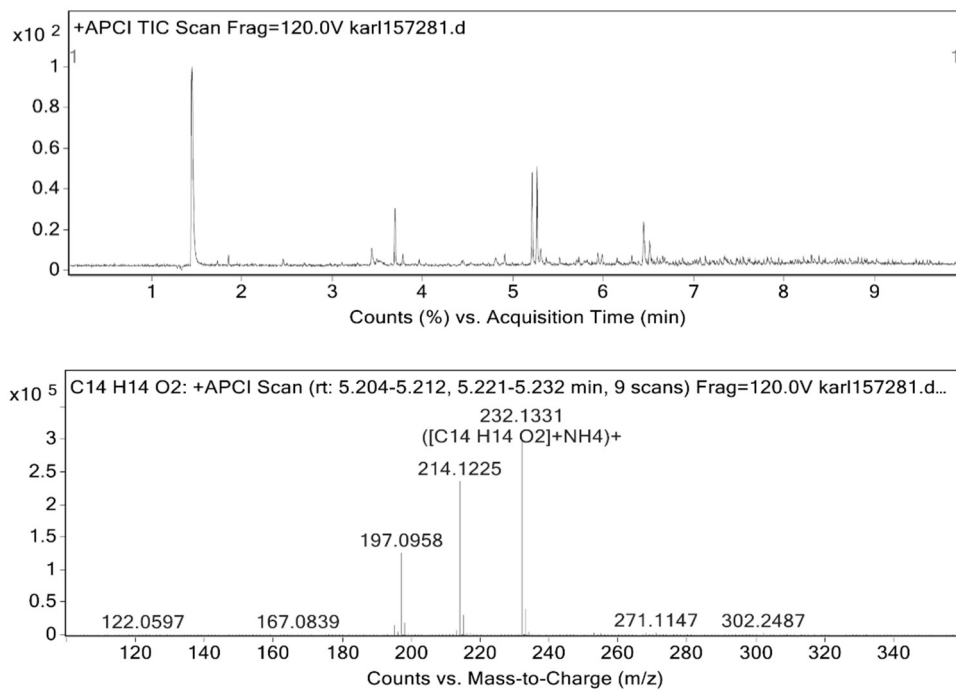
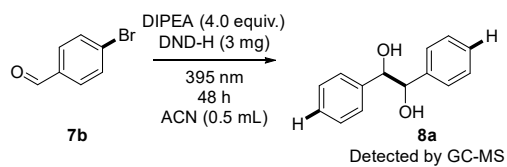


Figure S 10. Pinacol coupling of 4-bromobenzaldehyde: GC-MS trace and HRMS.

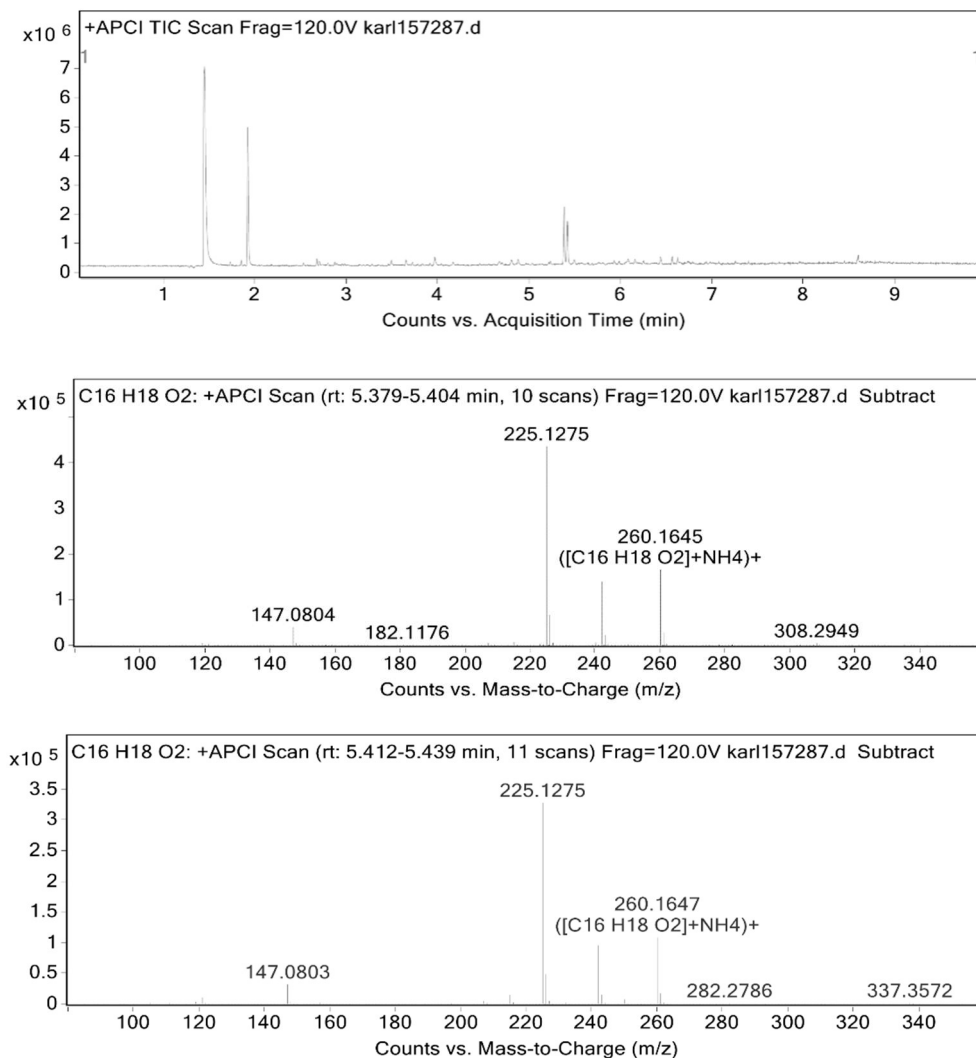
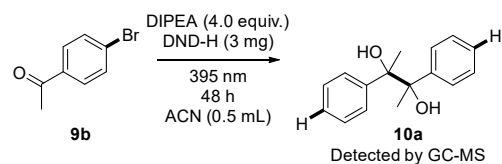


Figure S 11. Pinacol coupling of 4-bromoacetophenone: GC-MS trace and HRMS.

5.6.5.5 Unreactive Substrates

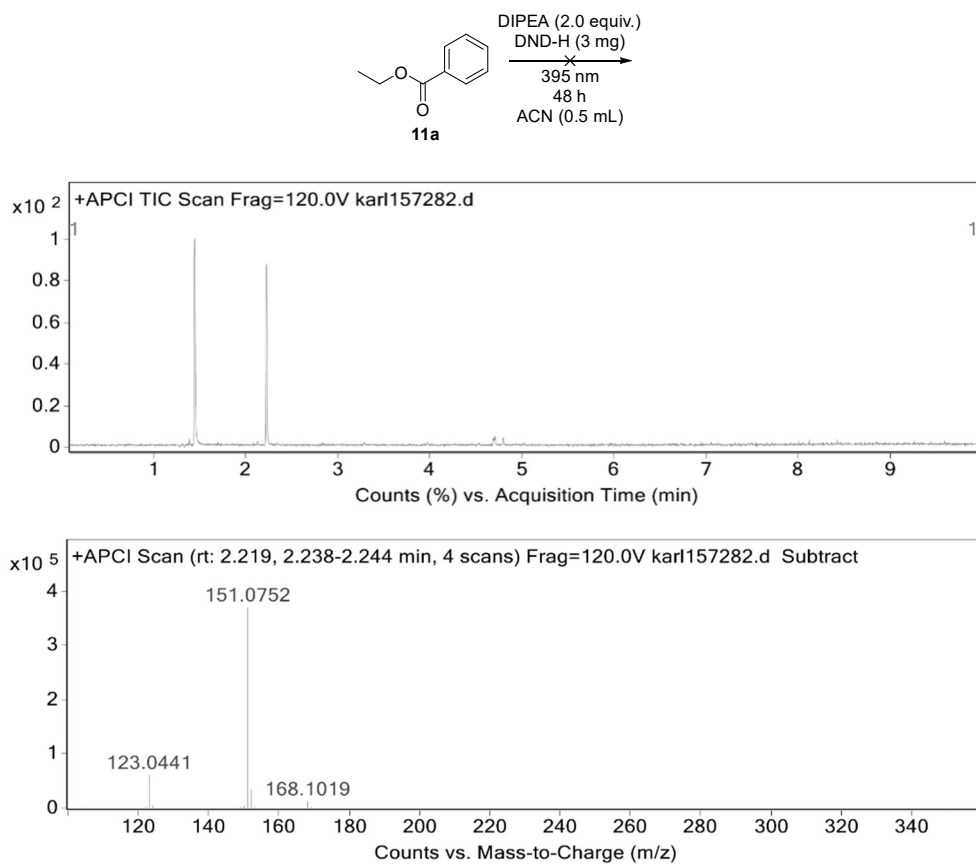


Figure S 12 Reduction of esters: GC-MS trace and HRMS.

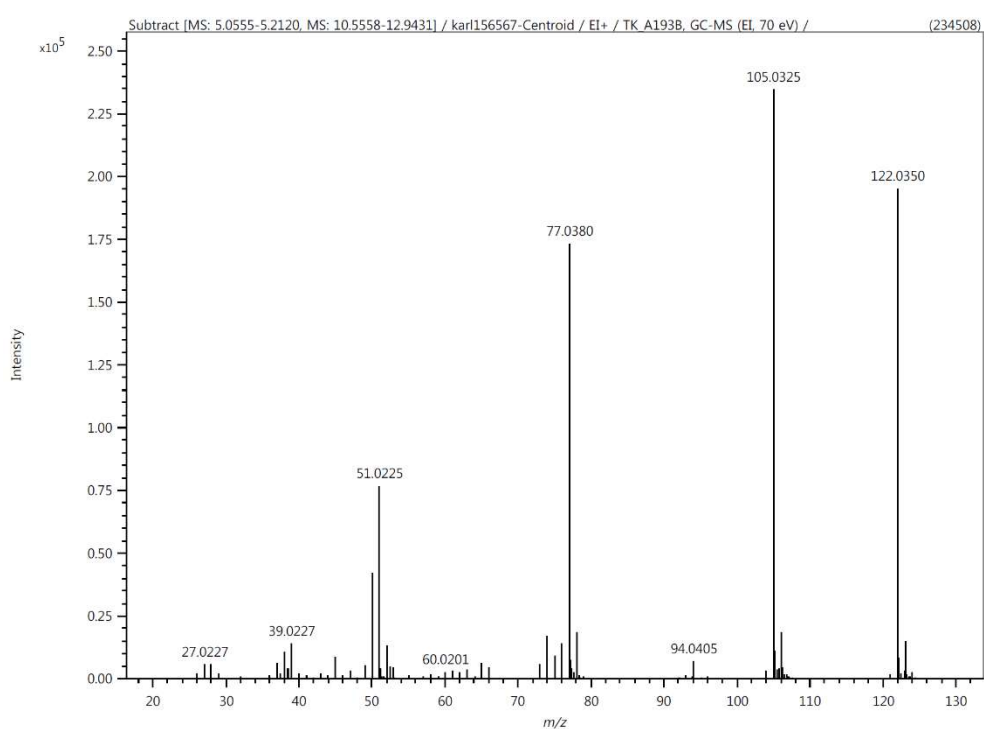
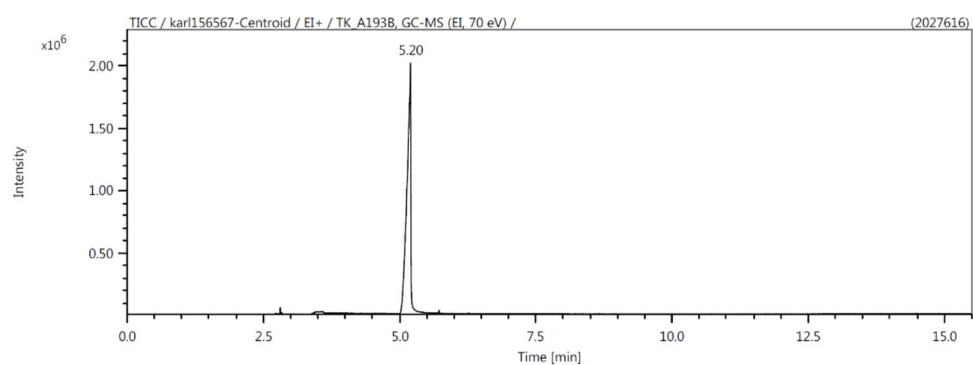
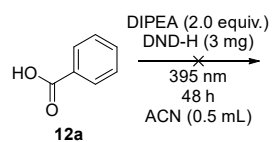


Figure S 13. Reduction of benzoic acid: GC-MS trace and HRMS.

5.6.6 Catalyst Recycling

General procedure D

For DND-H recycling we used 4-bromophenylether **1n** under standard reaction conditions (procedure **A**). The yield was determined according to procedure **B**, then the individual batches of catalyst (Table S8) were suspended in DCM, combined and transferred into one 1.5 mL Eppendorf Tube®. Centrifuged (2000 rpm) for 1 min the organic top layer was decanted. This procedure was repeated with PE, DCM and Acetone several times, till the top layer appeared colorless and the catalyst gray. Then, the open Eppendorf Tube® was placed in an oven (60°C) for 24 h. Before reuse, the dried catalyst was grinded with a spoon and a sample of recycled DND-H was taken for analytics.

Table S 8. Individual yields of recycled DND-H catalyst.

Reaction scheme: 4-bromophenylether (**1n**) reacts with DIPEA (2.0 equiv.), DND-H (3 mg) under UV light (395 nm) for 48 h in ACN (0.5 mL) to produce 4-phenylether (**2n**).

Entry ^a	Yield ₁ (%)	Yield ₂ (%)	Yield ₃ (%)	Yield ₄ (%)	Yield ₅ (%)
1	66	57	45	56	64
2	72	54	45	50	55
3	70	56	49	59	60
4	70	56	52	53	58
5	65	57	53	50	
6	67	47	56	59	
7	66	52	56		
8	63	49	57		
9	64	55			
10	70	49			
11	67				
12	65				

^a The number of reactions decreases because of sampling catalyst for surface analysis

5.6.7 Substrate Synthesis

Ethyl 2-(2-bromophenoxy)-2-methylpropanoate (1a_q):^[1] In a 50 mL Schlenk flask, a mixture of 2-bromophenol (650 μ L, 5.0 mmol, 1 equiv.), ethyl 2-bromoisobutyrate (595 μ L, 5.0 mmol, 1.0 equiv.) and K_2CO_3 (691 mg, 5 mmol, 1.0 equiv.) in dry ACN (10 mL) was refluxed for 18 h under nitrogen atmosphere. The mixture was cooled to room temperature and filtered, then washed with brine and dried over anhydrous Na_2SO_4 . The solvent was removed under reduced pressure and the crude was purified by flash column chromatography with PE/EA (95:5) to afford a colorless oil: 66% yield. **¹H NMR (400 MHz, $CDCl_3$)** δ_H [ppm] = 7.54 (dd, J = 7.8, 1.6 Hz, 1H), 7.16 (td, J = 8.0, 1.6 Hz, 1H), 6.90 – 6.84 (m, 2H), 4.25 (q, J = 7.1 Hz, 2H), 1.62 (s, 6H), 1.26 (t, J = 7.1 Hz, 3H). **¹³C NMR (101 MHz, $CDCl_3$)** δ_C [ppm] = 174.20, 152.73, 133.64, 128.05, 123.65, 119.52, 116.32, 80.94, 61.66, 25.32, 25.32, 14.21. **HRMS (ESI+)** m/z calcd. for $C_{12}H_{16}BrO_3$ + [$M+H$]+ = 287.0277, found 287.0277.

2-(4-chlorophenoxy)benzoic acid (1p):^[2] In a 100 mL Schlenk flask, a mixture of 4-chlorophenol (590 μ L, 6.0 mmol, 1.2 equiv.), 2-fluorobenzonitrile (543 μ L, 5.0 mmol, 1.0 equiv.) and K_2CO_3 (2.1 g, 15 mmol, 3 equiv.) in dry DMF (25 mL) was stirred under nitrogen atmosphere at 100°C for 10 h. The mixture was cooled to room temperature filtered and washed with ethyl acetate. Water (10 mL) was added to the solution and the organic phase was separated. Then, the aqueous phase was extracted with ethyl acetate (3x 20 mL) and the combined organic phase was washed with NaOH (5%) and brine. Dried over anhydrous Na_2SO_4 , the solvent was removed under reduced pressure. Without further purification, the crude was submitted to a mixture of NaOH (1.5 g, 37.5 mmol, 7.5 equiv.) in water/ethanol (1:1, 0.2 M) and stirred under reflux for 16 h. The mixture was cooled to room temperature, water (20 mL) was added and the mixture was extracted with ethyl acetate (20 mL). The aqueous solution was acidified with 1 N HCl and extracted with ethyl acetate (3x 20mL). Then, the combined organic phase was washed with brine and dried over anhydrous Na_2SO_4 . Solvent was removed under reduced pressure and the crude was purified by flash column chromatography (PE/EA) to afford a white solid: 85% yield. **¹H NMR (400 MHz, $CDCl_3$)** δ_H [ppm] = 11.10 (s, 1H), 8.13 (dd, J = 7.9, 1.7 Hz, 1H), 7.51 (td, J = 8.4, 1.8 Hz, 1H), 7.34 (d, J = 8.9 Hz, 2H), 7.23 (td, J = 7.9, 0.9 Hz, 1H), 6.99 (d, J = 8.9 Hz, 2H), 6.90 (d, J = 8.3 Hz, 1H). **¹³C NMR (101 MHz, $CDCl_3$)** δ_C [ppm] = 168.15, 156.98, 154.62, 135.00, 133.44, 130.22, 129.84, 124.13, 120.77, 119.27. **HRMS (EI+)** m/z calcd. for $C_{13}H_9O_3Cl$ + [M]+ = 248.02347, found 248.02403; MP: 130-132°C

5.6.8 GC-FID Calibration

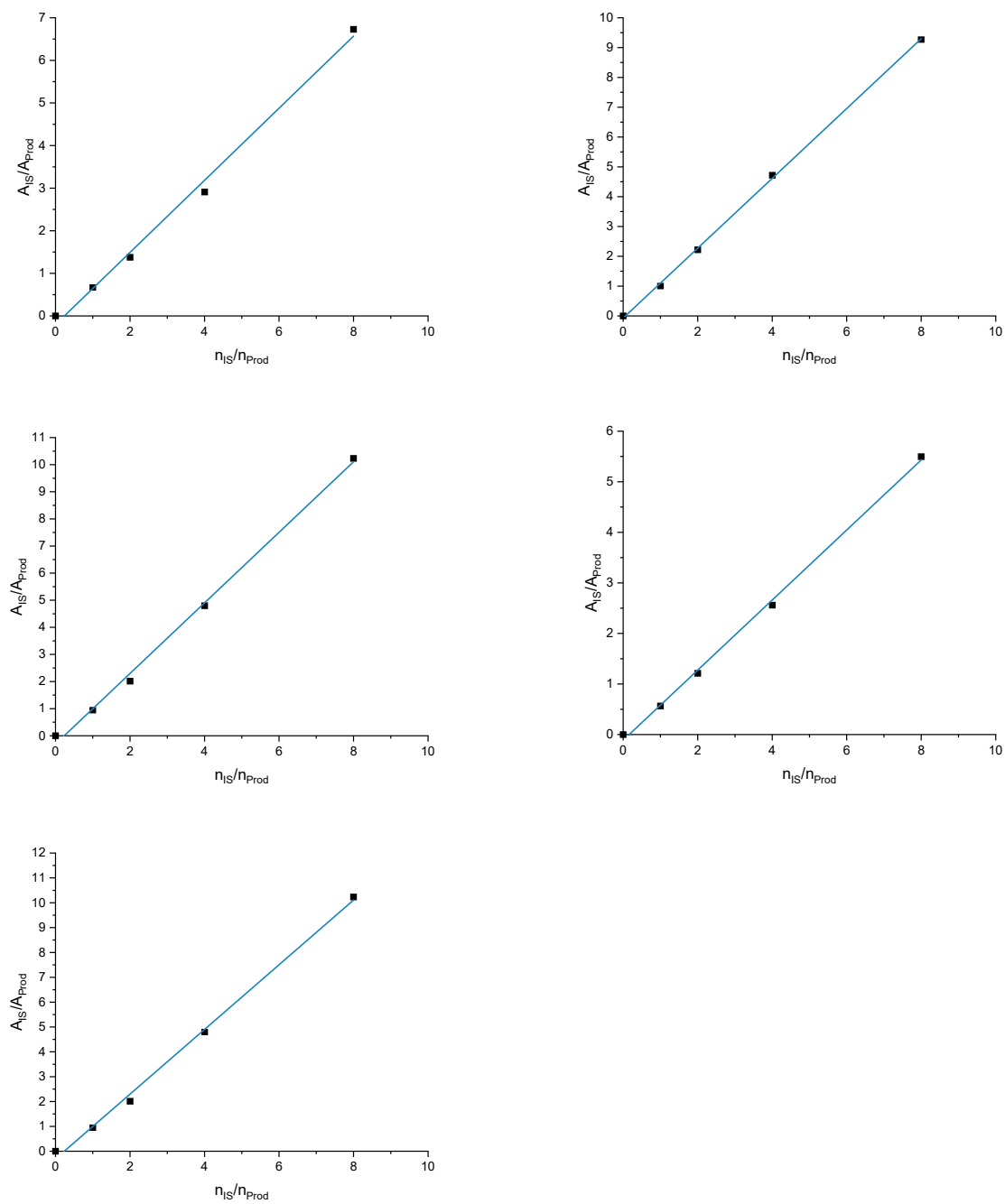


Figure S 14. GC-FID calibration curves of (top left) tertbutylbenzene, (top right) benzotrifluoride, (center left) ethylbenzene, (center right) diphenylether, (bottom left) benzene, with heptane as internal standard.

5.6.9 X-Ray Crystallography

Compound	V108_Wdh
Formula	C ₆ H ₁₆ BrN
$D_{calc.}/\text{g cm}^{-3}$	1.381
μ/mm^{-1}	5.719
Formula Weight	182.104
Color	clear colorless
Shape	prism-shaped
Size/mm ³	0.08×0.07×0.06
T/K	123.00(10)
Crystal System	monoclinic
Flack Parameter	0.004(16)
Hoof Parameter	0.004(16)
Space Group	$P2_1$
$a/\text{Å}$	7.7655(1)
$b/\text{Å}$	8.0280(1)
$c/\text{Å}$	7.8409(1)
α°	90
β°	116.385(2)
γ°	90
$V/\text{Å}^3$	437.892(12)
Z	2
Z'	1
Wavelength/Å	1.54184
Radiation type	Cu K α
Θ_{min}°	6.30
Θ_{max}°	75.23
Measured Refl's.	8988
Indep't Refl's	1794
Refl's $I \geq 2(I)$	1726
R_{int}	0.0517
Parameters	78
Restraints	4
Largest Peak	0.9627
Deepest Hole	-0.3355
GooF	1.0257
wR_2 (all data)	0.0834
wR_2	0.0829
R_1 (all data)	0.0327
R_1	0.0320

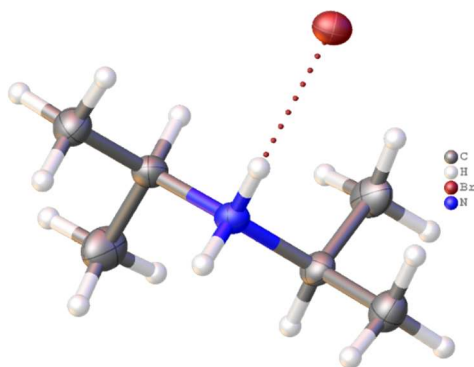
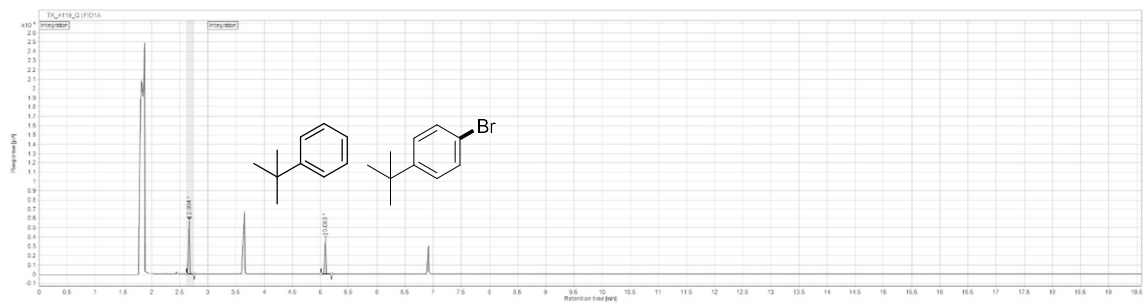


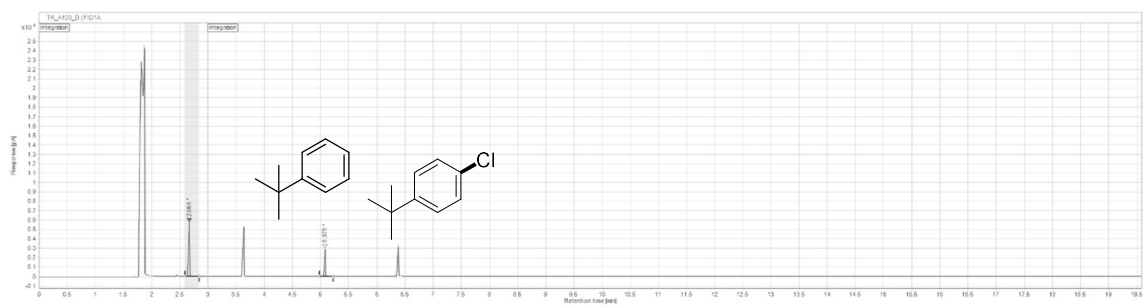
Figure S 15. Solid-state molecular structure of C₆H₁₆BrN. Thermal ellipsoids are set at the 50% probability level. C atoms are shown in grey, H atoms in white, N atoms in blue and Br atoms in red.

5.6.10 GC-FID Spectra

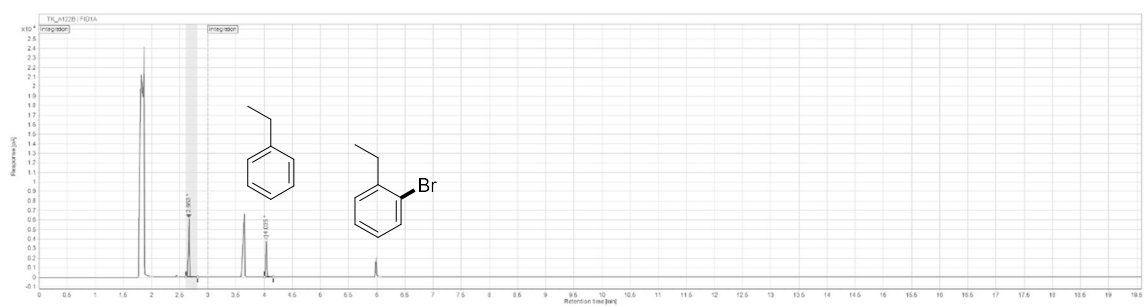
2a



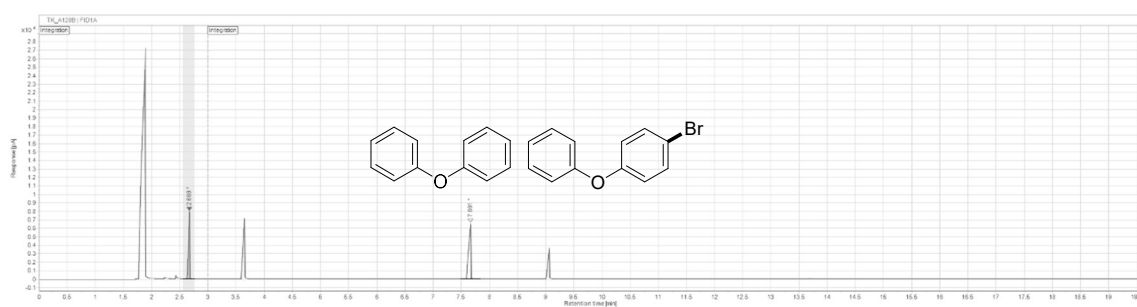
2b



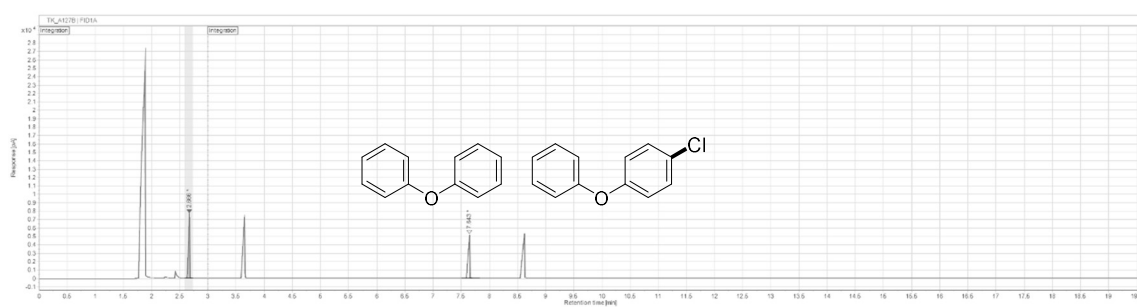
2c



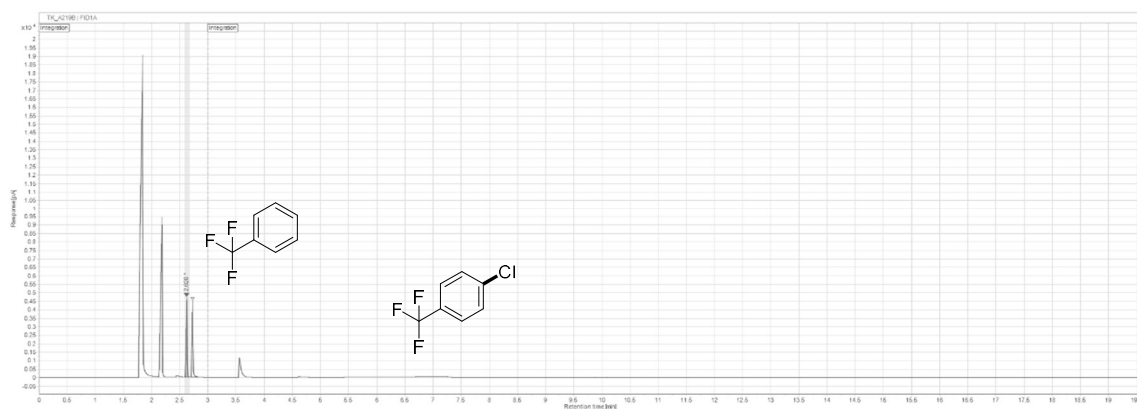
2n



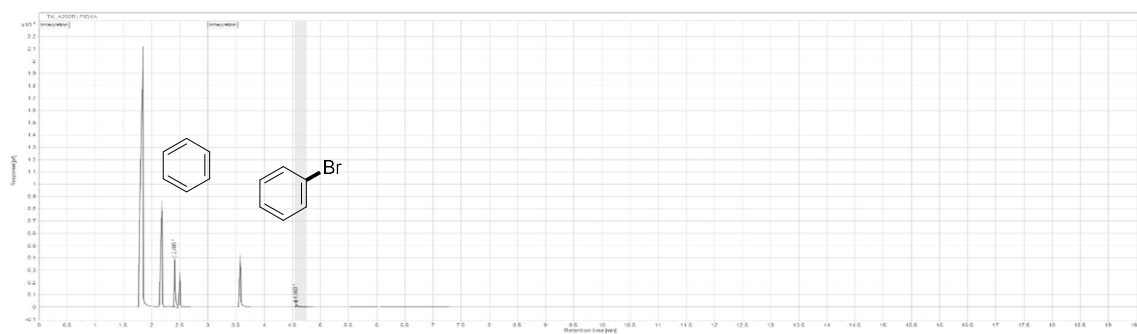
2o



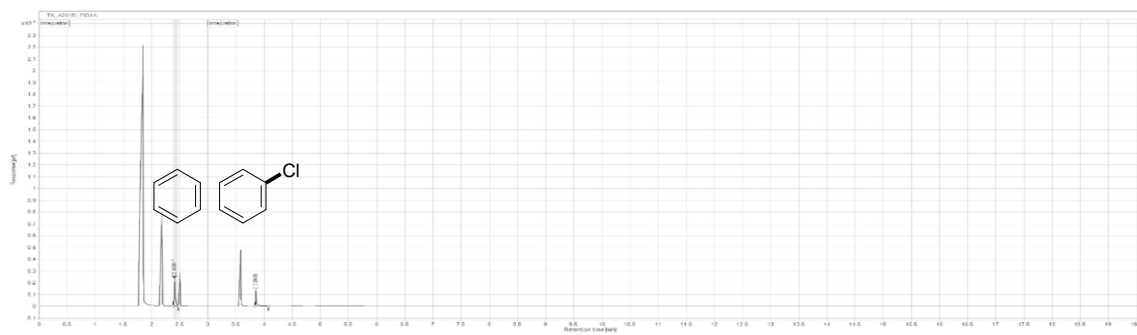
2s



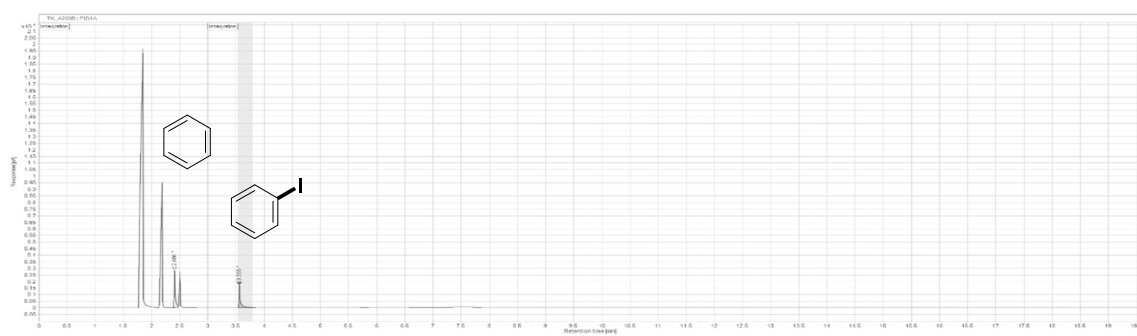
2at



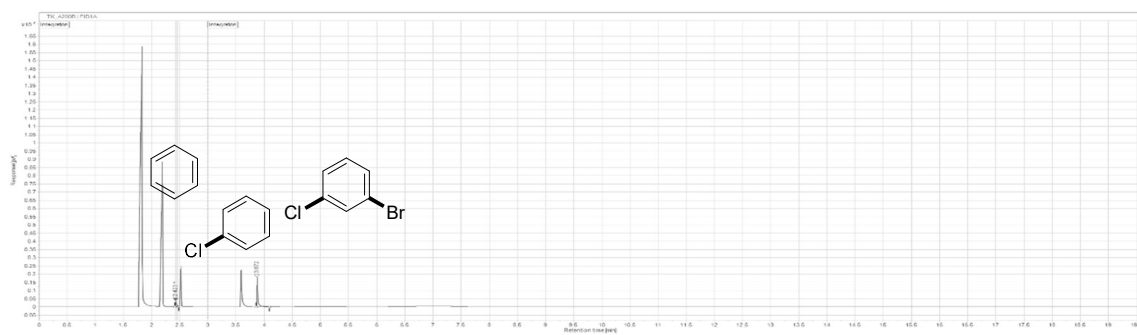
2au



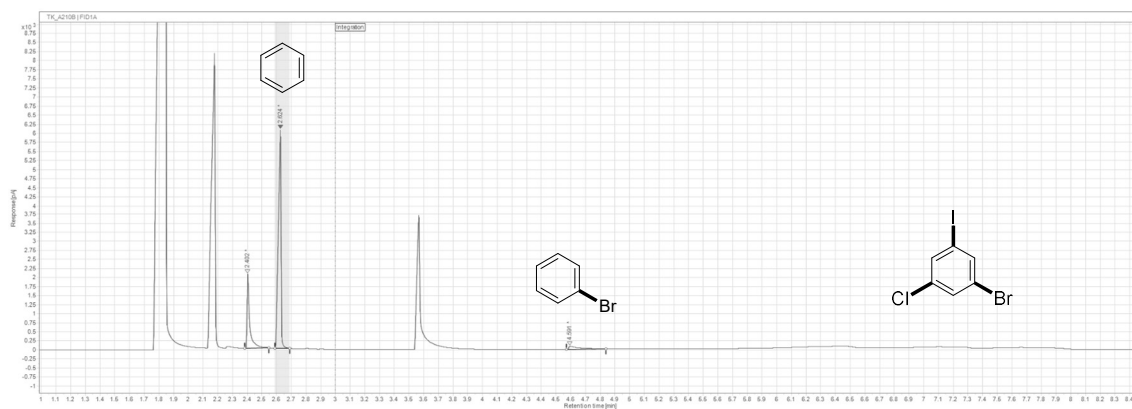
2av



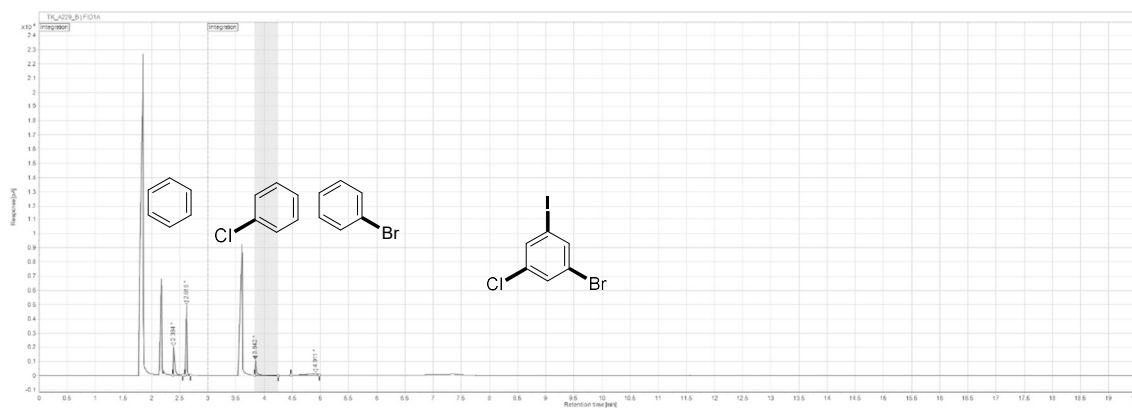
2aw



2ax

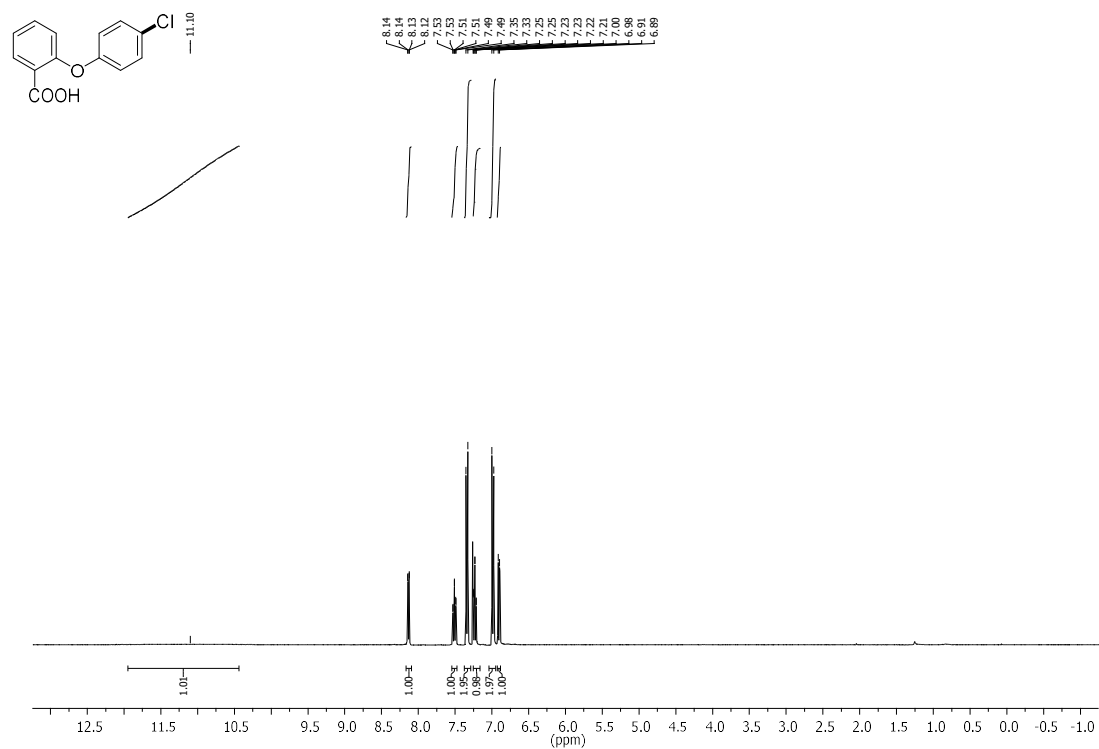
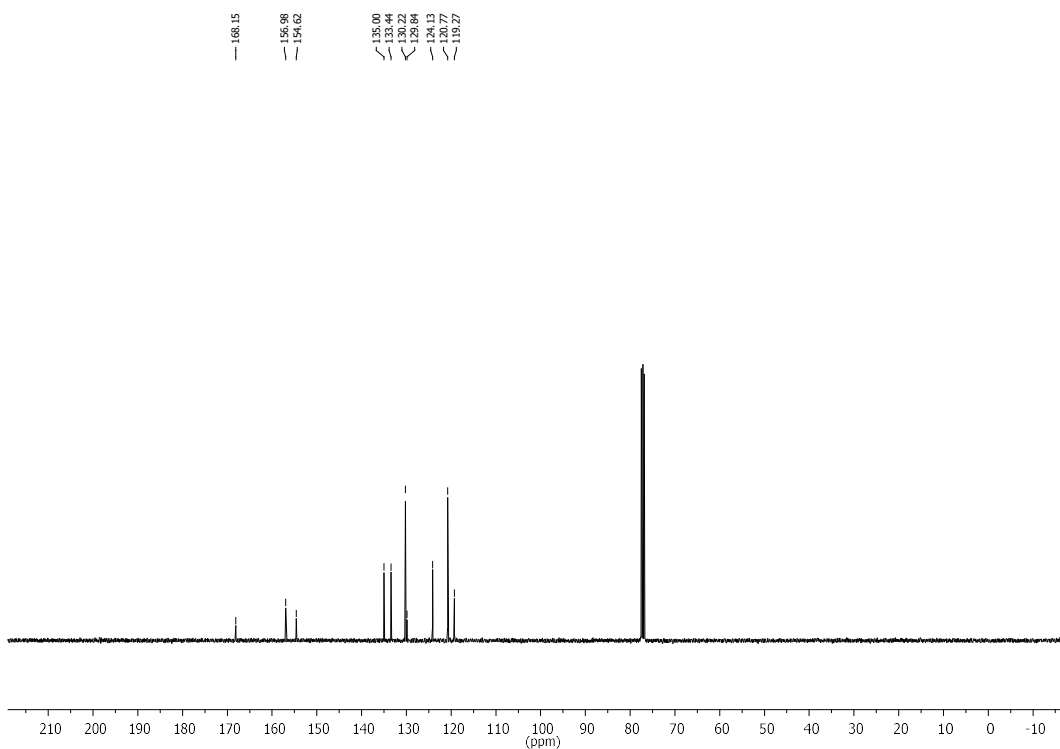


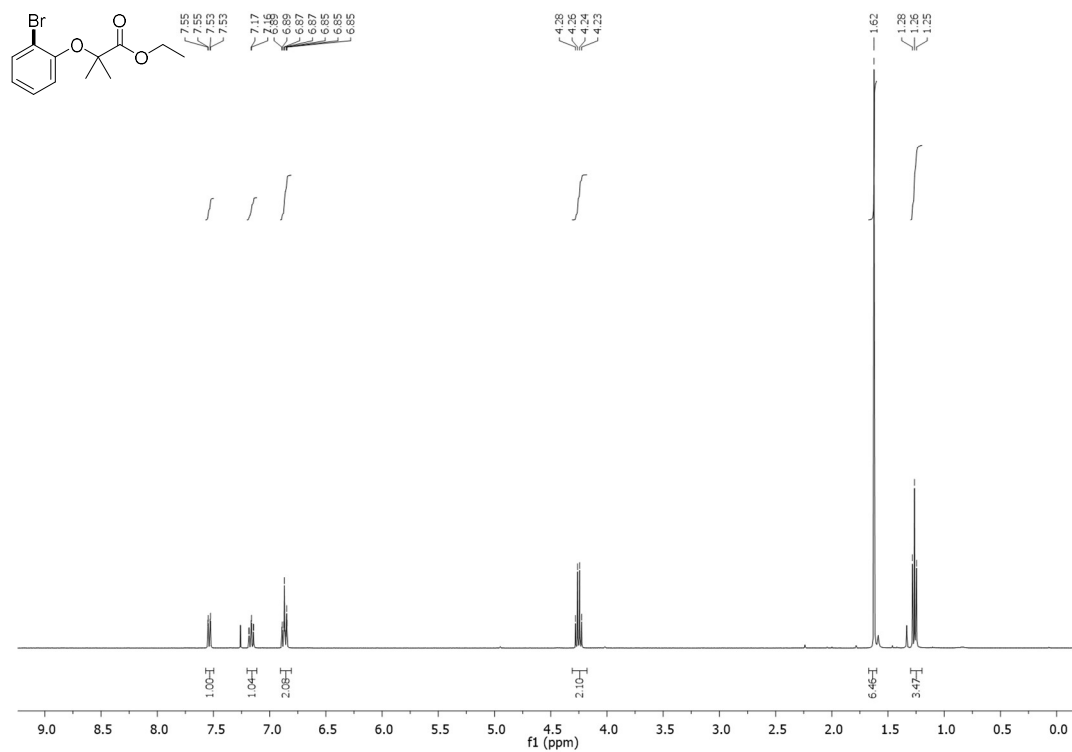
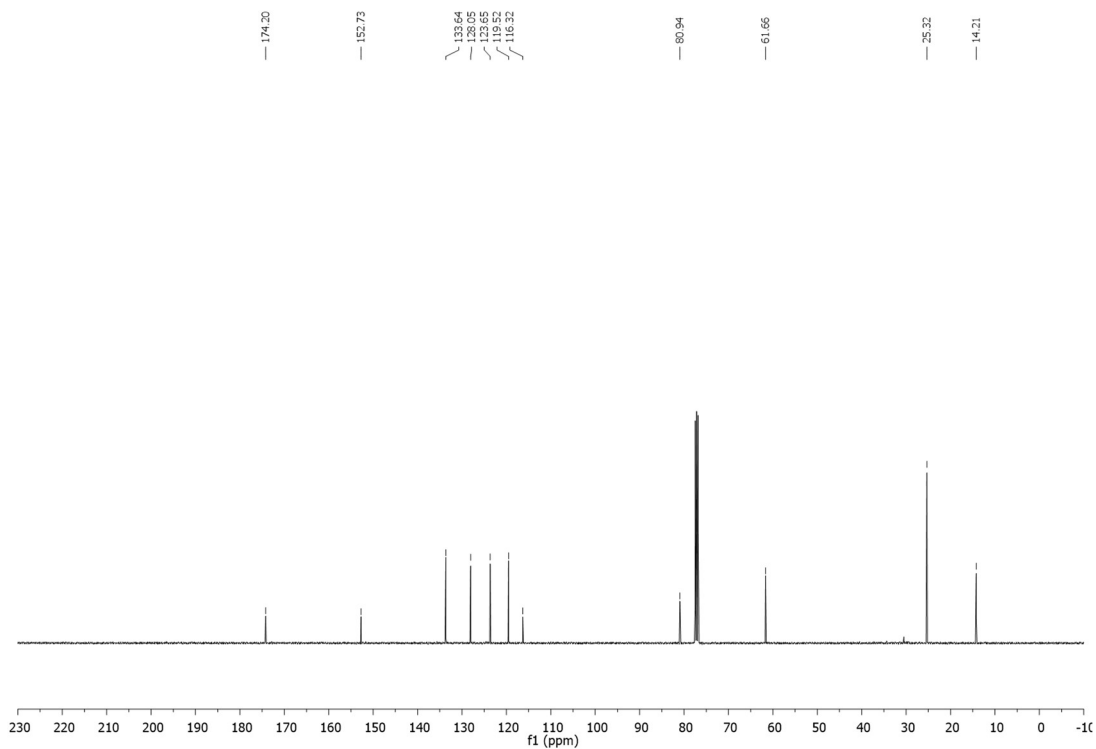
2az



5.6.11 NMR Spectra of Isolated Compounds

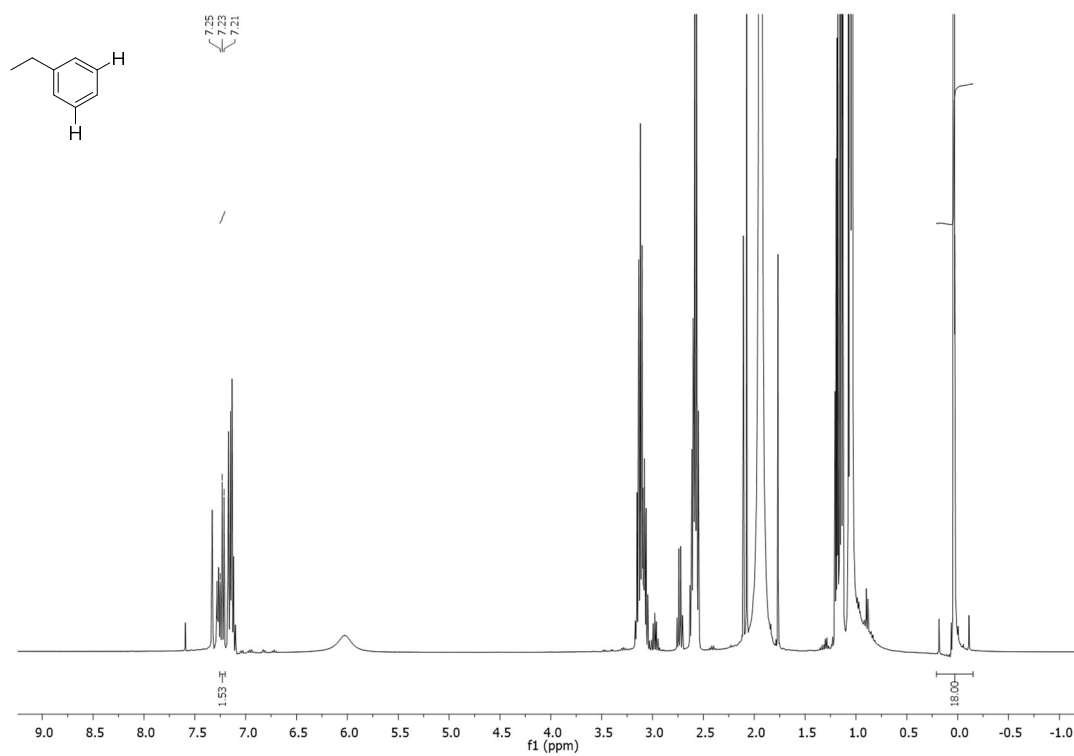
2-(4-chlorophenoxy)benzoic acid (1p):

 ^1H NMR (400 MHz, CDCl_3) ^{13}C NMR (101 MHz, CDCl_3)

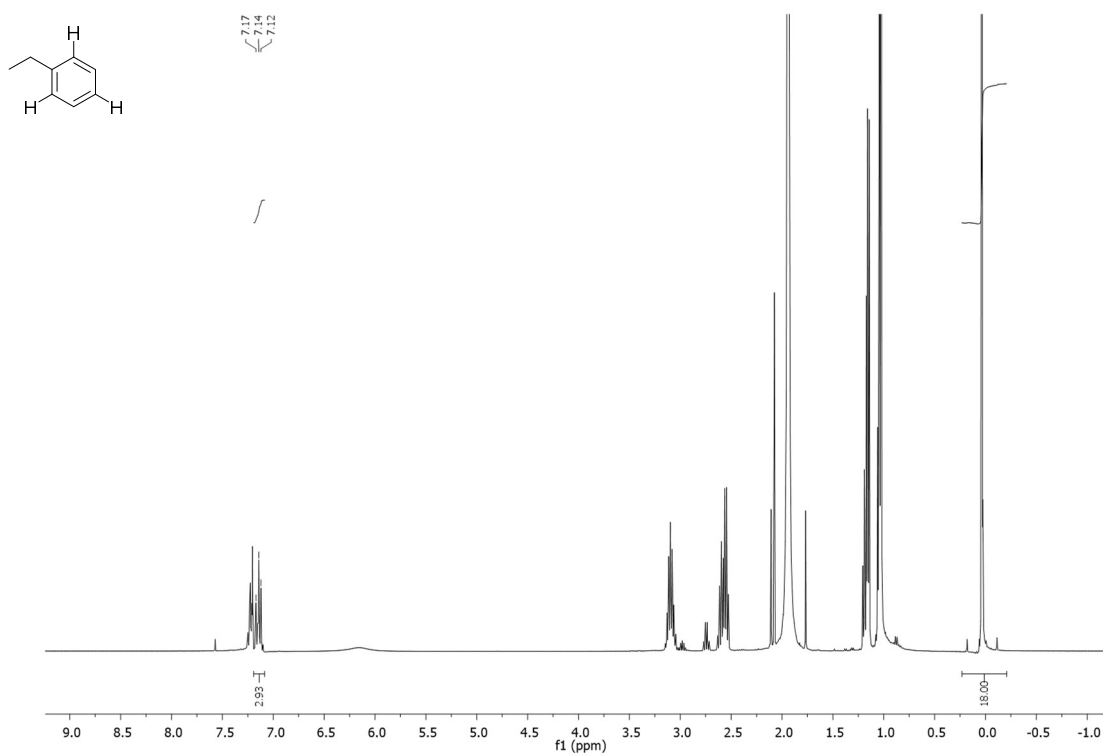
ethyl 2-(2-bromophenoxy)-2-methylpropanoate (1a): ^1H NMR (400 MHz, CDCl_3) ^{13}C NMR (101 MHz, CDCl_3)

5.6.12 NMR Spectra of Crude Mixtures

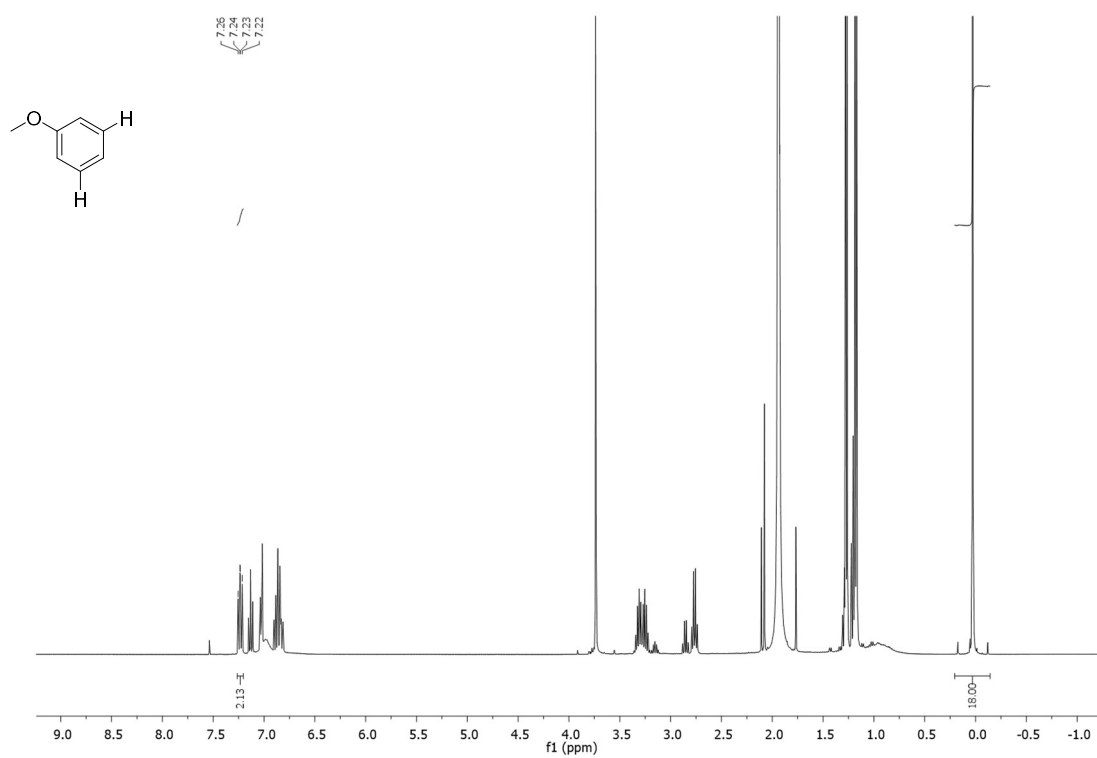
2d



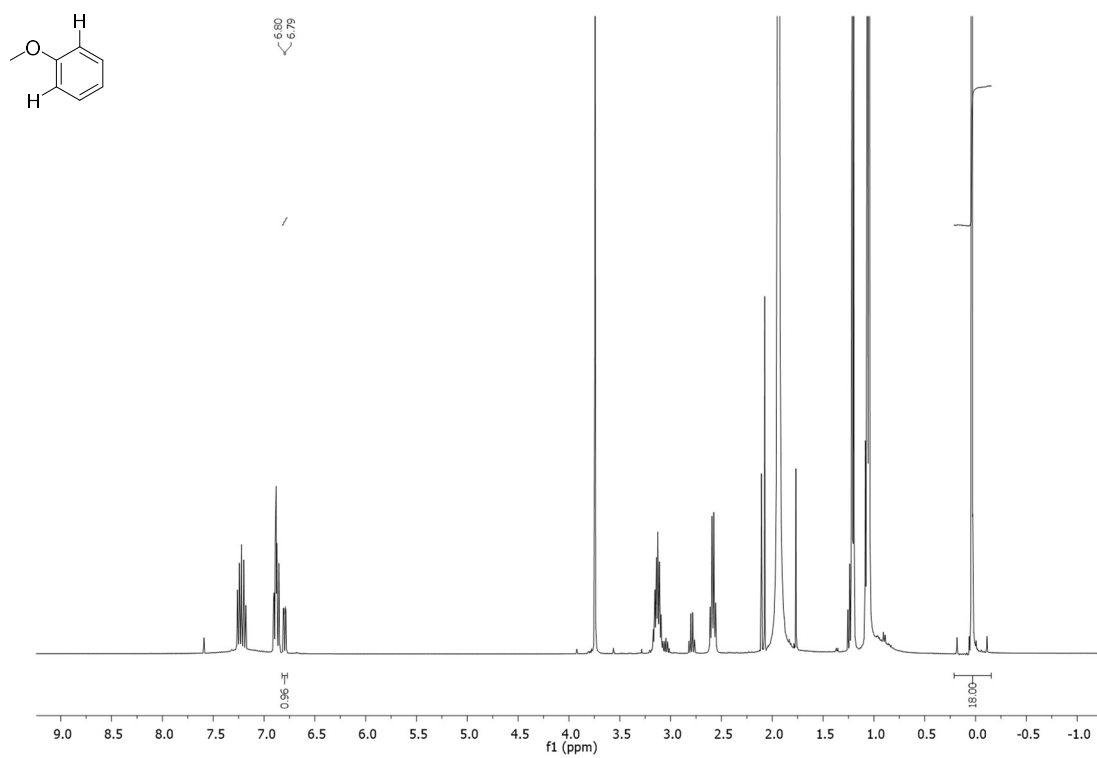
2e



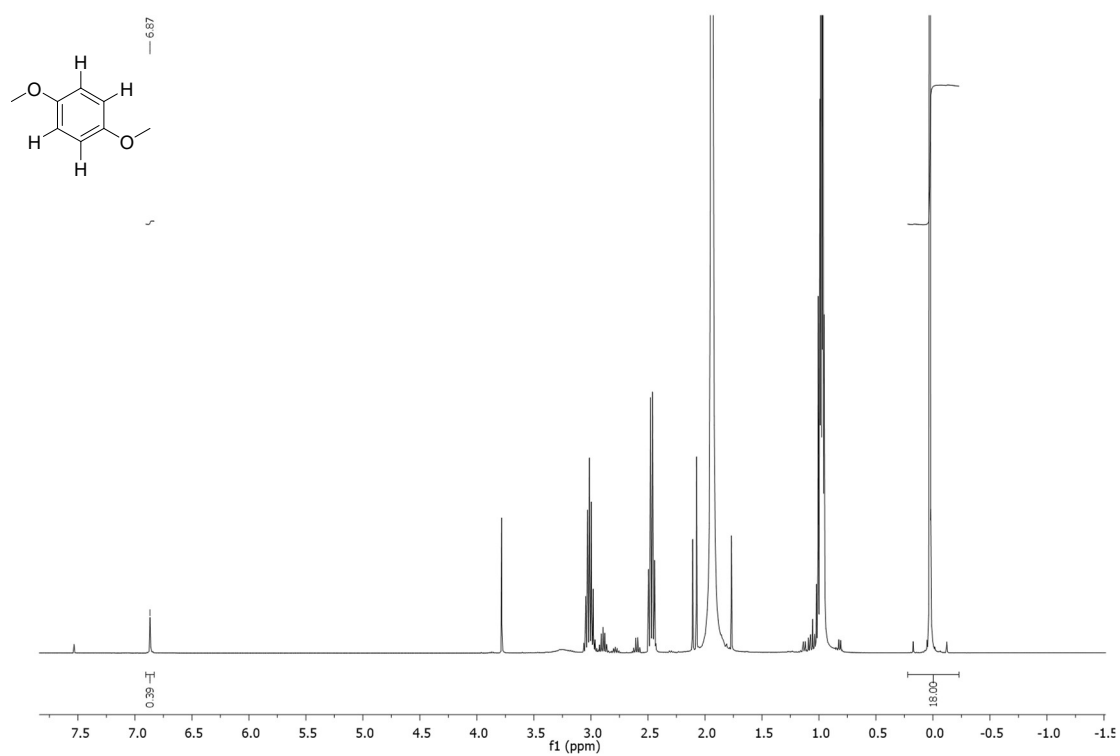
2f



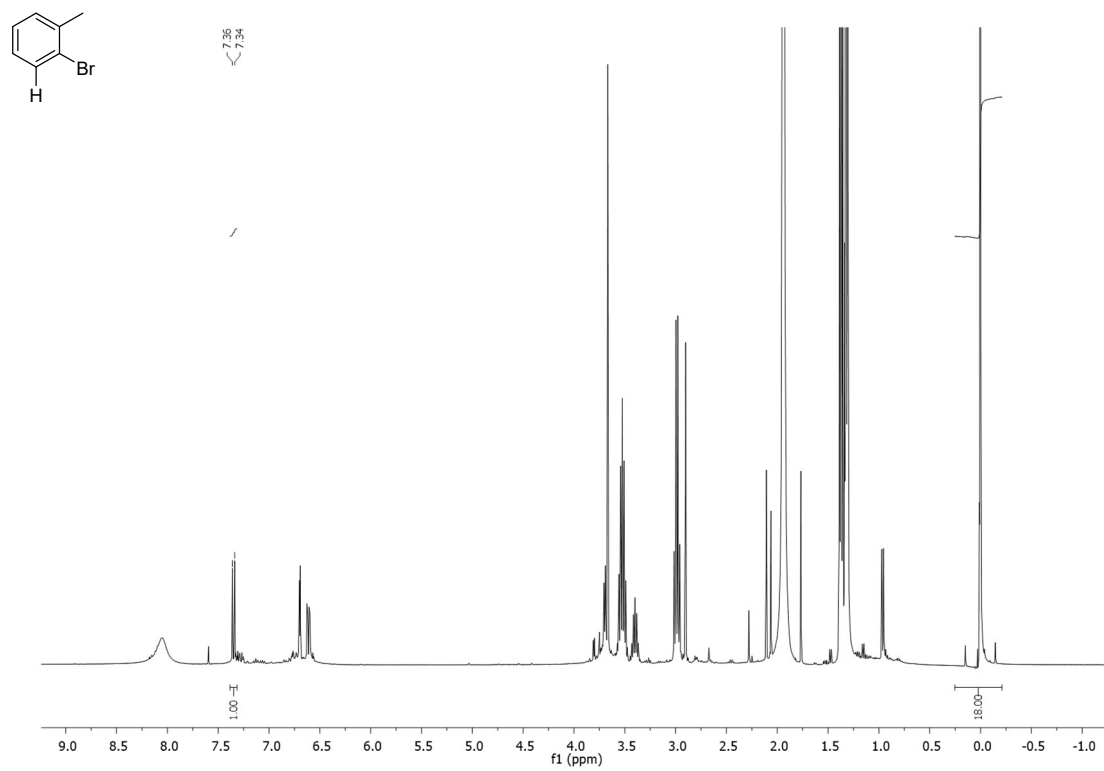
2g



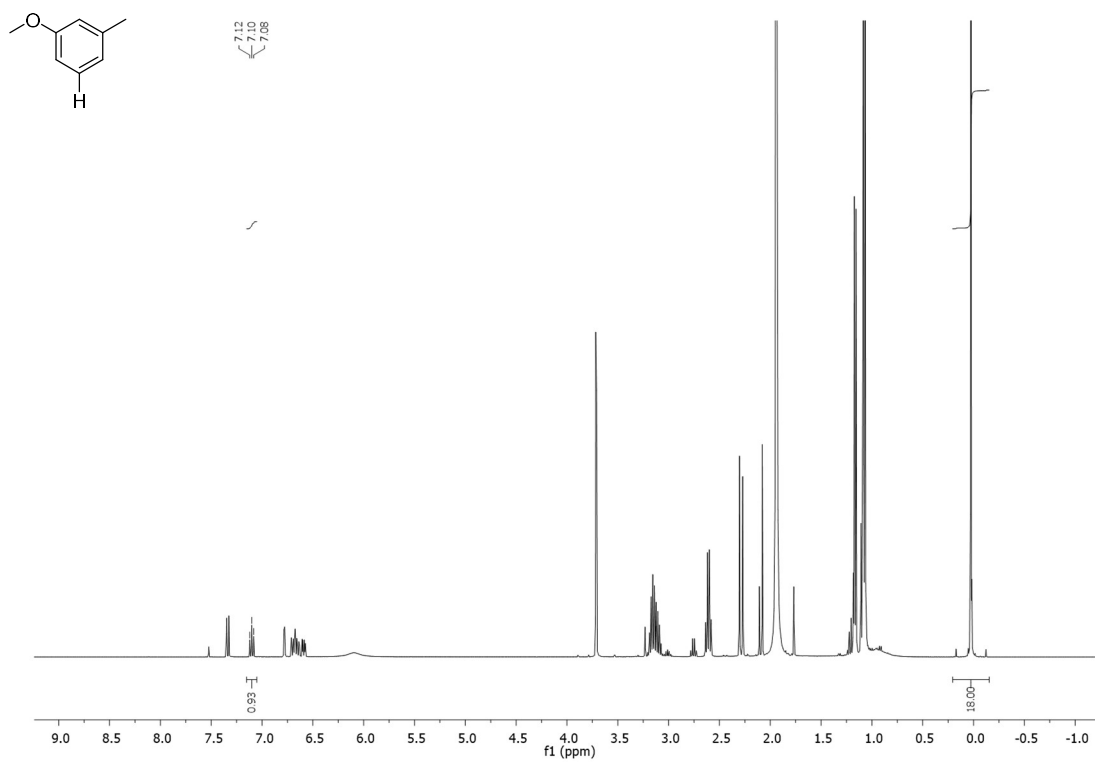
2k



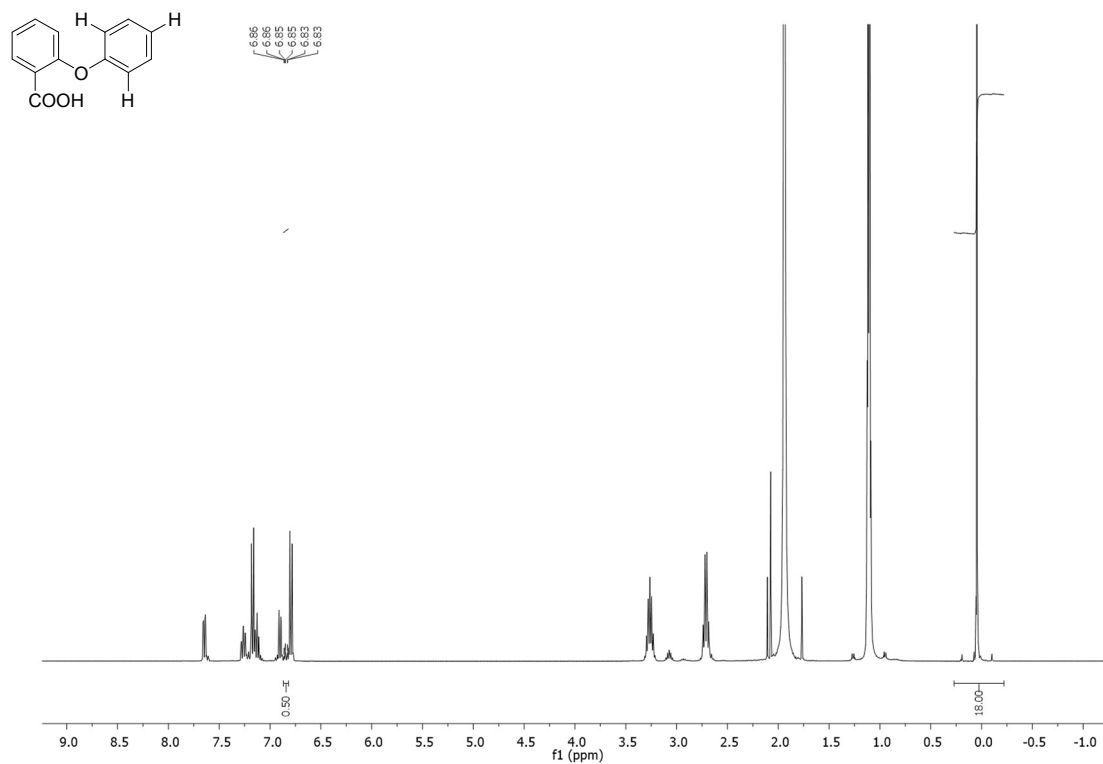
2l



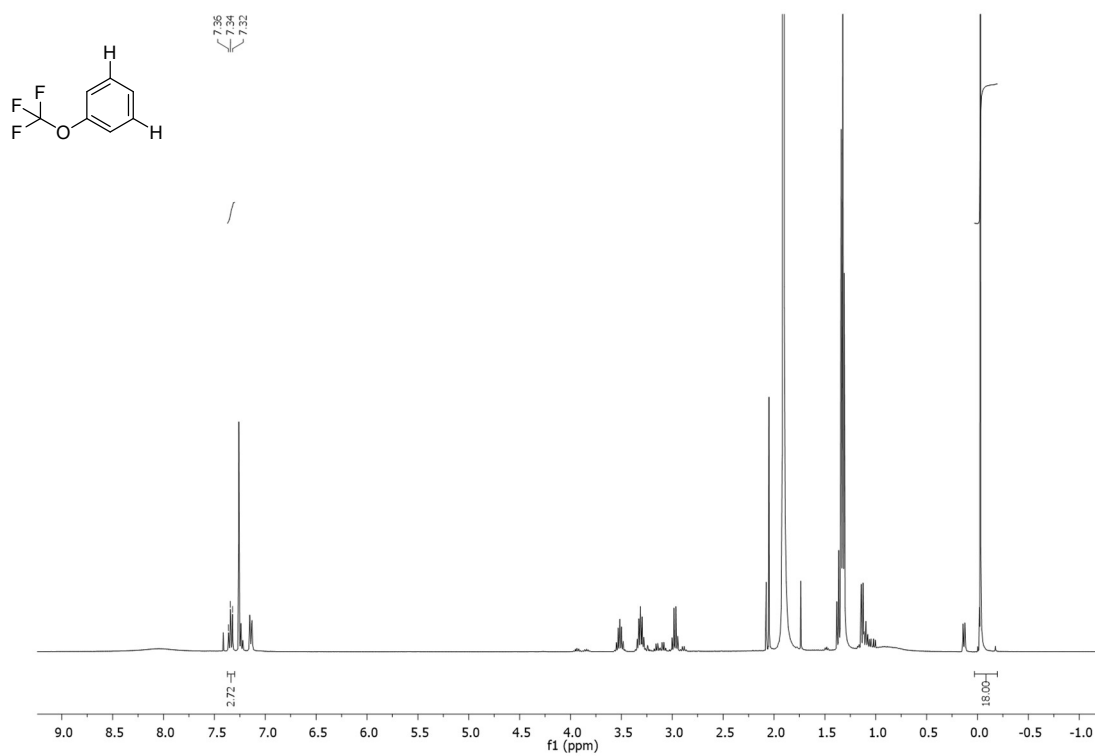
2m



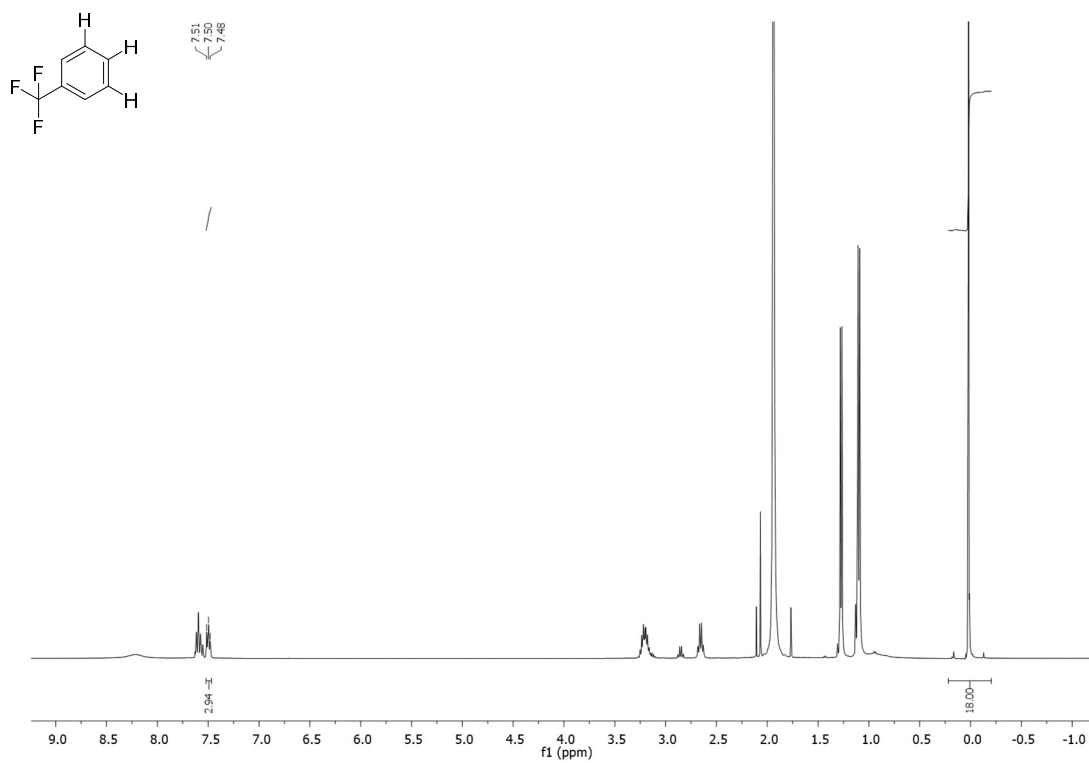
2p

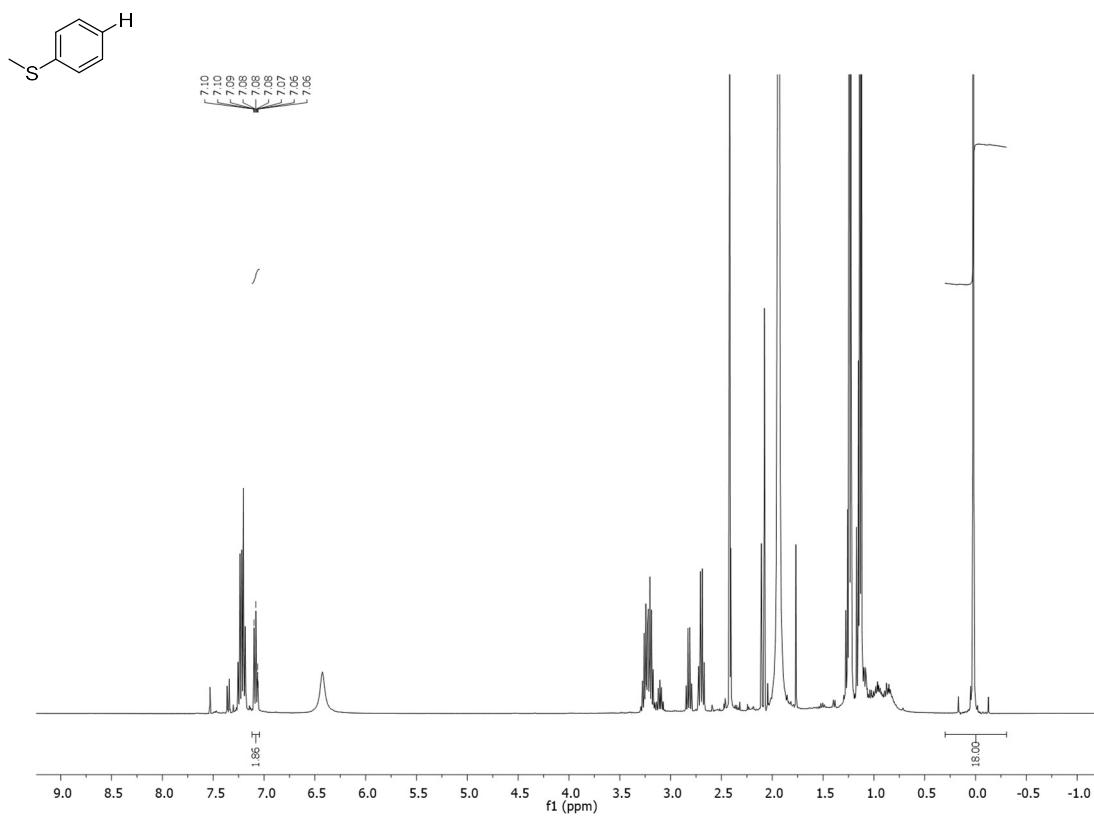
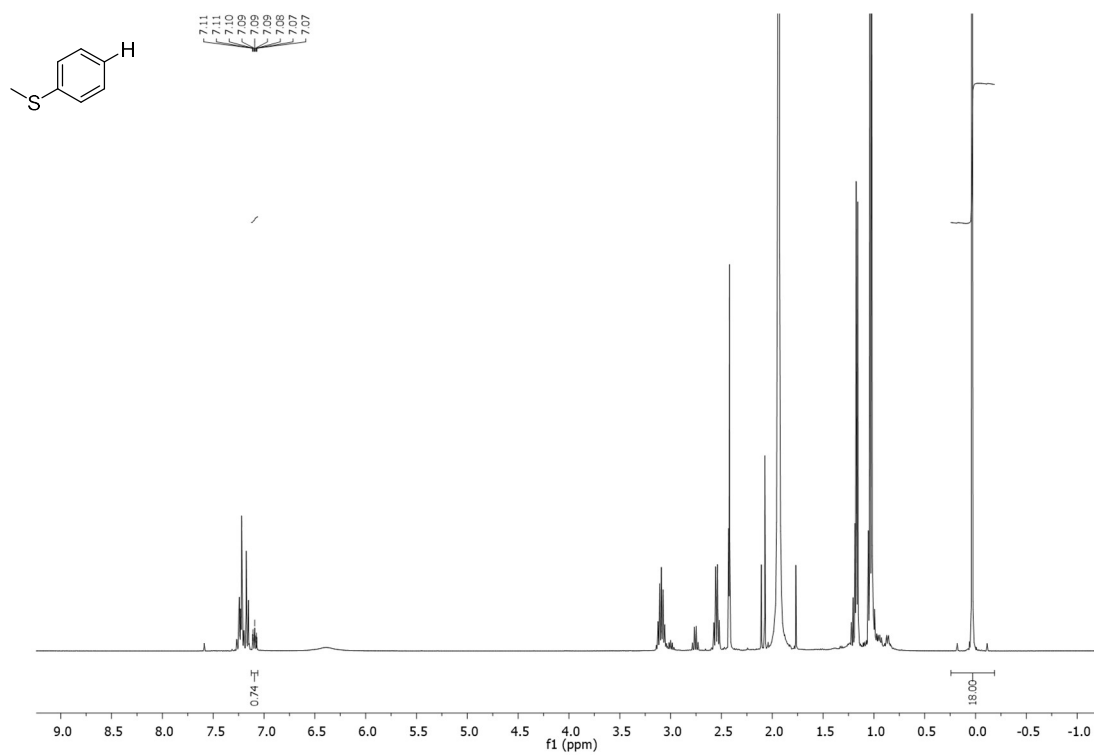


2q

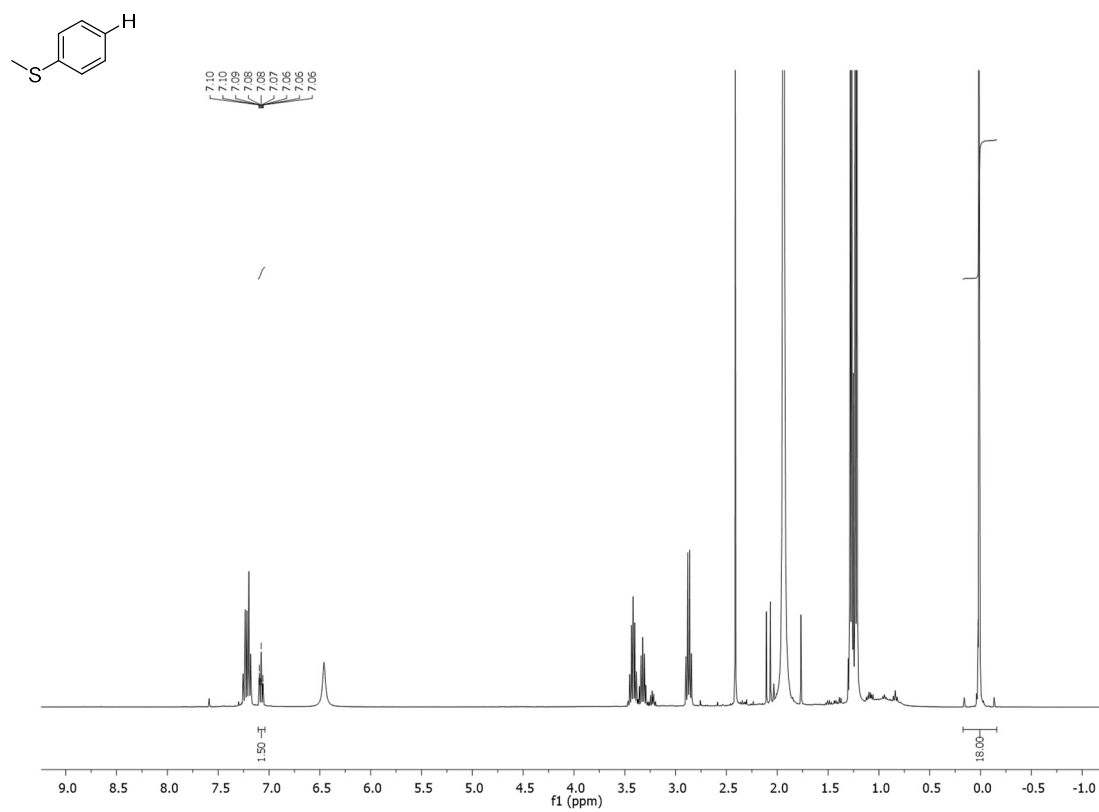


2s

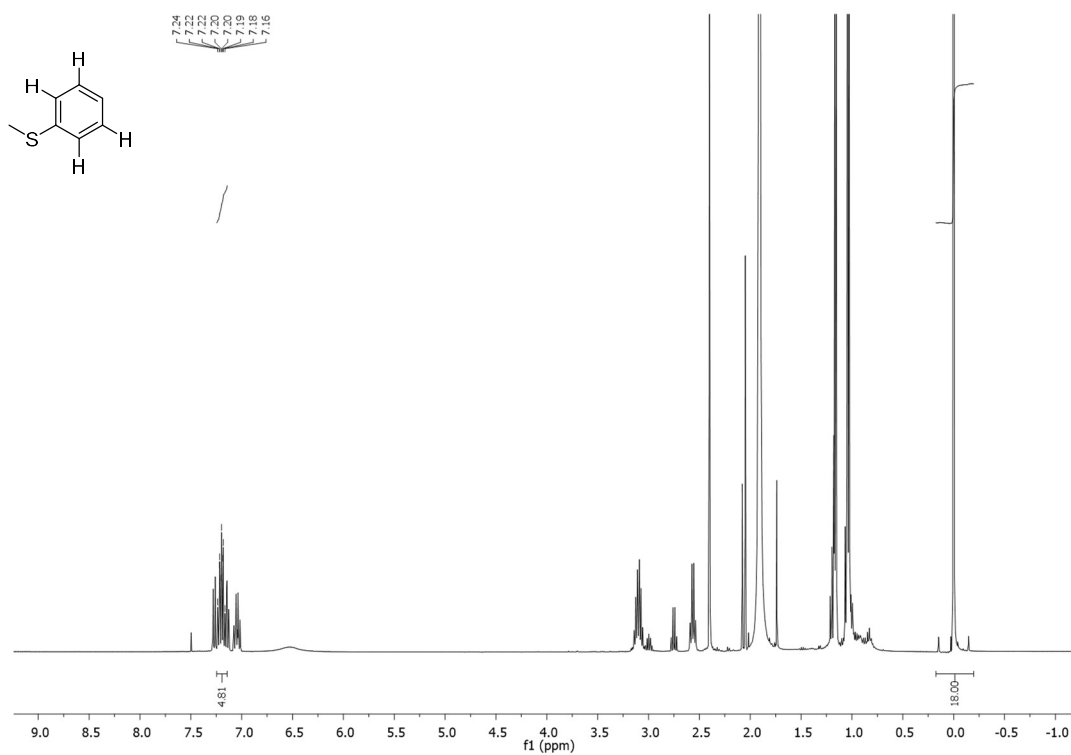


2t**2u**

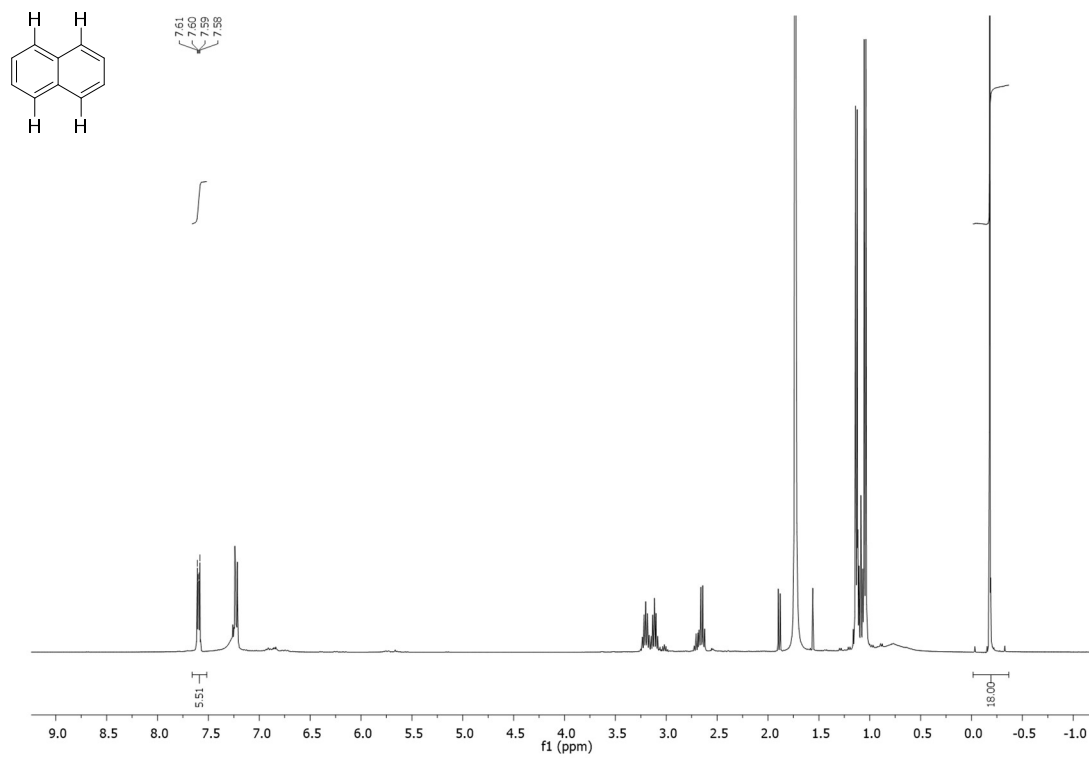
2v



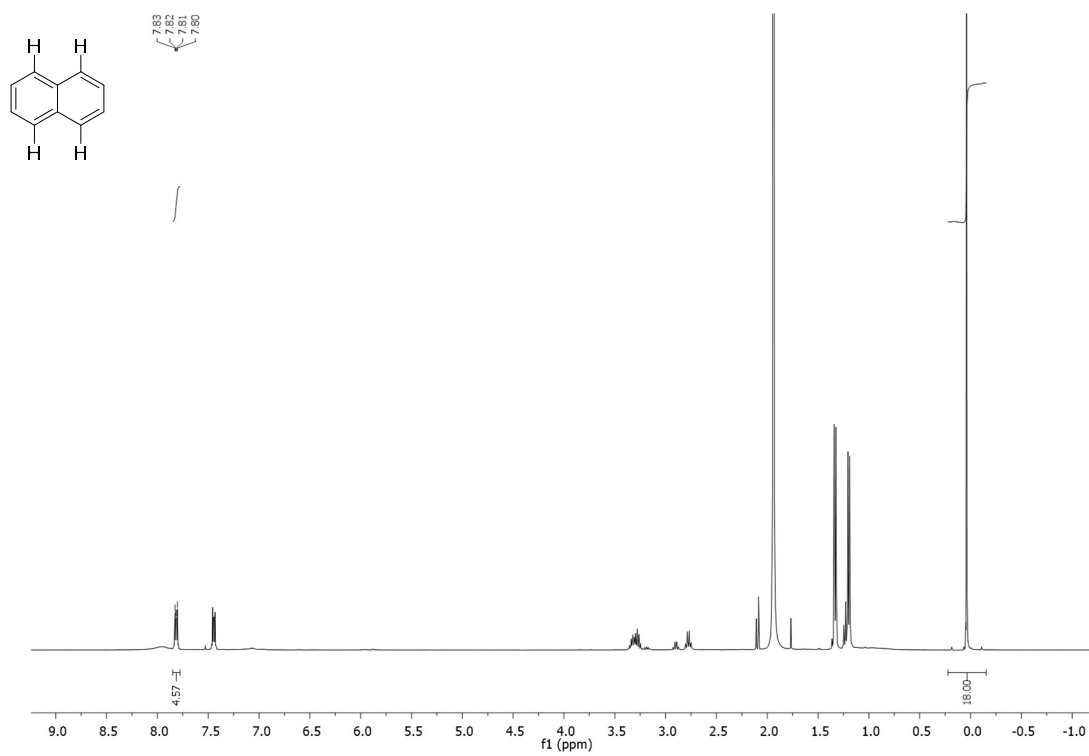
2w

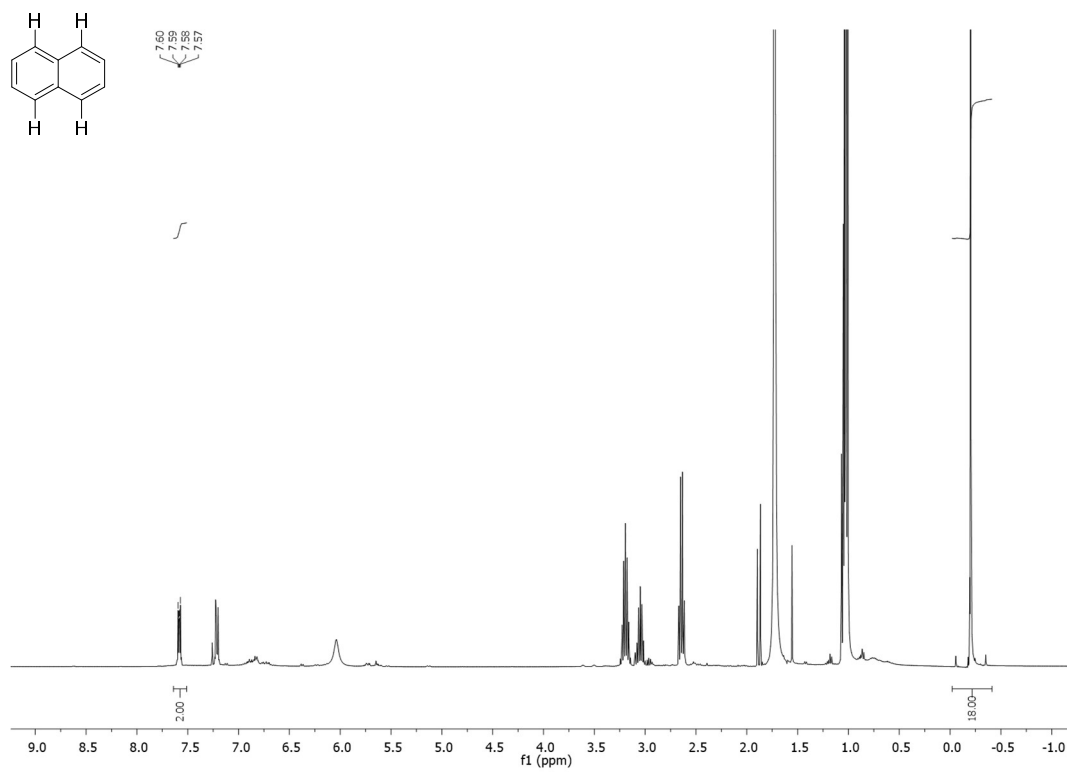
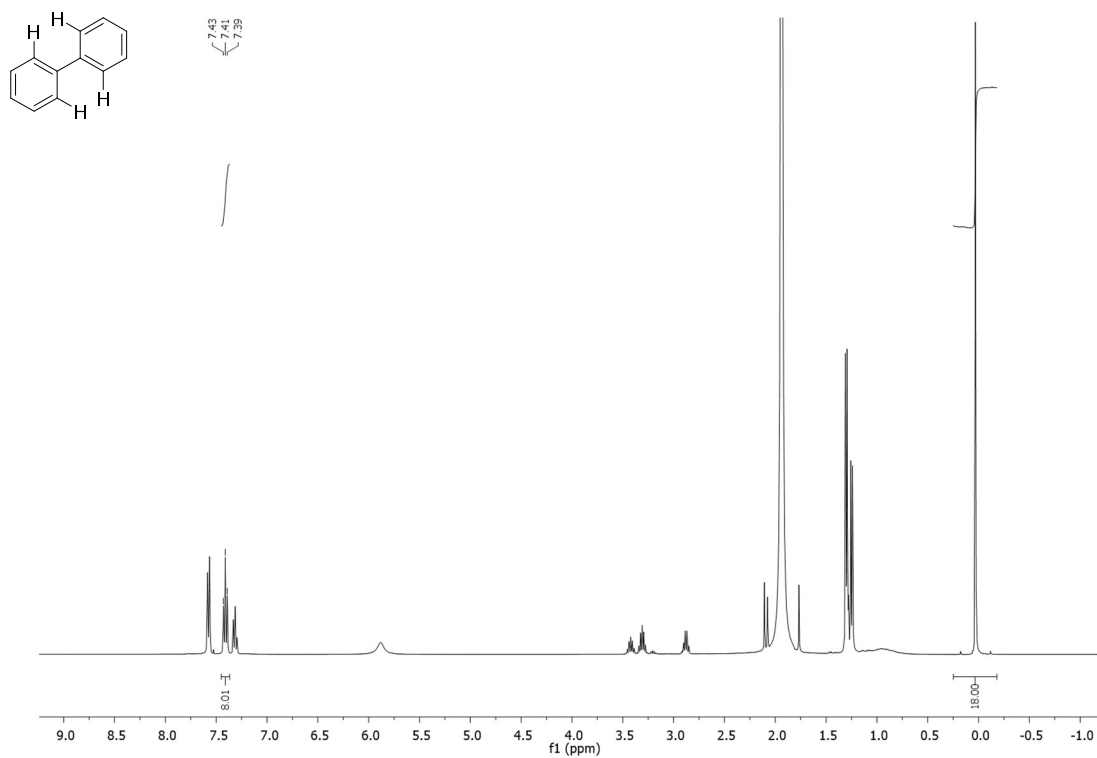


2x

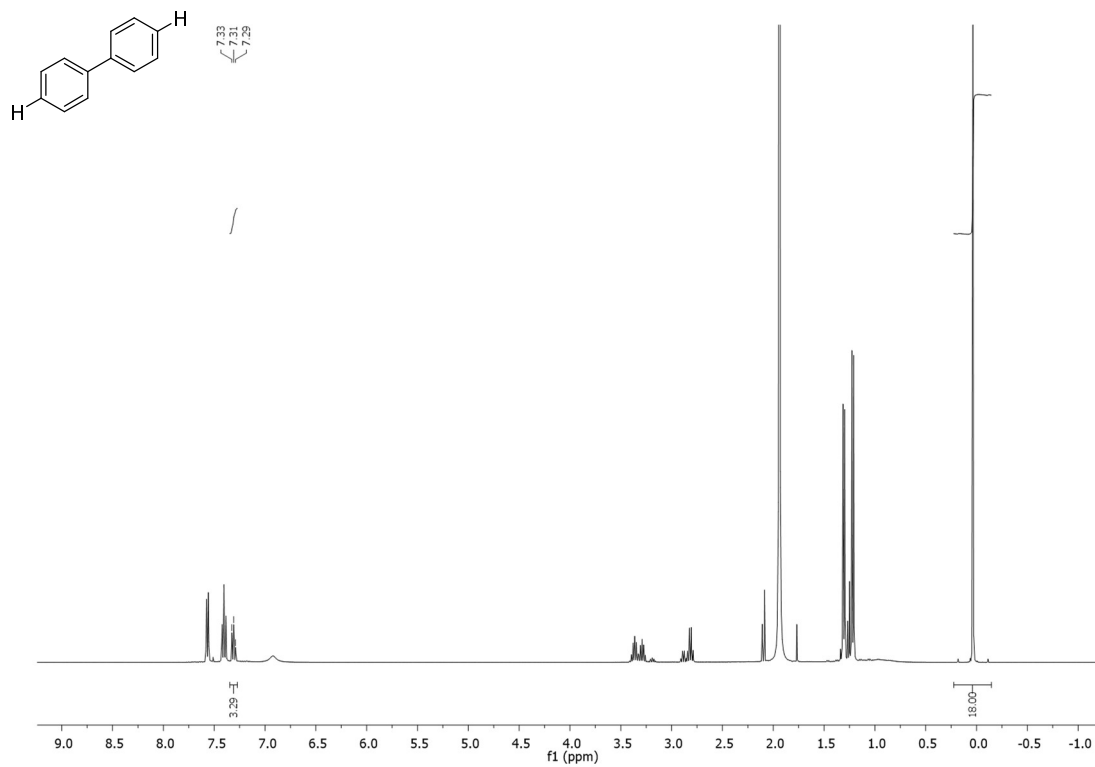


2y

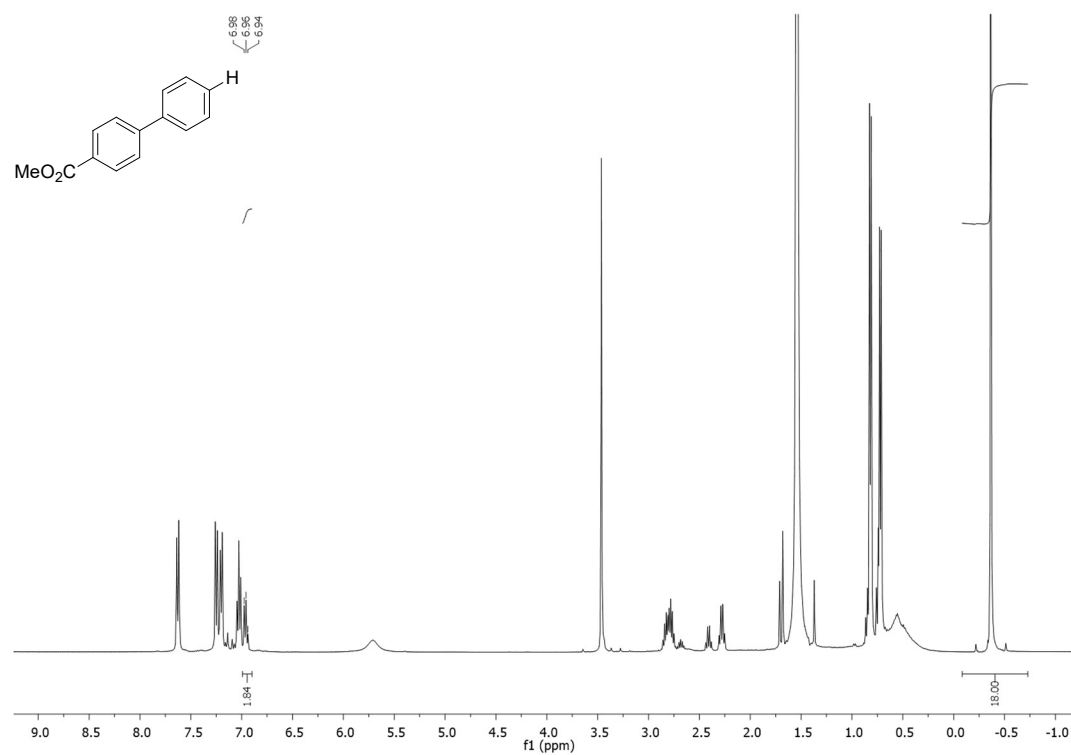


2z**2aa**

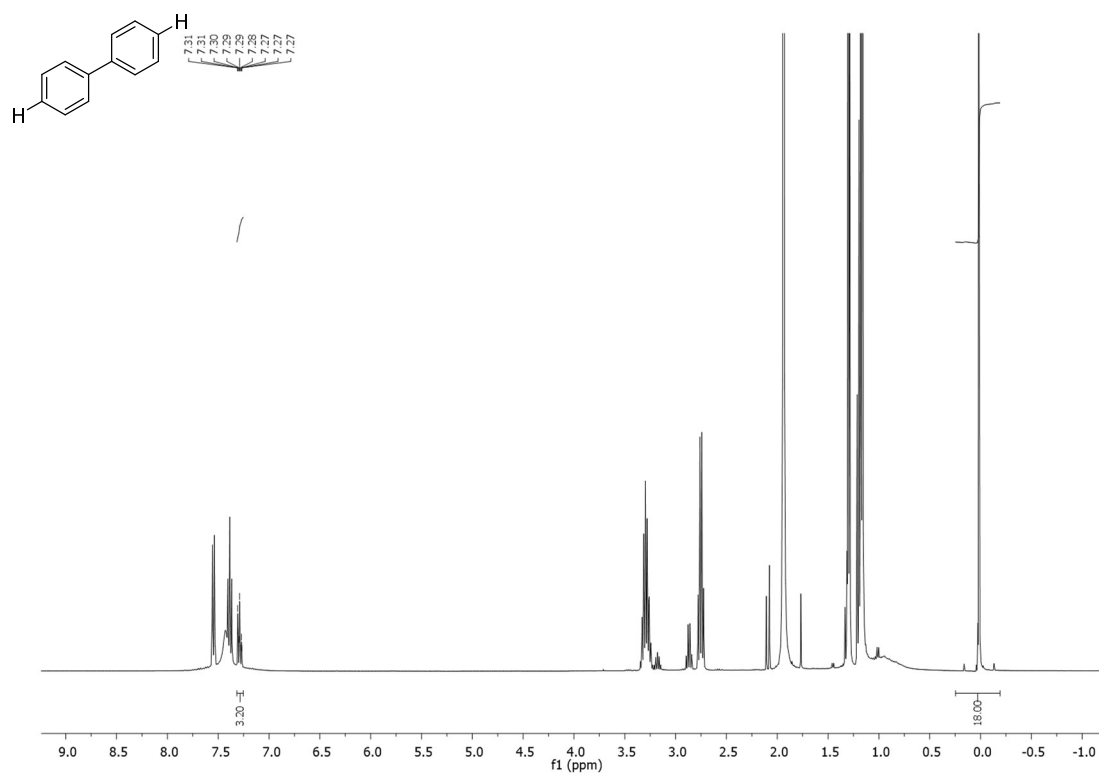
2ab



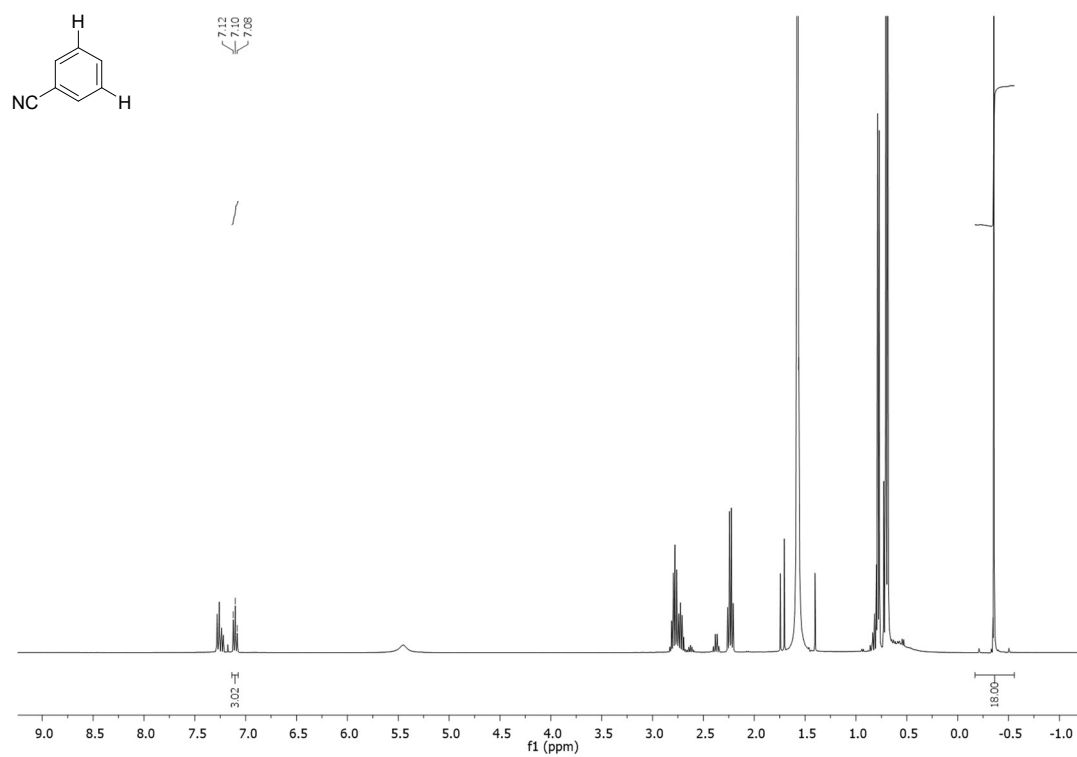
2ac



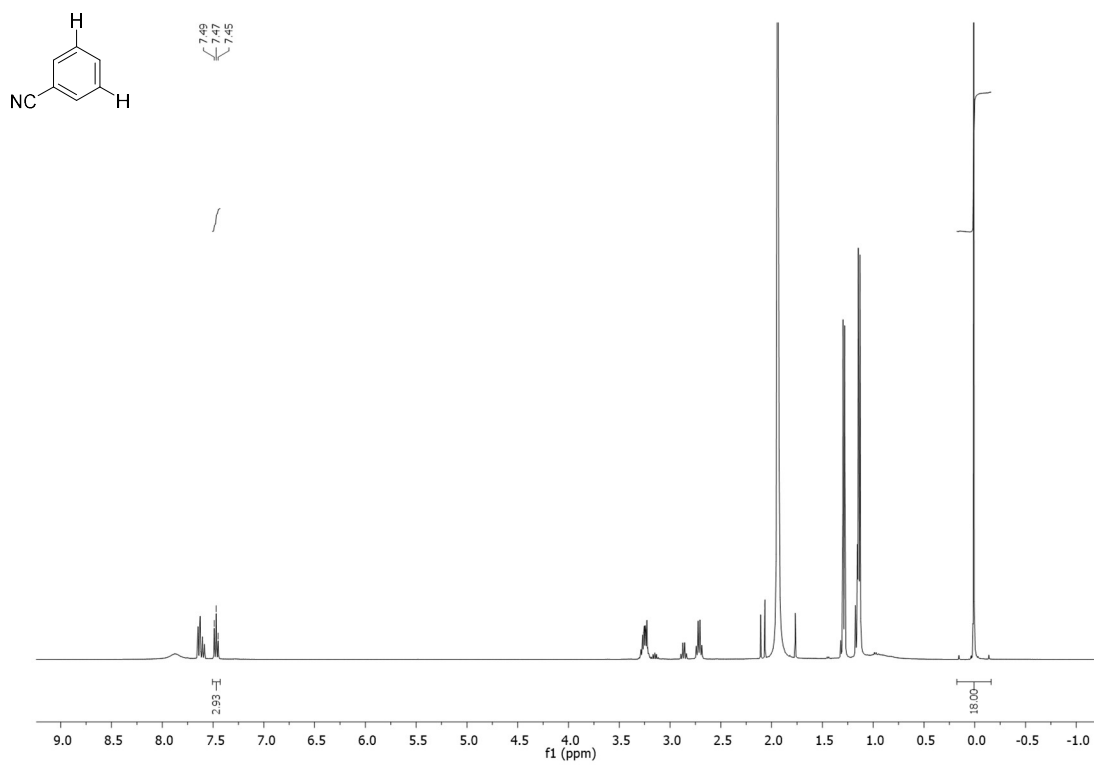
2ad



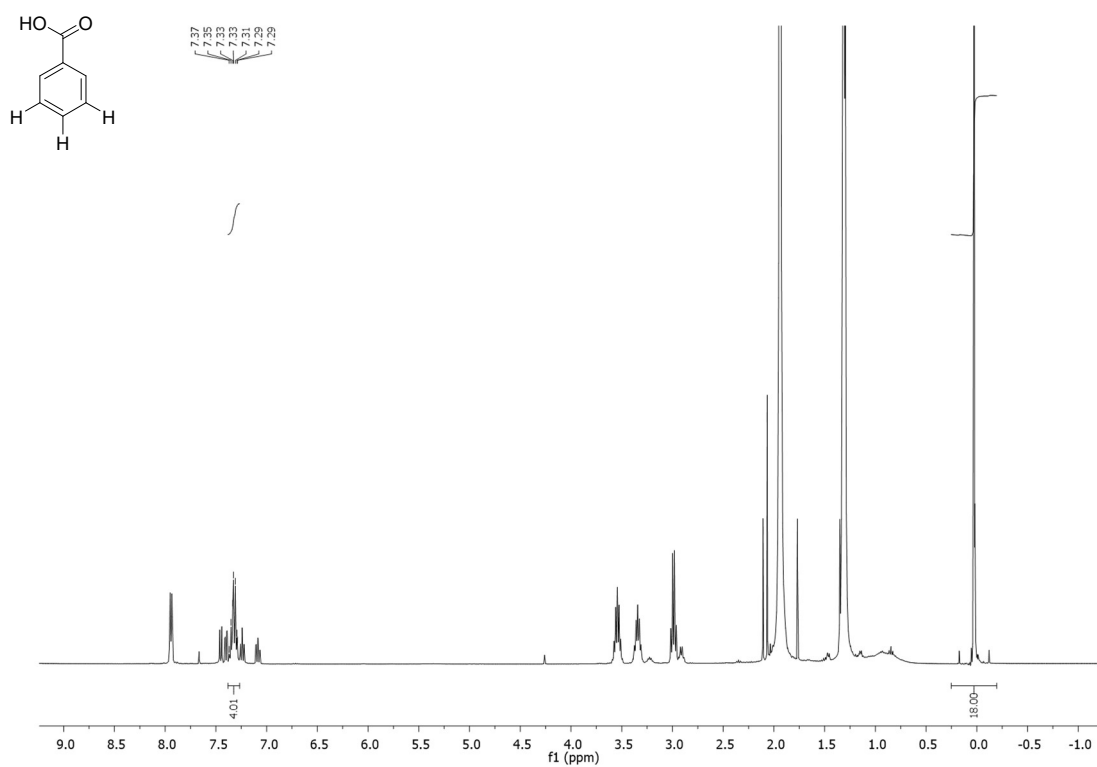
2ae



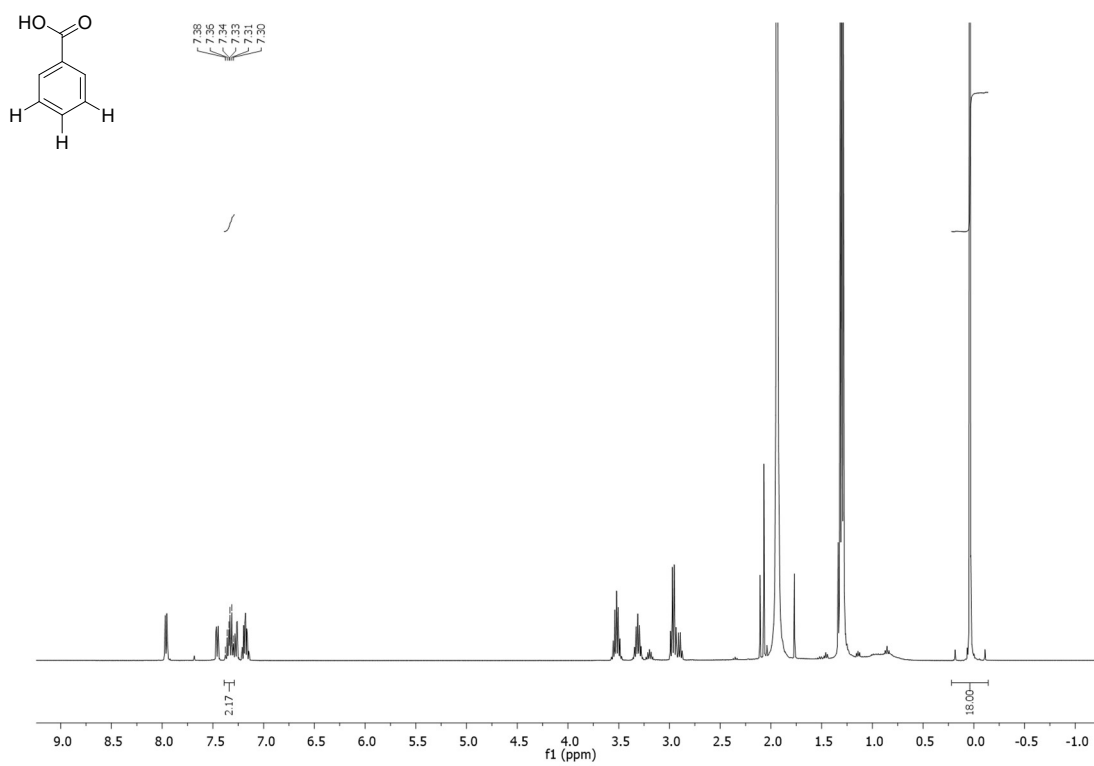
2af



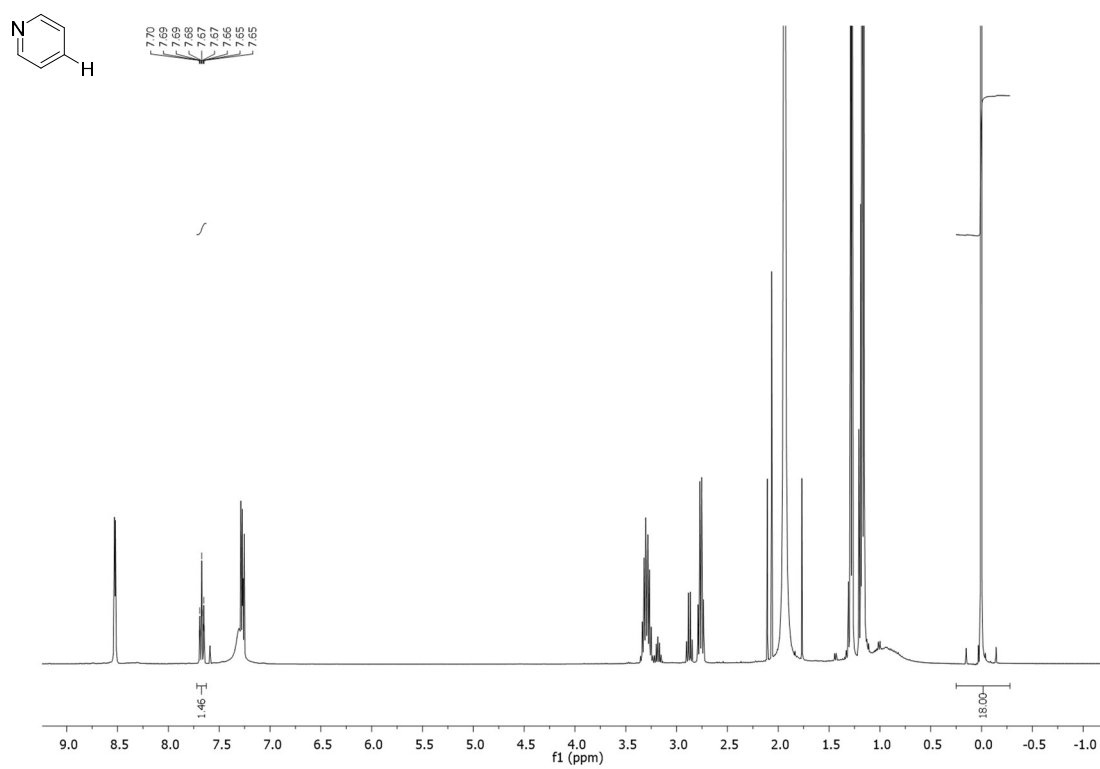
2ag

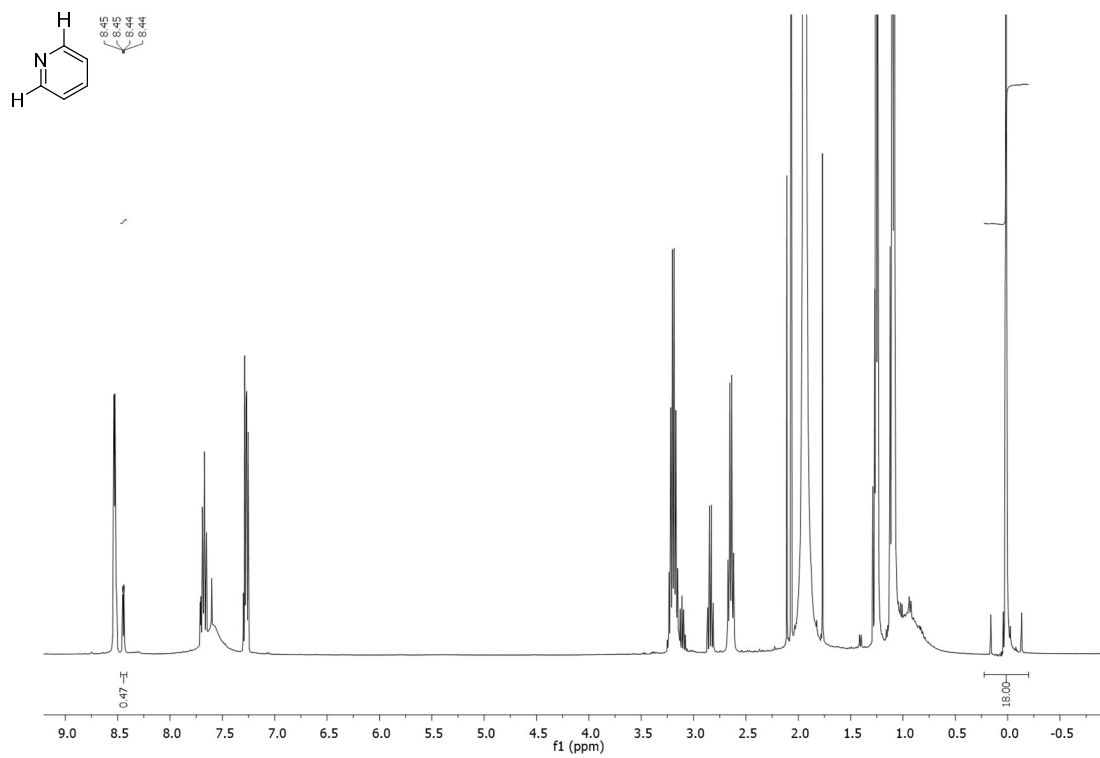
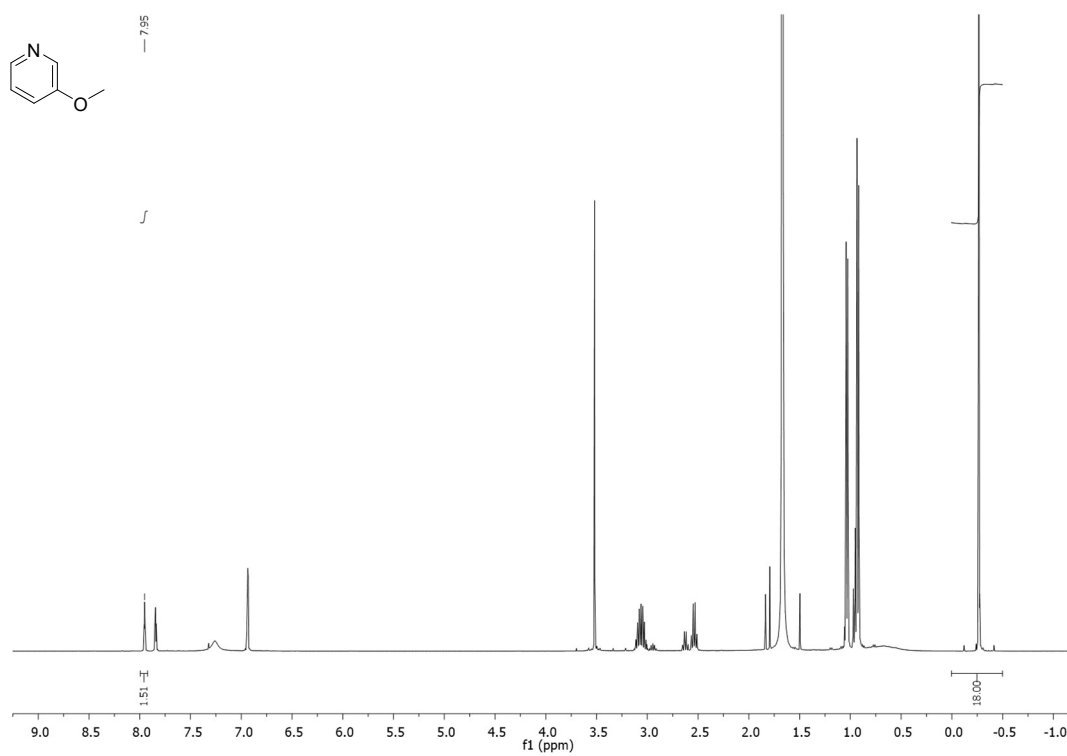


2ah

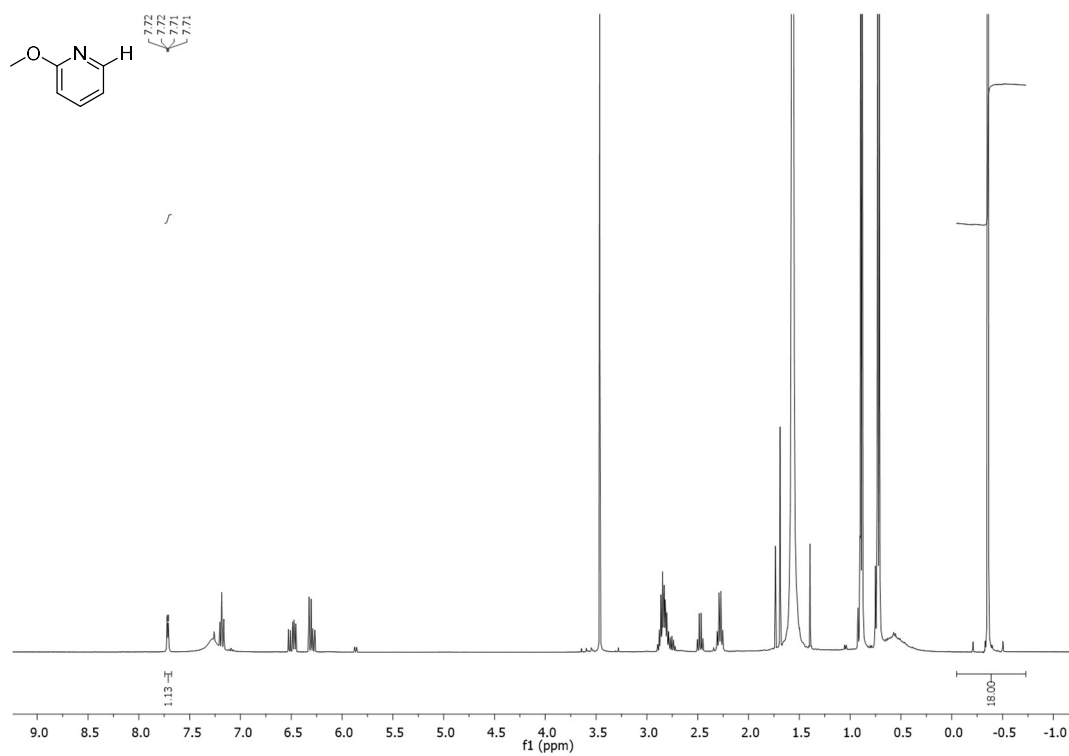


2ai

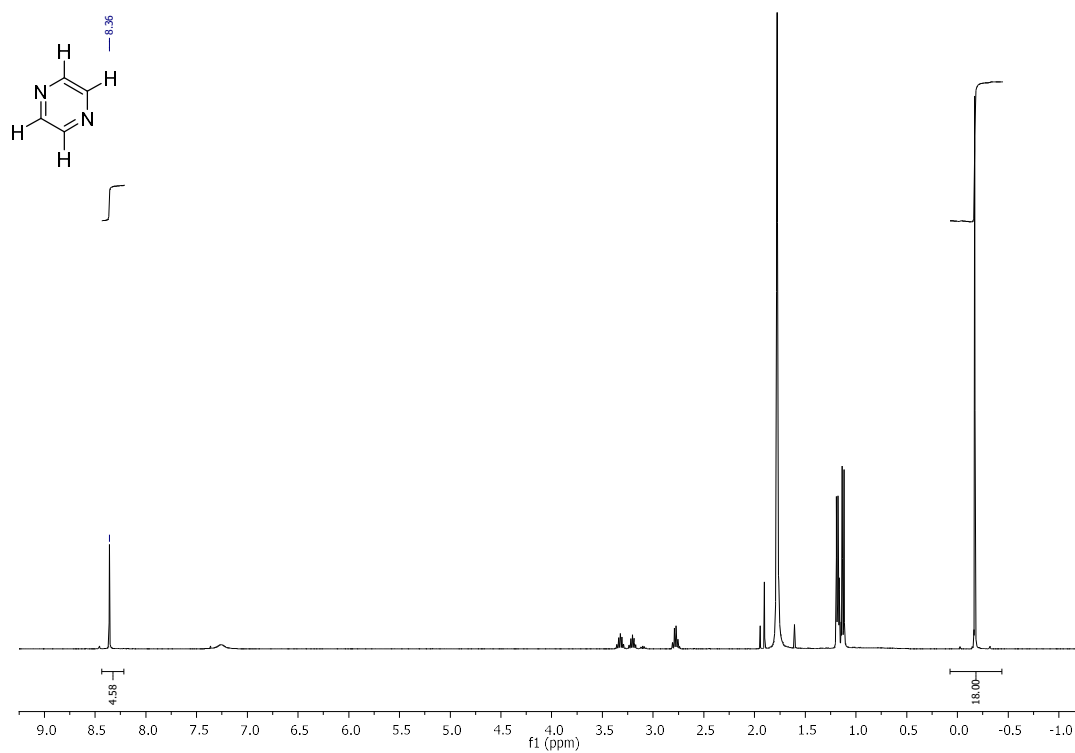


2aj**2ak**

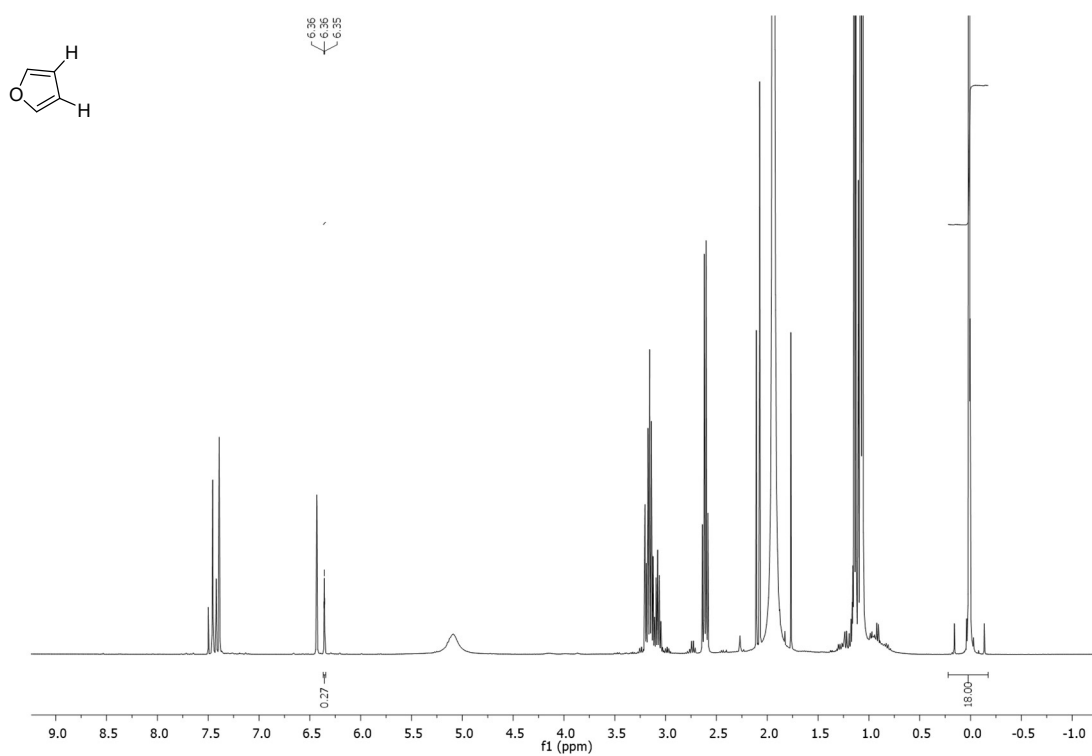
2al



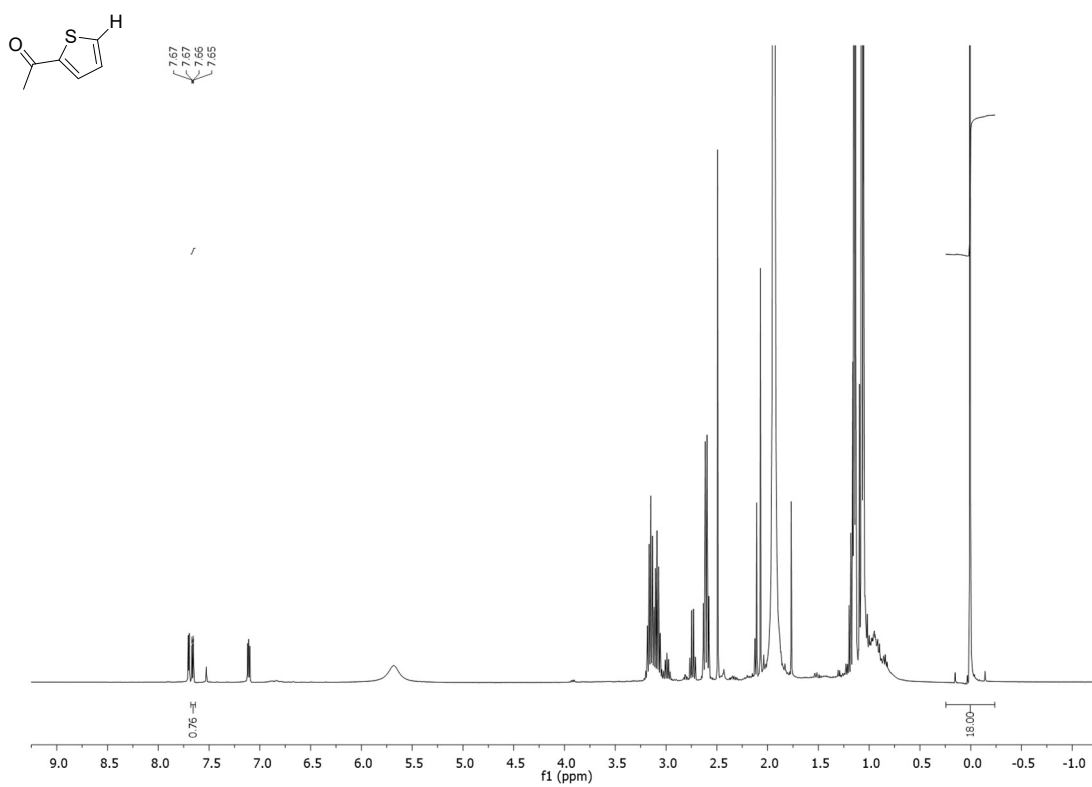
2am



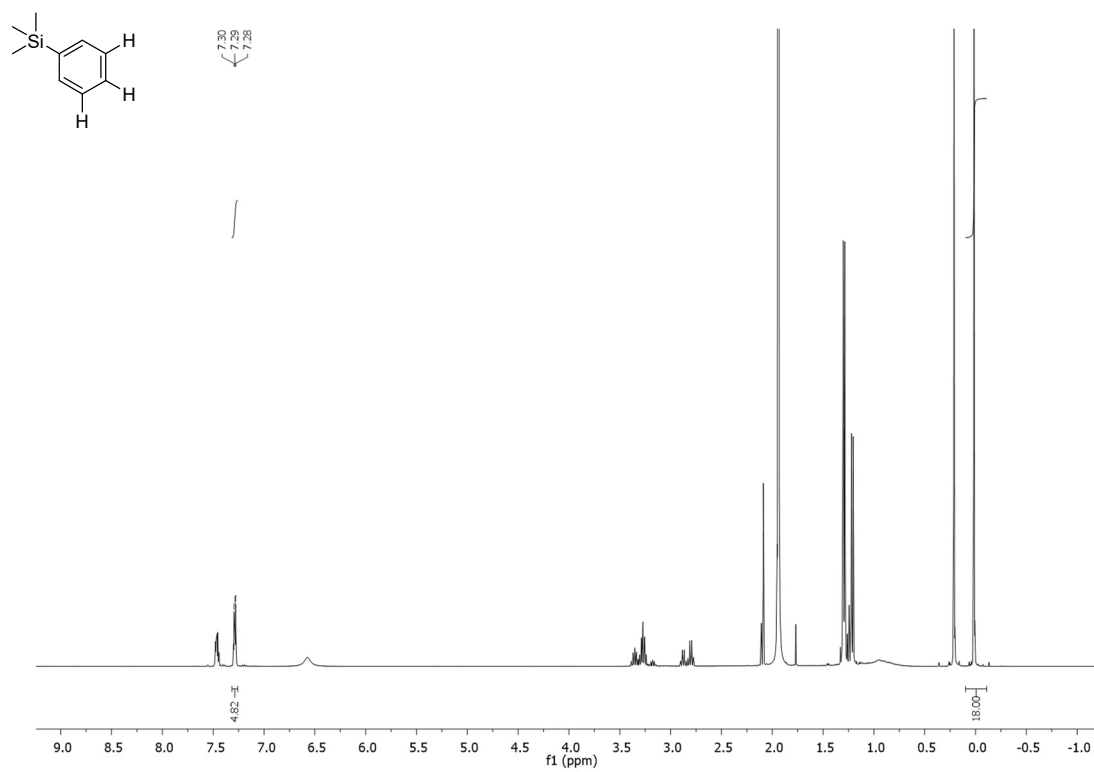
2ao



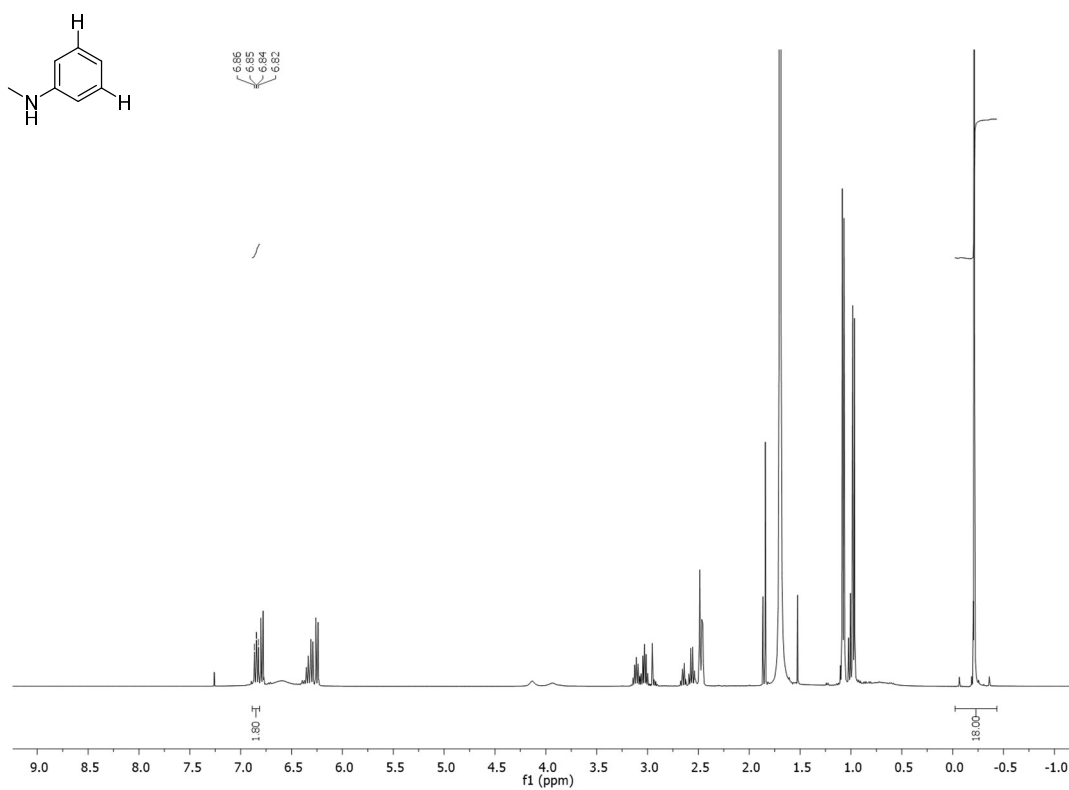
2ap



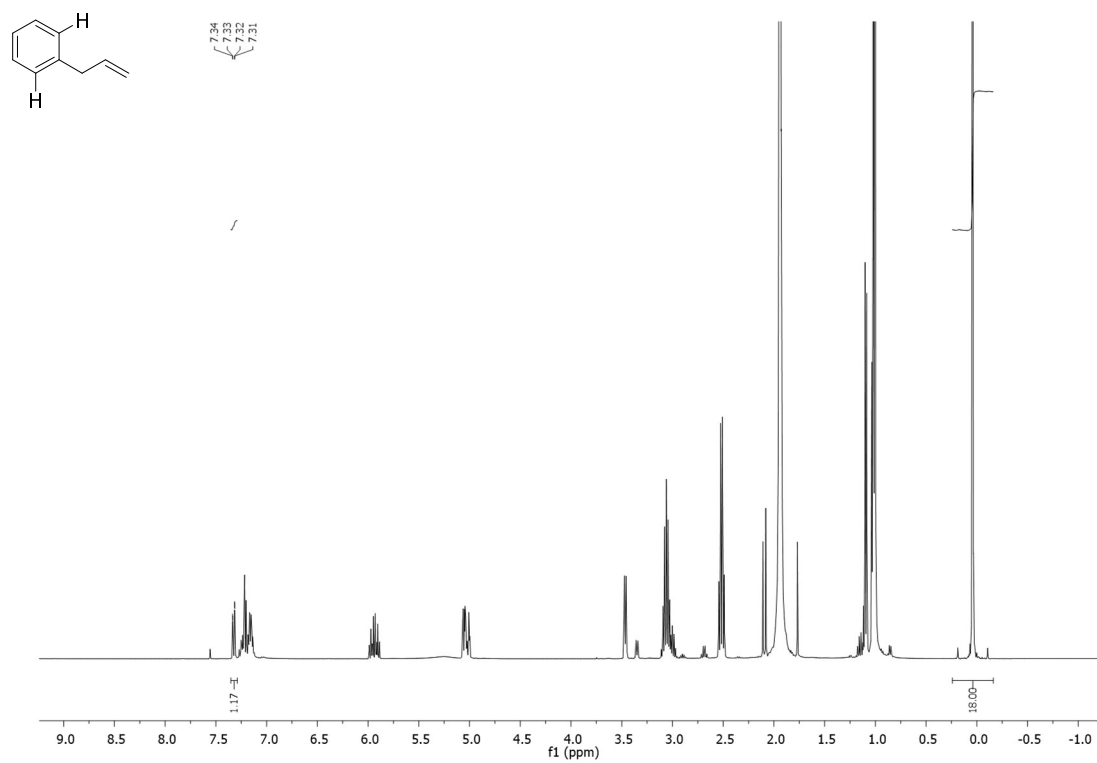
2aq



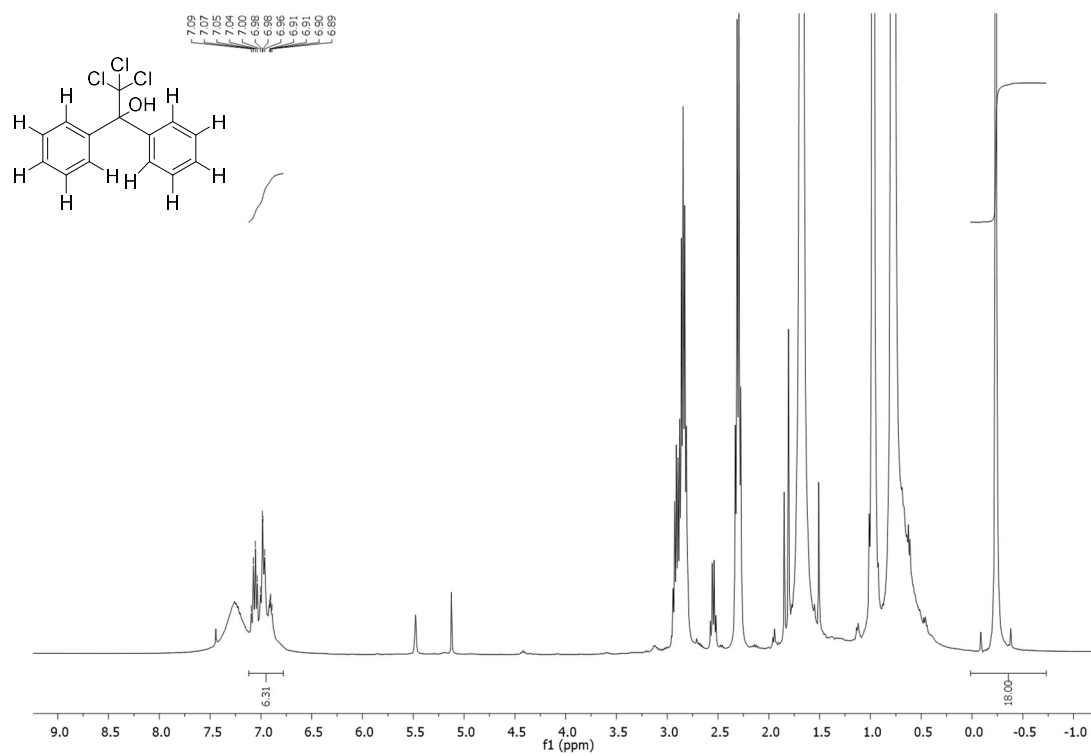
2ar



2as



Dicofol



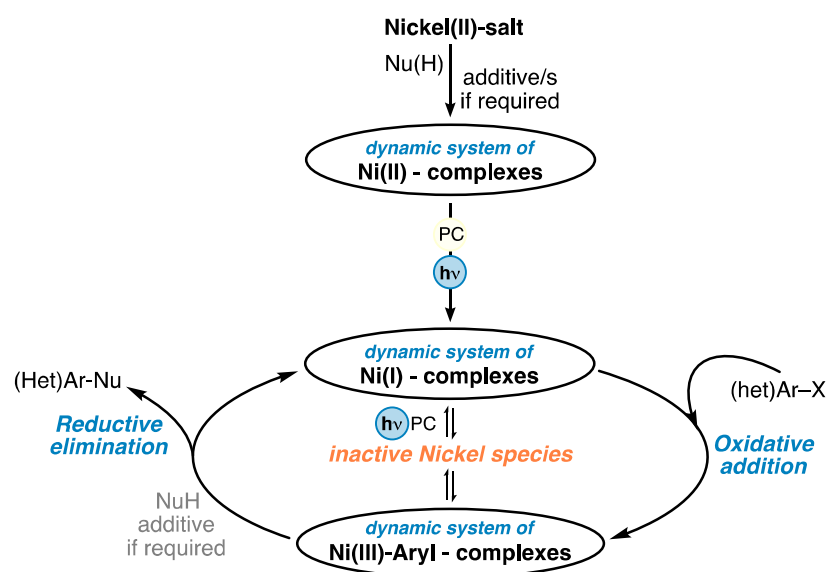
5.6.13 References

- [1] F. Del Bello, E. Diamanti, M. Giannella, V. Mammoli, L. Mattioli, F. Titomanlio, A. Piergentili, W. Quaglia, M. Lanza, C. Sabatini, G. Caselli, E. Poggesi and M. Pigni, *ACS Med. Chem. Lett.*, **2013**, *4*, 875–879.
- [2] A. Morishige, Y. Iyori and N. Chatani, *Helv. Chim. Acta*, **2021**, *104*, 8, e2100089
- [3] L. Palatinus, P. Brázda, P. Boullay, O. Perez, M. Klementová, S. Petit, V. Eigner, M. Zaarour and S. Mintova, *Science*, **2017**, *355*, 166–169.
- [4] L. Palatinus and A. van der Lee, *J. Appl. Crystallogr.* **2008**, *41*, 975–984.
- [5] L. Palatinus and G. Chapuis, *J. Appl. Crystallogr.* **2007**, *40*, 786–790.
- [6] L. J. Bourhis, O. V. Dolomanov, R. J. Gildea, J. A. K. Howard and H. Puschmann, *Acta Crystallogr. A Found. Adv.* **2015**, *71*, 59–75.
- [7] H. Puschmann, L. J. Bourhis, O. V. Dolomanov, R. J. Gildea and J. A. K. Howard, *Acta Crystallogr. A Found. Crystallogr.* **2011**, *67*, C593.

In the previous chapters, we have presented various synthetically useful tools ranging from SOE and e-PRC to conPET systems. The last chapter now deals with the combination of nickel and photoredox catalysis. Unlike before, we neither use completely new catalysts for this purpose, nor do we aim for extreme redox potentials, but rather we want to highlight the importance of photoredox catalysis for organic synthesis. Through this example, we intend to illustrate the possibilities that arise from the development of new catalytic systems and how they can be used for the synthesis of relevant molecules.

CHAPTER 6

6 A General Premise for Cross–Coupling Reactions with Adaptive Dynamic Homogeneous Catalysis



This chapter has been accepted and will be published soon: I. Ghosh, N. Shlapakov, T. A. Karl, J. Düker, M. Nikitin, J. V. Burykina, V. P. Ananikov and B. König *Nature* **2023**, by Springer Nature

T. A. Karl isolated compounds. 34 of which were included in the manuscript.

6.1 Abstract

Cross-coupling reactions are among the most important transformations in modern organic synthesis^[1-3]. Although the range of reported (het)arenes and nucleophile coupling partners are very large considering various protocols, the reaction conditions vary considerably between compound classes, necessitating renewed *case-by-case* optimization of reaction conditions^[4]. Here we introduce adaptive dynamic homogeneous catalysis (AD-HoC) with nickel and visible-light-driven redox processes for general C(sp²)-(het)atom coupling reactions. The self-adjustive nature of the catalytic system allowed the simple classification of dozens of various classes of nucleophiles in cross-coupling reactions. This is synthetically demonstrated in nine different bond-forming reactions (*i.e.*, C(sp²)-S, Se, N, P, B, O, C (sp³, sp², sp), Si, Cl) with hundreds of synthetic examples under very predictable reaction conditions. The catalytic reaction center(s) and conditions differ from one another by the added nucleophile, or if required, a commercially inexpensive amine base.

6.2 Introduction

Transition metal-mediated C(sp²)-(het)atom coupling reactions are among the most explored organic transformations enabling both efficient constructions of molecules and accessing molecular complexity for applications across many disciplines^[1-3]. Over the last five decades, a vast amount of literature evolved around palladium^[1,2], copper^[3], nickel^[5], and other metals^[6,7]. Despite significant achievements made in method developments, including the recent advancement of combining transition metals with photochemistry^[8,9], a large variety of required ligands, pre-catalysts, bases, additives, reaction conditions, electronics and/or structural diversities of coupling partners still pose challenges in selecting the right parameters for reaction efficiency and yield^[4,10,11]. Commercial sets of test-ligands and pre-catalysts, the advancement of rapid high-throughput screening methods^[12] evaluating hundreds of additives for reaction outcome, and the recent development of machine learning predictions^[13] facilitate the search for suitable conditions for specific coupling reactions but are associated with additional costs.

Instead of following the common notion of the use of pre-catalyst, ligands' design, base/additive screening, and other conditions noted above for case-by-case cross-coupling reactions, we report here adaptive dynamic homogeneous catalysis (AD-HoC) with nickel under visible-light-driven redox conditions for general C(sp²)-(het)atom coupling reactions. The adaptive part of AD-HoC with nickel relies on the formation of dynamic assembly of various nickel complexes, one or more species of which under photoredox reaction conditions meet the necessary electronic and coordination (geometry) requirements at the metal center to undergo the elementary catalytic steps (i.e., oxidative addition and reductive elimination) and yield the desired cross-coupled product. Keeping the electrophile, photocatalyst, and nickel constant, the conditions differ from one reaction to another by just the added nucleophile, or, if required, a commercially available inexpensive amine base. The self-adjustive nature makes the catalytic system universal, resulting in successful cross-coupling reactions with a range of electrophile/nucleophile combinations. In addition, general prediction of the reaction conditions could be delineated with the simple evaluation of only necessary and sufficient parameters (i.e., no or amine additive as a variable component). Figure 1 summarizes the general classification of commonly used nucleophiles and working strategies for coupling reactions using AD-HoC with nickel under photoredox reaction conditions.

6.3 Results and Discussion

A general trend between the different groups of nucleophiles was observed (Figure 1). Group I and group II (II') nucleophiles both coordinated with Ni(II). When the nucleophiles' presence and coordination result in catalytically competent nickel complexes for the necessary elementary catalytic steps, we classify them as group I. These nucleophiles coordinate to Ni(II), both without and with deprotonation forging in cases even polymeric nickel species (e.g., thiols, see SI). Group II nucleophiles showed a predominant tendency to coordinate with nickel without deprotonation. The cross-coupling reaction was efficient in the presence of a bicyclic tertiary amine as an additive. The presence of the latter allows the formation of catalytic species capable to undergo the elementary reaction steps and, moreover, neutralize the generated HBr or HCl (depending on the halide coupling partner). Relatively weak nucleophiles representing groups III and IV either did not coordinate to Ni(II) or showed coordination tendency only when deprotonated. The successful cross-coupling reactions as such rely on the presence of cyclohexylamine or TMG as additives, respectively in forming catalytically competent nickel complexes.

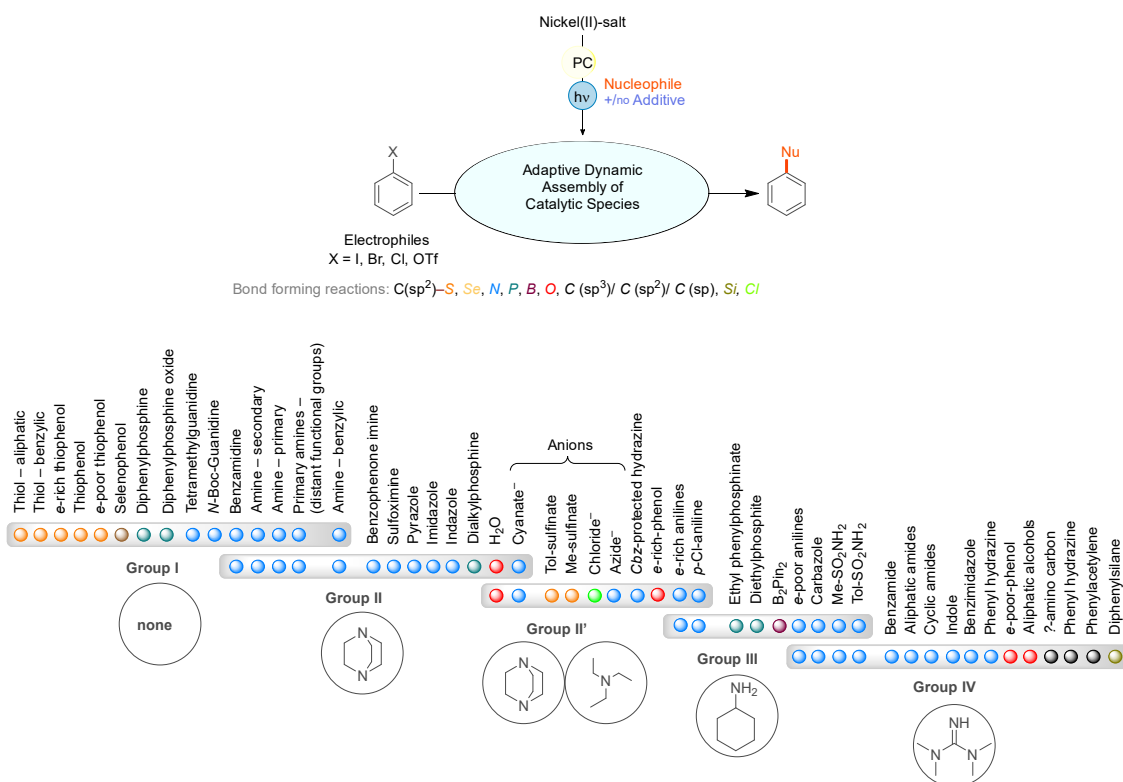


Figure 1. General classification of commonly used nucleophiles (according to the required additive) for cross-coupling reactions with Adaptive Dynamic Homogeneous Catalysis using nickel under visible-light-redox reaction conditions. The color of the circles reflects (het) atoms involved in the bond formation.

The presence of cyclohexylamine likely facilitates the oxidative addition of electrophiles and its relatively slow rate of reductive elimination allows reductive elimination for group II nucleophiles giving the desired product (see the discussion below). For very weak nucleophiles representing group IV, a more potent base, TMG, was effective as cyclohexylamine started competing in the reductive elimination step. We assume that due to very poor nucleophilicity, these nucleophiles alone suffer to coordinate with nickel even in the +III oxidation state. Similarly, to cyclohexylamine, TMG most likely has multiple roles. The increased basicity allows the required deprotonation of the nucleophile. Moreover, it is most likely involved as a ligand to render nickel more efficient in the elementary reaction steps.

We began our synthetic investigations with cyclohexanethiol representing group I in C(sp²)-S cross-coupling reactions (Figure 2). Upon addition to a dimethylacetamide (DMA) solution containing NiBr₂•glyme – a bench-stable commercial nickel source – and ethyl 4-bromobenzoate as a model substrate, an immediate color change was observed. The desired C(sp²)-S cross-coupling product **P**₉ was obtained in an excellent 92% isolated yield within one hour upon irradiation of the reaction mixture in the presence of 0.2 mol% 4CzIPN as an organic photocatalyst.^[14-17] Noteworthy, the simplicity of the reaction conditions goes against the general norm in reported traditional cross-coupling reactions since the coupling reaction is devoid of any base, conventional ligands, or other additives. Moreover, the use of 1.0 equiv. commercial 47% (*m/m*) HBr/H₂O solution allows the acceleration of the coupling reaction of 4-bromoaniline with different thiols (for example, **P**₂, **P**₁₄₆) in excellent isolated yields that were otherwise difficult to achieve. Several primary (**P**₁-**P**₈, including practical -SH surrogates^[18], **P**₁₄₅-**P**₁₅₉), secondary (**P**₉-**P**₁₂), and tertiary thiols (**P**₁₃-**P**₁₅), benzyl mercaptan (**P**₁₆-**P**₁₈), and thiophenol (**P**₁₉-**P**₂₅) were also no exception in giving the desired products in good to almost quantitative isolated yields. The simplicity of group I nucleophiles remained effective for a range of other bond-forming reactions (-P, -Se, -N) with different nucleophiles (e.g., selenophenol (**P**₁₃₅), diphenylphosphine or diphenylphosphine oxide (**P**₁₁₅-**P**₁₁₇), *N*-*tert*-boc-guanidine (**P**₂₇), among others) due to their facile coordination with Ni(II) species. However, the secondary amines^[19] required their presence in excess (see SI) to suppress the formation of the respective de-halogenated products – a process that can be tackled by replacing excess amines with a non-reactive bicyclic tertiary amine DABCO as an additive (see SI for further details).

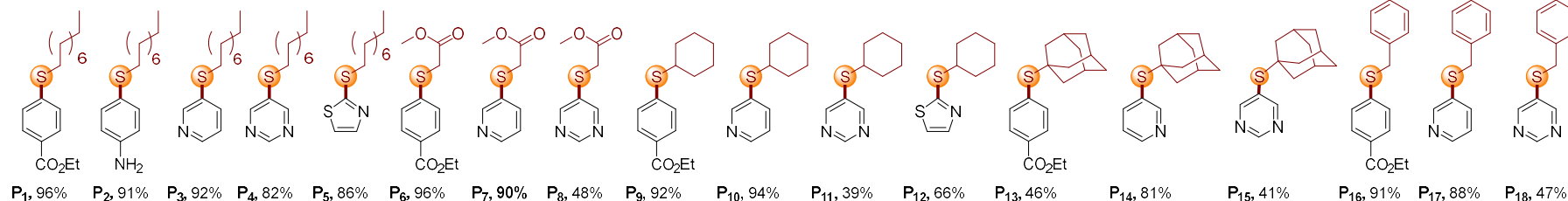
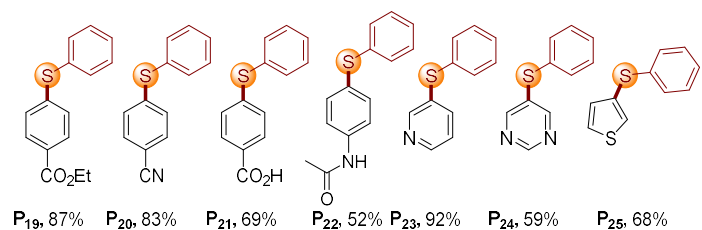
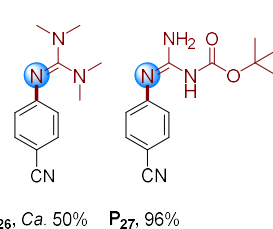
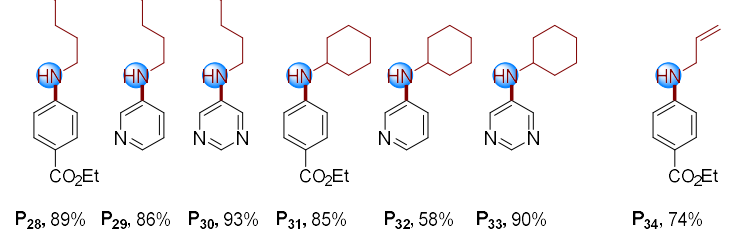
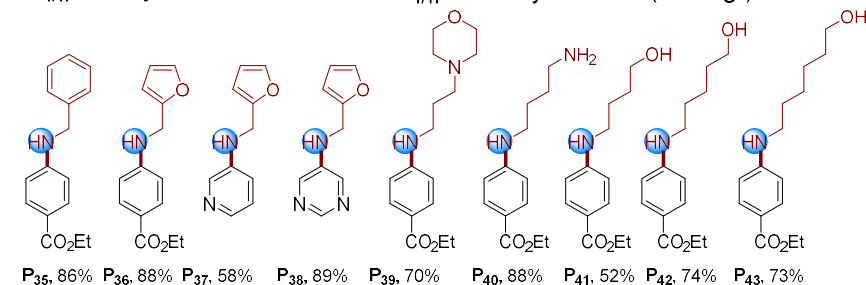
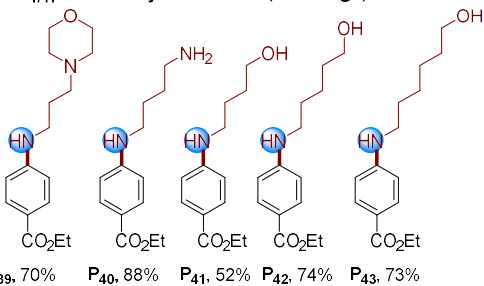
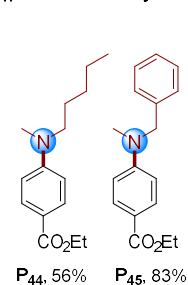
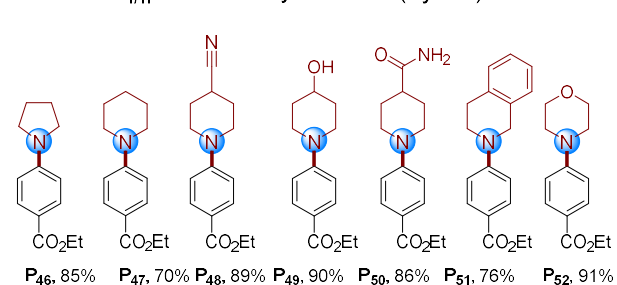
Group II nucleophiles also showed a predominant tendency to coordinate with nickel. We tested benzophenone imine as a candidate because it can serve as a convenient ammonia equivalent in (het)arene functionalizations.^[20] Benzophenone imine coordinates to Ni(II) species, but irradiation of the reaction mixture leads only to slow conversion of the aryl halide to the respective product.

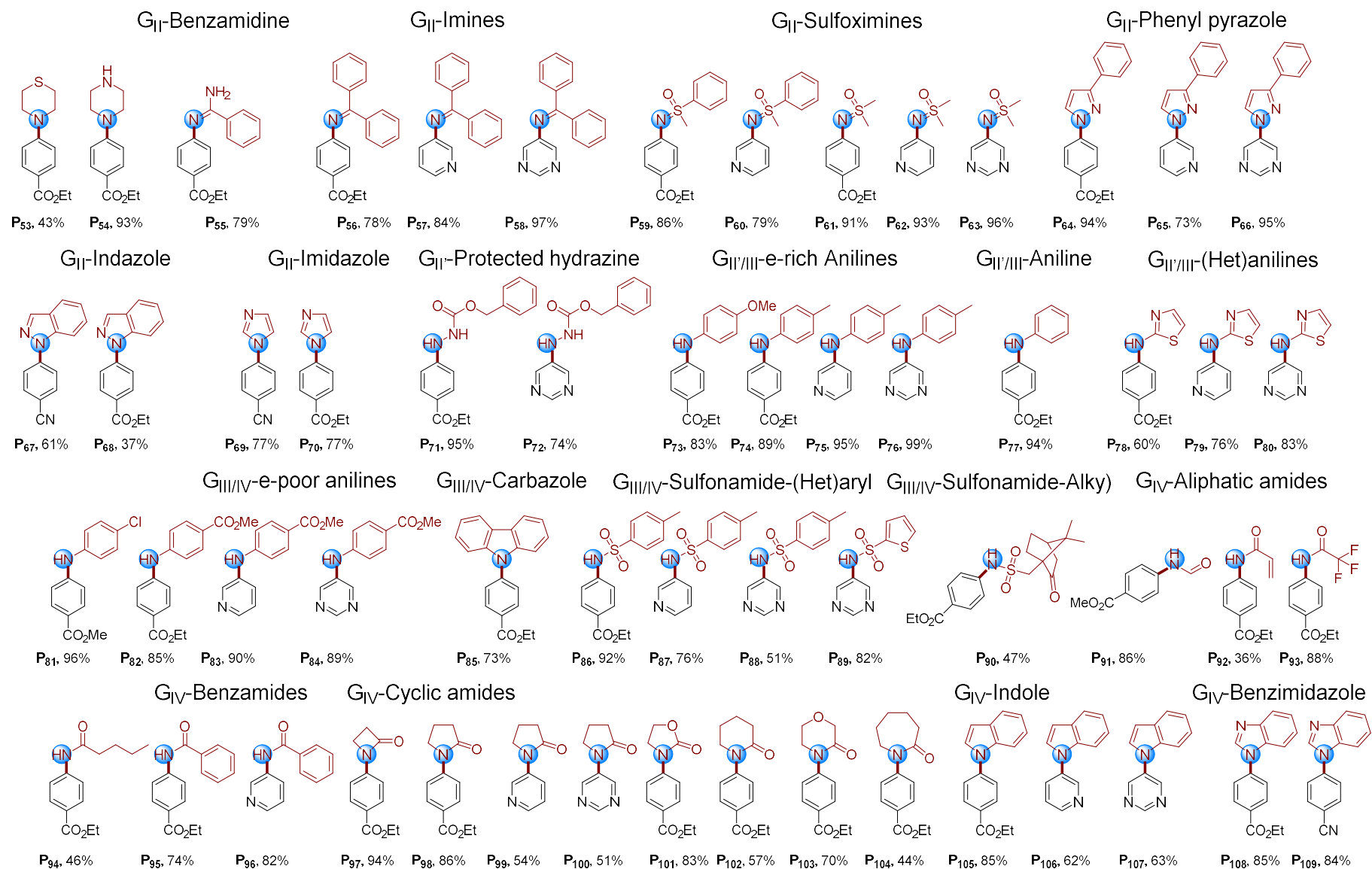
Synthetic examples with group I, II (II'), III, IV nucleophiles

Group I (G_I) - No added additives; **Group II (G_{II})** - DABCO; **Group II' (G_{II'})** - DABCO+Et₃N; **Group III (G_{III})** - Cyclohexylamine; **Group IV (G_{IV})** - TMG

Bond forming reactions: C(sp²)-S; C(sp²)-Se; C(sp²)-N; C(sp²)-P; C(sp²)-B; C(sp²)-O; C(sp²)-C(sp³/sp²/sp); C(sp²)-Si; C(sp²)-Cl

70+ different nucleophiles, 140+ examples

G_I-Alkyl thiolsG_I-ThiophenolsG_I-GuanidinesG_{I/II}-Primary aminesG_{I/II}-Benzylic aminesG_{I/II}-Primary amines (w.d.f.g.)G_{I/II}-Secondary aminesG_{I/II}-Secondary amines (cyclic)



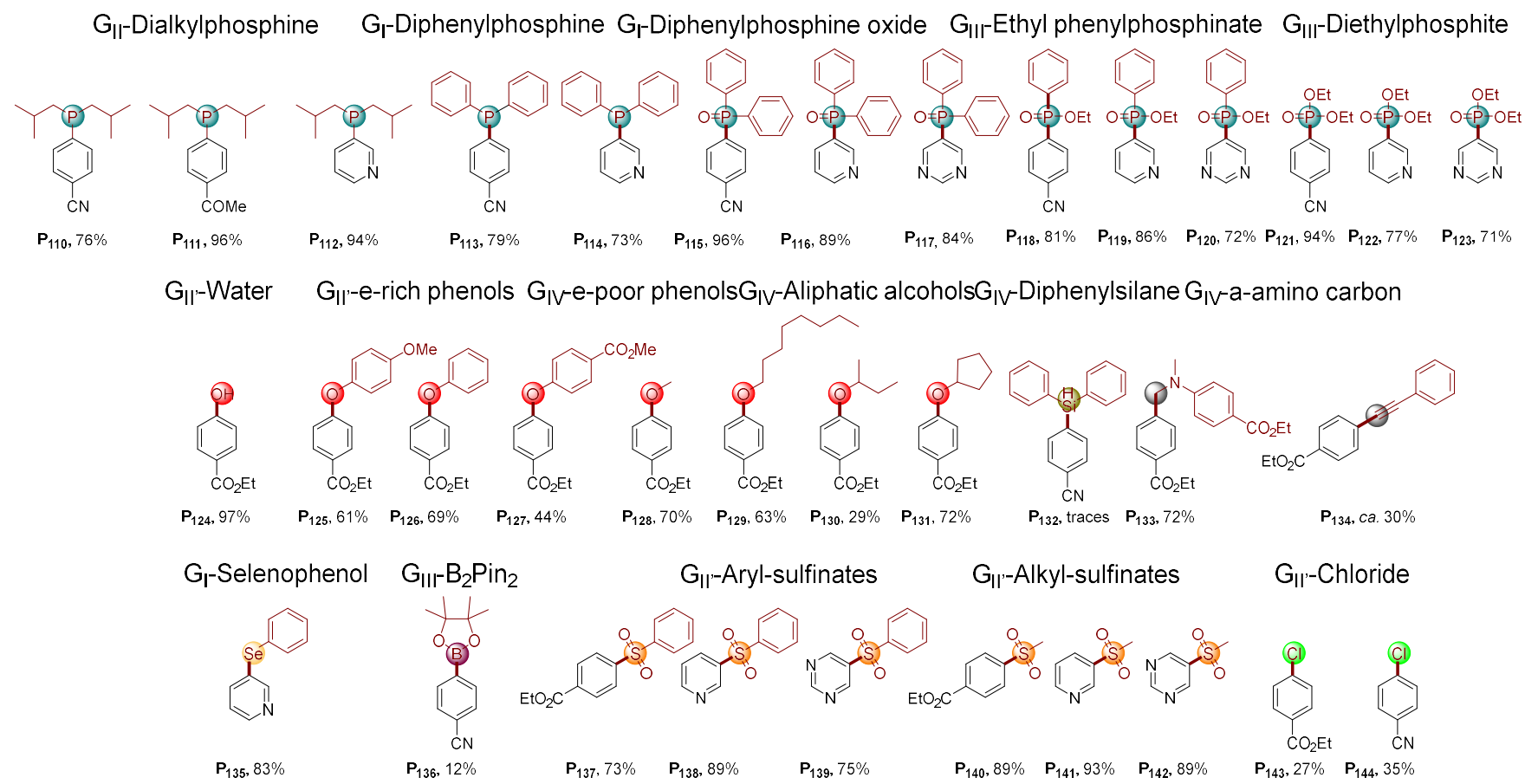


Figure 2. The nucleophiles' scope in $C(sp^2)$ -Br cross-coupling reactions. For more nucleophiles and electrophile scopes, see SI. Isolated yields are reported unless otherwise noted. For compounds **P₂₆** and **P₁₃₄** the formation of the desired product in synthetically useful yield was confirmed by GC/GC-MS analysis (see SI). The formation of the desired product **P₁₃₂** was confirmed by GC/GC-MS analysis.

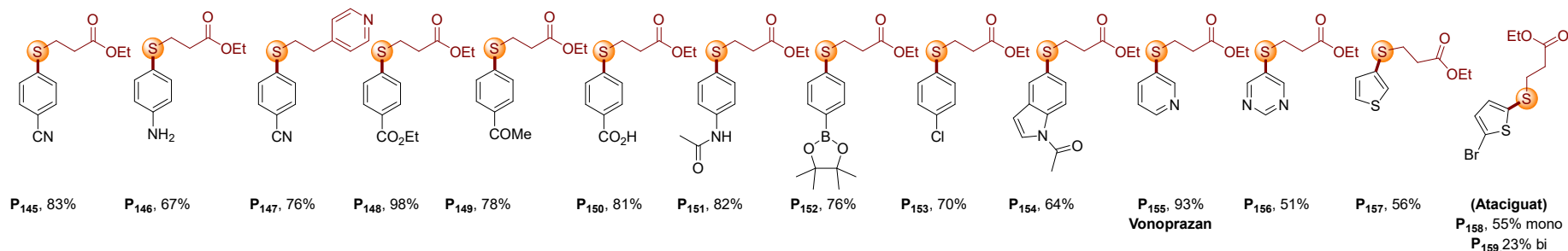
The addition of DABCO accelerated the reaction significantly giving the desired product in good to excellent yield (**P**₅₆–**P**₅₈). Similarly, sulfoximines (**P**₅₉–**P**₆₃), benzamidine (**P**₅₅), and a range of heterocycles such as pyrazole (**P**₆₄–**P**₆₆), imidazole (**P**₆₉–**P**₇₀), and dialkylphosphine (**P**₁₁₀–**P**₁₁₂) showed analogous reactivity pattern in giving the desired product in excellent yields.

Remarkably, the AD-HoC with nickel under visible-light-redox conditions was highly effective with a range of anions (they are capable of coordination with effective replacement of the bromide anions in nickel complexes, Group II^[21], (see SI for further details)) allowing even effective transformation of inexpensive commercial bulk chemicals into valuable functional groups (Figure 2 and 3). The applications include the use of aryl and alkyl sulfinates for the synthesis of respective sulfones (**P**₁₃₇–**P**₁₄₂) and LiCl (in combination with aryl bromides/iodides) in halogen exchange reactions (**P**₁₄₃–**P**₁₄₄). Effective *in situ* conversion of simple anions into valuable functional groups (Figure 3) was implemented with sodium cyanate (in the presence of various alcohols, **P**₁₆₀–**P**₁₇₁) or sodium azide (**P**₁₇₂–**P**₁₇₇) when used as nucleophiles. While the use of OCN[−] allowed the synthesis of protected anilines as carbamates – a common motif in an array of biologically active compounds^[22], the use of sodium azide allowed the installation of a free –NH₂ group onto (het)arenes in good to excellent yields.

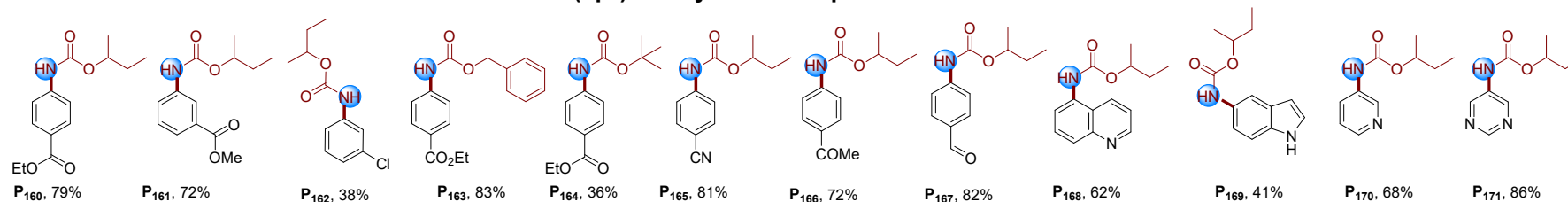
Synthetic examples using groups III and IV exemplify relatively weak nucleophiles. The use of cyclohexylamine and a guanidine base (in this case, 1,1,3,3-tetramethylguanidine (TMG)), respectively, allows the formation of catalytically competent nickel complexes. Electron-poor anilines and *p*-toluenesulfonamide were selected due to their poor coordination ability with Ni(II).^[23] The coupling reactions without any additive or with DABCO allowed only limited product yield with the relatively slow conversion of the (het)aryl halides. The addition of cyclohexylamine allowed the formation of the desired products in good to excellent yields.^[24] The use of TMG, a commercially available inexpensive guanidine base, became important for very weak nucleophiles (group IV) as cyclohexylamine started competing in the coupling reaction due also to its inherent reactivity.^[25] The use of TMG allowed a range of alkyl amides (**P**₉₁–**P**₉₄), benzamide (**P**₉₅–**P**₉₆), as well as four- to seven-membered cyclic amides (**P**₉₇–**P**₁₀₄), nitrogen (het)cycles such as indole (**P**₁₀₅–**P**₁₀₇) and benzimidazole (**P**₁₀₈–**P**₁₀₉), electron-poor phenols (**P**₁₂₇) to couple with (het)aryl halides giving the desired products in good to excellent yields. Additional examples include the use of aryl hydrazines in Suzuki-type synthesis of bi-(het)aryls (**P**₁₇₈–**P**₁₈₄). The coupling reactions can be executed with low amounts of catalyst loading (as reported here, with 4CzIPN and NiBr₂•glyme as low as 0.02 mol% and 1.0 mol% respectively), even with relatively inexpensive nickel salts (for example, NiCl₂•6H₂O), and in multi-gram synthetic transformation without significant impact on the reaction kinetics and yields of the desired product (see SI for further details). The use of cyclohexylamine additionally allowed a precipitate-free protocol, which is preferred in particular if the transformation is performed under flow conditions.^[26]

Effective conversion of simple reagents to important functional groups

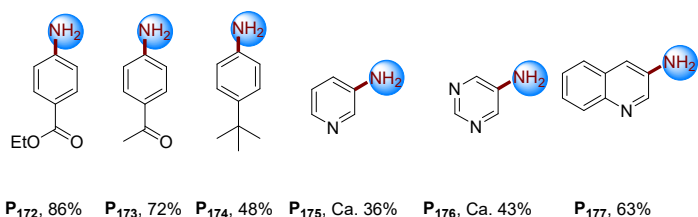
C(sp²)-S – installing practical thiol surrogate



C(sp²)-N – synthesis of protected anilines



C(sp²)-N – direct installation of free -NH₂ group



C(sp²)-C(sp²) – Suzuki type cross-coupling products

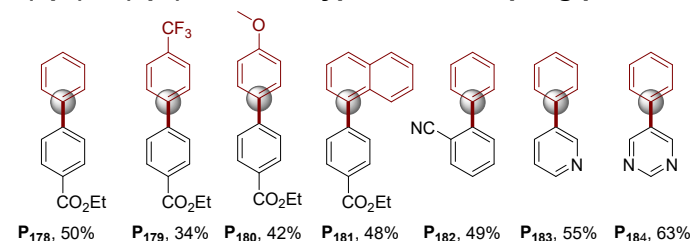


Figure 3. Installation of valuable functional groups onto (het)arenes using either simple nucleophiles or anions as practical surrogates. Isolated yields are reported. For compounds, **P₁₇₅** and **P₁₇₆** the formation of the desired product in synthetically useful yield was confirmed by GC/GC-MS analysis with an authentic sample.

Although relatively complex, a likely mechanism for the reported adaptive dynamic homogeneous catalysis with nickel involves a catalytic Ni(I)/Ni(III)^[27] cycle (see SI for more details), which may in part be self-sustained.^[28] A range of nucleophiles coordinate to NiBr₂·glyme in its air-stable +II oxidation state: either in the absence or in the presence of an added amine base, a dynamic equilibrium between differently coordinated species was observed (see SI for the UV and mass-spectrometric analyses). The dynamic nature of the assembly produces one or more species that are catalytically competent under the photoredox reaction conditions to undergo effective oxidative addition and reductive elimination. Mass spectrometric experiments revealed that thiols, representing group I nucleophiles, are able to coordinate and stabilize nickel complexes even in unstable oxidation states (*i.e.*, I and III), and the corresponding species can be detected by mass spectrometric methods (see SI for mass spectrometric analyses of nickel – nucleophile/additive mixtures). Thus, successful cross-coupling reactions can be implemented without any conventional ligand, base, or additives. For instance, methyl 3-mercaptopropionate complexed with Ni(II) species, and the formation of nickel polythiolate complexes containing Ni(I) and Ni(III) ions was observed. The second-order mass spectra confirmed the formation of polynuclear complexes containing Ni(I) species. Group II represents nucleophiles that coordinated to nickel without deprotonation and the addition of a tertiary amine DABCO allowed successful cross-coupling transformation. Their coordination ability facilitated the ligand exchange process and hence the successful reaction outcome. Group III/IV nucleophiles showed either very weak or no coordination to Ni(II) at all and exhibited the ability to coordinate only as a deprotonated anion. The successful cross-coupling reactions required cyclohexylamine or a more potent guanidine base (TMG, for Group IV) allowing the weak nucleophiles to interact with nickel effectively either in its +II-oxidation state (for visible effects in the absence and presence of TMG with methyl 4-aminobenzoate, *p*-toluenesulfonamide, indole, benzamide as nucleophiles see or at the ligand exchange step when nickel is present in its +III oxidation state. We postulate, that under the photoredox catalyst reaction condition, Ni(II) species are reduced to Ni(I) complexes which allow oxidative addition of (het)aryl halides to form Ni(III) species. Subsequent reductive elimination yields the respective cross-coupling product.

The AD-HoC with nickel and visible-light-driven redox processes proved to be highly efficient for the functionalization of complex bio-relevant molecules (**P**₁₈₅–**P**₂₃₀) or in the synthesis of (het)arenes (**P**₂₆₉–**P**₂₇₁), drugs (**P**₁₇₂, **P**₁₉₀, **P**₂₀₆), and valuable drugs intermediates (**P**₂₃₁–**P**₂₆₁), covering numerous functional groups in FDA-approved drugs. The applications include (het)arylation of amino acids, nucleosides, and drugs at their respective *S*-, *N*-, or *O*-atoms (**P**₁₈₅–**P**₂₀₆). Noteworthy are the synthetic results for selective C(sp²)-(het)atom cross-coupling reactions in the presence of other functional groups (*c.f.*, the C(sp²)-*S* arylation of glutathione (**P**₁₈₆) in the presence of free carboxylic and –NH₂ groups, and C(sp²)-*N* arylation of tryptamine (**P**₁₉₂), tyramine (**P**₁₉₃), and adenosine (**P**₁₉₉) in the presence of free indole, phenol, and free –OH

groups, respectively). Many five- and six-membered (het)aryl halides (-I, -Br, -Cl), triflates, and vinyl bromides were effective, including the C(sp²)-N coupling reactions of (het)aryl-iodides and -chlorides with 3-phenyl-1*H*-pyrazole and (het)aryl-bromides in one-pot carbamate synthesis offering a different selectivity from recent photocatalysis^[29] and traditional Pd-catalyzed protocols^[30] (see SI). The reactions with (het)aryl bromides and chlorides allowed late-stage functionalization of C(sp²)-Br/Cl bonds in drugs requiring only slightly elevated temperature for challenging chloride substrates as exemplified with NaOCN, aniline, carbazole, benzimidazole, ethyl 3-mercaptopropionate, and diphenylphosphine oxide as nucleophiles (**P**₂₀₇-**P**₂₃₀) in three-different (-N, -S, and -P) bond forming reactions.

The simplicity, versatility, and predictability of AD-HoC with nickel and visible-light-driven redox processes became more apparent when we turned our attention toward bi-functionalization reactions forging either one or two different chemical bonds for rapid construction of molecular complexity. The bi-functionalization reactions can be easily executed either on di-halo (het)arenes installing two different functional groups (**P**₂₆₂-**P**₂₆₉) or in molecules possessing both C(sp²)-Br bond and a nucleophile (**P**₂₇₂-**P**₂₇₆). Noteworthy is the "*simple reversal*" of the functionalization sequence (*c.f.*, **P**₂₇₄ and **P**₂₇₅) with the adjustment of the acidic or basic conditions using a commercial 47% (*m/m*) HBr/H₂O solution and cyclohexylamine

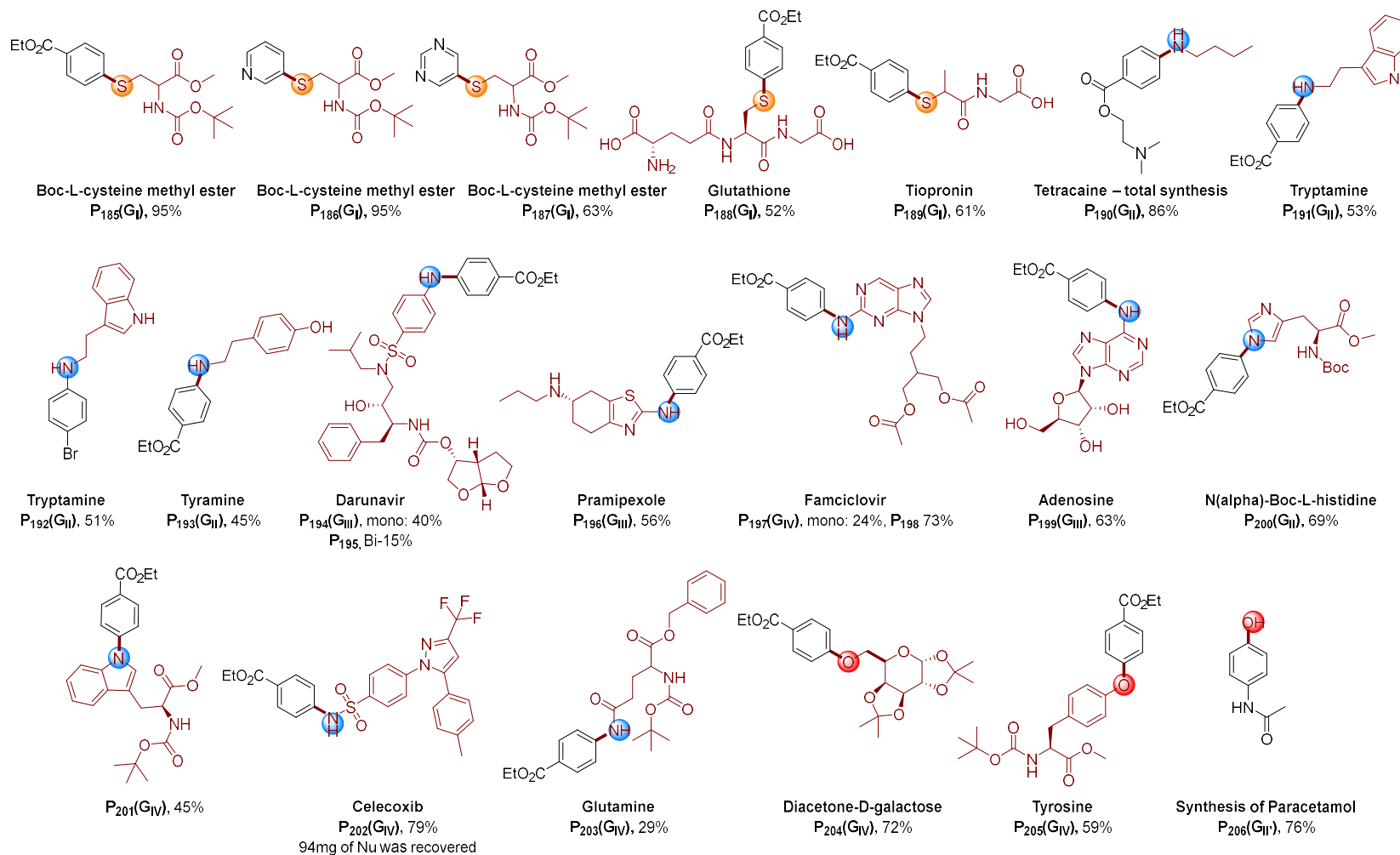
Implications for applications

Functionalization of bio-relevant molecules; Late-stage functionalizations; Synthesis of drugs' intermediates; Two-step transformations

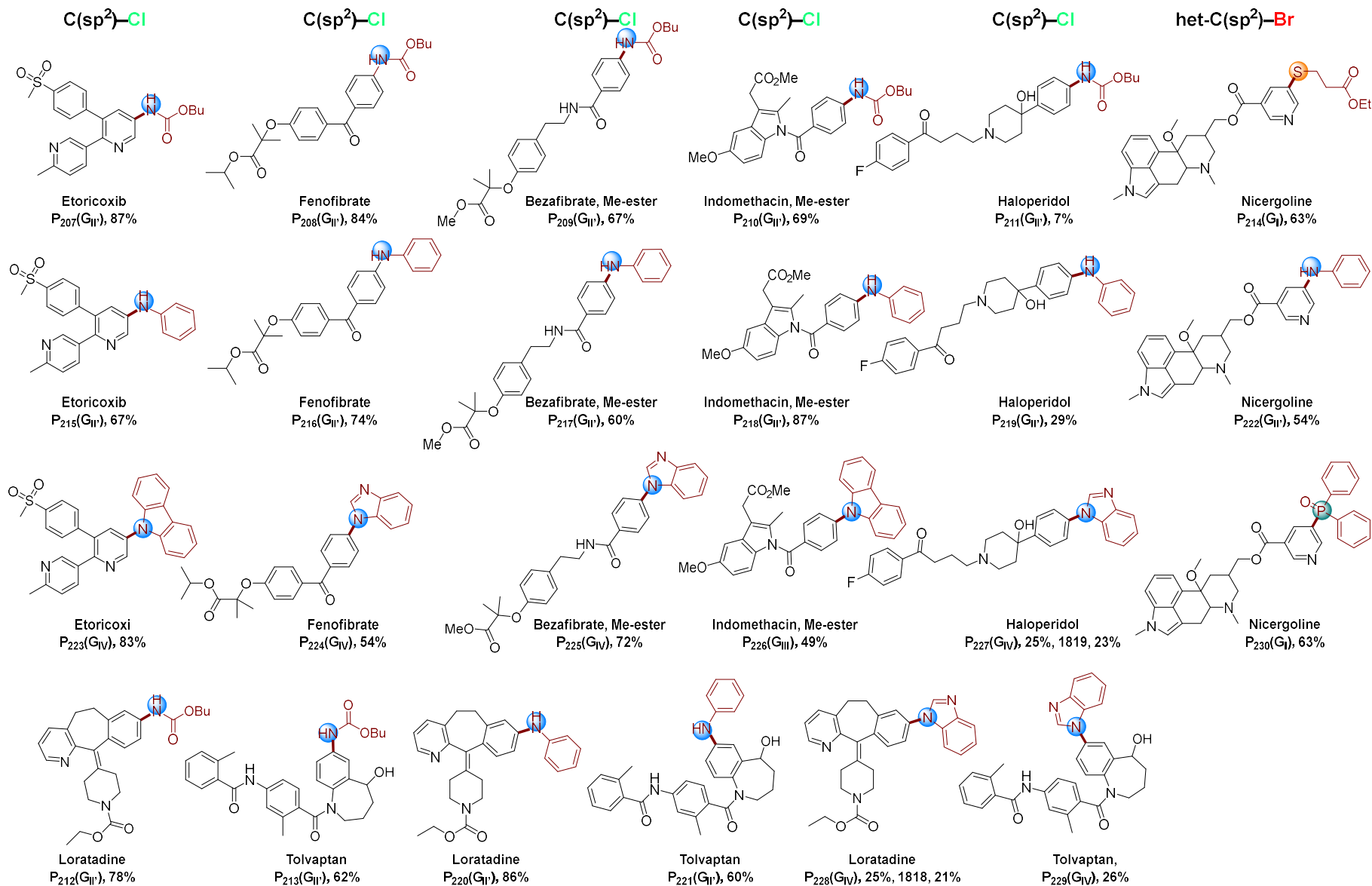
Bond forming reactions – C(sp²)-S; C(sp²)-N; C(sp²)-O

ca. 65 different nucleophiles; Electrophiles installed; ca. 90 Examples

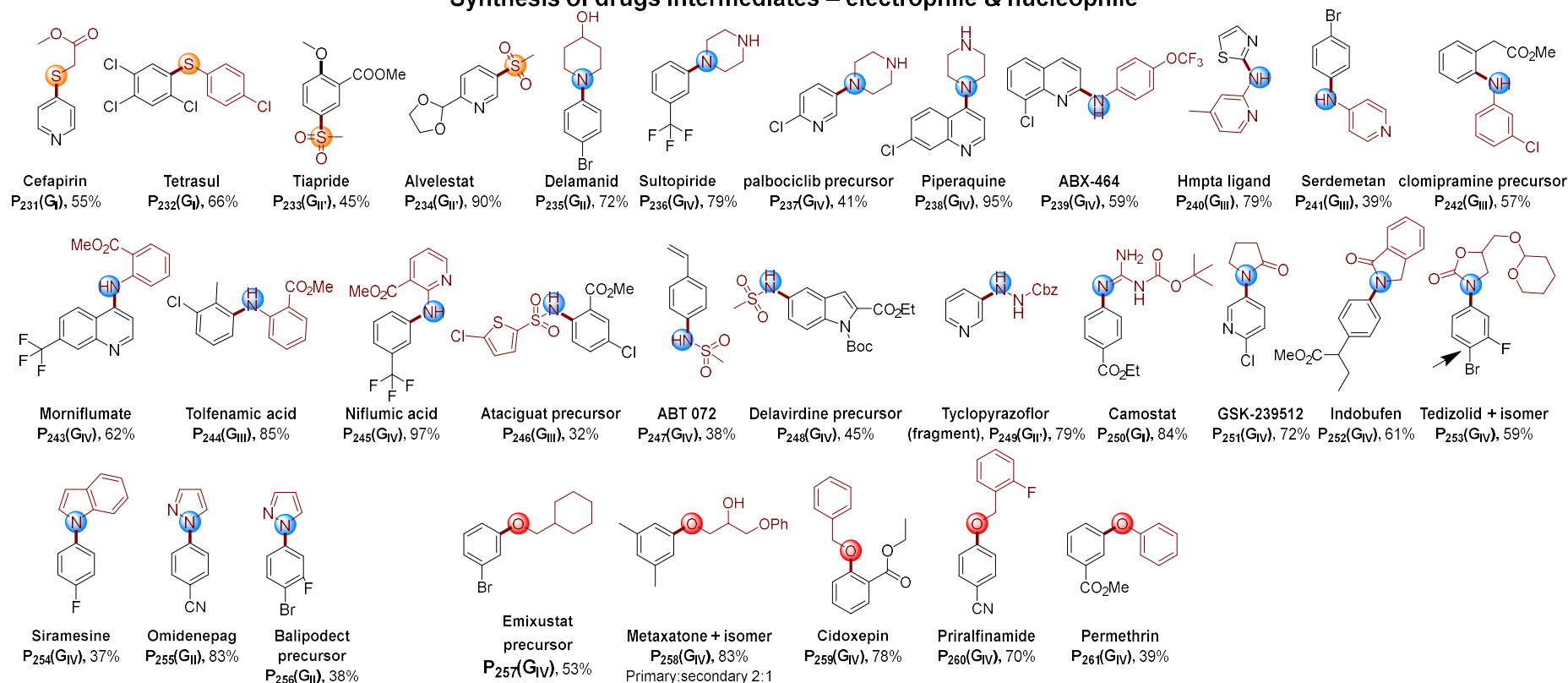
Nucleophiles – as amino acids & drugs



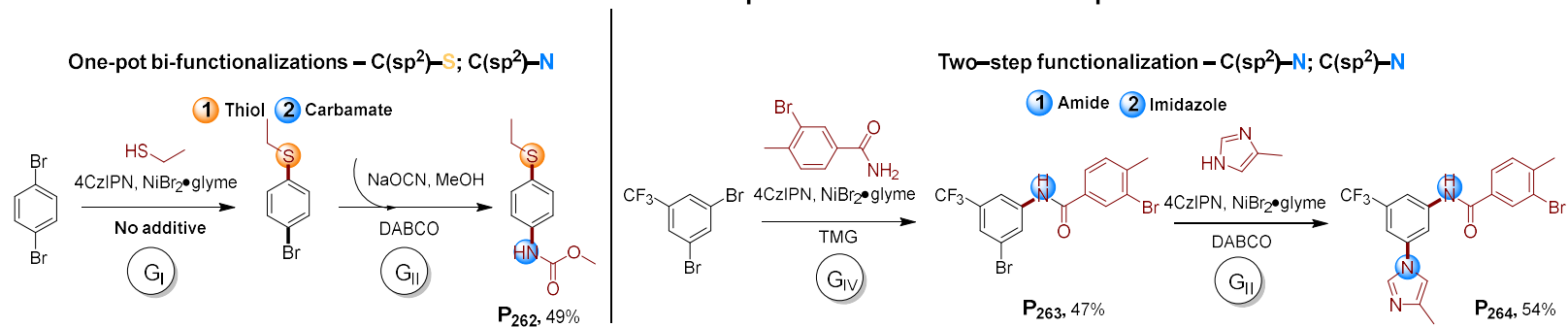
Electrophiles – as drugs

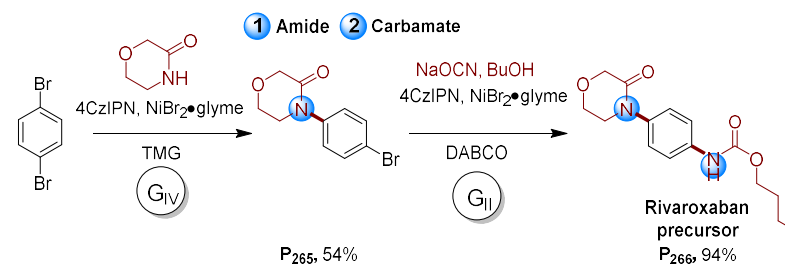


Synthesis of drugs intermediates – electrophile & nucleophile

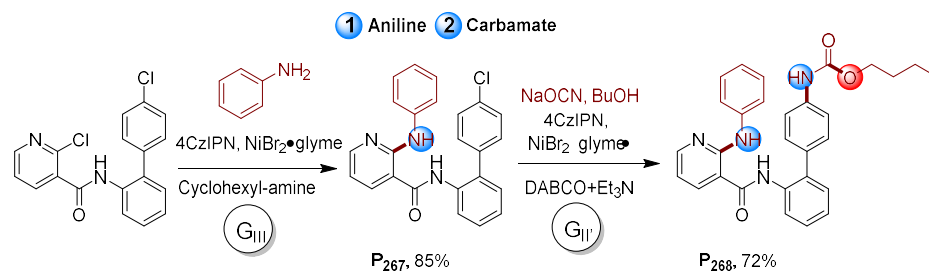
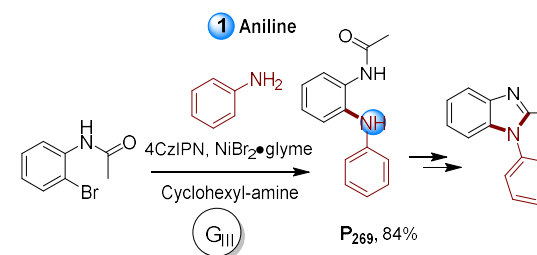
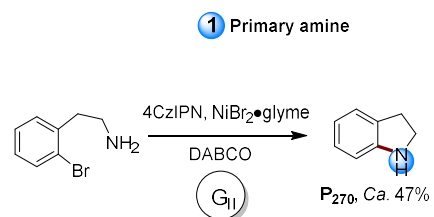
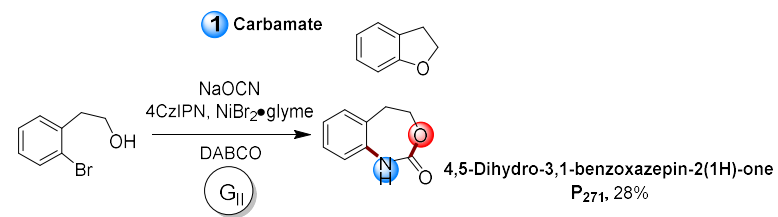


Two-step transformations – electrophile



Two-step functionalization – C(sp²)-N; C(sp²)-N

Two-step transformations – electrophile, syn of (het)aromatics

Two-step functionalization – C(sp²)-N; C(sp²)-NTwo-step functionalization – C(sp²)-N; C(sp²)-NTwo-step functionalization – C(sp²)-NTwo-step functionalization – C(sp²)-N; C(sp²)-O

One-pot two-step transformations – electrophiles & nucleophiles

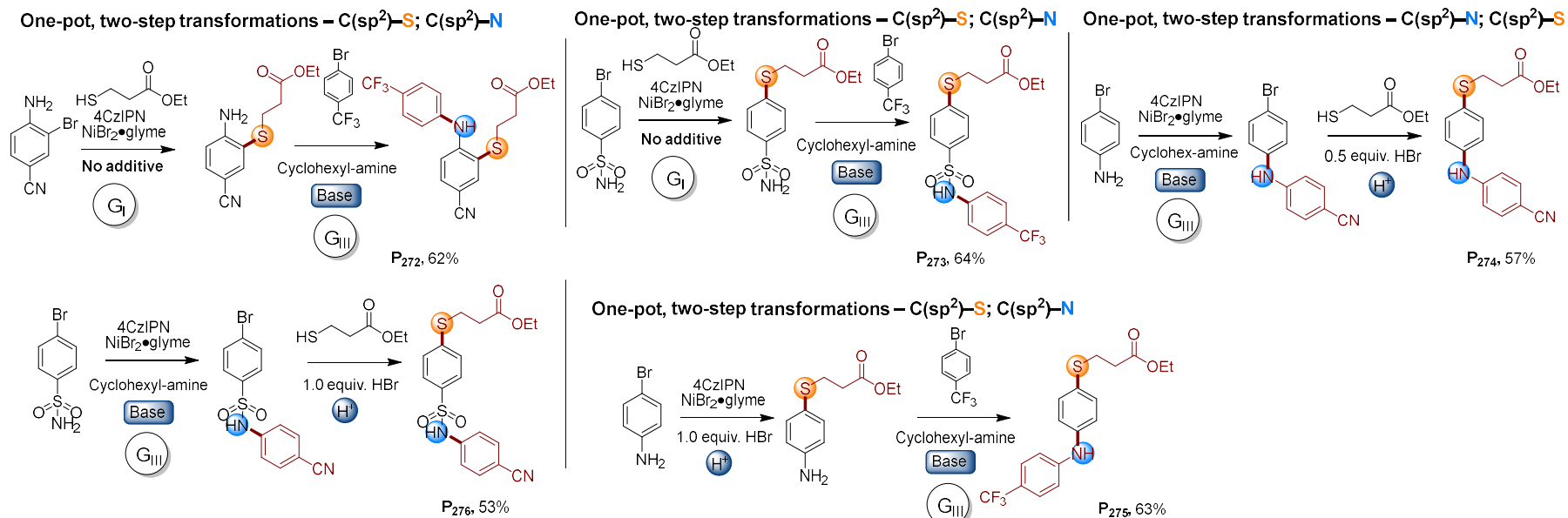
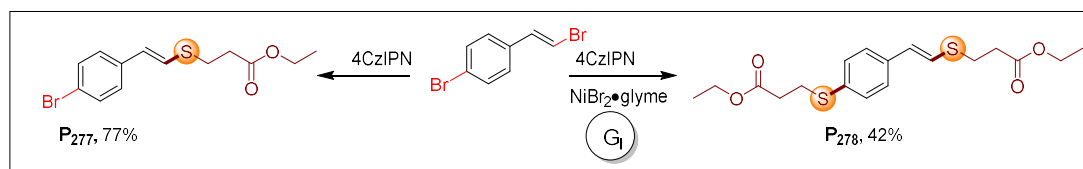
Two-step transformations *via* differential bond activation

Figure 4. Functionalization of bio-relevant molecules either as nucleophiles or electrophiles, synthesis of drugs, drug intermediates, and examples for two-step – either in tandem or one-pot – synthetic transformations. Isolated yields are reported. For compound P₂₇₀ the formation of the desired product was confirmed by GC and GC-MS analysis with an authentic sample, and no attempts were made for the purification of the desired product. The synthesis of P₂₇₇ can directly be performed with 4CzIPN^[31]

6.4 Conclusion

The adaptive dynamic homogeneous catalysis (Ad-HoC) with nickel and visible-light-driven redox processes relies on the formation of a dynamic assembly of catalytic species providing a simple platform for general cross-coupling reactions under very predictable reaction conditions. The ease of operation and effectiveness in solving numerous synthetic tasks are demonstrated in nine different bond-forming reactions (i.e., C(sp²)-S, Se, N, P, B, O, C (sp³, sp², sp), Si, Cl) covering various classes of nucleophiles and electrophiles. The reported simple, yet predictable, C(sp²)-X cross-coupling reaction conditions not only simplify the current approach of reaction condition screening for a specific cross-coupling transformation but also provide a general platform for artificial intelligence and machine learning processes. For the latter, one may consider, one reduced parameter is beneficial, and a generalization is pragmatic. We anticipate that applying the AD-HoC principle to other transition metal-mediated catalytic systems will accelerate the prediction of reaction conditions for different reactivity patterns.

6.5 References

- [1] N. Miyaura, A. Suzuki *Chem. Rev.* **1995**, *95*, 2457-2483.
- [2] P. Ruiz-Castillo, S. L. Buchwald *Chem. Rev.* **2016**, *116*, 12564-12649.
- [3] S. V. Ley, A. W. Thomas *Angew. Chem. Int. Ed.* **2003**, *42*, 5400-5449.
- [4] R. Dorel, C. P. Grugel, A.M. Haydl *Angew. Chem. Int. Ed.* **2019**, *58*, 17118-17129.
- [5] J. B. Diccianni, T. N. Diao, *Trends Chem.* **2019**, *1*, 830-844.
- [6] R. Jana, T. P Pathak, M. S. Sigman, *Chem. Rev.* **2011**, *111*, 1417-1492.
- [7] J. Zhang, S. Y. Wang, Y. Zhang, Z. Feng *Asian J. Org. Chem.* **2020**, *9*, 1519-1531.
- [8] M. H. Shaw, J. Twilton, D. W. C. MacMillan *J. Org. Chem.* **2016**, *81*, 6898-6926.
- [9] J. C. Tellis, D. N. Primer, G. A. Molander *Science* **2014**, *345*, 433-436.
- [10] M. S. Oderinde, M. Frenette, D. W. Robbins, B. Aquila, J. W. Johannes *J. Am. Chem. Soc.* **2016**, *138*, 1760-1763.
- [11] Y. Z. Qin, R. Sun, N. P. Gianoulis, D. G. Nocera *J. Am. Chem. Soc.* **2021**, *143*, 2005-2015.
- [12] C. N. P. Kullmer, J. A. Kautzky, S. W. Krska, T. Nowak D. W. MacMillan, *Science* **2022**, *376*, 532-539.
- [13] D. T. Ahneman, J. G. Estrada, S. S. Lin, S. D. Dreher, A. G. Doyle, *Science* **2018**, *360*, 186-190.
- [14] Our choice of 4CzIPN as a photocatalyst is based on its pure organic nature, easy synthesis on a multi-gram-scale (E. Speckmeier, T. G. Fischer, K. Zeitler *J. Am. Chem. Soc.* **2018**, *140*, 15353-15365.) excited-state lifetime (advantageous for short reaction times), and available ground and excited state redox potential window that allows easy manipulation of nickel's redox states. It is also to be noted here that the photocatalyst can also be functionalized under the photochemical reaction condition and may participate in the cross-coupling reaction (S. Grotjahn, B. König *Org. Lett.* **2021**, *23*, 8, 3146-3150).
- [15] E. Speckmeier, T. G. Fischer, K. Zeitler *J. Am. Chem. Soc.* **2018**, *140*, 15353-15365
- [16] S. Grotjahn, B. König *Org. Lett.* **2021**, *23*, 8, 3146-3150.
- [17] The cross-coupling reaction forging important C(sp²)-S bonds is also effective under air. However, and understandably so, relatively poor substrate conversion (and therefore, the yield of the desired product) was obtained as a result of quick consumption of the thiol nucleophile under air forming preferably di-sulfide.
- [18] T. Itoh, T. Mase *J. Org. Chem.* **2006**, *71*, 2203-2206.
- [19] The cross-coupling reactions were also effective for primary amines when used in excess and without any additives, however, the formation of the di-functionalized product led to the formation of the desired product relatively low in amount. The use of DABCO decreased the formation of the di-functionalized product yielding the desired product in excellent yield.
- [20] J. P. Wolfe, J. Ahman, J. P. Sadighi, R. A. Singer, S. L. Buchwald *Tetrahedron Lett.* **1997**, *38*, 6367-6370.
- [21] The addition of NEt₃ to DABCO was essential for anionic nucleophiles. The coupling reactions of anilines can also be facilitated with cyclohexylamine. See SI for a detailed listing.
- [22] A. K. Ghosh, M. J. Brindisi *Med. Chem.* **2015**, *58*, 2895-2940.
- [23] Y. Nakamura, K. Maruya, T. Mizoroki *Bull. Chem. Soc. Jpn.* **1980**, *53*, 3089-3092.
- [24] The coupling reactions with e-poor anilines, carbazole, Me-SO₂NH₂, and Tol-SO₂NH₂ are also effective in the presence of TMG, albeit with relatively slow reaction kinetics.
- [25] The cross-coupling reaction in the presence of cyclohexylamine did allow, in some cases, the formation of the desired product, however, in this case, cyclohexylamine is too good of a nucleophile and led to the formation of the byproduct (i.e., cyclohexylamine coupled product) in addition to the desired product. The use of other amidine bases, for example, 2-tert-butyl-1,1,3,3-tetramethylguanidine (Barton's base) or in general imine bases with very similar pK_a values for example 1,8-diazabicyclo[5.4.0]undec-7-en (DBU) or 7-methyl-1,5,7-triazabicyclo(4.4.0)dec-5-ene (MTBD) led to the formation of the desired products albeit with slower reaction kinetics and, in general, with the formation of more reduction product.
- [26] T. Noel, J. R. Naber, R. L. Hartman, J. P. McMullen, K. F. Jensen, S. L. Buchwald *Chem. Sci.* **2011**, *2*, 287-290.
- [27] It is to be noted here that we cannot completely rule out a Ni(0)/Ni(III) catalytic cycle, or the involvement of radicals with certain nucleophiles under photoredox reaction conditions. To determine which of the pathways are exclusively or simultaneously operative for a given nucleophile, a detailed mechanistic study is envisioned.
- [28] R. Sun, Y. Z. Qin, D. G. Nocera *Angew. Chem. Int. Ed.* **2020**, *59*, 9527-9533.
- [29] M. N. Lavagnino, T. Liang, D. W. C. MacMillan *Proc. Natl. Acad. Sci. U. S. A.* **2020**, *117*, 21058-21064.
- [30] E. V. Vinogradova, N. H. Park, B. P. Fors, S. L. Buchwald *Org. Lett.* **2013**, *15*, 1394-1397.
- [31] The reduction potential of 4CzIPN is enough for the activation of vinyl bromide.

6.6 Experimental Part

The following experimental part contains only the necessary information for the synthesis, isolation and characterization of the substances: P3, P6, P12, P13, P21, P24, P28, P35, P51, P57, P58, P63, P99, P106, P140, P150, P161, P162, P163, P167, P189, P196, P199, P201, P202, P205, P215, P220, P221, P228, P240, P250, P262 and P267.

For a detailed experimental part see: I. Ghosh, N. Shlapakov, T. A. Karl, J. Düker, M. Nikitin, J. V. Burykina, V. P. Ananikov and B. König *Nature* **2023**. (accepted article)

6.6.1 General Remarks

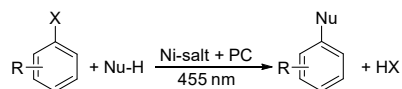
All reactions were carried out with dry solvents unless otherwise stated. The solvents (in this case, *N,N*-dimethylacetamide (DMA), *N,N*-dimethylformamide (DMF), acetonitrile (ACN), dimethyl sulfoxide (DMSO)) were dried with activated 3/4 Å molecular sieves following a reported procedure.^[1] Reagents were purchased at the highest commercial quality and used without further purification unless otherwise stated. The starting materials, whenever necessary, were synthesized according to the literature procedures. 1,2,3,5-Tetrakis(carbazol-9-yl)-4,6-dicyanobenzene (4CzIPN) was synthesized according to a reported protocol.^[2] Other photocatalysts (in this case, perylene) were commercially available and used without further purification. The nickel salts, nickel(II) bromide ethylene glycol dimethyl ether complex (NiBr₂•glyme), nickel(II)-bromide trihydrate (NiBr₂•3H₂O), nickel(II) chloride ethylene glycol dimethyl ether complex (NiCl₂•glyme), nickel(II) chloride hydrate (NiCl₂•xH₂O), nickel(II)-chloride hexahydrate (NiCl₂•6H₂O), nickel tetrafluoroborate hexahydrate (Ni(BF₄)₄•6H₂O), nickel(II)-acetate tetrahydrate (Ni(OAc)₂•4H₂O) were purchased at the highest commercial quality and used without further purification. The photochemical reactions were performed with 455 (±15) nm LEDs (OSRAM Oslon SSL 80 LDCQ7P-1U3U (*blue*, $\lambda_{max} = 455 (\pm 15) \text{ nm}$, $I_{max} = 1000 \text{ mA}$, radiant power ~ 500mW). The photochemical reactions under high-power LED illuminations were performed using either a photoreactor (*blue*, $\lambda_{max} = 455 (\pm 15) \text{ nm}$, $I_{max} = 1000 \text{ mA}$, radiant power ~ 1.4W) or photochemical immersion well reactor (*blue*, $\lambda_{max} = 455 (\pm 15) \text{ nm}$). For pictures of the irradiation set ups, see SI. Standard flash column chromatography was performed on a Biotage® Isolera™ Spektra system automated with high-performance flash purification system using silica gel 60 M (particle size 40–63 μm, 230–440 mesh, Merck) using petroleum ether (PE), ethyl acetate (EtOAc), dichloromethane (DCM), methanol (MeOH) as standard solvents. The reverse-phase column chromatography, whenever necessary, was performed with a reverse-phase column using water/acetonitrile as the solvent mixture. ¹H, ¹³C, ¹⁹F, and ³¹P NMR spectra were

recorded on Bruker Avance spectrometers (300 MHz, 75 MHz, 282 MHz, 121 MHz) or (400 MHz, 101 MHz, 376 MHz, 162 MHz) in CDCl₃, DMSO-*d*₆, and MeOH-*d*₄ solutions with internal solvent signals (for ¹H and ¹³C) as reference (7.26, 77.2 for CDCl₃, 2.50 and 39.5 for DMSO-*d*₆, and 3.31, 49.0 for MeOH-*d*₄). ¹H NMR data are reported as follows: chemical shift (ppm), multiplicity (s = singlet, br. s. = broad singlet, d = doublet, t = triplet, q = quartet, quint = quintet, sext = sextet, hept = heptet, dd = doublet of doublets, ddd = doublet of doublets of doublets, td = triplet of doublets, qd = quartet of doublets, m = multiplet), coupling constants (Hz), and numbers of protons. ¹⁹F data are reported as follows: chemical shift (ppm), multiplicity (wherever applicable, s = singlet, d = doublet, t = triplet, q = quartet), coupling constants (Hz), and numbers of fluorines (wherever applicable). Data for ¹³C NMR are reported in terms of chemical shift, multiplicity (wherever applicable, s = singlet, d = doublet, t = triplet, q = quartet), coupling constants (Hz), and no special nomenclature is used for equivalent carbons. Data for ³¹P NMR are reported in terms of chemical shift, multiplicity (wherever applicable, s = singlet, d = doublet, t = triplet, q = quartet), coupling constants (Hz), and no special nomenclature is used for equivalent phosphorus. High-resolution mass spectra (HRMS), low-resolution mass spectra (LRMS), and high-performance liquid chromatography-mass spectra (HPLC-MS) were obtained from the central analytic mass spectrometry facilities of the Faculty of Chemistry and Pharmacy, Regensburg University, and are reported according to the IUPAC recommendations 2013. UV-Vis measurements were performed with a Cary 4000 spectrometer. Electrochemical studies (in this case, cyclic voltammetry) were carried out under an argon atmosphere. The measurements were performed in respective solvents (DMA/DMF/ACN, DMSO) containing 0.1 M tetra-*n*-butylammonium tetrafluoroborate using ferrocene/ferrocenium (Fc/Fc⁺) as an internal reference. A glassy carbon electrode (working electrode), platinum wire counter electrode, and Ag quasi-reference electrode were employed. Gas chromatography (GC) and gas chromatography coupled to low-resolution mass spectrometry (GC-MS) analysis were performed using a capillary column (length: 30 m; diam.: 0.25 mm; film: 0.25 μM) using He gas as a carrier. GC was equipped with an FID detector. GC-MS was performed on 5975 MSD single quadrupole detector. For the reported GC-chromatograms of the cross-coupling reactions, the respective reduction products (as by-products, formed in minimal amounts) were identified by comparing them with authentic samples (GC/FID and GC-MS). Quantum yield measurements: The quantum yield was measured with a custom-made quantum yield determination setup^[3]: translation stages (horizontal and vertical): Thorlabs DT 25/M or DT S25/M; photographic lens with f = 50 mm; magnetic stirrer: Faulhaber motor (1524B024S R) with 14:1 gear (15A); PS19Q power sensor from Coherent; PowerMax software; adjustable power supply "Basetech BT-153 0–15 V/DC 0–3 A 45 W". High-resolution mass spectra were obtained on a Bruker maXis Q-TOF instrument (Bruker Daltonik GmbH, Germany) equipped with electrospray ionization (ESI) ion source. The experiments were performed in positive (+) MS ion mode (HV Capillary: 4500 V; HV End Plate Offset: - 500 V)

and negative (–) MS ion mode (HV Capillary: +4000 V; Spray Shield: –500 V) with a scan range of m/z 50–1500. External calibration of the mass spectrometer was performed using a low-concentration tuning mix solution (Agilent Technologies). Direct syringe injection was applied for the analyzed solutions in DMA (flow rate: $3.0 \mu\text{L}/\text{min}^{-1}$). Nitrogen was applied as nebulizer gas (1 bar) and dry gas ($4.0 \text{ L}/\text{min}$, $200 \text{ }^\circ\text{C}$). The spectra were processed using Bruker Data Analysis 5.1 software. The $\Delta\delta$ values for the Ni complexes in the article and in the SI are given for the most abundant signal in complex. Ultrahigh-resolution mass spectra (ESI-UHRMS) were acquired on a Bruker Solarix XR ion cyclotron resonance Fourier transform MS (Bremen, Germany) equipped with a 15 Tesla superconducting magnet and an Apollo II source in negative electrospray ionization mode. The sample was injected with a constant flow rate of $120 \mu\text{l}/\text{h}$, nebulizer gas pressure of 1 bar and drying gas ($200 \text{ }^\circ\text{C}$, $4.0 \text{ L}\times\text{min}^{-1}$). The accumulation time was 0.1 sec, the number of scans was 256, and the m/z range was 150–1500. The applied ESI voltage was a 3.6 kV capillary voltage and a –0.5 kV end plate offset. All spectra were acquired using a time transient of 2 MW. Transfer optic parameters were therefore ToF 1.3 msec, frequency 4 MHz and RF amplitude of 350 Vpp. In the ESI-MS spectra captions the appropriate composition for nickel complexes are given presumably and alternative structures may be assigned. Note: Due to a large number of synthetic examples in the SI, it was not possible to isolate all compounds (i.e., the desired product) and characterize them with NMR and high-resolution mass spectrometric analysis (HRMS).

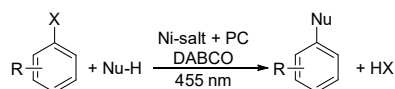
6.6.2 Synthetic Procedures of Cross-Coupling Reactions

General procedure I.



A 5 mL snap vial was charged with a magnetic stirring bar, (het)aryl halides (0.2 mmol, 1.0 equiv.), the respective coupling partner (0.3-0.5 mmol, 1.5-2.5 equiv.), 4CzIPN (0.1-0.5 mol%), and NiBr₂•glyme (5.0 mol%, unless otherwise stated). 0.4 mL solvent was used. The reaction mixture was then introduced to the nitrogen atmosphere either *via* applying reduced pressure and refilling (×3) or "pump-freeze-thaw" cycles (×3, important for low boiling reagents) with a syringe needle and irradiated under N₂ at 25 °C or 60 °C through the plane bottom side of the snap vial using a single blue LED (455 (± 15) nm). The reaction progress (in this case, mainly substrate consumption and the formation of desired product) was monitored by GC and GC-MS analysis. After completion, the reaction mixture was transferred (with the use of approx. 10 mL (×3) ethyl acetate) to a separating funnel. Then, approx. 10-15 mL of brine solution was added, shaken, and the organic layer was collected. The water layer was extracted again with ethyl acetate (3 × 20 mL). The combined organic layers were dried over MgSO₄, filtered, and concentrated under reduced pressure. Purification of the crude product was achieved by flash column chromatography using petrol ether/ethyl acetate or other appropriate solvent mixtures (PE/DCM, DCM/MeOH, EtOAc/MeOH, wherever applicable) as eluents on silica gel.

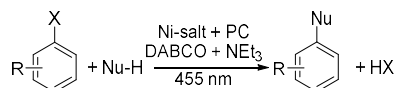
General procedure II.



A 5 mL snap vial was charged with a magnetic stirring bar, (het)aryl halides (0.2 mmol, 1.0 equiv.), the respective coupling partner 0.36 mmol, 1.8 equiv.), 1,4-diazabicyclo(2.2.2)octan (0.4 mmol, 2.2 equiv., unless otherwise stated), 4CzIPN (0.1-0.5 mol%), and a NiBr₂•glyme (5.0 mol%, unless otherwise stated). 0.4 mL solvent was used. The reaction mixture was then introduced to the nitrogen atmosphere either *via* applying reduced pressure and refilling (×3) or "pump-freeze-thaw" cycles (×3, important for low boiling reagents) with a syringe needle and irradiated under N₂ at 25 °C or 60 °C through the plane bottom side of the snap vial using a single blue LED (455 (± 15) nm). The reaction progress (in this case, mainly substrate consumption and the formation of desired product) was monitored by GC and GC-MS analysis. After completion, the reaction mixture was transferred (with the use of approx. 10 mL (×3) ethyl acetate to a separating funnel. Then, approx. 10-15 mL of brine solution was added, shaken, and the organic

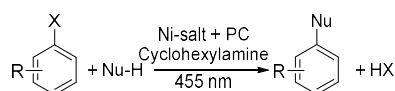
layer was collected. The water layer was extracted again with ethyl acetate (3 × 20 mL). The combined organic layers were dried over MgSO₄, filtered, and concentrated under reduced pressure. Purification of the crude product was achieved by flash column chromatography using petrol ether/ethyl acetate or other appropriate solvent mixtures (PE/DCM, DCM/MeOH, EtOAc/MeOH, wherever applicable) as eluents on silica gel.

General procedure II'.



A 5 mL snap vial was charged with a magnetic stirring bar, (het)aryl halides (0.2 mmol, 1.0 equiv.), the respective coupling partner (0.3-0.64 mmol, 1.5-3.2 equiv.), 1,4-diazabicyclo(2.2.2)octan (0.32-0.44 mmol, 1.6-2.2 equiv.), triethylamine (0.05-0.1 mmol, 0.25-0.5 equiv.), 4CzIPN (0.1-0.5 mol%), and a NiBr₂•glyme (5.0 mol%, unless otherwise stated). 0.4 mL–1.2 mL solvent was used. The reaction mixture was then introduced to the nitrogen atmosphere either *via* applying reduced pressure and refilling (×3) or "pump-freeze-thaw" cycles (×3) with a syringe needle and irradiated under N₂ at 25 °C or 60 °C through the plane bottom side of the snap vial using a single blue LED (455 (± 15) nm). The reaction progress (in this case, mainly substrate consumption and the formation of desired product) was monitored by GC and GC-MS analysis. After completion, the reaction mixture was transferred (with the use of 10 mL (×3) ethyl acetate to a separating funnel. Then, approx. 10-15 mL of brine solution was added, shaken, and the organic layer was collected. The water layer was extracted again with ethyl acetate (3 × 20 mL). The combined organic layers were dried over MgSO₄, filtered, and concentrated under reduced pressure. Purification of the crude product was achieved by flash column chromatography using petrol ether/ethyl acetate or other appropriate solvent mixtures (PE/DCM, DCM/MeOH, EtOAc/MeOH, wherever applicable) as eluents on silica gel.

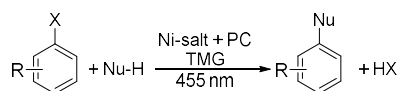
General procedure III.



A 5 mL snap vial was charged with a magnetic stirring bar, (het)aryl halides (0.2 mmol, 1.0 equiv.), the respective coupling partner (0.28-0.4 mmol, 1.4-2.0 equiv.), cyclohexylamine (0.26 mmol, 1.3 equiv.), 4CzIPN (0.1-0.5 mol%), and a NiBr₂•glyme (5.0 mol%, unless otherwise stated). 0.4 mL solvent was used. The reaction mixture was then introduced to the nitrogen atmosphere either *via* applying reduced pressure and refilling (×3) or "pump-freeze-thaw" cycles

(×3) with a syringe needle and irradiated under N₂ at 25 °C or 60 °C through the plane bottom side of the snap vial using a single blue LED (455 (± 15) nm). The reaction progress (in this case, mainly substrate consumption and the formation of desired product) was monitored by GC and GC-MS analysis. After completion, the reaction mixture was transferred (with the use of 10 mL (×3) ethyl acetate to a separating funnel. Then, approx. 10-15 mL of brine solution was added, shaken, and the organic layer was collected. The water layer was extracted again with ethyl acetate (3 × 20 mL). The combined organic layers were dried over MgSO₄, filtered, and concentrated under reduced pressure. Purification of the crude product was achieved by flash column chromatography using petrol ether/ethyl acetate or other appropriate solvent mixtures (PE/DCM, DCM/MeOH, EtOAc/MeOH, wherever applicable) as eluents on silica gel.

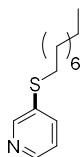
General procedure IV.



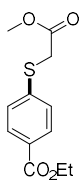
A 5 mL snap vial was charged with a magnetic stirring bar, (het)aryl halides (0.2 mmol, 1.0 equiv., unless otherwise stated), the respective coupling partner (0.36-0.6 mmol, 1.8-3.0 equiv.), 1,1,3,3-tetramethylguanidine (unless otherwise stated, 0.24 mmol, 1.2 equiv.), 4CzIPN (0.1-0.5 mol%), and a NiBr₂•glyme (5.0 mol%, unless otherwise stated). 0.4 mL solvent was used. The reaction mixture was then introduced to the nitrogen atmosphere either *via* applying reduced pressure and refilling (×3) or "pump-freeze-thaw" cycles (×3) with a syringe needle and irradiated under N₂ at 25 °C or 60 °C through the plane bottom side of the snap vial using a single blue LED (455 (± 15) nm). The reaction progress (in this case, mainly substrate consumption and the formation of desired product) was monitored by GC and GC-MS analysis. After completion, the reaction mixture was transferred (with the use of 10 mL (×3) ethyl acetate to a separating funnel. Then, approx. 10-15 mL of brine solution was added, shaken, and the organic layer was collected. The water layer was extracted again with ethyl acetate (3 × 20 mL). The combined organic layers were dried over MgSO₄, filtered, and concentrated under reduced pressure. Purification of the crude product was achieved by flash column chromatography using petrol ether/ethyl acetate or other appropriate solvent mixtures (PE/DCM, DCM/MeOH, EtOAc/MeOH, wherever applicable) as eluents on silica gel.

6.6.4 Characterization of Isolated Products

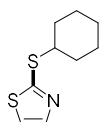
Note: The following products were synthesized by I. Ghosh and isolated by T. A. Karl.



3-(nonylthio)pyridine (P₃): The compound was prepared following the general *procedure I* using 3-bromopyridine (31.6 mg, 0.2 mmol, 1.0 equiv.), 1-nonanethiol (48.0 mg, 0.3 mmol, 1.5 equiv.), NiBr₂•glyme (3.2 mg, 0.01 mmol, 0.05 equiv.), and 4CzIPN (0.2 mol%, 0.0004 mmol, 0.002 equiv.). DMA (0.4 mL) was used as a solvent. The reaction mixture was irradiated under N₂ at 25 °C for 45 min using a single blue LED (455 (± 15) nm). After completion, the reaction mixture was subjected to the workup procedure outlined in general *procedure I* and purified using flash chromatography on silica gel using petroleum ether/ethyl acetate. Yield: 92%. ¹H NMR (CDCl₃, 400 MHz): 8.54 (1H, dd, *J* = 2.1, 0.5 Hz), 8.39 (1H, dd, *J* = 4.8, 1.6 Hz), 7.62 (1H, ddd, *J* = 7.9, 2.1, 1.6 Hz), 7.19 (1H, ddd, *J* = 7.9, 4.8, 0.5 Hz), 2.90 (2H, t, *J* = 7.4 Hz), 1.70-1.55 (2H, m), 1.49-1.34 (2H, m), 1.34-1.15 (10H, m), 0.86 (3H, t, *J* = 7.1 Hz). ¹³C NMR (CDCl₃, 100 MHz): 149.86, 146.74, 136.82, 134.38, 123.65, 33.79, 31.93, 29.52, 29.31, 29.22, 29.20, 28.81, 22.75, 14.19. HRMS: calculated for [M]⁺ C₁₄H₂₃NS⁺ 237.1546; found 237.1539.

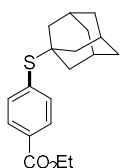


ethyl 4-((2-methoxy-2-oxoethyl)thio)benzoate (P₆): The compound was prepared following the general *procedure I* using ethyl 4-bromobenzoate (45.8 mg, 0.2 mmol, 1.0 equiv.), methyl thioglycolate (31.8 mg, 0.3 mmol, 1.5 equiv.), NiBr₂•glyme (3.2 mg, 0.01 mmol, 0.05 equiv.), and 4CzIPN (0.2 mol%, 0.0004 mmol, 0.002 equiv.). DMA (0.4 mL) was used as a solvent. The reaction mixture was irradiated under N₂ at 25 °C for 3 h using a single blue LED (455 (± 15) nm). After completion, the reaction mixture was subjected to the workup procedure outlined in general *procedure I* and purified using flash chromatography on silica gel using petroleum ether/ethyl acetate. Yield: 96%. ¹H NMR (CDCl₃, 400 MHz): 7.84 (2H, d, *J* = 8.5 Hz), 7.25 (2H, d, *J* = 8.5 Hz), 4.25 (2H, q, *J* = 7.1 Hz), 3.63 (3H, s), 3.62 (2H, s), 1.27 (3H, t, *J* = 7.1 Hz). ¹³C NMR (CDCl₃, 100 MHz): 169.70, 166.20, 141.82, 130.18, 128.27, 127.24, 61.09, 52.88, 34.97, 14.42. HRMS: calculated for [M]⁺ C₁₂H₁₄O₄S⁺ 254.0607; found 254.0603.

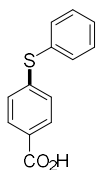


2-(cyclohexylthio)thiazole (P₁₂): The compound was prepared following the general *procedure I* using 2-bromothiazole (32.8 mg, 0.2 mmol, 1.0 equiv.), cyclohexanethiol (34.8 mg, 0.3 mmol, 1.5 equiv.), NiBr₂•glyme (3.2 mg, 0.01 mmol, 0.05 equiv.), and

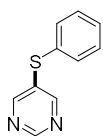
4CzIPN (0.2 mol%, 0.0004 mmol, 0.002 equiv.). DMA (0.4 mL) was used as a solvent. The reaction mixture was irradiated under N₂ at 25 °C for 3h using a single blue LED (455 (± 15) nm). After completion, the reaction mixture was subjected to the workup procedure outlined in general *procedure I* and purified using flash chromatography on silica gel using petroleum ether/ethyl acetate. Yield: 66%. **¹H NMR (CDCl₃, 400 MHz):** 7.68 (1H, d, *J* = 3.4 Hz), 7.21 (1H, d, *J* = 3.4 Hz), 3.60 (1H, tt, *J* = 10.4, 3.7 Hz), 2.15-2.03 (2H, m), 1.82-1.71 (2H, m), 1.66-1.56 (1H, m), 1.56-1.44 (2H, m), 1.44-1.24 (3H, m). **¹³C NMR (CDCl₃, 100 MHz):** 156.81, 155.86, 133.49, 33.64, 31.91, 29.50, 29.29, 29.18, 29.17, 28.73, 22.74, 14.17. **HRMS:** calculated for [M]⁺ C₉H₁₃NS₂⁺ 199.0484; found 199.0488.



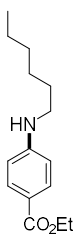
ethyl 4-(((3s,5s,7s)-adamantan-1-yl)thio)benzoate (P₁₃): The compound was prepared following the general *procedure I* using ethyl 4-bromobenzoate (45.8 mg, 0.2 mmol, 1.0 equiv.), 1-adamantanthiol (60.6 mg, 0.36 mmol, 1.8 equiv.), NiBr₂•glyme (3.2 mg, 0.01 mmol, 0.05 equiv.), and 4CzIPN (0.2 mol%, 0.0004 mmol, 0.002 equiv.). DMA (0.4 mL) was used as a solvent. The reaction mixture was irradiated under N₂ at 25 °C for 25h using a single blue LED (455 (± 15) nm). The reaction mixture was then subjected to the workup procedure outlined in general *procedure I* and purified using flash chromatography on silica gel using petroleum ether/ethyl acetate. Yield: 46%. **¹H NMR (CDCl₃, 400 MHz):** 7.97 (2H, d, *J* = 8.3 Hz), 7.55 (2H, d, *J* = 8.3 Hz), 4.37 (2H, q, *J* = 7.1 Hz), 2.06-1.94 (3H, m), 1.82 (6H, d, *J* = 2.5 Hz), 1.68-1.53 (6H, m), 1.39 (3H, t, *J* = 7.1 Hz). **¹³C NMR (CDCl₃, 100 MHz):** 166.42, 137.29, 136.85, 130.54, 129.34, 61.21, 49.01, 43.84, 36.19, 30.13, 14.45. **HRMS:** calculated for [M]⁺ C₁₉H₂₄O₂S⁺ 316.1492; found 316.1489.



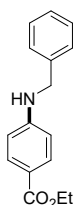
4-(phenylthio)benzoic acid (P₂₁): The compound was prepared following the general *procedure I* using 4-bromobenzoic acid (40.2 mg, 0.2 mmol, 1.0 equiv.), thiophenol (33.0 mg, 0.3 mmol, 1.5 equiv.), NiBr₂•glyme (3.2 mg, 0.01 mmol, 0.05 equiv.), and 4CzIPN (0.2 mol%, 0.0004 mmol, 0.002 equiv.). DMA (0.4 mL) was used as a solvent. The reaction mixture was irradiated under N₂ at 25 °C for 2 h using a single blue LED (455 (± 15) nm). After completion, the reaction mixture was subjected to the workup procedure outlined in general *procedure I* and purified using flash chromatography on silica gel using DCM/MeOH. Yield: 69%. **¹H NMR (CDCl₃, 300 MHz):** 11.52 (1H, br s), 7.96 (2H, d, *J* = 8.5 Hz), 7.61-7.47 (2H, m), 7.47-7.35 (3H, m), 7.21 (2H, d, *J* = 8.5 Hz). **¹³C NMR (CDCl₃, 75 MHz):** 172.02, 146.20, 134.26, 131.89, 130.80, 129.87, 129.08, 127.25, 126.45. **HRMS:** calculated for [M]⁺ C₁₃H₁₀O₂S⁺ 230.0396; found 230.0390.



5-(phenylthio)pyrimidine (P₂₄): The compound was prepared following the general *procedure I* using 3-bromopyrimidine (31.8 mg, 0.2 mmol, 1.0 equiv.), thiophenol (33.0 mg, 0.3 mmol, 1.5 equiv.), NiBr₂•glyme (3.2 mg, 0.01 mmol, 0.05 equiv.), and 4CzIPN (0.2 mol%, 0.0004 mmol, 0.002 equiv.). DMA (0.4 mL) was used as a solvent. The reaction mixture was irradiated under N₂ for 6h using a single blue LED (455 (± 15) nm). After completion, the reaction mixture was subjected to the workup procedure outlined in general *procedure I* and purified using flash chromatography on silica gel using petroleum ether/ethyl acetate. Yield: 59%. ¹H NMR (CDCl₃, 400 MHz): 9.01 (1H, s), 8.57 (2H, s), 7.48-7.28 (5H, m). ¹³C NMR (CDCl₃, 100 MHz): 157.10, 156.32, 133.65, 132.77, 131.72, 129.97, 128.89. HRMS: calculated for [M]⁺ C₁₀H₈N₂S⁺ 188.0403; found 188.0398.

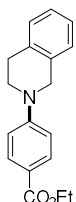


ethyl 4-(hexylamino)benzoate (P₂₈): The compound was prepared following the general *procedure II* using ethyl 4-bromobenzoate (45.8 mg, 0.2 mmol, 1.0 equiv.), hexylamine (36.4 mg, 0.36 mmol, 1.8 equiv.), 1,4-diazabicyclo[2.2.2]octane (49.3 mg, 0.44 mmol, 2.2 equiv.), NiBr₂•glyme (3.2 mg, 0.01 mmol, 0.05 equiv.), and 4CzIPN (0.5 mol%, 0.001 mmol, 0.005 equiv.). DMA (0.4 mL) was used as a solvent. The reaction mixture was irradiated under N₂ at 25 °C for 4h15min using a single blue LED (455 (± 15) nm). After completion, the reaction mixture was subjected to the workup procedure outlined in general *procedure II* and purified using flash chromatography on silica gel using petroleum ether/ethyl acetate. Yield: 89%. ¹H NMR (CDCl₃, 300 MHz): 7.86 (2H, d, *J* = 8.9 Hz), 6.55 (2H, d, *J* = 8.7 Hz), 4.31 (2H, q, *J* = 7.1 Hz), 4.3 (1H, br s), 3.19-3.11 (2H, m), 1.70-1.56 (2H, m), 1.48-1.72 (9H, m), 0.95-0.82 (3H, m). ¹³C NMR (CDCl₃, 75 MHz): 167.00, 152.05, 131.62, 118.71, 111.58, 60.25, 34.66, 31.69, 29.39, 26.86, 22.70, 14.58, 14.12. HRMS: calculated for [M+H]⁺ C₁₅H₂₄NO₂⁺ 250.1802; found 250.1804.

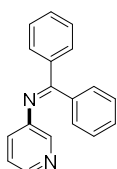


ethyl 4-(benzylamino)benzoate (P₃₅): The compound was prepared following the general *procedure II* using ethyl 4-bromobenzoate (45.8 mg, 0.2 mmol, 1.0 equiv.), benzylamine (38.52 mg, 0.36 mmol, 1.8 equiv.), 1,4-diazabicyclo[2.2.2]octane (49.3 mg, 0.44 mmol, 2.2 equiv.), NiBr₂•glyme (3.2 mg, 0.01 mmol, 0.05 equiv.), and 4CzIPN (0.5 mol%, 0.001 mmol, 0.005 equiv.). DMA (0.4 mL) was used as a solvent. The reaction mixture was irradiated under N₂ at 60 °C for 1.5h using a single blue LED (455 (± 15) nm). After completion, the reaction mixture was subjected to the workup procedure outlined in general *procedure II* and purified using flash chromatography on silica gel using petroleum ether/ethyl acetate. Yield: 86%. ¹H NMR (CDCl₃, 400 MHz): 7.89 (2H, d, *J* = 8.8 Hz), 7.42-7.33 (4H, m),

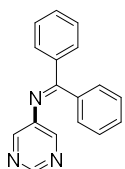
7.33-7.27 (1H, m), 6.59 (2H, d, $J = 8.8$ Hz), 4.63 (1H, br s), 4.38 (2H, s), 4.32 (2H, q, $J = 7.1$ Hz), 1.37 (3H, t, $J = 7.1$ Hz). ^{13}C NMR (CDCl_3 , 100 MHz): 166.93, 151.81, 138.51, 131.55, 128.80, 127.52, 127.42, 118.96, 111.68, 60.26, 47.66, 14.50. HRMS: calculated for $[\text{M}]^+$ $\text{C}_{16}\text{H}_{17}\text{NO}_2^+$ 255.1254; found 255.1249.



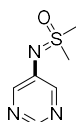
ethyl 4-(3,4-dihydroisoquinolin-2(1H)-yl)benzoate (P₅₁): The compound was prepared following the general *procedure II*, using ethyl 4-bromobenzoate (45.8 mg, 0.2 mmol, 1.0 equiv.), 1,2,3,4-tetrahydroisochinoline (47.9 mg, 0.36 mmol, 1.8 equiv.), 1,4-diazabicyclo[2.2.2]octane (49.3 mg, 0.44 mmol, 2.2 equiv.), $\text{NiBr}_2 \cdot \text{glyme}$ (3.2 mg, 0.01 mmol, 0.05 equiv.), and 4CzIPN (0.5 mol%, 0.001 mmol, 0.005 equiv.). DMA (0.4 mL) was used as a solvent. The reaction mixture was irradiated under N_2 at 25 °C for 3.5h using a single blue LED (455 (\pm 15) nm). After completion, the reaction mixture was subjected to the workup procedure outlined in general *procedure II* and purified using flash chromatography on silica gel using petroleum ether/ethyl acetate. Yield: 76%. ^1H NMR (d_6 -DMSO, 300 MHz): 7.81 (2H, d, $J = 9.0$ Hz), 7.31-7.14 (4H, m), 7.00 (2H, d, $J = 9.0$ Hz), 4.53 (2H, s), 4.24 (2H, q, $J = 7.1$ Hz), 3.64 (2H, t, $J = 5.9$ Hz), 2.93 (2H, t, $J = 5.9$ Hz), 1.29 (3H, t, $J = 7.1$ Hz). ^{13}C NMR (d_6 -DMSO, 75 MHz): 166.76, 152.79, 134.91, 134.01, 130.79, 128.10, 126.53, 126.49, 126.07, 117.29, 112.21, 59.77, 48.26, 44.27, 28.05, 14.35. HRMS: calculated for $[\text{M}]^+$ $\text{C}_{18}\text{H}_{19}\text{NO}_2^+$ 281.1410; found 281.1390.



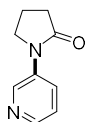
1,1-diphenyl-N-(pyridin-3-yl)methanimine (P₅₇): The compound was prepared following the general *procedure II*, using 3-bromopyridine (31.6 mg, 0.2 mmol, 1.0 equiv.), benzophenone imine (72.4 mg, 0.4 mmol, 2.0 equiv.), 1,4-diazabicyclo[2.2.2]octane (49.3 mg, 0.44 mmol, 2.2 equiv.), $\text{NiBr}_2 \cdot \text{glyme}$ (3.2 mg, 0.01 mmol, 0.05 equiv.), and 4CzIPN (0.5 mol%, 0.001 mmol, 0.005 equiv.). DMA (0.4 mL) was used as solvent. The reaction mixture was irradiated under N_2 at 60 °C for 12h using a single blue LED (455 (\pm 15) nm). After completion, the reaction mixture was subjected to the workup procedure outlined in general *procedure II* and purified using flash chromatography on silica gel using petroleum ether/ethyl acetate. Yield: 84%. ^1H NMR (d_6 -DMSO, 400 MHz): 8.09 (1H, dd, $J = 4.4, 1.6$ Hz), 7.95 (1H, dd, $J = 1.6, 0.6$ Hz), 7.77-7.62 (2H, m), 7.59-7.51 (1H, m), 7.51-7.42 (2H, m), 7.37-7.27 (3H, m), 7.20-7.09 (4H, m). ^{13}C NMR (d_6 -DMSO, 100 MHz): 169.51, 147.07, 144.08, 141.36, 138.23, 135.33, 131.35, 128.91, 128.78, 128.45, 128.20, 127.59, 123.22. HRMS: calculated for $[\text{M}]^+$ $\text{C}_{18}\text{H}_{14}\text{N}_2^+$ 258.1151; found 258.1153.



1,1-diphenyl-N-(pyrimidin-5-yl)methanimine (P₅₈): The compound was prepared following the general *procedure II*, using 3-bromopyrimidine (31.8 mg, 0.2 mmol, 1.0 equiv.), benzophenone imine (72.4 mg, 0.4 mmol, 2.0 equiv.), 1,4-diazabicyclo[2.2.2]octane (49.3 mg, 0.44 mmol, 2.2 equiv.), NiBr₂•glyme (3.2 mg, 0.01 mmol, 0.05 equiv.), and 4CzIPN (0.5 mol%, 0.001 mmol, 0.005 equiv.). DMA (0.4 mL) was used as a solvent. The reaction mixture was irradiated under N₂ at 60 °C for 12h using a single blue LED (455 (± 15) nm). After completion, the reaction mixture was subjected to the workup procedure outlined in general *procedure II* and purified using flash chromatography on silica gel using petroleum ether/ethyl acetate. Yield: 97%. **¹H NMR (d₆-DMSO, 400 MHz):** 8.72 (1H, s), 8.25 (2H, s), 7.77-7.66 (2H, m), 7.62-7.53 (1H, m), 7.53-7.45 (2H, m), 7.41-7.31 (3H, m), 7.27-7.16 (2H, m). **¹³C NMR (d₆-DMSO, 100 MHz):** 171.38, 153.23, 148.19, 145.17, 137.70, 134.70, 131.80, 129.11, 128.77, 128.56, 128.39. **HRMS:** calculated for [M]⁺ C₁₇H₁₃N₃⁺ 259.1104; found 259.1106.

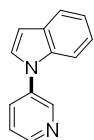


dimethyl(pyrimidin-5-ylimino)-λ⁶-sulfanone (P₆₃): The compound was prepared following the general *procedure II*, using 3-bromopyrimidine (31.8 mg, 0.2 mmol, 1.0 equiv.), iminodimethyl(6)sulfanone (29.8 mg, 0.32 mmol, 1.6 equiv.), 1,4-diazabicyclo[2.2.2]octane (40.3 mg, 0.36 mmol, 1.8 equiv.), NiBr₂•glyme (3.2 mg, 0.01 mmol, 0.05 equiv.), and 4CzIPN (0.5 mol%, 0.001 mmol, 0.005 equiv.). DMA (0.4 mL) was used as a solvent. The reaction mixture was irradiated under N₂ at 25 °C for 5h using a single blue LED (455 (± 15) nm). After completion, the reaction mixture was subjected to the workup procedure outlined in general *procedure II* and purified using flash chromatography on silica gel using petroleum ether/ethyl acetate. Yield: 96%. **¹H NMR (CDCl₃, 400 MHz):** 8.76 (1H, s), 8.44 (2H, s), 3.18 (6H, s). **¹³C NMR (CDCl₃, 100 MHz):** 151.96, 150.50, 140.81, 42.67. **HRMS:** calculated for [M]⁺ C₆H₉N₃OS⁺ 171.0461; found 171.0461.

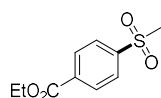


1-(pyridin-3-yl)pyrrolidin-2-one (P₉₉): The compound was prepared following the general *procedure IV*, using 3-bromopyridine (31.6 mg, 0.2 mmol, 1.0 equiv.), 2-pyrrolidone (30.6 mg, 0.36 mmol, 1.8 equiv.), 1,1,3,3-tetramethylguanidine (27.6 mg, 0.24 mmol, 1.2 equiv.), NiBr₂•glyme (3.2 mg, 0.01 mmol, 0.05 equiv.), and 4CzIPN (0.5 mol%, 0.001 mmol, 0.005 equiv.). ACN (0.5 mL) was used as a solvent. The reaction mixture was irradiated under N₂ at 60 °C for 30h using a single blue LED (455 (± 15) nm). After completion, the reaction mixture was subjected to the workup procedure outlined in general *procedure IV* and purified using flash chromatography on silica gel using petroleum ether/ethyl acetate. Yield: 54%. **¹H NMR (CDCl₃, 400 MHz):** 8.72 (1H, d, *J* = 2.4 Hz), 8.38 (1H, d, *J* = 4.7 Hz), 8.26 (1H, ddd,

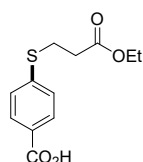
$J = 8.4, 2.4, 1.3$ Hz), 7.32 (1H, dd, $J = 8.4, 4.7$ Hz), 3.89 (2H, t, $J = 7.0$ Hz), 2.62 (2H, t, $J = 8.1$ Hz), 2.21 (2H, tt, $J = 8.1, 7.0$ Hz). ^{13}C NMR (CDCl_3 , 100 MHz): 174.90, 145.00, 140.13, 127.40, 123.69, 48.05, 32.42, 18.15. HRMS: calculated for $[\text{M}]^+ \text{C}_9\text{H}_{10}\text{N}_2\text{O}^+$ 162.0788; found 162.0785.



1-(pyridin-3-yl)-1H-indole (P₁₀₆): The compound was prepared following the general *procedure IV* using 3-bromopyridine (31.6 mg, 0.2 mmol, 1.0 equiv.), indole (70.2 mg, 0.6 mmol, 3.0 equiv.), 1,1,3,3-tetramethylguanidine (27.6 mg, 0.24 mmol, 1.2 equiv.), $\text{NiBr}_2 \bullet \text{glyme}$ (3.2 mg, 0.01 mmol, 0.05 equiv.), and 4CzIPN (0.5 mol%, 0.001 mmol, 0.005 equiv.). DMF (0.4 mL) was used as a solvent. The reaction mixture was irradiated under N_2 at 80 °C for 24h using a single blue LED (455 (\pm 15) nm). After completion, the reaction mixture was subjected to the workup procedure outlined in general *procedure IV* and purified using flash chromatography on silica gel using petroleum ether/ethyl acetate. Yield: 62%. ^1H NMR (CDCl_3 , 400 MHz): 8.85 (1H, dd $J = 2.5, 0.5$ Hz), 8.62 (1H, dd $J = 4.8, 1.5$ Hz), 7.85 (1H, ddd $J = 8.2, 2.5, 1.5$ Hz), 7.74-7.68 (1H, m), 7.56-7.51 (1H, m), 7.48 (1H, ddd $J = 8.2, 4.8, 0.5$ Hz), 7.33 (1H, d, $J = 3.3$), 7.30-7.24 (1H, m), 7.24-7.19 (1H, m), 6.75 (1H, dd, $J = 3.3, 0.7$). ^{13}C NMR (CDCl_3 , 100 MHz): 147.53, 145.70, 136.58, 135.88, 131.55, 129.61, 127.51, 124.25, 123.04, 121.52, 121.05, 110.09, 104.96. HRMS: calculated for $[\text{M}]^+ \text{C}_{13}\text{H}_{10}\text{N}_2^+$ 194.0838; found 194.0833.

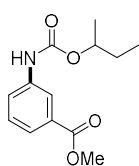


ethyl 4-(methylsulfonyl)benzoate (P₁₄₀): The compound was prepared following the general *procedure II'*, using ethyl 4-bromobenzoate (45.8 mg, 0.2 mmol, 1.0 equiv.), sodium methanesulfinate (36.7 mg, 0.36 mmol, 1.8 equiv.), 1,4-diazabicyclo[2.2.2]octane (49.3 mg, 0.44 mmol, 2.2 equiv.), triethylamine (10.1 mg, 0.1 mmol, 0.5 equiv.), $\text{NiBr}_2 \bullet \text{glyme}$ (3.2 mg, 0.01 mmol, 0.05 equiv.), and 4CzIPN (0.5 mol%, 0.001 mmol, 0.005 equiv.). DMA (1.2 mL) was used as a solvent. The reaction mixture was irradiated under N_2 at 25 °C for 3h using a single blue LED (455 (\pm 15) nm). After completion, the reaction mixture was subjected to the workup procedure outlined in general *procedure II'* and purified using flash chromatography on silica gel using petroleum ether/ethyl acetate. Yield: 89%. ^1H NMR (CDCl_3 , 400 MHz): 8.21 (2H, d, $J = 8.5$ Hz), 8.00 (2H, d, $J = 8.5$ Hz), 4.40 (2H, q, $J = 7.2$ Hz), 3.06 (3H, s), 1.40 (3H, t, $J = 7.2$ Hz). ^{13}C NMR (CDCl_3 , 100 MHz): 165.01, 144.23, 135.31, 130.56, 127.52, 61.91, 44.39, 14.31. HRMS: calculated for $[\text{M}]^+ \text{C}_{10}\text{H}_{12}\text{O}_4\text{S}^+$ 228.0451; found 228.0448.

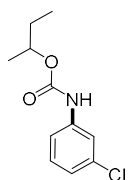


4-((3-ethoxy-3-oxopropyl)thio)benzoic acid (P₁₅₀): The compound was prepared following the general *procedure I*, using 4-bromobenzoic acid (40.2 mg, 0.2 mmol, 1.0 equiv.), ethyl 3-mercaptopropionate (40.2 mg, 0.3 mmol, 1.5 equiv.),

NiBr₂•glyme (3.2 mg, 0.01 mmol, 0.05 equiv.), and 4CzIPN (0.5 mol%, 0.001 mmol, 0.005 equiv.). DMA (0.4 mL) was used as a solvent. The reaction mixture was irradiated under N₂ at 25 °C for 4h using a single blue LED (455 (± 15) nm). After completion, the reaction mixture was subjected to the workup procedure outlined in general *procedure I* and purified using flash chromatography on silica gel using DCM/MeOH. Yield: 81%. ¹H NMR (CDCl₃, 400 MHz): 11.03, (1H, br s), 8.00 (2H, d, *J* = 8.3 Hz), 7.34 (2H, d, *J* = 8.3 Hz), 4.17 (2H, q, *J* = 7.1 Hz), 3.27 (2H, t, *J* = 7.4 Hz), 2.69 (2H, t, *J* = 7.4 Hz), 1.26 (3H, t, *J* = 7.1 Hz). ¹³C NMR (CDCl₃, 100 MHz): 171.91, 171.59, 144.25, 130.77, 126.91, 126.37, 61.10, 34.03, 27.24, 14.28. HRMS: calculated for [M]⁺ C₁₂H₁₄O₄S⁺ 254.0607; found 254.0611.

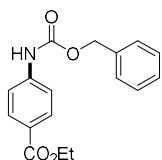


methyl 3-((sec-butoxycarbonyl)amino)benzoate (P₁₆₁): The compound was prepared following the general *procedure II'*, using methyl 3-bromobenzoate (43.0 mg, 0.2 mmol, 1.0 equiv.), sodium cyanate (19.5 mg, 0.3 mmol, 1.5 equiv.), 2-butanol (81.4 mg, 1.1 mmol, 5.5 equiv.), 1,4-diazabicyclo[2.2.2]octane (29.1 mg, 0.26 mmol, 1.3 equiv.), triethylamine (7.3 mg, 0.72 mmol, 0.36 equiv.), NiBr₂•glyme (3.2 mg, 0.01 mmol, 0.05 equiv.), and 4CzIPN (0.1 mol%, 0.0002 mmol, 0.001 equiv.). DMA (0.4 mL) was used as a solvent. The reaction mixture was irradiated under N₂ at 60 °C for 36h using a single blue LED (455 (± 15) nm). After completion, the reaction mixture was subjected to the workup procedure outlined in general *procedure II'* and purified using flash chromatography on silica gel using petroleum ether/ethyl acetate. Yield: 72%. ¹H NMR (CDCl₃, 400 MHz): 8.04 (1H, s), 7.77 (1H, d, *J* = 7.7 Hz), 7.70 (1H, d, *J* = 7.8 Hz), 7.41-7.31 (1H, m), 7.18 (1H, br s), 4.84 (1H, tq, *J* = 6.3, 6.3 Hz), 3.89 (3H, s), 1.72-1.47 (2H, m), 1.25 (3H, d, *J* = 6.3 Hz), 0.92 (3H, t, *J* = 7.5 Hz). ¹³C NMR (CDCl₃, 100 MHz): 167.07, 153.60, 138.77, 130.86, 129.18, 124.23, 123.05, 119.69, 73.57, 52.31, 29.06, 19.75, 9.74. HRMS: calculated for [M+NH₄]⁺ C₁₃H₂₁N₂O₄⁺ 269.1496; found 269.1497.

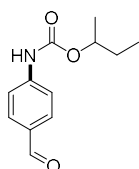


sec-butyl (3-chlorophenyl)carbamate (P₁₆₂): The compound was prepared following general *procedure II*, using 1-bromo-3-chlorobenzene (38.3 mg, 0.2 mmol, 1.0 equiv.), sodium cyanate (19.5 mg, 0.3 mmol, 1.5 equiv.), 2-butanol (40.74 mg, 0.55 mmol, 2.75 equiv.), 1,4-diazabicyclo[2.2.2]octane (29.1 mg, 0.26 mmol, 1.3 equiv.), NiBr₂•glyme (3.2 mg, 0.01 mmol, 0.05 equiv.), and 4CzIPN (0.5 mol%, 0.001 mmol, 0.005 equiv.). DMA (0.4 mL) was used as a solvent. The reaction mixture was irradiated under N₂ at 60 °C for 48h using a single blue LED (455 (± 15) nm). After completion, the reaction mixture was subjected to the workup procedure outlined in general *procedure II* and purified using flash chromatography on silica gel using petroleum ether/ethyl acetate. Yield: 38%. ¹H

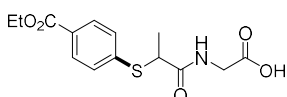
NMR (CDCl₃, 400 MHz): 7.52 (1H, s), 7.25-7.17 (2H, m), 7.05-6.98 (1H, m), 6.75 (1H, br s), 4.84 (1H, tq, *J* = 6.3, 6.3 Hz), 1.73-1.50 (2H, m), 1.26 (3H, d, *J* = 6.3 Hz), 0.93 (3H, t, *J* = 7.5 Hz). **¹³C NMR (CDCl₃, 100 MHz):** 153.33, 139.50, 134.82, 130.06, 123.31, 118.73, 116.63, 73.80, 29.06, 19.75, 9.76.



ethyl 4-(((benzyloxy)carbonyl)amino)benzoate (P₁₆₃): The compound was prepared following the general *procedure II*, using ethyl 4-bromobenzoate (45.8 mg, 0.2 mmol, 1.0 equiv.), sodium cyanate (19.5 mg, 0.3 mmol, 1.5 equiv.), benzyl alcohol (64.8 mg, 0.6 mmol, 3.0 equiv.), 1,4-diazabicyclo[2.2.2]octane (29.1 mg, 0.26 mmol, 1.3 equiv.), NiBr₂•glyme (3.2 mg, 0.01 mmol, 0.05 equiv.), and 4CzIPN (0.5 mol%, 0.001 mmol, 0.005 equiv.). DMA (0.4 mL) was used as a solvent. The reaction mixture was irradiated under N₂ at 60 °C for 24h using a single blue LED (455 (± 15) nm). After completion, the reaction mixture was subjected to the workup procedure outlined in general *procedure II* and purified using flash chromatography on silica gel using petroleum ether/ethyl acetate. Yield: 83%. **¹H NMR (CDCl₃, 400 MHz):** 7.99 (2H, d, *J* = 8.7 Hz), 7.47 (2H, d, *J* = 8.7 Hz), 7.43-7.28 (5H, m), 7.07 (1H, br s), 5.21 (2H, s), 4.35 (2H, q, *J* = 7.1 Hz), 1.37 (3H, t, *J* = 7.1 Hz). **¹³C NMR (CDCl₃, 100 MHz):** 166.36, 153.07, 142.18, 135.83, 130.99, 128.78, 128.61, 128.48, 125.32, 117.69, 67.42, 60.95, 14.45.

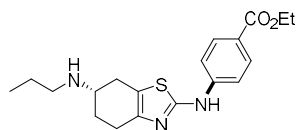


7sec-butyl (4-formylphenyl)carbamate (P₁₆₇): The compound was prepared following the general *procedure II*, using 4-bromobenzaldehyde (37.0 mg, 0.2 mmol, 1.0 equiv.), sodium cyanate (19.5 mg, 0.3 mmol, 1.5 equiv.), 2-butanol (81.4 mg, 1.1 mmol, 5.5 equiv.), 1,4-diazabicyclo[2.2.2]octane (29.1 mg, 0.26 mmol, 1.3 equiv.), NiBr₂•glyme (3.2 mg, 0.01 mmol, 0.05 equiv.), and 4CzIPN (0.5 mol%, 0.001 mmol, 0.005 equiv.). DMA (0.4 mL) was used as a solvent. The reaction mixture was irradiated under N₂ at 60 °C for 18h using a single blue LED (455 (± 15) nm). After completion, the reaction mixture was subjected to the workup procedure outlined in general *procedure II* and purified using flash chromatography on silica gel using petroleum ether/ethyl acetate. Yield: 82%. **¹H NMR (CDCl₃, 400 MHz):** 9.88 (1H, s), 7.81 (2H, d, *J* = 8.6 Hz), 7.59 (2H, d, *J* = 8.6 Hz), 7.38 (1H, br s), 4.85 (1H, tq, *J* = 6.3, 6.3 Hz), 1.71-1.48 (2H, m), 1.25 (3H, d, *J* = 6.3 Hz), 0.91 (3H, t, *J* = 7.4 Hz). **¹³C NMR (CDCl₃, 100 MHz):** 191.29, 153.09, 144.30, 131.39, 131.39, 118.02, 74.05, 28.98, 19.70, 9.72. **HRMS:** calculated for [M]⁺ C₁₂H₁₅NO₃⁺ 221,1046; found 221,1046.



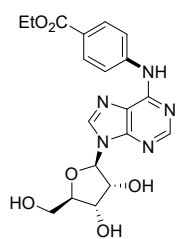
(2-((4-(ethoxycarbonyl)phenyl)thio)propanoyl)glycine (P₁₈₉): The compound was prepared following the general *procedure I*, using ethyl

4-bromobenzoate (45.8 mg, 0.2 mmol, 1.0 equiv.), tiopronin (34.2 mg, 0.21 mmol, 1.05 equiv.), NiBr₂•glyme (3.2 mg, 0.01 mmol, 0.05 equiv.), and 4CzIPN (0.5 mol%, 0.001 mmol, 0.005 equiv.). DMA (0.4 mL) was used as solvent. The reaction mixture was irradiated under N₂ for 6h using a single blue LED (455 (± 15) nm). After completion, the reaction mixture was subjected to the workup procedure outlined in general *procedure I* and purified using flash chromatography on silica gel. Yield: 61%. ¹H NMR (CDCl₃, 400 MHz): 7.92 (2H, d, *J* = 8.4 Hz), 7.34 (2H, d, *J* = 8.4 Hz), 7.20 (1H, t, *J* = 5.3 Hz), 6.19 (1H, br s), 4.35 (2H, q, *J* = 7.1 Hz), 4.03 (2H, d, *J* = 5.3 Hz), 3.98 (1H, q, *J* = 7.3 Hz), 1.60 (3H, d, *J* = 7.3 Hz), 1.37 (3H, t, *J* = 7.1 Hz). ¹³C NMR (CDCl₃, 100 MHz): 172.96, 172.66, 166.40, 140.43, 130.33, 128.79, 128.47, 61.32, 45.86, 41.54, 18.28, 14.43. HRMS: calculated for [M+H]⁺ C₁₄H₁₈NO₅S⁺ 312.0900; found 312.0908.



ethyl (R)-4-((6-(propylamino)-4,5,6,7-tetrahydrobenzo[d]thiazol-2-yl)amino)benzoate (P₁₉₆): The compound was prepared following the general *procedure III*, using ethyl 4-bromobenzoate (45.8 mg, 0.2

mmol, 1.0 equiv.), pramipexole (63.3 mg, 0.3 mmol, 1.5 equiv.), cyclohexylamine (25.7 mg, 0.26 mmol, 1.3 equiv.), NiBr₂•glyme (3.2 mg, 0.01 mmol, 0.05 equiv.), and 4CzIPN (0.5 mol%, 0.001 mmol, 0.005 equiv.). DMA (0.4 mL) was used as a solvent. The reaction mixture was irradiated under N₂ at 60 °C for 20h using a single blue LED (455 (± 15) nm). After completion, the reaction mixture was subjected to the workup procedure outlined in general *procedure III* and purified using flash chromatography on silica gel using DCM/MeOH. Yield: 56%. ¹H NMR (d₄-MeOH, 400 MHz): 7.92 (2H, d, *J* = 8.9 Hz), 7.59 (2H, d, *J* = 8.9 Hz), 4.32 (2H, q, *J* = 7.1 Hz), 3.14-3.05 (1H, m), 3.00 (1H, dd, *J* = 15.4, 5.0 Hz), 2.83-2.61 (4H, m), 2.50 (1H, dd, *J* = 15.4, 8.9 Hz), 2.21-2.11 (1H, m), 1.80-1.68 (1H, m), 1.59 (2H, qt, *J* = 7.4, 7.4 Hz), 1.36 (3H, t, *J* = 7.1 Hz), 0.97 (3H, t, *J* = 7.4 Hz). ¹³C NMR (d₄-MeOH, 100 MHz): 168.05, 162.98, 147.00, 146.63, 131.87, 123.68, 117.45, 117.12, 61.77, 55.36, 49.69, 29.41, 29.38, 26.11, 23.32, 14.67, 11.97. HRMS: calculated for [M+H]⁺ C₁₉H₂₆N₃O₂S⁺ 360.1740; found 360.1741.

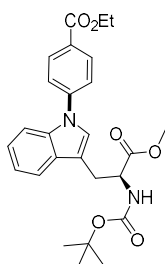


ethyl 4-((9-((2R,3R,4S,5R)-3,4-dihydroxy-5-(hydroxymethyl)tetrahydrofuran-2-yl)-9H-purin-6-yl)amino)benzoate (P₁₉₉): The compound was prepared following general *procedure III*, using ethyl

4-bromobenzoate (45.8 mg, 0.2 mmol, 1.0 equiv.), adenosine (106.8 mg, 0.4 mmol, 2.0 equiv.), cyclohexylamine (25.7 mg, 0.26 mmol, 1.3 equiv.),

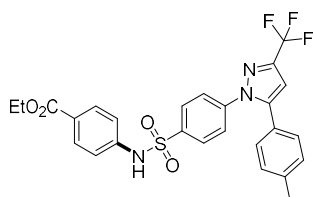
NiBr₂•glyme (3.2 mg, 0.01 mmol, 0.05 equiv.), and 4CzIPN (0.5 mol%, 0.001 mmol, 0.005 equiv.). DMA (0.4 mL) was used as solvent. The reaction mixture was irradiated under N₂ for 24h using a single blue LED (455 (± 15) nm). After completion, the reaction mixture was

subjected to the workup procedure outlined in general *procedure III* and purified using Reversed-phase flash chromatography using petroleum ether/ethyl acetate. Yield: 63%. **¹H NMR (d₄-MeOH, 400 MHz)**: 8.33 (1H, s), 8.22 (1H, s), 7.99 (2H, d, *J* = 9.0 Hz), 7.15 (2H, d, *J* = 9.0 Hz), 6.14-6.09 (1H, m), 5.21-5.13 (2H, m), 4.40-4.37 (1H, m), 4.33 (2H, q, *J* = 7.1 Hz), 3.95 (1H, dd, *J* = 12.6, 3.0 Hz), 3.95 (1H, dd, *J* = 12.6, 2.8 Hz), 1.37 (3H, t, *J* = 7.1 Hz). **¹³C NMR (d₄-MeOH, 100 MHz)**: 167.82, 163.16, 157.61, 153.59, 150.14, 142.13, 132.55, 124.66, 121.08, 116.44, 90.97, 85.71, 78.62, 74.45, 63.24, 61.91, 14.63. **HRMS**: calculated for [M+H]⁺ C₁₉H₂₂N₅O₆⁺ 416,1565; found 416,1570.



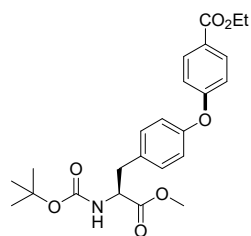
ethyl (S)-4-(3-(2-((tert-butoxycarbonyl)amino)-3-methoxy-3-oxopropyl)-1H-indol-1-yl)benzoate (P₂₀₁): The compound was prepared following general *procedure IV* using a syringe pump. The solution for syringe has been prepared from ethyl 4-bromobenzoate (91.6 mg, 0.4 mmol, 1.0 equiv.), 1,1,3,3-tetramethylguanidine (55.2 mg, 0.48 mmol, 1.2 equiv.) and DMA (600 μl), degassed and put into the syringe. methyl (*tert*-butoxycarbonyl)-*L*-tryptophanate

(254 mg, 0.8 mmol, 2.0 equiv.), NiBr₂•glyme (6.4 mg, 0.02 mmol, 0.05 equiv.), and 4CzIPN (1.6 mg, 0.002 mmol, 0.005 equiv.) have been dissolved in DMA (400 μl) and degassed in a crimp cap vial. The content of the syringe has been pushed into the reaction mixture *via* syringe pump for 40h during the photoirradiation under N₂ at 25 °C using a single blue LED (455 (± 15) nm). After the electrophile addition the reaction mixture has been irradiated for 8 h more. After completion, the reaction mixture was subjected to the workup procedure outlined in the general *procedure II* and purified using flash chromatography on silica gel using petroleum ether/ethyl acetate. Yield: 45%. **¹H NMR (CDCl₃, 400 MHz)**: 8.19 (2H, d, *J* = 8.6 Hz), 7.68-7.58 (2H, m), 7.55 (2H, d, *J* = 8.6 Hz), 7.30-7.23 (1H, m), 7.23-7.14 (2H, m), 5.14 (1H, d, *J* = 8.0 Hz), 4.34 (1H, dt, *J* = 8.0, 5.4 Hz), 4.42 (2H, q, *J* = 7.1 Hz), 3.72 (3H, s), 3.37 (1H, dd, *J* = 14.7, 5.4 Hz), 3.30 (1H, dd, *J* = 14.7, 5.4 Hz), 1.43 (3H, t, *J* = 7.1 Hz), 1.43 (9H, s). **¹³C NMR (CDCl₃, 100 MHz)**: 172.71, 166.04, 155.33, 143.51, 135.75, 131.34, 129.78, 128.04, 125.99, 123.30, 123.20, 120.97, 119.49, 112.92, 110.78, 80.07, 61.28, 54.12, 52.47, 28.45, 28.07, 14.50. **HRMS**: calculated for [M+H]⁺ C₂₆H₃₁N₂O₆⁺ 467,2177; found 467,2173.



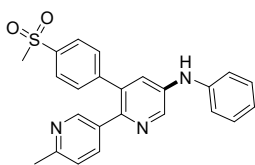
ethyl 4-((4-(5-(p-tolyl)-3-(trifluoromethyl)-1H-pyrazol-1-yl)phenyl)sulfonamido)benzoate (P₂₀₂): The compound was prepared following general *procedure IV*, using ethyl 4-bromobenzoate (45.8 mg, 0.2 mmol, 1.0 equiv.), celecoxib (152.4 mg, 0.4 mmol, 2.0 equiv.), NiBr₂•glyme (3.2 mg, 0.01 mmol, 0.05 equiv.), and 4CzIPN (0.5

mol%, 0.001 mmol, 0.005 equiv.), and 1,1,3,3-tetramethylguanidine (27.6 mg, 0.24 mmol, 1.2 equiv.). DMA (0.4 mL) was used as solvent. The reaction mixture was irradiated under N₂ at 60 °C for 24h using a single blue LED (455 (± 15) nm). After completion, the reaction mixture was subjected to the workup procedure outlined in general *procedure IV* and purified using flash chromatography on silica gel using petroleum ether/ethyl acetate. Yield: 79%. ¹H NMR (CDCl₃, 300 MHz): 10.92 (1H, br s), 7.86 (2H, d, *J* = 8.7 Hz), 7.85 (2H, d, *J* = 8.8 Hz), 7.51 (2H, d, *J* = 8.7 Hz), 7.22 (2H, d, *J* = 8.8 Hz), 7.16 (1H, s), 7.09 (2H, d, *J* = 8.4 Hz), 7.05 (2H, d, *J* = 8.4 Hz), 4.25 (2H, q, *J* = 7.1 Hz), 2.27 (3H, s), 1.27 (3H, d, *J* = 7.1 Hz). ¹³C NMR (CDCl₃, 75 MHz): 165.14, 145.31, 142.35 (q, *J*(C-F) = 37.5 Hz), 142.15, 141.92, 139.06, 138.82, 130.60, 129.29, 128.63, 128.09, 126.56, 125.19, 125.11, 121.25 (q, *J*(C-F) = 269.0 Hz), 118.91, 106.05, 60.59, 20.71, 14.14. HRMS: calculated for [M+H]⁺ C₂₆H₂₃F₃N₃O₄S⁺ 530,1356; found 530,1359.

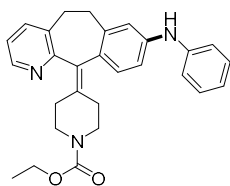


ethyl (R)-4-(4-(2-((tert-butoxycarbonyl)amino)-3-methoxy-oxopropyl)phenoxy)benzoate (P₂₀₅): The compound was prepared following general *procedure IV* using *syringe pump*. The solution for syringe has been prepared from ethyl 4-bromobenzoate (91.6 mg, 0.4 mmol, 1.0 equiv.), 1,1,3,3-tetramethylguanidine (55.2 mg, 0.48 mmol, 1.2

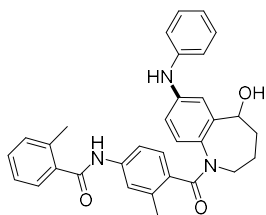
equiv.) and DMA (600 μl), degassed and put into the syringe. Methyl (tert-butoxycarbonyl)tyrosinate (236.3 mg, 0.8 mmol, 2 equiv.), NiBr₂•glyme (6.4 mg, 0.02 mmol, 0.05 equiv.), and 4CzIPN (1.6 mg, 0.002 mmol, 0.005 equiv.) have been dissolved in DMA (400 μl) and degassed in a crimp cap vial. The content of the syringe has been pushed into the reaction mixture *via* syringe pump for 40h during the photoirradiation under N₂ at 60 °C using a single blue LED (455 (± 15) nm). After the electrophile addition the reaction mixture has been irradiated for 8 h more. Upon completion, the reaction mixture was subjected to the workup procedure outlined in general *procedure X* and purified using flash chromatography on silica gel using petroleum ether/ethyl acetate. Yield: 59%. ¹H NMR (CDCl₃, 400 MHz): 8.00 (2H, d, *J* = 8.7 Hz), 7.14 (2H, d, *J* = 8.2 Hz), 6.98 (2H, d, *J* = 8.2 Hz), 6.96 (2H, d, *J* = 8.7 Hz), 5.03 (1H, d, *J* = 7.8 Hz), 4.59 (1H, dt, *J* = 7.8, 5.6 Hz), 4.35 (2H, q, *J* = 7.1 Hz), 3.72 (3H, s), 3.13 (1H, dd, *J* = 13.8, 5.6 Hz), 3.02 (1H, dd, *J* = 13.8, 5.6 Hz), 1.42 (9H, s), 1.38 (3H, t, *J* = 7.1 Hz). ¹³C NMR (CDCl₃, 100 MHz): 172.36, 166.22, 161.70, 155.15, 154.88, 132.36, 131.74, 130.99, 125.05, 120.12, 117.46, 80.12, 60.95, 54.58, 52.40, 37.96, 28.42, 14.48. HRMS: calculated for [M+Na]⁺ C₂₄H₂₉NNaO₇⁺ 466.1836; found 466.1843.



6'-methyl-3-(4-(methylsulfonyl)phenyl)-N-phenyl-[2,3'-bipyridin]-5-amine (P₂₁₅): The compound was prepared following the general *procedure II'*, using etoricoxib (71.8 mg, 0.2 mmol, 1.0 equiv.), aniline (37.2 mg, 0.4 mmol, 2.0 equiv.), 1,4-diazabicyclo[2.2.2]octane (49.3 mg, 0.44 mmol, 2.2 equiv.), triethylamine (5.05 mg, 0.25 mmol, 0.25 equiv.), NiBr₂•glyme (3.2 mg, 0.01 mmol, 0.05 equiv.), and 4CzIPN (0.1 mol%, 0.0002 mmol, 0.001 equiv.). DMA (0.4 mL) was used as a solvent. The reaction mixture was irradiated under N₂ at 80 °C for 24h using a single blue LED (455 (± 15) nm). After completion, the reaction mixture was subjected to the workup procedure outlined in general *procedure II'* and purified using flash chromatography on silica gel using petroleum ether/ethyl acetate. Yield: 67%. ¹H NMR (CDCl₃, 400 MHz): 8.51-8.44 (1H, m), 8.34 (1H, d, *J* = 1.9 Hz), 7.84 (2H, d, *J* = 8.0 Hz), 7.60-7.52 (1H, m), 7.39-7.33 (3H, m), 7.33-7.27 (2H, m), 7.15 (2H, d, *J* = 8.0 Hz), 7.09-6.96 (2H, m), 6.57 (1H, br s), 3.06 (3H, s), 2.51 (3H, s). ¹³C NMR (CDCl₃, 100 MHz): 156.75, 149.01, 145.37, 144.69, 141.04, 139.88, 139.68, 138.98, 137.93, 134.76, 132.67, 130.47, 129.75, 127.79, 124.08, 123.10, 122.97, 119.39, 44.60, 23.75. HRMS: calculated for [M+H]⁺ C₂₄H₂₂N₃O₂S⁺ 416,1427; found 416,1431.

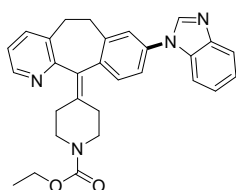


ethyl 4-(8-(phenylamino)-5,6-dihydro-11H-benzo[5,6]cyclohepta[1,2-b]pyridin-11-ylidene)piperidine-1-carboxylate (P₂₂₀): The compound was prepared following the general *procedure II'*, using loratadine (76.6 mg, 0.2 mmol, 1.0 equiv.), aniline (37.2 mg, 0.4 mmol, 2.0 equiv.), 1,4-diazabicyclo[2.2.2]octane (49.3 mg, 0.44 mmol, 2.2 equiv.), triethylamine (5.05 mg, 0.25 mmol, 0.25 equiv.), NiBr₂•glyme (3.2 mg, 0.01 mmol, 0.05 equiv.), and 4CzIPN (0.1 mol%, 0.0002 mmol, 0.001 equiv.). The 4CzIPN photocatalyst was added in 5 portions every 10 hours). DMA (0.4 mL) was used as a solvent. The reaction mixture was irradiated under N₂ at 80 °C for 48h using a single blue LED (455 (± 15) nm). After completion, the reaction mixture was subjected to the workup procedure outlined in general *procedure II'* and purified using flash chromatography on silica gel using petroleum ether/ethyl acetate. Yield: 86%. ¹H NMR (d₆-acetone, 300 MHz): 8.37 (1H, dd, *J* = 4.8, 1.4 Hz), 7.46 (1H, dd, *J* = 7.6, 1.1 Hz), 7.27-7.17 (2H, m), 7.15-7.07 (2H, m), 7.02 (2H, d, *J* = 8.0 Hz), 6.96-6.75 (3H, m), 5.83 (1H, br s), 4.12 (2H, q, *J* = 7.1 Hz), 4.00-3.66 (3H, m), 3.42-3.25 (2H, m), 3.21-3.04 (2H, m), 2.90-2.67 (2H, m), 2.65-2.58 (2H, m), 2.54-2.21 (4H, m). ¹³C NMR (d₆-acetone, 75 MHz): 157.91, 155.59, 145.95, 142.91, 142.64, 138.56, 137.80, 136.83, 134.37, 134.13, 131.24, 130.61, 129.38, 122.23, 121.10, 118.12, 117.75, 115.22, 69.59, 61.36, 53.88, 44.94, 44.83, 32.19, 31.82, 31.57, 29.33, 14.76. HRMS: calculated for [M+H]⁺ C₂₈H₃₀N₃O₂⁺ 440.2333; found 440.2336.



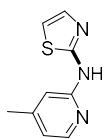
N-(4-(5-hydroxy-7-(phenylamino)-2,3,4,5-tetrahydro-1H-benzo[b]azepine-1-carbonyl)-3-methylphenyl)-2-methylbenzamide (P₂₂₁):

The compound was prepared following the general *procedure II'*, using tolvaptan (89.8 mg, 0.2 mmol, 1.0 equiv.), aniline (37.2 mg, 0.4 mmol, 2.0 equiv.), 1,4-diazabicyclo[2.2.2]octane (49.3 mg, 0.44 mmol, 2.2 equiv.), triethylamine (5.05 mg, 0.25 mmol, 0.25 equiv.), NiBr₂•glyme (6.4 mg, 0.02 mmol, 0.1 equiv.), and 4CzIPN (0.2 mol%, 0.0004 mmol, 0.002 equiv.). DMA (0.4 mL) was used as a solvent. The reaction mixture was irradiated under N₂ at 80 °C for 48h using a single blue LED (455 (± 15) nm). After completion, the reaction mixture was subjected to the workup procedure outlined in general *procedure II'* and purified using flash chromatography on silica gel using petroleum ether/ethyl acetate. Yield: 60%. ¹H NMR (d₆-acetone, 300 MHz): 9.59-9.09 (1H, m), 7.85-6.50 (15H, m), 5.46-4.71 (2H, m), 4.71-4.30 (1H, m), 4.10-3.14 (1H, m), 2.81-2.66 (1H, m), 2.64-2.33 (6H, m), 2.32-2.16 (1H, m), 1.89-1.56 (2H, m). ¹³C NMR (d₆-acetone, 75 MHz): 169.58, 168.70, 144.43, 144.28, 143.50, 140.22, 138.02, 137.19, 136.77, 133.64, 133.30, 131.50, 130.56, 129.93, 129.15, 127.90, 127.61, 126.39, 121.64, 121.10, 118.34, 116.56, 115.46, 113.69, 71.44, 47.11, 37.17, 27.08, 20.18, 19.76.

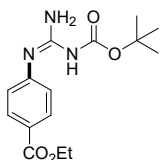


ethyl 4-(8-(1H-benzo[d]imidazol-1-yl)-5,6-dihydro-11H-benzo[5,6]cyclohepta[1,2-b]pyridin-11-ylidene)piperidine-1-carboxylate (P₂₂₈):

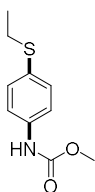
The compound was prepared following slightly modified general *procedure IV*, using loratadine (76.6 mg, 0.2 mmol, 1.0 equiv.), benzimidazole (70.8 mg, 0.6 mmol, 3.0 equiv.), 1,1,3,3-tetramethylguanidine (27.6 mg, 0.24 mmol, 1.2 equiv.), tributylamine (12.2 mg, 0.066 mmol, 0.33 equiv.), NiBr₂•glyme (3.2 mg, 0.01 mmol, 0.05 equiv.), and 4CzIPN (0.2 mol%, 0.0004 mmol, 0.0025 equiv.). DMA (0.4 mL) was used as solvent. The reaction mixture was irradiated under N₂ at 80 °C for 48h using a single blue LED (455 (± 15) nm). After completion, the reaction mixture was subjected to the workup procedure outlined in general *procedure IV* and purified using flash chromatography on silica gel using petroleum ether/ethyl acetate. Yield: 21%. ¹H NMR (CDCl₃, 300 MHz): 8.41 (1H, dd, *J* = 4.8, 1.4 Hz), 8.33 (1H, s), 7.79-7.70 (1H, m), 7.68-7.57 (2H, m), 7.54 (1H, d, *J* = 2.1 Hz), 7.49 (1H, dd, *J* = 8.1, 2.1 Hz), 7.40 (1H, d, *J* = 8.1 Hz), 7.34-7.26 (2H, m), 7.20 (1H, dd, *J* = 7.7, 4.8 Hz), 4.10 (2H, q, *J* = 7.1 Hz), 3.80-3.67 (2H, m), 3.63-3.41 (2H, m), 3.41-3.24 (2H, m), 3.07-2.93 (2H, m), 2.53-2.39 (2H, m), 2.38-2.19 (2H, m), 1.22 (3H, t, *J* = 7.1 Hz). ¹³C NMR (CDCl₃, 75 MHz): 158.39, 155.74, 147.44, 145.40, 143.53, 141.14, 139.88, 138.16, 137.93, 136.41, 135.25, 134.50, 134.47, 131.66, 125.30, 124.16, 123.18, 121.18, 121.96, 121.05, 111.51, 61.55, 45.69, 45.56, 32.48, 31.96, 31.59, 31.39, 15.02. HRMS: calculated for [M+H]⁺ C₂₉H₂₉N₄O₂⁺ 465.2285; found 465.2290.



N-(4-methylpyridin-2-yl)thiazol-2-amine (P₂₄₀): The compound was prepared following the general *procedure III*, using 2-bromothiazole (32.8 mg, 0.2 mmol, 1.0 equiv.), 4-methylpyridin-2-amine (32.4 mg, 0.3 mmol, 1.5 equiv.), cyclohexylamine (25.7 mg, 0.26 mmol, 1.3 equiv.), NiBr₂•glyme (3.2 mg, 0.01 mmol, 0.05 equiv.), and 4CzIPN (0.5 mol%, 0.001 mmol, 0.005 equiv.). DMA (0.4 mL) was used as a solvent. The reaction mixture was irradiated under N₂ at 25 °C for 19h using a single blue LED (455 (± 15) nm). After completion, the reaction mixture was subjected to the workup procedure outlined in general *procedure III* and purified using flash chromatography on silica gel using DCM/MeOH. Yield: 79%. ¹H NMR (d₆-acetone, 300 MHz): 10.65 (1H, br s), 8.19 (1H, d, *J* = 5.2 Hz), 7.41 (1H, d, *J* = 3.6 Hz), 6.97 (1H, s), 6.93 (1H, d, *J* = 3.6 Hz), 6.78 (1H, d, *J* = 5.2 Hz), 2.33 (3H, s). ¹³C NMR (d₆-acetone, 75 MHz): 161.56, 153.17, 149.79, 147.14, 138.04, 118.31, 111.63, 111.31, 21.09. **HRMS:** calculated for [M]⁺ C₉H₉N₃S⁺ 191.0512; found 191.0506.

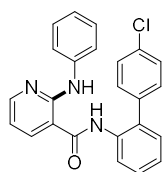


ethyl 4-(3-(tert-butoxycarbonyl)guanidino)benzoate (P₂₅₀): The compound was prepared following the general *procedure I*, using ethyl 4-bromobenzoate (45.8 mg, 0.2 mmol, 1.0 equiv.), *N*-boc-guanidine (79.5 mg, 0.5 mmol, 2.5 equiv.), NiBr₂•glyme (3.2 mg, 0.01 mmol, 0.05 equiv.), and 4CzIPN (0.5 mol%, 0.001 mmol, 0.005 equiv.). DMA (0.4 mL) was used as a solvent. The reaction mixture was irradiated under N₂ at 25 °C for 30h using a single blue LED (455 (± 15) nm). After completion, the reaction mixture was subjected to the workup procedure outlined in general *procedure I* and purified using flash chromatography on silica gel using petroleum ether/ethyl acetate. Yield: 84%. ¹H NMR (CDCl₃, 300 MHz): 7.99 (2H, d, *J* = 8.5 Hz), 7.10 (2H, d, *J* = 8.5 Hz), 6.96 (3H, br s), 4.33 (2H, q, *J* = 7.1 Hz), 1.36 (3H, t, *J* = 7.1 Hz), 1.28 (9H, s). ¹³C NMR (CDCl₃, 75 MHz): 166.40, 142.09, 131.28, 123.52, 81.03, 60.91, 28.06, 14.43. **HRMS:** calculated for [M+H]⁺ C₁₅H₂₂N₃O₄⁺ 308.1605; found 308.1607.



methyl (4-(ethylthio)phenyl)carbamate (P₂₆₂): The compound was prepared following the general *procedure I* using 1,4-dibromobenzene (47.2 mg, 0.2 mmol, 1.0 equiv.), ethyl mercaptan (13.7 mg, 0.22 mmol, 1.1 equiv.), NiBr₂•glyme (3.2 mg, 0.01 mmol, 0.05 equiv.), and 4CzIPN (0.2 mol%, 0.0004 mmol, 0.002 equiv.). DMA (0.4 mL) was used as a solvent. The reaction mixture was irradiated under N₂ for at 25 °C for 2h using a single blue LED (455 (± 15) nm). After irradiation, the reaction mixture was degassed properly to remove the traces of the thiol. Sodium cyanate (19.5 mg, 0.3 mmol, 1.5 equiv.), methanol (40 mL, 1.0 mmol, 5.0 equiv.) and 1,4-diazabicyclo[2.2.2]octane (29.1 mg, 0.26 mmol, 1.3 equiv.)

were added to the reaction mixture and after degassing was irradiated under N₂ for at 60 °C for 12h using a single blue LED (455 (± 15) nm). After completion, the reaction mixture was subjected to the workup procedure outlined in general *procedure I* and purified using flash chromatography on silica gel using petroleum ether/ethyl acetate. Yield: 49%. ¹H NMR (CDCl₃, 400 MHz): 7.31 (2H, *J* = 9.0 Hz), 7.28 (2H, *J* = 9.0 Hz), 6.95 (1H, br s), 3.75 (3H, s), 2.86 (2H, q, *J* = 7.4 Hz), 1.25 (3H, t, *J* = 7.4 Hz). ¹³C NMR (CDCl₃, 100 MHz): 154.19, 136.54, 131.25, 130.36, 119.37, 52.43, 28.86, 14.53. HRMS: calculated for [M]⁺ C₁₀H₁₃NO₂S⁺ 211,0662; found 211,0660.



***N*-(4'-chloro-[1,1'-biphenyl]-2-yl)-2-(phenylamino)nicotinamide (P₂₆₇):** The compound was prepared following the general *procedure III*, using boscalid (68.6 mg, 0.2 mmol, 1.0 equiv.), aniline (27.9 mg, 0.30 mmol, 1.5 equiv.), NiBr₂•glyme (3.2 mg, 0.01 mmol, 0.05 equiv.), and 4CzIPN (0.1 mol%, 0.0002 mmol, 0.001 equiv.), and cyclohexylamine (25.7 mg, 0.26 mmol, 1.3 equiv.). DMA (0.4 mL) was used as a solvent. The reaction mixture was irradiated under N₂ at 60 °C for 24h using a single blue LED (455 (± 15) nm). After completion, the reaction mixture was subjected to the workup procedure outlined in general *procedure III* and purified using flash chromatography on silica gel using petroleum ether/ethyl acetate. Yield: 85%. ¹H NMR (d₆-acetone, 300 MHz): 10.35 (1H, br s), 8.31 (1H, dd, *J* = 4.8, 1.8 Hz), 8.23 (1H, d, *J* = 7.8 Hz), 7.75 (1H, br s), 7.71-7.64 (2H, m), 7.51-7.43 (3H, m), 7.41-7.24 (7H, m), 7.08-6.99 (1H, m), 6.63 (1H, dd, *J* = 7.8, 4.8 Hz). ¹³C NMR (d₆-acetone, 75 MHz): 166.43, 155.68, 152.06, 139.88, 136.50, 135.16, 134.52, 134.14, 132.52, 130.70, 130.39, 129.55, 128.99, 128.91, 125.56, 122.91, 122.78, 120.75, 113.19, 110.90. HRMS: calculated for [M+H]⁺ C₂₄H₁₉ClN₃O⁺ 400.1211; found 400.1216.

6.6.5 References

- [1] D. Bradley, G. Williams, M. Lawton *J. Org. Chem.* **2010**, *75*, 8351-8354.
- [2] E. Speckmeier, T. G. Fischer, K. Zeitler *J. Am. Chem. Soc.* **2018**, *140*, 15353-15365.
- [3] U. Megerle, R. Lechner, B. König, E. Riedle *Photochem. Photobiol. Sci.* **2010**, *9*, 1400-1406.

SUMMARY

7 Summary

This dissertation discusses the development and investigation of new reactivities in organic chemistry. The work aims to bridge photoredox catalysis and organic electrochemistry. Both systems can provide extreme redox potentials and are therefore suitable for challenging activations in organic chemistry.

Chapter 1 reviews recent work on synthetic photoelectrochemistry (PEC). Electrochemically mediated photoredox catalysis (e-PRC) demonstrates selective reductive and oxidative activation of strong bonds. We give an overview of the most important classes of radical ion/ radical pre-catalysts, their properties and applications. New achievements in C(sp²/ sp³)-N, C-O bond formations and C(sp²)-X, C(sp³)-O cleavages are discussed in detail. We show the advantages of electro-recycling of photocatalysts and present examples from C(sp²)-H trifluoromethylation, C(sp²)-C(sp³) coupling and C(sp²)-O/N bond forming reactions. The electro-recycling of common and newly developed HAT catalysts is demonstrated on C(sp²)-C(sp³) and C(sp³)-N couplings, expanding PEC beyond previous applications. In addition to promising approaches to scale-up by recirculation or continuous flow, we also present new reactor platforms that feature reproducibility, excellent control of reaction variables and high throughput.

Since PEC requires similar equipment to SOE, both systems are constrained by limited access to electrochemical equipment. To solve this problem, we offer an alternative to commercial voltage sources (Chapter 2). An induction-based device recovers part of the rotational energy from magnetic stirrers, which is then available for synthetic electrochemistry. After rectification, the induced AC voltage was employable in constant current (c.c) or constant voltage (c.v) mode. In a comparative study with conventional devices on six different functionalizations including C-CF₃, C-Me, C-CO₂Me, C(sp²)-C(sp³), Si-O and C-N bond formation, the applicability of the device was demonstrated without significant deviations.

Despite the freely selectable voltage, electrochemistry is not the universal solution for extreme redox potentials. Selectivity problems that occur when several molecules/bonds have a similar redox potential can be circumvented with e-PRC. In chapter 3, we used a modified naphthalene diimide derivative (ⁿBuO-NpMI) in e-PRC for reductive cleavage of C(sp³)-O bonds. Under exceedingly mild conditions, phosphinates of aliphatic alcohols were reduced to carbanions, while halides/pseudohalides with similar or more accessible redox potentials remained untouched. The presence of a α -C(sp²)-X bond allows for *E*-selective olefination, which can be converted to *Z*-selectivity *via* a tandem reduction/photosensitization process. This photoisomerization occurs *via* energy transfer from the catalyst's lower-lying, longer-lived, excited state. The reduction of the phosphinates occurs from a different excited state (D_{n/n+1}). Based on calculations, it was shown that the electron density of the active catalyst is transferred

from the naphthalene to the *N*-aniline unit. The necessary spatial proximity between the catalyst and substrate makes the system highly selective despite the extreme redox potential.

To achieve a high redox potential for oxidative processes, we employed a catalyst that combines e-PRC and homogeneous photoredox catalysis. By accumulating the energy of more than one photon, consecutive photoinduced electron transfer (conPET) has proven to be a useful tool for expanding the accessible redox potential. We contribute to this field by the development of an oxidative conPET system based on cyclic planar triaryl amines (Chapter 4). As demonstrated by the oxidative coupling of electron-deficient halobenzenes with pyrazoles and purines, this system provides an oxidation power of $> +3$ V (vs. SCE). The feasibility of photoelectrocatalysis and the applicability of the catalysts for nucleophilic C-F substitution (S_NAr) extends the possible applications. In contrast to other reports, we observed neither reactivity from higher excited states nor pre-organization of catalyst and substrate. We also have spectroscopic evidence for productive reactivity from the lowest excited state of Ar_3N^+ . By limiting the rotational relaxation of the Ar_3N^+ , ridged systems were found to be more catalytically active than open systems.

In order to generate extreme redox potentials by means of heterogeneous photocatalysis, a semiconductor material with a suitable band structure is required. Diamond semiconductors have a unique negative electron affinity and high p-type surface conductivity, which is why the material has many applications in electrochemistry. How these properties can be harnessed for heterogeneous photocatalysis was investigated in chapter 5. Excitation of hydrogen-terminated detonation nanodiamonds (DND-H) at 395 nm releases a reduction potential of -3 V, which has been successfully used in the hydrodehalogenation of electron-rich aryl halides. While esters and acids are tolerated, ketones and aldehydes undergo Pinacol-type coupling reactions. Suggesting a radical mechanism, detailed studies including deuteration experiments, radical trapping and the use of an acid-terminated catalyst confirmed this hypothesis, excluding the involvement of solvated electrons or HAT. Reusability and low manufacturing costs make the material suitable for the detoxification of dioxins, pesticides, and PCBs.

Finally, to emphasize the importance of photoredox catalysis, an example of its applicability in the synthesis of valuable compounds is given. We introduce adaptive dynamic homogeneous catalysis (AD-HoC) for photoredox nickel co-catalytic C(sp²)-(het)atom coupling reactions. In contrast to previous reports, this platform allows the prediction of conditions for C(sp²)-S, Se, N, P, B, O, C (sp³, sp², sp), Si and Cl reactions and makes extensive optimization obsolete. Classification of nucleophiles regarding their ability to coordinate with nickel allowed us to define simple standard conditions which can be adjusted for each group by adding an amine base. Mass spectroscopic investigations revealed a dynamic Ni(I)/Ni(III) equilibrium involving more than one catalytically competent species. We propose that under photocatalytic conditions Ni(II) species are reduced to Ni(I) complexes, allowing for the oxidative addition of (het)aryl halides.

The resulting Ni(III) species then undergoes reductive elimination to yield the cross-coupling product. This method serves as a universal solution, demonstrated in hundreds of examples, including FDA-approved drugs. The simple scalability and the possibility to create rapid complexity *via* bi-functionalization reactions are additional benefits. The general classification of nucleophiles and the amount of created data can be a starting point for artificial intelligence and machine learning processes in cross-coupling reactions.

In our research for the development of new catalytic systems with extreme redox potentials, we have observed new reactivities in photo- and photoelectrocatalysis. The DND-H material, the presented triarylamine conPET system, and our ⁿBuONpMI e-PRC system all exhibit extreme redox strength. Extensive mechanistic studies explain the selectivity despite the high potential and synthetic examples demonstrate their applicability. Additional examples of electrochemistry and photo-nickel co-catalysis underline the importance of photo- and electrochemical processes in organic synthesis.

ZUSAMMENFASSUNG

8 Zusammenfassung

Diese Dissertation befasst sich mit der Entwicklung und Untersuchung von katalytischen Systemen in der organischen Chemie. Die Arbeit zielt darauf ab, eine Brücke zwischen der Photoredoxkatalyse und der organischen Elektrochemie zu schlagen. Beide Systeme können extreme Redoxpotentiale zur Verfügung stellen und eignen sich damit für die Realisierung anspruchsvoller Aufgabenstellungen. Es werden daher Verfahren der Photo- und Photoelektrokatalyse vorgestellt, die sich durch eben solche Redoxpotentiale auszeichnen.

Kapitel 1 gibt einen Überblick über die jüngsten Arbeiten zur synthetischen Photoelektrochemie (PEC). Die elektrochemisch vermittelte Photoredoxkatalyse (e-PRC) erlaubt eine selektive Aktivierung starker Bindungen, sowohl reduktiv als auch oxidativ. Wir geben hier einen Überblick über die wichtigsten Klassen von Radikationen/Radikal Katalysatoren, ihre Eigenschaften und Anwendungen. Neue Ergebnisse bei der Bildung von $C(sp^2/sp^3)$ -N und C-O-Bindungen sowie bei der Spaltung von $C(sp^2)$ -X und $C(sp^3)$ -O Bindungen werden ausführlich diskutiert. Wir erläutern die Vorteile des Elektro-Recyclings von Photokatalysatoren und präsentieren Beispiele von $C(sp^2)$ -H Trifluormethylierung, $C(sp^2)$ - $C(sp^3)$ - und $C(sp^2)$ -O/N Kupplungen. Das Elektro-Recycling gängiger und neu entwickelter HAT-Katalysatoren wird anhand von $C(sp^2)$ - $C(sp^3)$ - und $C(sp^3)$ -N Kupplungen demonstriert. Neben vielversprechenden Ansätzen zur Steigerung des Reaktionsdurchsatzes in kontinuierlichen Prozessen stellen wir auch gänzlich neue Reaktorplattformen vor.

Da für PEC und SOE identische Labornetzgeräte benötigt werden, ist ein einfacher Zugang zu geeigneten Spannungsquellen wünschenswert. Um diesen zu erleichtern, zeigen wir in Kapitel 2 eine Alternative zu kommerziellen Netzgeräten für den Einsatz im Syntheselabor. Hierfür wurde ein Gerät entwickelt, das durch Induktion einen Teil der Rotationsenergie von Magnetrührern zurückgewinnt und diese dann für die synthetische Elektrochemie zur Verfügung stellt. Nach Gleichrichtung kann die induzierte Wechselfeldspannung im galvanostatischen (c.c.) oder potentiostatischen (c.v.) Betrieb genutzt werden. Eine Vergleichsstudie zwischen konventionellen Spannungsquellen und diesem Gerät zeigt keine signifikanten Abweichungen der Ausbeuten. Untersucht wurden sechs verschiedene Funktionalisierungen organischer Moleküle, darunter C-CF₃, C-Me, C-CO₂Me, $C(sp^2)$ - $C(sp^3)$, Si-O und C-N-Bindungsknüpfungen. Die Anwendung in der organischen Elektrosynthese des Geräts wurde damit bewiesen.

Trotz der frei wählbaren Spannung ist die Elektrochemie nicht die Universallösung für extreme Redoxpotentiale. Auftretende Selektivitätsprobleme bei Molekülen und Bindungen mit ähnlichen Redoxpotentialen lassen sich mit der e-PRC umgehen. In Kapitel 3 kommt ein modifiziertes Naphthalin-Diimid-Derivat (ⁿBuO-NpMI) für die reduktive Spaltung von $C(sp^3)$ -O Bindungen mittels Photoelektrokatalyse zum Einsatz. Unter äußerst milden Bedingungen wurden

Phosphinate aliphatischer Alkohole zu Carbanionen reduziert, während Halogenide und Pseudohalogenide mit ähnlichen oder weniger negativen Redoxpotentialen nicht reagierten. Das Vorhandensein einer C(sp²)-X Bindung in α -Position ermöglicht eine *E*-selektive Olefinierung, die über einen Reduktions-/Photosensibilisierungsprozess in eine *Z*-Selektivität umgewandelt werden kann. Diese *E/Z*-Isomerisierung erfolgt durch Energieübertragung aus einem tief liegenden, langlebigen, angeregten Zustand des Katalysators. Die Reduktion der Phosphinate erfolgt aus einem anderen angeregten Zustand ($D_{n/n+1}$). Anhand von Berechnungen konnte gezeigt werden, dass die Elektronendichte des aktiven Katalysators vom Naphthalin auf die *N*-Anilineinheit übertragen wird. Die notwendige räumliche Nähe zwischen Katalysator und Substrat macht das System, trotz des extremen Redoxpotentials, sehr selektiv.

Um hohe Redoxpotentiale für oxidative Prozesse zu realisieren, wurde auf einen Katalysator übergegangen, der sich sowohl für die e-PRC als auch die homogene Photokatalyse eignet. Durch die Akkumulation der Energie von mehr als einem Photon hat sich der konsekutive photoinduzierte Elektronentransfer (conPET) als nützliches Instrument zur Erweiterung des zugänglichen Redoxpotentials erwiesen. In Kapitel 4 werden hierfür zyklische planare Triarylamine eingesetzt. An der oxidativen Kupplung von elektronenarmen Arylhalogeniden mit Pyrazolen und Purinen gezeigt, bietet dieses System eine Oxidationskraft von $> +3$ V (vs. SCE). Die Katalysatoren lassen sich zudem auch zur nukleophilen C-F-Substitution (S_NAr) von Fluorbenzolen einsetzen. Im Gegensatz zu früheren Arbeiten beobachten wir weder eine Reaktivität aus höher liegenden angeregten Zuständen noch eine Vororientierung von Katalysator und Substrat zueinander. Wir fanden außerdem spektroskopischen Nachweis für produktive Reaktivität aus dem niedrigsten angeregten Zustand des Ar_3N^{+} . Durch die Einschränkung der Rotation der Arylgruppen wird eine thermische Relaxation des angeregten Ar_3N^{+} gehemmt. Infolgedessen erwiesen sich geschlossene Systeme katalytisch aktiver als offene.

Als neue Katalysatoren für extreme Redoxpotentiale in der heterogenen Photoredoxkatalyse wurden Diamant-Materialien ausgewählt. Diamant-Halbleiter haben eine einzigartig negative Elektronenaffinität und einen hohen p-Typ-Charakter, weshalb das Material zahlreiche Anwendungen in der Elektrochemie findet. Wie diese Eigenschaften photokatalytisch nutzbar gemacht werden können, wurde in Kapitel 5 untersucht. Die Anregung von Detonationsnanodiamanten, deren Oberfläche mit Wasserstoff funktionalisiert wurde (DND-H), bei 395 nm, setzt ein Reduktionspotential von -3 V frei. Elektronenreiche Arylhalogenide ließen sich in einer Suspension von DND-H in Acetonitril damit erfolgreich hydrodehalogenieren. Während Ester- und Säurefunktionalitäten toleriert werden, kommt es bei Ketonen und Aldehyden zu Pinakol-Kopplungsreaktionen. Detaillierte Untersuchungen, darunter Deuterierungsexperimente und das Abfangen von Intermediaten, bestätigten die Hypothese eines radikalischen Mechanismus. Eine Beteiligung solvatisierter Elektronen oder ein Wasserstoffatomtransfer kann somit ausgeschlossen werden. Die Anwendung im katalytischen

Abbau von Dioxinen, Pestiziden und PCBs ist durch die Wiederverwendbarkeit und den niedrigen Preis des Materials denkbar.

Um die Bedeutung der Photoredoxkatalyse insgesamt zu verdeutlichen, zeigt das letzte Kapitel eine Anwendung zur Synthese komplexer Moleküle. Wir stellen die adaptive, dynamische, homogene Katalyse (AD-HoC) für Photo/Nickel-Kupplungsreaktionen vor. Im Gegensatz zu bisherigen Herangehensweisen bietet dieses System eine Plattform, von der aus Vorhersagen zu Reaktionsbedingungen für C(sp²)-S-, Se-, N-, P-, B-, O-, C- (sp³, sp², sp), Si- und Cl-Reaktionen getroffen werden können. Eine umfangreiche Optimierung wird damit überflüssig. Die Klassifizierung der Nukleophile hinsichtlich ihrer Fähigkeit, mit Nickel zu koordinieren, ermöglichte es uns, einfache Standardbedingungen zu definieren, die für jede Gruppe durch Zugabe einer Aminbase angepasst werden können. Diese Methode ist daher eine universelle Lösung die an hunderten von Beispielen, darunter auch von der FDA zugelassene Arzneimittel, nachgewiesen wurde. Die einfache Skalierbarkeit und die Möglichkeit in Reaktionskaskaden schnell komplexe Verbindungen zu erzeugen, sind weitere Vorteile. Die allgemeine Klassifizierung von Nukleophilen und die hierbei erzeugten Daten können zudem ein Ausgangspunkt für künstliche Intelligenz und maschinelle Lernprozesse bei Kreuzkupplungsreaktionen sein.

Abschließend lässt sich zusammenfassen, dass unseren Untersuchungen zu katalytischen Systemen mit extremen Redoxpotentialen neue Reaktivitäten der Photo- und Photoelektrokatalyse offengelegt haben. Mit DND-Materialien als heterogene Photoredoxkatalysatoren und zyklischen Triarylaminen als homogene Photoredoxkatalysatoren sowie NpMI-Derivaten als Vertreter der Photoelektrokatalyse wurden drei neue katalytische Systeme mit besonders hohem Redoxpotential vorgestellt. Zusätzliche Beispiele aus Elektrochemie und Photokatalyse unterstreichen die Bedeutung von photo- und elektrochemischen Prozessen in der organischen Synthese.

APPENDIX

9 Appendix

9.1 Abbreviations

4-CzIPN	1,2,3,5-tetrakis(carbazol-9-yl)-4,6-dicyanobenzene
4-DPAIPN	1,3-dicyano-2,4,5,6-tetrakis(diphenylamino)-benzene
a.u.	arbitrary unit
AC	alternating current
ACN	acetonitrile
AD-HoC	adaptive dynamic homogeneous catalysis
An	anthracene
BDE	bond dissociation enthalpy
BDFE	bond dissociation-free energies
BHT	butylated hydroxytoluene
BPI	benzo[ghi]perylene monoamide
Bpin	bis(pinacolato)diboron
bpy	2,2'-bipyridine
c.c.	constant current
c.v.	constant voltage
Cat	catalyst
CB	conducting band
CFL	compact fluorescent lamp
conPET	consecutive photoinduced electron transfer
CV	cyclic voltammetry
DABCO	1,4-diazabicyclo [2.2.2]octane
DADS	decay associated difference spectra
DBP	diodobis(difluoroboron)-1,2-bis((1 <i>H</i> -pyrrol-2-yl)methylene)hydrazine
DBU	1,8-diazabicyclo[5.4.0]undec-7-en

DC	direct current
DCA	9,10-dicyanoanthracene, 9,10-dicyanoanthracene
DDQ	2,3-dichloro-5,6-dicyano-1,4-benzoquinone
DFT	density functional theory
DIPEA	<i>N, N</i> -diisopropylethylamine
DMA	<i>N, N</i> -dimethylacetamide
dmb	4,4'-dimethyl-2,2'-bipyridine
DMF	<i>N, N</i> -dimethylformamide
DMSO	dimethyl sulfoxide
DND	detonation nanodiamond
DND-COOH	acid terminated nanodiamond
DND-H	hydrogen-terminated detonation nanodiamond
DPA	9,10-diphenyl anthracene
EDA	electron donor-acceptor
EH	energy harvesting
EPR	electron paramagnetic resonance
e-PRC	electrochemically-mediated photoredox catalysis
Fc	ferrocene
FID	flame ionization detector
GC	gas chromatography
glyme	ethylene glycol dimethyl ether complex
HAT	hydrogen atom transfer
HMDSO	hexamethyl disiloxane
HP	high power
HPLC	high-performance liquid chromatography
HRMS	high-resolution molecular spectroscopy
IC	internal conversion
IET	intermolecular vibronic energy transfer, intermolecular vibronic energy transfer
IR	infrared

IVR	intramolecular vibrational energy redistribution
LED	light-emitting diode
LMCT	ligand-to-metal charge transfer
MCRI	multireference configuration interaction
MeOH	methanol
Mes-Acr	9-mesityl-10-methyl acridinium
MTBD	7-methyl-1,5,7- triazabicyclo(4.4.0)dec-5-ene
NBS	<i>N</i> -bromosuccinimide
NCS	<i>N</i> -chlorosuccinimide
ND	neutral-density
NDI	naphthalene diimide
NEt ₃	triethylamine
NHPI	<i>N</i> -hydroxy phthalimide
NMR	nuclear magnetic resonance
NpMI	<i>N</i> -(2,6-di-iso-propylphenyl)naphthalene monoimide
PAT	process analytical technologies
PC	photocatalyst
PCB	polychlorinated biphenyl
PDI	perylene diimides
PE	petroleum ether
PEC	photoelectrochemistry
PRC	photoredox catalysis
Prod	product
PS	photosensitizer, power supply
PTZ	phenothiazine
RE	reference electrode
Rh6G	rhodamine 6G
rpm	rounds per minute
RVC	reticulated vitreous carbon

SAS	species-associated spectra
SCE	saturated calomel electrode
SET	single electron transfer
SnAr	nucleophilic aromatic substitution
SOE	synthetic organic electrochemistry
Sub	substrate
SVD	singular value decomposition
TAC	trisaminocyclopropenium
TBADT	tetra- <i>n</i> -butylammonium decatungstate
TBAP	tetrabutylammonium hexafluorophosphate
TCSPC	time-correlated single photon counting
TEMPO	2,2,6,6-tetramethylpiperidinyloxyl
TFE	trifluoroethanol
TLC	thin-layer chromatography
TMG	1,3,3-tetramethylguanidine
TPA	tri(<i>p</i> -substituted)arylamine
TPPD	tetraphenyl-para-phenylenediamine
TPTNP	tetraphenyltetranaphtho [2,3] porphyrin
TTA	triplet-triplet annihilation
TTBP	tetratertbutylperylene
TTET	triplet-triplet energy transfer
UV	ultra violet
VB	valence band
Vis	visible spectrum
WE	working electrode
ZPVE	zero-point vibrational energy

9.2 Curriculum Vitae

Personal Data

Name: Tobias Alwin Karl
Date and Place of birth: 03.06.1993, Neumarkt i. d. Opf.
Nationality: German

Education

10/2018 03/2023 **Ph.D. in Organic Chemistry**
Institute of Organic Chemistry, University of Regensburg
“New Concepts of Reactivity in Photo- & Photoelectrocatalysis”
Supervisor: Prof. Dr. Burkhard König
Funding: PhD Scholarship by Deutsche Bundesstiftung Umwelt (DBU)

04/2016 09/2018 **Master of Science in Chemistry**
Institute of Organic Chemistry, University of Regensburg
Master Thesis: *“Attempts Towards the Formation of Aryl Anions by Photoredox Catalysis”*
Supervisor: Prof. Dr. Burkhard König

10/2012 05/2016 **Bachelor of Science in Applied Chemistry**
Technical University of Nürnberg, Georg-Simon-Ohm
Bachelor Thesis: *“Pretreatment of Technical Ceramics for Electroless Chemical Metal Plating”*
Supervisor: Prof. Dr. Eberhard Aust
Company: SCHOTT AG, Landshut; Germany

03/2012 07/2012 **Allgemeine Fachhochschulreife (A-Levels)**
Technical Collage of Regensburg, Germany

09/2009 02/2012 **Vocational College**
Vocational College I Regensburg, Germany

Work Experience

08/2015 02/2016

Internship/Bachelor Thesis in Applied Chemistry

Company: SCHOTT AG, Landshut; Germany

“Pretreatment of Technical Ceramics for Electroless Chemical Metal Plating”

03/2014 06/2014

Internship in Applied Chemistry

Company: MAN Truck & Bus AG, Nürnberg, Germany

“Investigation of Deposits from Polyamide Components in the Vehicle Cooling System”

09/2009 06/2012

Vocational Training as a Mechatronics Engineer

Company: BMW AG, Regensburg, Germany

Internships Abroad

09/2019 10/2019

Research Internship

University of Ljubljana, Slovenia

Faculty of Chemistry and Chemical Technology

Supervisor: Prof. Dr. Jernej Iskra

Conferences & Summer Schools

09/2021 10/2022

CRC325Collaborative Research Centres by Deutsche Forschungsgemeinschaft (DFG) - *“Assembly Controlled Chemical Photocatalysis”*

03/2022

FloHet 2022

University of Florida, Gainesville, USA

Florida Heterocyclic and Synthetic Chemistry Conference

08/2019

29th Jyväskylä Summer School

Universität Jyväskylä, Finland

Electroorganic Synthesis by Prof. Dr. Siegfried R. Waldvogel

Publications

Ghosh I, Shlapakov N, **Karl TA**, Düker J, Nikitin M, Burykina JV, Ananikov VP, König B. A general premise for cross-coupling reactions with adaptive dynamic homogeneous catalysis. *Nature* 2023 (accepted article)

Karl TA, Seidl M, König B. Energy Harvesting: Synthetic Use of Recovered Energy in Electrochemical Late-Stage Functionalization. *Chem Electro Chem.* 2023;10, e202201097. doi:10.1002/celec.202201097.

Ritu, Das S, Tian YM, **Karl T**, Jain N, König B. Photocatalyzed Dehydrogenation of Aliphatic *N*-Heterocycles Releasing Dihydrogen. *ACS Catal.* 2022;12(16):10326-10332. doi:10.1021/acscatal.2c02830.

Wu S, Kaur J, **Karl TA**, Tian X, Barham JP. Synthetic Molecular Photoelectrochemistry: New frontiers in Synthetic Applications, Mechanistic Insights and Scalability. *Angew Chem Int Ed.* 2022;61(12). doi:10.1002/anie.202107811

Tian X, **Karl TA**, Reiter S, et al. Electro-mediated PhotoRedox Catalysis for Selective C(sp³)-O Cleavages of Phosphinated Alcohols to Carbanions. *Angew Chem Int Ed.* 2021;60(38):20817-20825. doi:10.1002/anie.202105895

Schirmer TE, Rolka AB, **Karl TA**, Holzhausen F, König B. Photocatalytic C-H Trifluoromethylthiolation by the Decatungstate Anion. *Org Lett.* 2021;23(15):5729-5733. doi:10.1021/acs.orglett.1c01870

Chen K, Schwarz J, **Karl TA**, Chatterjee A, König B. Visible light-induced redox neutral fragmentation of 1,2-diol derivatives. *Chem Commun.* 2019;55(87):13144-13147. doi:10.1039/C9CC06904F

Submitted Articles & Preprints

Bieszczad B, **Karl TA**, Rolka A, Nuernberger P, Kutta RJ, Koenig B, Oxidative conPET Catalysis for Arene Functionalization. *Chem. Rxiv.* 2022. <https://doi.org/10.26434/chemrxiv-2022-39x5>

DANKSAGUNG

10 Danksagung

Mein großer Dank gilt Prof. Dr. Burkhard König für die Möglichkeit der Promotion. Danke für das in mich gesetzte Vertrauen und die Unterstützung, sowohl in finanzieller als auch wissenschaftlicher Sicht. In den Jahren an Ihrem Lehrstuhl habe ich viel gelernt. Sie waren mir eine große Stütze bei der Entwicklung von Projekten und der Koordination von Kollaborationen. Darüber hinaus möchte ich mich für die Freiheit zur eigenständigen Verfolgung meiner Forschung und die Möglichkeit zur Teilnahme an nationalem und internationalem Austausch mit anderen Wissenschaftlern bedanken.

Für das Anfertigen des Zweitgutachtens danke ich Prof. Dr. Alexander Breder. Ich danke Prof. Dr. Michael Matysik für seine Rolle als Drittprüfer. Prof. Dr. Anke Bäumner danke ich für den Prüfungsvorsitz.

Ein besonderer Dank geht an die Deutsche Bundesstiftung Umwelt (DBU) und meinen Betreuer Dr. Hans-Christian Schäfer. Die finanzielle Förderung meiner Arbeit durch Ihr Stipendium hat mir sehr geholfen. Der durch Sie ermöglichte Austausch mit Stipendiaten aus ganz Deutschland war stets inspirierend und hat mein Umweltbewusstsein weiter geschärft.

Dem CRC 325: „Assembly Controlled Chemical Photocatalysis“ danke ich für die Möglichkeit meine Forschung auf interessanten sowie unterhaltsamen Seminartagen vorzustellen.

Für die wissenschaftliche Zusammenarbeit bedanke ich mich bei allen meinen zahlreichen Kooperationspartnern. Danke an: Dr. Joshua P. Barham, Dr. Bartosz Bieszczad, Dr. Anamitra Chatterjee, Dr. Kang Chen, Dr. Saikat Das, Jonas Düker, Dr. Indrajit Ghosh, Jaspreet Kaur, Prof. Dr. Anke Krüger, Dr. Roger-Jan Kutta, Prof. Dr. Patrick Nürnberger, Sebastian Reiter, Ritu, Alessa B. Rolka, Dr. Tobias E. Schirmer, Dr. Johanna Schwarz, Max Seidl, Nikita Shlapakov, Dr. Xianhai Tian, Dr. Ya-Ming Tian, Prof. Dr. Regina de Vivie-Riedle, Dr. Shangze Wu und Shahboz Yakubov. Ohne euch wären all die Projekte nicht möglich gewesen.

Den permanenten Mitarbeitern am Arbeitskreis König danke ich für einen reibungslosen Forschungsbetrieb. Mein Dank an: Barbara Bauer, Britta Badzuir, Dr. Petra Hilgers, Simone Strauß und Julia Zach für Hilfe bei Fragen aller Art. Ernst Lautenschlager danke ich für das Lösen jeglicher technischen Probleme, Dr. Rufolf Vasold für die schnelle und exzellente GC-FID und GC-MS Analysen und Regina Hoheisel für Ihre präzisen CV-Messungen.

In diesem Zug möchte ich mich auch bei den Mitarbeitern der Zentralen Analytik und der Elektrowerkstatt für die ausgezeichnete Arbeit bedanken.

Mein ganz besonderer Dank gilt denen Kollegen, die ich nun als Freunde bezeichnen darf. Ali, Uli, Julia, K-Boi, Indra und Tobi, ihr habt mir die Jahre versüßt.

Bei allen Weggefährten möchte ich mich für die Hilfsbereitschaft, gute Zusammenarbeit und ausgezeichnete Stimmung bedanken. Die Atmosphäre im Team hätte nicht besser sein können. Vor allem Karin Rustler, Alexander Wimmer, Andreas Graml, Bartosz Bieszad, Tanguy Saget, Grisa Princic, Michela Marcon, Rok Narobe, Karsten Donabauer, Nicolas Müller, Lea Müller, Alejandro Sanchez, Elina Taskiean und Dominik Birnthaler hatten daran sehr großen Anteil.

Meinen Studenten Baethe-Sandra Hoffelner, Benjamin Falge, Fiona Irlinger, Maximilian Phillip, Daniela Fritsch, Leon Ganser und Felix Müller danke ich für die tatkräftige Unterstützung.

Nicht zu vergessen sind die Mitglieder des wohl heißesten Beerpong Teams in der Geschichte des Arbeitskreises. Danke an Ulrike B. Wirth, Alessa B. Rolka und Ranit Lahmy für ihre zielsicheren Würfe und ihr geringes Gewicht. Ihr habt meine Leber und Bandscheiben geschont.

Den Bois: Johannes Moser, Dr. Matthias Ackermann, Dr. Karsten Donabauer und Vladas Maier verdanke ich die beste Zeit in Regensburg. Ihr seid Teil einer jeden guten Geschichte.

Mara Imdahl danke ich von tiefstem Herzen für die mir zuteil gewordene Unterstützung in jeder Hinsicht. Du hast die Jahre meiner Promotion maßgeblich mitbestimmt und dafür bin ich dir ewig dankbar.

Zu guter Letzt danke ich meiner Familie von ganzem Herzen. Meinen Geschwistern Bettina Kailer, Christina Sommerer und Simon Karl sowie meinen Eltern Irene und Georg Karl. Ohne euch stünde ich heute nicht hier.

11 Eidesstattliche Erklärung

- (1) Ich erkläre hiermit an Eides statt, dass ich die vorliegende Arbeit ohne unzulässige Hilfe Dritter und ohne Benutzung anderer als der angegebenen Hilfsmittel angefertigt habe; die aus anderen Quellen direkt oder indirekt übernommenen Daten und Konzepte sind unter Angabe des Literaturzitats gekennzeichnet.

- (2) Bei der Auswahl und Auswertung folgenden Materials haben mir die nachstehend aufgeführten Personen in der jeweils beschriebenen Weise entgeltlich/unentgeltlich geholfen:
 1. Das Manuskript zu Kapitel 1 wurde vor der Publikation durch J-P. Barham überarbeitet. S. Wu, J. Kaur und X. Tian haben den größten Teil des Artikels verfasst.
 2. Die in Kapitel 2 vorgestellte Apparatur wurde durch M. Seidl angefertigt.
 3. Die in Kapitel 3 gezeigten Produkte, Startmaterialien und Katalysatoren wurden durch X. Tian und S. Yakubov isoliert und charakterisiert. Alle gezeigten Berechnungen stammen von S. Reiter, R. de Vivie-Riedle und J-P. Barham.
 4. Das Konzept zu Kapitel 4 stammt von B. Bieszczad. Die gezeigten Produkte und Katalysatoren wurden zum größten Teil von B. Bieszczad isoliert und charakterisiert. A. B. Rolka hat einen Teil der Katalysatorsynthese übernommen. Das Manuskript, die Berechnungen und transiente Spektroskopie stammt von R. J. Kutta.
 5. Die Katalysatoren aus Kapitel 5 wurden von A. Krüger und Ihren Mitarbeitern hergestellt.
 6. I. Ghosh und N. Shlapakov führten die in Kapitel 6 gezeigten Reaktion durch. I. Ghosh, N. Shlapakov, J. Düker und M. Nikitin bereiteten Reaktionsansätze vor und isolierten Produkte. N. Shlapakov führte die Massenspektroskopischen Messungen durch. I. Ghosh führte die Auswertung der Ergebnisse und schrieb das Manuskript.

- (3) Weitere Personen waren an der inhaltlich-materiellen Herstellung der vorliegenden Arbeit nicht beteiligt. Insbesondere habe ich hierfür nicht die entgeltliche Hilfe eines Promotionsberaters oder anderer Personen in Anspruch genommen. Niemand hat von mir weder unmittelbar noch mittelbar geldwerte Leistungen für Arbeiten erhalten, die im Zusammenhang mit dem Inhalt der vorgelegten Dissertation stehen.
- (4) Die Arbeit wurde bisher weder im In- noch im Ausland in gleicher oder ähnlicher Form einer anderen Prüfungsbehörde vorgelegt

Regensburg, den 14.03.2023